INTERNAL COMBUSTION ENGINES

APPLIED THERMOSCIENCES

Colin R. Ferguson

Purdue University

JOHN WILEY & SONS

New York Chichester Brisbane Toronto Singapore

Library of Congress Cataloging in Publication Data:

Ferguson, Colin R.
Internal combustion engines, applied thermosciences.

Includes bibliographies and indexes.
1. Internal combustion engines. 2. Thermodynamics.
I. Title.
TJ756.F47 1985 621.43 85-6346
ISBN 0-471-88129-5

Printed in the United States of America

10 9 8 7 6 5 4 3 2 1

Preface

This book is intended first to demonstrate to the student the application of engineering sciences, especially thermal, and second it is a book about internal combustion engines. With respect to the latter, it is not all-encompassing. This approach is desirable because the design of internal combustion engines remains a highly empirical science. The development of such design requires the knowledge of methods and analysis that can be used to correlate or catalog the results of experiments and to design new ones.

Considerable effort is made at presenting the requisite thermodynamics. This is because most students have little, if any, experience applying the first law to unsteady processes in open systems or in differential form to closed systems and have experience with only the simplest of reacting gas mixtures.

Roughly two thirds of the book is devoted to thermodynamic analysis of internal combustion engines. In Chapter Two, processes are emphasized and equations of state are kept simple by assuming constant specific heats and analyzing heat engines rather than combustion engines. The first law of thermodynamics is applied to the engine cylinder treated as an open system during the intake and exhaust processes and as a closed system (when mass loss is neglected) during the compression, heat addition, and expansion processes. Methods of numerical integration of the unsteady conservation equations are discussed and employed. The use of professionally prepared subroutines available in math libraries is emphasized for solution.

Realistic equations of state, stoichiometry and predictions of chemical equilibrium are presented in Chapter Three and applied to the engine in chapter Four. The same processes introduced in Chapter Two for heat engines are used in Chapter Four but now applied to combustion engines. These chapters are rather vigorous and representative of the state of the art but are not necessarily cost effective in terms of teaching. For this reason cycle simulations are done using charts and tables provided in Appendix E. Here some of the rigor is relaxed so that the student can see more easily the most important features. The material is not, however, self-contained. This forces the student to read Chapters Three and Four and think through the applicable process relationships. I believe this brings to his or her attention how calcula-

INTERNAL COMBUSTION ENGINES

APPLIED THERMOSCIENCES

One
INTRODUCTION

This chapter is devoted to discussion of design and performance characteristics of basic engine types including conventional engines, state of the art engines, and alternative engines. Establishing nomenclature and explaining how engines work are emphasized.

1.1 SPARK IGNITION ENGINES

A schematic of a six cylinder Ford engine is shown in Figs. 1-1 and 1.2. Components of interest to us are labeled. Table 1-1 lists key dimensions, material, and performance parameters.

For any one cylinder, the crankshaft, connecting rod, piston, and head assembly can be represented by the mechanism shown in Fig. 1-3. Of particular interest are the following dimensions:

bore, b
connecting rod length, l
stroke, S
crank angle, θ

Top dead center of an engine refers to the crankshaft being in a position such that $\theta = 0°$. The volume in this position is minimum and is often called the *clearance volume*, V_0. *Bottom dead center* refers to the crankshaft being at $\theta = 180°$. The volume V_1, is maximum at bottom dead center.

The *compression ratio* is defined as the ratio of the maximum to minimum volume.

$$r = V_1/V_0 \tag{1.1}$$

The *displacement volume* is the difference between the maximum and minimum volume; for a single cylinder:

$$V_d = V_1 - V_0 = \frac{\pi}{4} b^2 S \tag{1.2}$$

For a multicylinder engine, multiply by the number of cylinders N_c. The Ford engine has six cylinders for a total displacement volume of 3.8 liters.

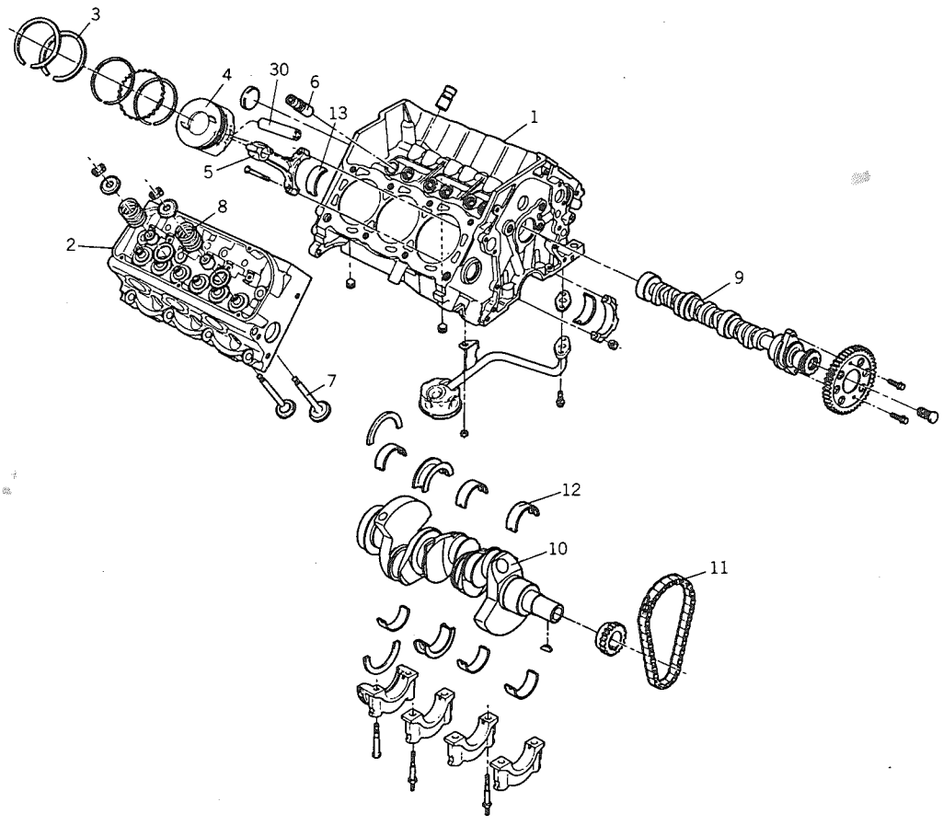

Key to Figs. 1-1 and 1-2

1 Cylinder block
2 Cylinder head
3 Piston ring
4 Piston
5 Connecting rod
6 Lifter
7 Valve
8 Valve spring
9 Camshaft
10 Crankshaft
11 Timing chain
12 Main bearing
13 Rod bearing
14 Carburetor
15 Throttle
16 Intake manifold
17 Thermostat
18 Flywheel
19 Distributor
20 Head gasket
21 Oil pan
22 Fuel pump
23 Water pump
24 Oil filter
25 Exhaust manifold
26 Rocker arm
27 Pushrod
28 Oil pump inside front cover
29 Spark plug

Figure 1-1 Ford 3.8 liter engine. Some of the engine's specifications are given in Table 1-1 (Armstrong and Stirrat, 1982). Reprinted with permission © 1982. Society of Automotive Engineers, Inc.

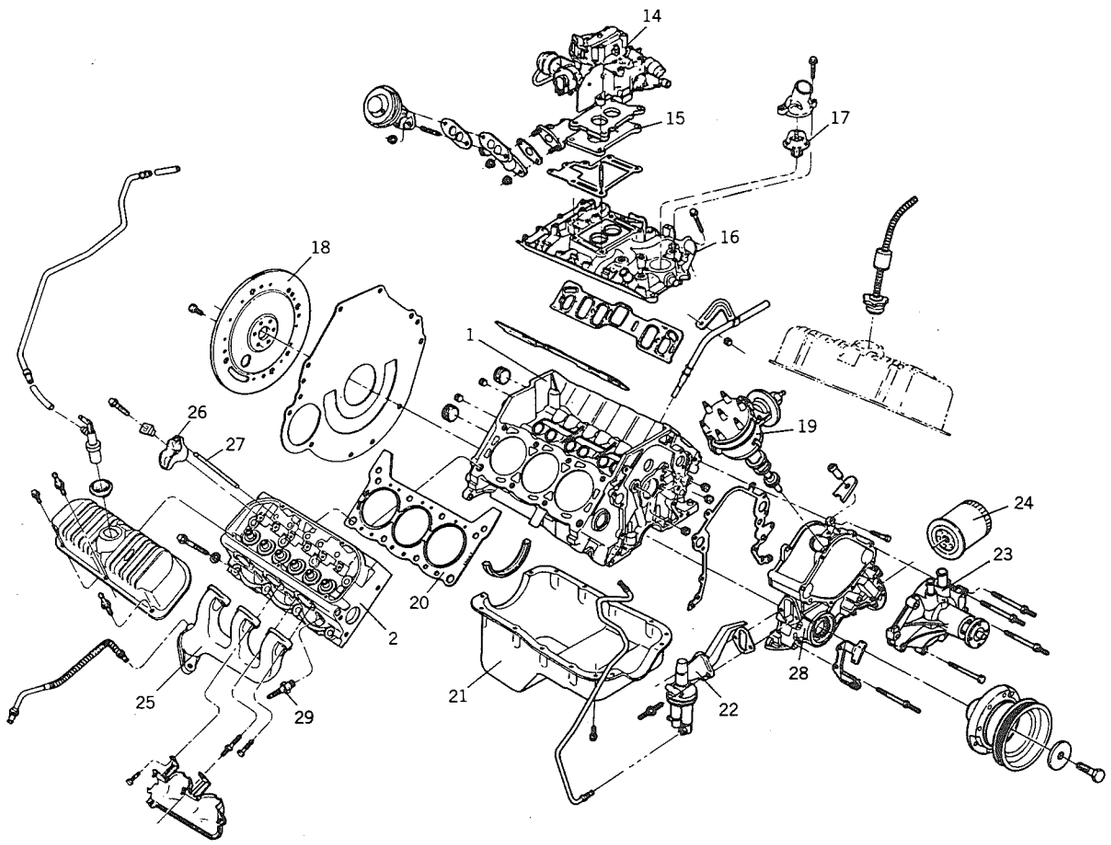

Figure 1-2 Ford 3.8 liter engine (Armstrong and Stirrat, 1982). Reprinted with permission © 1982. Society of Automotive Engineers, Inc.

Table 1-1 Example Automotive Engine Specifications

	FORD	GENERAL MOTORS	NISSAN
Number of cylinders	V-6	L-4	4, in line
Displacement, cm^3	3797	1991	1974
Bore, mm	96.8	89.0	84.5
Stroke, mm	86.0	80.0	88.0
Rod length, mm centerline to centerline	150.2	134.8	149.3
Bank angle, deg	90	NA	NA
Bank offset, mm	24.0	NA	NA
Bore spacing, mm	106.5	99.0	91.5
Compression ratio	8.6 : 1	9.0 : 1	8.5 : 1
Carburetor	Two Barrel Variable Venturi Downdraft	Staged two barrel (Varajet)	Two barrel
Valve lifters	Hydraulic	Hydraulic	OHC
Rocker arm ratio (nominal)	1.73 : 1	1.50 : 1	
Crankshaft main bearings	4	5	
Number of counterweights	2	4	4
Main bearing diameter, mm	64.0	63.35	53.0
Rod bearing diameter, mm	58.7	50.8	45.0
Piston pin diameter, mm	23.2	23.0	20.0
Valve head diameter, mm			
intake	45.3	40.6	40.0
exhaust	37.1	35.0	35.0
Valve lift, mm intake and exhaust	10.6	9.982	
Valve timing			
Intake opens, deg BTC	13	30	
Intake closes, deg ABC	56	90	
Exhaust opens, deg BBC	66	69	
Exhaust closes, deg ATC	17	51	
Valve spring load, Newtons			
Valve closed	311	384	
Valve open	912	933	
Material			
Cylinder block	Cast iron	Cast iron	Cast iron
Cylinder head	Semipermanent, mold aluminum	Cast iron	Die cast aluminum
Intake manifold	Die cast aluminum	Semipermanent, mold aluminum	Cast aluminum
Exhaust manifolds	Nodular cast iron	Nodular cast iron	Ductile cast iron
Crankshaft	Nodular cast iron	Nodular cast iron	Forged steel
Connecting rod	Forged steel	Forged steel	Forged steel
Piston	Permanent mold aluminum	Cast aluminum alloy	Cast aluminum alloy
Maximum power at rpm SAE gross, kW	102@4300	67.16@5000	66.0@5200
Maximum torque at rpm, SAE gross, Nm	271@2500	149.1@3600	155@2800
Firing order	1–4–2–5–3–6	1–3–4–2	
Oil flow, *l*/min at rpm	16@2500	9.0@2200	
Coolant flow, *l*/min at rpm	104@2500	51@2000	
Oil pressure, normal, KPA at rpm	345@2000	345@2000	
Mass, dressed kg	160	137	122

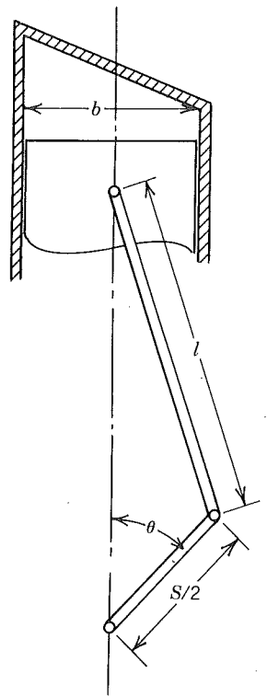

Figure 1-3 Slider crank model of piston cylinder geometry. Valid provided *wrist pin* is not offset. Using this geometry one can derive a relationship for piston position as a function of crank angle that will agree well with experimental values despite the finite bearing clearances in actual engines.

Engine speed R_s refers to the rotational speed of the crankshaft and is usually expressed as revolutions per minute. *Engine frequency* ω also refers to the rotation rate of the crankshaft but in units of radians per second. The *flywheel* is used to damp out fluctuations in engine speed that would be caused by the intermittent forcing torque.

Using the schematic shown in Fig. 1-3 as a model, a useful theoretical relationship can be derived for the instantaneous volume and piston speed for any given crank angle and engine frequency (see Homework Problem 1, this chapter). The *mean piston speed* is an important parameter in engine design since stresses and other factors *scale* with piston speed rather than with engine speed. Since the piston travels a distance of twice the stroke per revolution it should be clear that

$$\overline{U}_p = 2SR_s \tag{1.3}$$

Piston *rings* are used to seal the gases within the cylinder and to keep oil out. Notice that the rings have *gaps* to allow for thermal expansion during engine warm-up. As a result of the gaps, the seals are less effective and a certain amount of gas leaks out of the cylinder. This *blowby* degrades engine performance, as we shall see in Chapter 2. Similarly, a certain amount of oil leaks into the combustion chamber. However most of this oil is put to good use as a lubricant for the upper rings.

Gases are admitted and expelled from the cylinders by *valves* that open and close at the proper times. The *valve timing* is controlled by a *camshaft* that rotates at half the engine speed for a *four stroke* engine (see Fig. 1-4), as in the case of the Ford engine. In this example valve motion is controlled by *lobes* on the camshaft, *lifters*, *pushrods*, and *rocker arms*. Some engines use an *overhead camshaft* that eliminates pushrods and rocker arms, as in Fig. 1-5. The shape of the lobes determines when the valves open or close and what their rates of opening and closing will be.

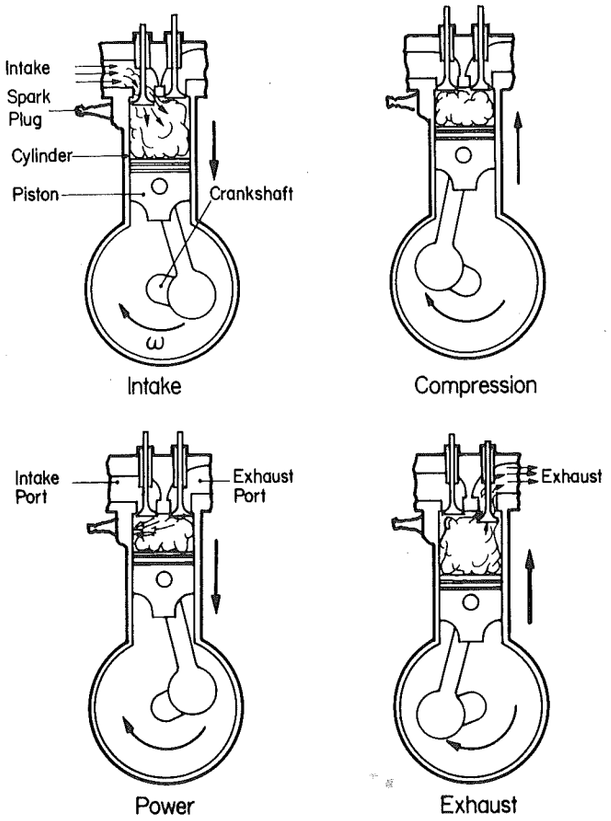

Figure 1-4 Four-stroke engine principle.

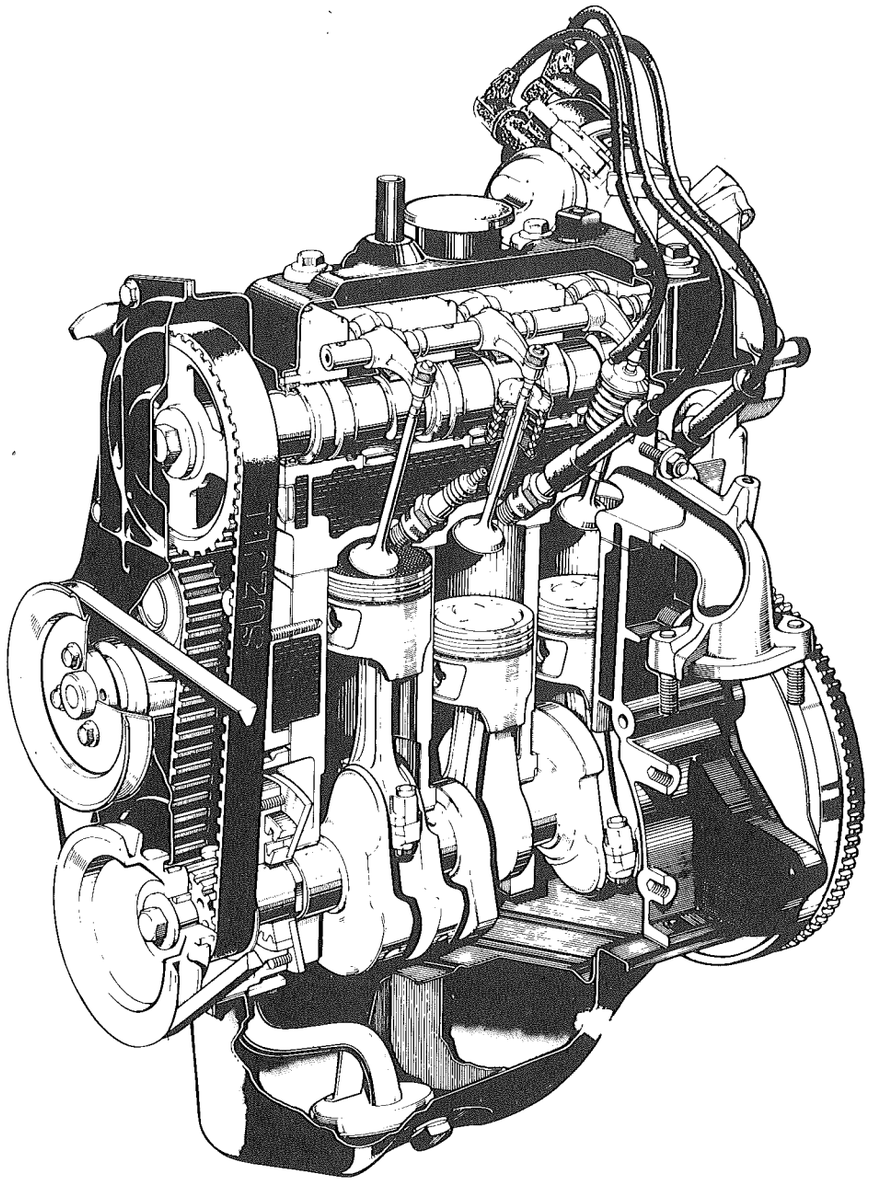

Figure 1-5 An overhead cam four-stroke engine. Notice that there are no pushrods, unlike the case in Fig. 1-1 and 1-2. Courtesy Suzuki Motor Co., LTD.

Examination of the general specifications of the Ford engine shows that the exhaust valve opens before the intake valve has shut. The period during which both valves are open simultaneously is called *overlap*. In this case the overlap is 122 deg. The *lift* specified refers to the maximum displacement of the valve. This is implied within the context of the specifications as *lift* may also refer to the instantaneous valve displacement.

Air and fuel enter the engine through the *carburetor*, whose function is to mix the fuel in proportion to the air flow. A *throttle* is part of the carburetor and is used to control the air inducted. Since the fuel flow is metered in proportion to the air flow, the throttle, in essence, controls the *power*. The *intake manifold* is a bundle of passages to distribute the fuel air mixture to individual cylinders. The *exhaust manifold* channels the exhaust from individual cylinders into a central pipe.

Some performance characteristics of the Ford engine are given in Fig. 1-6. The *brake* power refers to the power delivered by the engine; this is less than the boundary work done by the gas partly because of friction. The brake power $\mathbf{P}_b$ is the rate at which work is done; whereas *torque* τ is a measure of the work done per unit rotation (radians) of the crank. As we shall see when discussing *dynamometers* (used to measure torque), the two are related by

$$\mathbf{P}_b = 2\pi\tau R_s \tag{1.4}$$

The qualifications *gross* and *net* refer to definitions established by the Society of Automotive Engineers (SAE). The net power is from the complete engine;

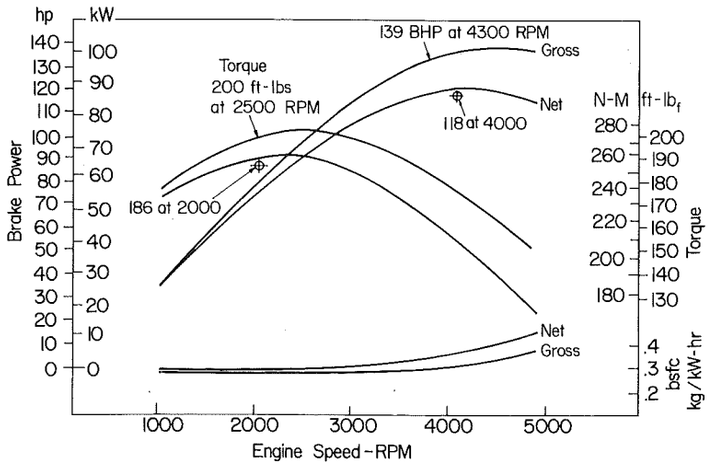

Figure 1-6 Wide open throttle performance of the Ford 3.8 liter engine. Measurements are made according to standards defined by the Society of Automotive Engineers, SAE J245 (Armstrong and Stirrat, 1982). Reprinted with permission © 1982. Society of Automotive Engineers, Inc.

whereas gross power is from an engine without the cooling fan, muffler, and tail pipe.

The results shown (Fig. 1-6) are at *wide open throttle*, WOT. The tests are run according to an SAE recommended procedure referred to as J245. As with most engines, the torque and power both exhibit maxima with engine speed. Maximum torque occurs at a lower speed than maximum power. Note that at high speeds the cooling fan requires considerable power.

The *brake specific fuel consumption*, bsfc, is a measure of engine efficiency. In fact bsfc and engine efficiency are inversely related, so that the lower the bsfc the better the engine. By definition the brake specific fuel consumption is the fuel flow rate $\dot{m}_f$, divided by the brake power $\mathbf{P}_b$

$$\text{bsfc} = \frac{\dot{m}_f}{\mathbf{P}_b} \tag{1.5}$$

Values of bsfc for the Ford engine given in Fig. 1-6 are typical of modern gasoline engines.

Engineers use bsfc rather than thermal efficiency primarily because a more or less universally accepted definition of thermal efficiency does not exist. We will explore why in Chapter 4. Note for now only that there is a problem with assigning a value to the energy content of the fuel. Let us call that available energy content a_c; the *brake thermal* efficiency is then

$$\eta = \frac{\mathbf{P}_b}{a_c \dot{m}_f} = \frac{1}{a_c \text{bsfc}} \tag{1.6}$$

Inspection of Eq. (1.6) shows that bsfc is a valid measure of efficiency provided a_c is held constant. Thus two different engines can be compared on a bsfc basis provided that they are operated on the same fuel.

Another performance parameter of importance is the *volumetric efficiency*, e_v. It is defined as the mass of fuel and air inducted into the cylinder divided by the mass that would occupy the displaced volume at the density ρ_i in the intake manifold.[1]

$$e_v = \frac{4\pi(\dot{m}_a + \dot{m}_f)}{\rho_i V_d \omega} = \frac{2(\dot{m}_a + \dot{m}_f)}{\rho_i V_d R_s} \tag{1.7}$$

As an aside, useful when deriving relationships for *two-stroke* versus four-stroke engines, it is often useful to write out the units in words, distinguishing cycles from revolutions. In a four-stroke engine there are two revolutions per cycle

[1] In Eq. (1.7), $\dot{m}_f$ is the flow rate of the fuel inducted. For a direct injection engine $\dot{m}_f = 0$. Related to volumetric efficiency is a parameter termed the *delivery ratio* defined in terms of the air flow only and the ambient air density instead of the intake manifold density.

but in a two-stroke engine there is only one. For example the factor 4 in equation 1.7 is clearly identified in the following equation.

$$e_v = \frac{\left(2\frac{\text{rev}}{\text{cycle}}\right)\left(\frac{2\pi \text{ rad}}{\text{rev}}\right)\left(\frac{\text{g}}{\text{s}}\right)}{\left(\frac{\text{g}}{\text{cm}^3}\right)\left(\frac{\text{cm}^3}{\text{cycle}}\right)\left(\frac{\text{rad}}{\text{s}}\right)} \tag{1.8}$$

Note the displacement volume is written as volume per cycle.

It is desirable to maximize the volumetric efficiency of an engine since the amount of fuel that can be burned for a given engine displacement (hence size and weight) is maximized. Although it does not influence in any way the thermal efficiency of the engine, it will influence the efficiency of the *system* in which it is installed. Clearly heavier engines in a vehicle will reduce the fuel economy. Thus if one can realize the same power from an engine that is lighter but of thermal efficiency comparable to the heavier one, the fuel economy will go up.

The volumetric efficiency is influenced by a number of engine parameters including valve size, valve lifts, valve timings, and intake manifold configuration. Figure 1-7 shows several configurations considered by Ford engineers and Fig. 1-8 shows the resulting volumetric efficiencies.

A major concern in intake manifold design is the ability to achieve a uniform fuel/air distribution from cylinder to cylinder. The *air–fuel ratio* of an engine is the ratio of air to fuel by mass in the inducted charge. This

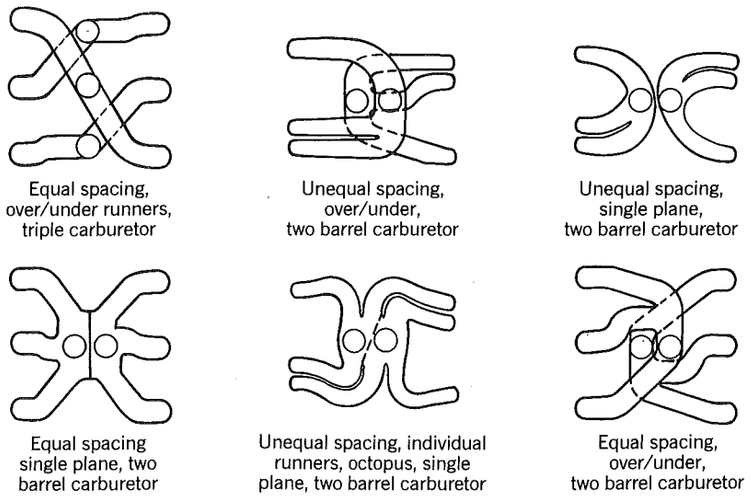

Figure 1-7 Intake manifold runner alternatives considered in the design of a Ford V-6 engine (Armstrong and Stirrat, 1982). Reprinted with permission © 1982. Society of Automotive Engineers, Inc.

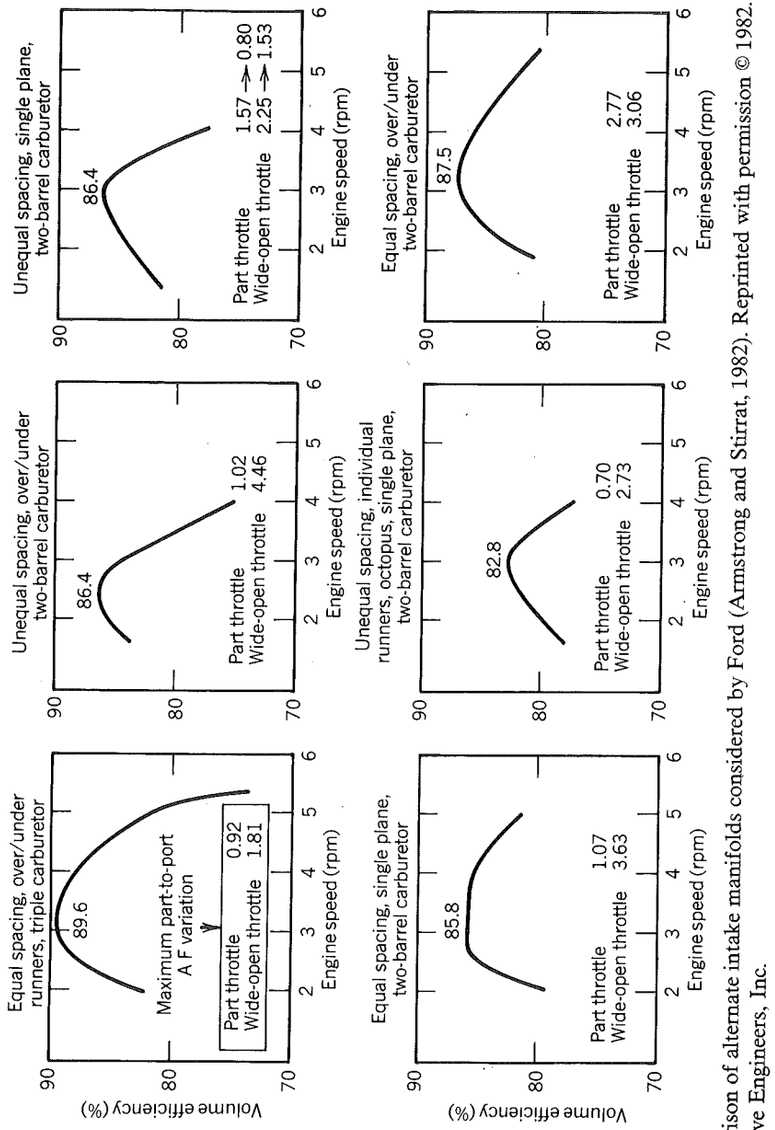

Figure 1-8 Comparison of alternate intake manifolds considered by Ford (Armstrong and Stirrat, 1982). Reprinted with permission © 1982. Society of Automotive Engineers, Inc.

Table 1-2 Computer Aided Inlet Manifold Design By Chevrolet[a]

ORIGINAL MODEL

(a)

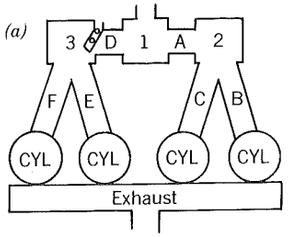

BASELINE VALUES

Plenum 1 = 278 cm^3
Plenum 2 and 3 = 131 cm^3 each
Pipes A and D = 14.5 cm^2 area, 6.1 cm long
Pipes B, C, F, E = 9.7 cm^2 area, 22.4 cm long
Exhaust plenum = 1311 cm^3 volume

CHANGES	Δ TORQUE@2500 rpm	Δ TORQUE@5000 rpm
Pipe area − 10%	+1.0%	−5.0%
Pipe area − 20%	+1.5%	−16.0%
Pipe area + 10%	−0.5%	+1.3%
Plenum − 40%	+1.0%	0.0%
Pipe length + 17%	+2.0%	−6.5%
Pipe area + 10%, Plenum − 40% Pipe length + 17%	+0.5%	+1.3%

DESIGN MODEL

(b)

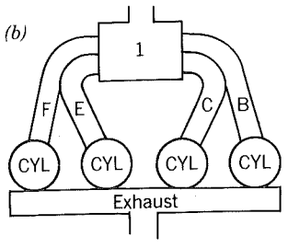

BASELINE VALUES

Plenum 1 = 418 cm^3 volume
Pipes B, C, F, E = 7.9 cm^2 area, 26.4 cm long
Exhaust plenum = 1311 cm^3 volume

CHANGES	Δ TORQUE@2500 rpm	Δ TORQUE@5000 rpm
Pipe area − 10%	+2.5%	−10.0%
Pipe area + 10%	−1.0%	+5.0%
Pipe area + 20%	−2.2%	+5.5%
Plenum − 20%	0.0%	0.0%
Pipe length − 15%	−0.5%	+0.5%
Plenum − 20%, Pipe area + 15%, Pipe length − 8%	−1.0%	+5.0%

FINAL DESIGN

(c)

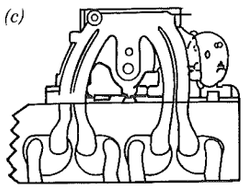

Plenum volume = 343 cm^3 volume
Pipe area = 9.4 cm^2 area
Pipe length = 24 cm long

Source: (Walker, 1982). Reprinted with Permission © 1982, Society of Automotive Engineers, Inc.
[a]See Homework Problem 12.

number is typically 15. It is desirable to deliver the same air–fuel ratio to each cylinder. As can be seen in Fig. 1-7, the maximum difference from cylinder to cylinder can vary anywhere from 0.70 to 4.46 or regularly 5 to 30%. The *two barrel* (i.e., two independent air passages) carburetor with single plane runners and unequal port spacing design was selected as the best compromise between maximizing volumetric efficiency and minimizing cylinder to cylinder air–fuel ratio variations. The single plane configuration also permitted use of a low height, low weight, and low cost die-cast aluminum manifold.

The design of intake manifolds is one example of where cut and try empiricism must be used, and where computer modeling of the fluid flows helps designers minimize the number of configurations cut and tried. Table 1-2 illustrates use of a computer engine simulation employed by Chevrolet to design the intake manifolds for the GM 1.8 and 2.0 liter four-cylinder engines.

Configuration (A) is the baseline case designed from experience with other engines. Parameters listed are changed to study their effects on volumetric efficiency as measured by changes in torque. To package the engine in the new J-car line and minimize weight, it was desirable to reduce the total plenum volume and increase the runner length. The simulation showed that this could be done only if the runner cross-sectional area was increased at the same time. A modified design based on these results and the aforementioned packaging criteria was then tried as a new baseline (B) the design model. Further exercise of the computer program showed that the plenum volume could be reduced further and there was still room for improvement with larger runner cross-sectional area. The final design reflects these results although the computer model would not be able to include all the details of the final design.

A schematic of the Chevrolet engine is shown in Fig. 1-9 with specifications provided in Table 1-1. Wide open throttle performance is given in Fig. 1-10. As these engines differ in size from the Ford engine, comparison is difficult although some of the trends look similar. A parameter that *scales out* the effect of engine size is the *brake mean effective pressure*, bmep. The bmep is the work done per unit displacement volume; thus for a four stroke engine

$$\text{bmep} = \frac{4\pi\tau}{V_d} = \frac{2\mathbf{P}_b}{V_d R_s} \tag{1.9}$$

On this basis, the Ford and GM engines are compared in Fig. 1-11. Notice that the differences are now seen to be rather small. In fact, when *scaled* correctly, all piston engines are remarkably *similar*, as Table 1-3 illustrates. There is good reason for this; all engines tend to be made from similar materials. The small differences noted can be attributed to different service criteria for which the engine was designed. The automotive engine is more highly stressed and lighter than the diesel stationary engine. Since material stress in an engine depends on a first approximation only on the bmep and mean piston speed, it follows that for the same stress limit imposed by the material, all engines should have the same bmep and mean piston speed. Since *specific* power, power per unit piston area, is the product of bmep and mean piston speed it too is more or less fixed.

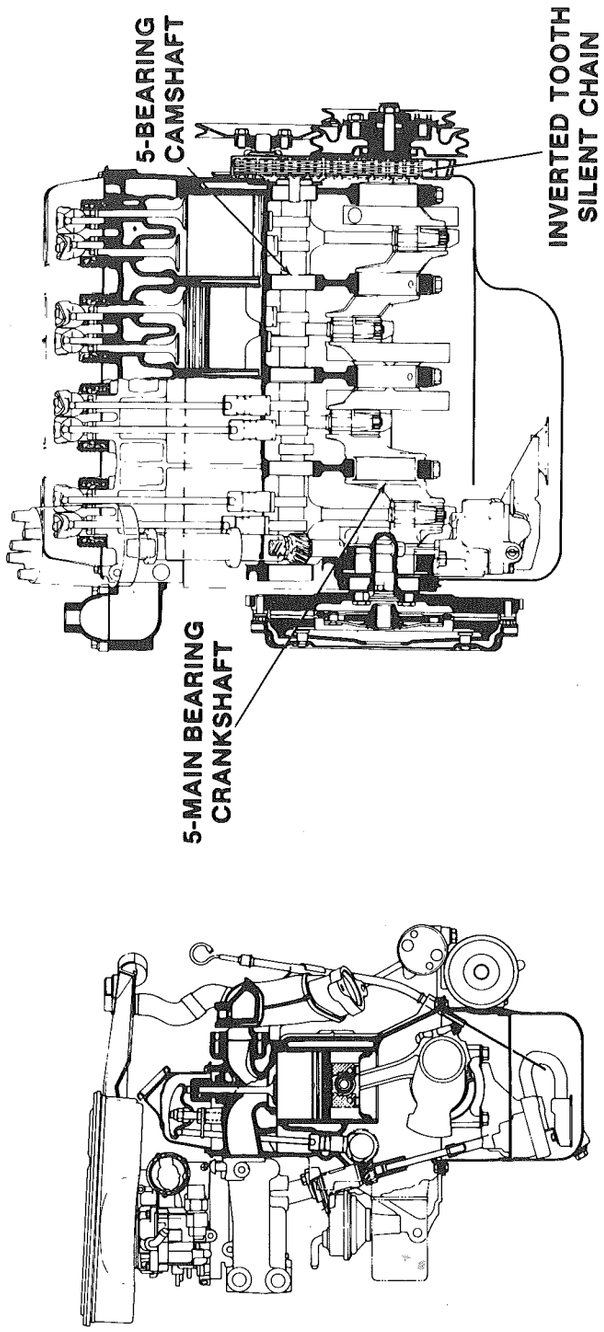

Figure 1-9 Chevrolet L-4 engine. Some of the engine's specifications are given in Table 1-1 (Walker, 1982). Reprinted with permission © 1982. Society of Automotive Engineers, Inc.

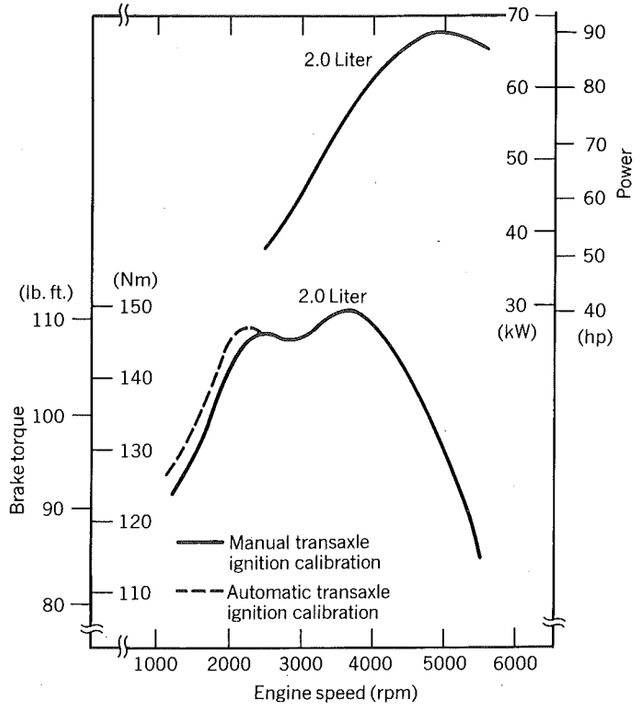

Figure 1-10 Wide-open throttle performance of GM L-4 engine. Note that engine is smaller than the Ford engine, has less power and torque, but operates at higher engine speeds (Walker, 1982). Reprinted with permission © 1982. Society of Automotive Engineers, Inc.

Finally, since the engines geometrically resemble one another independent of size, the mass per unit displacement volume is more or less independent of engine size.

The lubrication system of the GM engines is shown in Fig. 1-12. Oil is pumped from the *oil pan* to the *oil filter*. If the oil filter is plugged with dirt, then oil is bypassed. Oil is distributed from the main oil gallery to the valve train and crankshaft. Oil flows through the lifters and pushrods to the rocker arms. That oil then dribbles back to the pan. Oil exits the main gallery through drilled holes to the *timing chain* and to each *camshaft bearing*. From the camshaft bearings, oil then flows to each main bearing and then through passages in the crankshaft to the connecting *rod bearings*. The oil leaving the rod and main bearings is thrown off the crankshaft arms and counter weights in a spray. This spray provides oil to lubricate the cylinder and the piston pins (it also coats the piston). That oil and the oil sprayed on other surfaces then dribbles back to the pan.

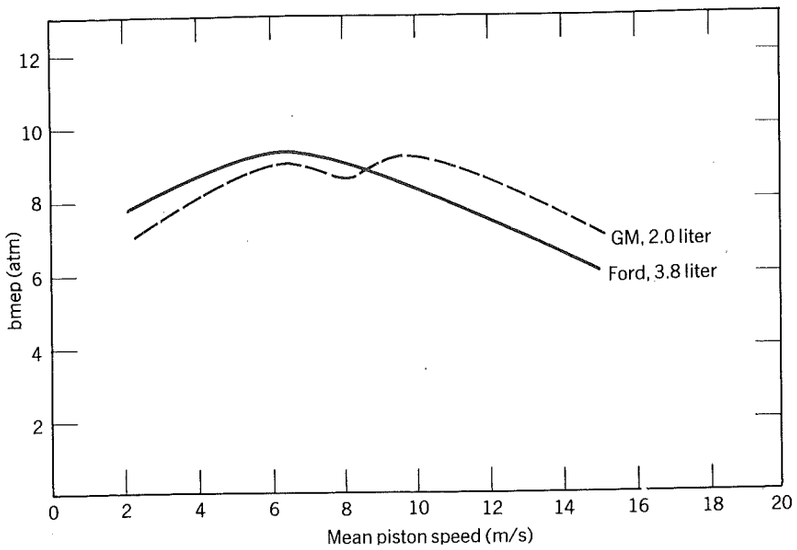

Figure 1-11 Brake mean effective pressure at WOT versus mean piston speed of two automotive engines. Notice that when performance is scaled to be size independent there is considerable similarity.

Table 1-3 Comparison of a Large Diesel Engine with an Automotive Gasoline Engine and a Model Airplane Engine

CHARACTERISTICS	MODEL AIRPLANE[a]	AUTOMOTIVE[b]	LARGE DIESEL[a]
Extensive			
Bore, mm	12.6	89	737
Stroke, mm	13.1	80	1016
Displacement (one cylinder), l	1.6×10^{-3}	0.498	433
Power per cylinder, watt	100	1.68×10^{4}	5.29×10^{5}
Engine speed, rpm	11,400	5000	164
Mass per cylinder, kg	0.12	34.3	3.56×10^{4}
Power per liter^3, Watt/l	6.25×10^{4}	3.37×10^{4}	1.22×10^{3}
Intensive			
Bmep, atm	3.2	8.0	4.5
Mean piston speed, m/s	5.0	13.3	5.6
Specific output, Watt/cm^2	80	270	124
Mass/displacement, kg/l	75	82	69

[a] From Taylor (1977), Chapter 11. (Both engines are two-stroke, loop scavenged. Model airplane has crankcase compression.)
[b] GM, L-4 engine, four stroke.

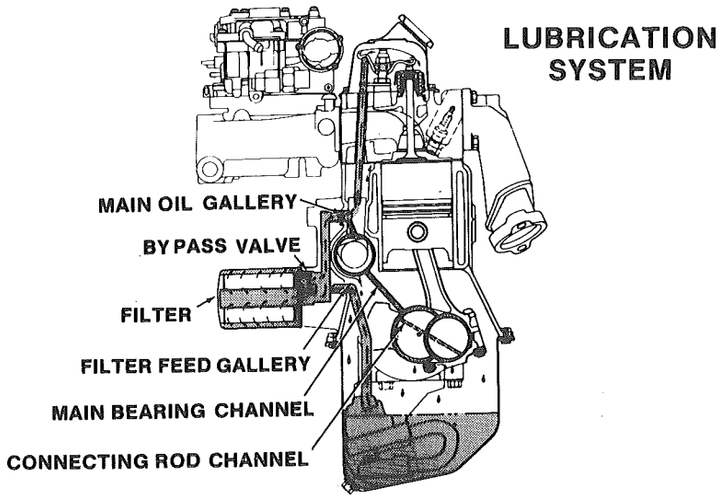

Figure 1-12 Component lubrication, GM L-4 (Walker, 1982). Reprinted with permission © 1982. Society of Automotive Engineers, Inc.

The cooling system of the GM engines is shown in Fig. 1-13. A *water pump* pumps the coolant through passages in the block and head that surround the combustion chambers. Warm coolant flows through the intake manifold to warm it and thereby assist in vaporizing the fuel. Coolant flows through the heater-core heat exchanger and back to the radiator. When the engine is cold, a *thermostat* prevents coolant from returning to the radiator so that in effect it is eliminated from the system, resulting in a more rapid warm-up of the engine.

The power required to drive the water pump is a part of the difference between the work done by the gas or *indicated horsepower* and the brake horsepower. It has already been mentioned that friction is part of the difference. The difference is also caused by power being required to drive *accessories* such as the air conditioner, power steering pump, air pump, and alternator, as illustrated in Fig. 1-14. Other power robbing devices, though small by comparison to those mentioned, include the *distributor*, the *oil pump*, and the *fuel pump*. Some engines use a cooling fan which at high speeds, as already mentioned for the Ford engine, consumes considerable power. Some manufacturers, Nissan for example, use an electric cooling fan that operates only at low speeds.

Revolutionary changes have taken place with *engine controls* in recent years and the progress continues. Conventional carburetors are being replaced by *throttle body fuel injection* as illustrated in Fig. 1-15. A *microcomputer* specifies the mass of fuel to be injected and thereby inducted for each intake-valve open period. The mass injected is controlled by the *duration* of the *solenoid* actuated fuel injector upstream of the throttle.

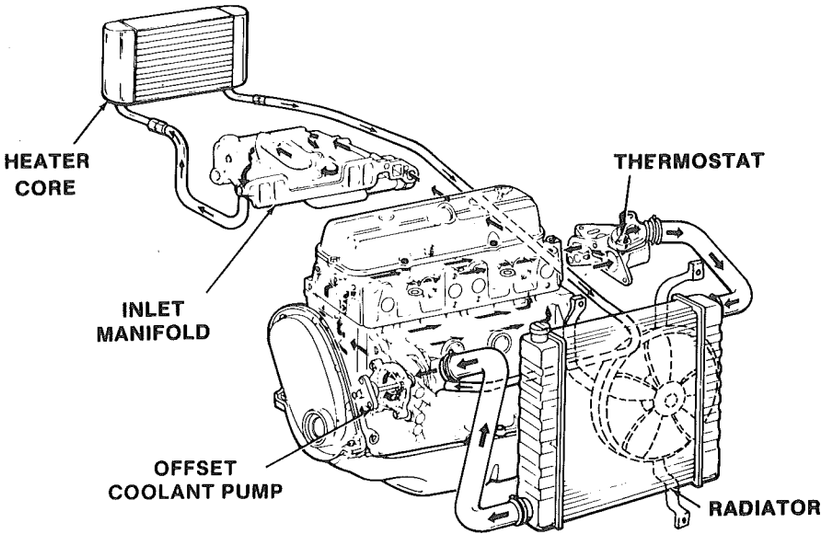

Figure 1-13 Parallel coolant flow, GM L-4 (Walker, 1982). Reprinted with permission © 1982. Society of Automotive Engineers, Inc.

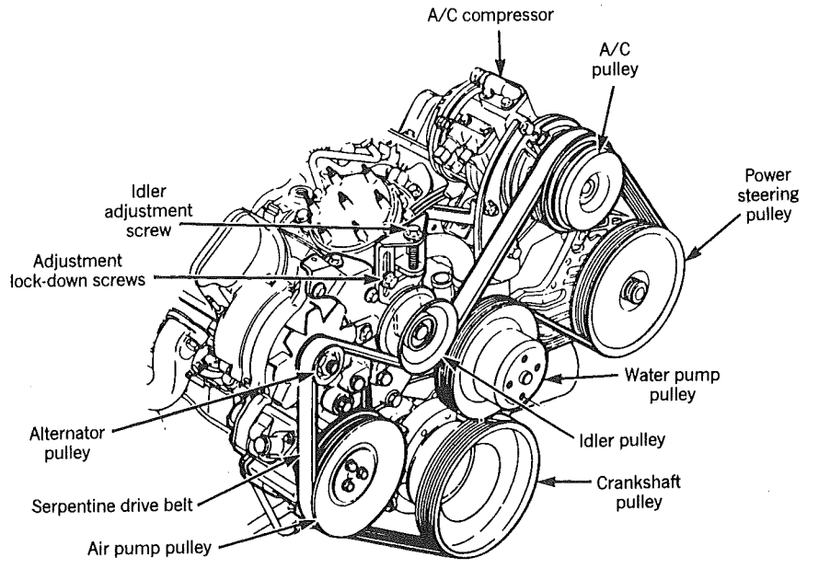

Figure 1-14 Accessory drive, Ford 3.8 liter (Armstrong and Stirrat, 1982). Reprinted with permission © 1982. Society of Automotive Engineers, Inc.

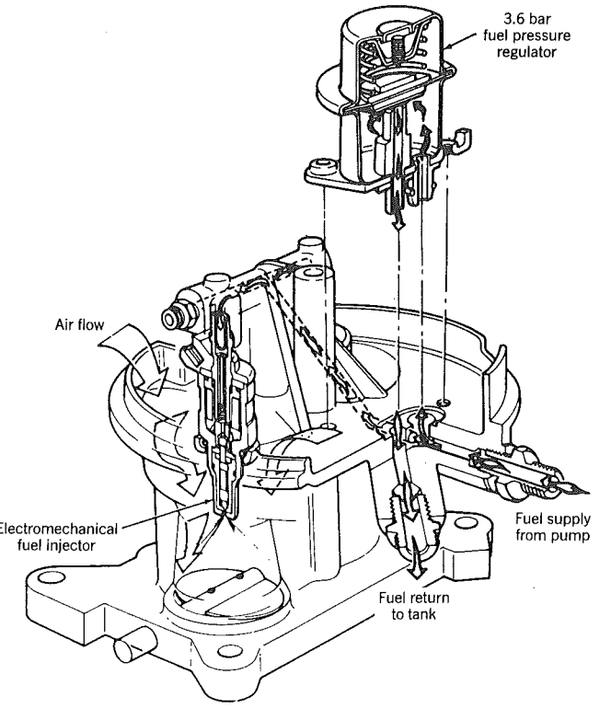

Figure 1-15 Cutaway of fuel charging assembly, Ford (Czadzeck and Reid, 1979). Reprinted with permission © 1979. Society of Automotive Engineers, Inc.

Sensors or transducers are used to provide the computer with the following information:

Throttle position
Rate of change of throttle position
Intake manifold pressure
Atmospheric pressure
Coolant temperature
Intake charge temperature
Exhaust gas recirculation valve position
Crank angle
Exhaust oxygen concentration
Occurrence of knock

With this knowledge of the engine operation as input, the computer can be

programmed to control the following:

Fuel injection duration
Ignition timing
Start of the air pump
Shift of the transmission
Turning on of a warning light
Reprogramming of the computer

The latter control possibility is called *closed loop control.* It can compensate for differences due to normal manufacturing tolerances and for slight changes due to wear or buildup of deposits. For example, the exhaust oxygen concentration is a measure of the air–fuel ratio. The computer is programmed to deliver the proper air–fuel ratio and can use the exhaust oxygen as a check. If the oxygen is too high, it will compensate by providing more fuel; whereas if it is too low, it can provide less fuel. Thus if gum starts to reduce the flow area in the fuel injector, the system can compensate, up to a point. If the buildup is too large, then a warning light is turned on.

The ignition signal is typically sent to a solid state switch called an SCR, that turns the switch on and, as illustrated in Fig. 1-16, a capacitor then discharges through the primary circuit of the ignition *coil.* This generates a high voltage in the secondary circuit which is connected to the appropriate *spark plug* through contacts in the spark plug through contacts in the *distributor*. Timing is completely controlled by the computer. Between firing of the plugs, the capacitor is recharged. Clearly the RC (resistance-capacitance) time constant must be small compared to the engine period.

All the engines discussed so far are *naturally aspirated*, not *supercharged* or *turbocharged*. The concept of turbocharging is illustrated in Fig. 1-17. Exhaust gas leaving an engine is further expanded through a *turbine* that drives a *compressor*. The compressor raises the density of the incoming charge so that more fuel and air can be delivered to the cylinder to increase the power.

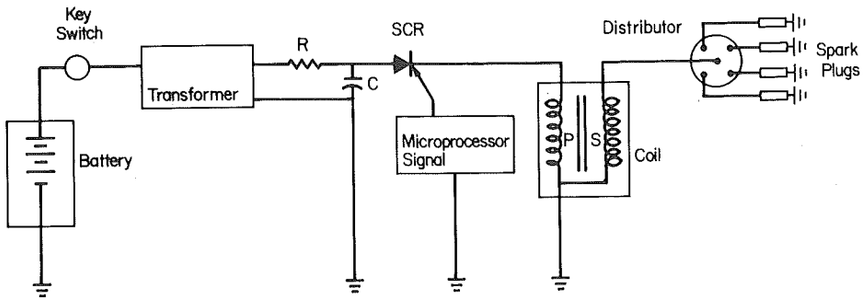

Figure 1-16 Capacitive discharge ignition system. This is not a literal representation of any system used in practice, it is much simpler so as to focus on the most important concepts.

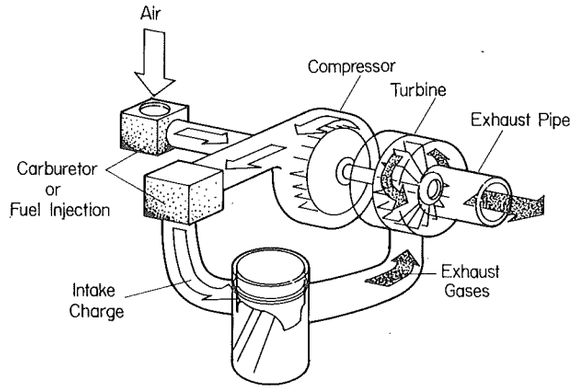

Figure 1-17 Turbocharged engine principle (Wallace, 1978). Reprinted with permission © 1978. Society of Automotive Engineers, Inc.

The benefits are twofold: (1) the engine is more efficient because energy that would have otherwise been wasted is recovered from the exhaust gas; (2) a smaller engine can be constructed to produce a given power because it is more efficient and because the density of the incoming charge is greater. A supercharger utilizes a compressor driven by the engine itself rather than by a turbine. Superchargers are limited to applications in which the increased density is desirable at all engine speeds, such as in racing.

The power available to drive the compressor when turbocharging is a nonlinear function of engine speed such that at low speeds there is little if any

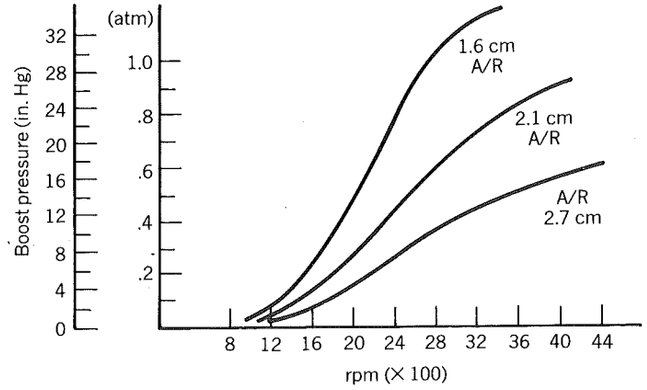

Figure 1-18 The effect of various A/R turbines on manifold pressure on a Buick engine. The A/R parameter is the ratio of the turbine inlet nozzle area to the radius of the centroid of that area (Wallace, 1978). Reprinted with permission © 1978. Society of Automotive Engineers, Inc.

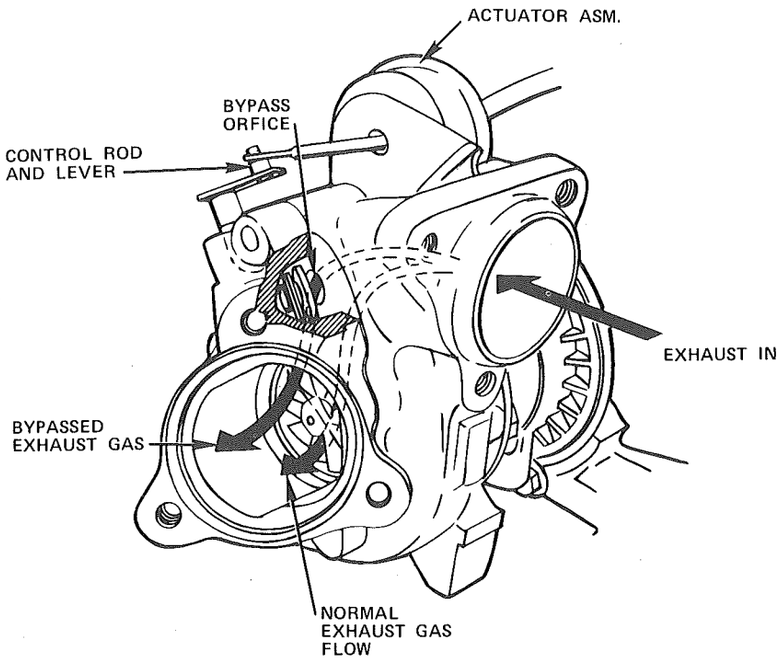

Figure 1-19 Wastegate control valve used by Buick (Wallace, 1978). Reprinted with permission © 1978. Society of Automotive Engineers, Inc.

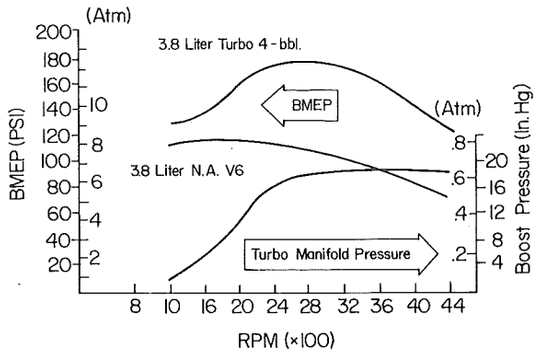

Figure 1-20 Manifold pressure and bmep of Buick turbocharged engine at WOT. The notation N.A. means naturally aspirated and 4-bbl means the engine has a four-barrel carburetor (Wallace, 1978). Reprinted with permission © 1978. Society of Automotive Engineers, Inc.

boost (density increase), whereas at high speeds the boost is maximum. It is also low at part throttle and high at wide open throttle. These are desirable characteristics for an automotive engine since throttling or *pumping* losses are minimized.

One result of this nonlinearity is consumer perception of a performance lag. This can be dealt with in a number of ways. For example, Fig. 1-18 shows for a Buick system, the effect on boost of varying the ratio of turbine inlet nozzle area to the radius of the centroid of that area, the A/R ratio. A lower value of A/R provides a smaller effective nozzle, thereby increasing turbine speed for a fixed gas flow. The increased speed produces more boost at all engine speeds.

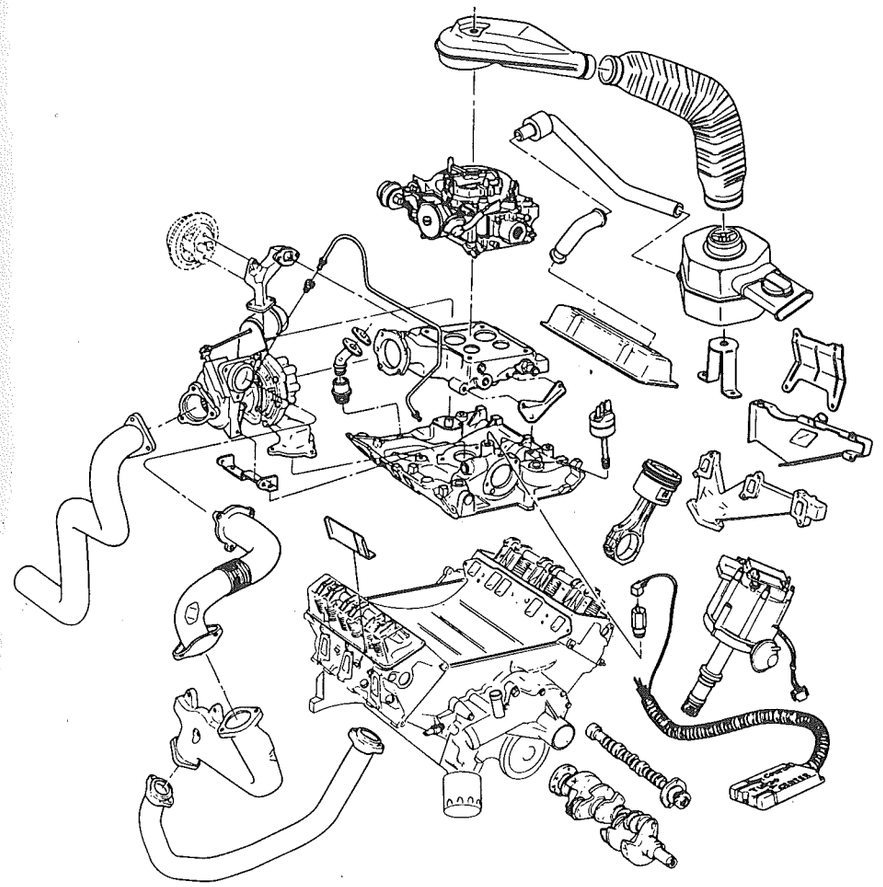

Figure 1-21 New and redesigned Buick turbocharged V-6 engine components (Wallace, 1978). Reprinted with permission © 1978. Society of Automotive Engineers, Inc.

The problem encountered is that for manifold boost greater than about 0.7 bars the engine will knock. Therefore to maintain boost at low and mid speed and avoid knock at high speed a *wastegate* is installed on the turbocharger. As shown in Fig. 1-19 if the boost is too high, some of the exhaust gas is routed to bypass the turbine. In this example, the bypass is controlled by a diaphragm that senses boost. In other engines it is controlled by the microcomputer when knock is sensed.

Performance characteristics of the turbocharged Buick 3.8 liter V-6 engine are given in Fig. 1-20. The effect of the wastegate control is noticed when the boost curve is compared to the corresponding $A/R = 2.1$ cm curve in Fig. 1-18. For comparison, the bmep of the naturally aspirated version of the same engine is also shown in Fig. 1-20.

Matching the turbocharger to the engine gives the designer new degrees of freedom that could not be considered when building a naturally aspirated engine. Thus in optimizing the vehicle system many parts are different in the turbocharged engine compared with the naturally aspirated engine. Fig. 1-21 shows the new and redesigned parts of the Buick engine.

1.2 COMPRESSION IGNITION ENGINES

Spark ignition engines are often called gasoline engines and compression ignition engines are often called *diesel engines*. The basic difference between the two is the means by which the fuel and air are mixed and burned. In a gasoline engine, fuel and air are mixed external to the cylinder volume; during intake a fuel–air mixture is inducted through the intake valve into the cylinder. In a diesel engine, fuel and air are mixed internally; during intake only air is inducted into the cylinder.

If the compression ratio of a gasoline engine is too high, then some of the mixture will *autoignite* and burn so quickly that it will rattle the engine parts; the attendant noise is called *knock*. Autoignition occurs because compression of the fuel–air mixture raises its temperature too high. Since knock is undesirable, the engine designer must limit the compression ratio so that it does not occur. As we shall see, this is one factor that limits the efficiency of gasoline engines.

Diesel engines are able to operate at higher compression ratios than gasoline engines because the fuel is mixed with air at the time combustion is to commence. The compression ratio is deliberately selected to be high enough so that the gases near the end of the compression stroke are hot enough so that the fuel autoignites very soon after injection starts. The remaining fuel to be injected can then burn no faster than it is injected. The period between the start of injection and autoignition is called the *ignition delay*. Its duration depends upon the engine design and the fuel type. The designer strives for a small ignition delay, for once the mixture autoignites all the fuel already injected burns very quickly. If too much fuel burns in this phase instead of at a rate limited by the fuel injection, the engine will knock intolerably. Diesel fuel

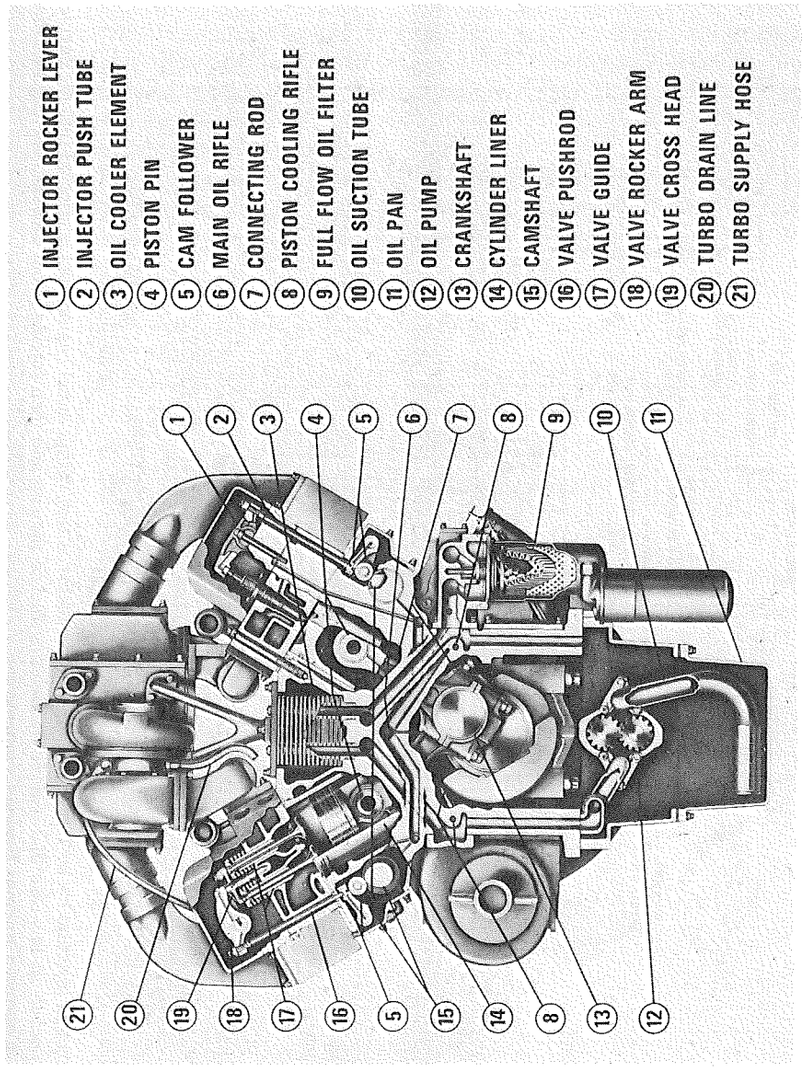

Figure 1-22 A Cummins direct-injection diesel engine. Courtesy Cummins Engine Company, Inc.

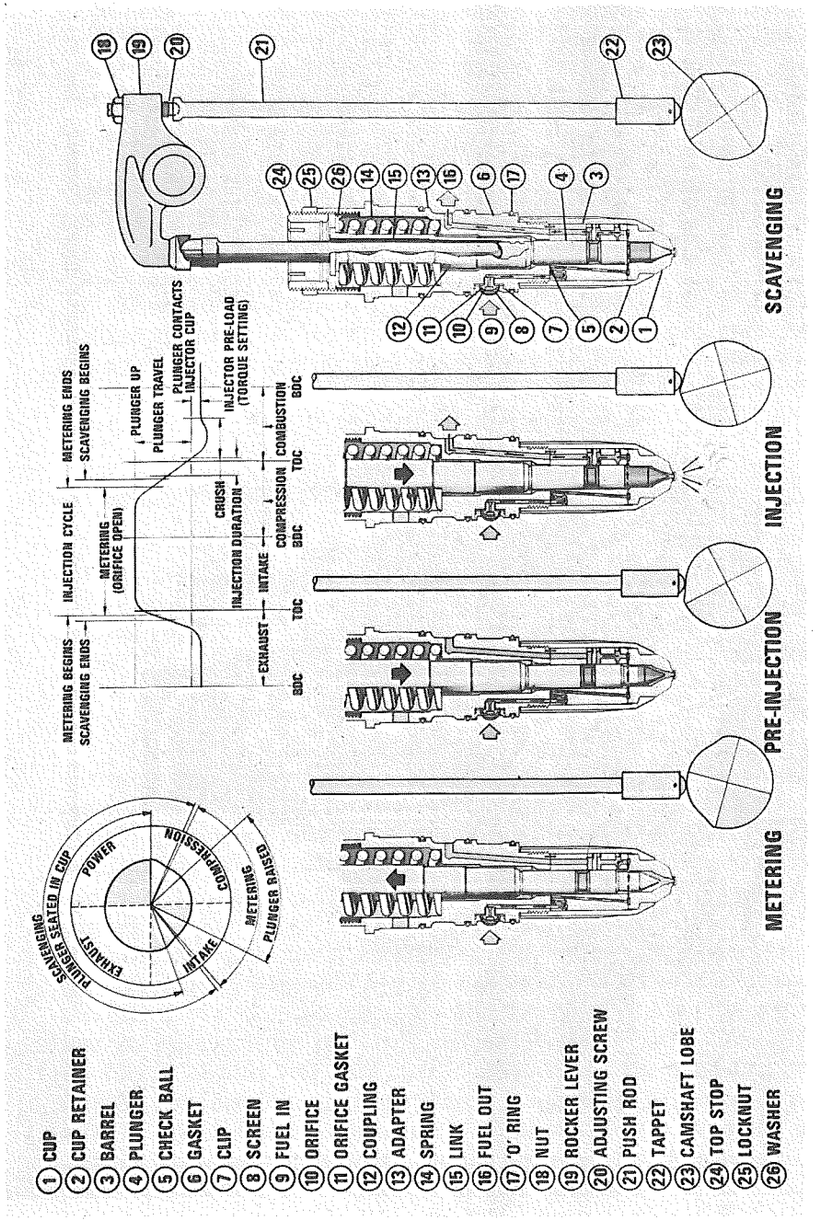

Figure 1-23 Cummins fuel injection cycle. The important thing to realize is that with a diesel engine, fuel is injected into the engine at the time combustion is to occur. In this case that is done by metering fuel to the cup and then forcing it out and into the engine cylinder by means of the plunger. Courtesy Cummins Engine Company, Inc.

should possess the ability to autoignite easily, whereas gasoline should resist autoignition. Clearly, gasoline would make a poor diesel fuel and vice versa.

As an example of a diesel engine, Fig. 1-22 shows a *direct injection* or *open chamber* engine. Most of the parts shown are familiar to the reader from examining spark ignition engines. Apart from differences in structural integrity of the various parts, a fundamental change is the appearance of a *fuel injection* system in lieu of the carburetor and attendant throttle (or throttle body fuel injection as the case may be).

The fuel injection system used in the Cummins engine is illustrated in Fig. 1-23 (see also Fig. 7-52 and its discussion). When the *plunger* is raised, in the metering stroke, a fuel pump delivers fuel under pressure through the

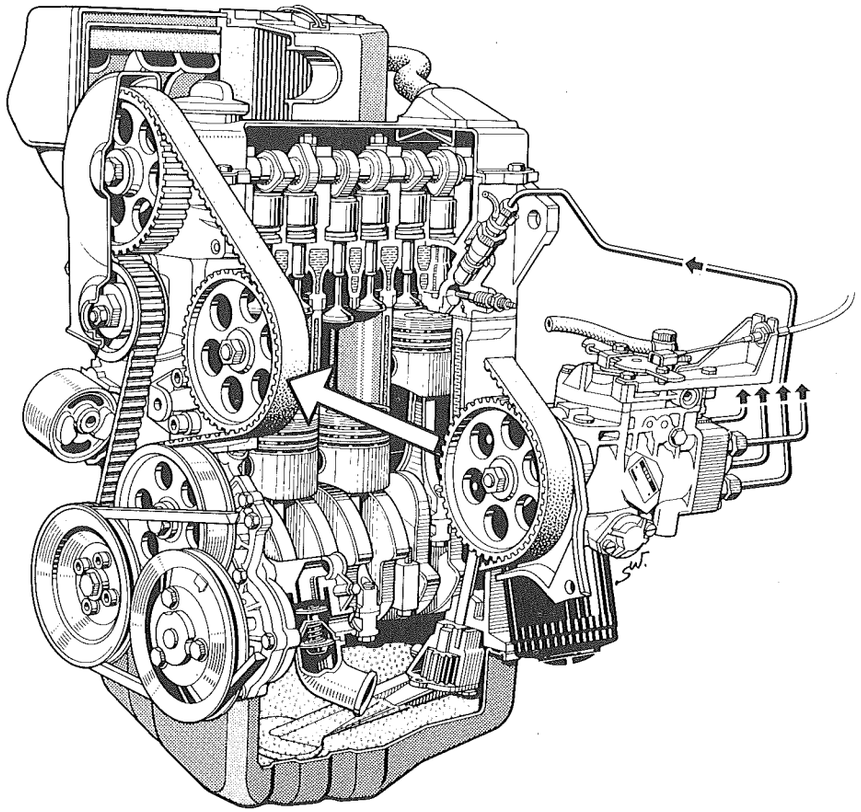

Figure 1-24 Volkswagen diesel engine. Fuel injection occurs via a pumping plunger within the fuel pump. The stroke of that plunger determines the mass of fuel to be injected. When the plunger starts to move, a needle valve within the injector is closed and the fuel pressure in the fuel line rapidly rises to a value that ultimately lifts the needle valve off its seat allowing fuel to be injected into the combustion chamber (Hofbauer and Sator, 1977). Reprinted with permission © 1974. Society of Automotive Engineers, Inc.

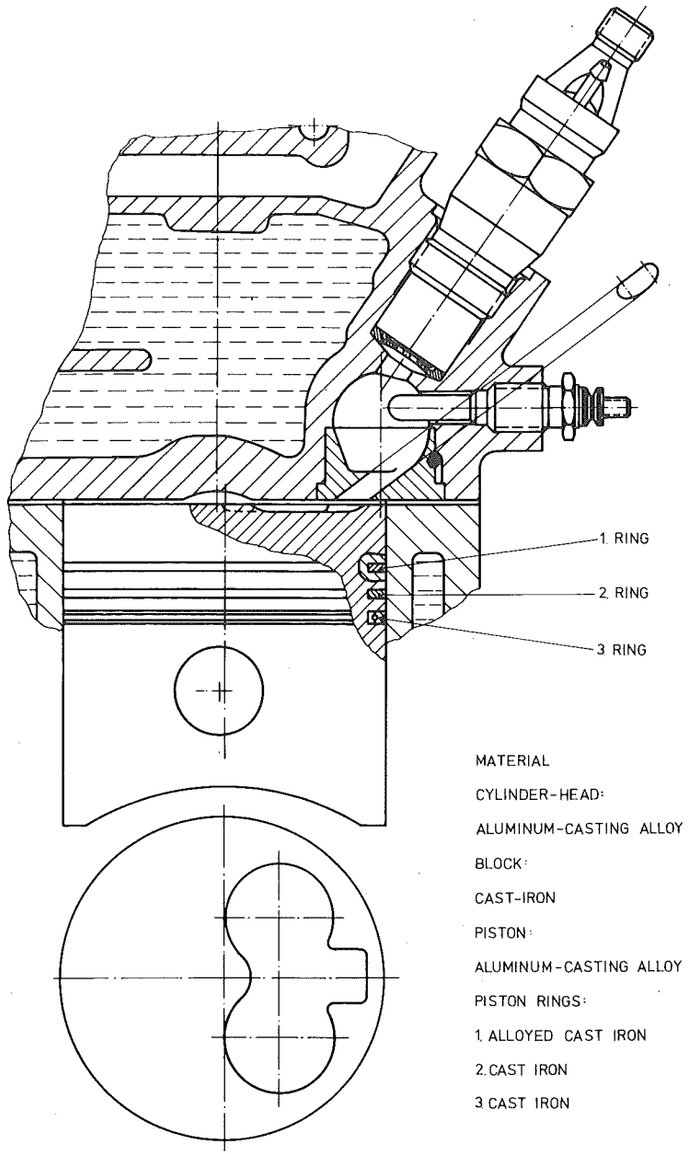

Figure 1-25 Volkswagen combustion chamber (Hofbauer and Sator, 1977). Reprinted with permission © 1977. Society of Automotive Engineers, Inc.

orifice and into the *cup*. At the proper time, defined by the cam, the plunger moves down to close the orifice, open the *bypass* passage, and compress the fuel forcing it through the *nozzle orifices* into the combustion chamber. The only high pressure in the system is developed at this time. The flow through the nozzle orifices *atomizes* the liquid fuel into fine droplets so that evaporation will be quick ensuring a short ignition delay. The bypass flow continues through the purging phase and is the means by which the injector is cooled. The mass of fuel injected is varied by changing fuel-pump delivery pressure.

An example of an *indirect injection* or *divided chamber* diesel engine is shown in Fig. 1-24. In this type of engine the combustion chamber is two volumes connected by a passage. The Volkswagen combustion chamber is isolated in Fig. 1-25 to show this point. Notice that during compression, gases will be forced to enter the spherical *swirl chamber* through a tangential passage. This creates a rotating or swirling flow in the chamber and assists mixing of the fuel and air during injection. Since the swirl is high, less demand is put on the injector to produce a finely atomized spray. During combustion the flow will reverse itself and rich combustion products will flow back into the

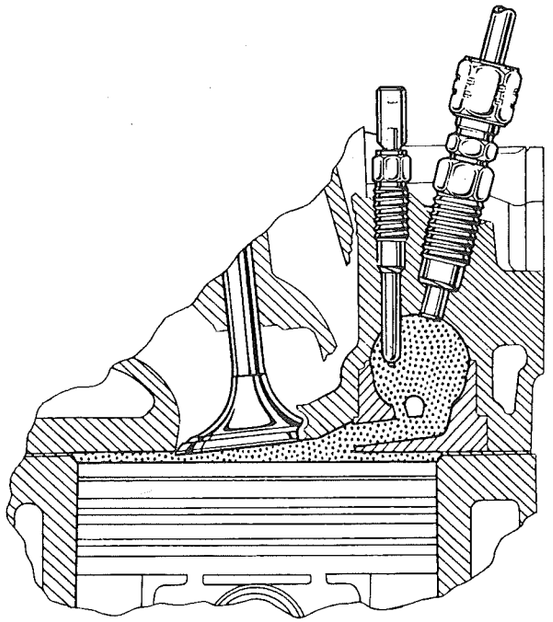

Figure 1-26 Oldsmobile 4.3 liter V6—swirlchamber. Notice the little dam at the entrance to the swirl chamber (Leonard and Johnson, 1982). Reprinted with permission © 1982. Society of Automotive Engineers, Inc.

cylinder or *main chamber*. Recesses are in the piston surface to direct that flow and mix it with air to complete combustion.

Notice, too, that this engine has a *glow plug*. The swirling air motion also enhances convective heat transfer. One result is that in a cold engine the gases compressed into the swirl chamber lose so much heat that ignition may be difficult or impossible to achieve. The glow plug is a resistance heater turned on at this time to aid in starting. After the engine has fired a few times, the walls of the swirl chamber become hot, thereby reducing the heat loss during compression. The glow plug is thus used only for starting.

Divided-chamber engines tend to be used where the engine is expected to perform over a wide range of speeds and loads such as in an automobile. When

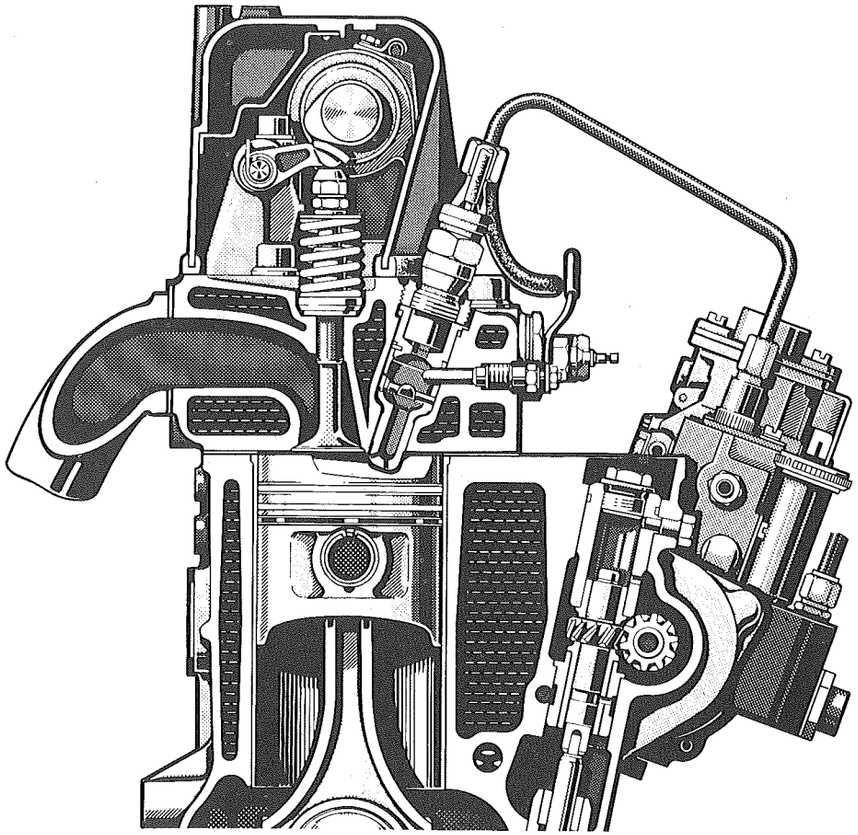

Figure 1-27 Daimler–Benz prechamber passenger car engine. Because of restrictions at the prechamber throat, the flows in and out of this prechamber will be at higher speeds than in either the Volkswagen or General Motors engines in Fig. 1-25 and 1-26 (Hoffman, 1971). Reprinted with permission © 1971. Society of Automotive Engineers, Inc.

the operating range of the engine is less broad such as in trucks, ships, locomotives, or electric power generation, open chamber engines predominate. Figures 1-26 through 1-30 show different combustion chambers to illustrate that a great deal of flexibility exists in the design of diesel engines. That each engine manufacturer has worked to optimize the design for a particular application and that each manufacturer has produced an engine with unique characteristics illustrates that the optimum design is highly dependent upon the specific application.

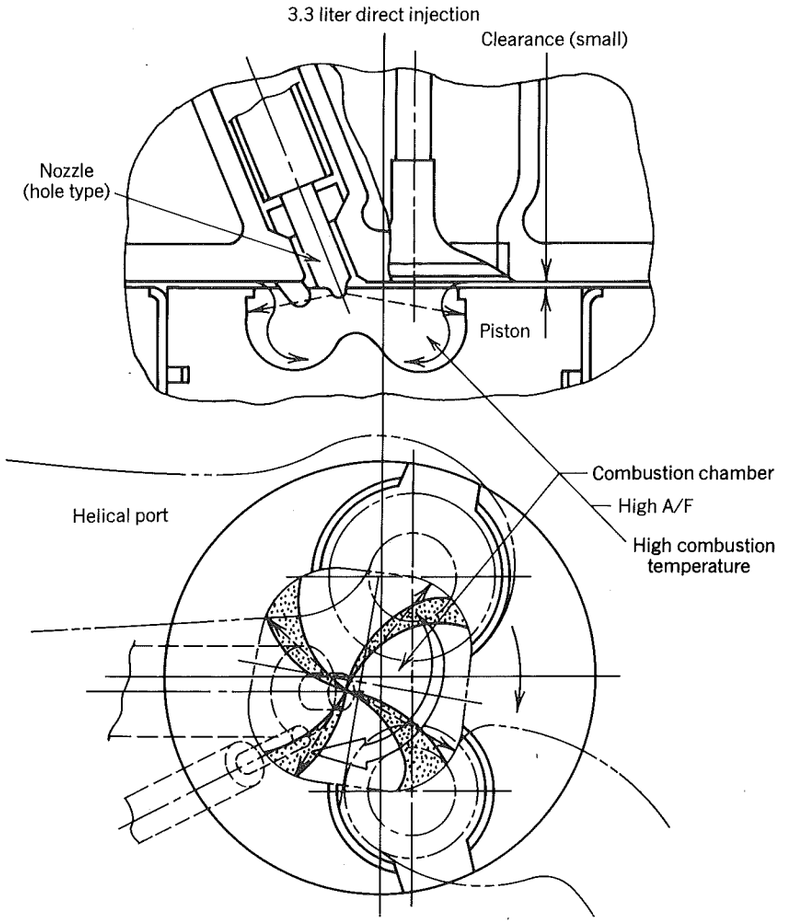

Figure 1-28 Isuzu–medium swirl. The square cup in the piston is believed to generate small recirculation zones in each corner that are counter rotating with respect to the swirl and thus promote mixing of fuel with air (Kawamura, Kihara and Kinbara, 1982). Reprinted with permission © 1982. Society of Automotive Engineers, Inc.

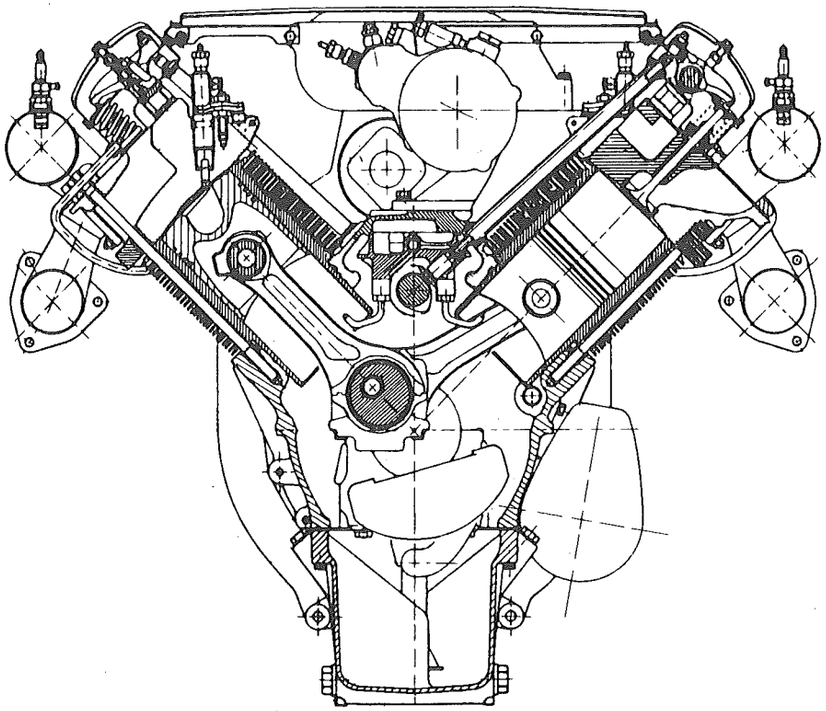

Figure 1-29 Deutz FL 413–air cooled, high swirl direct injection engine. The swirling air distributes injected fuel throughout the cylinder (Finsterwalder, 1972). Reprinted with permission © 1972. Society of Automotive Engineers, Inc.

As an example consider the results of experiments done by General Motors in the course of developing a 5.7 liter V-8 engine. Figure 1-31 shows three nozzle locations considered.

(A) directs fuel tangentially in the direction of swirl and along a plane offset from the swirl chamber's plane of symmetry.

(B) directs fuel across the swirl chamber along a plane offset from the swirl chamber's plane of symmetry.

(C) directs fuel through the center of the swirl chamber.

It was determined that:

(A) produced the lowest efficiency, lowest *nitric oxide* pollutant (NO_x), lowest noise, and highest *hydrocarbon* pollutant (HC).

(B) produced intermediate efficiency and HC with highest NO_x and noise.

(C) produced highest efficiency with lowest HC and intermediate noise and NO_x.

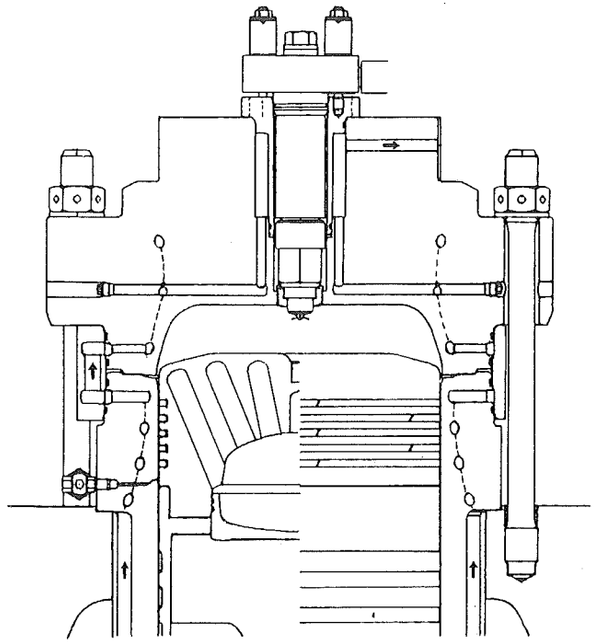

Figure 1-30 Sulzer RLA-56–a quiescent direct injection engine. The fuel injection itself is relied upon to create the necessary air motion required to mix the fuel and air (Eberle, 1980). Reprinted with permission © 1980 ASME.

Experiments were also done varying the number of holes in the fuel injector nozzle holding the total flow area fixed. Results are given in Fig. 1-32 for the nozzle location (A). Our theoretical understanding is such that we believe we understand the processes in principle but must admit that only order of magnitude estimates can be made and that, in practice, experimentation has to be employed in engine development.

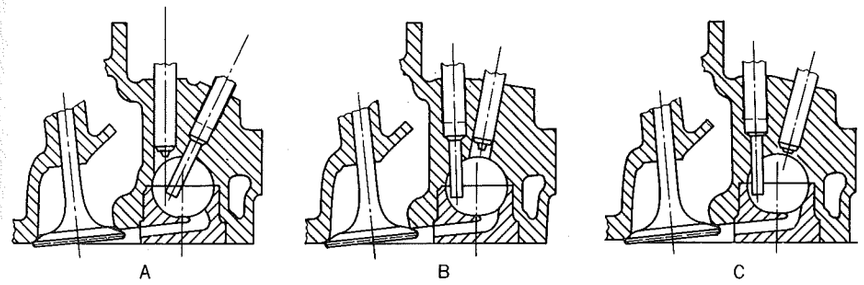

Figure 1-31 Three nozzle positions evaluated by Oldsmobile engineers (Jones, Kingsbury, Lyon, Mutley and Thurston, 1978). Reprinted with permission © 1978. Society of Automotive Engineers, Inc.

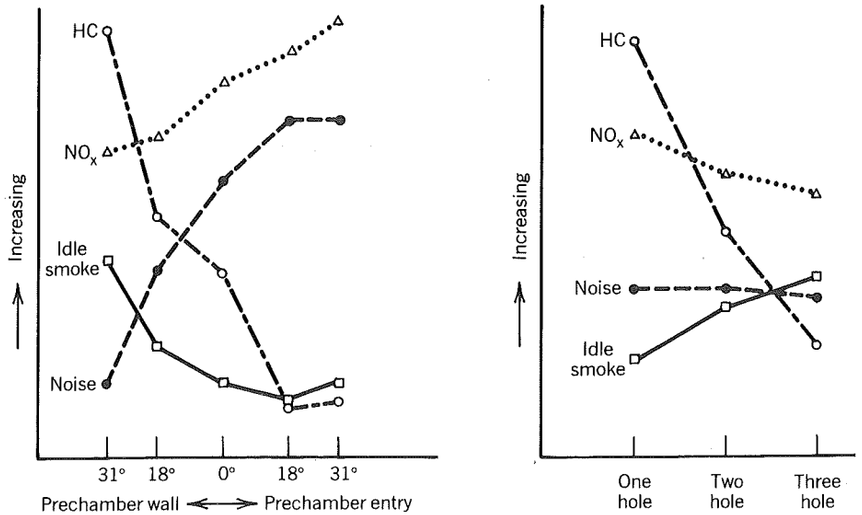

Figure 1-32 Effect of nozzle hole angle and effect of multiple holes (constant total flow area) in fuel injection nozzle for position A in Fig. 1-31 (Jones *et al.*, 1978). Reprinted with permission © 1978. Society of Automotive Engineers, Inc.

Diesel engines, whether open or divided chamber engines, suffer from a *smoke limit*, the limit to how much fuel can be burned per unit air before significant quantities of smoke are formed. The particles that comprise smoke are undesirable since they are unsightly, contaminate the engine oil, and radiate heat to the walls during combustion and expansion, and because they have toxic substances adsorbed to them.

Smoke forms because the combustion is heterogeneous. Consider as a model the following reaction path for a hydrocarbon fuel:

First stage

$$C_\alpha H_\beta + \chi O_2 \nearrow \quad \alpha CO + \frac{\beta}{2} H_2 + (2\chi - \alpha) O_2 \quad \text{clean} \qquad \chi \geq 2\alpha$$

$$\searrow \quad \frac{\chi}{2} CO + \left(\alpha - \frac{\chi}{2}\right) C(s) + \frac{\beta}{2} H_2 \quad \text{sooting} \qquad \chi < 2\alpha$$

Second stage

$$CO + \tfrac{1}{2} O_2 \rightarrow CO_2$$
$$C(s) + O_2 \rightarrow CO_2$$
$$H_2 + \tfrac{1}{2} O_2 \rightarrow H_2O$$

According to this model, combustion takes place in two stages. If there is enough oxygen present, that is, $\chi \geq 2\alpha$, then the flame is clean since no solid carbon is formed. The products of the first stage are then carbon monoxide and hydrogen. The second stage burns the first stage products to completion.

If in the first stage there is not enough oxygen present to convert all the fuel carbon to carbon monoxide, that is, $\chi < 2\alpha$, then solid carbon is produced. This is likely to occur locally within the fuel spray injected into the engine since it takes time for air and its attendant oxygen to be mixed in with the fuel. Mixing is a continual process within the cylinder during combustion and expansion. When only trace quantities of solid carbon appear in the exhaust it is because air was mixed into the fuel-rich pockets early enough during expansion so that the second stage of combustion could proceed. But if too much fuel is injected, even though the engine may be lean overall, some fuel-rich pockets will form and proceed through the first stage of combustion; by the time enough oxygen is added to these pockets to complete the second stage, the piston will have expanded the cylinder contents, thereby dropping the temperatures enough to freeze the reactions and prevent completion of the second stage.

Even if they are operated fuel rich, spark ignition engines do not have a problem with smoke since the fuel and air are premixed. However there is a problem with carbon monoxide because when fueled rich there is not enough

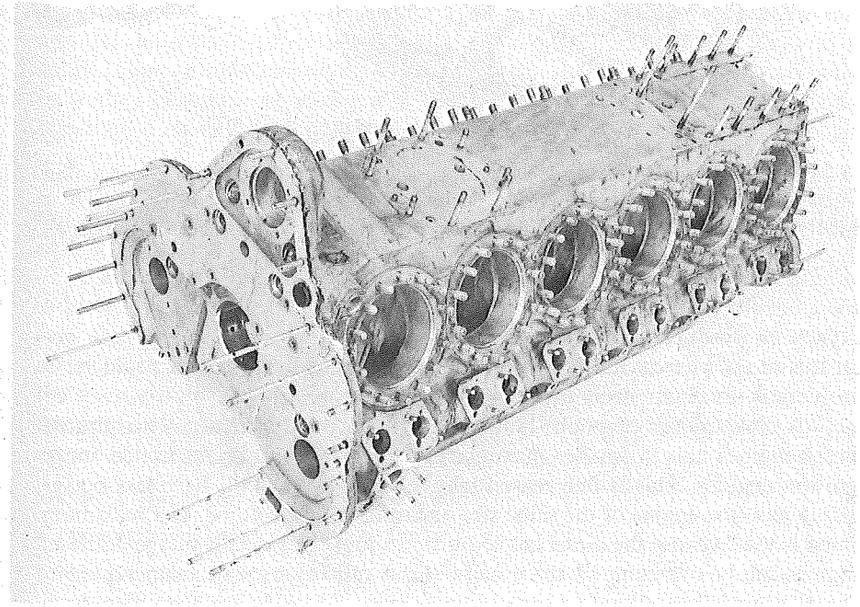

Figure 1-33 AVCR 1360-2–engine crankcase. This is a high bmep diesel engine; accordingly the crankcase is rather sturdy (Grundy, Kiley, and Brevick, 1976). Reprinted with permission © 1976. Society of Automotive Engineers, Inc.

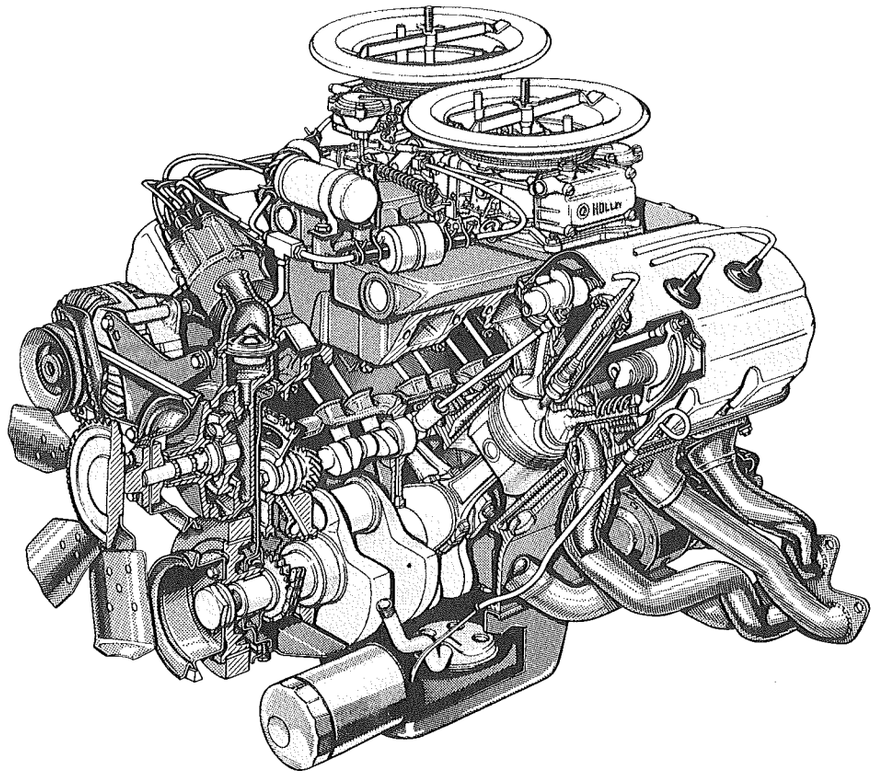

Figure 1-34 1965 Chrysler Corporation hemispherical-combustion chamber, acceleration engine used for drag racing (Weertman and Lechner, 1966). Reprinted with permission © 1966. Society of Automotive Engineers, Inc. (Illustration courtesy of Chrysler Corporation.)

oxygen to produce carbon dioxide (CO_2 requires two atoms of oxygen per carbon atom whereas CO requires only one). Of course, smoke could be a problem if the engine were fueled abnormally rich.

A consequence of smoke-limited performance is that naturally aspirated diesel engines have a smaller maximum bmep than naturally aspirated spark ignition engines. This is one reason why a diesel engine will have less power than a gasoline engine of the same size or displacement volume. The maximum bmep is less because the diesel has to burn less fuel. This disadvantage of diesel engines can be overcome by the use of either a turbocharger or a supercharger. Diesel engines can tolerate a greater boost since knock is not a problem with them. Consequently one can build a diesel engine to produce a greater bmep than a gasoline engine.

Consider the AVCR 1360-2 supercharged diesel engine built by Teledyne Continental for military application. The crankcase of this engine is shown in Fig. 1-33. Note the large number of bolts required to clamp the cylinder head to the block. This engine operates with a bmep of 24 atm at 2200 rpm. Compare that to the Chrysler hemi[2] drag engine shown in Fig. 1-34. This engine produces a maximum bmep of 12.9 atm at 5000 rpm.

Still it is true that for automotive sizes[3] gasoline engines can be built to produce more power per unit displacement volume, a rough measure of power per unit weight. This is because fuel injection systems used in diesel engines limit the maximum useful speed (see Eq. 7.91). The AVCR 1360-2 produces 48.8 kW/*l* at 2600 rpm, whereas the Chrysler hemi produces 64.1 kW/*l* at 6400 rpm. For large engines in which the rotational speeds are considerably less, there is more time for fuel injection and the difference thus disappears.

1.3 STRATIFIED CHARGE ENGINES

Although there remains a great deal of flexibility in the design of diesel engines (as evidenced by the large variation seen even among manufacturers competing in the same market, implying that the optimum solution has not yet been found), the same cannot be said of the spark ignition engines already discussed. This is primarily because the fuel–air mixture is more or less homogeneous at the time of spark. Engine manufacturers have long recognized this and thus have explored ways to produce a heterogeneous mixture at the time of spark. Thus stratified charge engines have been developed. But only recently have they become cost effective in certain applications because of changing constraints on engine design imposed to control emissions and burn poorer quality fuels.

Like diesel engines, stratified charge engines have two basic configurations: open chamber and divided chamber. The Honda engine shown in Fig. 1-35 is a good example of the latter.

The Honda engine has three valves. A rich premixed fuel–air charge is inducted into the prechamber and a lean premixed fuel–air charge is inducted into the main chamber. This flow and subsequent compression sets up a distribution in the fuel–air ratio varying from rich at the spark plug to lean at the main chamber valves, as the diagrams indicate. There are more degrees of freedom in the design of this engine than in a conventional spark ignited engine. These include:

- ratio of prechamber to clearance volume
- cross-sectional area of passage throat
- ratio of prechamber to main chamber fuel–air ratio

[2] This refers to the fact that the combustion chamber is hemispherical in shape.

[3] The term *automotive size* does not preclude trucks. It is in reference to an order of magnitude.

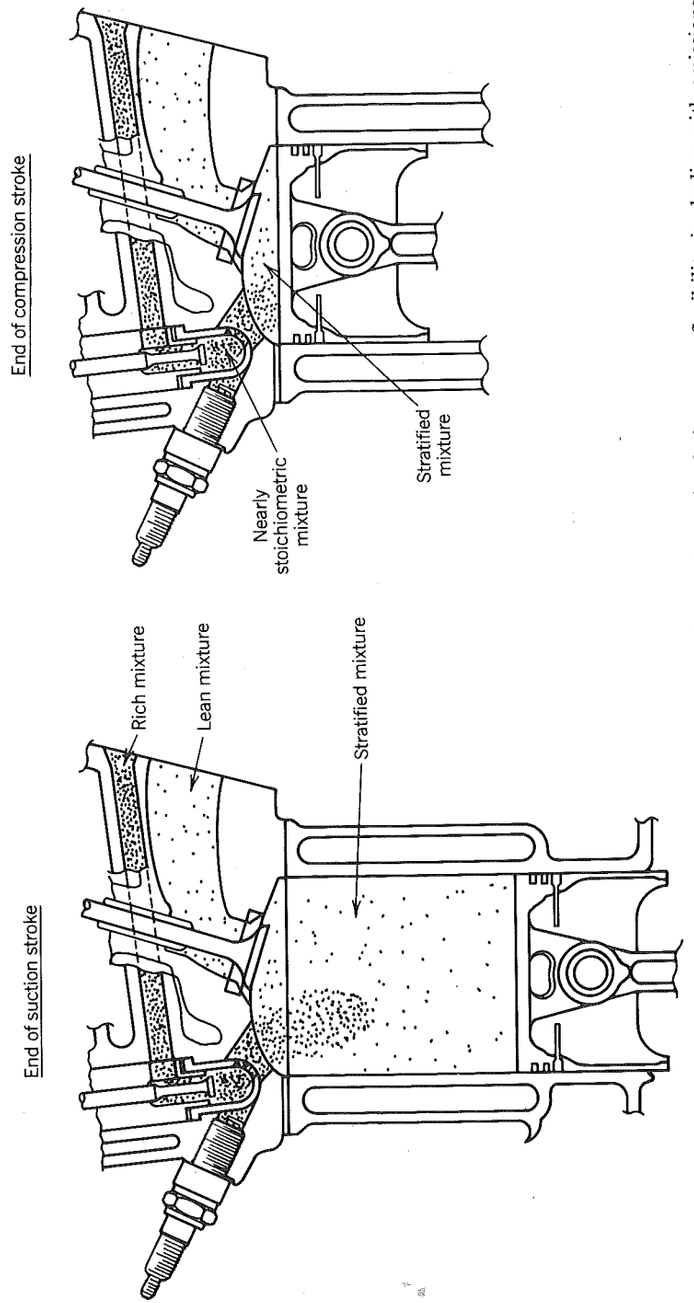

Figure 1-35 Divided chamber stratified charge engine. Stratifying the charge allows the designer new flexibility in dealing with emissions and knock constraints (Date *et al.*, 1974). Reprinted with permission © 1974. Society of Automotive Engineers, Inc. (Courtesy Honda R & D Co., Ltd.)

- third valve size and timing
- passage angle

These extra degrees of freedom allow lower emissions and a lower *octane* requirement (i.e., gasoline less resistant to autoignition is required) with no sacrifice in indicated thermal efficiency.

An example of a direct injection stratified charge engine is shown in Fig. 1-36. The extra degrees of freedom afforded in this concept relative to conventional spark ignition engines include:

- fuel injection timing
- fuel nozzle orientation and number of holes
- distance between injector and spark plugs
- ratio of cup volume to clearance volume
- fuel pressure

Again, these extra degrees of freedom allow construction of a better engine. In fact, dependent upon the fuel-injection timing, the engine can operate anywhere from more or less homogeneous combustion to combustion as heterogeneous as in a diesel engine.

If, for example, fuel is injected early in the intake stroke, there is plenty of time for the fuel to evaporate and mix thoroughly with the air prior to spark ignition. But if the fuel is injected later when it is intended to burn, then no more time for mixing is available than in a diesel engine. With late injection the engine is a multifuel engine since autoignition is not relied upon to start the combustion (ignition delay is fixed by the time required for fuel to traverse from the injector to the spark plug) and combustion can be limited by the rate of fuel injection. If a high quality diesel fuel is burned in the late injection stratified charge engine such that ignition delay is less than the time required for fuel to reach the spark plug, no problem is created since the fuel will autoignite and subsequently burn at a rate limited by the fuel injection. If a poor quality diesel fuel is burned, such as gasoline or, worse yet, methanol, still no problem arises since the spark limits the ignition delay, thereby preventing a large amount of fuel from burning rapidly once autoignition occurs, as would be the case in a diesel engine.

In fact, a very appealing piston engine vehicle can be constructed. Powered by a direct injection stratified charge engine fueled with methanol, it would have the advantages of a diesel engine, high compression ratio and no air throttling, but not the disadvantage of a smoke limited bmep because there is no smoke limit due to the presence of oxygen already in the fuel (CH_3OH). However, one must recognize that consumers try to maximize kilometers traveled per dollar rather than per liter. Although it is very fuel efficient, this car would not sell if the manufacturing of the fuel were inefficient and therefore expensive. To date the tradeoffs involved have not favored such construction.

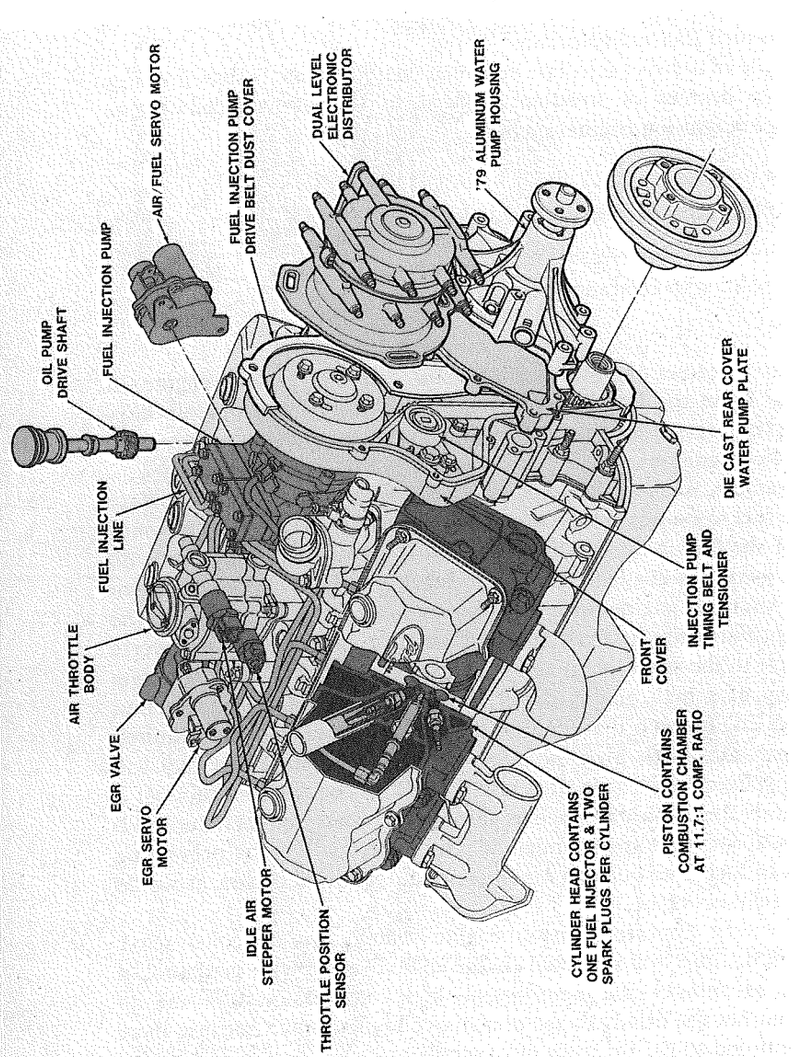

Figure 1-36 Ford's prototype open-chamber, stratified-charge engine. The fuel is directly injected into the cylinder but earlier in the compression stroke than with a diesel engine allowing use of a lower injection pressure. Two spark plugs ensure reliable ignition. Courtesy Ford Motor Company.

1.4 TWO-STROKE ENGINES

As the name implies, two-stroke engines need only two strokes of the piston or one revolution to complete a cycle. Thus there is a power stroke every revolution instead of every two revolutions as for four stroke engines.

The principle of operation is illustrated in Fig. 1-37. During compression, a subatmospheric pressure is created in the crankcase. In the example shown, this opens a *reed valve* letting air rush into the crankcase. Once the piston reverses direction during combustion and expansion begins, the air in the crankcase closes the reed valve so that the air is compressed. As the piston travels further, it uncovers holes or *exhaust ports*, and exhaust gases begin to leave, rapidly dropping the cylinder pressure to that of the atmosphere. Then the intake ports are opened and compressed air from the crankcase flows into the cylinder pushing out the remaining exhaust gases. This pushing out of exhaust by the incoming air is called *scavenging*.

Herein lies one problem with two-stroke engines: the scavenging is not perfect; some of the air will go straight through the cylinder and out the exhaust port, a process called *short circuiting*. Some of the air will also mix with exhaust gases and a portion of this mixture will be pushed out by the remaining incoming air. The magnitude of the problem is strongly dependent on the port designs and the shape of the piston top. Less than perfect scavenging is of particular concern if the engine is a carbureted gasoline engine, for instead of air being in the crankcase there is a fuel–air mixture. Some of this fuel–air mixture will thus appear in the exhaust, wasting fuel and emitting *hydrocarbon* pollutants.

Carbureted two-stroke engines are used where efficiency is not of primary concern and advantage can be taken of the engine's simplicity; this translates into lower cost and higher power per unit weight. Familiar examples include motorcycles, chain saws, outboard motors, and model airplane engines. However, use in motorcycles is decreasing because they have poor emission characteristics.

Two-stroke industrial engines are mostly diesel and typically *supercharged*. An example using both a supercharger and a turbocharger is shown in Figure 1-38. The supercharger is driven by the engine and is used with the turbocharger instead of the crankcase to compress in two stages the incoming air. The engine shown illustrates one of many different porting arrangements used in practice. In this case the incoming air enters through ports around the cylinder circumference located so as to open and close at the correct time. Combustion products are exhausted through cam actuated poppet valves located in the cylinder head.

Because there is a significant difference between the mass of air[4] m_a that enters the cylinder and the mass of air that is retained or *trapped* m_a^t, the

[4]If the engine is carbureted, replace the word *air* with *fuel air mixture* and *ambient density* with *mixture density at ambient pressure and temperature* in this discussion.

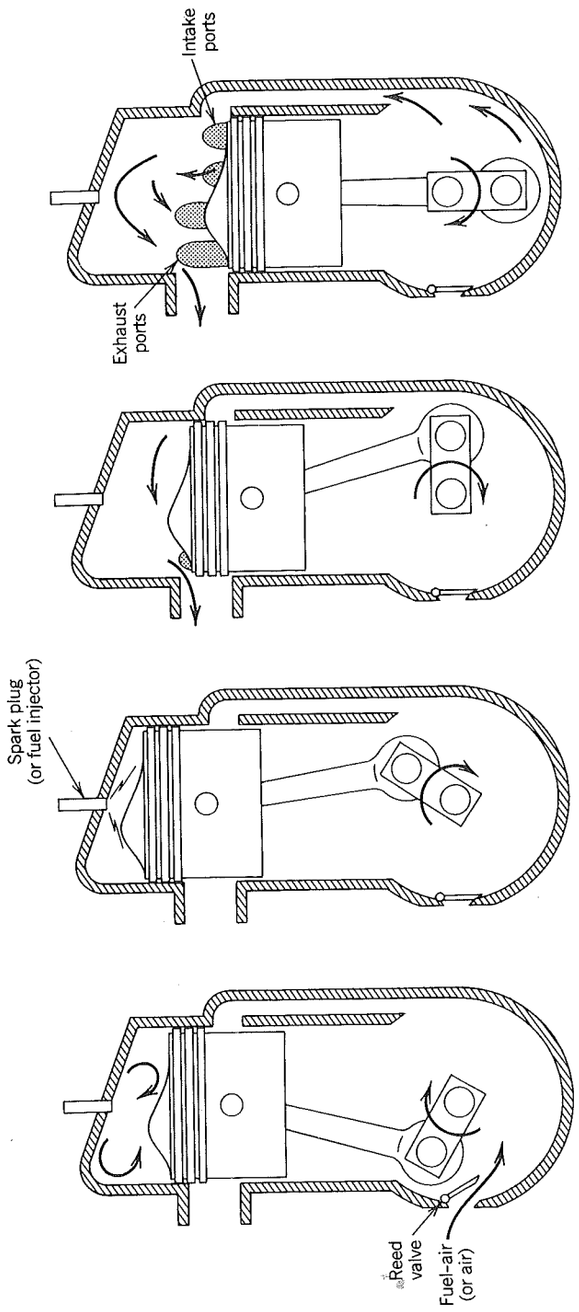

Figure 1-37 Cross-scavenged two-stroke engine.

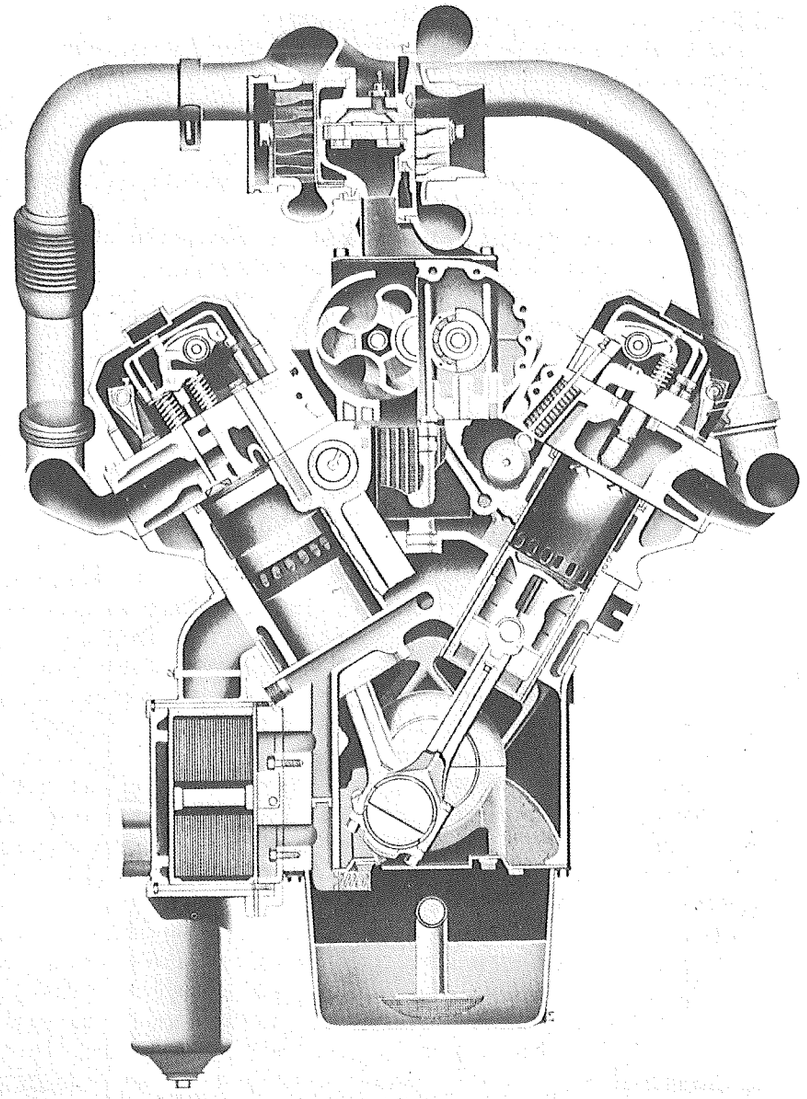

Figure 1-38 Detroit Diesel Allison (DDA), two-stroke turbo and supercharged diesel engine. This engine is called a through-scavenged engine because air flows in at the bottom of cylinder and out of the top during the intake process. Courtesy Detroit Diesel Allison.

concept of volumetric efficiency is replaced by a *delivery ratio* D_r, a *scavenging efficiency* e_s, and a *trapping efficiency* Γ.

The delivery ratio is the ratio of entering or delivered air mass m_a to the ideal air mass at ambient density

$$D_r = \frac{m_a}{\rho_\infty V_d} \tag{1.10}$$

where, as before, V_d is the displacement volume. The subscript ∞ is used on the density to denote the ambient density.

The scavenging efficiency is the ratio of the delivered air retained, or trapped air mass, to the mass of trapped charge in the cylinder

$$e_s = \frac{m_a'}{m} \tag{1.11}$$

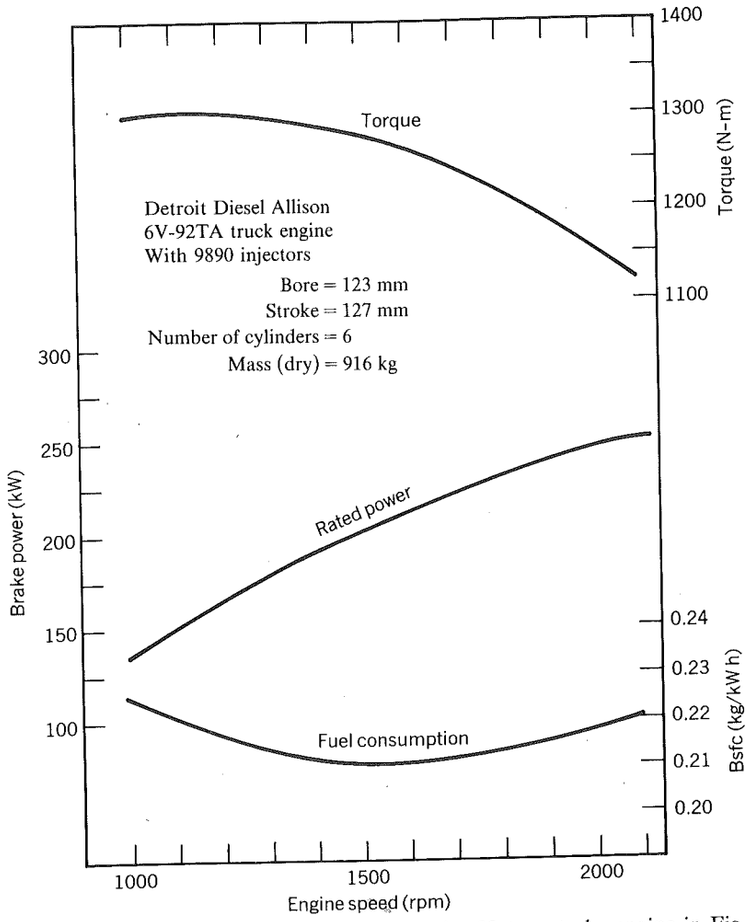

Figure 1-39 Performance data for DDA series 92 two-stroke engine in Fig. 1-38.

The scavenging efficiency is less than unity because of the presence of exhaust gas left over from the previous cycle. The trapping efficiency is the ratio of the air mass trapped to the mass of air delivered; thus

$$\Gamma = \frac{m_a'}{m_a} \tag{1.12}$$

The brake mean effective pressure is still the appropriate way to *scale* the work done. However for two-stroke engines Eq. 1.9 is replaced by

$$\text{bmep} = \frac{2\pi\tau}{V_d} \tag{1.13}$$

The difference is a factor of 2, the origin of which can be appreciated by writing out the units as in Eq. 1.8. Brake specific fuel consumption is the appropriate measure of efficiency and Eq. 1.4 through 1.6 still apply.

Some performance data for a carbureted engine are given in Homework Problem 5 which also illustrates the effects exhaust tuning can have. Performance data for the turbo and supercharged Detroit Diesel engine are given in Fig. 1-39.

1.5 STATE OF THE ART ENGINES

The AVCR-1360-2 engine built by Teledyne Continental Motors has already been mentioned. A unique feature of this engine is that the *compression ratio varies* with load to control combustion pressure. This is done via hydraulic actuators in the piston. As in Fig. 1-40, the piston consists of two main parts, the piston ring carrier and the piston pin carrier.

The piston pin carrier is connected to the connecting rod. The piston ring carrier is free to move within predetermined limits relative to the piston pin carrier. This movement varies the height from the center of the piston pin to the top of the piston crown. Thus the compression ratio is varied via an accompanying change in the clearance volume.

Oil from the lubricating system fills the upper chamber with pressurized oil through a nonreturn oil supply valve moving the piston ring carrier to its position of maximum compression ratio. Oil also enters the lower chamber through an orifice from the upper chamber. The piston is in the high compression ratio mode until the load increases and the increased cylinder gas pressure causes the preset oil discharge valve to release oil from the upper chamber. Cylinder pressure is regulated until the low compression ratio is reached.

Oil in the lower chamber, which is free to flow back to the upper chamber through the connecting orifice, controls the amount of movement between the piston pin carrier and piston ring carrier during the exhaust and intake strokes. At these times inertial forces tend to move the ring carrier upwards.

The piston described has also been used in an experimental automotive diesel engine. Although it has not proven to be cost effective, it does present an alternative solution to using glow plugs for cold starting. In addition, use of a high compression ratio at light loads reduces noise and hydrocarbon emissions.

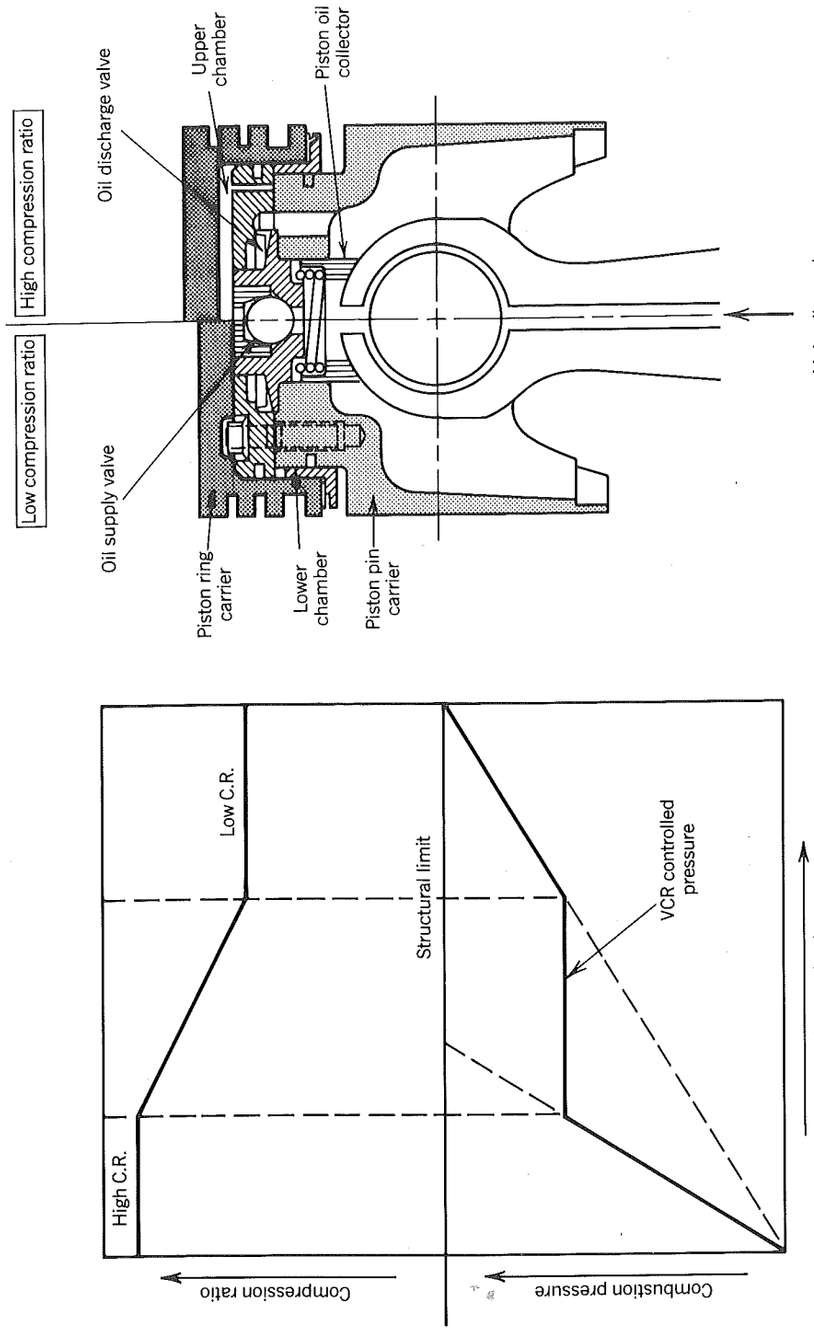

Figure 1-40 Variable compression ratio piston used in AVCR 1360-2 engine (see Fig. 1-33). This piston design allows the compression ratio to vary with load yielding better efficiency at part load, better cold start characteristics, and ability to operate on a broader range of diesel fuels (Hill and Dodd, 1978). Reprinted with permission © 1978. Society of Automotive Engineers, Inc.

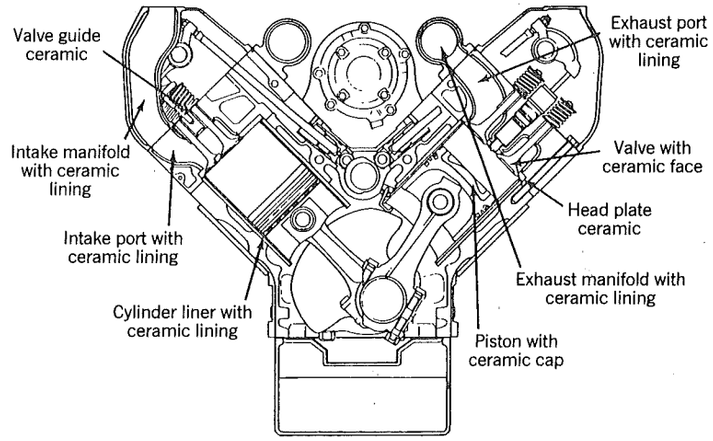

Figure 1-41 Cummins prototype insulated diesel engine. This engine requires no explicit cooling system (Bryzik and Kamo, 1983). Reprinted with permission © 1983. Society of Automotive Engineers, Inc.

The Cummins Engine Company has demonstrated that it is possible to build an engine without an explicit cooling system and with a brake thermal efficiency of $\eta_t \approx 50\%$. The basic idea, as Fig. 1-41 illustrates, is to line the combustion chamber with an *insulating material*. This reduces the heat loss from the gas in the cylinder, which leads to a small increase in efficiency but, more importantly, increases the energy of the exhaust gases. Since the exhaust turbine can then do more work than an inlet air compressor may need, a second turbine is installed and geared to the crankshaft; this is called *turbo-compounding*.

Although Cummins has successfully achieved a life of 250 hours on an insulated research engine and this success has prompted initiation of similar programs by other engine manufacturers, achieving the life of 10,000 to 15,000 hours required to be practical remains a challenge.

Lubrication is one problem. Since the walls of an insulated engine are considerably hotter than those in conventional engines, they thin out conventional lubricants and cause irreversible chemical changes. Possible solutions to this problem include using gas lubrication or solid lubricant coatings. Designing an engine requiring no oil may be feasible.

Many clever mechanisms have been patented that allow variable compression ratio, variable stroke, or complete expansion; see, for example, the book *Some Unusual Engines* by Setright (1975). To date, none have proven to be cost effective because extra mechanisms are involved. The advantages of such engines are often lost because of increased friction, reduced maximum speed, or increased weight.

The so-called K-cycle engine in this family has received considerable recent attention. Fig. 1-42 shows a prototype. The cylinders rotate about the shaft, sliding along a surface called a seal plate. During compression and

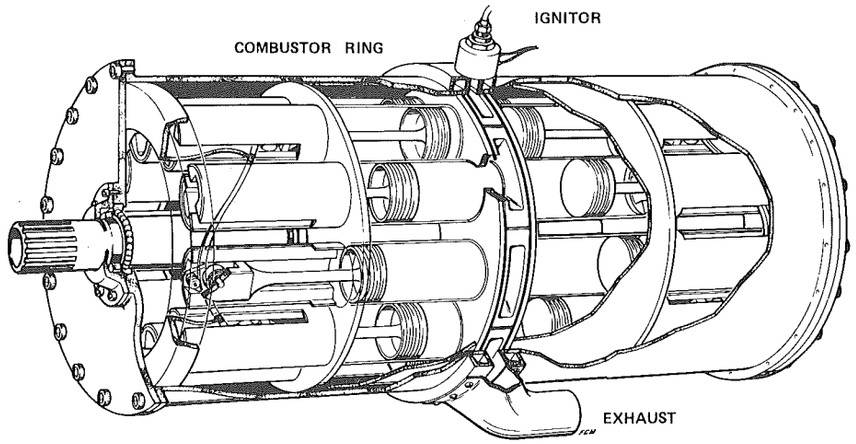

NOTE — This view demonstrates the power and exhaust strokes. The intake and compression strokes would be viewed from the other side of the engine.

Figure 1-42 Side view of K-cycle engine, a clever design that allows for an expansion stroke greater than the compression stroke. This view demonstrates the power and exhaust strokes. The intake and compression strokes would be viewed from the other side of the engine. Courtesy Kristiansen Cycle Engines Ltd.

expansion, the seal plate seals the gases within the cylinder. Ports located at the proper angular and radial position on the seal plate admit and expel gases during intake and exhaust.

Reciprocation of the pistons is controlled by the stationary cam shown in Fig. 1-43. The shape of the cam allows the expansion stroke to be longer than the compression stroke, which offers significant improvements in efficiency. Likewise, the cam can be contoured so that piston motion is rather small near

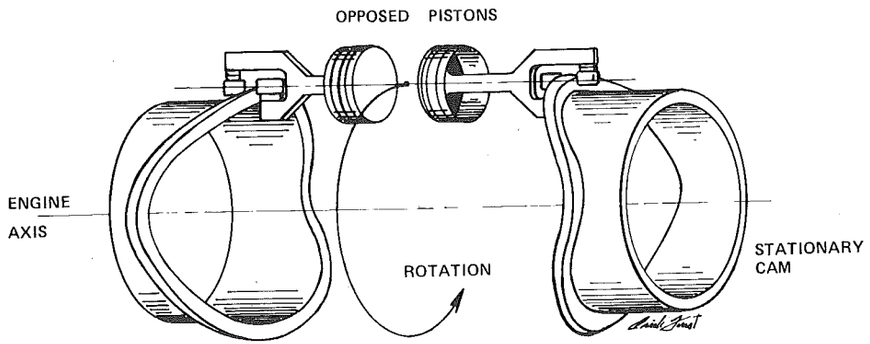

Figure 1-43 K-cycle engine opposed cam and piston assembly. Courtesy Kristiansen Cycle Engines Ltd.

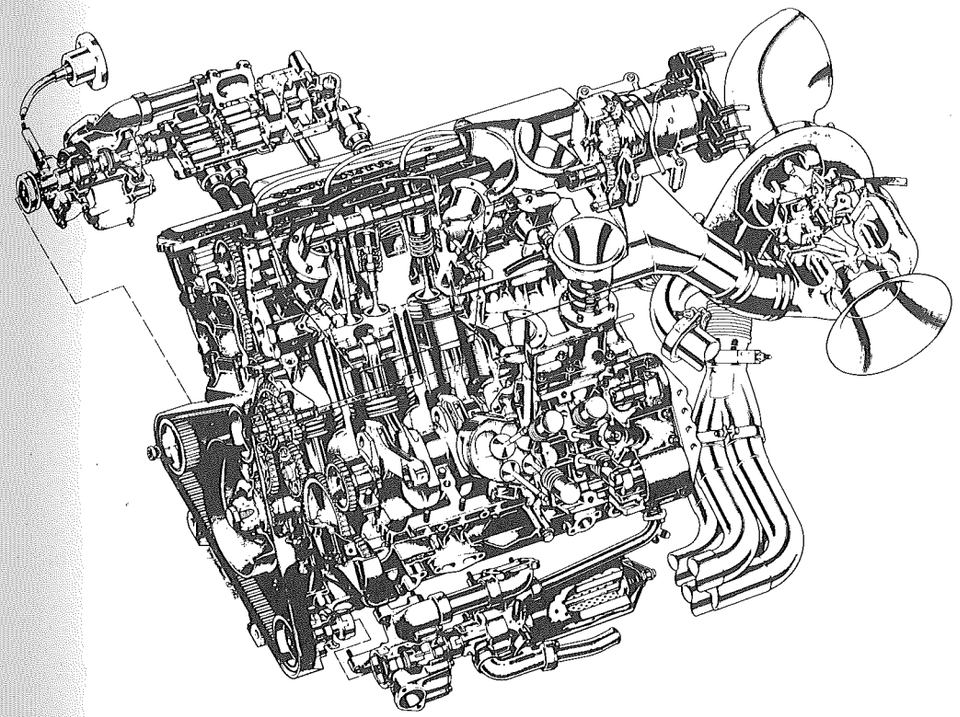

Figure 1-44 Cosworth DFX racing engine. The four valves per cylinder allow for a greater mass flow rate and higher engine speeds. © Tony Matthews.

top dead center, thereby achieving combustion closer to the ideal that occurs at constant volume.

The Cosworth 2.65 liter engine type DFX is an aluminum block V-8 built for racing (used in such races as the Indianapolis 500). A schematic of the engine is shown in Fig. 1-44. The engine is spark ignited and designed to run on port-injected methanol. Methanol offers several advantages when used to fuel spark ignition engines. The resistance to knock is high, thus allowing the Cosworth engine to run at a compression ratio of 10.5 with the turbocharged boost set at 0.6 atm. The stoichiometric fuel–air ratio is about twice that of gasoline and the latent heat of evaporation is about three times that of gasoline. This means that significant cooling of the air charge will occur as the methanol evaporates (about six times more than can be obtained with gasoline). By using fuel considerably richer than stoichiometric, this after-cooling is used to maximum advantage, even though fuel is wasted, and it is done without using the added bulk and weight of a heat exchanger. "Fueling rich" also adds to the knock resistance. The Cosworth engine produces a maximum bmep of 22.3 atm and a specific power on the order of 1100 W/cm^2. Because knock is not a problem, the maximum bmep is comparable to that of the AVCR-1360-2

turbocharged diesel engine. Because the engine does not rely on combustion limited by the rate of fuel injection, its maximum speed is 10,500 rpm. The combination of high speed, high compression ratio, and turbocharging nets a specific power, on a modest boost, of about twice that produced by the Chrysler hemi drag engine or the AVCR diesel engine. At higher boosts, specific powers of 2500 W/cm^2 and bmeps of 50 atm appear attainable. On such exotic fuels as nitromethane or pentaborane even higher specific powers can be attained although a great price is paid in engine life (state of the art engines for drag racing that need to last only five or six seconds appear to have specific powers of 2500 W/cm^2).

One of the distinguishing features of the Cosworth engine is the use of an aluminum alloy for the block and other parts. There are racing engines that use titanium connecting rods and/or magnesium parts such as the oil pan or gear covers. That new technology often appears in racing engines is not unusual because they can tolerate more costly parts than mass produced engines. The racing industry thus acts as a proving ground for new ideas.

For example, the Ford Motor Company has contracted Polimotor Research Inc. to build racing engines from fiber-reinforced plastic, also called

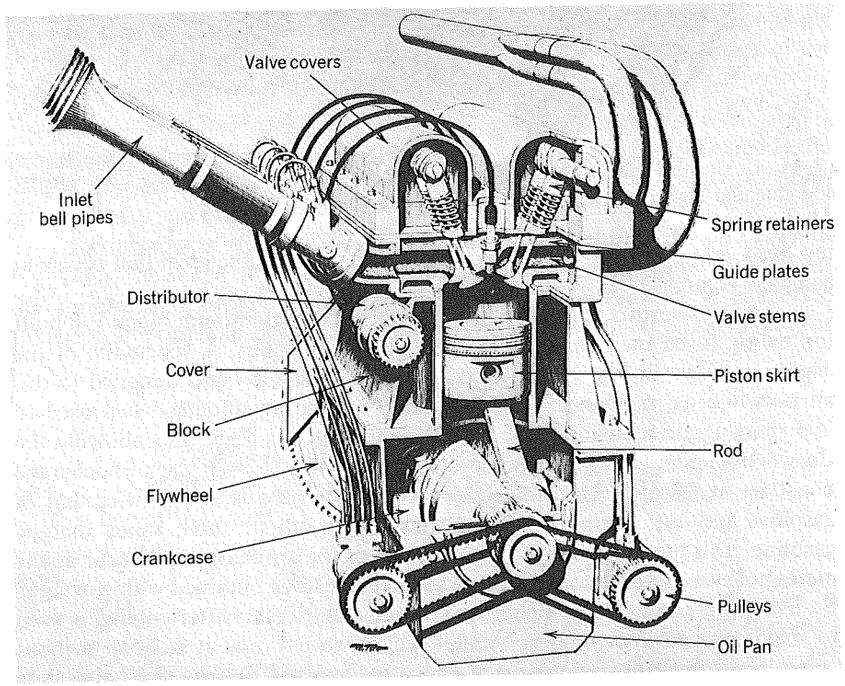

Figure 1-45 A semiplastic engine built by Polimotor Research Inc. under contract to Ford Motor Co. The fiber reinforced plastic parts are labeled. Note how the head, block, and structurally loaded oil pan are fastened with through-bolts. Reprinted from *Popular Science* with permission © 1982. Times Mirror Magazine, Inc.

composites. A plastic engine is shown in Fig. 1-45. Labeled parts are made of composite material. The Ford production engine (2.3 liter, four cylinder) has a mass of 188 kg; whereas the Polimotor twin cam engine, which uses the same crankshaft, has a mass of 69 kg. The plastic engine's weight is only 37% of that of production engine.

The reduced weight is an obvious advantage. Not as apparent is that higher piston speeds are possible because the mass of the reciprocating parts is reduced and there is increased strength due to the ability to line fibers in the direction of maximum stress. This means that for a given maximum power, the engine can be made even smaller, thus realizing further weight and bulk reductions.

1.6 ALTERNATIVE ENGINES

Reciprocating piston internal combustion engines are built that can deliver a power anywhere from 0.01 to 5×10^4 kW. They compete in the market place with electric motors, gas turbines, steam engines, Stirling engines, and rotary engines.

Prior to World War II, aircraft relied almost exclusively on piston engines. Today gas turbines are the dominant power plant in large planes and piston engines dominate the market in small planes. Ships and railroad locomotives used to run by steam engines; today diesel engines are the dominant power plant. In 1900 most automobiles were steam or electrically powered, by 1940 most automobiles were powered by gasoline engines (Amann, 1980).

In this section each of the alternative powerplants will be discussed in terms of a particular application where it dominates the field by having some advantage over the internal combustion engine.

First consider electric motors, which compete in the range of powers less than about 500 kW. They are used, for example, in forklifts operated within a factory or warehouse. Internal combustion engines are not applied in this case because they would build up high levels of pollutants such as carbon monoxide or nitric oxide.

Proponents of electric vehicles point out that almost any fuel can be used to generate electricity, therefore we can reduce our dependence upon petroleum by switching to electric vehicles. There would be no exhaust emissions emitted throughout an urban environment. The emmissions produced by the new electric generating stations could be localized geographically so as to minimize the effect.

But because of the batteries, the electric vehicles that have been built to date have a limited range, on the order of one fifth of what can be easily realized with a gasoline engine powered vehicle. It is generally recognized that a breakthrough in battery technology is required if electric vehicles are to become a significant part of the automotive fleet.

However, electric motors are found in a variety of applications, such as where the noise and vibration of a piston engine or the handling of a fuel are

unacceptable. Other examples are easy to think of in both industrial and residential sectors. Electric motors will run in the absence of air, such as in outer space or under water; they are explosion proof; and they can operate at cryogenic temperatures.

An exploded view of an electric motor is shown in Fig. 1-46. Only the simplest of two-stroke engines have so few parts; this translates to ease in repair and maintenance.

If one can generalize, one might state with respect to electric motors that internal combustion engines tend to be found in applications where mobility is a requirement or electricity is not available.

Gas turbine engines compete with internal combustion engines on the other end of the power spectrum, at powers greater than about 500 kW. The advantages offered depend on the application. Factors to consider are the efficiency and power per unit weight.

A gas turbine consists basically of a compressor–burner–turbine combination which provides a supply of hot, high-pressure gas. This may then be expanded through a nozzle (turbojet), through a turbine, to drive a fan, and then through a nozzle (turbofan), through a turbine, to drive a propeller (turboprop), or through a turbine to spin a shaft in a stationary or vehicular application.

A schematic and a cutaway view of a Pratt and Whitney PW2037 turbofan engine are shown in Fig. 1-47. One advantage a gas turbine engine offers to the designer is that the hardware responsible for compression, combustion, and expansion are three different devices, whereas in a piston engine all these processes are done within the cylinder. Thus the hardware for

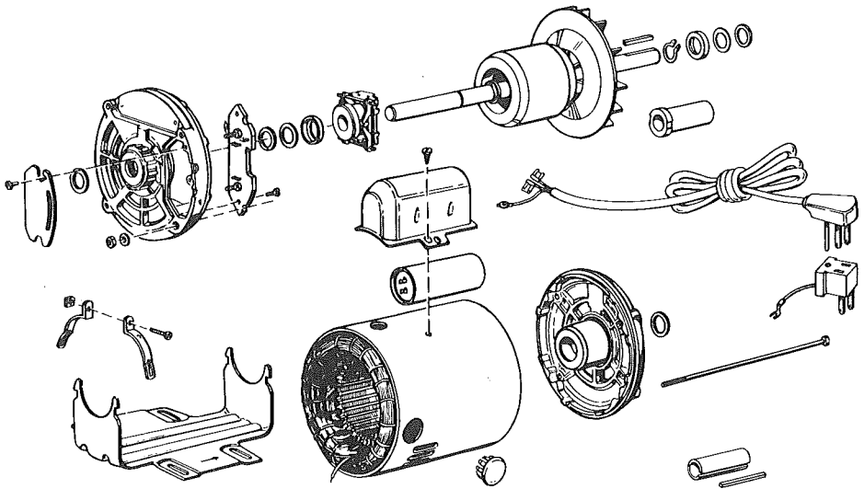

Figure 1-46 Typical electric motor; only the simplest of two-stroke engines have so few parts. Electric motors displace internal combustion engines at the low end of the power spectrum. By permission, Sears, Roebuck and Co.

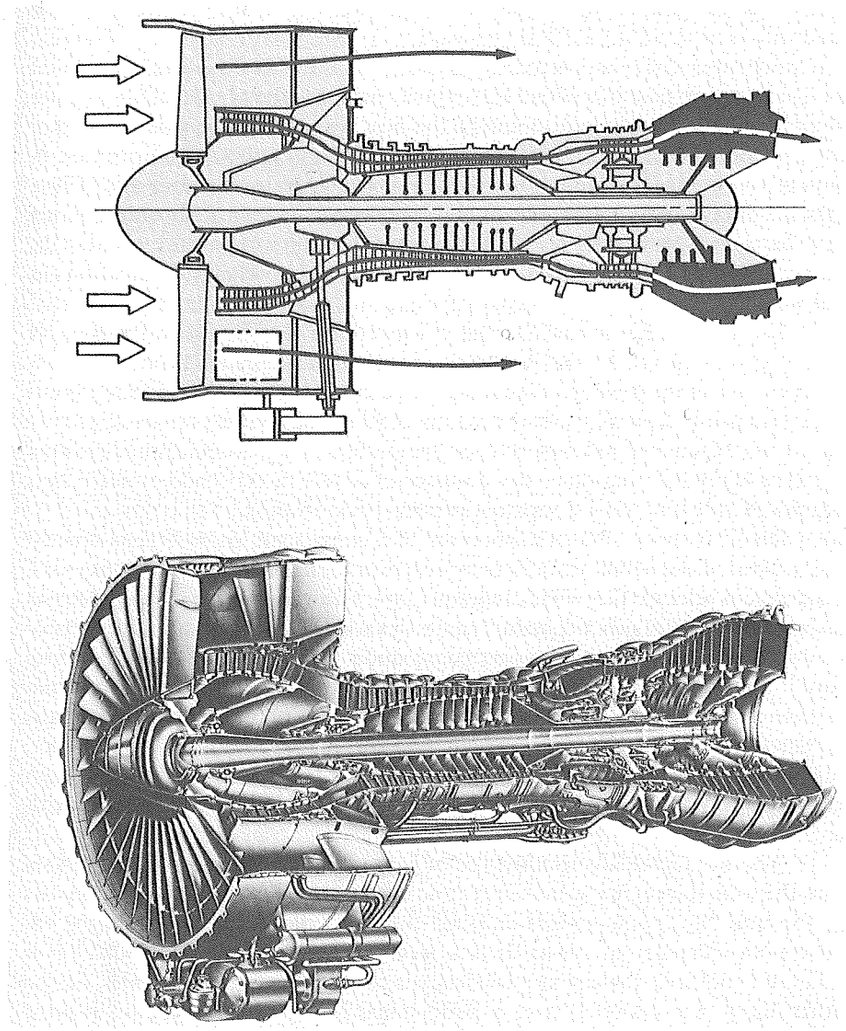

Figure 1-47 Pratt and Whitney PW 2037 gas turbine engine. Gas turbines displace piston engines at the high end of the power spectrum in cases where mobility is a requirement.

each process in a gas turbine engine can be optimized separately; whereas in a piston engine compromises must be made with any given process since the hardware is expected to do all three tasks.

One advantage the internal combustion engine offers to a designer is that the gases at any position within the engine vary periodically from hot to cold. Thus the average temperature during the heat transfer to the walls is neither very hot nor cold. On the other hand, the gas temperature at any position in the gas turbine is steady, and the turbine inlet temperature is always very hot, thus tending to warm material at this point to a greater temperature than anywhere in a piston engine. With temperature limits imposed by materials, the reciprocating engine can have a greater peak cycle temperature than the gas turbine engine.

As an aside, the trade offs just discussed are also found in the K-cycle engine discussed earlier and in conventional piston engines. The stationary cams in the K-cycle allow a designer some new degrees of freedom toward separate optimization of the compression, combustion, and expansion processes but at the expense of lower peak-cycle temperatures. It should also be pointed out that turbocharging gives the designer of conventional engines some new degrees of freedom toward separate process optimization.

Recall that the adiabatic efficiency of a compressor or turbine is defined as the ratio of the actual work done or received for a given pressure ratio to the isentropic work for the same pressure ratio. The thermal efficiency of a gas turbine engine is highly dependent upon the adiabatic efficiency of its components which in turn is highly dependent upon their size and their operating conditions. Large turbomachinery tends to be more efficient than small turbomachinery. That airliners are larger than automobiles is one reason gas turbines have displaced piston engines in airliners but not in automobiles. Likewise gas turbines are beginning to penetrate the marine industry, though not as rapidly as power per unit weight is not as important with ships as with airplanes.

Another factor favoring the use of gas turbines in airliners (and ships) is that the time the engine spends operating at part or full load is small compared to the time the engine spends cruising, thus the engine can be optimized for maximum efficiency at cruise. It is a minor concern that at part load or at take-off conditions the engine's efficiency is compromised. Automobiles, on the other hand, are operated over a wide range of load and speed so a good efficiency at all conditions is better than a slightly better efficiency at the most probable operating condition and a poorer efficiency at all the rest. Since long-distance trucks are larger than cars and spend proportionately more time at cruise, it is reasonable to expect gas turbines to appear in trucks before in cars (although it is not clear whether or not they will).

Steam engines (or to admit the possibility of some of the fluorocarbons developed for this use, vapor-cycle engines) are less efficient than internal combustion engines. They are used today almost totally in stationary applications and where the energy source precludes the use of internal combustion engines. Such energy sources include coal, garbage, nuclear, and solar, and

waste heat in the exhaust gas of combustion devices including internal combustion engines. In some applications the emission characteristics might be a factor. In the early 1970s, in fact, a great deal of development work was done toward producing an automotive steam engine when it was not known whether the emissions from the internal combustion engine could be reduced enough to meet the standards dictated by concern for public health.

An interesting application of steam engines is in underwater propulsion and power generation. Figure 1-48 shows the features of a proposed underwater power plant using a boron slurry, with its attendant high energy density, as the fuel and oxygen as the oxidant (Burkland, 1969). Solid fuels such as boron or coal are more difficult to handle and deliver to a combustor than liquid fuels. Slurries composed of fine solid particles, anywhere from 50 to 80% by weight, mixed with water can be pumped and thus handled as a liquid.

The combustion products of a slurry contain small, abrasive particles which if used in a piston or turbine expander will cause intolerable wear rates. However, they cause little if any problem when passed through a heat exchanger and are thus suitable for use in a steam engine.

There should be renewed interest in steam engines for transportation because of their ability to use coal slurries. Current interest in trying to operate diesel or gas turbine engines on coal seems misplaced. As gasoline and diesel fuel can be made from coal, successful displacement of internal combustion engines by steam engines will depend upon whether it is cheaper to operate a vehicle with a poor efficiency (steam engine) using a cheap fuel (coal slurry) or with a high efficiency (gasoline engine) using an expensive fuel (coal or shale-oil-derived gasoline).

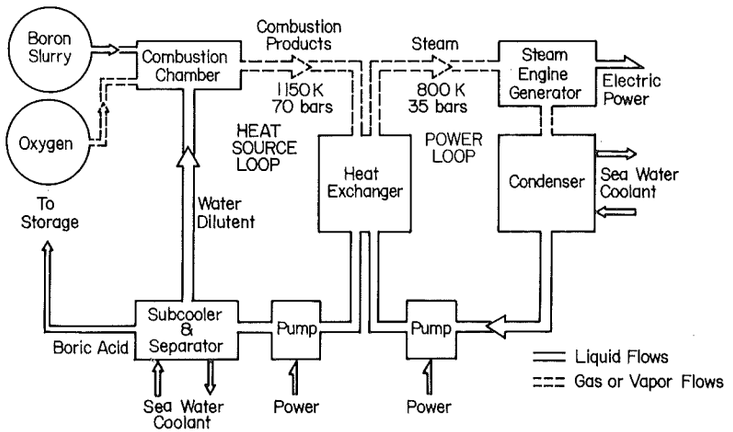

Figure 1-48 Boron thermochemical power plant cycle—boron slurry/oxygen-steam engine. Rankine cycle based engines are especially appropriate for solid fuels or when the combustion products are expected to contain small abrasive particles as with boron or coal slurries (Burkland, 1969). Reprinted with permission © 1969. Society of Automotive Engineers, Inc.

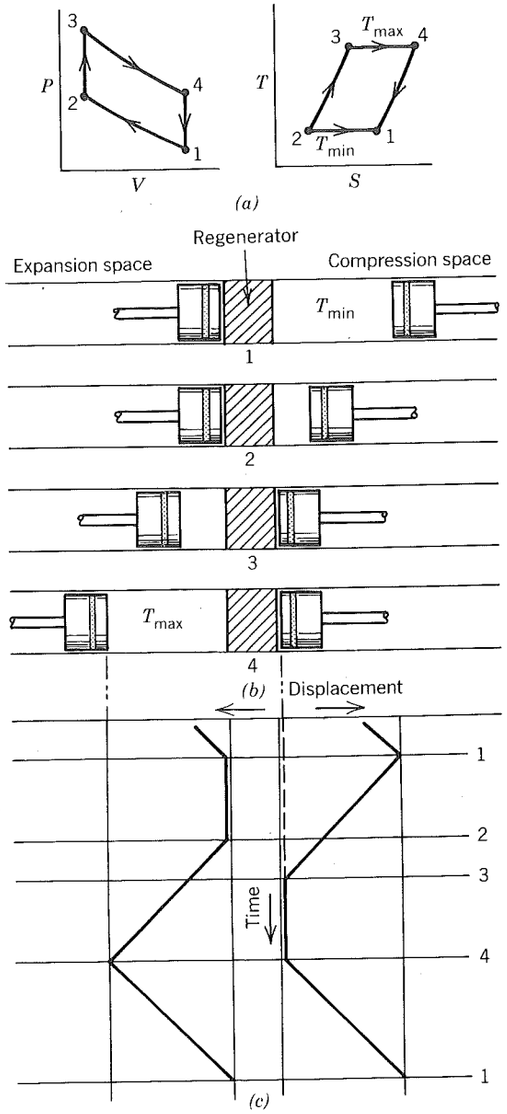

Figure 1-49 The Stirling cycle. (*a*) P–V and T–S diagrams. (*b*) Piston arrangement at the terminal points of the cycle. (*c*) Time-displacement diagram. Walker (1973), Reprinted with permission © 1973. Oxford University Press.

Stirling engines are attractive because they, like steam engines, are heat or external combustion engines and can thus use a multitude of energy sources. Their ideal thermodynamic cycle more closely approximates a Carnot cycle than any of the Rankine, Brayton or Otto cycles, the ideal cycles for steam, gas turbine, and piston engines, respectively. They are attractive combustion engines because their exhaust emissions are controllable without catalytic convertors or particulate traps.

The Stirling cycle is illustrated in Fig. 1-49, where two opposed pistons separated by a regenerator are shown. The regenerator acts as a thermal capacitance that alternately releases and absorbs heat. It is designed to have a high heat transfer coefficient and low flow resistance to any gas that flows through it. The compression space is maintained at a low temperature and the expansion space at a high temperature (when reduced to hardware, the temperature of the expansion is then material limited).

The gas is compressed isothermally from (1) to (2) and heat is rejected to the low-temperature sink. From (2) to (3) the gas is displaced from the compression space to the expansion space. This is accomplished by moving both pistons to the left, holding the volume between them constant. The gases flowing through the regenerator absorb heat and flow into the expansion at space T_{max}.

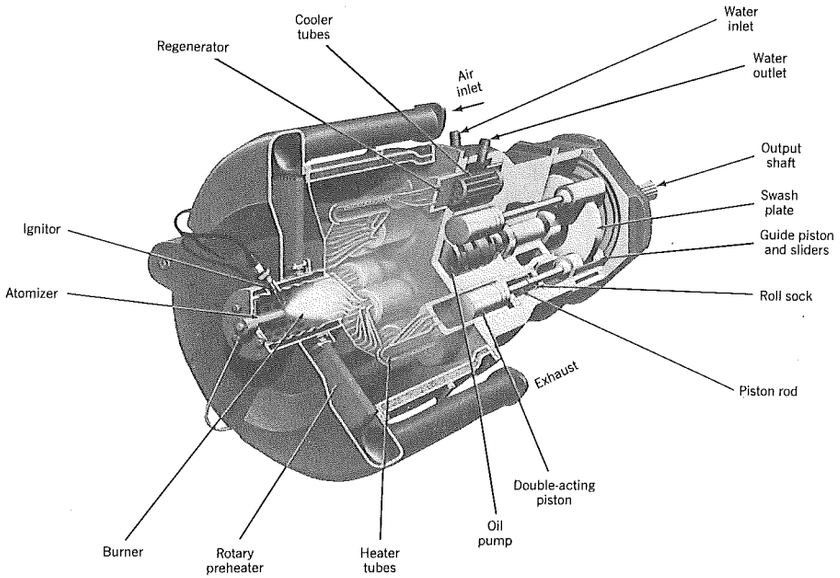

Figure 1-50 A swash-plate drive stirling engine. The swash plate controls the piston reciprocation in a manner not unlike that of the cam employed in the K-cycle engine. See Fig. 1-43 (Postma, Van Giessel, and Reinink, 1973). Reprinted with permission © 1973. Society of Automotive Engineers, Inc.

By adding heat from (3) to (4), the gases are isothermally expanded. The final displacement at constant volume from (4) to (1) returns the heat previously drawn by the gas from the regenerator back to the regenerator cooling the gas down to the temperature T_{min}.

Fig. 1-50 and 1-51 illustrate a swash-plate and a rhombic-drive Stirling engine, respectively. Neither style engine poses a threat to the internal combustion engine in any of its current applications. Experience gained in building the prototypes should suggest that Stirling engines will be too expensive because

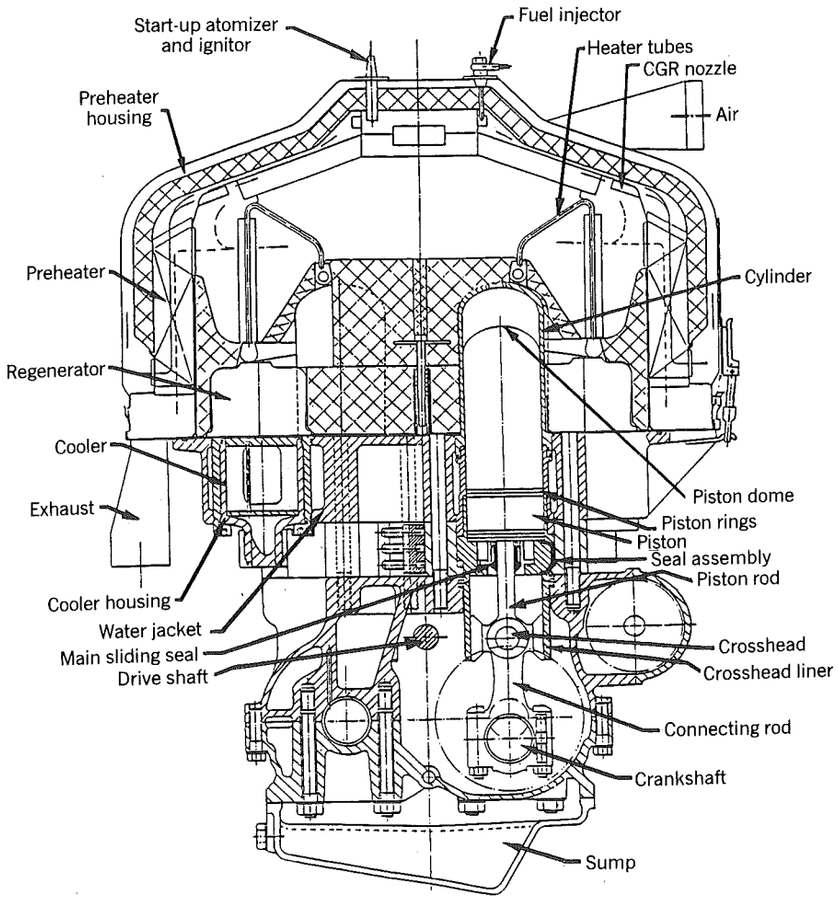

Figure 1-51 Rhombic-drive stirling engine. Stirling engines are external combustion engines. The working gas, usually hydrogen, is separate and distinct from the fuel, air, and combustion products. As with any external combustion engine, the potential for operation on solid fuels is higher than with internal combustion engines. Courtesy Mechanical Technology Inc.

they need a complicated control network, an exhaust-gas/inlet-air preheater, high quality materials in the expansion space, and the use of high pressure hydrogen working gas which is hard to contain (Fagenbaum, 1983).

The modern Stirling engine may find its first application in systems where synergism can be exploited. For example, a concept for a heat pump system is shown in Fig. 1-52. Using a Stirling engine to power the heat pump eliminates the need to purchase electricity to drive an electric motor to power the same heat pump. This is more efficient but not necessarily cost effective. An electric powered heat pump delivers to the indoor heat exchanger only that heat delivered by the heat pump (54 kW in this case). Using a Stirling engine to drive the heat pump allows one to deliver to the indoor heat exchanger heat that is rejected to the coolant (33 kW in this case).

This is synergystic in that normally the heat rejected to the coolant of an engine is wasted. Used to replace an electric motor, the total effect is greater than the sum of the effects taken independently. The Stirling engine is better suited to this application because, compared to an internal combustion engine, more of the heat rejected appears in the coolant than in the exhaust.

The last engine considered here as an alternative to reciprocating piston engines is the Wankel engine. This is the most highly developed engine in a

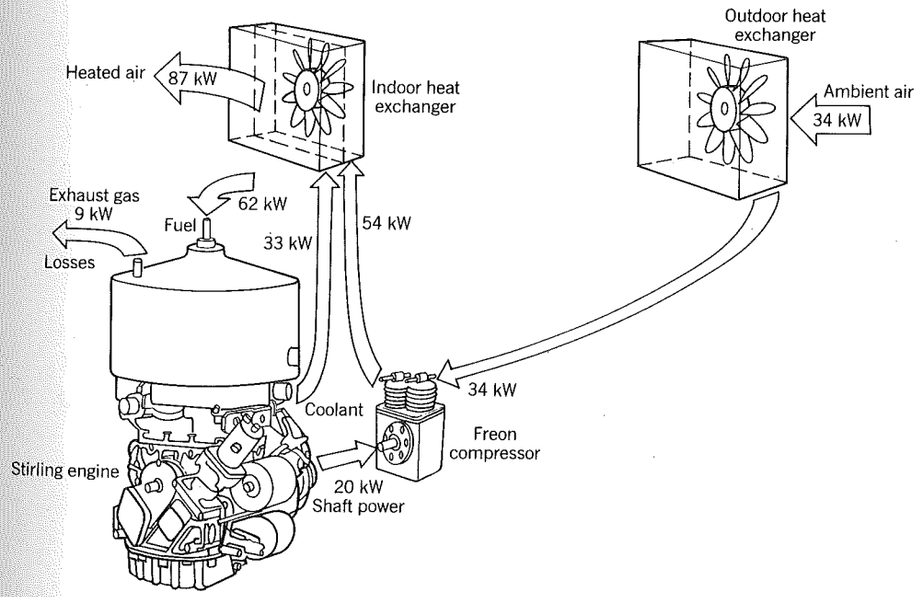

Figure 1-52 Stirling driven heat pump. Most of the heat rejected by stirling engines appears in the coolant, which can be exploited to good advantage as in this heat pump. (Fagenbaum, 1983). Reprinted with permission © 1983. ASME.

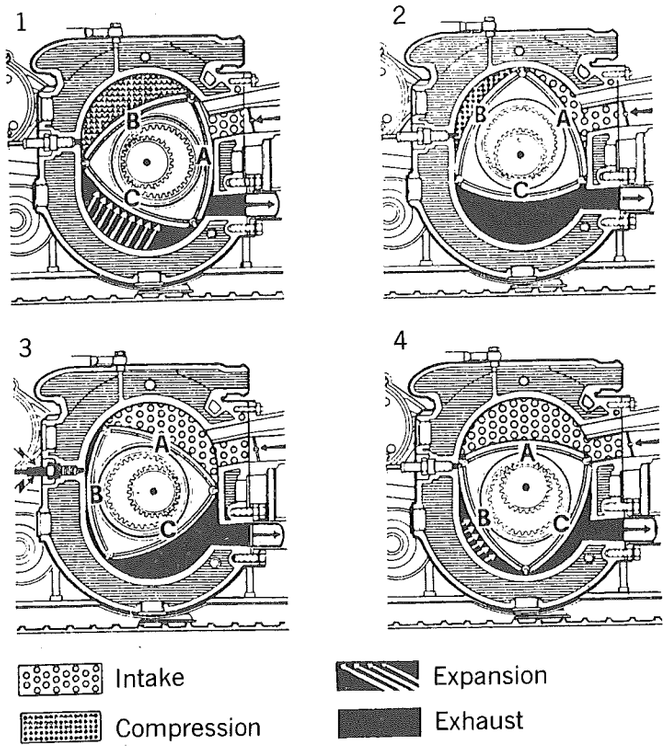

Figure 1-53 In the four-stroke Wankel, all three working chambers are in continuous action. Although rotor face (A) is sweeping out the remaining exhaust gases and preparing to begin a new intake phase, chamber (B) is beginning compression and chamber (C) is about to complete its expansion phase. In the second sketch, chamber (A) goes ahead with its intake, while chamber (B) approaches maximum compression. Chamber (C) has just started its exhaust phase. In the third sketch, ignition takes place in chamber (B), chamber (A) is about to complete its intake phase, and chamber (C) is in the middle of the exhaust phase. The fourth sketch shows expansion in chamber (B), completion of intake in chamber (A), and continued scavenging in chamber (C) (rotor revolves CCW). From *The Wankel Engine* by J. Norbye © 1971. Reprinted with the permission of the author.

larger family of rotary engines. Figure 1-53 illustrates how a Wankel operates. Notice that it is a four-stroke engine. It can be built as a homogeneous or stratified-charge spark ignition engine or as a compression ignition engine. Because its thermodynamic cycle is the same as that in a conventional engine it offers no greater potential as a thermodynamic machine. Like the K-cycle or gas turbine it could suffer a material limitation on peak-cycle temperature but

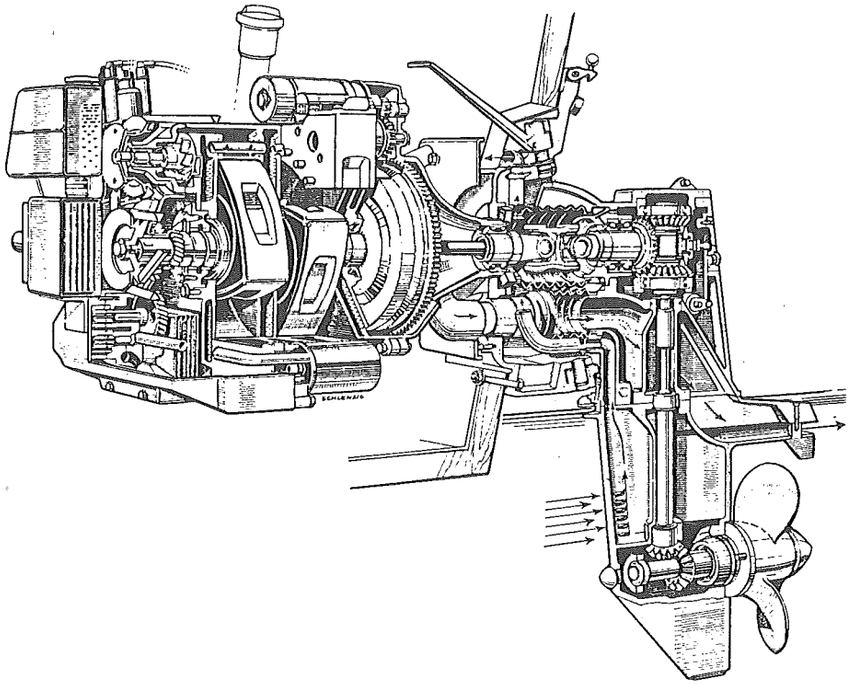

Figure 1-54 The marine version of the NSU Ro-80 engine forms a very compact power unit for an inboard/outboard installation. From *The Wankel Engine* by J. Norbye © 1971. Reprinted with permission of the author.

unlike these engines it offers no corresponding advantage in terms of separate-process optimization. Its primary advantages are a better power to weight ratio and inherent dynamic balance. Wankel engines are competing with conventional engines in small sports cars, motorcycles, chain saws and, as Fig. 1-54 shows, in small boats, all applications where its advantages outweigh its inferior fuel economy.

1.7 GENERAL REFERENCES

Annand, W. J. D., and G. E. Roe, *Gas Flow in the Internal Combustion Engine*, G. T. Foulis, Somerset, England, 1974.

Ansdale, R. F., *The Wankel RC Engine*, A. S. Barnes, New York, 1969.

Benson, R. S. and N. D. Whitehouse, *Internal Combustion Spark and Compression Ignition Engines, Their Design and Development*, Pergamon, New York, 1979.

Burman, P. G. and F. DeLuca, *Fuel Injection and Controls for Internal Combustion Engines*, Simmons–Boardman, New York, 1962.

Campbell, A. S., *Thermodynamic Analysis of Combustion Engines*, Wiley, New York, 1979.

Collie, M. J., (Ed.), *Stirling Engine*: *Design and Feasibility for Automotive Use*, Noyles Data, New Jersey, 1979.

Cummins, C. L., Jr., *Internal Fire*, Carnot Press, Lake Oswego, Oregon, 1976.

Diesel, E., G. Goldbeck, and F. Schildberger, *From Engines to Autos*: *Five Pioneers in Engine Development and Their Contributions to the Automotive Industry*, Henry Regnery, Chicago, 1960.

Hartley–Smith, D. I., *Diesel Engine Maintenance*, Iliffe, London, 1964.

Henein, N. A. and D. J. Patterson, *Emission from Combustion Engines and Their Control*, Science, Ann Arbor, 1972.

Hill, P. G. and C. R. Peterson, *Mechanics and Thermodynamics of Propulsion*, Addison–Wesley, Reading, Massachusetts, 1970.

Judge, A. W., *Automobile Engines*: *In Theory*, *Design*, *Construction*, *Operation and Testing*, *Motor Manuals* Volume 1, Robert Bentley, Cambridge, Massachusetts, 1972.

Lichty, L. C., *Combustion Engine Processes*, McGraw–Hill, New York, 1967.

Mackerle, J., *Air Cooled Motor Engines*, Cleaver–Hume Press, Ltd., London, 1961.

Norbye, J. P., *The Wankel Engine*, Chilton, Philadelphia, 1971.

Obert, E. F., *Internal Combustion Engines and Air Pollution*, Harper & Row, New York, 1973.

Rogowski, A. R., *Elements of Internal Combustion Engines* McGraw–Hill, New York, 1953.

Sawyer, J. W., Ed., *Sawyer's Gas Turbine Engineering Handbook*, Gas Turbine Publications, Stamford, Connecticut, 1976.

Schmidt, F. A. F., *The Internal Combustion Engine*, translated by R. W. S. Mitchell and J. Horne, Chapman & Hall, London, 1965.

Schweitzer, P. H., *Scavenging of Two-Stroke Cycle Diesel Engines*, Macmillan, New York, 1959.

Setright, L. J. K., *Some Unusual Engines*, Mechanical Engineering Publ. Ltd., London, 1975.

Springer, G. S. and D. S., Patterson, (Eds.), *Engine Emissions*: *Pollutant Formation and Measurement*, Plenum New York, 1973.

Taylor, C. F., *The Internal-Combustion Engine in Theory and Practice*, Vols. 1 and 2, MIT Press, Cambridge, Massachusetts, 1977.

Transactions of The Society of Automotive Engineers. [This is a primary reference for engineers working with engines. An author index, subject index, and collation of abstracts is in the reference section of most libraries.]

Walker, G., *Stirling Cycle Machines*, Oxford University Press (Clarendon), London/New York, 1973.

Yamamoto, K., *Rotary Engine*, Sankaido Co. Ltd., Japan, 1981.

1.8 SPECIFIC REFERENCES

Alperstein, M., G. H. Schafer, and F. J. Vilforth, III. (1974), "Texaco's Stratified Charge Engine," SAE paper 740563.

Amann, C. A. (1980), "Why *Not* a New Engine," SAE Trans., Vol. 89, p. 4561, paper 801428.

Armstrong, D. L. and G. F. Stirrat (1982), "Ford's 1982 3.8L V6 Engine," SAE SP-510 p. 33, paper 820112.

Bryzik, W. and R. Kamo (1983), "TACOM/Cummins Adiabatic Engine Program," SAE paper 830314.

Burkland, C. V. (1969), "A Rankine Cycle Powerplant with Boron Slurry Fuel," SAE paper 690732.

Butler, J. L., J. H. Garrett, and J. L. Hoch (1974), "Cummins K-Series Engines," SAE paper 740030.

Czadzeck, G. H. and R. A. Reid (1979), "Ford's 1980 Central Fuel Injection System," SAE SP-477, p. 27, paper 790742.

Date, T., S. Yagi, A. Ishizuya, and I. Fuji (1974), "Research and Development of the Honda CVCC Engine," SAE paper 740605.

Eberle, M. K. (1980), "The Marine Diesel Engine—The Answer to Low Grade Fuels," ASME paper 80-DGP-16.

Fagenbaum, J. (1983), "The Stirling–A Hot Engine for the 80's," *Mechanical Engineering*, **105** (5), p. 18–29.

Field, D. B. and S. J. Hinkle (1974), "Detroit Diesel Allison's Series 92 Engines," SAE paper 740037.

Finsterwalder, G. (1972), "A New Deutz Multifuel System," SAE paper 720103.

Grundy, J. R., L. R. Kiley, and E. A. Brevick (1976), "AVCR 1360-2 High Specific Output Variable Compression Ratio Diesel Engine," SAE paper 760051.

Herrmann, R. (1980), "PA.4-200 Engines with Variable Geometry Precombustion Chamber and Two Stage Turbocharging System," ASME paper 80-DGP-22.

Heywood, J. B. (1976), "Pollutant Formation and Control in Spark Ignition Engines," *Prog. Energy Combust. Sci.* Vol. 1, pp. 135–164.

Hill, S. W. and J. L. Dodd (1977), "A Low NO_x Lightweight Car Engine," SAE Trans., Vol. 86, paper 770430.

Hisatomi, T. and H. Iida (1982), "Nissan Motor Company's New 2.0 Liter Four Cylinder Gasoline Engine," SAE-510, p. 53, paper 820113.

Hofbauer, P. and K. Sator (1977), "Advanced Automotive Power Systems—Part 2: A Diesel for a Subcompact Car," SAE Trans., Vol. 86, p. 400, paper 770113.

Hoffman, H., (1971), "Development Work on the Mercedes-Benz Commercial Diesel Engine, Model Series 400," SAE paper 710558.

Huntington, R., (1981), *Design and Development of the Indy Car*, H. P. Books, Tucson, Arizona.

Jones, J. A., W. L. Kingsbury, H. H. Lyon, P. R. Mutly, and K. W. Thurston (1979), "Development of a 5.7 Liter V8 Automotive Diesel Engine," SAE Trans., Vol. 87, paper 78042.

Kamo, R. and W. Bryzik (1981), "Cummins—TARADCOM Adiabatic Turbocompound Engine Program," SAE paper 810070.

Kawamura, H., R. Kihara, and M. Kinbara (1982), "Isuzu's New 3.27 L Small Direct Injection Diesel," SAE paper 820032.

Leonard, T. R. and A. R. Johnson (1982), "Architecture of the New GM 4.3 Liter Diesel Engine Designed by Oldsmobile," SAE SP-510, paper 820117.

Postma, N. D., R. Van Giessel, and F. Reinink (1973), "The Stirling Engine for Passenger Car Application," SAE paper 730648.

Scussel, A. J., A. O. Simko, and W. R. Wade (1978), "The Ford PROCO Engine Update," SAE Trans., Vol. 87, paper 780699.

Walker, J. W. (1982), "The GM 1.8 Liter L-4 Gasoline Engine Designed by Chevrolet," SAE SP-510, p. 1, Paper 820111.

Wallace, T. F. (1978), "Buick's Turbocharged V-6 Powertrain for 1978," SAE Trans., Vol. 87, p. 1947, paper 780413.

Weertmar, W. L. and R. J. Lechner (1966), "Chrysler Corporation's New Hemi Head High Performance Engine," SAE Trans., Vol. 75, paper 660342.

1.9 HOMEWORK

1. With reference to Figure 1-3:
   a. Find the cylinder volume V at any crank angle θ. Present your result in the dimensionless form

$$\frac{V(\theta)}{V(0)} = \tilde{V}(\theta, r, \epsilon)$$

   where

$$r = \frac{V(\pi)}{V(0)} \text{ is the compression ratio}$$

$$\epsilon = \frac{S}{2l} \text{ is a geometric ratio}$$

   b. Expand the function $\tilde{V}$ in a Taylor Series to show that for small ϵ, $\tilde{V}$ is asymptotic to

$$\tilde{V}(\theta, r, \epsilon) \sim 1 + \frac{r-1}{2}(1 - \cos\theta) \qquad \epsilon \to 0$$

   c. Show that the piston speed is

$$U(\theta) = \frac{\omega S}{r-1}\frac{d\tilde{V}}{d\theta}$$

   or

$$\frac{U(\theta)}{\omega S} = \frac{\sin\theta}{2}\left[1 + \frac{\epsilon\cos\theta}{(1-\epsilon^2\sin^2\theta)^{1/2}}\right]$$

   [where ω is the engine frequency.]
2. If the energy content of gasoline is $a_c = 18{,}000$ Btu/lb, what is the maximum gross thermal efficiency at WOT of the Ford Engine in Fig. 1-6?
3. To illustrate the effect of combustion chamber geometry on swirl amplification consider an axisymmetric engine where at bottom dead center the

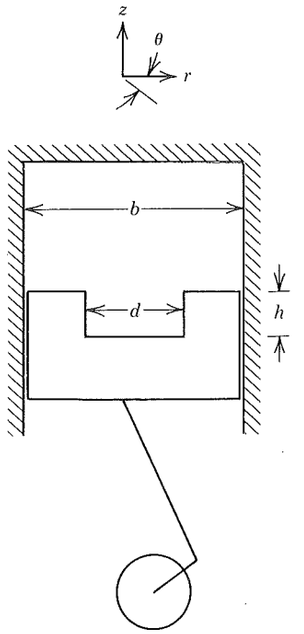

Figure 1-55 Illustration for Homework Problem 3.

velocity field of the air inside the cylinder is approximately

$$v_r = v_z = 0$$

$$v_\theta = V_o(2r/b)$$

The motion is said to be solid body since the gas is swirling as though it were a solid. If at top dead center the motion is also solid body and angular momentum is conserved during compression, what is the ratio of initial to final swirl (i.e., angular frequency) in terms of the compression ratio and/or the dimensionless lengths d/b, h/b?
(*Hint*: Evaluate the moment of inertia about the cylinder axis at top and bottom dead center.) Consider the case in which the volume at top dead center is entirely within the piston cup.

4. The velocity of air going into a swirl or prechamber may be computed from mass conservation assuming the density is spatially uniform. For example, consider the SEMT engine shown in Fig. 1-56. For a control volume containing both the prechamber and mainchamber we know that the mass is constant, that is,

$$\frac{dm}{dt} = 0 = \frac{d}{dt}\left[\rho(V_p + V_m)\right]$$

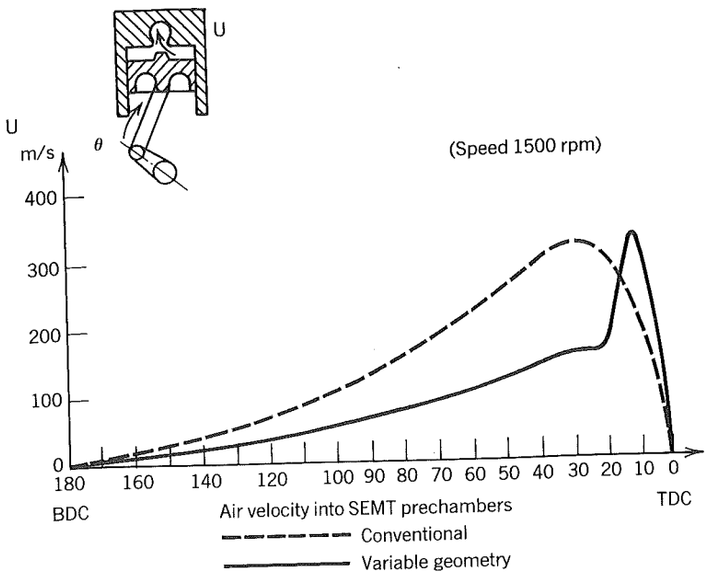

Figure 1-56 From (Herrmann, 1980). Reprinted with permission © 1980. ASME.

where

ρ = gas density

m = cylinder contents mass

V_p = prechamber volume

V_m = mainchamber volume

However the density is increasing with time because of the compression process. Hence neither $d\rho/dt$ nor dV_m/dt are zero and they must balance according to

$$(V_p + V_m)\frac{d\rho}{dt} + \rho\frac{dV_m}{dt} = 0$$

Denoting the mass of gas in the prechamber as $m_p = \rho V_p$, it follows that

$$\frac{dm_p}{dt} = V_p\frac{d\rho}{dt} = -\frac{\rho V_p}{V_p + V_m}\frac{dV_m}{dt}$$

The mass of gas in the prechamber increases with time as long as the density is increasing. The equation of continuity (mass conservation) applied to the prechamber leads to the conclusion that

$$\frac{dm_p}{dt} = \dot{m}_{\text{in}} = \rho UA$$

where U is the gas velocity in the connecting passage of cross-sectional area A. Finally, relating the rate of change of mainchamber volume to the instantaneous piston speed U_p, we have

$$U = U_p\frac{\frac{\pi}{4}b^2}{A}\frac{V_p}{V_p + V_m}$$

This illustrates clearly how the gas is accelerated because of a small throat of area A. That gas motion is used to mix the air and fuel together during ignition delay and the subsequent combustion. Our analysis neglects the combustion and thus establishes the flow into which the fuel will be injected. Here the flow is driven by the piston but later it will reverse itself and be driven by the combustion.

Results applied to the SEMT engine are given in the Fig. 1-56. Given that at bottom dead center

$$b = 200 \text{ mm} \qquad S = 210 \text{ mm}$$

$$\frac{V_p}{V_p + V_m} = 0.30 \qquad \epsilon = 0.25$$

$$R_s = 1500 \text{ rpm}$$

find the area A as a function of crank angle θ for both the conventional and variable geometry prechambers. Make a dimensionless plot of the variable area divided by conventional area versus crank angle.

5. Following are data from a fuel inducted 380 cc single cylinder two-stroke engine manufactured by Greeves Motorcycles for use in motor cross competition (reported by G. P. Blair and W. L. Cahoon, "A More Complete Analysis of Unsteady Flow through a High-Specific-Output Two-Cycle Engine," SAE Trans., Vol. 81, paper 720156)

For the MK1 at 5500 rpm (assume $\rho_\infty = 1.21$ kg/m^3) find:

a. The air flow rate, g/s

b. The fuel–air ratio (Hint: The bsfc and bmep are known.)

ENGINE TYPE	ENGINE SPEED (rpm)	BMEP (atm)	DELIVERY RATIO (%)	TRAPPING[a] EFFICIENCY (%)	BSFC (g/kW H)
MK1	5500	6.81	74.8	62.5	490
Peak bmep	7000	6.23	69.1	62.1	457
Peak $\mathbf{P}_b$	7500	5.55	60.6	60.0	507
MK2	5500	6.72	74.9	92.7	516
Peak bmep	6500	7.29	70.0	77.0	436
Peak $\mathbf{P}_b$	7000	6.83	68.0	71.1	426

[a] Estimated

The engine dimensions are given in Table 1-4.

Table 1-4 Engine Dimensions

ENGINE DETAILS	MK1	MK2
Bore, mm	82	82
Stroke, mm	72	72
Connecting-rod centers, mm	139.7	139.7
Geometric compression ratio	14	14
Trapped compression ratio	6.57	8.3
Crankcase compression ratio	1.6	1.6
Exhaust opens, deg atdc	96	96
Inlet opens, deg btdc	76	78
Transfer opens, deg atdc	115	111
Exhaust ports width, mm	58	58
Inlet port width, mm	46	58
Transfer port width, mm	64	62
Carburetor flow diameter, mm	32	34
Inlet pipe length, mm	178	178
Transfer pipe length, mm	100	100
Exhaust pipe lengths and diameters, mm (see figure)		
K1	432	406
K9	584	635
K2	813	787
K3	813	914
K4	1041	1117
K5	1422	1346
D1	49.5	44.7
D9	74.7	70.1
D2	92.1	101
D3	92.1	101
D4	41.3	28.6
D5	41.3	28.6

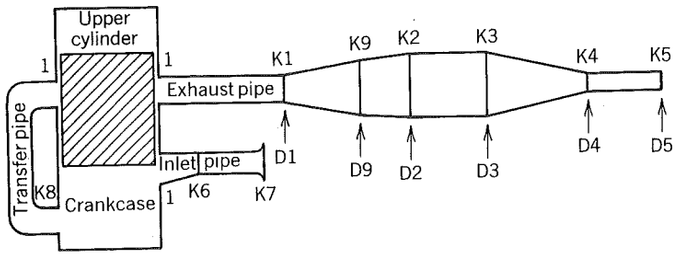

Mathematical model of two-cycle engine as used for development of THROUGHFLOW computer program.

6. Assuming that the mean effective pressure, mean piston speed, specific power, and mass per unit displacement volume are all size independent (i.e., universal constants) how will the power per unit weight of engines depend upon the number of cylinders employed at fixed total displacement volume? As this is an order of magnitude analysis, you may assume that the bore and stroke are equal.
7. Compute for the following engines the mean piston speed (m/s) and the specific power (W/cm^2).

ENGINE	BORE (in.)	STROKE (in.)	CYLINDERS	POWER/SPEED (hp/rpm)
AVCR 1360-2	5.375	5.000	12	1500/2600
Chrysler Hemi	4.250	3.750	8	600/6400
Cosworth DFX	3.373	2.256	8	700/10500

8. For the two-stroke engine in Fig. 1-39 compare the bmep (atm), the specific power (W/cm^2), the mean piston speed (m/s), and the engine mass per unit displacement volume (kg/l). Do the computations for an engine speed of 2100 rpm. Compare with values given in Table 1-3 for the other engines.
9. How much overlap does the GM engine in Table 1-1 have?
10. For the engines listed in problem 7, compute the bmep (bar) and the torque (N-m).
11. Suppose the volumetric efficiency of the AVCR diesel engine in problem 7 is 80% and the inlet manifold density is 50% greater than standard atmospheric density. What is the air flow rate (kg/min) if $R_s = 2600$ rpm?
12. In Table 1-2, changes in torque are assumed to be the result of changes in volumetric efficiency, a reasonable assumption. Show that if the bsfc, intake manifold gas density, and air to fuel ratio are independent of manifold changes, then torque is directly proportional to the volumetric efficiency.
13. Each throttle body fuel injector (there are two) in Fig. 1-15 serves three of the Ford's six cylinders. Each of the cylinders requires a fuel delivery once per four-stroke cycle. How many times is an injector opened in two engine revolutions? The mass of fuel injected is proportional to the duration the injector is actuated. How should the duration change with engine speed if the same mass of fuel is to be injected per cycle? How about the frequency of injector actuation?

Two

GAS CYCLES

A study of gas cycles as models of internal combustion engines is useful for qualitatively illustrating some of the important parameters influencing engine performance, that is, the engine's efficiency and work output. It also provides a review of thermodynamics. Gas-cycle calculations treat the combustion process as an equivalent heat transfer. The efficiency is then well defined in terms of that heat transfer.

Eventually we will model the combustion process using relationships that the student has been introduced to but probably has not applied to an analysis (showing how work can be produced by burning a fuel). The definition of efficiency in this case can be rigorously defined but the student may feel uncomfortable with the definition since it is rarely used in practice.

The gas cycle also serves to introduce many of the ideal processes to be used in these latter models, called fuel–air cycles. Then when we treat combustion more rigorously the student will already have been introduced to many of the ideal processes used in the fuel air cycles.

This chapter is broken into sections dealing with closed-system models and open-system models.

2.1 CONSTANT VOLUME HEAT ADDITION

This cycle is often referred to as the Otto cycle and models the special case of an internal combustion engine whose combustion is so rapid that the piston hardly moves during the event and thus combustion occurs at constant volume. The cycle for analysis is shown in Fig. 2-1. The four basic processes are:

1 to 2 isentropic compression
2 to 3 constant-volume heat addition
3 to 4 isentropic expansion
4 to 1 constant-volume heat rejection

The working fluid is an ideal gas and let us assume, to keep our mathematics simple, that it has constant specific heats. This assumption is acceptable since we will eventually dispense with gas cycles anyway.

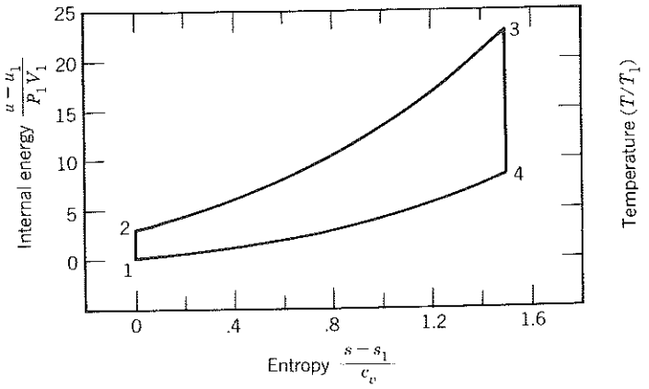

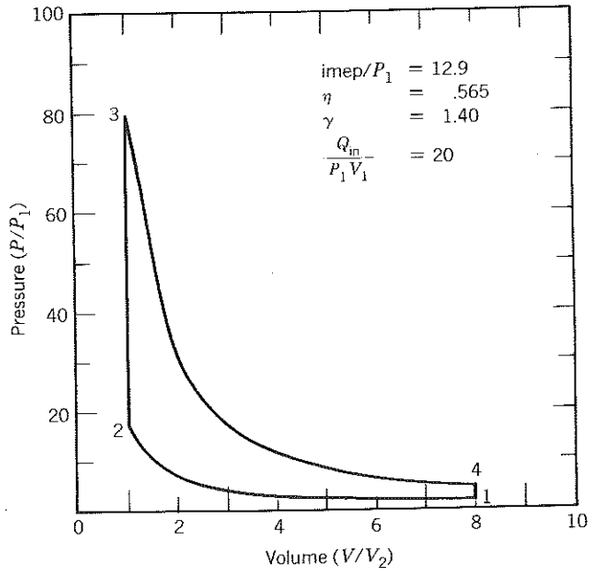

Figure 2-1 Otto cycle.

The student should be able to show that the following relationships are valid:

Heat addition

$$Q_{in} = mc_v(T_3 - T_2) \tag{2.1}$$

Heat rejection

$$Q_{out} = mc_v(T_4 - T_1) \tag{2.2}$$

Compression stroke

$$\frac{P_2}{P_1} = r^{\gamma} \qquad \frac{T_2}{T_1} = r^{\gamma-1} \tag{2.3}$$

Expansion stroke

$$\frac{P_4}{P_3} = \left(\frac{1}{r}\right)^{\gamma} \qquad \frac{T_4}{T_3} = \left(\frac{1}{r}\right)^{\gamma-1} \tag{2.4}$$

where

m = mass of gas in the cylinder

c_v = specific heat

r = compression ratio

γ = ratio of specific heats

The compression ratio of an engine is defined to be

$$r = V_1/V_2 \tag{2.5}$$

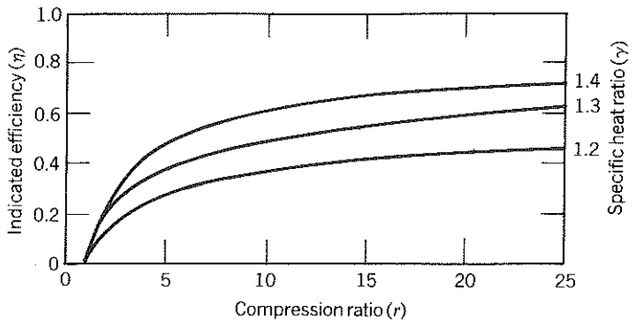

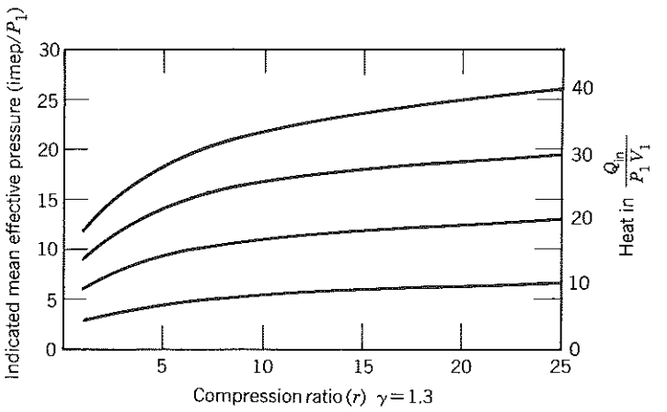

Figure 2-2 Otto cycle characteristics.

In this case the expansion ratio and compression ratio are equal so that

$$\frac{1}{r} = V_3/V_4 = V_2/V_1 \tag{2.6}$$

For a thermodynamic cycle such as this, the thermal efficiency is

$$\eta = \frac{W_{\text{out}}}{Q_{\text{in}}} = 1 - \frac{Q_{\text{out}}}{Q_{\text{in}}} \tag{2.7}$$

If we introduce the previously cited relations for Q_{in} and Q_{out}, we get

$$\eta = 1 - \frac{T_4 - T_1}{T_3 - T_2} = 1 - \frac{1}{r^{\gamma-1}} \tag{2.8}$$

The efficiency of the Otto cycle depends on the specific heat ratio and on the compression ratio. A plot of efficiency over the same range of compression ratios found in actual engines is shown in Fig. 2-2. The efficiencies we have computed are about twice as large as measured for actual engines. There are a number of reasons for this. We have not accounted for internal friction within the engine; actual engines burn a fuel and do not use heat transfer to increase the entropy of the charge; and we have ignored heat losses.

2.2 CONSTANT PRESSURE HEAT ADDITION

This cycle is often referred to as the Diesel cycle and models the special case of an internal combustion engine whose combustion is controlled so that the beginning of the expansion stroke occurs at constant pressure. The cycle for analysis is shown in Fig. 2-3. The four basic processes are:

1 to 2 isentropic compression
2 to 3 constant pressure heat addition
3 to 4 isentropic expansion
4 to 1 constant volume heat rejection

Again assuming constant specific heats, the student should recognize the following differences

Heat addition

$$Q_{\text{in}} = mc_p(T_3 - T_2) \tag{2.9}$$

Expansion stroke

$$\frac{P_4}{P_3} = \left(\frac{\beta}{r}\right)^{\gamma} \qquad \frac{T_4}{T_3} = \left(\frac{\beta}{r}\right)^{\gamma-1} \tag{2.10}$$

where we have defined the parameter β as

$$\beta = V_3/V_2 \tag{2.11}$$

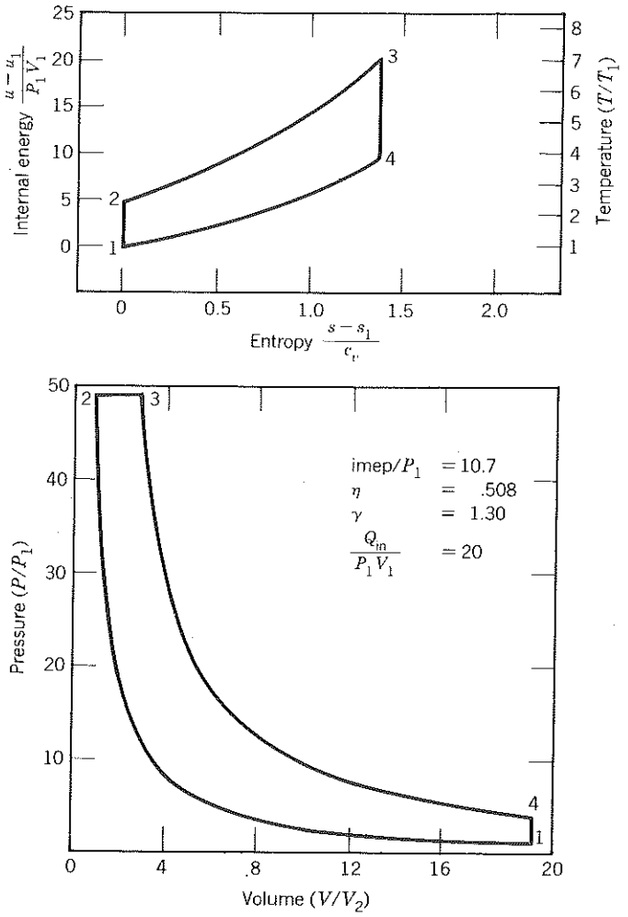

Figure 2-3 Diesel cycle.

In this case the indicated efficiency is

$$\eta = 1 - \frac{1}{r^{\gamma-1}} \frac{\beta^{\gamma} - 1}{\gamma(\beta - 1)} \tag{2.12}$$

Although Eq. (2.12) is correct, the utility suffers somewhat in that β is not a natural choice of independent variable. Rather, in engine operation, we think more in terms of the heat transferred in. The two are related according to Eq. (2.13).

$$\beta = 1 + \frac{\gamma - 1}{\gamma}\left(\frac{Q_{\text{in}}}{P_1V_1}\right)\frac{1}{r^{\gamma-1}} \tag{2.13}$$

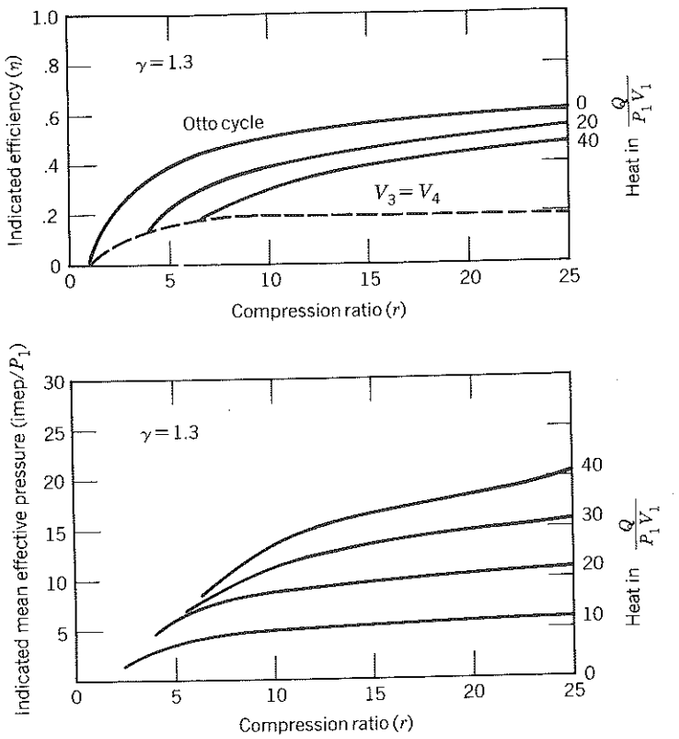

Figure 2-4 Diesel cycle characteristics.

Diesel cycle efficiencies are shown in Fig. 2-4. They illustrate that high compression ratios are desirable and that the efficiency decreases as the heat added increases.

2.3 DUAL CYCLE

Modern compression ignition engines resemble neither the constant-volume nor the constant-pressure cycle but rather an intermediate in which some of the heat is added at constant volume and then the remaining heat is added at constant pressure. The distribution of heat added in the two processes is something the designer can specify approximately by choice of fuel, fuel injection system, and engine geometry, usually to limit the peak pressure in the cycle. Consequently this cycle is also referred to as the limited-pressure cycle.

The cycle notation is illustrated in Fig. 2-5. In this case we have the following difference:

Heat addition

$$Q_{\text{in}} = mc_v(T_{2.5} - T_2) + mc_p(T_3 - T_{2.5}) \tag{2.14}$$

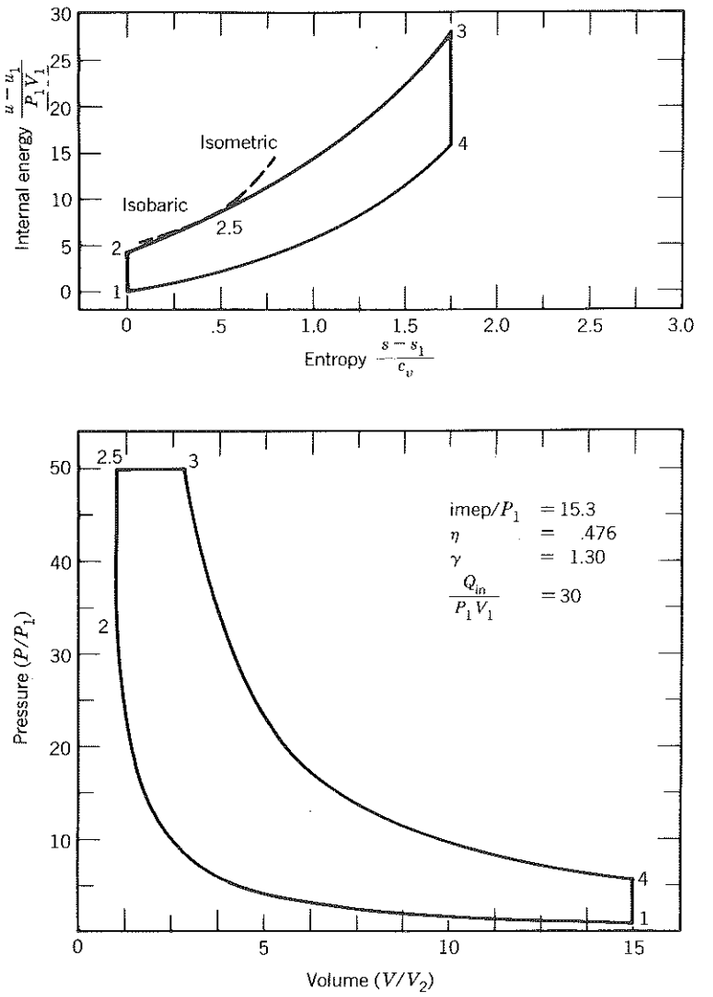

Figure 2-5 Dual cycle.

The expansion stroke is still described by Eq. (2.11) provided we write $\beta = V_3/V_{2.5}$. In terms of $\alpha = P_3/P_2$, it can be shown that

$$\eta = 1 - \left(\frac{1}{r}\right)^{\gamma-1}\left[\frac{\alpha\beta^{\gamma} - 1}{(\alpha - 1) + \gamma\alpha(\beta - 1)}\right] \tag{2.15}$$

The constant-volume and constant-pressure cycles can be considered as special cases of the Dual cycle in which $\beta = 1$ and $\alpha = 1$, respectively. Intermediate results are shown in Fig. 2-6. Transformation of β and α to more natural

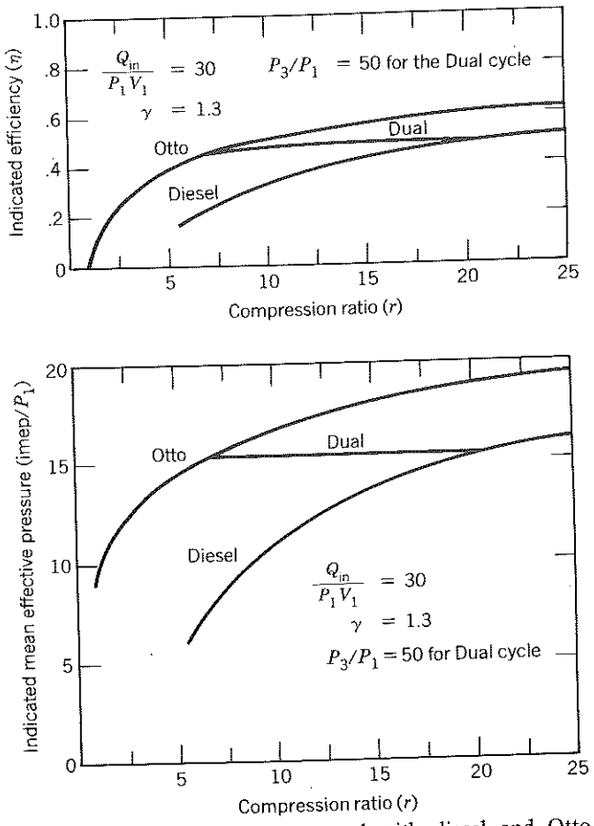

Figure 2-6 Dual cycle compared with diesel and Otto cycles.

variables yields

$$\beta = 1 + \frac{\gamma - 1}{\alpha\gamma}\left[\frac{Q_{in}}{P_1V_1}\frac{1}{r^{\gamma-1}} - \frac{\alpha - 1}{\gamma - 1}\right] \tag{2.16}$$

$$\alpha = \frac{1}{r^{\gamma}}\frac{P_3}{P_1} \tag{2.17}$$

2.4 DISCUSSION

The pressure–volume diagram of an engine is often called the indicator diagram. The area within the cycle is a good measure of the work done by the gas. Some of the work is dissipated by the friction of the moving parts so that the work delivered by the engine is reduced. It is possible to measure both the work done by the gas and the work delivered to the crankshaft. To distinguish

between the two, the following definitions are used:

Indicated work is work done by the gas.

Brake work is work done by the crankshaft.

The difference between the indicated work and the brake work is the work done against friction that is dissipated as heat, and the work required to pump the fluids in and out of the engine.

In theoretical cycles such as these air cycles or the fuel air cycles to be discussed later we are computing the indicated work and the indicated efficiency.

As far as thermodynamics is concerned, the efficiency and work per unit mass of gas are the parameters of primary interest. Expressing the work analogously as an intensive thermodynamic property is convenient because for many systems the analysis is then independent of size.

Such an approach would be satisfactory too, for internal combustion engines, if engine size scaled with the mass of air within the cylinders. As we shall learn later, the amount of mass within the cylinders is sometimes varied to control engine loads. It has thus been found convenient to compare engines of different sizes in terms of the work per unit displacement volume of an engine. The work so expressed is called the mean effective pressure because it has the units of pressure and because it can be though of as the constant pressure that if applied to the piston during the expansion stroke would yield the work of the cycle. The indicated mean-effective pressure according to any of the gas cycle models is

$$\frac{\text{imep}}{P_1} = \frac{Q_{in}}{P_1V_1}\frac{r}{r-1}\eta \tag{2.18}$$

Maximizing the mean effective pressure is important in engine design so that one can build a smaller, lighter engine to produce a given amount of work. (This may not be as important for stationary engines.) There are evidently two ways to do this: to increase the compression ratio and to increase the heat input. However there are practical limitations to these approaches. For spark-ignition engines of conventional design, the compression ratio must be low enough to avoid engine knock (the subject of Chapter 9); whereas for diesel engines increasing engine friction limits the utility of increasing compression ratio. Other more complicated factors influence the selection of compression ratio, especially constraints imposed by emission standards and, for some diesel engines, problems of startability.

One might expect that we increase Q_{in} by increasing the fuel flow rate delivered to an engine. As we shall see in our studies of fuel–air cycles, this is not always correct, for in fuel rich mixtures a lot of energy is not used because there is not enough oxygen to burn the carbon monoxide to carbon dioxide nor the hydrogen to water. The fuel–air cycle predicts that the efficiency decreases the richer the mixture is beyond stoichiometric.

The fuel–air cycle adequately models conventional spark-ignition engines but is not as useful for an engine as heterogeneous as a typical diesel engine.

Diesel engine fuel-flow rates are limited by the appearance of solid carbon in exhaust that did not burn to carbon monoxide or carbon dioxide. This occurs even though the engine is running lean and is not predicted by fuel–air cycles. A more sophisticated model is required. These exist but are beyond the scope of this text.

According to the gas cycles (and indeed to the fuel–air cycles later discussed), the efficiency is greatest if heat can be added at constant volume

$$\eta_{\text{otto}} > \eta_{\text{dual}} > \eta_{\text{diesel}} \tag{2.19}$$

Why then do we build engines that resemble constant pressure heat addition when we recognize that constant volume heat addition would be better? To illustrate how complicated that question is let us ask the following: Suppose that the maximum pressure in the cycle must be less than $P_{\max}$. How should the heat be added to produce the required work? The answer is now

$$\eta_{\text{diesel}} > \eta_{\text{dual}} > \eta_{\text{otto}} \tag{2.20}$$

The mathematics can be used to show this is true but it is easier to demonstrate in terms of a temperature entropy diagram. The Otto cycle 1–2–3–4 and the Diesel cycle 1–2–3–4 are drawn on such a diagram so that the work done in each cycle is the same. It can then be seen that the diesel is rejecting less heat and must therefore be the most efficient.

2.5 ARBITRARY HEAT RELEASE

All the previous cycles yielded results that could be expressed in closed form, that is, by an equation. Now we will study influences due to the relative timing of the heat addition. In this case the heat addition may be a prescribed function of crank angle. For example, for spark ignition engines it is found that the following works reasonably well

$$x = \frac{1}{2}\left\{1 - \cos\left[\frac{\pi(\theta - \theta_s)}{\theta_b}\right]\right\} \tag{2.21}$$

where x is the fraction of the heat release, θ refers to crank angle, θ_s is the start of heat release, and θ_b is its duration. Equation (2.21) is applied only during the time of heat release; $\theta_s < \theta < \theta_s + \theta_b$

Another function generally used is

$$x = 1 - \exp\left[-\left(\frac{\theta - \theta_s}{\theta_b}\right)^n\right] \tag{2.22}$$

In this case θ_b is the time scale for heat release but the duration is some multiple of θ_b. Equation (2.22) is applied until x is close enough to unity for practical purposes. (This is illustrated in the following example.)

For either of these functions, the parameters θ_s and θ_b as well as n are used to curve fit experimental data. They are not known a priori. The functions are useful for extrapolation from conditions with which one has experimented, using the same engine (the parameters are engine dependent).

In any case, assume that $x(\theta)$ can be prescribed. The equation of state for an ideal gas is

$$PV = mRT \tag{2.23}$$

Taking the logarithm of both sides and differentiating with respect to crank angle gives

$$\frac{1}{P}\frac{dP}{d\theta} + \frac{1}{V}\frac{dV}{d\theta} = \frac{1}{T}\frac{dT}{d\theta} \tag{2.24}$$

The first law of thermodynamics in differential form for an ideal gas with constant specific heat is

$$mc_v\frac{dT}{d\theta} = \frac{dQ}{d\theta} - P\frac{dV}{d\theta} \tag{2.25}$$

Dividing the left-hand side by mRT and the right-hand side by PV, and rearranging then yields

$$\frac{1}{T}\frac{dT}{d\theta} = (\gamma - 1)\left(\frac{1}{PV}\frac{dQ}{d\theta} - \frac{1}{V}\frac{dV}{d\theta}\right) \tag{2.26}$$

Combining Eq. (2.25) and (2.26) and introduction of $dQ = Q_{\text{in}}\,dx$ produces

$$\frac{dP}{d\theta} = -\gamma\frac{P}{V}\frac{dV}{d\theta} + (\gamma - 1)\frac{Q_{\text{in}}}{V}\frac{dx}{d\theta} \tag{2.27}$$

In practice, it is convenient to normalize the equation by letting

$$\tilde{P} = P/P_1 \qquad \tilde{V} = V/V_1 \qquad \tilde{Q} = Q_{\text{in}}/P_1V_1 \tag{2.28}$$

in which case we obtain

$$\frac{d\tilde{P}}{d\theta} = -\gamma\frac{\tilde{P}}{\tilde{V}}\frac{d\tilde{V}}{d\theta} + (\gamma - 1)\frac{\tilde{Q}}{\tilde{V}}\frac{dx}{d\theta} \tag{2.29}$$

The volume V and its derivative $dV/d\theta$ are known functions of the crank angle θ. Likewise by either prescription (2.21) or (2.22) the derivative $dx/d\theta$ can be evaluated. Therefore, given the specific heat ratio γ and the total heat transferred into the system $\tilde{Q}$, Eq. (2.29) is of the following form:

$$\frac{d\tilde{P}}{d\theta} = f(\theta, \tilde{P}) \tag{2.30}$$

which is a linear first-order differential equation and easily solved by numerical integration. Solution yields $\tilde{P}(\theta)$, which once determined allows computation of the work of the cycle, the indicated mean effective pressure, and the indicated efficiency.

EXAMPLE 2.1

Assume for a particular spark-ignition engine the following data:

$$r = 10 \qquad \gamma = 1.3 \qquad \tilde{Q} = 20$$

$$\tilde{V} = \left[1 + \frac{r-1}{2}(1 - \cos\theta)\right]/r$$

Given that Eq. (2.22) is applicable with

$$n = 4 \qquad \theta_b = 40° \qquad \theta_s = -40°$$

find the indicated efficiency and mean effective pressure. Compare the result with an equivalent Otto cycle. Draw a P–V diagram.

SOLUTION:

Although Eq. (2.30) can be integrated alone to generate $\tilde{P}(\theta)$ and then find the work, it is convenient to integrate for the work simultaneously. The differential equation for the work is

$$\frac{d\tilde{W}}{d\theta} = \frac{1}{P_1 V_1}\frac{dW}{d\theta} = \tilde{P}\frac{d\tilde{V}}{d\theta} \tag{2.31}$$

Equations (2.30) and (2.31) are a pair of linear first-order differential equations that can be simultaneously integrated. A convenient way to solve this problem is to use a "canned" subroutine. The following program employs the routine DVERK from the International Mathematical and Statistical Library (IMSL) which is available in most computing centers. For convenience, the instructions for using DVERK are given in Appendix A.

```
      EXTERNAL FCN
      DIMENSION Y(2), C(24), W(2,9)
      DATA N/2/, X/-180./, Y/1.0, 0.0/, XEND/-170./, TOL/.001/,
     &     IND/1/, NW/2/
      WRITE(6,10)
10    FORMAT(6X,'THETA',6X,'PRESSURE',6X,'WORK')
      WRITE(6,20) X, Y
20    FORMAT(3(2X,1PE11.4))
      DO 30 I = 1,36
      CALL DVERK(N, FCN, X, Y, XEND, TOL, IND, C, NW, W, IER)
      WRITE(6,20) XEND, Y
      X = XEND
30    XEND = X + 10.
      STOP
      END
C
      SUBROUTINE FCN(N, THETA, Y, YPRIME)
      REAL Y(N), YPRIME(N)
      DATA GAMMA/1.3/, Q/20.0/, PI/3.141593/, R/10.0/, THETAS/-40.0/,
     &     THETAB/40.0/, EN/4.0/
      V = (1.0 + (R - 1.0)/2.0*(1.0 - COS(THETA*PI/180.0)))/R
      DV = (R - 1.0)/2.*SIN(THETA*PI/180.)/R*PI/180.
      DX = 0.
      IF( THETA .LE. THETAS ) GO TO 10
      X = 1.0 - EXP(-((THETA - THETAS)/THETAB)**EN)
      DX = (1.0 - X)*EN*((THETA - THETAS)/THETAB)**(EN - 1.0)/THETAB
10    YPRIME(1) = - GAMMA*Y(1)*DV/V + (GAMMA - 1.0)*Q*DX/V
      YPRIME(2) = Y(1)*DV
      RETURN
      END
```


The output from running this program is given below

THETA	PRESSURE	WORK
-1.8000e+02	1.0000e+00	0.0000e+00
-1.7000e+02	1.0090e+00	-6.8670e-03
-1.6000e+02	1.0364e+00	-2.7627e-02
-1.5000e+02	1.0842e+00	-6.2766e-02
-1.4000e+02	1.1556e+00	-1.1312e-01
-1.3000e+02	1.2559e+00	-1.7993e-01
-1.2000e+02	1.3929e+00	-2.6489e-01
-1.1000e+02	1.5784e+00	-3.7026e-01
-1.0000e+02	1.8303e+00	-4.9898e-01
-9.0000e+01	2.1753e+00	-6.5480e-01
-8.0000e+01	2.6549e+00	-8.4242e-01
-7.0000e+01	3.3332e+00	-1.0676e+00
-6.0000e+01	4.3107e+00	-1.3366e+00
-5.0000e+01	5.7401e+00	-1.6557e+00
-4.0000e+01	7.8334e+00	-2.0268e+00
-3.0000e+01	1.0953e+01	-2.4409e+00
-2.0000e+01	1.7543e+01	-2.8894e+00
-1.0000e+01	3.4065e+01	-3.3732e+00
0.0000e+00	5.8915e+01	-3.6625e+00
1.0000e+01	6.9609e+01	-3.1967e+00
2.0000e+01	5.9193e+01	-1.8788e+00
3.0000e+01	4.4020e+01	-1.8789e-01
4.0000e+01	3.1915e+01	1.4946e+00
5.0000e+01	2.3387e+01	3.0067e+00
6.0000e+01	1.7563e+01	4.3065e+00
7.0000e+01	1.3581e+01	5.4028e+00
8.0000e+01	1.0817e+01	6.3201e+00
9.0000e+01	8.8630e+00	7.0845e+00
1.0000e+02	7.4572e+00	7.7194e+00
1.1000e+02	6.4310e+00	8.2438e+00
1.2000e+02	5.6749e+00	8.6731e+00
1.3000e+02	5.1167e+00	9.0193e+00
1.4000e+02	4.7082e+00	9.2915e+00
1.5000e+02	4.4173e+00	9.4966e+00
1.6000e+02	4.2227e+00	9.6398e+00
1.7000e+02	4.1108e+00	9.7244e+00
1.8000e+02	4.0743e+00	9.7524e+00

The pressure volume diagram is compared with an equivalent Otto cycle in Fig. 2.7.

Note the large difference between peak pressures. This difference is characteristic of actual cycles. Notice too that the exhaust temperature (at point 4) is larger than in the Otto cycle, hence more heat is rejected and the cycle is less efficient. This is not characteristic of actual cycles because heat loss during the expansion stroke drops point 4 further. However, a larger exhaust temperature is a qualitative indicator of engine inefficiency.

The efficiency is computed directly from its definition

$$\eta = \frac{\tilde{W}}{\tilde{Q}} = \frac{9.7524}{20} = 0.488$$

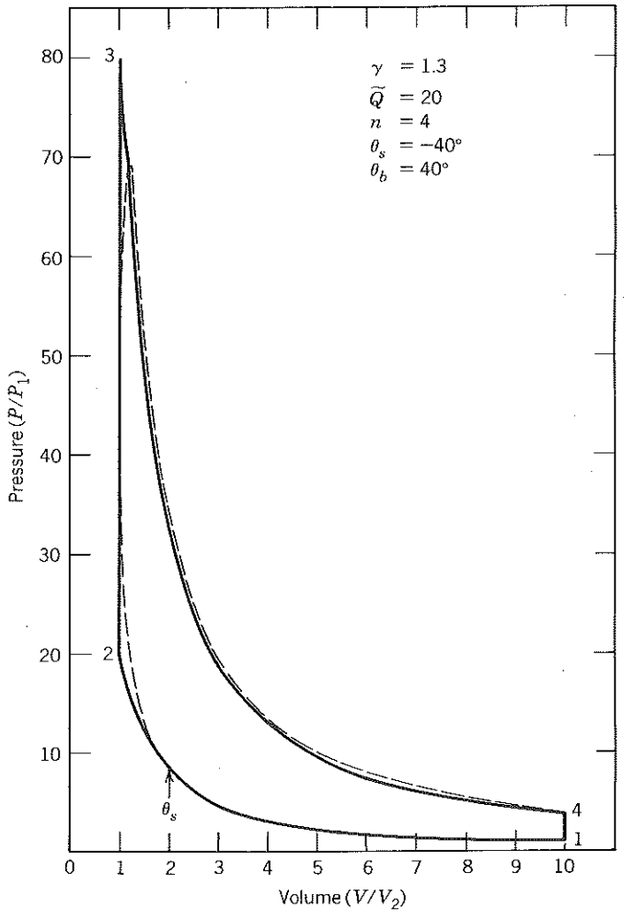

Figure 2-7 Pressure–volume diagram of Example 2.1. The dashed line is the result obtained for an arbitrary heat release; the solid line is the equivalent Otto cycle.

The imep is then computed using Eq. (2.18)

$$\frac{\text{imep}}{P_1} = \eta \tilde{Q} \frac{r}{r-1} = 10.8$$

The equivalent Otto cycle efficiency is $\eta_{\text{otto}} = 0.499$, hence

$$\frac{\eta}{\eta_{\text{otto}}} = \frac{\eta}{1-\left(\frac{1}{r}\right)^{\gamma-1}} = 0.978$$

Inclusion of heat loss during expansion into the analysis would lower that ratio to about 0.9.

It is important that the reader understand the methodology by which the solution was achieved. This is just one of many examples to follow wherein a set of first-order ordinary differential equations is solved to model an engine process.

In the present case, with reference to Appendix A, note the following:

- In order to tabulate the pressure and the work as a function of crank angle every 10 deg, the integration was put into a do loop. Integration was then done in 10-deg chunks.
- Initial conditions are specified in a data statement in the main program.
- The units of the derivatives are (crank angle) deg^{-1}, hence we need the factor $\pi/180$ at the end of the expression for DV $(= d\tilde{V}/d\theta)$.

The results of some numerical computations for efficiency as functions of heat release parameters are shown in Fig. 2-8. They illustrate the importance of establishing the correct timing for the start of heat release. They also show that the efficiency at the optimum timing is a rather weak function of the duration and very nearly equal to that of the Otto cycle. As we shall see later, this is also true of actual spark-ignition engines; the efficiency at optimum spark timing is very nearly equal to that of the constant volume fuel–air cycle.

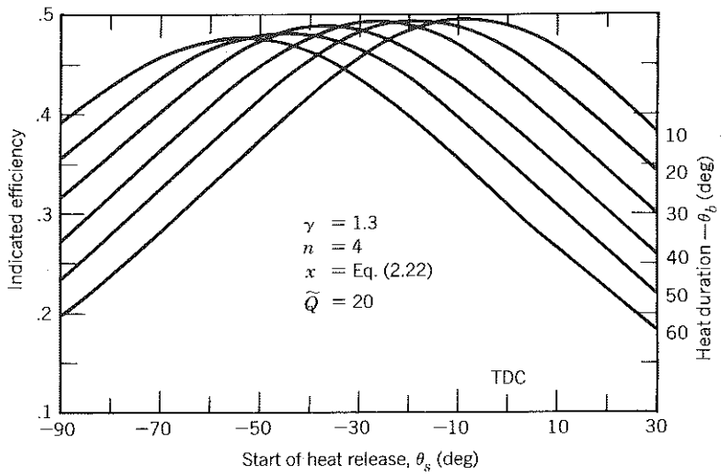

Figure 2-8 The influence of timing and duration of heat release on efficiency.

2.6 HEAT LOSS

Equation (2.26) is valid whether or not dQ is interpreted as the heat addition due to combustion or the heat lost by the gases in the cylinder because of convection. To admit both possibilities write

$$dQ = Q_{\text{in}}\,dx - dQ_l \tag{2.32}$$

where dQ_l is the heat loss. From the definition of the heat transfer coefficient, the heat loss is

$$\frac{dQ_l}{dt} = \mathbf{h}A(T - T_w) \tag{2.33}$$

where

$\mathbf{h}$ = heat transfer coefficient (not to be confused with enthalpy)

A = surface area in contact with the gases

T_w = wall temperature

When dimensionless variables are introduced

$$\tilde{Q} = \frac{Q_{\text{in}}}{P_1V_1} \qquad \tilde{T} = \frac{T}{T_1} \qquad \tilde{Q}_l = \frac{Q_l}{P_1V_1}$$

$$\tilde{\mathbf{h}} = \frac{\mathbf{h}T_1(A_o - 4V_o/b)}{P_1V_1\omega} \qquad \beta = \frac{4V_1}{b(A_o - 4V_o/b)}$$

and A_o is the area of the combustion chamber in contact with the gases at top center, the dimensionless heat loss is then

$$\frac{d\tilde{Q}_l}{d\theta} = \tilde{\mathbf{h}}(1 + \beta\tilde{V})(\tilde{P}\tilde{V} - \tilde{T}_w) \tag{2.34}$$

and substitution into Eq. (2.26) yields

$$\frac{d\tilde{P}}{d\theta} = -\gamma\frac{\tilde{P}}{\tilde{V}}\frac{d\tilde{V}}{d\theta} + \frac{(\gamma - 1)}{\tilde{V}}\left[\tilde{Q}\frac{dx}{d\theta} - \tilde{\mathbf{h}}(1 + \beta\tilde{V})(\tilde{P}\tilde{V} - \tilde{T}_w)\right] \tag{2.35}$$

Note that the efficiency of an adiabatic engine depends on the compression ratio, the stroke to rod length, the dimensionless heat added during the combustion, and the parameters of the burn law. When heat losses are admitted there is an additional dependence on the dimensionless wall temperature, heat transfer coefficient, and surface area of the combustion chamber.

EXAMPLE 2.2

For the same engine as in Example 2.1, find the efficiency when heat loss is accounted for. In this case assume

$$\tilde{\mathbf{h}} = 0.20 \qquad \beta = 1.5 \qquad \tilde{T}_w = 1.2$$

SOLUTION:

Integrate Eq. (2.31), (2.34), and (2.35) simultaneously using the routine DVERK introduced earlier.

```
      EXTERNAL FCN
      DIMENSION Y(3), C(24), W(3,9)
      DATA N/3/, X/-180./, Y/1.0, 2*0.0/, XEND/-170./, TOL/.001/,
     &     IND/1/, NW/3/
      WRITE(6,10)
10    FORMAT(6X,'THETA',6X,'PRESSURE',6X,'WORK',8X,'HEAT LOSS')
      WRITE(6,20) X, Y
20    FORMAT(4(2X,1PE11.4))
      DO 30 I = 1,36
      CALL DVERK(N, FCN, X, Y, XEND, TOL, IND, C, NW, W, IER)
      WRITE(6,20) XEND, Y
      X = XEND
30    XEND = X + 10.
      STOP
      END
C
      SUBROUTINE FCN(N, THETA, Y, YPRIME)
      REAL Y(N), YPRIME(N)
      DATA GAMMA/1.3/, Q/20.0/, PI/3.141593/, R/10.0/, THETAS/-40.0/,
     &     THETAB/40.0/, EN/4.0/, H/0.2/, BETA/1.5/, TW/1.2/
      V = (1.0 + (R - 1.0)/2.0*(1.0 - COS(THETA*PI/180.0)))/R
      DV = (R - 1.0)/2.*SIN(THETA*PI/180.)/R*PI/180.
      DX = 0.
      IF( THETA .LE. THETAS ) GO TO 10
      X = 1.0 - EXP(-((THETA - THETAS)/THETAB)**EN)
      DX = (1.0 - X)*EN*((THETA - THETAS)/THETAB)**(EN - 1.0)/THETAB
10    YPRIME(1) = - GAMMA*Y(1)*DV/V + (GAMMA - 1.0)/V*(Q*DX
     &          - H*(1.0 + BETA*V)*(Y(1)*V - TW)*PI/180.)
      YPRIME(2) = Y(1)*DV
      YPRIME(3) = H*(1.0 + BETA*V)*(Y(1)*V - TW)*PI/180.
      RETURN
      END
```

The output obtained follows and the heat loss is plotted in Fig. 2-9.

THETA	PRESSURE	WORK	HEAT LOSS
-1.8000e+02	1.0000e+00	0.0000e+00	0.0000e+00
-1.7000e+02	1.0141e+00	-6.8907e-03	-1.7144e-02
-1.6000e+02	1.0468e+00	-2.7814e-02	-3.3356e-02
-1.5000e+02	1.0998e+00	-6.3388e-02	-4.8189e-02
-1.4000e+02	1.1766e+00	-1.1457e-01	-6.1242e-02
-1.3000e+02	1.2826e+00	-1.8271e-01	-7.2157e-02
-1.2000e+02	1.4259e+00	-2.6959e-01	-8.0632e-02
-1.1000e+02	1.6184e+00	-3.7756e-01	-8.6414e-02
-1.0000e+02	1.8780e+00	-5.0959e-01	-8.9298e-02
-9.0000e+01	2.2320e+00	-6.6948e-01	-8.9121e-02
-8.0000e+01	2.7218e+00	-8.6192e-01	-8.5740e-02
-7.0000e+01	3.4120e+00	-1.0926e+00	-7.9025e-02
-6.0000e+01	4.4029e+00	-1.3677e+00	-6.8830e-02
-5.0000e+01	5.8464e+00	-1.6931e+00	-5.4975e-02
-4.0000e+01	7.9516e+00	-2.0705e+00	-3.7247e-02
-3.0000e+01	1.1074e+01	-2.4900e+00	-1.5241e-02

-2.0000e+01	1.7627e+01	-2.9421e+00	1.6766e-02
-1.0000e+01	3.3979e+01	-3.4265e+00	8.3843e-02
0.0000e+00	5.8394e+01	-3.7144e+00	2.2536e-01
1.0000e+01	6.8516e+01	-3.2547e+00	4.4716e-01
2.0000e+01	5.7736e+01	-1.9636e+00	7.0204e-01
3.0000e+01	4.2492e+01	-3.2294e-01	9.5146e-01
4.0000e+01	3.0474e+01	1.2925e+00	1.1881e+00
5.0000e+01	2.2080e+01	2.7284e+00	1.4140e+00
6.0000e+01	1.6387e+01	3.9487e+00	1.6316e+00
7.0000e+01	1.2516e+01	4.9655e+00	1.8431e+00
8.0000e+01	9.8404e+00	5.8056e+00	2.0502e+00
9.0000e+01	7.9543e+00	6.4965e+00	2.2539e+00
1.0000e+02	6.5986e+00	7.0624e+00	2.4548e+00
1.1000e+02	5.6074e+00	7.5232e+00	2.6532e+00
1.2000e+02	4.8733e+00	7.8948e+00	2.8491e+00
1.3000e+02	4.3257e+00	8.1899e+00	3.0422e+00
1.4000e+02	3.9173e+00	8.4182e+00	3.2322e+00
1.5000e+02	3.6160e+00	8.5876e+00	3.4189e+00
1.6000e+02	3.4005e+00	8.7039e+00	3.6019e+00
1.7000e+02	3.2566e+00	8.7716e+00	3.7808e+00
1.8000e+02	3.1753e+00	8.7936e+00	3.9554e+00

As before

$$\eta = \frac{\tilde{W}}{\tilde{Q}} = \frac{8.7936}{20} = 0.440$$

$$\frac{\text{imep}}{P_1} = \eta\tilde{Q}\frac{r}{r-1} = 9.77$$

$$\frac{\eta}{\eta_{\text{otto}}} = \frac{\eta}{1-\left(\frac{1}{r}\right)^{\gamma-1}} = 0.881$$

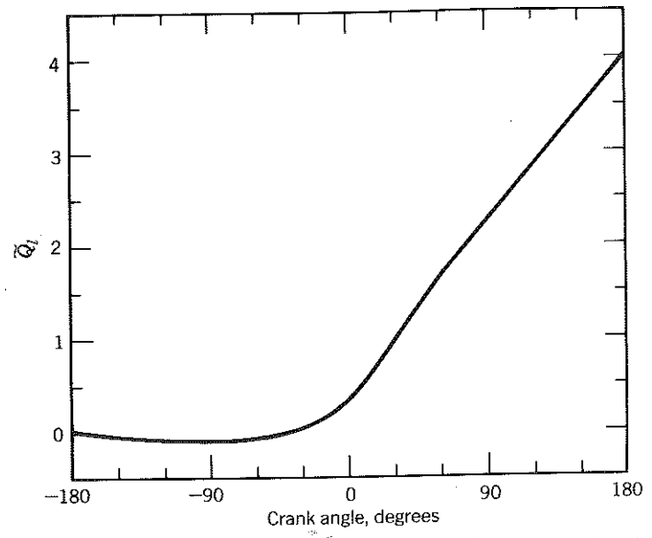

Figure 2-9 Heat loss in Example 2.2. Notice that compression is nearly isentropic.

Accounting for blowby will lower the ratio of η/η_{otto} to about 0.87. Notice that the heat loss is about 20% of the input energy,

$$\frac{\tilde{Q}_l}{\tilde{Q}} = \frac{3.9554}{20} = 0.198$$

With respect to the program, note the following changes:

- N = 3 and W is dimensioned (3, 9).
- Three initials conditions for Y are now specified in the main program data statement.
- YPRIME (1) is given by Eq. 2.35.
- YPRIME (3) is given by Eq. 2.34.

Internal combustion engines do not operate on closed thermodynamic cycles—rather, there is an induction of fresh charge and expulsion of combustion products. Furthermore, there is leakage of charge past the rings. In the next sections, simple models of the intake, exhaust, and leakage process will be presented.

2.7 MASS LOSS (BLOWBY)

Consider an engine in which when the valves are shut, mass is transferred from the cylinder to the crankcase. As the mass in the cylinder is no longer constant, Eq. (2.24) is no longer valid. Rather we must write

$$\frac{1}{P}\frac{dP}{d\theta} + \frac{1}{V}\frac{dV}{d\theta} = \frac{1}{m}\frac{dm}{d\theta} + \frac{1}{T}\frac{dT}{d\theta} \tag{2.36}$$

Similarly, the first law of thermodynamics in differential form applicable to an open system must be used.

$$mc_v\frac{dT}{d\theta} + c_vT\frac{dm}{d\theta} = \frac{dQ}{d\theta} - P\frac{dV}{d\theta} - \frac{\dot{m}_l c_p T}{\omega} \tag{2.37}$$

Where $\dot{m}_l$ is the instantaneous leakage or blowby rate and is assumed to be always out of the cylinder and taking with it gas characterized by the enthalpy of the cylinder contents, that is, c_pT.

Eliminating $dT/d\theta$ between Eq. (2.36) and (2.37) yields the following

$$\frac{dP}{d\theta} = -\gamma\frac{P}{V}\frac{dV}{d\theta} + \frac{(\gamma-1)}{V}\frac{dQ}{d\theta} - \frac{\gamma\dot{m}_l}{\omega m} \tag{2.38}$$

Elimination of $dm/d\theta$ requires use of the equation of continuity for mass conservation

$$\frac{dm}{d\theta} = -\frac{\dot{m}_l}{\omega} \tag{2.39}$$

Introducing $C = \dot{m}_l/m$, analyzing as before, and employing Eq. (2.32) finally

gives

$$\frac{d\tilde{P}}{d\theta} = -\gamma\frac{\tilde{P}}{\tilde{V}}\frac{d\tilde{V}}{d\theta} + \frac{(\gamma-1)}{\tilde{V}}\left[\tilde{Q}\frac{dx}{d\theta} - \tilde{\mathbf{h}}(1+\beta\tilde{V})(\tilde{P}\tilde{V}/\tilde{m} - \tilde{T}_w)\right] - \frac{\gamma C\tilde{P}}{\omega} \tag{2.40}$$

$$\frac{d\tilde{W}}{d\theta} = \tilde{P}\frac{d\tilde{V}}{d\theta} \tag{2.41}$$

$$\frac{d\tilde{Q}_l}{d\theta} = \tilde{\mathbf{h}}(1+\beta\tilde{V})(\tilde{P}\tilde{V}/\tilde{m} - \tilde{T}_w) \tag{2.42}$$

$$\frac{d\tilde{m}}{d\theta} = -\frac{C\tilde{m}}{\omega} \tag{2.43}$$

Equations (2.40) through (2.43) represent a set of four ordinary differential equations that can be solved simultaneously provided the parameter C can be specified. Specification of C is discussed in Chapter 8, here it will be assumed to be a constant.

EXAMPLE 2.3

Repeat Example 2.2 accounting for blowby and the associated enthalpy leakage from the cylinder. Assume the following additional data:

$$C = 0.8/s \qquad \omega = 200/s$$

SOLUTION:

Numerical integration is left as a student exercise (Homework problem 12) since by now he or she should be able to follow the lead of previous examples and use DVERK.

At the end of expansion, results obtained are

$$\tilde{P} = 3.0947 \qquad \tilde{Q}_l = 3.9767$$

$$\tilde{W} = 8.6989 \qquad \tilde{m} = 0.9752$$

Hence

$$\eta = 0.435 \qquad \frac{\tilde{Q}_l}{\tilde{Q}} = 0.199$$

$$\frac{\text{imep}}{P_1} = 9.67 \qquad \tilde{m}_l = 0.025$$

$$\frac{\eta}{\eta_{\text{otto}}} = 0.872$$

Note that the constant C is expected to be a strong function of ring design and vary considerably from engine to engine because of normal tolerancing practice. The value chosen was selected to model an engine in good condition, built to the normal dimensions; 2.5% of the charge was lost.

Also note that it is possible to integrate Eq. (2.43) analytically. One obtains

$$\tilde{m} = \exp\left[\frac{-C(\theta+\pi)}{\omega}\right]$$

Hence for $\theta = \pi$, $\tilde{m} = 0.9752$, which agrees with the numerical answer to all significant figures shown. Comparing a numerical answer with an analytic answer is a good way to check a numerical integration procedure.

2.8 IDEAL FOUR-STROKE PROCESS

The exhaust valve is supposed to open at bottom dead center and close at top dead center. The intake valve opens at the top dead center of exhaust valve closing and remains open until bottom dead center of the compression stroke. The intake and exhaust valve overlap, that is, the time during which they are open simultaneously, is assumed to be zero.

Referring to Fig. 2.10, the ideal processes are all adiabatic and are as follows:

4 to 5a	constant cylinder volume blowdown
5a to 6	constant pressure exhaustion
6 to 7	constant cylinder volume reversion
7 to 1	constant pressure induction

At the end of the expansion stroke 3 to 4, the pressure in the cylinder is larger than the exhaust pressure. Hence when the exhaust valve opens, the gases will flow out of the cylinder even if the piston does not move. Typically the pressure ratio P_4/P_e is such that sonic flow occurs at the valve so that blowdown is very quick and the constant volume approximation is justified.

Notice that no work is done on the piston during blowdown and that during the constant pressure exhaustion, work is required to expel the gas

$$W_{5a-6} = \int_{5a}^{6} P\,dV = -P_e V_d \tag{2.44}$$

A first-law analysis applied to the control mass defined in Fig. 2-11 during 5 to 6 leads to

$$\Delta H = 0 \tag{2.45}$$

since the pressure is constant. For ideal gases the enthalpy depends only on temperature, so the process is also isothermal and incompressible. Hence the fraction of the control mass still within the engine (called the residual fraction) is

$$f = \frac{V_6/v_6}{V_4/v_4} = \frac{1}{r}\frac{v_4}{v_6} = \frac{1}{r}\frac{T_4}{T_e}\frac{P_e}{P_4} \tag{2.46}$$

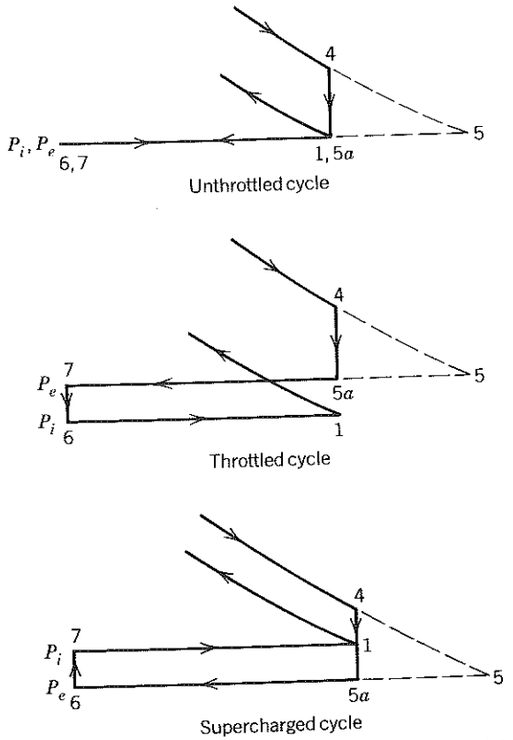

Figure 2-10 Four-stroke inlet and exhaust model. P_i = inlet pressure, P_e = exhaust pressure.

The intake stroke is better analyzed in terms of the cylinder as a control volume. The unsteady first law of thermodynamics is to be applied.

$$\left(\frac{dE}{dt}\right)_{\text{c.v.}} = \dot{Q} - \dot{W}_{\text{c.v.}} + \dot{m}_{\text{in}} h_{\text{in}} - \dot{m}_{\text{out}} h_{\text{out}} \tag{2.47}$$

Let

t_6 = time at beginning of intake

t_1 = time at the end of intake

Integrating the energy equation for an adiabatic process yields

$$E_1 - E_6 = -\int_6^1 P\,dV + \int_6^1 (\dot{m}_{\text{in}} h_{\text{in}} - \dot{m}_{\text{out}} h_{\text{out}})\,dt \tag{2.48}$$

To generate specific results we need to distinguish three cases dependent upon the ratio of inlet to exhaust pressure.

If the inlet pressure is less than the exhaust pressure, the engine is said to be throttled. In this ideal case there is flow from the cylinder into the intake

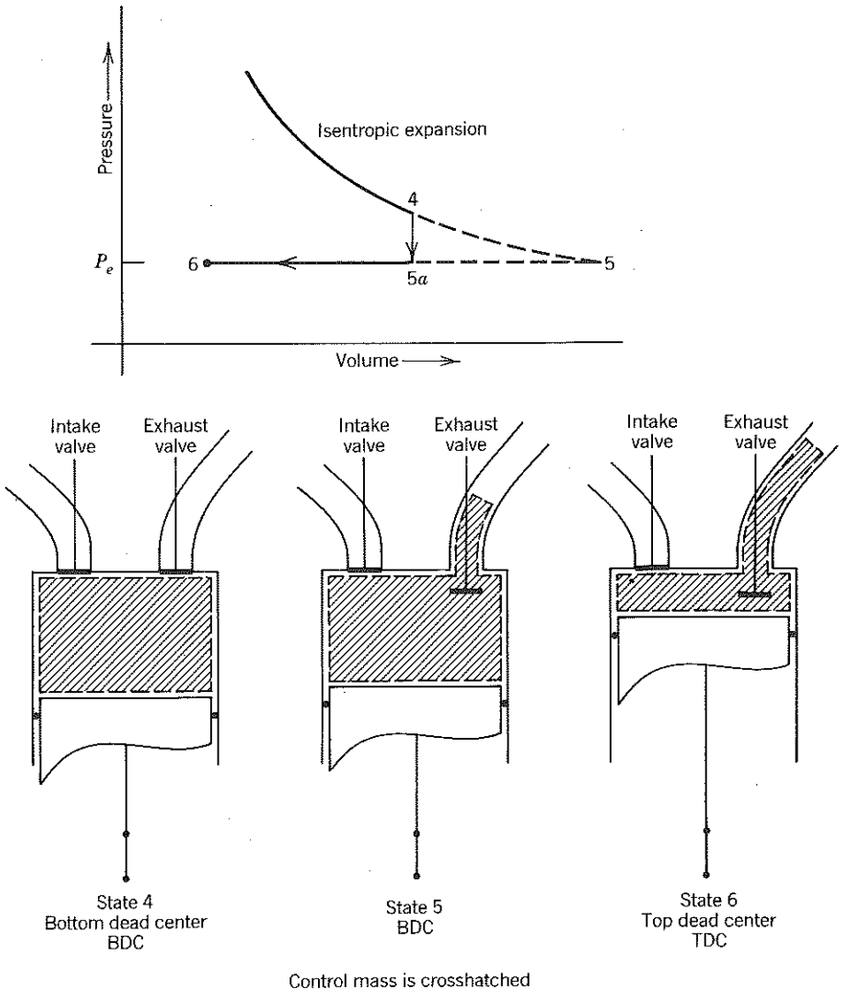

Figure 2-11 Exhaust stroke (4 to 5 to 6) illustrating residual mass. Note that while the blowdown is assumed to occur at constant cylinder volume, the control mass is assumed to expand isentropically.

pipe during the period of constant volume reversion. After the cylinder pressure and inlet pressure equilibrate, the piston moves down and draws mixture into the cylinder. In the initial portion of the stroke, it is inducting mostly combustion products that had flowed into the inlet pipe during reversion. In the latter portion of the stroke, the mixture flowing in is fresh charge, undiluted by any combustion products.

It follows that

$$E_1 - E_6 = P_i(V_6 - V_1) + m_i h_i \tag{2.49}$$

where

m_i = mass of fresh charge inducted

h_i = enthalpy of fresh charge

Algebraic manipulation to find T_1 is as follows:

$$H_1 - H_6 = (P_i - P_e)V_6 + m_i h_i \tag{2.50}$$

$$T_1 = (1-f)T_i + fT_e\left[1 - \left(1 - \frac{P_i}{P_e}\right)\left(\frac{\gamma - 1}{\gamma}\right)\right] \tag{2.51}$$

The volumetric efficiency is given by

$$e_v = \frac{m_i}{\rho_i V_d} = 1 - \frac{P_e/P_i - 1}{\gamma(r-1)} \tag{2.52}$$

If the inlet pressure is greater than the exhaust pressure, the engine is said to be supercharged (turbocharging is a special case of supercharging in which a compressor driven by an exhaust turbine raises the pressure of atmospheric air delivered to an engine). In this case during reversion there is flow from the intake pipe into the engine until the pressure equilibrates. In actual engines, because of valve overlap, there may be a flow of fresh mixture from the inlet to the exhaust pipe, which can waste fuel and be a source of hydrocarbon exhaust emissions. The analyses that we have done are still valid and Eq. (2.48) through (2.52) may be applied.

The last case to be considered is when inlet and exhaust pressures are equal; the engine is then said to be unthrottled. Again, Eq. (2.48) through (2.52) are applicable.

During the intake process work is done by the gas within the control volume since the piston is expanding the cylinder volume. During exhaust, work is done on the gas. The net effect during the intake and exhaust strokes is

$$W_{5a\text{ to }1} = (P_i - P_e)V_d \tag{2.53}$$

The negative of that work is called pumping work since it is a loss of useful work for the throttled engine. The pumping mean effective pressure defined as the pumping work per unit displacement volume is then

$$\text{pmep} = P_e - P_i \tag{2.54}$$

The indicated mean effective pressure is defined as the work per unit displacement volume done by the gas during the compression and expansion stroke. Some people like to define it as the work done by the control volume for the whole cycle, that is, including pumping. We shall call the work of the whole cycle the net indicated mean effective pressure. The following relations should be clear:

$$(\text{imep})_{\text{net}} = \text{imep} - \text{pmep} \tag{2.55}$$

$$\eta_{\text{net}} = \eta(1 - \text{pmep}/\text{imep}) \tag{2.56}$$

Finally, prior to doing a computation, the reader should be careful to distinguish the mass in quantities that are mass intensive. To illustrate, consider that in engine design the delivered-fuel-to-inducted-air ratio is specified. In a gas cycle it is analogous to specifying the heat added per unit mass of gas inducted, q. Hence the heat added is

$$Q_{\text{in}} = mq(1-f) \tag{2.57}$$

Now suppose that we compute the work done during compression as

$$w_{1\text{ to }2} = c_v(T_1 - T_2) \tag{2.58}$$

In our system of units the work is expressed as J/g. Confusion can arise as to whether that is per gram of gas in the cylinder (it is!) or per gram of gas inducted. The reader is advised to beware because here and in the literature the meaning is implicit in the context in which the symbol in question appears.

EXAMPLE 2.4

Compute cycle temperatures and pressures, the net efficiency, and the net mean effective pressure of an engine that operates on the ideal Otto cycle with ideal four-stroke intake and exhaust whose specifications are

$r = 10$	$\gamma = 1.25$	$T_i = 300$ K
$P_e = 1$ atm	$P_i/P_e = 0.50$	$q = 600$ cal/g
$M = 29$		

SOLUTION:

First let us calculate the gas constant and specific heat

$$R = \frac{1.987 \text{ cal/mole K}}{29 \text{ g/mole}} = 0.06852 \frac{\text{cal}}{\text{g K}}$$

$$c_v = \frac{R}{\gamma - 1} = \frac{0.06852}{0.25} = 0.2741 \frac{\text{cal}}{\text{g K}}$$

To begin our computation let us assume, based on our experience with engines, that

$$f = 0.05 \qquad T_e = 1000 \text{ K}$$

The temperature at the start of the compression is given by Eq. 2.51

$$T_1 = (1-f)T_i + fT_e\left[1 - \left(1 - \frac{P_i}{P_e}\right)\frac{\gamma - 1}{\gamma}\right] = 330 \text{ K}$$

The pressure is equal to the inlet pressure

$$P_1 = 0.5 \text{ atm}$$

The gases are then isentropically compressed

$$P_2 = P_1 r^{\gamma} = 8.89 \text{ atm}$$

$$T_2 = T_1 r^{\gamma-1} = 587 \text{ K}$$

Heat is now added at constant volume

$$T_3 = T_2 + \frac{(1-f)q}{c_v} = 2667 \text{ K}$$

$$P_3 = P_2(T_3/T_2) = 40.4 \text{ atm}$$

and the gases are expanded isentropically

$$P_4 = P_3(1/r)^{\gamma} = 2.27 \text{ atm}$$

$$T_4 = T_3(1/r)^{\gamma-1} = 1500 \text{ K}$$

Whereas blowdown occurs at constant cylinder volume, we assume that the control mass expands isentropically to the exhaust pressure. Hence

$$T_5 = T_4\left(\frac{P_e}{P_4}\right)^{(\gamma-1)/\gamma} = T_e = 1273 \text{ K}$$

Finally the residual mass fraction is

$$f = \frac{1}{r}\frac{T_4}{T_e}\frac{P_e}{P_4} = 0.0519$$

The computed residual mass fraction and exhaust temperature are improved estimates over our initial guess. We must iterate until both agree with our input values. An iteration table follows.

Iteration Table

ITERATE	1	2	3
f	0.05	0.0519	0.0532
T_e	1000	1273	1291
T_1	330	344	346
P_1	0.5	0.5	0.5
T_2	587	612	616
P_2	8.89	8.89	8.89
T_3	2667	2687	2688
P_3	40.4	39.0	38.8
T_4	1500	1511	1512
P_4	2.27	2.20	2.18
T_e	1273	1291	1294
f	0.0519	0.0532	0.0536

Rarely will one have to iterate more than three times.

With the thermodynamic state of the key points established in the cycle we can compute the efficiency and the work.

$$\eta = 1 - \left(\frac{1}{10}\right)^{0.25} = 0.4377$$

$$\text{imep} = P_1\left[q\frac{(1-f)}{RT_1}\right]\frac{\eta}{1-1/r} = 5.82 \text{ atm}$$

$$\text{pmep} = 0.5 \text{ atm}$$

$$\eta_{\text{net}} = 0.4377(1 - 0.5/5.82) = 0.400$$

$$(\text{imep})_{\text{net}} = 5.82 - 0.5 = 5.32 \text{ atm}$$

Constant pressure intake and exhaust processes occur only at low engine speeds. A more realistic computation models the instantaneous pressure drops across the valves and further would account for the heat transfer which is especially significant during the exhaust. Such an analysis is deferred to Chapter 7.

2.9 TWO-STROKE ENGINES

Chapter 7 discusses two-stroke engines in considerable detail. In this type of engine, both the inlet and exhaust ports are open near bottom dead center. The inlet pressure is greater than the exhaust pressure so that when the ports are uncovered there is a flow of fresh mixture into the cylinder that forces exhaust gases to escape. This process is called scavenging. The fresh mixture trapped in the cylinder at the end of the scavenging depends on many factors.

The ideal process assumes

- constant cylinder volume (V_1) and constant pressure (P_1) scavenging
- adiabatic scavenging

The residual fraction is determined entirely by the scavenging process and can be taken as an independent parameter in the gas-cycle analysis.

2.10 DIMENSIONAL ANALYSIS

For a gas-cycle analysis of a piston engine, the indicated efficiency is a function of the following variables

r, γ	Otto
$\tilde{Q}, \theta_b, \theta_s, \text{n}$	Heat Release
$\tilde{\mathbf{h}}, \beta, \tilde{T}_w$	Heat Loss
C/ω	Mass Loss

Addition of the ideal intake exhaust model accounts for the pumping loss. The net efficiency then depends on the parameters listed and introduces a

dependence on the engine pressure ratio

$$P_e/P_i - \text{four stroke}$$

In the case of a two-stroke engine, the residual fraction is specified

$$f - \text{two stroke}$$

Introduction of friction in Chapter 6 will add a Reynolds number to the list for brake efficiency

$$\frac{\bar{U}_p b}{\nu_o} - \text{friction}$$

where ν_o is the oil viscosity and $\bar{U}_p$ is the mean piston speed.

Consideration of the actual intake and exhaust in Chapter 7 will introduce

Z_i, Z_e	Mach index through valves or ports
$\tilde{d}_i, \tilde{d}_e$	valve or port diameters
$\tilde{l}_i, \tilde{l}_e$	valve lifts
$\theta_{io}, \theta_{eo}, \theta_{ic}, \theta_{ec}$	valve or port timing
$\tilde{d}_{ip}, \tilde{d}_{ep}$	pipe diameter
$\tilde{L}_{ip}, \tilde{L}_{ep}$	pipe lengths

A problem with gas cycle analysis is: How does one choose γ and $\tilde{Q}$? For hydrocarbon fuels one can choose

$$\gamma = 1.4 - 0.16\phi \tag{2.59}$$

$$q(\text{cal/g}) = \begin{cases} \left[\left(\dfrac{\phi F_s}{1+\phi F_s}\right)10{,}660\right] & \phi \le 1 \\ \left\{\dfrac{\phi F_s}{1+\phi F_s}[10{,}660 - 930(\phi - 1)]\right\} & \phi > 1 \end{cases} \tag{2.60}$$

where ϕ is the fuel air equivalence ratio and F_s the stoichiometric fuel air ratio.

Equation (2.60) accounts for the fact that in rich combustion not all the heat of combustion is released. Equations (2.59) and (2.60) are forced to approximate the right answer which can come only from analysis of the combustion instead of a fictitious heat transfer. Herein lies the basic problem with gas cycles analysis: If one has analyzed the combustion to obtain equations like (2.59) and (2.60) then in so doing one has obtained the right answer and need no longer consider the gas cycle. For this reason, in Chapter 3, we introduce the thermodynamics of combustion and in Chapter 4 we use the results for cycle analysis. In so doing we delete γ, $\tilde{Q}$ from our list and

replace them with:

H/C	hydrogen-to-carbon ratio of the fuel
ϕ	fuel–air equivalence ratio
M	molecular weight of the fuel
$\tilde{Q}_c$	heat of combustion of the fuel
$\tilde{Q}_v$	heat of vaporization of the fuel
$\tilde{a}_c$	available energy of combustion of the fuel

If the fuel is not a hydrocarbon we would add further

O/C	oxygen-to-carbon ratio of the fuel
N/C	nitrogen-to-carbon ratio of the fuel

Now all the variables we will consider have been listed. The list can go on to include parameters of intake and exhaust manifold design for multicylinder engines, bearing sizes, ring design, turbo or supercharge parameters, and the like. It is hoped that the reader can appreciate that, in part, engine development continues today because there are so many variables that not all possible combinations have yet been tested.

2.11 REFERENCES

Van Wylen, G. J., and R. E. Sonntag, *Fundamentals of Classical Thermodynamics*, Wiley, New York, 1985.

Taylor, C. F., *The Internal Combustion Engine in Theory and Practice*, Vol. 1, MIT Press, Cambridge, Massachusetts, 1977.

2.12 HOMEWORK

1. **a.** Show for an Otto cycle that $T_3/T_2 = T_4/T_1$.
   b. Derive the result in Eq. (2.8).
2. **a.** Show that for a Diesel cycle $(T_3/T_2)^\gamma = T_4/T_1$.
   b. Derive eq. (2.12) and (2.13).
3. For equal maximum temperature and work done, which cycle will be more efficient, the Diesel or Otto? The two cycles should have a common state corresponding to the start of compression.
4. Show that as $r \to 1$, $\text{imep}/P_1 \to \tilde{Q}(\gamma - 1)$ for the Otto cycle. The dimensionless heat transfer in is $\tilde{Q} = Q_{\text{in}}/P_1V_1$
5. Repeat Example 2.2 using Eq. (2.21) instead of (2.22).
6. With reference to Section 2.6 on heat loss, show that for a cylindrical combustion chamber

$$\beta = 2\frac{S}{b}\frac{r}{r-1}$$

What effect at constant S/b and r will valve pockets on the piston have

on β? How would β for a hemispherical combustion chamber compare with that of a cylindrical chamber?

7. Study the effect of wall temperature by using the program in Example 2.2. Plot the indicated efficiency versus dimensionless wall temperature. At what wall temperature would the engine be "adiabatic" in the sense that heat loss during expansion is balanced by heat gain during compression?
8. Two gasoline engines have the same dimensionless parameters

$$\gamma = 1.3 \quad r = 8 \quad \tilde{Q} = 30$$
$$\theta_s = 35° \quad \theta_b = 40° \quad n = 4,$$
$$\tilde{\mathbf{h}} = 0.15 \quad \beta = 1.4 \quad \tilde{T}_w = 1.3$$
$$\epsilon = 0.25$$

Dimensionally they are quite different.

	ENGINE A	ENGINE B
b(cm)	10	100
S(cm)	8	80
P_i(atm)	0.5	2.0
T_i(K)	320	400
Engine speed (rpm)	1500	200

How will their indicated efficiencies compare according to our closed-system gas-cycle model? How will then indicated mean effective pressure compare? Be sure to explain your reasoning.

9. Analyze a Diesel cycle, (along the lines used in Example 2.4) with the following data:

$$r = 22 \quad \gamma = 1.3 \quad T_i = 300 \text{ K}$$
$$P_e = 1 \text{ atm} \quad P_i/P_e = 0.98 \quad q = 500 \text{ cal/g}$$
$$M = 29$$

10. If the engine in Example 2.4 were a four-cylinder, four-stroke engine with a 10-cm bore and an 8-cm stroke operating at 2000 rpm, how much indicated power (kW) would it produce? What if it were a two-stroke engine?
11. In Example 2.4, T_e is the exhaust temperature during the constant pressure exhaust stroke. It is not the same as the average temperature of the gases exhausted. Explain.
12. Study the effect of blowby on performance and efficiency by writing a computer program to solve Example 2.3. Vary the engine frequency over the following range $50 < \omega < 5000/s$. Explain physically why the blowby should decrease with increasing engine speed.
13. The blowby model in this chapter does not account for the fact that during the compression stroke the blowby gas might contain fuel. Explain how this lost fuel will further degrade the engine's performance. Contrast the significance of this effect for a gasoline engine with that for a diesel engine.

14. ***Complete Expansion Engine*** By clever geometrical linkage, as in the K-cycle, or by closing the inlet valve late, an engine can be constructed with an expansion ratio greater than the compression ratio. Model this engine by the cycle shown.

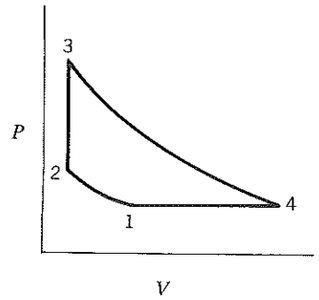

1 to 2 isentropic compression
2 to 3 constant volume heat in
3 to 4 isentropic expansion
4 to 1 constant pressure heat out

Derive an expression for the efficiency in terms of

$$\gamma, \alpha = V_4/V_3, \text{ and } \beta = V_1/V_4.$$

15. ***Reciprocating Brayton Cycle*** Derive an expression for the efficiency of a complete expansion engine in which the heat is added at constant pressure. Express the result in terms of the pressure ratio $\alpha = P_2/P_1$.
16. ***Stirling Cycle*** The Stirling engine is of interest because its theoretical efficiency is equal to the Carnot efficiency. Show that this is true if and only if the heat in from 2 to 3 comes from the heat out of 4 to 1 (regeneration).

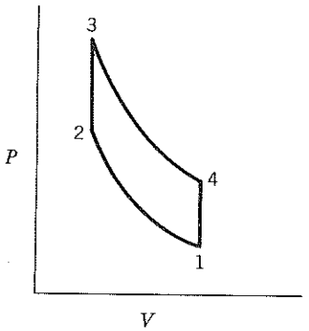

1 to 2 isothermal compression
2 to 3 constant volume heat in
3 to 4 isothermal expansion
4 to 1 constant volume heat out

17. ***Variable Specific Heats*** Use the Air Tables in Appendix D to analyze a Diesel cycle in which

$$r = 10 \quad T_1 = 300 \text{ K}$$
$$\frac{Q_{in}}{P_1 V_1} = 15 \quad P_1 = 1 \text{ bar}$$

Compare the predicted efficiency with that given by Eq. (2.12) for the case $\gamma = 1.4$.

Three

FUEL, AIR, AND COMBUSTION THERMODYNAMICS

It has already been mentioned that an understanding of combustion engines will require better thermodynamic models than those used in Chapter 2. In this chapter we review the thermodynamics of combustion by casting it into a form suitable for application to internal combustion engines.

A few words about air are in order first. The properties of air vary geographically, with altitude and with time. We will assume that air is 21% oxygen and 79% nitrogen by volume. Extension of our analyses to different air encountered in practice will be obvious. The most frequent differences accounted for are the presence of water and argon in air.

3.1 IDEAL GAS EQUATIONS OF STATE

The mass of a mixture is the sum of the mass of all J components

$$m = \sum_{i=1}^{J} m_i \tag{3.1}$$

The mass fraction of any given species is defined as

$$x_i = m_i/m \tag{3.2}$$

and it should be clear that

$$1 = \sum_{i=1}^{J} x_i \tag{3.3}$$

The internal energy of a mixture is the sum of the energy of all J components

$$U = \sum_{i=1}^{J} m_i u_i \tag{3.4}$$

where the u_i are understood to be mass intensive as opposed to molar

intensive. The mass intensive internal energy is

$$u = \sum_{i=1}^{J} x_i u_i \tag{3.5}$$

Analogous relations for the enthalpy are

$$H = \sum_{i=1}^{J} m_i h_i \tag{3.6}$$

$$h = \sum_{i=1}^{J} x_i h_i \tag{3.7}$$

The moles of mixture is the sum of moles of all J components

$$N = \sum_{i=1}^{J} N_i \tag{3.8}$$

and the mole fraction of any given species is

$$y_i = N_i/N \tag{3.9}$$

The internal energy of a mixture can also be written as

$$U = \sum_{i=1}^{J} N_i u_i \tag{3.10}$$

where now the u_i are understood to be molar intensive. The molar intensive internal energy is thus

$$u = \sum_{i=1}^{J} y_i u_i \tag{3.11}$$

Likewise the enthalpy is

$$H = \sum_{i=1}^{J} N_i h_i \tag{3.12}$$

$$h = \sum_{i=1}^{J} y_i h_i \tag{3.13}$$

Notice that capital letters have been adopted for extensive variables and lower-case letters are reserved for intensive variables. No attempt has been made to distinguish between molar intensive and mass intensive quantities since the meaning should be clear from the context in which they are used.

The molecular weight of a mixture

$$M = \sum_{i=1}^{J} y_i M_i \tag{3.14}$$

is the conversion factor required between molar intensive and mass intensive units. For example, the mass intensive (specific) gas constant is related to the

molar intensive (universal) gas constant by

$$R = R_u/M \tag{3.15}$$

The subscript u may or may not be used again since the use of R should be clear from the context.

The familiar relationships between pressure, temperature, and volume are

$$\begin{aligned} PV &= NRT \\ PV &= mRT \\ Pv &= RT \end{aligned} \tag{3.16}$$

The entropy of a mixture is also the sum of the entropies of each component

$$S = \sum_{i=1}^{J} m_i s_i = \sum_{i=1}^{J} N_i s_i \tag{3.17}$$

but unlike enthalpy, where the enthalpy of a component is evaluated at the total pressure ($h_i = u_i + Pv_i$), the entropy of a component is evaluated at its partial pressure. The partial pressure of a component is

$$P_i = y_i P \tag{3.18}$$

and the entropy of any component is

$$s_i = s_i^o - R_i \ln (P_i/P_o) \tag{3.19}$$

where s_i^o depends only on temperature and is the entropy of that component when $P_i = P_o$. Substitution of Eq. (3.19) into Eq. (3.17) yields the convenient relations

$$s = -R \ln (P/P_o) + \sum_{i=1}^{J} x_i (s_i^o - R_i \ln y_i) \tag{3.20}$$

$$s = -R \ln (P/P_o) + \sum_{i=1}^{J} y_i (s_i^o - R \ln y_i) \tag{3.21}$$

Thermodynamic data for elements, combustion products, and many pollutants are available in a compilation published by the National Bureau of Standards, called the JANAF Tables (1971). For single component fuels the data presented by Stull, Westrum and Sinke, (1969) is in the same format as that of the JANAF Tables. In addition to these two references a compilation by Rossini (1953) is useful for hydrocarbon fuels at temperatures as high as 1500 K. The data we need from these sources is given in Appendix F.

For computer calculations it is awkward to deal with tabular data. For this reason the specific heats are curve fitted to polynomials by minimizing the least-squares error. The function we will employ for any given species is

$$\frac{c_p}{R} = a_1 + a_2 T + a_3 T^2 + a_4 T^3 + a_5 T^4 \tag{3.22}$$

Table 3.1 Thermo Data ($300 \le T \le 1000$ K)

i	SPECIES	a_{11}	a_{12}	a_{13}	a_{14}	a_{15}	a_{16}	a_{17}
0	Gasoline[a] C_7H_{17}	0.406E + 01	0.601E − 01	−0.188E − 05	−0	0	−0.4053E + 05	−0.28325E + 01
1	CO_2	0.24007797E + 01	0.87350957E − 05	−0.66070878E − 05	0.20021861E − 08	0.63274039E − 15	−0.48377527E + 05	0.96951457E + 01
2	H_2O	0.40701275E + 01	−0.11084499E − 02	0.41521180E − 05	−0.29637404E − 08	0.80702103E − 12	−0.30279722E + 05	−0.32270046E + 00
3	N_2	0.36748261E + 01	−0.12081500E − 02	0.23240102E − 05	−0.63217559E − 09	−0.22577253E − 12	−0.10611588E + 04	0.23580424E + 01
4	O_2	0.36255985E + 01	−0.18782184E − 02	0.70554544E − 05	−0.67635137E − 08	0.21555993E − 11	−0.10475226E + 04	0.43052778E + 01
5	CO	0.37100928E + 01	−0.16190964E − 02	0.36923594E − 05	−0.20319674E − 08	0.23953344E − 12	−0.14356310E + 05	0.2955535E + 01
6	H_2	0.30574451E + 01	0.26765200E − 02	−0.58099162E − 05	0.55210391E − 08	−0.18122739E − 11	−0.98890474E + 03	−0.22997056E + 01
7	H	0.25000000E + 01	0	0	0	0	0.25471627E + 05	−0.46011762E + 00
8	O	0.29464287E + 01	−0.16381665E − 02	0.24210316E − 05	−0.16028432E − 08	0.38906964E − 12	0.29147644E + 05	0.29639949E + 01
9	OH	0.38375943E + 01	−0.10778858E − 02	0.96830378E − 06	0.18713972E − 09	−0.22571094E − 12	0.36412823E + 04	0.49370009E + 00
10	NO	0.40459521E + 01	−0.34181783E − 02	0.79819190E − 05	−0.61139316E − 08	0.15919076E − 11	0.97453934E + 04	0.29974988E + 01

Source: From Gordon and McBride (1971).

[a]Estimated properties of AL Label 7927G, see Table 10-8.

It follows that the enthalpy and entropy at atmospheric pressure are

$$\frac{h}{RT} = a_1 + \frac{a_2}{2}T + \frac{a_3}{3}T^2 + \frac{a_4}{4}T^3 + \frac{a_5}{5}T^4 + \frac{a_6}{T} \tag{3.23}$$

$$\frac{s^o}{R} = a_1 \ln T + a_2 T + \frac{a_3}{2}T^2 + \frac{a_4}{3}T^3 + \frac{a_5}{4}T^4 + a_7 \tag{3.24}$$

where a_6 and a_7 are constants of integration determined by matching the enthalpy and entropy at some reference temperature. Values of the constants for several species of interest to us are given in Table 3-1. The reference temperature is chosen to be 298 K with the enthalpy of H_2, O_2, N_2, and C(s) set to zero.

EXAMPLE 3.1

Compute the enthalpy, internal energy, entropy, and specific volume of a gas mixture at $T = 500$ K, $P = 15$ bars. The constituents and their mole fractions are

i	SPECIES	y_i
1	CO_2	0.091
2	H_2O	0.138
3	CO	0.052
4	H_2	0.022
5	N_2	0.697

The list below was prepared from the thermodynamic data in Appendix F.

i	h_i (kcal/mole)	u_i^a (kcal/mole)	s_i^o (cal/mole K)	M_i (g/mole)
1	−92.067	−93.061	56.122	44.010
2	−56.144	−57.138	49.334	18.016
3	−25.000	−25.994	50.841	28.011
4	1.406	0.412	34.806	2.016
5	1.413	0.419	49.386	28.013

[a]Recall that $u = h - Pv$.

The properties of the mixture are

$$h = -16.410 \text{ kcal/mole} = -0.596 \text{ kcal/g}$$
$$u = -17.404 \text{ kcal/mole} = -0.362 \text{ kcal/g}$$
$$s = 46.288 \text{ cal/mole K} = 1.682 \text{ cal/g K}$$
$$v = 2735 \text{ cm}^3\text{/mole} = 99.40 \text{ cm}^3\text{/g}$$

3.2 STOICHIOMETRY AND FUEL–AIR–RESIDUAL COMPOSITION

Let us represent the chemical formula of a fuel as $C_\alpha H_\beta O_\gamma N_\delta$. A stoichiometric reaction is defined such that the only products are carbon dioxide and water. Let us write

$$\epsilon\phi C_\alpha H_\beta O_\gamma N_\delta + (0.21\ O_2 + 0.79\ N_2) \rightarrow \nu_1 CO_2 + \nu_2 H_2O + \nu_3 N_2 \quad (3.25)$$

and solve for ϵ, the molar fuel–air ratio, and the coefficients ν_i $(i = 1, 2, 3)$ that describe the product composition. We know that atoms are conserved, so we can write

C	$\epsilon\alpha$	$= \nu_1$
H	$\epsilon\beta$	$= 2\nu_2$
O	$\epsilon\gamma + 2(0.21) = 2\nu_1 + \nu_2$	
N	$\epsilon\delta + 2(0.79) = 2\nu_3$	

Solution of these four equations gives

$$\begin{aligned}
\nu_1 &= 0.210\alpha/(\alpha + 0.25\beta - 0.5\gamma) \\
\nu_2 &= 0.105\beta/(\alpha + 0.25\beta - 0.5\gamma) \\
\nu_3 &= 0.790 + 0.105\delta/(\alpha + 0.25\beta - 0.5\gamma) \\
\epsilon &= 0.210/(\alpha + 0.25\beta - 0.5\gamma)
\end{aligned} \quad (3.26)$$

The stoichiometric fuel–air ratio by mass is

$$F_s = \frac{\epsilon(12.01\alpha + 1.008\beta + 16.00\gamma + 14.01\delta)}{28.85} \quad (3.27)$$

Typical values are given in Table 3-2. Notice that for hydrocarbons ($\gamma = \delta = 0$) the stoichiometric fuel–air ratio by mass is not a particularly strong function of type. For typical fuels the stoichiometric air–fuel ratio is 15 or $F_s \approx 0.067$.

Table 3-2 Stoichiometric Fuel–Air Ratios, Mole and Mass Fractions

FUEL	ϵ	F_s	y_s	x_s
C_2N_2	0.1050	0.1894	0.0950	0.1592
H_2	0.4200	0.0293	0.2958	0.0285
NH_3	0.2800	0.1653	0.2188	0.1419
CH_4	0.1050	0.0584	0.1000	0.0552
C_3H_8	0.0420	0.0642	0.0403	0.0603
C_8H_{18}	0.0168	0.0665	0.0165	0.0624
$C_{15}H_{32}$	0.0091	0.0672	0.0090	0.0630
$C_{20}H_{40}$	0.0070	0.0681	0.0070	0.0638
C_2H_2	0.0840	0.0758	0.0775	0.0705
$C_{10}H_8$	0.0175	0.0777	0.0172	0.0721
CH_4O	0.1400	0.1555	0.1228	0.1346
C_2H_6O	0.0700	0.1118	0.0654	0.1006
CH_3NO_2	0.2800	0.5924	0.2188	0.3720

The table also shows the mole and mass fraction of fuel in a stoichiometric fuel–air mixture.

$$y_s = \frac{\epsilon}{1+\epsilon} \qquad x_s = \frac{F_s}{1+F_s} \quad (3.28)$$

The fuel–air equivalence ratio is defined as the actual fuel–air ratio divided by the stoichiometric fuel–air ratio

$$\phi = F/F_s \quad (3.29)$$

If $\phi < 1$ the mixture is called lean, if $\phi > 1$ the mixture is said to be rich and if $\phi = 1$ the mixture is said to be stoichiometric.

At low temperatures (such as in the exhaust) and carbon to oxygen ratios less than one, the overall combustion reaction can be written

$$\phi\epsilon C_\alpha H_\beta O_\gamma N_\delta + (0.21\ O_2 + 0.79\ N_2) \rightarrow \nu_1 CO_2 + \nu_2 H_2O + \nu_3 N_2 + \nu_4 O_2 + \nu_5 CO + \nu_6 H_2 \quad (3.30)$$

For reactant C/O ratios greater than one we would have to add solid carbon C(s) and several other species as we shall see.

Convenient approximations for lean and rich combustion are

$$\begin{cases} \phi < 1 & \nu_5 = \nu_6 = 0 \\ \phi > 1 & \nu_4 = 0 \end{cases}$$

For the lean or stoichiometric cases, atom-balance equations are sufficient to determine the product composition (four equations and four unknowns). For the rich case we introduce an equilibrium constant for the reaction

$$CO_2 + H_2 \rightleftharpoons CO + H_2O \qquad K = \frac{\nu_2\nu_5}{\nu_1\nu_6} \quad (3.31)$$

Solutions for both rich and lean cases are given in Table 3-3.

Table 3-3 Low Temperature Combustion Products, ν_i (moles/mole of air)

i	SPECIES	$\phi \le 1$	$\phi > 1$
1	CO_2	$\alpha\phi\epsilon$	$\alpha\phi\epsilon - \nu_5$
2	H_2O	$\beta\phi\epsilon/2$	$0.42 - \phi\epsilon(2\alpha - \gamma) + \nu_5$
3	N_2	$0.79 + \delta\phi\frac{\epsilon}{2}$	$0.79 + \delta\phi\frac{\epsilon}{2}$
4	O_2	$0.21(1 - \phi)$	0
5	CO	0	ν_5
6	H_2	0	$0.42(\phi - 1) - \nu_5$

Source: Hires, Ekchian, Heywood, Tabczynski, and Wall (1976).

In the rich case the parameter ν_5 is given by the solution of a quadratic equation

$$\nu_5 = \frac{-b + \sqrt{b^2 - 4ac}}{2a} \tag{3.32}$$

where

$$a = 1 - \mathrm{K}$$
$$b = 0.42 - \phi\epsilon(2 - \gamma) + \mathrm{K}[0.42(\phi - 1) + \alpha\phi\epsilon]$$
$$c = -0.42\alpha\phi\epsilon(\phi - 1)\mathrm{K}$$

EXAMPLE 3.2

Find the composition of combustion products of C_8H_{18} at $\phi = 1.2$, $T = 1000$ K, and $P = 100$ atm.

SOLUTION:

The equilibrium constant curve fitted to JANAF Table data is given by $\ln \mathrm{K} = 2.743 - 1.761/t - 1.611/t^2 + 0.2803/t^3$ where $t = T/1000$ and T is in degrees Kelvin. In this case $\mathrm{K} = 0.706$ ($\mathrm{K} = 0.693$ if determined directly from tables). The curve fit applies to $400 < T < 3200$ K. The fuel parameters are

$$\alpha = 8 \quad \beta = 18 \quad \gamma = 0 \quad \delta = 0 \quad \epsilon = 0.01680$$

The quadratic equation leads to

$$a = 0.3066 \quad b = 0.2675 \quad c = -0.00949 \quad \nu_5 = 0.0387$$

The remaining coefficients are

$$\nu_1 = 0.1226 \quad \nu_3 = 0.7900$$
$$\nu_2 = 0.1362 \quad \nu_6 = 0.0453$$

The mole fraction of any species is

$$y_i = \nu_i \Big/ \sum_{i=1}^{6} \nu_i \tag{3.33}$$

Solutions are

$$y_1 = 0.1082 \quad y_3 = 0.6974 \quad y_5 = 0.0342$$
$$y_2 = 0.1202 \quad y_4 = 0 \quad y_6 = 0.0400$$

The molecular weight is

$$M = \sum_{i=1}^{6} y_i M_i = 27.50$$

and the mass fraction of any species is

$$x_i = \frac{M_i}{M} y_i$$

In this particular case

$$x_1 = 0.1732 \quad x_3 = 0.7103 \quad x_5 = 0.0348$$
$$x_2 = 0.0788 \quad x_4 = 0 \quad x_6 = 0.0029$$

We have learned to determine the composition of fuel–air mixtures and their combustion products at low temperatures. In reciprocating engines we have seen that there is residual gas mixed with the fuel and air. We need to determine the composition of such a mixture for analysis of the compression stroke and later the unburned mixture ahead of the flame.

The residual mass fraction f is a convenient parameter to deal with. Let us rewrite the combustion equation as

$$\nu_0' C_\alpha H_\beta O_\gamma N_\delta + \nu_4' O_2 + \nu_3' N_2 \rightarrow \nu_1'' CO_2 + \nu_2'' H_2O + \nu_3'' N_2 + \nu_4'' O_2 + \nu_5'' CO + \nu_6'' H_2 \tag{3.34}$$

where

ν_i' = reactant coefficient

ν_i'' = product coefficient

Adopting similar notation for other symbols, it should be clear that for a mixture of residual gas and premixed fuel–air

$$x_i = (1 - f)x_i' + fx_i'' \qquad i = 0, 6 \tag{3.35}$$

The mole fractions are given by

$$y_i = (1 - y_r)y_i' + y_r y_i'' \tag{3.36}$$

Where the residual mole fraction is

$$y_r = \left[1 + \frac{M''}{M'}\left(\frac{1}{f} - 1\right)\right]^{-1} \tag{3.37}$$

3.3 A SUBROUTINE FOR FUEL–AIR RESIDUAL GAS

```
C*****************************************************************
C
      SUBROUTINE FARG (P, T, PHI, F, H, U, V, S, Y, CP, DLVLT, DLVLP)
C
C     PURPOSE:
C        COMPUTE THE PROPERTIES OF A FUEL, AIR, RESIDUAL
C        GAS MIXTURE
C
C     GIVEN:
C        P       - PRESSURE (BARS)
C        T       - TEMPERATURE (K)
C        PHI     - FUEL AIR EQUIVALENCE RATIO
C        F       - RESIDUAL MASS FRACTION
```

```
C
C      RETURNS:
C         H        - ENTHALPY (J/G)
C         U        - INTERNAL ENERGY (J/G)
C         V        - SPECIFIC VOLUME (CM**3/G)
C         S        - ENTROPY (J/G/K)
C         Y        - A SIX DIMENSIONAL COMPOSITION VECTOR OF
C                    MOLE FRACTIONS
C                    1=CO2, 2=H2O, 3=N2, 4=O2, 5=CO, 6=H2
C         CP       - SPECIFIC HEAT AT CONSTANT PRESSURE (J/G/K)
C         DLVLT    - DERIVATIVE OF LOG VOLUME WITH RESPECT TO LOG
C                    TEMPERATURE AT CONSTANT PRESSURE
C         DLVLP    - DERIVATIVE OF LOG VOLUME WITH RESPECT TO LOG
C                    PRESSURE AT CONSTANT TEMPERATURE
C
C      REMARKS:
C         1. VALID FOR 300 < T < 1000
C         2. ASSUMES THE FUEL IS GASOLINE. TO CHANGE FUELS
C            ONLY THE FUEL DATA STATEMENT NEEDS MODIFICATION.
C         3. ENTHALPIES OF O2, H2, N2 AND C(S) ARE SET TO ZERO
C            AT 298K
C         4. THE FUEL MOLE FRACTION IS UNITY MINUS THE SUM OF Y(I)
C
C*************************************************************
C
      REAL M, MW, MRES, MFA, MFUEL, K, NU, N2
      LOGICAL RICH,LEAN
      DIMENSION A(7,6), TABLE(6), M(6), NU(6), Y(6), CP0(6), H0(6),
     &          S0(6)
C
C     FUEL DATA
C
      DATA ALPHA/7.0/, BETA/17.0/, GAMMA/0./, DELTA/0./,
     &     A0/4.0652/, B0/6.0977E-02/, C0/-1.8801E-05/, D0/-3.5880E+04/,
     &     E0/15.45/
C
C     TABLE 3.1, I = 1,6
C
      DATA A/
     1 .24007797E+01, .87350957E-02, -.6607878E-05, .20021861E-08,
     1 .63274039E-15, -.48377527E+05, .96951457e+01,
     2 .40701275E+01, -.11084499E-02, .41521180E-05, -.29637404E-08,
     2 .80702103E-12, -.30279722E+05, -.32270046E+00,
     3 .36748261E+01, -.12081500E-02, .23240102E-05, -.63217559E-09,
     3 -.22577253E-12, -.10611588E+04, .23580424E+01,
     4 .36255985E+01, -.18782184E-02, .70554544E-05, -.67635137E-08,
     4 .21555993E-11, -.10475226E+04, .43052778E+01,
     5 .37100928E+01, -.16190964E-02, .36923594E-05, -.20319674E-08,
     5 .23953344E-12, -.14356310E+05, .29555355E+01,
     6 .30574451E+01, .26765200E-02, -.58099162E-05, .55210391E-08,
     6 -.18122739E-11, -.98890474E+03, -.22997056E+01/
C
C     OTHER DATA
C
      DATA RU/8.315/, TABLE/-1.,1.,0.,0.,1.,-1./, M/44.01, 18.02,
     &         28.008, 32.000, 28.01, 2.016/
C
C     COMPUTE RESIDUAL GAS COMPOSITION ACCORDING TO TABLE 3.3
C
      RICH = PHI .GT. 1.0
      LEAN = .NOT. RICH
```



```
      DLVLT =  1.0
      DLVLP = -1.0
      EPS = .21/(ALPHA + 0.25*BETA - 0.5*GAMMA)
      IF (RICH) GO TO 10
      NU(1) = ALPHA*PHI*EPS
      NU(2) = BETA*PHI*EPS/2.
      NU(3) = 0.79 + DELTA*PHI*EPS/2.
      NU(4) = 0.21*(1.0 - PHI)
      NU(5) = 0.
      NU(6) = 0.
      DCDT = 0.
      GO TO 20
10    Z = 1000./T
      K = EXP(2.743 + Z*(-1.761 + Z*(-1.611 + Z*.2803)))
      DKDT = -K*(-1.761 + Z*(-3.222 + Z*.8409))/1000.
      A1 = 1.0 - K
      B = .42 - PHI*EPS*(2.*ALPHA - GAMMA) + K*(.42*(PHI - 1.) +
     &    ALPHA*PHI*EPS)
      C = -.42*ALPHA*PHI*EPS*(PHI - 1.0)*K
      NU(5) = (-B + SQRT(B*B - 4.*A1*C))/2./A1
      DCDT = DKDT*(NU(5)**2 - NU(5)*(.42*(PHI - 1.) + ALPHA*
     &       PHI*EPS) + .42*ALPHA*PHI*EPS*(PHI - 1.))/
     &       (2.*NU(5)*A1 + B)
      NU(1) = ALPHA*PHI*EPS - NU(5)
      NU(2) = .42 - PHI*EPS*(2.*ALPHA - GAMMA) + NU(5)
      NU(3) = .79 + DELTA*PHI*EPS/2.
      NU(4) = 0.
      NU(6) = .42*(PHI - 1.) - NU(5)
C
C     COMPUTE MOLE FRACTIONS AND MOLECULAR WEIGHT OF RESIDUAL
C
20    TMOLES = 0.
      DO 30 I = 1,6
30    TMOLES = TMOLES + NU(I)
      MRES = 0.
      DO 40 I = 1,6
      Y(I) = NU(I)/TMOLES
40    MRES = MRES + Y(I)*M(I)
C
C     COMPUTE MOLE FRACTIONS AND MOLECULAR WEIGHT OF FUEL-AIR
C
      FUEL = EPS*PHI/(1. + EPS*PHI)
      O2 = .21/(1. + EPS*PHI)
      N2 = .79/(1. + EPS*PHI)
      MFA = FUEL*(12.01*ALPHA + 1.008*BETA + 16.*GAMMA + 14.01*
     &      DELTA) + 32.*O2 + 28.02*N2
C
C     COMPUTE MOLE FRACTIONS OF FUEL-AIR-RESIDUAL GAS
C
      YRES = F/(F + MRES/MFA*(1. - F))
      DO 50 I = 1,6
50    Y(I) = Y(I)*YRES
      YFUEL = FUEL*(1. - YRES)
      Y(3) = Y(3) + N2*(1. - YRES)
      Y(4) = Y(4) + O2*(1. - YRES)
C
C     COMPUTE COMPONENT PROPERTIES
C
      DO 60 I = 1,6
      CP0(I) = A(1,I) + A(2,I)*T + A(3,I)*T**2 + A(4,I)*T**3 +
     &         A(5,I)*T**4
```

```
      HO(I) = A(1,I) + A(2,I)/2.*T + A(3,I)/3.*T**2 + A(4,I)/4.*
     &        T**3 + A(5,I)/5.*T**4 + A(6,I)/T
60    SO(I) = A(1,I)*ALOG(T) + A(2,I)*T + A(3,I)/2.*T**2 +
     &        A(4,I)/3.*T**3 + A(5,I)/4.*T**4 + A(7,I)
C
      MFUEL = 12.01*ALPHA + 1.008*BETA + 16.000*GAMMA + 14.01*DELTA
      CPFUEL = A0 + B0*T + C0*T**2
      HFUEL = A0 + B0/2.*T + C0/3.*T**2 + D0/T
      SOFUEL = A0*ALOG(T) + B0*T + C0/2.*T**2 + E0
C
C     COMPUTE PROPERTIES OF MIXTURE
C
      H = HFUEL*YFUEL
      S = (SOFUEL - ALOG(YFUEL))*YFUEL
      CP = CPFUEL*YFUEL
      MW = MFUEL*YFUEL
      DO 70 I = 1,6
      H = H + HO(I)*Y(I)
      S = S + Y(I)*(SO(I) - ALOG(Y(I)))
      CP = CP + CPO(I)*Y(I) + HO(I)*T*TABLE(I)*DCDT*YRES/TMOLES
70    MW = MW + Y(I)*M(I)
C
      R = RU/MW
      H = R*T*H
      U = H - R*T
      V = 10.*R*T/P
      S = R*(-ALOG(.9869*P) + S)
      CP = R*CP
C
      RETURN
      END
```

The subroutine FARG is written for the case in which the fuel is gasoline. To change to other fuels the FUEL DATA STATEMENT must be modified. Constants for some fuels we will consider later are given here:

FUEL	a_o	b_o	c_o	d_o	e_o
CH_3NO_2	1.412633	2.087101E − 02	−8.142134E − 06	−1.026351E + 04	1.917126E + 01
CH_4	1.971324	7.871586E − 03	−1.048592E − 06	−9.930422E + 03	8.873728
CH_3OH	1.779819	1.262503E − 02	−3.624890E − 06	−2.525420E + 04	1.50884E + 01
C_6H_6	−2.545087	4.79554E − 02	−2.030765E − 05	8.782234E + 03	3.348825E + 01
C_7H_{17}[a]	4.0652	6.0977E − 02	−1.8801E − 05	−3.5880E + 04	1.545E + 01
$C_{14.4}H_{24.9}$[b]	7.9710	1.1954E − 01	−3.6858E − 05	−1.9385E + 04	−1.7879

[a] Gasoline.
[b] Diesel fuel.

The constants give the ideal gas properties of the fuel according to

$$\frac{c_p}{R} = a_o + b_o T + c_o T^2$$

$$\frac{h}{RT} = a_o + \frac{b_o}{2}T + \frac{c_o}{3}T^2 + \frac{d_o}{T}$$

$$\frac{s^o}{R} = a_o \ln T + b_o T + \frac{c_o}{2}T^2 + e_o$$

3.4 EQUILIBRIUM COMBUSTION PRODUCTS

In general, we often consider a problem in which T, P are specified and

$$\epsilon\phi C_\alpha H_\beta O_\gamma N_\delta + 0.21O_2 + 0.79N_2 \rightarrow \nu_1 CO_2 + \nu_2 H_2O + \nu_3 N_2 + \nu_4 O_2 + \nu_5 CO + \nu_6 H_2 + \nu_7 H + \nu_8 O + \nu_9 OH + \nu_{10} NO + \nu_{11} N + \nu_{12} C(s) + \nu_{13} NO_2 + \nu_{14} CH_4 + \cdots \quad (3.38)$$

For a mixture of n species, the Gibbs free energy is

$$g = \sum_{j=1}^{n} \mu_j \nu_j \quad (3.39)$$

where the chemical potential of species j is defined by

$$\mu_j = \left(\frac{\partial g}{\partial \nu_j}\right)_{T,P,\nu_{i\neq j}} \quad (3.40)$$

The equilibrium state is determined by minimizing the Gibbs free energy subject to the constraints imposed by atom conservation, that is,

$$\sum_{j=1}^{n} a_{ij}\nu_j = b_i^o \qquad i = 1, \ldots, l$$

or

$$\sum_{j=1}^{n} a_{ij}\nu_j - b_i - b_i^o = 0 \qquad i = 1, \ldots, l \quad (3.41)$$

where a_{ij} is the number of atoms of element i in species j, b_i^o is the number of atoms of element i in the reactants, and

$$b_i = \sum_{j=1}^{n} a_{ij}\nu_j \quad (3.42)$$

is the number of atoms of element i in the products.

Defining a term G to be

$$G = g + \sum_{i=1}^{l} \lambda_i (b_i - b_i^o) \quad (3.43)$$

where λ_i are Lagrangian multipliers, the condition for equilibrium becomes

$$0 = \delta G = \sum_{j=1}^{n} \left(\mu_j + \sum_{i=1}^{l} \lambda_i a_{ij}\right)\delta\nu_j + \sum_{i=1}^{l} (b_i - b_i^o)\,\delta\lambda_i \quad (3.44)$$

Treating the variations $\delta\nu_j$ and $\delta\lambda_i$ as independent gives

$$\mu_j + \sum_{i=1}^{l} \lambda_i a_{ij} = 0 \qquad j = 1, \ldots, n \quad (3.45)$$

For ideal gases

$$\mu_j = \mu_j^o + RT\ln(\nu_j/\nu) + RT\ln(P/P_o) \tag{3.46}$$

so that

$$\frac{\mu_j^o}{RT} + \ln(\nu_j/\nu) + \ln(P/P_o) + \sum_{i=1}^{l} \pi_i a_{ij} = 0 \qquad j = 1,\ldots,n \tag{3.47}$$

where $\pi_i = \lambda_i/RT$.

For a given temperature and pressure (T, P) Eq. (3.47) is a set of n equations for the n unknown ν_j, l unknown π_i, and ν.

Equation (3.41) provides an additional l equations and we close the set with

$$\nu = \sum_{j=1}^{n} \nu_j \tag{3.48}$$

We have to solve a set of $n + l + 1$ equations.

EXAMPLE 3.3

Find the equilibrium composition for the reaction

$$N_2 \rightarrow \nu_1 N_2 + \nu_2 N$$

at $T = 5000$ K, $P = 100$ atm.

SOLUTION:

In this case we have $n = 2$, $l = 1$ so we will have to solve four equations for four unknowns. Equation (3.41) becomes $b_1 - 2 = 0$ and Eq. (3.42) yields

$$b_1 = 2\nu_1 + \nu_2$$

where we have labeled $j = 1$ for N_2 and $j = 2$ for N. Combining these results we get

$$2\nu_1 + \nu_2 = 2$$

a result that should be clear.

We need the chemical potential at the standard state for both species in Eq. (3.47). This data is in the JANAF Tables (see Appendix F). Mixing the notation there and ours we get

$$\frac{\mu_j^o}{RT} = \frac{(F^o - H_{298}^o)/T}{R} + \frac{\Delta H_{f,298}^o}{RT} \tag{3.49}$$

Hence

$$\frac{\mu_1^o}{RT} = \frac{-60.322}{1.9872} + 0 = -30.355$$

$$\frac{\mu_2^o}{RT} = \frac{-45.971}{1.9872} + \frac{112{,}965}{1.987(5000)} = -11.764$$

Our Eqs. (3.47), (3.41), and (3.48) are

$$-25.750 + \ln(\nu_1/\nu) + 2\pi_1 = 0$$

$$-7.159 + \ln(\nu_2/\nu) + \pi_1 = 0$$

$$2 = 2\nu_1 + \nu_2$$

$$\nu = \nu_1 + \nu_2$$

Solution leads to

$$\nu_1 = 0.9984 \qquad \nu_2 = 0.0032 \qquad \nu = 1.0016 \qquad \pi_1 = 12.8766$$

Recall that the thermodynamic state may be specified by any two independent properties. For example, for constant pressure combustion, instead of temperature the enthalpy is known. In this case temperature is unknown and we add an additional equation to our set,

$$H = \sum_{j=1}^{n} \nu_j h_j \tag{3.50}$$

For an isentropic compression or expansion or expansion to a specified pressure, the entropy is given instead of enthalpy or temperature. In this case we add

$$S = \sum_{j=1}^{n} \nu_j \left(s_j^o - R\ln(\nu_j/\nu) + R\ln P\right) \tag{3.51}$$

Finally, if in any case specific volume rather than pressure is known, then we have to minimize the Helmholtz free energy. In this case a similar analysis (Gordon and McBride, 1971) shows that Eq. (3.47) is replaced by

$$\frac{\mu_j^o}{RT} + \ln(\nu_j/\nu) + \ln(RT/v) + \sum_{i=1}^{l} \pi_i a_{ij} = 0 \qquad j = 1,\ldots,n \tag{3.52}$$

For constant volume combustion we include

$$U = \sum_{j=1}^{n} \nu_j (h_j - RT) \tag{3.53}$$

For an isentropic expansion or compression to a specified volume we include

$$S = \sum_{j=1}^{n} \nu_j \left(s_j^o - R\ln(\nu_j/\nu) + R\ln(RT/v)\right) \tag{3.54}$$

A summary of the appropriate sets of equations to solve for given thermodynamic variables follows.

GIVEN PROPERTIES	EQUATIONS REQUIRED
T, P	(3.41), (3.48), (3.47)
H, P	(3.41), (3.48), (3.47), (3.50)
S, P	(3.41), (3.48), (3.47), (3.51)
T, V	(3.41), (3.48), (3.52)
U, V	(3.41), (3.48), (3.52), (3.53)
S, V	(3.41), (3.48), (3.52), (3.54)

Solution of these problems for practical application requires numerical iteration on a computer. Fortunately, there are now several canned computer programs available.

Thermodynamic properties computed using a NASA program called TRANS72 (Svhela and McBride, 1973) for hydrocarbon–air mixtures in which $\beta/\alpha = 2.25$ are given in the chart found on the back cover for the special cases $\phi = 0.8$, 1.0, and 1.2. Results illustrating composition shifts with temperature and equivalence ratio are given in Fig. 3-1 and 3-2 for the case in which $P =$ 50 atm.

Composition as a function of temperature is shown in Fig. 3-2. At this pressure, the composition predicted using Table 3-3 is a good approximation for temperatures less than about 2000 K. At lower pressures, dissociation is even greater, so that at atmospheric pressure Table 3-3 is valid for temperatures less than about 1500 K. Notice that at high temperatures there is a significant amount of nitric oxide (NO). If any gas in an engine cylinder is raised to these high temperatures, that gas will tend toward equilibrium at a rate determined by chemical kinetics. Since the chemistry for most species that contribute to the thermodynamic properties is fast enough in many cases local equilibrium may be assumed. Nitric oxide, however, is significant because it is an air pollutant. Unlike the species of thermodynamic importance, its chemistry is not fast enough to assume that it is in equilibrium concentrations. Likewise, once formed, its chemistry freezes during the expansion stroke so that even in the low-temperature exhaust gases nitric oxides are found. This will be discussed more fully when we deal with emissions.

Composition as a function of equivalence ratio is illustrated in Fig. 3-2. The results show the general trends expected from Fig. 3-1 and Table 3-3 but emphasize that if the equivalence ratio is greater than about 4 the species list becomes quite large and includes solid carbon C(s), hydrogen cyanide HCN, acetylene C_2H_2, and methane CH_4. Thus if anywhere in the cylinder there are fuel air pockets where $\phi \geq 3$, such as in diesel or stratified charge engines, there will be a tendency for these species to form. Similar to nitric oxides, they may freeze when mixed with leaner pockets or when the temperature drops, so these species can appear in the exhaust. With diesel engines, the maximum power is limited by the appearance of solid carbon (smoke) in the exhaust even though the engine is running lean.

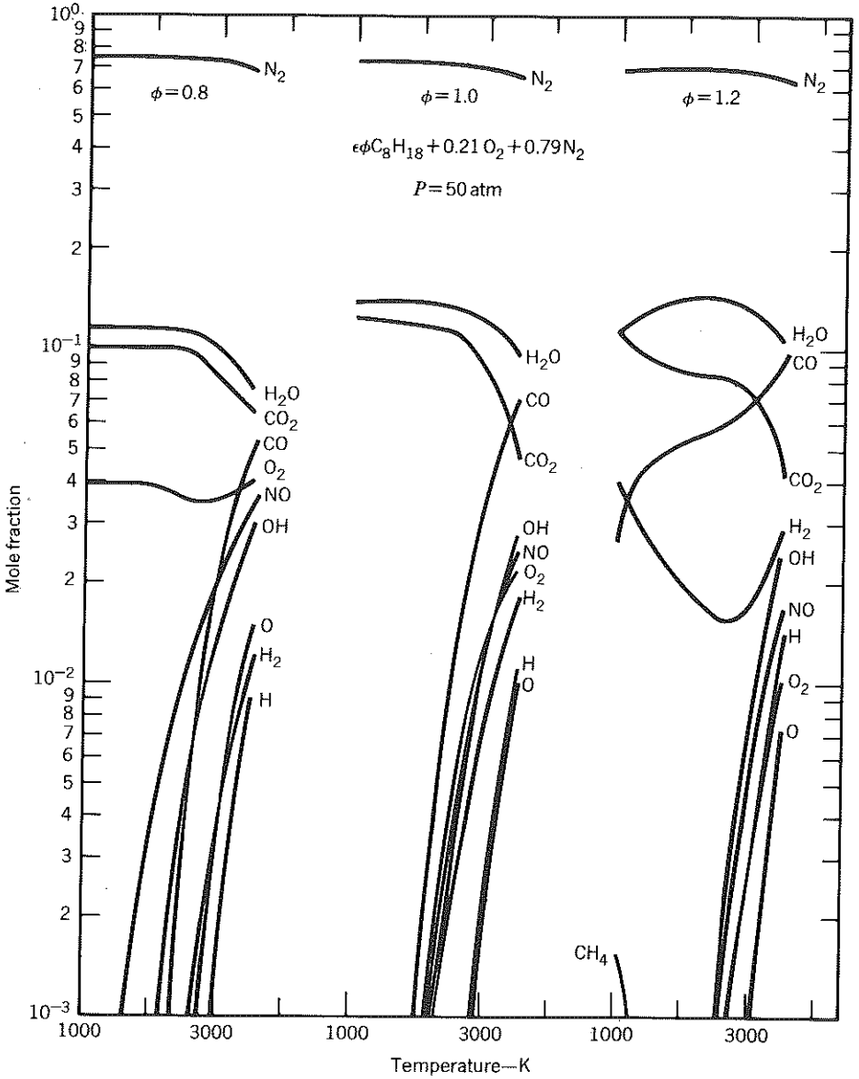

Figure 3-1 Composition of octane–air mixtures at equilibrium for different temperatures at $\phi = 0.8$, 1.0, and 1.2.

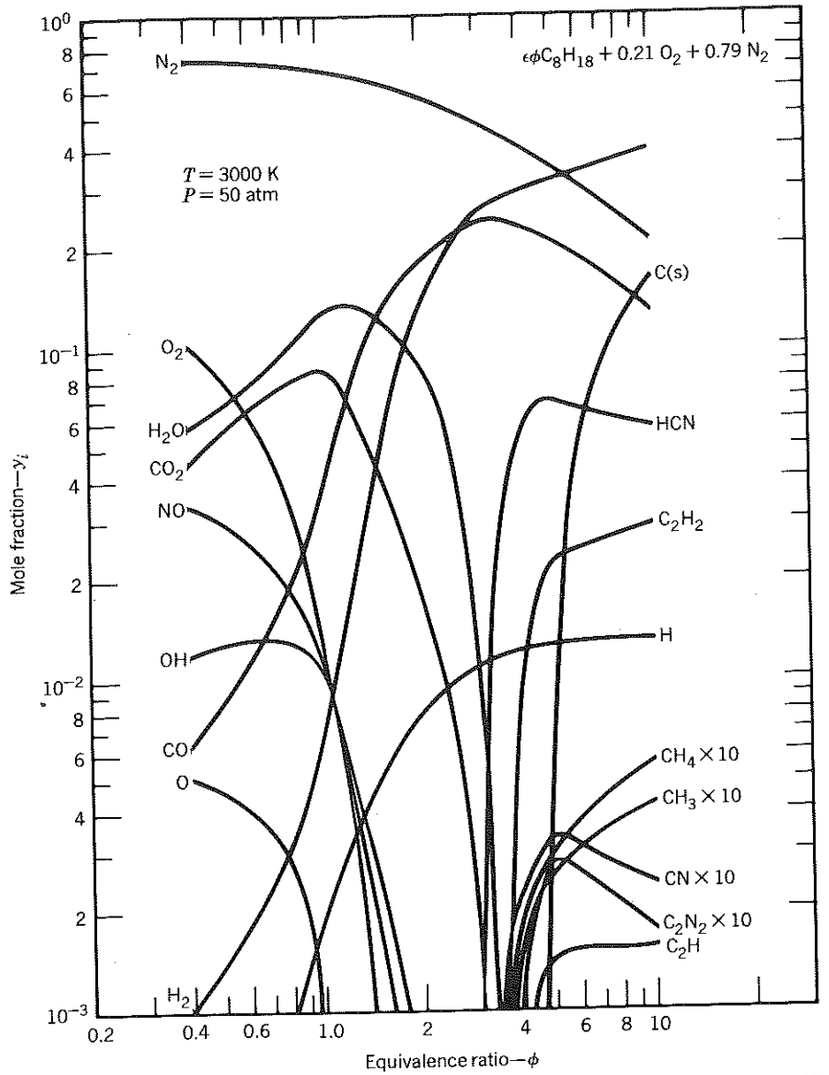

Figure 3-2 Equilibrium composition of octane–air mixture at $T = 3000$ K, P = 50 atm.

3.5 PRACTICAL CHEMICAL EQUILIBRIUM—FORMULATION

Inspection of Figs. 3-1 and 3-2 shows that provided $\phi < 3$, the only species of importance because of dissociation are O, H, OH, and NO. Thus the species list in Eq. (3.38) can be terminated at $i = 10$; that is, we need to consider only 10 species. It is important to recognize that this is not known a priori; it is known from computing with a much larger species list and inspecting the results.

Let us consider the following problem

$$\epsilon\phi C_\alpha H_\beta O_\gamma N_\delta + 0.21O_2 + 0.79N_2 \rightarrow \nu_1 CO_2 + \nu_2 H_2O + \nu_3 N_2 + \nu_4 O_2 + \nu_5 CO + \nu_6 H_2 + \nu_7 H + \nu_8 O + \nu_9 OH + \nu_{10} NO \qquad (3.55)$$

Atom balancing yields the following four equations:

$$\text{C} \quad \epsilon\phi\alpha = (y_1 + y_5)\text{N} \qquad (3.56)$$

$$\text{H} \quad \epsilon\phi\beta = (2y_2 + 2y_6 + y_7 + y_9)\text{N} \qquad (3.57)$$

$$\text{O} \quad \epsilon\phi\gamma + 0.42 = (2y_1 + y_2 + 2y_4 + y_5 + y_8 + y_9 + y_{10})\text{N} \qquad (3.58)$$

$$\text{N} \quad \epsilon\phi\delta + 1.58 = (2y_3 + y_{10})\text{N} \qquad (3.59)$$

where $N = \sum_{i=1}^{10} \nu_i$ is the total number of moles. By definition, the following can be written

$$\sum_{i=1}^{10} y_i - 1 = 0 \qquad (3.60)$$

Introduction of six equilibrium constants will yield eleven equations for the ten unknown mole fractions y_i and the number of moles N. As reactions, consider the following

$$\frac{1}{2}H_2 \rightleftharpoons H \qquad K_1 = \frac{y_7 P^{1/2}}{y_6^{1/2}} \qquad (3.61)$$

$$\frac{1}{2}O_2 \rightleftharpoons O \qquad K_2 = \frac{y_8 P^{1/2}}{y_4^{1/2}} \qquad (3.62)$$

$$\frac{1}{2}H_2 + \frac{1}{2}O_2 \rightleftharpoons OH \qquad K_3 = \frac{y_9}{y_4^{1/2} y_6^{1/2}} \qquad (3.63)$$

$$\frac{1}{2}O_2 + \frac{1}{2}N_2 \rightleftharpoons NO \qquad K_4 = \frac{y_{10}}{y_4^{1/2} y_3^{1/2}} \qquad (3.64)$$

$$H_2 + \frac{1}{2}O_2 \rightleftharpoons H_2O \qquad K_5 = \frac{y_2}{y_4^{1/2} y_6 P^{1/2}} \qquad (3.65)$$

$$CO + \frac{1}{2}O_2 \rightleftharpoons CO_2 \qquad K_6 = \frac{y_1}{y_5 y_4^{1/2} P^{1/2}} \qquad (3.66)$$

Use of equilibrium constants is identical to maximizing the entropy of the gas. This method is simpler when considering restricted species lists such as the present case.

With the composition known, one can proceed to compute the thermodynamic properties of interest: enthalpy, entropy, specific volume, and internal energy. The equilibrium specific heats are computed along the lines outlined in Homework problem 7. A subroutine that does all this is presented in Section 3.7. The next section presents a method of solving the 11 nonlinear equations Eq. (3.56) to (3.66) in 11 unknowns.

3.6 PRACTICAL CHEMICAL EQUILIBRIUM—SOLUTION

This section presents a method developed by Olikara and Borman (1975) to solve for the composition, the equilibrium specific heats, and other partial derivatives useful in thermodynamic analysis.

The unit of pressure in the six equations Eq. (3.61) to (3.66) is the atmosphere. Olikara and Borman (1975) have curve fitted the equilibrium constants to JANAF Table data. Their expressions are of the form

$$\log K_p = A \ln(T/1000) + B/T + C + DT + ET^2 \tag{3.67}$$

where T is in Kelvin. For the range $600 < T < 4000$ K their results are summarized in Table 3-4.

The expressions for equilibrium constants can be rearranged to express mole fractions of all the species in terms of y_3, y_4, y_5, and y_6, the mole fractions of N_2, O_2, CO, and H_2, respectively.

$$y_7 = c_1 y_6^{1/2} \qquad \text{where } c_1 = K_1/P^{1/2} \tag{3.68}$$

$$y_8 = c_2 y_4^{1/2} \qquad \text{where } c_2 = K_2/P^{1/2} \tag{3.69}$$

$$y_9 = c_3 y_4^{1/2} y_6^{1/2} \qquad \text{where } c_3 = K_3 \tag{3.70}$$

$$y_{10} = c_4 y_4^{1/2} y_3^{1/2} \qquad \text{where } c_4 = K_4 \tag{3.71}$$

$$y_2 = c_5 y_4^{1/2} y_6 \qquad \text{where } c_5 = K_5 P^{1/2} \tag{3.72}$$

$$y_1 = c_6 y_4^{1/2} y_5 \qquad \text{where } c_6 = K_6 P^{1/2} \tag{3.73}$$

Table 3-4

	A	B	C	D	E
K_1	0.432168E + 00	−0.112464E + 05	0.267269E + 01	−0.745744E − 04	0.242484E − 08
K_2	0.310805E + 00	−0.129540E + 05	0.321779E + 01	−0.738336E − 04	0.344645E − 08
K_3	−0.141784E + 00	−0.213308E + 04	0.853461E + 00	0.355015E − 04	−0.310227E − 08
K_4	0.150879E − 01	−0.470959E + 04	0.646096E + 00	0.272805E − 05	−0.154444E − 08
K_5	−0.752364E + 00	0.124210E + 05	−0.260286E + 01	0.259556E − 03	−0.162687E − 07
K_6	−0.415302E − 02	0.148627E + 05	−0.475746E + 01	0.124699E − 03	−0.900227E − 08

The number of moles can be eliminated by dividing Eq. (3.57) by Eq. (3.56). One obtains

$$2y_2 + 2y_6 + y_7 + y_9 - \frac{\beta}{\alpha}(y_1 + y_5) = 0 \tag{3.74}$$

Likewise we can divide Eq. (3.58) and Eq. (3.59) to obtain

$$2y_1 + y_2 + 2y_4 + y_5 + y_8 + y_9 + y_{10} - \left[\left(\gamma + \frac{0.42}{\epsilon\phi}\right)\frac{1}{\alpha}(y_1 + y_5)\right] = 0 \tag{3.75}$$

$$2y_3 + y_{10} - \left[\left(\delta + \frac{1.58}{\epsilon\phi}\right)\frac{1}{\alpha}(y_1 + y_5)\right] = 0 \tag{3.76}$$

Defining the ratios

$$d_1 = \frac{\beta}{\alpha} \qquad d_2 = \frac{\gamma}{\alpha} + \frac{0.42}{\epsilon\phi\alpha} \qquad d_3 = \frac{\delta}{\alpha} + \frac{1.58}{\epsilon\phi\alpha}$$

and substituting Eq. (3.68) through Eq. (3.73) into Eq. (3.74) through (3.76) and into (3.60) one obtains four equations in four unknowns y_3, y_4, y_5, and y_6. The resulting equations are nonlinear and best solved by Newton–Raphson iteration.

The four equations Eq. (3.60) and (3.74) through (3.76) may be written as

$$f_j(y_3, y_4, y_5, y_6) = 0 \qquad j = 1,2,3,4 \tag{3.77}$$

An approximate solution can be obtained by using Table 3-3. Denote this vector as the first approximation

$$\left[y_3^{(1)}, y_4^{(1)}, y_5^{(1)}, y_6^{(1)}\right] \tag{3.78}$$

which is reasonably close to the solution vector

$$\left(y_3^*, y_4^*, y_5^*, y_6^*\right) \tag{3.79}$$

The functions on the left-hand side of Eq. (3.77) can be expanded into a Taylor Series about the known vector. Let

$$\Delta y_1 = y_i^* - y_i^{(1)} \tag{3.80}$$

Then, neglecting second-order and higher derivatives, one obtains four equations that yield approximations to Δy_i; $i = 3,4,5,6$.

$$f_j + \frac{\partial f_j}{\partial y_3}\Delta y_3 + \frac{\partial f_j}{\partial y_4}\Delta y_4 + \frac{\partial f_j}{\partial y_5}\Delta y_5 + \frac{\partial f_j}{\partial y_6}\Delta y_6 \approx 0 \qquad j = 1,2,3,4 \tag{3.81}$$

This set of linear equations can be solved for Δy_i; $i = 3,4,5,6$ using a matrix algebra subroutine employing Gaussian elimination. The second approximation is then

$$y_i^{(2)} = y_i^{(1)} + \Delta y_i \qquad i = 3,4,5,6 \tag{3.82}$$

Using this second approximation as a new first approximation, the procedure is repeated again and again until the changes and the f_j are small

$$|\Delta y_i| \leq \xi \ll 1 \tag{3.83}$$

where ξ is some specified tolerance. A relative change was not used in this case because some of the y_i may be smaller than the uncertainty due to roundoff. Thus one cannot be sure that $|\Delta y_i| \ll y_i^{(2)}$ for every species.

For convenience, define the following partial derivatives

$$D_{ij} = \frac{\partial y_i}{\partial y_j} \quad \begin{matrix} i = 1,2,7,8,9,10 \\ j = 3,4,5,6 \end{matrix}$$

$$D_{jj} = \frac{\partial y_j}{\partial y_j} = 1$$

From Eqs. (3.68) through (3.73) one obtains the following nonzero derivatives

$$D_{76} = \frac{1}{2}\frac{c_1}{y_6^{1/2}} \qquad D_{103} = \frac{1}{2}\frac{c_4 y_4^{1/2}}{y_3^{1/2}}$$

$$D_{84} = \frac{1}{2}\frac{c_1}{y_4^{1/2}} \qquad D_{26} = c_5 y_4^{1/2}$$

$$D_{94} = \frac{1}{2}\frac{c_3 y_6^{1/2}}{y_4^{1/2}} \qquad D_{24} = \frac{1}{2}\frac{c_5 y_6}{y_4^{1/2}}$$

$$D_{96} = \frac{1}{2}\frac{c_3 y_4^{1/2}}{y_6^{1/2}} \qquad D_{14} = \frac{1}{2}\frac{c_6 y_5}{y_4^{1/2}}$$

$$D_{104} = \frac{1}{2}\frac{c_4 y_3^{1/2}}{y_4^{1/2}} \qquad D_{15} = c_6 y_4^{1/2}$$

Writing Eq. (3.81) in matrix notation as $[A][Z] - [B] = 0$ the matrix elements are then

$$[B] = [-f]$$
$$[Z] = [\Delta y]$$

and

$$A_{11} = \frac{\partial f_1}{\partial y_3} = 1 + D_{103}$$

$$A_{12} = \frac{\partial f_1}{\partial y_4} = D_{14} + D_{24} + 1 + D_{84} + D_{104} + D_{94}$$

$$A_{13} = \frac{\partial f_1}{\partial y_5} = D_{15} + 1$$

$$A_{14} = \frac{\partial f_1}{\partial y_6} = D_{26} + 1 + D_{76} + D_{96}$$

$$A_{21} = \frac{\partial f_2}{\partial y_3} = 0$$

$$A_{22} = \frac{\partial f_2}{\partial y_4} = 2D_{24} + D_{94} - d_1 D_{14}$$

$$A_{23} = \frac{\partial f_2}{\partial y_5} = -d_1 D_{15} - d_1$$

$$A_{24} = \frac{\partial f_2}{\partial y_6} = 2D_{26} + 2 + D_{76} + D_{96}$$

$$A_{31} = \frac{\partial f_3}{\partial y_3} = D_{103}$$

$$A_{32} = \frac{\partial f_3}{\partial y_4} = 2D_{14} + D_{24} + 2 + D_{84} + D_{94} + D_{104} - d_2 D_{14}$$

$$A_{33} = \frac{\partial f_3}{\partial y_5} = 2D_{15} + 1 - d_2 D_{15} - d_2$$

$$A_{34} = \frac{\partial f_3}{\partial y_6} = D_{26} + D_{96}$$

$$A_{41} = \frac{\partial f_4}{\partial y_3} = 2 + D_{103}$$

$$A_{42} = \frac{\partial f_4}{\partial y_4} = D_{104} - d_3 D_{14}$$

$$A_{43} = \frac{\partial f_3}{\partial y_5} = d_3 D_{15} - d_3$$

$$A_{44} = \frac{\partial f_4}{\partial y_6} = 0$$

Solution of the matrix equation $[A][\Delta y] + [f] = 0$ yields the Δy_i required in Eq. (3.82).

Evaluating the equilibrium specific heat requires the change in mole fraction due to a change in temperature (refer to Homework problem 7).

Examination of Eq. (3.68) through (3.73) reveals that four independent derivatives are required, that is,

$$\frac{\partial y_i}{\partial T} \qquad i = 3,4,5,6$$

since the remaining derivatives can be expressed in terms of this independent set.

$$\frac{\partial y_7}{\partial T} = y_6^{1/2}\frac{\partial c_1}{\partial T} + D_{76}\frac{\partial y_6}{\partial T} \tag{3.84}$$

$$\frac{\partial y_8}{\partial T} = y_4^{1/2}\frac{\partial c_2}{\partial T} + D_{84}\frac{\partial y_4}{\partial T} \tag{3.85}$$

$$\frac{\partial y_9}{\partial T} = y_4^{1/2}y_6^{1/2}\frac{\partial c_3}{\partial T} + D_{94}\frac{\partial y_4}{\partial T} + D_{96}\frac{\partial y_6}{\partial T} \tag{3.86}$$

$$\frac{\partial y_{10}}{\partial T} = y_4^{1/2}y_3^{1/2}\frac{\partial c_4}{\partial T} \tag{3.87}$$

$$\frac{\partial y_2}{\partial T} = y_4^{1/2}y_6\frac{\partial c_5}{\partial T} + D_{24}\frac{\partial y_4}{\partial T} + D_{26}\frac{\partial y_6}{\partial T} \tag{3.88}$$

$$\frac{\partial y_1}{\partial T} = y_4^{1/2}y_5\frac{\partial c_6}{\partial T} + D_{14}\frac{\partial y_4}{\partial T} + D_{15}\frac{\partial y_5}{\partial T} \tag{3.89}$$

The independent set of derivatives is obtained by solution of the matrix equation that results from differentiating Eq. (3.77) with respect to T

$$\frac{\partial f_j}{\partial T} + \frac{\partial f_j}{\partial y_3}\frac{\partial y_3}{\partial T} + \frac{\partial f_j}{\partial y_4}\frac{\partial y_4}{\partial T} + \frac{\partial f_j}{\partial y_5}\frac{\partial y_5}{\partial T} + \frac{\partial f_j}{\partial y_6}\frac{\partial y_6}{\partial T} = 0 \tag{3.90}$$

$$j = 1,2,3,4$$

In matrix form

$$[A]\left[\frac{\partial y}{\partial T}\right] + \left[\frac{\partial f}{\partial T}\right] = 0 \tag{3.91}$$

where the matrix A is seen to be identical to that used earlier in the Newton–Raphson iteration. To evaluate $\partial f/\partial T$, define

$$x_i = \frac{y_i}{c_{i-6}} \qquad \text{where } i = 7,\ldots,10$$

$$x_1 = \frac{y_1}{c_6}$$

$$x_2 = \frac{y_2}{c_5} \tag{3.92}$$

Inspection of Eq. (3.68) through (3.73) reveals that x_i are functions of y_i; $i = 3,4,5,6$ only.

Substitution of x_i into Eq. (3.74) through (3.76) and into (3.60) followed by differentiation with respect to T yields

$$\frac{\partial f_1}{\partial T} = \frac{\partial c_6}{\partial T}x_1 + \frac{\partial c_5}{\partial T}x_2 + \frac{\partial c_1}{\partial T}x_7 + \frac{\partial c_2}{\partial T}x_8 + \frac{\partial c_3}{\partial T}x_9 + \frac{\partial c_4}{\partial T}x_{10} \tag{3.93}$$

$$\frac{\partial f_2}{\partial T} = 2\frac{\partial c_5}{\partial T}x_2 + \frac{\partial c_1}{\partial T}x_7 + \frac{\partial c_3}{\partial T}x_9 - d_1\frac{\partial c_6}{\partial T}x_1 \tag{3.94}$$

$$\frac{\partial f_3}{\partial T} = 2\frac{\partial c_6}{\partial T}x_1 + \frac{\partial c_5}{\partial T}x_2 + \frac{\partial c_2}{\partial T}x_8 + \frac{\partial c_3}{\partial T}x_9 + \frac{\partial c_4}{\partial T}x_{10} - d_2\frac{\partial c_6}{\partial T}x_1 \tag{3.95}$$

$$\frac{\partial f_4}{\partial T} = \frac{\partial c_4}{\partial T}x_{10} - d_3\frac{\partial c_6}{\partial T}x_1 \tag{3.96}$$

From the expressions for c_i

$$\frac{\partial c_1}{\partial T} = \frac{1}{P^{1/2}}\frac{d\mathrm{K}_1}{dT} \qquad \frac{\partial c_4}{\partial T} = \frac{d\mathrm{K}_4}{dT}$$

$$\frac{\partial c_2}{\partial T} = \frac{1}{P^{1/2}}\frac{d\mathrm{K}_2}{dT} \qquad \frac{\partial c_5}{\partial T} = P^{1/2}\frac{d\mathrm{K}_5}{dT}$$

$$\frac{\partial c_3}{\partial T} = \frac{d\mathrm{K}_3}{dT} \qquad \frac{dc_6}{dT} = P^{1/2}\frac{d\mathrm{K}_6}{dT}$$

From Eq. (3.67) it follows that

$$\frac{d\mathrm{K}_i}{dT} = 2.302585\mathrm{K}_i\left[\frac{A}{T} - \frac{B}{T^2} + D + 2ET\right]$$

A reacting mixture of ideal gases has an enthalpy dependent on temperature *and* pressure. For this reason partial derivatives with respect to pressure are also useful. Their evaluation is along the lines of Eq. (3.84) through (3.96) with $\partial/\partial P$ replacing $\partial/\partial T$. Note that neither c_3 nor c_4 depends on pressure, hence terms containing $\partial c_3/\partial P$ and $\partial c_4/\partial P$ drop out. The other derivatives required are

$$\frac{\partial c_1}{\partial P} = -\frac{1}{2}\frac{c_1}{P} \qquad \frac{\partial c_5}{\partial P} = \frac{1}{2}\frac{c_5}{P}$$

$$\frac{\partial c_2}{\partial P} = -\frac{1}{2}\frac{c_2}{P} \qquad \frac{\partial c_6}{\partial P} = \frac{1}{2}\frac{c_6}{P}$$

where P is in bars (or whatever unit is preferred; however in Eq. (3.68) through (3.73) P must be in atmospheres). Solution of all these equations, starting with Eq. (3.89) yields $\partial y_i/\partial T$ and $\partial y_i/\partial P$ for $i = 1,\ldots,10$.

The thermodynamic derivatives sought are

$$c_P = \left(\frac{\partial h}{\partial T}\right)_P = \frac{1}{M}\left[\sum_{i=1}^{10}\left(y_i c_{p_i} + h_i\frac{\partial y_i}{\partial T}\right) - \frac{hM_T}{M}\right] \tag{3.97}$$

$$\left(\frac{\partial \ln v}{\partial \ln T}\right)_P = 1 - \frac{TM_T}{M} \tag{3.98}$$

$$\left(\frac{\partial \ln v}{\partial \ln P}\right)_T = -1 - \frac{PM_P}{M} \tag{3.99}$$

where

$$M_T = \frac{\partial M}{\partial T} = \sum_{i=1}^{10} M_i \frac{\partial y_i}{\partial T} \tag{3.100}$$

$$M_P = \frac{\partial M}{\partial P} = \sum_{i=1}^{10} M_i \frac{\partial y_i}{\partial P} \tag{3.101}$$

The specific heat data from Gordon and McBride (1971) required for Eq. (3.22) through (3.24) are given in the computer subroutine of the next section. The format used is identical to that employed to enter Table 3-1 into the subroutine FARG previously considered.

3.7 A SUBROUTINE FOR EQUILIBRIUM COMBUSTION PRODUCTS

```
C*****************************************************************
C
      SUBROUTINE ECP (P, T, PHI, H, U, V, S, Y, CP, DLVLT, DLVLP, IER)
C
C     PURPOSE:
C        COMPUTE THE PROPERTIES OF EQUILIBRIUM COMBUSTION
C        PRODUCTS
C
C     GIVEN:
C        P       - PRESSURE (BARS)
C        T       - TEMPERATURE (K)
C        PHI     - FUEL AIR EQUIVALENCE RATIO
C
C     RETURNS:
C        H       - ENTHALPY (J/G)
C        U       - INTERNAL ENERGY (J/G)
C        V       - SPECIFIC VOLUME (CM**3/G)
C        S       - ENTROPY (J/G/K)
C        Y       - A TEN DIMENSIONAL COMPOSITION VECTOR OF
C                  MOLE FRACTIONS
C                  1=CO2, 2=H2O, 3=N2, 4=O2, 5=CO, 6=H2
C                  7=H, 8=O, 9=OH, 10=NO
C        CP      - SPECIFIC HEAT AT CONSTANT PRESSURE (J/G/K)
C        DLVLT   - DERIVATIVE OF LOG VOLUME WITH RESPECT TO LOG
C                  TEMPERATURE AT CONSTANT PRESSURE
C        DLVLP   - DERIVATIVE OF LOG VOLUME WITH RESPECT TO LOG
C                  PRESSURE AT CONSTANT TEMPERATURE
C        IER     - AN ERROR MESSAGE
C              0 - NORMAL
C              1 - CONVERGENCE FAILURE: COMPOSITION LOOP
C              2 - CALLED WITH TOO HIGH AN EQUIVALENCE RATIO; C(S)
C                  AND OTHER SPECIES WOULD FORM
C
C     REMARKS:
C        1. VALID FOR 300 < T < 4000
C        2. ASSUMES THE FUEL IS GASOLINE. TO CHANGE FUELS
C           ONLY THE FUEL DATA STATEMENT NEEDS MODIFICATION.
C        3. THE ENTHALPIES OF H2, O2, N2 AND C(S) ARE SET TO
C           ZERO AT 298K
C        4. SUBROUTINES REQUIRED: FARG, LEQIF (IMSL)
```



```
C        5. IF ESTIMATES OF Y(I) I=1,10 ARE AVAILBLE THEY SHOULD
C           BE INPUT THROUGH THE ARGUMENT LIST. OTHERWISE INPUT
C           ZERO'S AND THE ROUTINE WILL MAKE ITS OWN ESTIMATES
C
C*****************************************************************
C
      REAL M, MW, K, KP, MT, MP
      LOGICAL CHECK
      DIMENSION M(10), K(6), C(6), Y(10), D(3), B(4), A(4,4), YD(6),
     &          KP(5,6), DFDT(4), DCDT(6), DKDT(6), DCDP(6),
     &          DYDT(10), DYDP(10), AO(7,10), DFDP(4), CPO(10), HO(10),
     &          SO(10), WK(12)
C
C     FUEL DATA
C
      DATA ALPHA/7.0/, BETA/17.0/, GAMMA/0./, DELTA/0./
C
C     SPECIFIC HEAT DATA FROM GORDON AND MCBRIDE (1971)
C
      DATA AO/
     1  .44608041E+01,  .30981719E-02, -.12392571E-05,  .22741325E-09,
     1 -.15525954E-13, -.48961442E+05, -.98635982E+00,
     2  .27167633E+01,  .29451374E-02, -.80224374E-06,  .10226682E-09,
     2 -.48472145E-14, -.29905826E+05,  .66305671E+01,
     3  .28963194E+01,  .15154866E-02, -.57235277E-06,  .99807393E-10,
     3 -.65223555E-14, -.90586184E+03,  .61615148E+01,
     4  .36219535E+01,  .73618264E-03, -.19652228E-06,  .36201558E-10,
     4 -.28945627E-14, -.12019825E+04,  .36150960E+01,
     5  .29840696E+01,  .14891390E-02, -.57899684E-06,  .10364577E-09,
     5 -.69353550E-14, -.14245228E+05,  .63479156E+01,
     6  .31001901E+01,  .51119464E-03,  .52644210E-07, -.34909973E-10,
     6  .36945345E-14, -.87738042E+03, -.19629421E+01,
     7  .25000000E+01, 0., 0., 0., 0.,  .25471627E+05, -.46011763E+00,
     8  .55420596E+01, -.27550619E-04, -.31028033E-08,  .45510674E-11,
     8 -.43680515E-15,  .29230803E+05,  .49203080E+01,
     9  .29106427E+01,  .95931650E-03, -.19441702E-06,  .13756646E-10,
     9  .14224542E-15,  .39353815E+04,  .54423445E+01,
     #  .31890000E+01,  .13382281E-02, -.52899318E-06,  .95919332E-10,
     # -.64847932E-14,  .98283290E+04,  .67458126E+01/
C
C     EQUILIBRIUM CONSTANT DATA FROM OLIKARA AND BORMAN (1975)
C
      DATA KP/
     1  .432168E+00, -.112464E+05, .267269E+01, -.745744E-04,
     1  .242484E-08,
     2  .310805E+00, -.129540E+05, .321779E+01, -.738336E-04,
     2  .344645E-08,
     3 -.141784E+00, -.213308E+04, .853461E+00, .355015E-04,
     3 -.310227E-08,
     4  .150879E-01, -.470959E+04, .646096E+00, .272805E-05,
     4 -.154444E-08,
     5 -.752364E+00,  .124210E+05, -.260286E+01, .259556E-03,
     5 -.162687E-07,
     6 -.415302E-02,  .148627E+05, -.475746E+01, .124699E-03,
     6 -.900227E-08/
C
C     MOLECULAR WEIGHTS
C
      DATA M/44.01, 18.02, 28.008, 32., 28.01, 2.018, 1.009, 16.,
     &       17.009, 30.004/
```

```
C
C     OTHER DATA
C
      DATA MAXITS/100/, TOL/3.0E-05/, RU/8.31434/
C
C     MAKE SURE SOLID CARBON WILL NOT FORM
C
      IER = 2
      EPS = .210/(ALPHA + 0.25*BETA - 0.5*GAMMA)
      IF( PHI .GT. (.210/EPS/(0.5*ALPHA - 0.5*GAMMA)) ) RETURN
      IER = 0
C
C     DECIDE IF AN INTIAL ESTIMATE TO THE COMPOSITION IS
C     REQUIRED OR IF T < 1000 IN WHICH CASE FARG WILL SUFFICE
C
C
      SUM = 0.
      DO 10 I = 1,10
10    SUM = SUM + Y(I)
      IF( T .GT. 1000. .AND. SUM .GT. 0.998 ) GO TO 20
      CALL FARG(P,T,PHI,1.,H,U,V,S,YO,CP,DLVLT,DLVLP)
      DO 30 I = 1,10
30    Y(I) = 0.
      DO 40 I = 1,6
40    Y(I) = YO(I)
      IF( T .LE. 1000. ) RETURN
20    CONTINUE
C
C     EVALUATE THE REQUISITE CONSTANTS
C
      PATM = .9869233*P
      DO 50 I = 1,6
50    K(I) = 10.**(KP(1,I)*ALOG(T/1000.) + KP(2,I)/T + KP(3,I) +
     &       KP(4,I)*T + KP(5,I)*T*T)
      C(1) = K(1)/SQRT(PATM)
      C(2) = K(2)/SQRT(PATM)
      C(3) = K(3)
      C(4) = K(4)
      C(5) = K(5)*SQRT(PATM)
      C(6) = K(6)*SQRT(PATM)
      D(1) = BETA/ALPHA
      D(2) = (GAMMA + .42/EPS/PHI)/ALPHA
      D(3) = (DELTA + 1.58/EPS/PHI)/ALPHA
C
C     SET UP ITERATION LOOP FOR NEWTON-RAPHSON ITERATION AND
C     INTRODUCE TRICK TO PREVENT INSTABILITIES NEAR PHI = 1.0
C     AT LOW TEMPEARTURES ON 24 BIT MACHINES (VAX). SET
C     TRICK = 1.0 ON 48 BIT MACHINES (CDC)
C
      TRICK = 10.
      CHECK = ABS(PHI - 1.0) .LT. TOL
      IF(CHECK) PHI = PHI*(1.0 + SIGN(TOL,PHI - 1.0))
      ICHECK = 0
      DO 5 J = 1,MAXITS
      DO 4 JJ = 1,10
4     Y(JJ) = AMIN1(1.0,AMAX1(Y(JJ),1.0E-25))
      D76 = 0.5*C(1)/SQRT(Y(6))
      D84 = 0.5*C(1)/SQRT(Y(4))
      D94 = 0.5*C(3)*SQRT(Y(6)/Y(4))
      D96 = 0.5*C(3)*SQRT(Y(4)/Y(6))
```



```
      D103 = 0.5*C(4)*SQRT(Y(4)/Y(3))
      D104 = 0.5*C(4)*SQRT(Y(3)/Y(4))
      D24 = 0.5*C(5)*Y(6)/SQRT(Y(4))
      D26 = C(5)*SQRT(Y(4))
      D14 = 0.5*C(6)*Y(5)/SQRT(Y(4))
      D15 = C(6)*SQRT(Y(4))
      A(1,1) = 1. + D103
      A(1,2) = D14 + D24 + 1. + D84 + D104 + D94
      A(1,3) = D15 + 1.0
      A(1,4) = D26 + 1.0 + D76 + D96
      A(2,1) = 0.0
      A(2,2) = 2.0*D24 + D94 - D(1)*D14
      A(2,3) = -D(1)*D15 - D(1)
      A(2,4) = 2.0*D26 + 2.0 + D76 + D96
      A(3,1) =  D103
      A(3,2) = 2.0*D14 + D24 + 2.0 + D84 + D94 + D104 - D(2)*D14
      A(3,3) = 2.0*D15 + 1.0 - D(2)*D15 - D(2)
      A(3,4) = D26 + D96
      A(4,1) = 2.0 + D103
      A(4,2) = D104 - D(3)*D14
      A(4,3) = -D(3)*D15 - D(3)
      A(4,4) = 0.
C
C     SOLVE THE MATRIX EQUATIONS 3.81 FOR COMPOSITION CORRECTIONS
C
      SUM = 0.
      DO 55 I = 1,10
55    SUM = SUM + Y(I)
      B(1) = -(SUM - 1.0)
      B(2) = -(2.0*Y(2) + 2.0*Y(6) + Y(7) + Y(9) - D(1)*Y(1) -
     &         D(1)*Y(5))
      B(3) = -(2.0*Y(1) + Y(2) + 2.0*Y(4) + Y(5) + Y(8) + Y(9)
     &     +   Y(10) -   D(2)*Y(1) - D(2)*Y(5))
      B(4) = -(2.0*Y(3) + Y(10) - D(3)*Y(1) - D(3)*Y(5))
      CALL LEQIF(A, 4, 4, 4, B, 4, 1, 0, WK, IERROR)
      ERROR = 0.
      DO 56 L = 3,6
      LL = L - 2
      Y(L) = Y(L) + B(LL)/TRICK
      ERROR = AMAX1(ERROR,ABS(B(LL)))
      Y(L) = AMIN1(1.0,AMAX1(Y(L),1.0E-25))
56    CONTINUE
      Y(7) = C(1)*SQRT(Y(6))
      Y(8) = C(2)*SQRT(Y(4))
      Y(9) = C(3)*SQRT(Y(4)*Y(6))
      Y(10)= C(4)*SQRT(Y(4)*Y(3))
      Y(2) = C(5)*SQRT(Y(4))*Y(6)
      Y(1) = C(6)*SQRT(Y(4))*Y(5)
      IF(ERROR .LT. TOL)  ICHECK = ICHECK + 1
      IF(ERROR .LT. TOL .AND. ICHECK .GE. 2) GO TO 57
5     CONTINUE
      IER = 1
C
C     COMPUTE THE REQUISITE CONSTANTS TO FIND PARTIAL DERIVATIVES
C
57    DO 60 I = 1,6
60    DKDT(I) = 2.302585*K(I)*(KP(1,I)/T - KP(2,I)/T/T + KP(4,I)
     &        + 2.0*KP(5,I)*T)
      DCDT(1) = DKDT(1)/SQRT(PATM)
      DCDT(2) = DKDT(2)/SQRT(PATM)
```

```
      DCDT(3) = DKDT(3)
      DCDT(4) = DKDT(4)
      DCDT(5) = DKDT(5)*SQRT(PATM)
      DCDT(6) = DKDT(6)*SQRT(PATM)
      DCDP(1) = -0.5*C(1)/P
      DCDP(2) = -0.5*C(2)/P
      DCDP(5) =  0.5*C(5)/P
      DCDP(6) =  0.5*C(6)/P
      X1 = Y(1)/C(6)
      X2 = Y(2)/C(5)
      X7 = Y(7)/C(1)
      X8 = Y(8)/C(2)
      X9 = Y(9)/C(3)
      X10= Y(10)/C(4)
      DFDT(1) = DCDT(6)*X1 + DCDT(5)*X2 + DCDT(1)*X7 + DCDT(2)*X8
     &        + DCDT(3)*X9 + DCDT(4)*X10
      DFDT(2) = 2.0*DCDT(5)*X2 + DCDT(1)*X7 + DCDT(3)*X9 -
     &          D(1)*DCDT(6)*X1
      DFDT(3) = 2.0*DCDT(6)*X1 + DCDT(5)*X2 + DCDT(2)*X8
     &        + DCDT(3)*X9 + DCDT(4)*X10 - D(2)*DCDT(6)*X1
      DFDT(4) = DCDT(4)*X10 - D(3)*DCDT(6)*X1
      DFDP(1) = DCDP(6)*X1 + DCDP(5)*X2 + DCDP(1)*X7 + DCDP(2)*X8
      DFDP(2) = 2.0*DCDP(5)*X2 + DCDP(1)*X7 - D(1)*DCDP(6)*X1
      DFDP(3) = 2.0*DCDP(6)*X1 + DCDP(5)*X2 + DCDP(2)*X8 -
     &          D(2)*DCDP(6)*X1
      DFDP(4) = -D(3)*DCDP(6)*X1
C
C     SOLVE THE MATRIX EQUATIONS 3.91 FOR THE INDEPENDENT DERIVATIVES
C     AND THEN DETERMINE THE DEPENDENT DERIVATIVES
C
      DO 70 I = 1,4
70    B(I) = -DFDT(I)
      CALL LEQIF(A, 4, 4, 4, B, 4, 1, 1, WK, IERROR)
      DYDT(3) = B(1)
      DYDT(4) = B(2)
      DYDT(5) = B(3)
      DYDT(6) = B(4)
      DYDT(1) = SQRT(Y(4))*Y(5)*DCDT(6) + D14*DYDT(4) + D15*DYDT(5)
      DYDT(2) = SQRT(Y(4))*Y(6)*DCDT(5) + D24*DYDT(4) + D26*DYDT(6)
      DYDT(7) = SQRT(Y(6))*DCDT(1) + D76*DYDT(6)
      DYDT(8) = SQRT(Y(4))*DCDT(2) + D84*DYDT(4)
      DYDT(9) = SQRT(Y(4)*Y(6))*DCDT(3) + D94*DYDT(4) + D96*DYDT(6)
      DYDT(10)= SQRT(Y(4)*Y(3))*DCDT(4) + D104*DYDT(4) + D103*DYDT(3)
C
      DO 80 I = 1,4
80    B(I) = -DFDP(I)
      CALL LEQIF(A, 4, 4, 4, B, 4, 1, 1, WK, IERROR)
      DYDP(3) = B(1)
      DYDP(4) = B(2)
      DYDP(5) = B(3)
      DYDP(6) = B(4)
      DYDP(1) = SQRT(Y(4))*Y(5)*DCDP(6) + D14*DYDP(4) + D15*DYDP(5)
      DYDP(2) = SQRT(Y(4))*Y(6)*DCDP(5) + D24*DYDP(4) + D26*DYDP(6)
      DYDP(7) = SQRT(Y(6))*DCDP(1) + D76*DYDP(6)
      DYDP(8) = SQRT(Y(4))*DCDP(2) + D84*DYDP(4)
      DYDP(9) = D94*DYDP(4) + D96*DYDP(6)
      DYDP(10)= D104*DYDP(4) + D103*DYDP(3)
C
C
C     COMPUTE THE THERMODYNAMIC PROPERTIES
```



```
C
      DO 90 I = 1,10
      CPO(I) = AO(1,I) + AO(2,I)*T + AO(3,I)*T*T + AO(4,I)*T**3
     &       + AO(5,I)*T**4
      HO(I) = AO(1,I) + AO(2,I)/2.*T + AO(3,I)/3.*T*T + AO(4,I)/4.*
     &        T**3 + AO(5,I)/5.*T**4 + AO(6,I)/T
90    SO(I) = AO(1,I)*ALOG(T) + AO(2,I)*T + AO(3,I)/2.*T**2
     &      + AO(4,I)/3.*T**3 + AO(5,I)/4.*T**4 + AO(7,I)
C
C     Y(1),Y(2) ARE REEVALUTED TO CLEAN UP ANY ROUND-OFF ERRORS WHICH
C     CAN OCCUR FOR THE LOW TEMPERATURE STOICHIOMETRIC SOLUTIONS
C
      Y(1) = (2.*Y(3) + Y(10))/D(3) - Y(5)
      Y(2) = (D(1)/D(3)*(2.*Y(3) + Y(10)) - 2.*Y(6) - Y(7) - Y(9))/2.
C

      MW = 0.
      CP = 0.
      H = 0.
      S = 0.
      MT = 0.
      MP = 0.
      DO 100 I = 1,10
      IF( Y(I) .LE. 1.0E-25 ) GO TO 100
      H = H + HO(I)*Y(I)
      MW = MW + M(I)*Y(I)
      MT = MT + M(I)*DYDT(I)
      MP = MP + M(I)*DYDP(I)
      CP = CP + Y(I)*CPO(I) + HO(I)*T*DYDT(I)
      S = S + Y(I)*(SO(I) - ALOG(Y(I)))
100   CONTINUE
C
      R = RU/MW
      V = 10.*R*T/P
      CP = R*(CP - H*T*MT/MW)
      DLVLT =  1.0 + AMAX1(-T*MT/MW,0.)
      DLVLP = -1.0 - AMAX1( P*MP/MW,0.)
      H = H*R*T
      S = R*(-ALOG(PATM) + S)
      U = H - R*T
      RETURN
      END
```

3.8 LIQUIDS AND LIQUID–VAPOR–GAS MIXTURES

The thermodynamics involved with fuel injection, carburetion, water injection, and water condensation can be complicated. Fortunately, we can make some simplifications that are quite accurate for our intended use.

First let us consider a pure substance in terms of its compressed liquid, saturated liquid, saturated vapor, and superheated vapor states. The simplifications that we will introduce are

- Compressed and saturated liquids are incompressible.
- Saturated and superheated vapors are ideal gases.

For an incompressible substance, it can be shown that the internal energy and entropy depend only on temperature. Hence the approximation for compressed liquids can be

$$u = u_f(T) \tag{3.102}$$

$$s = s_f(T) \tag{3.103}$$

where the notation $u_f(T)$ and $s_f(T)$ denote the internal energy and entropy of saturated liquid at the temperature T.

The enthalpy of an incompressible substance depends on pressure, and it is consistent with Eq. (3.102) and (3.103) to assume that

$$h = h_f^o(T) + (P - P_{\text{atm}})v \tag{3.104}$$

where h_f^o is the enthalpy at atmospheric pressure. The only property remaining to be prescribed is the specific volume. Let us choose it to be the specific volume of compressed liquid at atmospheric pressure as these data are readily available.

$$v = v^o(T_1) \tag{3.105}$$

where T_1 is the initial temperature in the process being analyzed.

To introduce the enthalpy of vaporization into our equations of state for the liquids is convenient since these data are usually easier to find than the

Table 3-5 Ideal Gas Enthalpy, Enthalpy of Vaporization, Saturation Vapor Pressure, and Specific Volume of Some Liquid Fuels at $T = 298$ K

FORMULA	NAME	h_g^a (kJ/mole)	h_{fg} (kJ/mole)	P_{sat} (bar)	v^o (cm^3/g)
CH_3NO_2	Nitromethane	−74.73	38.37	0.050	0.879
CH_4O	Methanol	−201.17	37.92	0.186	1.264
C_2H_6O	Ethanol	−234.81	42.34	0.084	1.267
$C_4H_{10}O$	Ethyl ether	−252.21	26.53	0.733	1.413
C_5H_{12}	n-pentane	−146.00	26.44	0.710	1.597
C_6H_{14}	Hexane	−167.19	31.49	0.242	1.514
C_6H_6	Benzene	+82.93	34.02	0.129	1.138
C_7H_{17}	Gasoline[b]	−267.12	38.51	[c]	1.449
C_8H_{18}	Octane	−208.45	41.51	0.022	1.423
C_8H_{18}	Isooctane	−224.14	35.11	0.071	1.445
C_8H_{10}	Ethylbenzene	+29.29	42.01	0.013	1.153
$C_{12}H_{26}$	n-dodecane	−290.87	61.32	< 0.001	1.336
$C_{14}H_{30}$	Tetradecane	−332.13	71.24	< 0.001	1.311
$C_{14.4}H_{24.9}$	T–T diesel fuel[b]	−100.00	74.08	[c]	1.176
$C_{16}H_{34}$	Hexadecane (cetane)	−373.34	81.14	< 0.001	1.293
$C_{19}H_{40}$	Nonadecane	−435.14	95.03	< 0.001	1.286
H_2O	Water	−241.83	44.02	0.031	1.000

Source: P_{sat} and v^o are from the CRC Handbook (1975–1976); h_{fg} is from N. B. Vargaflik (1975); and h_g is from Stull et al. (1969).

[a] Also called the enthalpy of formation at $T = 298$ K.

[b] Estimated for typical fuel.

[c] Applies only to a pure substance.

saturated liquid data. We then have

$$h = h_g - h_{fg} + (P - P_{\text{atm}})v \tag{3.106}$$

Unlike specific volume, data for the enthalpy of vaporization at saturation pressure are readily available. Hence we choose

$$h_{fg} = h_{fg}(T_1) \tag{3.107}$$

where, again, T_1 is the temperature as the start of the process being analyzed.

Typically

$$|P - P_{\text{atm}}|v \ll |h_{fg}| \quad \text{and} \quad |Pv| \ll |h| \tag{3.108}$$

so that in many cases we can write for liquids

$$h \approx h_g - h_{fg} \tag{3.109}$$

$$u \approx h \tag{3.110}$$

Table 3-5 gives the enthalpy of vaporization, the ideal gas enthalpy, the specific volume of compressed liquid, and the saturation pressure of several substances at $T = 298$ K. Table 3-6 gives most of the same data for octane but at different temperatures.

We will also deal with mixtures of gases in contact with a liquid phase. In these cases we assume

- The liquid contains no dissolved gases.
- The gases are ideal.
- At equilibrium the partial pressure of the liquid's vapor is equal to the saturation pressure corresponding to the mixture temperature.

Let χ denote the quality of the condensable substance, that is, the ratio of vapor to liquid and vapor. The enthalpy of the system is then

$$H = (1 - \chi)m_1(h_{g,1} - h_{fg}) + \chi m_1 h_1 + \sum_{i=1}^{n} m_i h_i \tag{3.111}$$

Table 3-6 Enthalpy of Vaporization, Saturation Vapor Pressure, and Atmospheric Specific Volume of Octane

T (K)	h_{fg} (kJ/mole)	P_{sat} (bar)	v^o (cm^3/g)
298	41.50	0.018	1.432
325	39.99	0.075	1.479
350	38.22	0.211	1.527
375	36.45	0.503	1.579
400	34.46	1.058	1.639
425	32.35	2.003	1.708
450	30.07	3.500	1.789
475	27.49	5.707	1.890
500	24.32	8.837	2.022
550	20.35	13.21	2.214

Source: Vargaftik (1975).

or

$$h = \sum_{i=1}^{n} x_i h_i - (1-\chi) x_1 h_{fg} \tag{3.112}$$

The indexing is chosen so that $i = 1$ corresponds to the condensable substance and $i = 2, \ldots, n$ corresponds to all other gases.

Likewise, the system volume is

$$V = (1-\chi) m_1 (v_{g,1} - v_{fg}) + \chi m_1 v_g + \sum_{i=2}^{n} m_i v_i \tag{3.113}$$

and the specific volume is

$$v = \sum_{i=1}^{n} x_i v_i - (1-\chi) x_1 v_{fg} \tag{3.114}$$

where the v_i are computed at the total pressure (Amagat–Leduc Law of Additive Volumes).

3.9 ISENTROPIC PROCESSES

We wish to compute the change of state due to an isentropic compression or expansion to a specified pressure or specific volume. For a mixture of ideal gases that chemically reacts to changing constraints, such as volume or pressure, simple relationships cannot be derived and we resort to the computer.

Note that the subroutines FARG and ECP both compute the entropy given the temperature and pressure. Represent that computation by

$$s = s(T, P) \tag{3.115}$$

For an isentropic process from P_1 to P_2, it follows by definition that $s_2 = s_1$. To find the unknown temperature, an iteration is required. An efficient means of doing this is provided by the Newton–Raphson method. For this purpose define

$$f = s_2 - s(T_2, P_2) \tag{3.116}$$

Denote the correct solution to the problem as T_2^* and let $T_2^{(1)}$ represent a first approximation to T_2^*. The function $f(T_2)$ can be expanded into a Taylor Series about T_2^*. Let $\Delta T_2 = T_2^* - T_2^{(1)}$; then, neglecting higher order terms, one obtains

$$f + \frac{\partial f}{\partial T_2} \Delta T_2 = 0 \tag{3.117}$$

The derivative is evaluated at $T_2^{(1)}$ and can be expressed in terms of variables returned by FARG and ECP. In fact, any thermodynamic derivative can be expressed in terms of the three derivatives returned by FARG and ECP. The

FORTRAN variable names given to the three derivatives returned are:

$$\text{CP} = c_P = \left(\frac{\partial h}{\partial T}\right)_P$$

$$\text{DLVLP} = \left(\frac{\partial \ln v}{\partial \ln P}\right)_T$$

$$\text{DLVLT} = \left(\frac{\partial \ln v}{\partial \ln T}\right)_P$$

For example, the ratio of specific heats is given by

$$\gamma = \frac{c_P}{c_v} = \frac{c_P}{c_P + \dfrac{Pv}{T}\left(\dfrac{\partial \ln v}{\partial \ln T}\right)_P^2 \Big/ \left(\dfrac{\partial \ln v}{\partial \ln P}\right)_T} \tag{3.118}$$

The derivative required in Eq. (3.117) is

$$\frac{\partial f}{\partial T_2} = -\left(\frac{\partial s}{\partial T}\right)_P = -\frac{c_P}{T} \tag{3.119}$$

These relationships and others found in Lewis and Randall (1961) are summarized in Appendix C.

Substitution of Eq. (3.119) and (3.117) yields

$$\Delta T_2 = \frac{f T_2}{c_{P_2}} \tag{3.120}$$

Hence, an improved estimate of the temperature is given by

$$T_2^{(2)} = T_2^{(1)} + \frac{f T_2^{(1)}}{c_{P_2}} \tag{3.121}$$

Using this second approximation as a new first approximation, the procedure is repeated again and again until ΔT_2 is small; that is,

$$\frac{|\Delta T_2|}{T_2^{(2)}} \le \epsilon \tag{3.122}$$

where ϵ is some specified tolerance.

EXAMPLE 3.4

Fuel, air, and residual gas at $T_1 = 300$ K, $P_1 = 1$, $\phi = 0.8$, and $f = 0.10$ is compressed isentropically to $P_2 = 20$ bars. Find the work $w_{1\to 2}$ and T_2.

SOLUTION:

```
C
      DIMENSION Y(6)
      DATA MAXITS/50/, TOL/.001/
```

```
C
C       ESTABLISH INITIAL CONDITIONS
C
        T1 = 300.
        P1 = 1.0
        PHI = 0.8
        F = 0.1
        CALL FARG(P1, T1, PHI, F, H1, U1, V1, S1, Y, CP, DLVLT, DLVLP)
C
C       MAKE INITIAL ESTIMATE
C
        P2 = 20.
        GAMMA = CP/(CP + P1*V1/T1/10.*DLVLT**2/DLVLP)
        T2 = T1*(P2/P1)**((GAMMA - 1.)/GAMMA)
C
C       DO ITERATION
C
        DELT2 = 2000.
        DO 10 I = 1,MAXITS
        CALL FARG(P2, T2, PHI, F, H2, U2, V2, S2, Y, CP, DLVLT, DLVLP)
        IF( ABS(DELT2)/T2 .LT. TOL ) GO TO 20
        F0 = S1 - S2
        DELT2 = F0*T2/CP
        T2 = T2 + DELT2
10      CONTINUE
        WRITE(6,30)
30      FORMAT(' CONVERGENCE CRITERIA NOT MET ')
20      CONTINUE
C
C       FIND THE WORK FROM FIRST LAW
C
        W12 = -(U2 - U1)
C
C       WRITE THE ANSWERS
C
        WRITE(6,40) T2, W12
40      FORMAT(' T2(K) = ',1PE11.4,2x,' W12(J/G) = ',1PE11.4)
        STOP
        END
```

Running the program above yields:

```
T2(K) = 6.4498E+02        W12(J/G) = -2.8321E+02
```

For an isentropic process from v_1 to v_2, it follows by definition that $s_2 = s_1$. Therefore, we can write two equations in two unknowns to find T_2 and P_2. They are

$$s_2 - s(T_2, P_2) = 0 \tag{3.123}$$

$$v_2 - v(T_2, P_2) = 0 \tag{3.124}$$

Solution is best achieved, again, by Newton–Raphson iteration. To this end we define the following:

$$f_1(x_1, x_2) = s_2 - s(x_1, x_2) \tag{3.125}$$

$$f_2(x_1, x_2) = v_2 - v(x_1, x_2) \tag{3.126}$$

Denote the correct solution to the problem as $x_1^* = T_2$, $x_2^* = P_2$, and let $x_1^{(1)}$ and $x_2^{(2)}$ represent an estimate of the solution. The functions f_1 and f_2 can be expanded into a Taylor Series about x_1^* and x_2^*.

$$\Delta x_i = x_i^* - x_i^{(1)} \qquad i = 1, 2 \tag{3.127}$$

Then, neglecting second-order and higher derivatives, one obtains

$$f_1 + \frac{\partial f_1}{\partial x_1}\Delta x_1 + \frac{\partial f_1}{\partial x_2}\Delta x_2 \approx 0 \tag{3.128}$$

$$f_2 + \frac{\partial f_2}{\partial x_1}\Delta x_1 + \frac{\partial f_2}{\partial x_2}\Delta x_2 \approx 0 \tag{3.129}$$

where

$$\frac{\partial f_1}{\partial x_1} = -\left(\frac{\partial s}{\partial T}\right)_P \qquad \frac{\partial f_1}{\partial x_2} = -\left(\frac{\partial s}{\partial P}\right)_T \tag{3.130}$$

$$\frac{\partial f_2}{\partial x_1} = -\left(\frac{\partial v}{\partial T}\right)_P \qquad \frac{\partial f_2}{\partial x_2} = -\left(\frac{\partial v}{\partial P}\right)_T \tag{3.131}$$

The derivatives are evaluated at $x_1^{(1)}$ and $x_2^{(1)}$. They can be evaluated in terms of derivatives returned by the subroutines, FARG and ECP.

$$\text{CP} = c_P \qquad \text{DLVLP} = \left(\frac{\partial \ln v}{\partial \ln P}\right)_T \qquad \text{DLVLT} = \left(\frac{\partial \ln v}{\partial \ln T}\right)_P$$

The relations needed are

$$-\left(\frac{\partial s}{\partial P}\right)_T = \left(\frac{\partial v}{\partial T}\right)_P = \frac{v}{T}\left(\frac{\partial \ln v}{\partial \ln T}\right)_P \tag{3.132}$$

$$\left(\frac{\partial s}{\partial T}\right)_P = \frac{c_P}{T} \tag{3.133}$$

$$\left(\frac{\partial v}{\partial P}\right)_T = \frac{v}{P}\left(\frac{\partial \ln v}{\partial \ln P}\right)_T \tag{3.134}$$

Equations (3.128) and (3.129) contain two unknowns, Δx_1 and Δx_2. Solution yields

$$\Delta x_1 = \frac{\dfrac{T}{P}\left(\dfrac{\partial \ln v}{\partial \ln P}\right)_T f_1 + \left(\dfrac{\partial \ln v}{\partial \ln T}\right)_P f_2}{\dfrac{c_P}{P}\left(\dfrac{\partial \ln v}{\partial \ln P}\right)_T + \dfrac{v}{T}\left(\dfrac{\partial \ln v}{\partial \ln T}\right)_P^2} \tag{3.135}$$

$$\Delta x_2 = \frac{-\left(\dfrac{\partial \ln v}{\partial \ln T}\right)_P f_1 + \dfrac{c_P}{v} f_2}{\dfrac{c_P}{P}\left(\dfrac{\partial \ln v}{\partial \ln P}\right)_T + \dfrac{v}{T}\left(\dfrac{\partial \ln v}{\partial \ln T}\right)_P^2} \tag{3.136}$$

It follows from Eq. 3.127 that an improved estimate is

$$x_i^{(2)} = x_i^{(1)} + \Delta x_i \qquad i = 1, 2 \tag{3.137}$$

Using this second approximation as a new first approximation, the procedure is repeated again and again until the relative changes are small; that is,

$$\frac{|\Delta x_i|}{x_i^{(2)}} \leq \xi \qquad i = 1,2 \tag{3.138}$$

where ξ is some specified tolerance.

EXAMPLE 3.5

Find the temperature and specific volume after expanding equilibrium combustion products of gasoline and air at $T_1 = 2000$ K, $P_1 = 50$ bars, and $\phi = 1.0$ by a volume ratio $v_2/v_1 = 8$. How much work was done by the gas?

SOLUTION:

```
C
      DIMENSION Y(10)
      DATA MAXITS/50/, TOL/.001/, DX1/2000./, DX2/100./, Y/10*0./
C
C     ESTABLISH INITIAL CONDITIONS
C
      T1 = 2000.
      P1 = 50.
      PHI = 1.0
      CALL ECP(P1,T1,PHI,H1,U1,V1,S1,Y,CP,DLVLT,DLVLP,IER)
      IF( IER .NE. 0) WRITE(6,10) IER
10    FORMAT(' ERROR 10: ECP RETURNED IER = ',I2)
C
C     MAKE AN INITIAL ESTIMATE
C
      V2 = 8.0*V1
      GAMMA = CP/(CP + P1*V1/T1/10.*DLVLT**2/DLVLP)
      T2 = T1*(V1/V2)**(GAMMA - 1.0)
      P2 = P1*(V1/V2)**GAMMA
C
C     DO ITERATION
C
      DO 20 I = 1,MAXITS
      CALL ECP(P2,T2,PHI,H2,U2,V2,S2,Y,CP,DLVLT,DLVLP,IER)
      IF( IER .NE. 0) WRITE(6,30) IER
30    FORMAT(' ERROR 30: ECP RETURNED IER = ',I2)
      IF( ABS(DX1)/T2 .LT. TOL .AND. ABS(DX2)/P2 .LT. TOL ) GO TO 40
      F1 = S1 - S2
      F2 = 8.0*V1 - V2
      DET = CP/P2*DLVLP + V2/10./T2*DLVLT**2
      DX1 = (T2/P2*DLVLP*F1 + DLVLT*F2/10.)/DET
      DX2 = (-DLVLT*F1 + CP/V2*F2)/DET
      T2 = T2 + DX1
      P2 = P2 + DX2
20    CONTINUE
      WRITE(6,50)
50    FORMAT(' CONVERGENCE FAILURE')
40    CONTINUE
C
C     COMPUTE WORK FROM FIRST LAW
```



```
C
      W12 = -(U2 - U1)
C
C     WRITE ANSWERS
C
      WRITE(6,60) T2, V2, W12
60    FORMAT(' T2(K) = ',1PE11.4,2X,' V2(CM**3/G) = ',1PE11.2,2X,
     &       ' W12(J/G) = ',1PE11.4)
      STOP
      END
```

The output of the program is:

```
T2(K) = 1.151E+03   V2(CM**3/G) = 9.35E+02   W12(J/G) = 9.4205E+02
```

3.10 COMBUSTION

Thermodynamics is able to predict the equilibrium state that results from burning a fuel–air mixture given only the initial conditions. In this section we discuss constant pressure and constant volume combustion to illustrate the principles. We also introduce the heat of combustion and the adiabatic flame temperature.

Let us first consider the case in which combustion occurs at constant pressure. Suppose that the fuel and air are premixed to a homogeneous state. Application of the first law leads to

$$\boxed{\Delta h = q} \tag{3.139}$$

That is, the enthalpy of the products is equal to the enthalpy of the reactants plus any heat transferred to the system. In this case, given the heat transferred per unit mass, we can solve for the temperature, specific volume, internal energy, and the like of the products by Newton–Raphson iteration. For the special case of adiabatic combustion, the resultant temperature is called the adiabatic flame temperature.

EXAMPLE 3.6

A stoichiometric mixture of gasoline C_7H_{17}(g), air, and residual gas is burned at constant pressure. Given that $T_1 = 298$ K, $P_1 = 1.013$ bar, and $f_1 = 0.10$, compute the adiabatic flame temperature.

SOLUTION:

```
C
      DIMENSION Y1(6), Y2(10)
      DATA MAXITS/50/, TOL/.001/
C
C     ESTABLISH INTIAL CONDITIONS
C
      T1 = 298.
```

```
      P1 = 1.01325
      PHI = 1.0
      F = 0.1
      CALL FARG(P1,T1,PHI,F,H1,U,V,S,Y1,CP,DLVLT,DLVLP)
C
C     MAKE AN INITIAL ESTIMATE
C
      P2 = P1
      T2 = 2000.
C
C     DO THE ITERATION
C
      DO 10 I = 1,MAXITS
      CALL ECP(P2,T2,PHI,H2,U,V,S,Y2,CP,DLVLT,DLVLP,IER)
      IF( IER .NE. 0 ) WRITE(6,25) IER
25    FORMAT(' ECP RETURNED IER = ',I3)
      F = H1 - H2
      DELT2 = F/CP
      T2 = T2 + DELT2
      IF(ABS(DELT2)/T2 .LT. TOL) GO TO 20
10    CONTINUE
      WRITE(6,30)
30    FORMAT(' CONVERGENCE FAILURE')
20    CONTINUE
C
C     WRITE THE ANSWER
C
      WRITE(6,40) T2
40    FORMAT(' T2(K) = ',1PE11.4)
      STOP
      END
```

The answer is T2(K) = 2.1229E + 03.

Adiabatic flame temperatures for several fuels burned in air from $T_1 = 298$ K and $P_1 = 1$ atm are shown in Fig. 3-3 as functions of equivalence ratio. There is little dependence on fuel type among the hydrocarbons. Other calculations show that the adiabatic flame temperature decreases with residual fraction and slightly decreases with pressure.

The heat of combustion of a fuel is defined as the heat transferred out of a system per unit mass or mole of fuel when the initial and final states are at the same temperature and pressure. Furthermore, the fuel is assumed to burn completely to carbon dioxide and water. The analyses that led to Table 3-3 for the lean or stoichiometric case can be used to compute the heat of combustion. Restricting our attention to $T = 298$ K, it can be shown that

$$-q_{c,298} = \alpha h_{CO_2,298} + \frac{\beta}{2}\left[h_{H_2O,298} - (1-\chi)h_{fg,H_2O,298}\right] - h_{C_\alpha H_\beta O_\gamma N_\delta,298} \tag{3.140}$$

Two values are recognized: The lower heat of combustion is defined so that all of the water in the products is gaseous (the quality is $\chi = 1.0$), and the higher

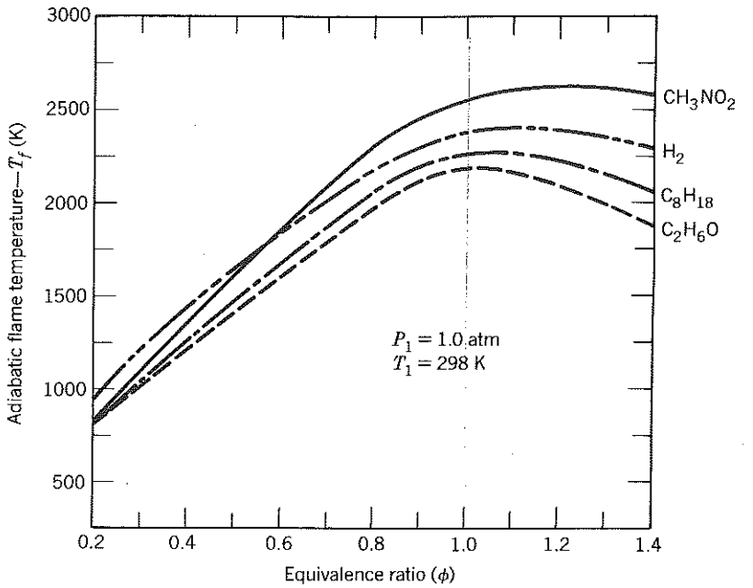

Figure 3-3 Adiabatic flame temperature of some fuels initially at atmospheric pressure and temperature.

heat of combustion is defined so that all of the water in the products is liquid ($\chi = 0.0$).

The higher heat of combustion and stoichiometric adiabatic flame temperature of several fuels are given in Table 3-7.

The heat of combustion is used primarily in two ways: (1) in some cases, such as in the gas cycles or when solving reacting Navier–Stokes equations, it

Table 3-7 Higher Heat of Combustion and Stoichiometric Adiabatic Flame Temperature of Some Fuels at $P = 1.0$ atm, $T = 298$ K.

FUEL		$q_{c,298}$ (kJ/g)	$T_{f,\phi=1.0}$ (K)
C_2N_2 (g)	Cyanogen	21.0	2596
H_2 (g)	Hydrogen	141.6	2383
NH_3 (g)	Ammonia	22.5	2076
CH_4 (g)	Methane	55.5	2227
C_3H_8 (g)	Propane	50.3	2268
C_8H_{18} (l)	Octane	47.9	2266
$C_{15}H_{32}$ (l)	Pentadecane	47.3	2269
$C_{20}H_{40}$ (g)	Eicosane	47.3	2291
C_2H_2 (g)	Acetylene	49.9	2540
$C_{10}H_8$ (s)	Naphthalene	40.3	2328
CH_4O (l)	Methanol	22.7	2151
C_2H_6O (l)	Ethanol	29.7	2197
CH_3NO_2 (l)	Nitromethane	11.6	2545

is desirable to relax the rigor of the thermodynamics by using the heat of combustion to define an equivalent heat release; (2) for practical fuels, discussed in Chapter 10, the enthalpy at $T = 298$ can be determined inexpensively by measurement of the heat combustion.

An analogous discussion could be presented for constant-volume combustion where

$$\Delta u = q \tag{3.141}$$

However, as a rule of thumb, when the heat of combustion or adiabatic flame temperature is referred to without qualification, constant pressure combustion is implied.

Once again, the equilibrium state is best determined by using Newton–Raphson iteration. The derivatives required include:

$$\left(\frac{\partial u}{\partial T}\right)_P = c_P - \frac{Pv}{T}\left(\frac{\partial \ln v}{\partial \ln T}\right)_P \tag{3.142}$$

$$\left(\frac{\partial u}{\partial P}\right)_T = -v\left[\left(\frac{\partial \ln v}{\partial \ln T}\right)_P + \left(\frac{\partial \ln v}{\partial \ln P}\right)_T\right] \tag{3.143}$$

3.11 REFERENCES

CRC Handbook of Chemistry and Physics, (1975–1976), 56th ed., CRC, Cleveland, Ohio.

Gordon, S. and B. McBride (1971), "Computer Program for Calculation of Complex Chemical Equilibrium Compositions, Rocket Performance, Incident and Reflected Shocks, and Chapman-Jouquet Detonations," NASA SP-273.

Hires, S. D., A. Ekchian, J. B. Heywood, R. J. Tabaczynski, and J. C. Wall (1976), "Performance and NO_x Emissions Modeling of a Jet Ignition Pre-Chamber Stratified Charge Engine," SAE Trans., Vol. 85, paper 760161.

JANAF Thermochemical Tables, (1971), 2nd ed., National Bureau of Standards Publications, NSRDS-N35 37, Washington D.C.

Lewis, G. N. and M. Randall, (1961), *Thermodynamics*, McGraw-Hill, New York, p. 665–668.

Olikara, C. and G. L. Borman (1975), "A Computer Program for Calculating Properties of Equilibrium Combustion Products with Some Applications to I.C. Engines," SAE paper 750468.

Rossini, F. D., (1953), *Selected Values of Physical and Thermodynamic Properties of Hydrocarbons and Related Compounds*, Carnegie Press, Pittsburgh.

Stull, D. R., E. F. Westrum, Jr. and G. C. Sinke (1969), *The Chemical Thermodynamics of Organic Compounds*, Wiley, New York.

Svehla, R. A. and B. H. McBride (1973), "Fortran IV Computer Program for Calculation of Thermodynamic and Transport Properties of Complex Chemical Systems," NASA TND-7056.

Vargaftik, N. B. (1975), *Tables on the Thermophysical Properties of Liquids and Gases*, Wiley, New York.

3.12 HOMEWORK

1. Using Table 3-1, verify that the enthalpy and entropy of CO_2 in Example 3.1 are correct.
2. Why does Eq. (3.20) contain y_i? Why is R in the summation in Eq. (3.21) not suscripted with i?
3. Verify Table 3-3.
4. What is the molar C/O ratio of the products in Eq. (3.25)?
5. Repeat Example 3.2 for Methanol CH_3OH at $\phi = 1.0$.
6. Derive Eqs. (3.36) and (3.37).
7. The specific heat at constant pressure is defined as

$$c_P = \left(\frac{\partial h}{\partial T}\right)_P$$

Substitution into Eq. (3.13) yields

$$c_P = \sum_{i=1}^{J}\left(y_i c_{P_i} + h_i \frac{\partial y_i}{\partial T}\right)$$

The specific heat so computed is called the equilibrium specific heat. Another specific heat is recognized, the frozen specific heat, which is computed holding the composition constant. It follows that

$$c_{P,f} = \sum_{i=1}^{J} y_i c_{P_i}$$

To compute the equilibrium specific heat of a fuel, air, and residual gas mixture, consider Eq. (3.36) and differentiate with respect to T

$$\frac{\partial y_i}{\partial T} = y_r \frac{\partial y_i''}{\partial T}$$

In differentiating, it was recognized that neither y_r nor y_i' depend on temperature. It is also true that $\Sigma_{i=1}^{6} \nu_i$ for either the lean or rich cases in Table 3-3 does not depend on temperature. It follows that

$$\frac{\partial y_i}{\partial T} = y_r \frac{1}{\Sigma \nu_i} \frac{\partial \nu_i}{\partial T}$$

Inspection of the table reveals that none of the lean ν_i depend on T; whereas, for the rich case, those with ν_5 do depend on T, as can be seen through solution of the quadratic equation Eq. (3.32). Hence we can write

$$\frac{\partial y_i}{\partial T} = 0 \qquad \text{(lean)}$$

$$\frac{\partial y_i}{\partial T} = y_r \frac{1}{\Sigma \nu_i} \frac{\partial \nu_i}{\partial \nu_5} \frac{\partial \nu_5}{\partial \mathrm{K}} \frac{\partial \mathrm{K}}{\partial T} \qquad \text{(rich)}$$

The subroutine FARG stores $\partial \nu_i / \partial \nu_5$ in the vector TABLE (6) and defines

$$\mathrm{DCDT} = \frac{\partial \nu_5}{\partial \mathrm{K}} \frac{\partial \mathrm{K}}{\partial T}$$

Show that for the rich case

a. y_r, y_i', and $\Sigma\nu_i$ do not depend on temperature.

b.
$$\frac{\partial \nu_5}{\partial \mathrm{K}} = \frac{\nu_5^2 - \nu_5(0.42(\phi-1)+\alpha\phi\epsilon)+0.42\alpha\phi\epsilon(\phi-1)}{(2\nu_5 a+b)}$$

c.
$$\frac{\partial \mathrm{K}}{\partial T} = \frac{\partial \mathrm{K}}{\partial t}\frac{\partial t}{\partial T}$$
$$\frac{\partial \mathrm{K}}{\partial T} = \left(\frac{1.761}{t^2}+\frac{3.222}{t^3}-\frac{0.8409}{t^4}\right)\frac{\mathrm{K}}{1000}.$$

d. Verify the FORTRAN expressions in FARG used for DCDT and DKDT. Verify the DATA given for TABLE.

e. Show that the molecular weight of the products is independent of temperature.

8. Repeat Example 3.3 for the reaction

$$O_2 \rightarrow \nu_1 O_2 + \nu_2 O$$

Verify your result by using the equilibrium constants given in the JANAF Tables, see Appendix F.

9. Explain why lines of constant temperature are horizontal at low entropy but not at larger entropies on the large chart on the back cover.

10. At what equivalence ratio for octane–air mixtures does the carbon to oxygen ratio of the system equal unity? Why do you think this is of interest?

11. A system whose composition is

i	SPECIES	y_i
1	H_2O	0.141
2	CO_2	0.125
3	N_2	0.734

is at equilibrium at $T = 298$ K and $P = 1$ atm. What is the enthalpy (J/g) and specific volume (cm^3/g)?

12. Equilibrium combustion products at $\phi = 1.0$ of octane C_8H_{18} (l) are expanded isentropically from $T_1 = 2000$ K, $P_1 = 10$ atm to a pressure of 1 atm. Find the final temperature and the work done. (Use the chart found on the back cover rather than the computer.)

13. Equilibrium combustion products of isooctane $C_8H_{18}(g)$ are expanded isentropically by a volume ratio of 10 : 1. For $\phi = 1.0$ and an initial state of $T_1 = 3000$ K, $P_1 = 50$ atm, find the final state (T_2, P_2) and the work done. (Use the chart found on the back cover of the book.)

14. Repeat Example 3.4 for $P_2 = 10$ bars, $\phi = 1.25$, $T_1 = 300$ K, $P_1 = 0.75$ bars, and $f = 0.15$.

15. Use Eq. (3.118) to calculate the ratio of specific heats for fuel–air–residual gas as a function of equivalence ratio. Graph your results over $0 < \phi < 1.5$ at $T = 298$ K, $P = 1.0$ bar, and $f = 0.10$.

16. Repeat H.W. 14 for the equilibrium combustion products at $T_1 = 1500$ K, $P_1 = 5.0$ bar, and $P_2 = 1.0$ bar.

17. Repeat Example 3.5 for $v_2/v_1 = 10$.

18. Prepare a subroutine CMPRSS for fuel–air residual gas. Consider modifying Example 3.4. The routine will be given:

V	specific volume (cm^3/g)
S	entropy (J/g/K)
PHI	fuel–air equivalence ratio
F	residual mass fraction

and will return:

T	temperature (K)
P	pressure (bar)
U	internal energy (J/g)

19. Prepare a subroutine EXPAND following Example 3.5. The routine will be given:

V	specific volume (cm^3/g)
S	entropy (J/g/K)
PHI	fuel–air equivalence ratio

and will return:

P	pressure (bar)
T	temperature (K)
U	internal energy (J/g)

20. Repeat Example 3.5 for $\phi = 0.8$.

21. Implicit in Eq. (3.139) and later (3.141) is that the variables are mass intensive. Recognize that in a chemical reaction, mass is conserved but moles are not. Explain why Eq. (3.139) is not valid for molar–intensive variables.

22. Compute the adiabatic flame temperature for constant volume combustion of a stoichiometric mixture of gasoline, C_7H_{17} (g), air, and residual gas given that $T_1 = 298$ K, $P_1 = 1$ atm, and $f = 0.10$.
Prepare a subroutine COMBST with the following input/output:
Given:

V	specific volume (cm^3/g)
U	internal energy (J/g)
PHI	fuel–air equivalence ratio

Returns:

P	pressure (bar)
T	temperature (K)
S	entropy (J/g/K)

The subroutine will be used later when we analyze the Otto fuel–air cycle.

23. Compute the higher, lower, and equilibrium heat of combustion for cetane, $C_{16}H_{34}$ (l). The equilibrium computation determines the quality of the water in the products at atmospheric pressure.

24. The heat of combustion could have been defined without requiring complete conversion to carbon dioxide and water. What would the lower heat of combustion be for the case $\phi = 1.4$, fuel = C_8H_{18} (l) (octane), $T_o = 298$ K, $P_o = 1$ atm?

Enthalpies (kJ/mole) at $T = 298$ K that you will need are:

H_2O	−241.83	H_2	0.0
CO_2	−393.52	N_2	0.0
CO	−110.53	O_2	0.0

Assume the water quality is zero, that Table 3-3 is applicable, and that $K = 9.95 \times 10^{-6}$

Four

FUEL–AIR CYCLES

The groundwork for introducing the fuel–air cycles was laid in Chapter 2, where the basic processes are presented, and in Chapter 3, where the required thermodynamic equations of state are given. We now bring all that we have learned into analysis of the efficiency and work produced by an internal combustion engine.

4.1 EFFICIENCY

The appropriate definition of efficiency for any of the gas cycles is clear. When a fuel is burned rather than heat being transferred to produce work, it is usually assumed that the efficiency is the ratio of the net work done per unit mass of fuel inducted to the heat of combustion of the fuel. According to the principles of thermodynamics, this definition is not necessarily correct if we prefer that

$$\eta = \frac{W_{\text{c.v.}}}{(W_{\text{c.v.}})_{\text{maximum possible}}} \tag{4.1}$$

Consider the first law of thermodynamics as applied to the control volume shown in Fig. 4-1 (Obert, 1968).

$$\left(\frac{dE}{dt}\right)_{\text{c.v.}} = \dot{Q}_{\text{c.v.}} - \dot{W}_{\text{c.v.}} + \sum_{\text{in}} \dot{m}h - \sum_{\text{out}} \dot{m}h \tag{4.2}$$

Let us integrate over one period of the engine's cycle

$$0 = Q_{\text{c.v.}} - W_{\text{c.v.}} + \sum_{\text{in}} mh - \sum_{\text{out}} mh \tag{4.3}$$

The maximum work is obtained only if the process is reversible, in which case

$$Q_{\text{c.v.}} = T_o\left(\sum_{\text{out}} ms - \sum_{\text{in}} ms\right) \tag{4.4}$$

Hence

$$(W_{\text{c.v.}})_{\text{maximum possible}} = m_f q_{c,T_o,P_o} + T_o\left(\sum_{\text{out}} ms - \sum_{\text{in}} ms\right) \tag{4.5}$$

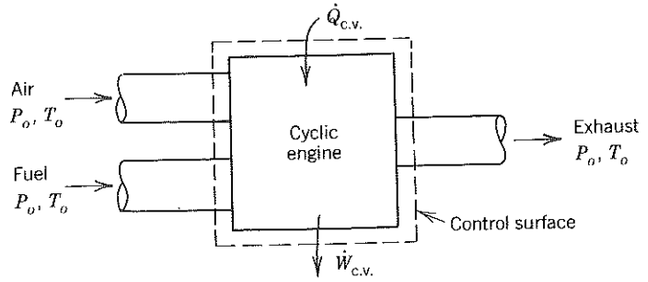

Figure 4-1 Control volume for analyzing maximum work that a cyclic engine can produce by burning a fuel.

Introducing the available energy of combustion defined as

$$a_c = q_c + T_o\left(\sum_{\text{out}} ms - \sum_{\text{in}} ms\right)/m_f \tag{4.6}$$

the efficiency is

$$\eta = \frac{W_{c.v.}}{m_f a_c} \tag{4.7}$$

Fig. 4-2 compares the available energy of combustion with the heat of combustion at $T_o = 298$ K, $P_o = 1$ atm. The maximum work is attained only if the exhaust is in equilibrium at the state T_o, P_o; thus the exhaust water quality is evaluated by setting the partial pressure of the vapor equal to the saturation vapor pressure at $T = T_o$.

It is evident from Fig. 4-2 that more energy is available per unit mass of fuel if an engine is fueled lean than if it is fueled rich. Equation (4.7) is appropriate only when the exhaust of the engine is used as fuel for some other device. In the more usual case, a definition that reflects the waste of energy by running rich is called for. For this reason, we will base our efficiency on the maximum available energy of combustion which occurs for very lean equivalence ratios. Thus, letting

$$a_o = a_{c,\phi=0.01} \tag{4.8}$$

the efficiency is defined to be

$$\eta = \frac{W_{c.v.}}{m_f a_o} = \frac{w_{c.v.}(1+\phi F_s)}{\phi F_s (1-f) a_o} \tag{4.9}$$

where $w_{c.v.}$ the work per unit mass done by the system.

To a certain extent, the definition of efficiency is equivocal. It seems impractical to take into account the small amount of work that can in principal be realized because the exhaust composition is different from that of the atmosphere. The arguments presented could be extended to recognize that

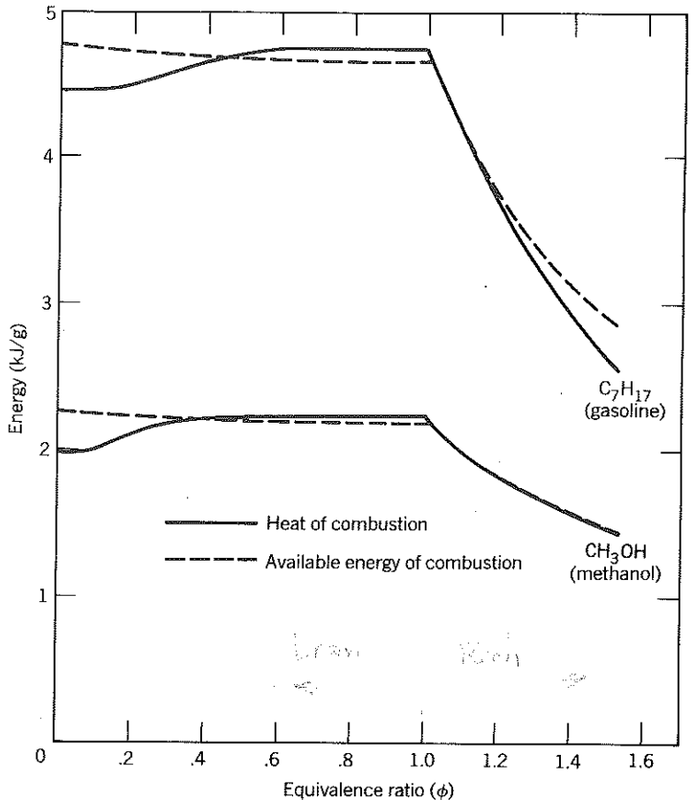

Figure 4-2 Available energy and heat of combustion for liquid gasoline and methanol. Fuel and air are unmixed, $P_o = 1$ atm., $T_o = 298$ K. Products are mixed with equilibrium water quality.

more energy is available on a cold day than on a hot day. Thus, rather than $T_o = 298$ K, one should evaluate a_o at the temperature equal to that of the coldest day ever recorded at Antarctica since in principle one could run all engines down there on the coldest of days. This concept is easily dismissed if one recognizes the practical constraints.

Speaking then of practical constraints, the only way in which the reversible heat transfer of Eq. (4.4) can occur between an engine and its surroundings is via an intervening Carnot engine. One may then make a case for defining efficiency in terms of the heat of combustion on the premise that never will a heat engine of any sort, including the Carnot engine, be used to reduce the irreversibilities associated with the heat transfer. By inspection of Fig. 4-2, one would then use the stoichiometric heat of combustion, for here the heat of combustion is maximum. Arguments can also be made, though not very

convincingly, for use of either the lower or the higher heat of combustion rather than the equilibrium heat of combustion.

The choice of $\phi = 0.01$ in Eq. (4.8) is also equivocal. Fig. 4-1 suggests taking the limit of $\phi \to 0$ to evaluate a_o. Strictly speaking, that limit does not exist, for it would imply that thermodynamic states exist with no bound in volume. Indeed if one tries to evaluate the limit one will find it blows up. Thus $\phi = 0.01$ was chosen as being close enough to zero for practical purposes. Indeed it is unlikely that any engine would be operated significantly leaner than this.

It was mentioned in Chapter 1 that many engineers prefer to measure engine efficiency using the specific fuel consumption because its definition is unequivocal. In situations in which fuel type is not varied, this is a useful approach. To compare diesel engines with gasoline engines or to properly consider alternative fuels, Eq. (4.9) seems to be the best compromise between the conflicting demands of the real and the ideal.

To compute the maximum available energy of combustion, note that in the limit of there being no fuel, the heat of combustion corresponds to the lower heat. The exhaust water is in a gaseous state. Results assuming that the fuel and air are initially unmixed are given in Table 4-1. Notice that for the most part there is little difference between the lower heat of combustion and the maximum available energy.

Table 4-1 Maximum Available Energy of Combustion[a] Compared with the Lower Heat of Combustion

FUEL		h_{298} (kJ/mole)	s^o_{298} (J/mole/K)	q_c (kJ/g)	a_o (kJ/g)
C_2N_2 (g)	Cyanogen	309.1	241.5	21.06	21.29
H_2 (g)	Hydrogen	0.0	130.6	119.95	119.52
NH_3 (g)	Ammonia	−45.7	192.6	18.61	20.29
CH_4 (g)	Methane	−74.9	186.2	50.01	52.42
C_3H_8 (g)	Propane	−103.9	269.9	46.36	49.16
C_7H_{17} (*l*)	Gasoline[b]	−305.6	345.8	44.51	47.87
C_8H_{18} (*l*)	Octane	−249.5	360.8	44.43	47.67
C_8H_{18} (*l*)	Isooctane	−259.3	328.0	44.35	47.67
$C_{14.4}H_{24.9}$ (*l*)	T–T diesel[b]	−174.0	525.9	42.94	45.73
$C_{15}H_{32}$ (*l*)	Pentadecane	−428.9	587.5	43.99	47.22
C_2H_2 (g)	Acetylene	226.7	200.8	48.22	48.58
C_6H_6 (*l*)	Benzene	48.91	173.0	40.14	42.14
$C_{10}H_8$ (s)	Naphthalene	78.1	166.9	38.86	40.84
CH_4O (*l*)	Methanol	−239.1	126.8	19.91	22.68
C_2H_6O (*l*)	Ethanol	−277.2	160.7	26.82	29.71
CH_3NO_2 (*l*)	Nitromethane	−113.1	171.8	10.54	12.43
C (s)	Graphite	0.0	5.7	32.76	33.70
$C_{176}H_{144}O_8N_3$ (s)	Good coal[b]	−10000.0	3000.0	31.57	33.57

[a] Based on equilibrium water quality, lean combustion at $\phi = 0.01$ and unmixed reactants.
[b] Estimated for typical fuel.

In the rich case, there is significant carbon monoxide and hydrogen in the exhaust. Thus not all of the heat is released and the exhaust gases could in principle be used as a fuel for some other engine. In practice, however, those gases are usually exhausted to the atmosphere and the energy is wasted.

4.2 OTTO CYCLE

The Otto cycle models engines whose combustion is rapid enough that it occurs at constant volume near top dead center. It is generally most applicable to homogeneous charge spark ignition engines. The basic processes are

1 to 2	Isentropic compression of fuel, air, and residual gases
2 to 3	Adiabatic, isometric combustion
3 to 4	Isentropic expansion of equilibrium combustion products

The following example illustrates how to apply the thermodynamics developed in Chapter 3 to the Otto fuel–air cycle.

EXAMPLE 4.1 OTTO FUEL AIR CYCLE

```
C
C     GIVEN:
C       COMPRESSION RATIO - R
C       FUEL AIR EQUIVALENCE RATIO - PHI
C       RESIDUAL MASS FRACTION - F
C       INITIAL PRESSURE - P1 (BAR)
C       INITIAL TEMPERATURE - T1 (K)
C       FUEL - GASOLINE
C
C     FIND:
C       INDICATED THERMAL EFFICIENCY - ETA
C       INDICATED MEAN EFFECTIVE PRESSURE - IMEP (BAR)
C       PEAK PRESSURE - P3 (BAR)
C
C     NOTE:
C       THE SUBROUTINES CMPRSS, EXPAND AND COMBUST DEVELOPED
C       IN THE HOMEWORK ASSIGNMENTS OF CHAPTER 3 WILL BE USED
C
      REAL IMEP
      DIMENSION Y1(10)
      DATA AO/47870./, FS/.06548/
      R = 10.
      PHI = 0.8
      F = .10
      P1 = 1.0
      T1 = 350.
C
C     ESTABLISH INITIAL STATE
C
      CALL FARG(P1, T1, PHI, F, H1, U1, S1, Y1, CP, DLVLT, DLVLP)
C
C     ISENTROPIC COMPRESSION OF FUEL-AIR-RESIDUAL GAS
C
      V2 = V1/R
```

```
      S2 = S1
      CALL CMPRSS(V2, S2, PHI, F, T2, P2, U2)
C
C     ADIABATIC, CONSTANT VOLUME COMBUSTION
C
      V3 = V2
      U3 = U2
      CALL COMBST(V3, U3, PHI, P3, T3, S3)
C
C     ISENTROPIC EXPANSION OF EQUILIBRIUM COMBUSTION PRODUCTS
C
      V4 = R*V3
      S4 = S3
      CALL EXPAND(V4, S4, PHI, P4, T4, U4)
C
C     COMPUTE AND WRITE THE ANSWERS
C
      W = U1 - U4
      ETA = W*(1.0 + PHI*FS)/PHI/FS/(1.0 - F)/AO
      IMEP = W/(V1 - V2)*10.
C
      WRITE(6,10) ETA, IMEP, P3
10    FORMAT(' ETA = ',1PE11.4,2X,'IMEP = ',1PE11.4,2X,'P3 = ',1PE11.4)
      STOP
      END
```

SOLUTION:

The output obtained is

```
ETA = 4.6028E-01      IMEP = 1.1198E+01      P3 = 7.6520E+01
```

Results obtained using the code in Example 4.1 for different equivalence ratios and different compression ratios are given in Fig. 4-3 and 4-4. Some important conclusions and others derived by varying the initial temperature and pressure are:

1. Indicated efficiency increases with compression ratio, is maximized by lean combustion, and is practically independent of the initial temperature and initial pressure.
2. Indicated mean effective pressure increases with compression ratio, is maximized slightly rich of stoichiometric, and drops linearly with the initial density (i.e., imep $\propto P_1$ and imep $\propto 1/T_1$).
3. For a given compression ratio, the peak pressure is proportional to the indicated mean effective pressure.
4. Peak temperatures in the cycles are maximum for equivalence ratios slightly rich of stoichiometric.

Similar results are more extensively presented by Taylor (1977) for the fuel octane. In fact, the results shown are characteristic of most hydrocarbon

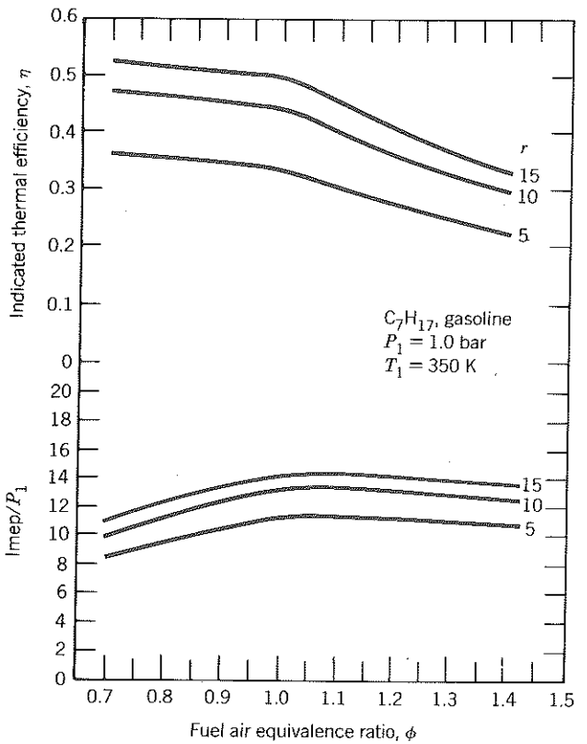

Figure 4-3 Otto fuel–air cycle characteristics. Efficiency is maximum for lean mixtures; whereas imep is maximum for slightly rich mixtures. In actual engines, maximum efficiency occurs at stoichiometric or slightly lean; excessive dilution of the charge with air degrades the combustion.

fuels. It is of interest to explore the influence of fuel properties for some alternative fuels as we look to the future. Table 4.2 presents results obtained for two different compression ratios and five different fuels. Notice that there is very little difference among hydrocarbons. According to this analysis, diesel fuel would be just as good as gasoline in a homogeneous-charge spark-ignition engine; in reality, of course, knock would be a problem. That nitromethane is a good racing fuel is clear for it produced a much larger imep than any of the other fuels considered.

Because one technique for emission control is exhaust gas recirculation, it is also of interest to examine the influence of the residual fraction. By pumping exhaust gas into the intake manifold and mixing it with the fuel and air, one has, in essence, increased the residual gas fraction. Although the exhaust gas so recirculated is cooled before introduction into the induction system, it is still considerably warmer than the inlet air. Therefore we will increase the inlet

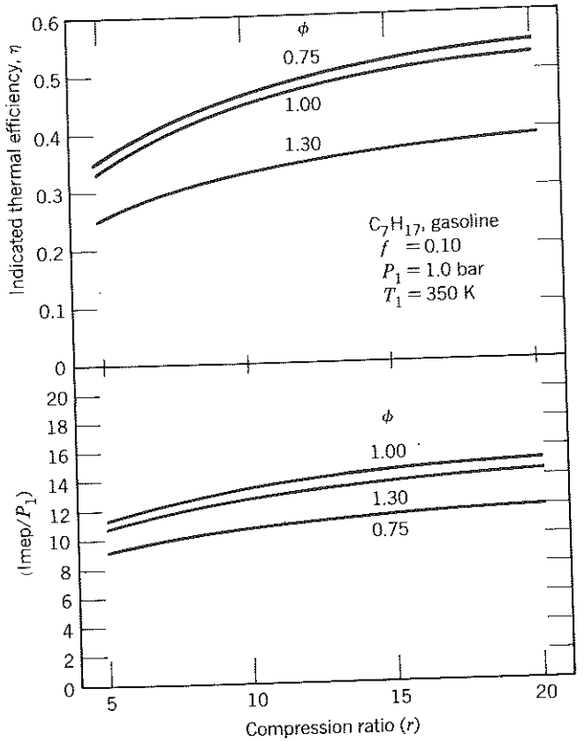

Figure 4-4 Otto fuel–air cycle characteristics. Both efficiency and imep increase with compression ratio.

Table 4-2 Otto Fuel–Air Cycle—Effect of Fuel Type[a]

FUEL		r	η_t	imep (BAR)	COMMENTS
Benzene	C_6H_6	10	0.438	13.5	Aromatic hydrocarbons, low H/C ratio
		15	0.492	14.6	
Diesel	$C_{14.4}H_{24.9}$	10	0.439	13.7	T–T, see Table 10-5(a), very low octane
		15	0.495	14.9	
Gasoline	C_7H_{17}	10	0.440	13.3	Unleaded, see Table 10-3, AL7927G
		15	0.495	14.4	
Methane	CH_4	10	0.443	12.2	gaseous, high H/C ratio
		15	0.496	13.1	
Methanol	CH_3OH	10	0.430	13.1	future fuel from coal?
		15	0.483	14.2	
Nitromethane	CH_3NO_2	10	0.388	21.0	racing fuel
		15	0.433	23.1	

[a]All calculations use $\phi = 1.0$, $f = 0.10$, $P_1 = 1.0$ bar, $T_1 = 350$ K.

temperature in our computations simultaneously to examine the overall effect. To illustrate, assume $T_1 = (330 + 200f)$ in degrees Kelvin. The results obtained for gasoline are given in Fig. 4-5. Notice that the efficiency increases slightly with increasing dilution of the charge by residual gas. Notice too that imep falls with increasing f; it falls because the residual gas displaces fuel–air and because it warms the fuel–air, thereby reducing the charge density.

The indicated efficiency and mean effective pressure of actual engines are determined in practice by measuring the cylinder pressure as a function of cylinder volume and integrating $\int P\,dV$ to find the work. It is also possible to measure the residual fraction and charge density trapped within the cylinder. Otto fuel–air cycles, with P_1, T_1, and f chosen such that the charge density and entropy are matched to the conditions in the cylinder at the time of inlet valve closing, overpredict the work and efficiency by a factor of only 1.1 to 1.2.

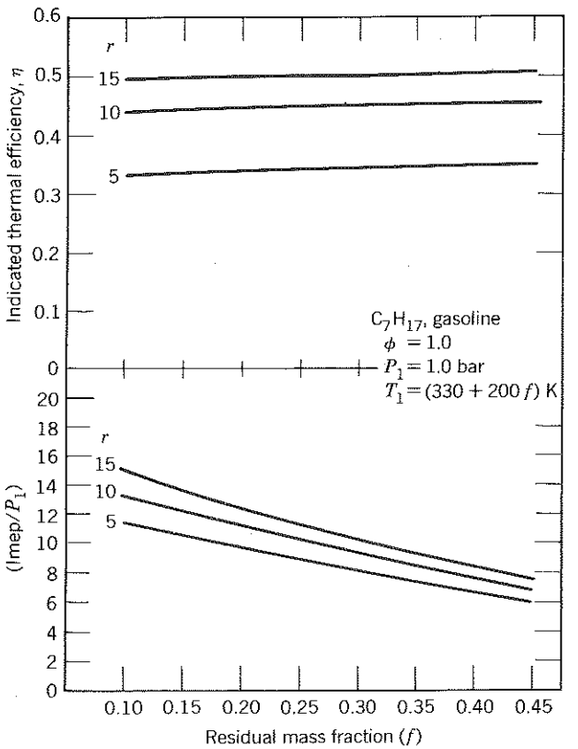

Figure 4-5 Otto fuel–air cycle characteristics. Dilution of the charge by residual gas increases the efficiency a negligible amount but drops the imep significantly. If misfire did not occur at large residual fractions, exhaust gas recirculation could be used to control engine torque.

Stated differently, the ratio of the actual efficiency to that of the Otto fuel air cycle is

$$\eta/\eta_{\text{otto}} \approx 0.8 \text{ to } 0.9$$

Based on the analysis done in Chapter 2, this is to be expected, and the difference is attributed mainly to heat loss but also to mass loss and the finite burning rate. As will be shown later, a small part of the discrepancy can be attributed to opening the exhaust valve prior to bottom dead center because blowdown also occurs at a finite rate.

For a given engine operated at optimum spark timing, the ratio η/η_{otto} is nearly independent of the fuel–air equivalence ratio, the inlet temperature, the inlet pressure, the exhaust gas recirculation, and the engine speed. Thus all the trends predicted by the Otto fuel–air cycle are in fact observed in practice. All the conclusions drawn from Fig. 4-3 to 4-5 apply to actual engines, provided that they are operated at optimum spark timing.

It is also instructive to consider the Otto fuel–air cycle with the ideal inlet and exhaust processes. In this case, the variables T_1, P_1, and f are no longer the independent variables. Instead, the intake pressure P_i, the exhaust pressure P_e, and the intake temperature T_i are the independent variables.

The additional processes, introduced in Chapter 2, are reiterated here:

4 to 5	isometric blowdown
5 to 6	isobaric exhaust
6 to 7	isometric reversion
7 to 1	isobaric intake

The blowdown is considered to be isentropic as far as the control mass is concerned. One solves for the temperature T_5 by requiring that $s_5 = s_4$ and $P_5 = P_e$. Application of the first law to the control mass during exhaust leads to the conclusion that

$$h_6 = h_5 \qquad P_6 = P_5$$
$$T_6 = T_5 \qquad v_6 = v_5$$

These are still valid conclusions even though now we are treating the exhaust gas as equilibrium combustion products.

The residual fraction is given by

$$f = \frac{1}{r}\frac{v_4}{v_6} \tag{4.10}$$

The energy equation applied to the cylinder control volume during intake is given in Eq. (2.48), (2.49), and (2.50). Note that Eq. (2.51) is no longer valid since it assumes constant specific heats. In this case Eq. (2.51) is replaced by

$$h_1 = f\left[h_6 + (P_i - P_e)v_6\right] + (1-f)h_i \tag{4.11}$$

and, of course, it is still true that

$$P_1 = P_i \tag{4.12}$$

The volumetric efficiency and pumping work are

$$e_v = \frac{m_i}{\rho_i V_d} = \frac{r(1-f)v_i}{(r-1)v_1} \tag{4.13}$$

$$\text{pmep} = P_e - P_i \tag{4.14}$$

Finally, the net work and thermal efficiency are

$$(\text{imep})_{\text{net}} = \text{imep} - \text{pmep} \tag{4.15}$$

$$\eta_{\text{net}} = \eta\left(1 - \frac{\text{pmep}}{\text{imep}}\right) \tag{4.16}$$

As in Example 2.4, analysis of the cycle requires iteration. Example 4.2 illustrates the procedure.

EXAMPLE 4.2 FOUR-STROKE OTTO FUEL AIR CYCLE WITH IDEAL INTAKE AND EXHAUST

```
C
C       GIVEN:
C         COMPRESSION RATIO - R
C         FUEL AIR EQUIVALENCE RATIO - PHI
C         INTAKE PRESSURE - PI (BAR)
C         INTAKE TEMPERATURE - TI (K)
C         EXHAUST PRESSURE - PE (BAR)
C         FUEL - GASOLINE
C
C       FIND:
C         NET INDICATED THERMAL EFFICIENCY - ETANET
C         INDICATED MEAN EFFECTIVE PRESSURE - IMEP (BAR)
C         PUMPING MEAN EFFECTIVE PRESSURE - PMEP (BAR)
C         RESIDUAL MASS FRACTION - F
C         VOLUMETRIC EFFICIENCY - EV
C
C       NOTE:
C         TWO NEW SUBROUTINES ARE REQUIRED TO HANDLE BLOWDOWN
C         AND COMPUTE THE TEMPERATURE AT THE START OF THE
C         COMPRESSION STROKE. THEY ARE BLWDWN & TSTART RESPECTIVELY.
C
      REAL IMEP
      DIMENSION Y1(6), Y(6)
      DATA AO/47870./, FS/.06548/, MAXITS/25/, TOL/.001/
C
      R = 10.
      PHI = 0.8
      PI = 0.75
      TI = 300.
      PE = 1.05
C
C     FIND ENTHALPY OF INTAKE FUEL AIR MIXTURE
C
      CALL FARG(PI, TI, PHI, 0., HI, U, VI, S, Y, CP, DLVLT, DLVLP)
C
      P1 = PI
C
C     GUESS AT RESIDUAL FRACTION AND INITIAL TEMPERATURE
```

```
C
      F = .10
      T1 = 350.
C
C     DO ITERATION USING SUCCESSIVE APPROXIMATION
C
      DO 10 I = 1,MAXITS
C
C     ESTABLISH INITIAL STATE
C
      CALL FARG(P1, T1, PHI, F, H1, U1, V1, S1, Y1, CP, DLVLT, DLVLP)
C
C     ISENTROPIC COMPRESSION OF FUEL-AIR-RESIDUAL GAS
C
      V2 = V1/R
      S2 = S1
      CALL CMPRSS(V2, S2, PHI, F, T2, P2, U2)
C
C     ADIABATIC, CONSTANT VOLUME COMBUSTION
C
      V3 = V2
      U3 = U2
      CALL COMBST(V3, U3, PHI, P3, T3, S3)
C
C     ISENTROPIC EXPANSION OF EQUILIBRIUM COMBUSTION PRODUCTS
C
      V4 = R*V3
      S4 = S3
      CALL EXPAND(V4, S4, PHI, P4, T4, U4)
C
C     ISENTROPIC BLOWDOWN OF THE CONTROL MASS TO EXHAUST PRESSURE
C
      P5 = PE
      S5 = S4
      CALL BLWDWN(P5, S5, PHI, V5, T5, H5)
C
C     COMPUTE THE RESIDUAL FRACTION
C
      FOLD = F
      V6 = V5
      F = V4/V6/R
C
C     CONSTANT PRESSURE INTAKE AND EXHAUST
C
      H6 = H5
      H1 = F*(H6 + (PI - PE)*V6/10.) + (1. - F)*HI
      T1OLD = T1
      CALL TSTART(H1,PI,PHI,F,T1)
C
C     CONVERGENCE CHECK
C
      ERROR = AMAX1(ABS(1. - FOLD/F), ABS(1. - T1OLD/T1))
      IF( ERROR .LT. TOL ) ICHECK = ICHECK + 1
      IF( ICHECK .GE. 2 ) GO TO 20
10    CONTINUE
      WRITE(6,30)
30    FORMAT(' CONVERGENCE FAILURE')
20    CONTINUE
C
C     COMPUTE AND WRITE THE ANSWERS
C
      W = U1 - U4
```



```
      ETA = W*(1.0 + PHI*FS)/PHI/FS/(1.0 - F)/AO
      IMEP = W/(V1 - V2)*10.
C
      PMEP = PE - PI
      ETANET = ETA*(1. - PMEP/IMEP)
      EV = R*(1. - F)*VI/(R - 1.)/V1
C
      WRITE(6,40) ETANET, IMEP, PMEP, F, EV
40    FORMAT(' ETANET = ',1PE11.4,2X,'IMEP = ',1PE11.4,2X,'PMEP = ',
     &       1PE11.4,2X,'F = ',1PE11.4,2X,'EV = ',1PE11.4)
      STOP
      END
```

SOLUTION:

Execution of the program in Example 4.2 gives

```
ETANET = 4.4273e-01      IMEP = 9.3955e+00      PMEP = 3.0000e-01
F = 3.8623e-02      EV = 9.5863e-01
```

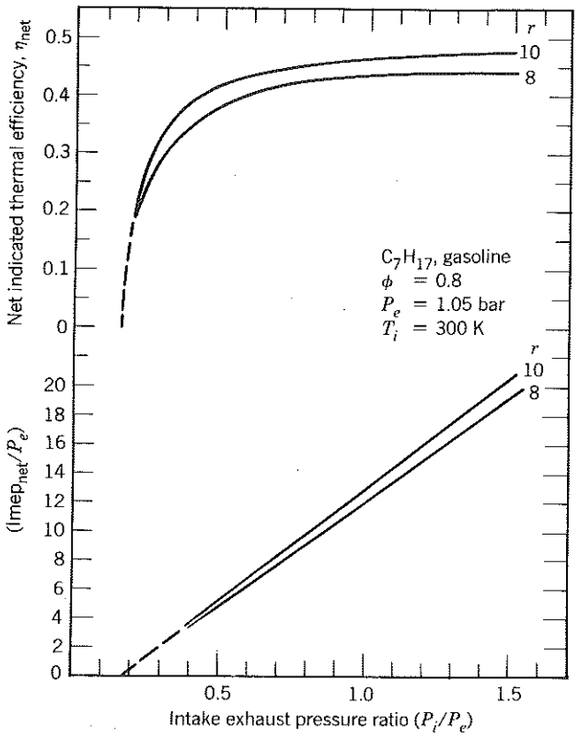

Figure 4-6 Characteristics of the Otto fuel–air cycle coupled with the ideal four-stroke intake and exhaust model. The efficiency drops dramatically below intake to exhaust pressure ratios of 0.5 because of the pumping loss.

Results obtained by varying the intake to exhaust pressure ratio and the compression ratio are given in Fig. 4-6 and 4-7. The net efficiency and the net indicated mean effective pressure are each seen to be a strong function of the pressure ratio. The advantage to turbocharging and the disadvantage of throttling are clear. For pressure ratios corresponding to supercharging, the curves are not representative, for one would have to account for the work to drive the compressor.

Notice that throttling also hurts the volumetric efficiency, mainly because of an increase in the residual fraction. The residual fraction decreases with compression ratio as one would expect.

The intake and exhaust portion of the cycle analyzed is not nearly as good as the compression, combustion, and expansion portion of the cycle. This

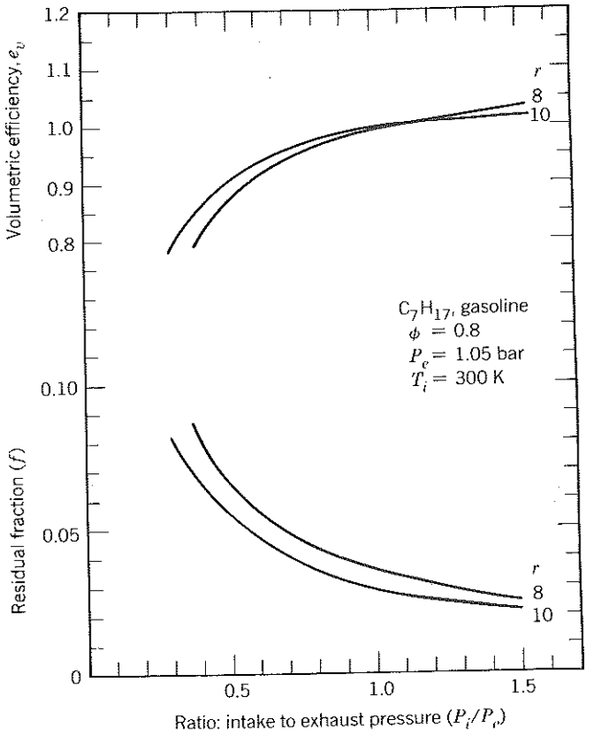

Figure 4-7 Characteristics of the Otto fuel–air cycle and four-stroke ideal intake and exhaust model. The volumetric efficiency drops and the residuals increase for pressure ratios less than 1 because of the reversion process. For pressure ratios greater than 1, the volumetric efficiency increases with pressure ratio because the incoming charge compresses the residual fraction in the clearance volume before filling the displaced volume.

is because of the neglect of heat transfer and the assumptions of isobaric intake and exhaust processes. As will be shown in Chapter 7, neglect of the heat transfer causes the residual fraction to be underpredicted by a factor on the order of 2. It will also be shown that the processes are isobaric only at very low piston speeds; consequently, at high piston speeds, the pumping mean effective pressure can be in considerable error and can even have the wrong sign for super- or turbo-charged engines.

4.3 FUEL-INJECTED LIMITED-PRESSURE CYCLE

This cycle models diesel engines and fuel injected stratified charge engines in which the fuel is injected at the time it is intended to burn. The processes are:

1 to 2	Isentropic compression of air and residual gas
2 to 2.5	Constant volume, adiabatic fuel injection, and combustion
2.5 to 3	Constant pressure, adiabatic fuel injection, and/or combustion
3 to 4	Isentropic expansion

These engines, in general, are fueled over all lean. In this case, the air residual gas mixture is equivalent to equilibrium combustion products at an equivalence ratio given by

$$\phi_{12} = \frac{f\phi}{1+(1-f)\phi F_s} \tag{4.17}$$

Thus the thermodynamic state during compression can be determined using the subroutine ECP with the equivalence ratio ϕ_{12} used as an argument. (In fact, the subroutine EXPAND already developed can be used here.)

The details of the fuel injection and combustion are of no concern. We need only assume that at state 3 the gases in the cylinder are equilibrium combustion products at the overall fuel–air equivalence ratio. To specify the state, we know that

$$P_3 \le P_{\text{limit}} \tag{4.18}$$

and we apply the energy equation to the process 2 to 3.

$$\Delta U = m_3u_3 - m_2u_2 = m_fh_f - P_3(m_3v_3 - m_2v_2) \tag{4.19}$$

Let us define the residual fraction to be the ratio of the residual mass to the cylinder gas mass prior to fuel injection (an assumption already used in Eq. (4.17)). It follows that

$$\frac{m_2}{m_3} = \frac{m_a + m_r}{m_a + m_r + m_f} = \frac{1}{1+(1-f)\phi F_s} \tag{4.20}$$

$$\frac{m_f}{m_3} = \frac{(1-f)\phi F_s}{1+\phi F_s(1-f)} \tag{4.21}$$

and the enthalpy at state 3 is

$$h_3 = \frac{u_2 + P_3v_2 + (1-f)\phi F_s h_f}{1+(1-f)\phi F_s} \tag{4.22}$$

The pressures during fuel injection P_f are high enough that Eq. (3.104) should be used in lieu of (3.109) to evaluate the fuel enthalpy. Hence

$$h_f = h_f^0 + v^0\left(P_f - P^0\right) \tag{4.23}$$

where the superscript zero denotes conditions at atmospheric pressure ($P^0 = 1.01325$ bar).

In doing a computation, one should first assume that the combustion and fuel injection are entirely at constant volume. If the resultant P_3 satisfies Eq. (4.18), then indeed the process is at constant volume. However if Eq. (4.18) is not satisfied, then $P_3 = P_{\text{limit}}$ and one solves Eq. (4.22) to find the state 3.

The expansion occurs to a specific volume at state 4 different than that at state 1 because of the fuel injected. It can be shown that expansion must satisfy the following constraints:

$$s_4 = s_3 \tag{4.24}$$

$$v_4 = \frac{rv_2}{1 + (1-f)\phi F_s} \tag{4.25}$$

To evaluate the work, it is convenient to split it into three parts due to the change in mass and energy by fuel injection. The works expressed per unit mass *after* fuel injection are

$$w_{12} = \frac{u_1 - u_2}{1 + \phi F_s(1-f)} \tag{4.26}$$

$$w_{23} = P_3\left[v_3 - \frac{v_2}{1 + \phi F_s(1-f)}\right] \tag{4.27}$$

$$w_{34} = u_3 - u_4$$

$$w_{\text{c.v.}} = w_{12} + w_{23} + w_{34} \tag{4.28}$$

The efficiency and imep are given by

$$\eta = \frac{w_{\text{c.v.}} m_3}{m_f a_o} = \frac{w_{\text{c.v.}}\left[1 + \phi F_s(1-f)\right]}{\phi F_s a_o (1-f)} \tag{4.29}$$

$$\text{imep} = \frac{w_{\text{c.v.}}\left[1 + \phi F_s(1-f)\right]}{v_1 - v_2} \tag{4.30}$$

Example (4.3), following, illustrates how to apply these equations to a stratified charge engine with diesel fuel injected at the time combustion is to commence.

EXAMPLE 4.3 FUEL INJECTED LIMITED PRESSURE FUEL AIR CYCLE


```
C
C      GIVEN:
C        COMPRESSION RATIO - R
C        FUEL AIR EQUIVALENCE RATIO - PHI
C        RESIDUAL MASS FRACTION - F
C        INITIAL PRESSURE - P1 (BAR)
C        INITIAL TEMPERATURE - T1 (K)
C        PLIM - LIMIT PRESSURE (BAR)
C        FUEL - T:T DIESEL
C
C      FIND:
C        INDICATED THERMAL EFFICIENCY - ETA
C        INDICATED MEAN EFFECTIVE PRESSURE - IMEP (BAR)
C        RATIO OF ETA TO ETA(OTTO) - ERATIO
C
C      NOTE:
C        1. SUBROUTINE FIBURN IS INTRODUCED TO HANDLE FUEL INJECTION
C           AND COMBUSTION ACCORDING TO EQUATION 4.22
C        2. THE EQUIVALENT OTTO CYCLE IS COMPUTED ASSUMING CONSTANT
C           VOLUME FUEL INJECTION AND COMBUSTION
C        3. THE FUEL INJECTION PRESSURE IS ASSUMED TO BE 150 BAR
C           THE FUEL TEMPERATURE IS ASSUMED TO BE 298 (K)
C        4. THE FUEL DATA STATEMENT IN ECP MUST BE MODIFIED TO
C           ACCOMODATE THE T-T DIESEL FUEL
C
      REAL IMEP, MFUEL
      DIMENSION Y1(10)
      DATA AO/45730./, FS/.06907/, HFUEL/-174000./, VFUEL/1.189/,
     &     PFUEL/150./, MFUEL/199.15/
      R = 15.
      F = .05
      P1 = 1.0
      T1 = 325.
      PHI = .50
      PLIM = 50.
C
C***     DO EQUIVALENT OTTO CYCLE FIRST   *****
C
C
C     ESTABLISH INITIAL STATE
C
      PHI12 = F*PHI/(1. + (1. - F)*PHI*FS)
      CALL ECP(P1, T1, PHI12, H1, U1, V1, S1, Y1, CP, DLVLT, DLVLP,IER)
C
C     ISENTROPIC COMPRESSION OF AIR & RESIDUAL GAS
C
      V2 = V1/R
      S2 = S1
      CALL EXPAND(V2, S2, PHI12, P2, T2, U2)
      IF( P2 .GT. PLIM ) GO TO 90
C
C     ADIABATIC, CONSTANT VOLUME FUEL INJECTION AND COMBUSTION
C
      V3 = V2/(1. + (1. - F)*PHI*FS)
      HF = HFUEL/MFUEL + (PFUEL - 1.01325)*VFUEL/10.
      U3 = (U2 + (1. - F)*PHI*FS*HF)/(1. + (1. - F)*PHI*FS)
      CALL COMBST(V3, U3, PHI, P3, T3, S3)
C
C     ISENTROPIC EXPANSION OF EQUILIBRIUM COMBUSTION PRODUCTS
C
      V4 = R*V3
      S4 = S3
      CALL EXPAND(V4, S4, PHI, P4, T4, U4)
C
```

```
C       COMPUTE ETAOTT
C
        W12 = (U1 - U2)/(1. + PHI*FS*(1. - F))
        W34 = U3 - U4
        W = W12 + W34
        ETAOTT = W*(1.0 + PHI*FS*(1.0 - F))/PHI/FS/(1.0 - F)/AO
C
C       COMPARE P3 WITH PLIM
C
        ERATIO = 1.
        IF( P3 .LT. PLIM ) GO TO 110
C
C***    NOW DO LIMITED PRESSURE FUEL INJECTION & COMBUSTION    ****
C
        P3 = PLIM
        H3 = (U2 + P3*V2/10. + (1. - F)*PHI*FS*HF)/(1. + (1. - F)*PHI*FS)
        CALL FIBURN(P3, H3, PHI, T3, U3, V3, S3)
C
C       ISENTROPIC EXPANSION
C
        S4 = S3
        CALL EXPAND(V4, S4, PHI, P4, T4, U4)
C
C       COMPUTE AND WRITE THE ANSWERS
C
        W12 = (U1 - U2)/(1. + PHI*FS*(1. - F))
        W23 = P3*(V3 - V2/(1. + PHI*FS*(1. - F)))/10.
        W34 =  U3 - U4
        W = W12 + W23 + W34
        ETA = W*(1. + PHI*FS*(1. - F))/PHI/FS/(1. - F)/AO
        ERATIO = ETA/ETAOTT
110     IMEP = W*(1. + PHI*FS*(1. - F))/(V1 - V2)*10.
        WRITE(6,10) ETA, ERATIO, IMEP
10      FORMAT(' ETA, ERATIO, IMEP = ',3(1PE11.4,2X))
        GO TO 80
90      WRITE(6,70)
70      FORMAT(' COMPRESSION RATIO IS TOO HIGH ')
80      STOP
        END
```

SOLUTION:

Execution of this program yields the following:

```
ETA, ERATIO, IMEP = 5.2553e-01   9.2586e-01   8.6166e+00
```

Results obtained via the method in Example 4.3 for different compression ratios and equivalence ratios are given in Fig. 4-8 and 4-9. Important conclusions are:

- The efficiency decreases with increased equivalence ratio.
- imep increases with equivalence ratio as one might expect.

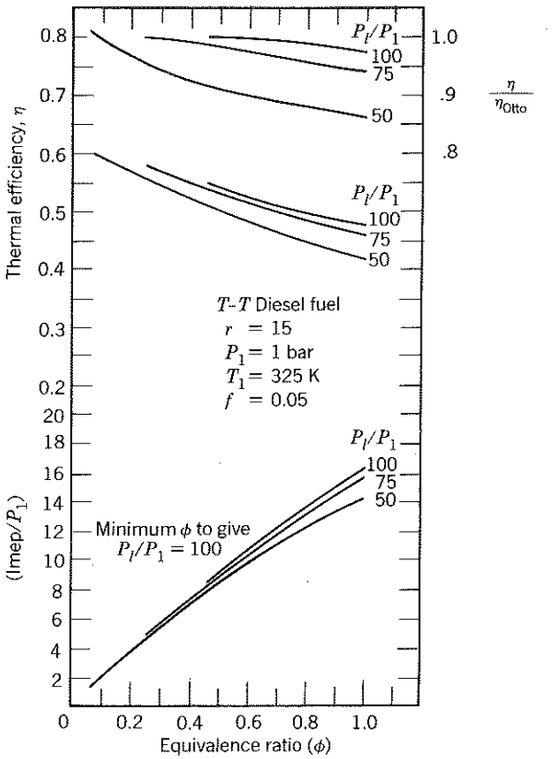

Figure 4-8 Characteristics of the limited pressure fuel injected fuel–air cycle. Again, the thermal efficiency is increased as the charge is burned leaner. The imep increases with equivalence ratio and, since the combustion is heterogeneous, the engine's torque can be controlled without throttling the air.

- Both efficiency and imep increase with increasing limit pressure.
- Even in the absence of heat and mass loss the ratio η/η_{otto} may be as low as 0.85.

In practice, the ratio η/η_{otto} for diesel and fuel injected stratified engines is more sensitive to the particular design and the operating conditions than it is for homogeneous-charge spark-ignition engines. Thus a greater range of indicated efficiencies exists among engines made by different manufacturers and among engines of different sizes.

Divided-chamber engines usually have a smaller ratio than openchamber engines partly because of throttling losses through the throat between chambers and but mainly because of a greater heat loss.

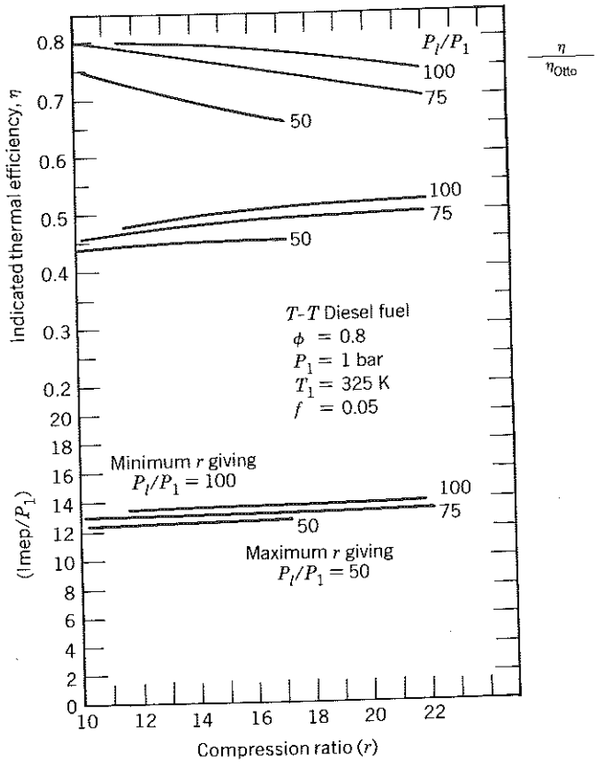

Figure 4-9 Characteristics of the limited pressure fuel injected fuel–air cycle. The constraint on peak pressure results in the efficiency and imep being insensitive to compression ratio.

4.4 ARBITRARY HEAT RELEASE—FUEL INDUCTED ENGINES

Here we analyze a cycle in which fuel and air are inducted through the inlet valve. As in Chapter 2, a differential form of the energy conservation equation applied to an open system is solved. For a control volume encasing the cylinder contents, the energy equation is

$$m\frac{du}{d\theta}+u\frac{dm}{d\theta}=\frac{dQ}{d\theta}-P\frac{dV}{d\theta}-\frac{\dot{m}_l h_l}{\omega} \tag{4.31}$$

Equation (2.37), considered earlier, is a special case of Eq. (4.31) where the specific heats of the fluid are constant. That assumption will no longer be employed; rather the fluid will have internal energy and enthalpy dependent upon temperature and pressure according to the relations programmed into the subroutines FARG and ECP.

An empirical relationship expressing the fraction of the heat added at any time to the crank angle was employed in Chapter 2. In this analysis those

same empirical functions, Eq. (2.21) or (2.22), will be employed, but x will be defined as the mass fraction of the cylinder contents that have been burned. The energy of the system is then assumed to be

$$u=\frac{U}{m}=xu_b+(1-x)u_u \tag{4.32}$$

where u_b is the energy of the burned gas that is at a temperature T_b and u_u is the energy of the unburned gas at a temperature T_u. Likewise, the specific volume of the system is given by

$$v=\frac{V}{m}=xv_b+(1-x)v_u \tag{4.33}$$

We will derive a set of ordinary differential equations describing the rates of change of pressure, work, and heat loss with respect to crank angle. By simultaneously integrating these equations from the start of compression until the end of expansion, the pressure–volume diagram, the indicated efficiency, and indicated mean effective pressure are determined.

To this end let us represent the functional relationship between v_b, T_b, and P as

$$v_b=v_b(T_b,P) \tag{4.34}$$

and differentiate this expression with respect to crank angle. It follows that

$$\frac{dv_b}{d\theta}=\frac{\partial v_b}{\partial T_b}\frac{dT_b}{d\theta}+\frac{\partial v_b}{\partial P}\frac{dP}{d\theta} \tag{4.35}$$

and we can see the emergence of one of the derivatives we seek, that is, $dP/d\theta$.

The subroutine ECP was programmed to return the requisite partial derivatives in logarithmic form. Substitution of the logarithmic derivatives into Eq. (4.35) yields

$$\frac{dv_b}{d\theta}=\frac{v_b}{T_b}\frac{\partial \ln v_b}{\partial \ln T_b}\frac{dT_b}{d\theta}+\frac{v_b}{P}\frac{\partial \ln v_b}{\partial \ln P}\frac{dP}{d\theta} \tag{4.36}$$

By analogy

$$\frac{dv_u}{d\theta}=\frac{v_u}{T_u}\frac{\partial \ln v_u}{\partial \ln T_u}\frac{dT_u}{d\theta}+\frac{v_u}{P}\frac{\partial \ln v_u}{\partial \ln P}\frac{dP}{d\theta} \tag{4.37}$$

The relationship between u_b, T_b, and p is represented as

$$u_b=u_b(T_b,P) \tag{4.38}$$

and

$$\frac{du_b}{d\theta}=\frac{\partial u_b}{\partial T_b}\frac{dT_b}{d\theta}+\frac{\partial u_b}{\partial P}\frac{dP}{d\theta} \tag{4.39}$$

Introducing the partial derivatives returned by ECP through Eq. (3.142) and (3.143) leads to

$$\frac{du_b}{d\theta}=\left(c_{Pb}-\frac{Pv_b}{T_b}\frac{\partial \ln v_b}{\partial \ln T_b}\right)\frac{dT_b}{d\theta}-v_b\left(\frac{\partial \ln v_b}{\partial \ln T_b}+\frac{\partial \ln v_b}{\partial \ln P}\right)\frac{dP}{d\theta} \tag{4.40}$$

Likewise for the unburned gas

$$\frac{du_u}{d\theta}=\left(c_{Pu}-\frac{Pv_u}{T_u}\frac{\partial \ln v_u}{\partial \ln T_u}\right)\frac{dT_u}{d\theta}-v_u\left(\frac{\partial \ln v_u}{\partial \ln T_u}+\frac{\partial \ln v_u}{\partial \ln p}\right)\frac{dP}{d\theta} \tag{4.41}$$

One comment is in order before proceeding. We have tacitly assumed that the pressures of the burned and unburned gas are equal, which, as mentioned earlier, is a good approximation for open-chamber engines.

Let us now consider the energy equation Eq. (4.31) term by term. By Eq. (4.32), the first term on the left is developed as follows:

$$m\frac{du}{d\theta}=\left[x\frac{du_b}{d\theta}+(1-x)\frac{du_u}{d\theta}+(u_b-u_u)\frac{dx}{d\theta}\right]m \tag{4.42}$$

Substitution of Eqs. (4.40) and (4.41) then give

$$\begin{aligned}m\frac{du}{d\theta}=&\,mx\left(c_{Pb}-\frac{Pv_b}{T_b}\frac{\partial \ln v_b}{\partial \ln T_b}\right)\frac{dT_b}{d\theta}+m(1-x)\left(c_{Pu}-\frac{Pv_u}{T_u}\frac{\partial \ln v_u}{\partial \ln T_u}\right)\frac{dT_u}{d\theta}\\&-\left[mxv_b\left(\frac{\partial \ln v_b}{\partial \ln T_b}+\frac{\partial \ln v_b}{\partial \ln P}\right)+m(1-x)v_u\left(\frac{\partial \ln v_u}{\partial \ln T_u}+\frac{\partial \ln v_u}{\partial \ln p}\right)\right]\frac{dP}{d\theta}\\&+m(u_b-u_u)\frac{dx}{d\theta}\end{aligned} \tag{4.43}$$

The remaining term on the left-hand side requires introduction of mass conservation and an algorithm to compute the blowby. As before, we shall write

$$\frac{dm}{d\theta}=\frac{-\dot m_l}{\omega}=\frac{-Cm}{\omega} \tag{4.44}$$

where C is the blowby constant dependent upon ring design, a discussion of which is deferred to Chapter 8.

The heat into the system, on the right-hand side of Eq. (4.31), will be expressed in terms of the heat loss

$$\frac{dQ}{d\theta}=\frac{-\dot Q_l}{\omega}=\frac{-\dot Q_b-\dot Q_u}{\omega} \tag{4.45}$$

from the burned and unburned gas, respectively.

To express the heat loss in terms of temperature requires the introduction of a heat transfer coefficient $\mathbf{h}$

$$\dot Q_b=\mathbf{h}A_b(T_b-T_w) \tag{4.46}$$

$$\dot Q_u=\mathbf{h}A_u(T_u-T_w) \tag{4.47}$$

where A_b and A_u are the areas of burned and unburned gas in contact with the cylinder walls at temperature T_w. To calculate the areas A_b and A_u, let us

suppose that

$$A_b=\left(\frac{\pi b^2}{2}+\frac{4V}{b}\right)x^{1/2} \tag{4.48}$$

$$A_u=\left(\frac{\pi b^2}{2}+\frac{4V}{b}\right)1-x^{1/2} \tag{4.49}$$

Equations (4.48) and (4.49) are empirical functions that have the correct limits in the case of a cylinder where $x\to 0$ and when $x\to 1$. The fraction of cylinder area contacted by burned gas is assumed to be proportional to the square root of the mass fraction burned to reflect the fact, because of the density difference between burned and unburned gas, the burned gas occupies a larger volume fraction of the cylinder than the unburned gas.

In practice, the exponent on x may be left as a free parameter to be determined from experiments, or a more complicated scheme may be used based on an assumption about the flame shape. We have assumed, for convenience, that $\mathbf{h}_u=\mathbf{h}_b=\mathbf{h}=$ constant. Again one will find a more realistic approach used in practice, which in this case we defer to Chapter 8.

The work term in Eq. (4.31) requires no further explanation, but we need to specify the enthalpy of the mass loss due to blowby. Early in the combustion process, unburned gas leaks past the rings. Late in the combustion process, burned gas leaks past the rings. In the spirit of being conceptually correct while deviating from what might be done in practice, let us assume that

$$h_l=(1-x^2)h_u+x^2h_b \tag{4.50}$$

which has the correct limits and recognizes that a larger portion of unburned gas will be leaking than the unburned mass fraction. Finally, to complete Eq. (4.50), the equations of state must now include

$$h_u=h_u(T_u,P) \tag{4.51}$$

$$h_b=h_b(T_b,P) \tag{4.52}$$

and are computed by subroutines FARG and ECP, respectively.

Examination of all the terms of Eq. (4.31) just discussed reveals the following derivatives in that equation

$$\frac{dP}{d\theta},\frac{dT_b}{d\theta},\frac{dT_u}{d\theta},\frac{dV}{d\theta},\frac{dx}{d\theta} \tag{4.53}$$

and the following variables

$$P,T_b,T_u \tag{4.54}$$

$$u_b,u_u,v_b,v_u,h_b,h_u \tag{4.55}$$

$$\frac{\partial \ln v_b}{\partial \ln T_b},\frac{\partial \ln v_u}{\partial \ln T_u},\frac{\partial \ln v_b}{\partial \ln P},\frac{\partial \ln v_u}{\partial \ln P},c_{Pb},c_{Pu} \tag{4.56}$$

$$m,V,x \tag{4.57}$$

$$C,\omega,\mathbf{h},b \tag{4.58}$$

The variables in (4.58) are all constants specified according to the engine type and operating characteristics.

The variables in Eq. (4.57) are all known functions of crank angle. The mass at any angle is

$$m = m_1 \exp\left[-C(\theta - \theta_1)/\omega\right] \tag{4.59}$$

which follows from integration of Eq. (4.44). The initial mass m_1 at $\theta = \theta_1$ (start of compression) is specified from knowledge of the volumetric efficiency and residual fraction. The cylinder volume is known from the compression ratio r, volume at *tdc* V_0, and $\epsilon = S/2l$ (S = stroke, l = rod length) to be

$$V = V_o\left[\left[1 + \frac{r-1}{2}\left\{1 - \cos\theta + \frac{1}{\epsilon}\left[1 - (1 - \epsilon^2 \sin^2\theta)^{1/2}\right]\right\}\right]\right] \tag{4.60}$$

The mass fraction burned is known from the empirical burning law, for example

$$x = \begin{cases} 0 & \theta < \theta_s \\ \frac{1}{2}\left\{1 - \cos\left[\dfrac{\pi(\theta - \theta_s)}{\theta_b}\right]\right\} & \theta_s < \theta < \theta_s + \theta_b \\ 1 & \theta > \theta_s + \theta_b \end{cases} \tag{4.61}$$

All the variables in the lists (4.55) and (4.56) are thermodynamic properties and known functions (via ECP and FARG) of P, T_b, and T_u.

The derivatives $dV/d\theta$ and $dx/d\theta$ in Eq. (4.53) are known by differentiating (4.60) and Eq. (4.61), respectively. The energy equation (4.31) is thus seen to be a relationship among three derivatives, their integrals, and parameters dependent upon the integrals. In other words, we have an equation of the following form:

$$f\left(\theta, \frac{dP}{d\theta}, \frac{dT_b}{d\theta}, \frac{dT_u}{d\theta}, P, T_b, T_u\right) = 0 \tag{4.62}$$

If we can find two more equations, then we can rearrange them into the standard form used to numerically integrate a set of ordinary differential equations.

$$\frac{dP}{d\theta} = f_1(\theta, P, T_b, T_u) \tag{4.63}$$

$$\frac{dT_b}{d\theta} = f_2(\theta, P, T_b, T_u) \tag{4.64}$$

$$\frac{dT_u}{d\theta} = f_3(\theta, P, T_b, T_u) \tag{4.65}$$

We will find it convenient to integrate simultaneously for the work done, the heat lost, and the enthalpy lost.

$$\frac{dW}{d\theta} = f_4(\theta, P) \tag{4.66}$$

$$\frac{dQ_l}{d\theta} = f_5(\theta, P, T_b, T_u) \tag{4.67}$$

$$\frac{dH_l}{d\theta} = f_6(\theta, P, T_b, T_u) \tag{4.68}$$

One of the requisite equations can be derived from Eq. (4.33) for the specific volume of the system. Differentiating it and incorporating Eq. (4.36) and (4.37) yield

$$\frac{1}{m}\frac{dV}{d\theta} - \frac{V}{m^2}\frac{dm}{d\theta} = x\frac{dv_b}{d\theta} + (1-x)\frac{dv_u}{d\theta} + (v_b - v_u)\frac{dx}{d\theta}$$

$$\frac{1}{m}\frac{dV}{d\theta} + \frac{VC}{m\omega} = x\frac{v_b}{T_b}\frac{\partial \ln v_b}{\partial \ln T_b}\frac{dT_b}{d\theta} + (1-x)\frac{v_u}{T_u}\frac{\partial \ln v_u}{\partial \ln T_u}\frac{dT_u}{d\theta}$$

$$+\left[x\frac{v_b}{P}\frac{\partial \ln v_b}{\partial \ln P} + (1-x)\frac{v_u}{P}\frac{\partial \ln v_u}{\partial \ln P}\right]\frac{dP}{d\theta} + (v_b - v_u)\frac{dx}{d\theta} \tag{4.69}$$

The remaining equation comes from introduction of the unburned gas entropy into the analysis. Treating the unburned gas as an open system losing mass via leakage and combustion, it can be shown that

$$-\dot{Q}_u = \omega m(1-x)T_u\frac{ds_u}{d\theta} \tag{4.70}$$

To utilize Eq. (4.70), the equation of state relating entropy to temperature and pressure must be introduced.

$$s_u = s_u(T_u, p) \tag{4.71}$$

From which it follows that

$$\frac{ds_u}{d\theta} = \left(\frac{\partial s_u}{\partial T_u}\right)\frac{dT_u}{d\theta} + \left(\frac{\partial s_u}{\partial P}\right)\frac{dP}{d\theta} \tag{4.72}$$

$$\frac{ds_u}{d\theta} = \left(\frac{c_{Pu}}{T_u}\right)\frac{dT_u}{d\theta} - \frac{v_u}{T_u}\frac{\partial \ln v_u}{\partial \ln T_u}\frac{dP}{d\theta} \tag{4.73}$$

Elimination of $ds_u/d\theta$ between Eq. (4.70) and (4.73) gives

$$c_{Pu}\frac{dT_u}{d\theta} - v_u\frac{\partial \ln v_u}{\partial \ln T_u}\frac{dP}{d\theta} = \frac{-\mathbf{h}\left(\dfrac{\pi b^2}{2} + \dfrac{4V}{b}\right)}{\omega m}\frac{(1-x^{1/2})}{(1-x)}(T_u - T_w) \tag{4.74}$$

The three equations that will produce Eq. (4.63) through (4.65) are thus Eq.

(4.31), (4.69), and (4.74). For convenience, let us define the following variables:

$$A = \frac{1}{m}\left(\frac{dV}{d\theta} + \frac{VC}{\omega}\right) \tag{4.75}$$

$$B = \mathbf{h}\frac{\left(\frac{\pi b^2}{2} + \frac{4V}{b}\right)}{\omega m}\left[\frac{v_b}{c_{Pb}}\frac{\partial \ln v_b}{\partial \ln T_b}x^{1/2}\frac{T_b - T_w}{T_b} + \frac{v_u}{c_{Pu}}\frac{\partial \ln v_u}{\partial \ln T_u}(1 - x^{1/2})\frac{T_u - T_w}{T_w}\right] \tag{4.76}$$

$$\mathbf{C} = -(v_b - v_u)\frac{dx}{d\theta} - v_b\frac{\partial \ln v_b}{\partial \ln T_b}\frac{h_u - h_b}{c_{Pb}T_b}\left[\frac{dx}{d\theta} - \frac{(x - x^2)C}{\omega}\right] \tag{4.77}$$

$$D = x\left[\frac{v_b^2}{c_{Pb}T_b}\left(\frac{\partial \ln v_b}{\partial \ln T_b}\right)^2 + \frac{v_b}{P}\frac{\partial \ln v_b}{\partial \ln P}\right] \tag{4.78}$$

$$E = (1 - x)\left[\frac{v_u^2}{c_{Pu}T_u}\left(\frac{\partial \ln v_u}{\partial \ln T_u}\right)^2 + \frac{v_u}{P}\frac{\partial \ln v_u}{\partial \ln P}\right] \tag{4.79}$$

Finally, the six equations to be integrated are:

$$\frac{dP}{d\theta} = \frac{A + B + \mathbf{C}}{D + E} \tag{4.80}$$

$$\frac{dT_b}{d\theta} = \frac{-\mathbf{h}\left(\frac{\pi b^2}{2} + \frac{4V}{b}\right)x^{1/2}(T_b - T_w)}{\omega m c_{Pb}x} + \frac{v_b}{c_{Pb}}\frac{\partial \ln v_b}{\partial \ln T_b}\left(\frac{A + B + \mathbf{C}}{D + E}\right) + \frac{h_u - h_b}{xc_{Pb}}\left[\frac{dx}{d\theta} - (x - x^2)\frac{C}{\omega}\right] \tag{4.81}$$

$$\frac{dT_u}{d\theta} = \frac{-\mathbf{h}\left(\frac{\pi b^2}{2} + \frac{4V}{b}\right)(1 - x^{1/2})(T_u - T_w)}{\omega m c_{Pu}(1 - x)} + \frac{v_u}{c_{Pu}}\frac{\partial \ln v_u}{\partial \ln T_u}\left(\frac{A + B + \mathbf{C}}{D + E}\right) \tag{4.82}$$

$$\frac{dW}{d\theta} = P\frac{dV}{d\theta} \tag{4.83}$$

$$\frac{dQ_l}{d\theta} = \frac{\mathbf{h}}{\omega}\left(\frac{\pi}{2}b^2 + \frac{4V}{b}\right)\left[x^{1/2}(T_b - T_u) + (1 - x^{1/2})(T_u - T_w)\right] \tag{4.84}$$

$$\frac{dH_l}{d\theta} = \frac{Cm}{\omega}\left[(1 - x^2)h_u + x^2 h_b\right] \tag{4.85}$$

EXAMPLE 4.4 ARBITRARY HEAT RELEASE (FUEL INDUCTED)

```
C
C       GIVEN IN BLOCK DATA SUBPROGRAM:
C         COMPRESSION RATIO - R
C         BORE - B (CM)
C         STROKE - S (CM)
C         HALF STROKE TO ROD RATIO - EPS
C         ENGINE SPEED - RPM
C         HEAT TRANSFER COEFFICIENT - H (J/S/M**2/K)
C         BLOWBY COEFFICIENT - C (1/S)
C         EQUIVALENCE RATIO - PHI
C         RESIDUAL FRACTION - F
C         INITIAL PRESSURE  - P1 (BAR)
C         INITIAL TEMPERATURE - T1 (K)
C         WALL TEMPERATURE - TW (K)
C         BURN ANGLE - THETAB (DEG)
C         START OF HEAT RELEASE - THETAS (DEG ATDC)
C
C       FIND:
C         INDICATED THERMAL EFFICIENCY - ETA
C         INDICATED MEAN EFFECTIVE PRESSURE - IMEP (BAR)
C
C       NOTE:
C         1. COSINE BURNING LAW IS EMPLOYED, EQN. 4.61
C         2. FUEL - GASOLINE (C7H17)
C
        EXTERNAL RATES
        REAL IMEP, MNOT, M
        COMMON /ENGINE/ R, B, S, EPS, RPM, H, C, THETAB, THETAS,
     &                  PHI, F, P1, T1, TW, MNOT, OMEGA, UNOT, UFINAL
        DIMENSION Y1(6), Y2(10), Y(6), COM(24), WM(6,9)
        DATA AO/47870./, FS/.06548/, Y/1., 10000., 350., 3*0.0/,
     &       N/6/, THETA/-180./, THETAE/-179./, TOL/.001/, IND/1/,
     &       NW/6/, PI/3.141593/, Y2/10*0.0/
C
C       LABEL HEADER ON OUTPUT PAGE AND PRINT INITIAL CONDITIONS
C
        OMEGA = RPM*PI/30.
        CALL AUXLRY(THETA, V, X, EM)
        Y(1) = P1
        Y(3) = T1
        CALL FARG(Y(1), Y(3), PHI, F, HU, U, VU, SU, Y1, CP, DLVLT,
     &       DLVLP)
        MNOT = V/VU
        UNOT = MNOT*U
        WRITE(6,10)
10      FORMAT(5X,'THETA',4X,'VOLUME',3X,'BURN FRAC',2X,'PRESSURE',3X,
     &         'BURN TEMP',2X,'T UNBURN',3X,'WORK',3X,'HEAT LOSS',5X,
     &         'MASS',3X,'H-LEAK')
        WRITE(6,15)
15      FORMAT(4X,'DEG ATDC',2X,'CM**3',6X,'--',8X,'BARS',7X,'KELVIN',
     &         5X,'KELVIN',3X,'JOULES',4X,'JOULES',6X,'GRAMS',2X,
     &         'JOULES')
        WRITE(6,20) THETA, V, X, (Y(I),I=1,5), MNOT, Y(6)
20      FORMAT(4X,F5.0,6X,F5.0,4X,F5.3,6X,F5.2,7X,F5.0,5X,F5.0,
     &         5X,F5.0,3X,F5.0,7X,F5.3,3X,F5.2)
C
```

```
C
C       INTEGRATE THE RATE EQUATIONS 4.80 - 4.85 AND PRINT ANSWERS
C       EVERY 10 DEGREES
C
        DO 30 I = 1,36
        DO 25 J = 1,10
        CALL DVERK (N, RATES, THETA, Y, THETAE, TOL, IND, COM, NW, WM,
     &              IERROR)
        CALL AUXLRY(THETAE, V, X, EM)
        M = EM*MNOT
        THETA = THETAE
        THETAE = THETA + 1.
        IF(THETAS .GE. THETA .AND. THETAS .LT. THETAE)
     &  CALL TINITL(Y(1), Y(3), PHI, F, Y(2))
        IF(THETA .GT. THETAS + THETAB) Y(3) = 10000.
25      CONTINUE
        WRITE(6,20) THETA, V, X, (Y(J),J=1,5), M, Y(6)
30      CONTINUE
C
C       COMPUTE AND WRITE THE ETA, IMEP AND ERRORS
C
        CALL ECP(Y(1), Y(2), PHI, HB, U, VB, SB, Y2, CP, DLVLT, DLVLP,
     &           IER)
        UFINAL = U*M
        ERROR1 = 1.0 - VB*M/V
        ERROR2 = 1.0 + Y(4)/(UFINAL - UNOT + Y(5) + Y(6))
        ETA = Y(4)/MNOT*(1. + PHI*FS*(1. - F))/PHI/FS/(1. - F)/AO
        IMEP = Y(4)/(PI/4.*B**2*S)*10.
        WRITE(6,40) ETA, IMEP, ERROR1, ERROR2
40      FORMAT('ETA = ',1PE11.4,' IMEP = ',1PE11.4,' ERROR1 =',1PE11.4,
     &         ' ERROR2 = ',1PE11.4)
        STOP
        END
C
C
        SUBROUTINE RATES(N, THETA, Y, YPRIME)
        DIMENSION Y1(6), Y2(10)
        REAL Y(N), YPRIME(N), M, MNOT
        COMMON /ENGINE/ R, BORE, STROKE, EPS, RPM, HEAT, CEE, THETAB,
     &                  THETAS, PHI, F, P1, T1, TW, MNOT, OMEGA, UNOT,
     &                  UFINAL
        DATA PI/3.141593/, Y2/10*0.0/
        CALL AUXLRY(THETA, V, X, EM)
        M = EM*MNOT
        RAD = THETA*PI/180.
        DUMB = SQRT(1. - (EPS*SIN(RAD))**2)
        DV = PI/8.*BORE**2*STROKE*SIN(RAD)*(1. + EPS*COS(RAD)/DUMB)
        A = (DV + V*CEE/OMEGA)/M
        C1 = HEAT*(PI*BORE**2/2. + 4.*V/BORE)/OMEGA/M/10000.
        C0 = SQRT(X)
C
C       THREE DIFFERENT COMPUTATIONS ARE REQUIRED DEPENDING
C       UPON THE SIZE OF THE MASS FRACTION BURNED
C
        IF( X .GT. .999 ) GO TO 20
        IF( X .GT. .001 ) GO TO 10
C
C       COMPRESSION
C
```



```
        CALL FARG(Y(1), Y(3), PHI, F, HL, U, VU, S, Y1, CP, DLVLT,
     &            DLVLP)
        B = C1*VU/CP*DLVLT*(1.0 - TW/Y(3))
        C = 0.
        D = 0.
        E = VU**2/CP/Y(3)*DLVLT**2 + 10.*VU/Y(1)*DLVLP
        YPRIME(1) = (A + B + C)/(D + E)*10.
        YPRIME(2) = 0.
        YPRIME(3) = -C1/CP*(Y(3) - TW) + VU/CP*DLVLT*YPRIME(1)/10.
        GO TO 30
C
C       COMBUSTION
C
10      CALL FARG(Y(1), Y(3), PHI, F, HU, U, VU, S, Y1, CPU, DLVLTU,
     &            DLVLPU)
        CALL ECP(Y(1), Y(2), PHI, HB, U, VB, S, Y2, CPB, DLVLTB, DLVLPB,
     &       IER)
        B = C1*(VB/CPB*DLVLTB*C0*(1. - TW/Y(2)) + VU/CPU*DLVLTU*
     &      (1. - C0)*(1. - TW/Y(3)))
        DX = 0.5*SIN(PI*(THETA - THETAS)/THETAB)*180./THETAB
        C = -(VB - VU)*DX - VB/Y(2)*DLVLTB*(HU - HB)/CPB*(DX - (X -
     &      X**2)*CEE/OMEGA)
        D = X*(VB**2/CPB/Y(2)*DLVLTB**2 + 10.*VB/Y(1)*DLVLPB)
        E = (1. - X)*(VU**2/CPU/Y(3)*DLVLTU**2 + 10.*VU/Y(1)*DLVLPU)
        HL = (1.0 - X**2)*HU + X**2*HB
        YPRIME(1) = (A + B + C)/(D + E)*10.
        YPRIME(2) = -C1/CPB/C0*(Y(2) - TW) + VB/CPB*DLVLTB*
     &              YPRIME(1)/10. + (HU - HB)/CPB*(DX/X - (1. - X)*
     &              CEE/OMEGA)
        YPRIME(3) = -C1/CPU/(1. + C0)*(Y(3) - TW) + VU/CPU*DLVLTU*
     &              YPRIME(1)/10.
        GO TO 30
C
C       EXPANSION
C
20      CALL ECP(Y(1), Y(2), PHI, HL, U, VB, S, Y2, CP, DLVLT, DLVLP,
     &           IER)
        B = C1*VB/CP*DLVLT*(1. - TW/Y(2))
        C = 0.
        D = VB**2/CP/Y(2)*DLVLT**2 + 10.*VB/Y(1)*DLVLP
        E = 0.
        YPRIME(1) = (A + B + C)/(D + E)*10.
        YPRIME(2) = -C1/CP*(Y(2) - TW) + VB/CP*DLVLT*YPRIME(1)/10.
        YPRIME(3) = 0.
C
C       ALL CASES
C
30      YPRIME(4) = Y(1)*DV/10.
        YPRIME(5) = C1*M*(C0*(Y(2) - TW) + (1. - C0)*(Y(3) - TW))
        YPRIME(6) = CEE*M/OMEGA*HL
        DO 40 I = 1,N
40      YPRIME(I) = YPRIME(I)*PI/180.
        RETURN
        END
C
C
        SUBROUTINE AUXLRY(THETA, V, X, EM)
        COMMON /ENGINE/ R, B, S, EPS, RPM, H, C, THETAB, THETAS,
     &                  PHI, F, P1, T1, TW, EMNOT, OMEGA, UNOT, UFINAL
```

```
      DATA PI/3.141593/
      RAD = THETA*PI/180.
      VTDC = PI/4.*B**2*S/(R - 1.)
      V = VTDC*(1. + (R - 1.)/2.*(1. - COS(RAD) + 1./EPS*(1. -
     &     SQRT(1. - (EPS*SIN(RAD))**2))))
      X = 0.5*(1. - COS(PI*(THETA - THETAS)/THETAB))
      IF(THETA .LE. THETAS) X = 0.
      IF(THETA .GE. THETAS + THETAB) X = 1.
      EM = EXP(-C*(RAD + PI)/OMEGA)
      RETURN
      END
C
C
      BLOCK DATA
      COMMON /ENGINE/ R, B, S, EPS, RPM, H, C, THETAB, THETAS,
     &                PHI, F, P1, T1, TW, EMNOT, OMEGA, UNOT, UFINAL
      DATA R/10./, B/10./, S/8./, EPS/.25/, RPM/2000./, H/500./,
     &     C/0.8/, THETAB/60./, THETAS/-35./,  PHI/0.8/, F/.1/,
     &     P1/1.0/, T1/350./, TW/420./
      END
C
C
      SUBROUTINE TINITL(P, TU, PHI, F, TB)
      DIMENSION Y1(6), Y2(10)
      DATA MAXITS/50/, TOL/.001/, Y2/10*0.0/
      TB = 2000.
      CALL FARG(P, TU, PHI, F, HU, U, V, S, Y1, CP, DLVLT, DLVLP)
      DO 10 I = 1,MAXITS
      CALL ECP(P, TB, PHI, HB, U, V, S, Y2, CP, DLVLT, DLVLP, IER)
      DELT = (HU - HB)/CP
      TB = TB + DELT
      IF(ABS(DELT/TB) .LT. TOL) RETURN
10    CONTINUE
      WRITE(6,20)
20    FORMAT('CONVERGENCE FAILURE IN TINITL')
      RETURN
      END
```

SOLUTION:

THETA DEG ATDC	VOLUME CM**3	BURN FRAC --	PRESSURE BARS	BURN TEMP KELVIN	T UNBURN KELVIN	WORK JOULES	HEAT LOSS JOULES	MASS GRAMS	H-LEAK JOULES
-180.	698.	0.	1.00	*****	350.	0.	0.	0.714	0.
-170.	695.	0.	1.01	*****	353.	-0.	-1.	0.714	-0.14
-160.	684.	0.	1.04	*****	357.	-1.	-2.	0.713	-0.28
-150.	666.	0.	1.08	*****	362.	-3.	-4.	0.713	-0.42
-140.	641.	0.	1.14	*****	369.	-6.	-4.	0.712	-0.56
-130.	609.	0.	1.23	*****	377.	-10.	-5.	0.712	-0.69
-120.	571.	0.	1.35	*****	386.	-15.	-6.	0.711	-0.81
-110.	527.	0.	1.50	*****	398.	-21.	-6.	0.711	-0.93
-100.	477.	0.	1.72	*****	413.	-29.	-7.	0.710	-1.05
-90.	424.	0.	2.01	*****	430.	-39.	-7.	0.710	-1.15
-80.	368.	0.	2.43	*****	451.	-51.	-6.	0.709	-1.25
-70.	312.	0.	3.02	*****	476.	-67.	-6.	0.709	-1.34
-60.	257.	0.	3.91	*****	507.	-85.	-5.	0.708	-1.41
-50.	205.	0.	5.24	*****	544.	-109.	-4.	0.708	-1.46
-40.	160.	0.	7.28	*****	588.	-137.	-2.	0.708	-1.49
-30.	122.	0.017	10.90	2143.	647.	-170.	-0.	0.707	-1.49
-20.	93.	0.146	20.93	2296.	752.	-232.	5.	0.707	-1.45
-10.	76.	0.371	38.59	2439.	863.	-262.	14.	0.706	-1.34

THETA DEG ATDC	VOLUME CM**3	BURN FRAC --	PRESSURE BARS	BURN TEMP KELVIN	T UNBURN KELVIN	WORK JOULES	HEAT LOSS JOULES	MASS GRAMS	H-LEAK JOULES
0.	70.	0.629	56.28	2514.	936.	-289.	27.	0.706	-1.15
10.	76.	0.654	61.31	2497.	952.	-253.	41.	0.705	-0.91
20.	93.	0.983	52.13	2400.	916.	-152.	57.	0.705	-0.68
30.	122.	1.000	37.80	2248.	*****	-26.	73.	0.704	-0.53
40.	160.	1.000	26.80	2098.	*****	94.	88.	0.704	-0.50
50.	205.	1.000	19.40	1948.	*****	198.	104.	0.703	-0.58
60.	257.	1.000	14.51	1822.	*****	284.	119.	0.703	-0.75
70.	312.	1.000	11.24	1734.	*****	355.	134.	0.702	-0.99
80.	368.	1.000	8.99	1621.	*****	411.	149.	0.702	-1.30
90.	424.	1.000	7.42	1541.	*****	457.	165.	0.701	-1.67
100.	477.	1.000	6.29	1472.	*****	493.	180.	0.701	-2.09
110.	527.	1.000	5.47	1412.	*****	522.	195.	0.700	-2.54
120.	571.	1.000	4.86	1360.	*****	545.	210.	0.700	-3.03
130.	609.	1.000	4.40	1315.	*****	563.	225.	0.700	-3.55
140.	641.	1.000	4.05	1276.	*****	576.	240.	0.699	-4.10
150.	666.	1.000	3.79	1241.	*****	586.	255.	0.699	-4.67
160.	684.	1.000	3.60	1212.	*****	593.	269.	0.698	-5.26
170.	695.	1.000	3.47	1186.	*****	596.	283.	0.698	-5.86
180.	698.	1.000	3.39	1165.	*****	598.	297.	0.697	-6.48

ETA = 3.8821e-01 IMEP = 9.5102e+00 ERROR1 = -5.2238e-04 ERROR2 = 1.0633e-04

Some comments are in order regarding the preceding program.

Otto Cycle The equivalent fuel—air Otto cycle predicts $\eta = 0.460$, hence $\eta/\eta_{\text{otto}} = 0.845$.

Losses The efficiency is less than that of the equivalent Otto cycle because of the finite burning angle, the heat loss, and the blowby. The analysis in Chapter 2 estimated well the contributions to η/η_{otto} that can be attributed to the finite burning angle and the heat loss. But that analysis underestimates the effect of blowby because it fails to account for the fact that for part of the time, fuel may be leaking out reducing the heat released. That effect has been accounted for in the analysis presented here. Executing the same program with the blowby constant set of zero ($C = 0$) yields $\eta = 0.397$ and $\eta/\eta_{\text{otto}} = 0.863$.

Enthalpy Finally, the enthalpy that leaked out is indeed a negative number. This is a confusing and esoteric point related to the fact that energy can only be defined to within some arbitrary constant. The blowby manifests itself in the energy balance through two terms in Eq. 4.31,

$$u\frac{dm}{d\theta} \text{ and } \frac{-\dot{m}_l h_l}{\omega}$$

Equation (4.85) has kept track of only one of these terms for later use in a double check of the accuracy of the numerical integration.

Output Format For $\theta < \theta_s$, burned gas does not yet exist; therefore T_b was set to a large number in order to overflow the specified field, thereby causing asterisks to be printed. A similar tactic was employed on T_u for $\theta > \theta_s + \theta_b$.

Initial Burned Temperature It is assumed that as $x \to 0$ then $h_u \to h_b$ and the initial burned gas temperature is the adiabatic flame temperature based on the enthalpy at the time of spark. The subroutine TINITL performs the requisite

computation when $\theta \le \theta_s < \theta + 1°$. The integration is split into two nested do loops in order to call TINITL at the appropriate time.

Double Check The following errors are computed once the cycle is completely determined:

$$\epsilon_1 = 1 - vm/V \tag{4.86}$$

$$\epsilon_2 = 1 + \frac{W}{\Delta(mu) + Q_l + H_l} \tag{4.87}$$

where Q_l is the heat lost, H_l is the enthalpy that leaked out, and W is the work done. That these errors are both small gives confidence that the analysis and its programming are both correct.

Limits In the limit cases $x \to 0$ or $x \to 1$, the computer will encounter limits of the type zero divided by zero which it cannot handle. Therefore if $x < 0.001$, the system is treated as consisting of only unburned gas and if $x > 0.999$, it is treated as being entirely composed of burned gas.

IMSL The IMSL routine DVERK was used for integration because the reader is already familiar with its use. This is probably not the optimum routine to use for this problem as the derivative evaluations are expensive. Another routine based on a different method, such as DGEAR, may be better suited. No matter what method is used, one always has to write a subroutine such as RATES that embodies the physics of the model. The rest of the program is more or less dealing with input/output management.

4.5 ARBITRARY HEAT RELEASE—FUEL INJECTED ENGINES

The fluids in fuel-injected engines are by no means homogeneous. The fuel is often in two phases and is distributed very nonuniformly within the cylinder. It is common to ignore these details and empirically determine a fictitious fuel injection rate from a measured pressure–volume diagram. The parameters of that fictitious process are correlated with actual parameters. The problem when inverted will yield the measured pressure–volume diagram when the actual parameters are inputed. When the correlation is extrapolated to new circumstances, we have an analytical (though strictly empirical) tool for predicting pressure–volume diagrams and hence the indicated work.

To illustrate the correlation we will use for $\theta > \theta_s$ is

$$\frac{\dot{m}_{fi}}{m_{fi}} = \frac{\omega}{\theta_d \Gamma(n)} \left(\frac{\theta - \theta_s}{\theta_d} \right)^{n-1} \exp\left[\frac{-(\theta - \theta_s)}{\theta_d} \right] \tag{4.88}$$

where $\Gamma(n) = \int_o^\infty t^{n-1} e^{-t}\, dt$ is the gamma function (Abramowitz and Stegun, 1972), θ_s is the start of fuel injection, θ_d is a measure of the injection duration,

and m_{fi} is the total mass of fuel to be injected. The gamma function may be evaluated accurately from the asymptotic formula if $n > 1$.

$$\ln \Gamma(n) = \left(n - \frac{1}{2}\right)\ln(n) - n + \frac{1}{2}\ln(2\pi) + \frac{1}{12n} - \frac{1}{360n^3} + \frac{1}{1260n^5} - \frac{1}{1680n^7} \tag{4.89}$$

The relationship between the injection duration, θ_{99} is the angular change over which 99% of the fuel is injected, and the duration measure θ_d for different values of the shape parameter n is shown in Fig. 4-10. The different shapes that can be achieved via variation of n are illustrated in Fig. 4-11 for the case of $\theta_{99} = 50°$. From these curves, the following values of n are expected:

$1 \le n \le 2$ open chamber

$3 \le n \le 5$ divided chamber

The exact value is highly dependent upon the engine design and the fuel employed.

The rate of change of "burned fuel" in the cylinder is given by

$$\frac{dm_f}{d\theta} = \frac{1}{\omega}\left(\dot{m}_{fi} - \frac{\dot{m}_l \phi F_s}{1 + \phi F_s} \right) \tag{4.90}$$

where $\dot{m}_{fi}$ is zero for $\theta < \theta_s$ and is given by Eq. (4.88) for $\theta > \theta_s$. The blowby

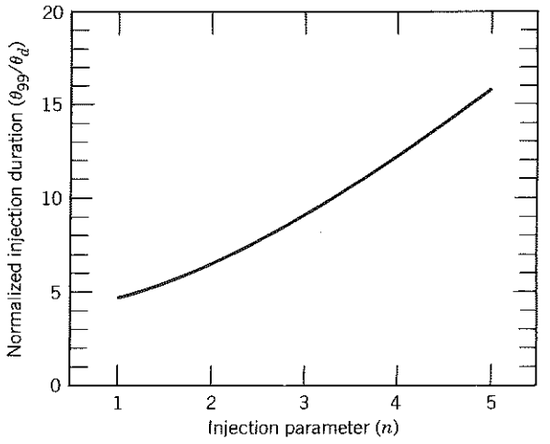

Figure 4-10 Here θ_{99} is the change in crank angle required to inject 99% of the fuel if the fuel is injected according to Eq. (4.88). An engineer might use a curve like this with knowledge of θ_{99} and n to find the parameter θ_d in order to use Eq. (4.88) as an empirical approximation.

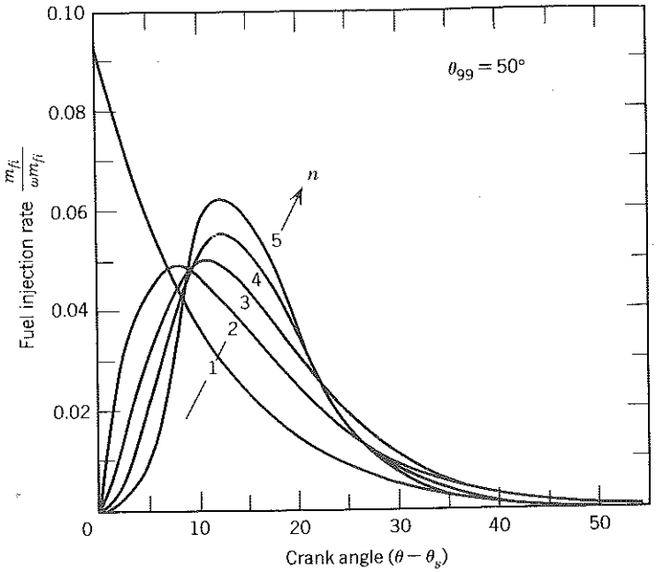

Figure 4-11 The effect of the injection parameter n on the injection rate shape. Smaller values of n result in a larger fraction of fuel being injected earlier in the injection process.

$\dot{m}_l$ is, as in Chapter 2, assumed to be

$$\dot{m}_l = Cm \tag{4.91}$$

Likewise, the rate of change of "burned air" within the cylinder is

$$\frac{dm_a}{d\theta} = \frac{-\dot{m}_l/\omega}{1 + \phi F_s} \tag{4.92}$$

and the equivalence ratio at any time is

$$\phi = \frac{m_f}{F_s m_a} \tag{4.93}$$

The mass in the cylinder at any time is

$$m = m_a + m_f \tag{4.94}$$

The energy equation applied to the cylinder contents gives

$$\frac{dU}{d\theta} = -\frac{\dot{Q}_l}{\omega} - P\frac{dV}{d\theta} - \frac{\dot{m}_l h_l}{\omega} + \frac{\dot{m}_{fi} h_f}{\omega} \tag{4.95}$$

By use of a fictitious fuel injection rate, we have tacitly assumed the system to

be homogeneous. In this case

$$U = mu = mu(T, P, \phi) \tag{4.96}$$

$$V = mv = mv(T, P, \phi) \tag{4.97}$$

$$h_l = h = h(T, P, \phi) \tag{4.98}$$

where the functional relationships indicated are for equilibrium combustion products, that is, the subroutine ECP.

The heat loss rate is given by

$$\dot{Q}_l = \mathbf{h}\left(\frac{\pi b^2}{2} + \frac{4V}{b}\right)(T - T_w) \tag{4.99}$$

which assumes a cylindrical combustion chamber with walls at temperature T_w.

An initial-value problem has been established; by simultaneous integration of Eq. (4.90), (4.92), and (4.95), one obtains m_f, m_a, and U as functions of time. Solutions of the algebraic equations give m, θ, P, T, h_l, and $\dot{Q}_l$ as functions of time. The volume as a function is known from the engine geometry and engine speed. The following illustrates one way to solve the equations.

EXAMPLE 4.5 ARBITRARY HEAT RELEASE (FUEL INJECTED AT TIME OF COMBUSTION)

```
C       GIVEN IN BLOCK DATA SUBPROGRAM:
C         COMPRESSION RATIO - R
C         BORE - B(CM)
C         STROKE - S(CM)
C         HALF STROKE TO ROD RATIO - EPS
C         ENGINE SPEED - RPM
C         HEAT TRANSFER COEFFICIENT - H
C         BLOWBY COEFFICIENT - C
C         EQUIVALENCE RATIO - PHI
C         RESIDUAL FRACTION - F
C         INITIAL PRESSURE - P
C         INITIAL TEMPERATURE - T
C         WALL TEMPERATURE - TW
C         START OF INJECTION - THETAS (DEG ATDC)
C         INJECTION DURATION PARAMETER - THETAD (DEG)
C         INJECTION PARAMETER - EN
C
C       FIND:
C         INDICATED THERMAL EFFICIENCY - ETA
C         INDICATED MEAN EFFECTIVE PRESSURE - IMEP(BAR)
C
C       NOTE:
C         1. FICTITIOUS INJECTION RATE - EQUATION 4.88
C         2. FUEL - T:T DIESEL
C
      EXTERNAL RATES
      REAL IMEP, MFUEL, MFI, MNOT, MDOTFI, M
```

```
      COMMON /ENGINE/ R, B, S, EPS, RPM, H, C, THETAS, THETAD,
     &                EN, PHI, F, P, T, TW, OMEGA, UNOT,
     &                MFI, HF, GAMMA
      DIMENSION Y1(10), Y(6), COM(24), WM(6,9)
      DATA AO/45730./, FS/.06907/, HFUEL/-174000./, VFUEL/1.189/,
     &     PFUEL/150./, MFUEL/199.15/, Y/6*0.0/, N/6/, THETA/-180./,
     &     THETAE/-170./, TOL/.001/, IND/1/, NW/6/, PI/3.141593/
C
C
C     LABEL HEADER ON OUTPUT PAGE AND PRINT INITIAL CONDITIONS
C
      OMEGA = RPM*PI/30.
      CALL AUXLRY(THETA, V, XDOT)
      PHI12 = F*PHI/(1.0 + (1.0 - F)*PHI*FS)
      CALL ECP(P, T, PHI12, H1, U, V1, S1, Y1, CP, DLVLT, DLVLP, IER)
      MNOT = V/V1
      UNOT = U*MNOT
      MDOTFI = 0.
      M = MNOT
      Y(1) = UNOT
      Y(5) = MNOT/(1.0 + PHI12*FS)
      Y(6) = Y(5)*PHI12*FS
      MFI = PHI*FS*(1.0 - F)*MNOT
      HF = HFUEL/MFUEL + (PFUEL - 1.01325)*VFUEL/10.
      GAMMA = (EN - 0.5)*ALOG(EN) - EN + 0.5*ALOG(2.*PI) + 1./12./
     &        EN - 1./360./EN**3 + 1./1260./EN**5 - 1./1680./EN**7
      GAMMA = EXP(GAMMA)
      WRITE(6,10)
10    FORMAT(4X,'THETA',5X,'VOLUME',4X,'MDOTFI',3X,'PRESSURE',1X,
     &       'TEMP',6X,'MASS',6X,'ENERGY',4X,'WORK',4X,'HEAT LOSS',
     &       1X,'H-LEAK')
      WRITE(6,20)
20    FORMAT(4X,'DEG ATDC',2X,'CM**3',5X,'GM/SEC',3X,'BARS',5X,
     &       'KELVIN',4X,'GRAMS',5X,'JOULES',4X,'JOULES',4X,'JOULES',
     &       2X,'JOULES')
      WRITE(6,30) THETA, V, MDOTFI, P, T, M, (Y(I),I=1,4)
30    FORMAT(4X,F5.0,5X,F5.1,5X,F6.3,1X,F6.2,4X,F5.0,5X,F6.4,
     &       4X,F6.0,3X,F6.1,4X,F6.2,4X,F6.3)
C
C     INTEGRATE RATE EQUATIONS AND PRINT EVERY 10 DEGREES
C
      DO 40 I = 1,36
      CALL DVERK(N, RATES, THETA, Y, THETAE, TOL, IND, COM, NW, WM,
     &           IERROR)
      CALL AUXLRY(THETAE, V, XDOT)
      MDOTFI = MFI*XDOT
      CALL STATE(Y(1), Y(5), Y(6), V, P, T, HL)
      M = Y(5) + Y(6)
      WRITE(6,30) THETAE, V, MDOTFI, P, T, M, (Y(J),J=1,4)
      THETA = THETAE
40    THETAE = THETA + 10.
C
C
C     COMPUTE AND WRITE THE ETA, IMEP AND ERRORS
C
      ETA = Y(2)/MFI/AO
      VD = PI/4.*B**2*S
      IMEP = Y(2)/VD*10.
      ERROR1 = 1. - PHI*FS/Y(6)*Y(5)
      W = -(Y(1) - UNOT) - Y(3) - Y(4) + MFI*HF
```



```
      ERROR2 = 1. - Y(2)/W
      WRITE(6,50) ETA, IMEP, ERROR1, ERROR2
50    FORMAT(' ETA = ',1PE11.4,' IMEP = ',1PE11.4,' ERROR1 = ',
     &       1PE11.4,' ERROR2 = ',1PE11.4)
      STOP
      END
C
C
C
      SUBROUTINE RATES(N, THETA, Y, YPRIME)
      DIMENSION Y1(10)
      REAL Y(N), YPRIME(N), M, MDOTFI, MFI
      COMMON /ENGINE/ R, B, S, EPS, RPM, H, C, THETAS, THETAD,
     &                EN, PHI, F, P, T, TW, OMEGA, UNOT,
     &                MFI, HF, GAMMA
      DATA PI/3.141593/, Y1/10*0.0/
      CALL AUXLRY(THETA, V, XDOT)
      MDOTFI = XDOT*MFI
      RAD = THETA*PI/180.
      DUMB = SQRT(1. - (EPS*SIN(RAD))**2)
      DV = PI/8.*B**2*S*SIN(RAD)*(1. + EPS*COS(RAD)/DUMB)
      CALL STATE(Y(1), Y(5), Y(6), V, P, T, HL)
      M = Y(5) + Y(6)
C
      YPRIME(2) = P*DV/10.
      YPRIME(3) = H*(PI*B**2/2. + 4.*V/B)*(T - TW)/OMEGA/10000.
      YPRIME(4) = C*M*HL/OMEGA
C
      YPRIME(1) = -YPRIME(2) - YPRIME(3) - YPRIME(4) + MDOTFI*HF/
     &            OMEGA
C
      YPRIME(5) = -C*Y(5)/OMEGA
      YPRIME(6) = (MDOTFI - C*Y(6))/OMEGA
C
      DO 10 I = 1,N
10    YPRIME(I) = YPRIME(I)*PI/180.
      RETURN
      END
C
C
      SUBROUTINE STATE(ENERGY, AIR, FUEL, VOL, P, T, H)
C
      DIMENSION Y(10)
      DATA MAXITS/50/, TOL/.001/, Y/10*0.0/, FS/.06535/
      U = ENERGY/(AIR + FUEL)
      V = VOL/(AIR + FUEL)
      ERROR = 1.0
      PHI = FUEL/AIR/FS
      DO 10 I = 1,MAXITS
      CALL ECP(P,T,PHI,H,U2,V2,S,Y,CP,DLVLT,DLVLP,IER)
      IF ( ERROR .LT. TOL ) GO TO 20
      F1 = U - U2
      F2 = V - V2
      DET = V2**2/T*((-10.*CP*T/P/V2 + DLVLT)*(-DLVLP) + DLVLT*(DLVLT
     &    + DLVLP))
      DELT = -V2*(10.*F1/P*DLVLP + F2*(DLVLT + DLVLP))/DET
      DELP = -P*V2/T*((10.*CP*T/P/V2 - DLVLT)*F2 - 10.*F1/P*DLVLT)/DET
      T = T - DELT
      P = P - DELP
      ERROR = AMAX1(ABS(DELT/T),ABS(DELP/P))
```

```
10      CONTINUE
        WRITE(6,30)
30      FORMAT(' CONVERGENCE FAILURE IN STATE' )
20      CONTINUE
        IF ( IER .NE. 0 ) WRITE(6,15) IER
15      FORMAT(' ECP RETURNED IER = ',I2,'FROM STATE')
        RETURN
        END
C
C
        SUBROUTINE AUXLRY(THETA, V, XDOT)
        COMMON /ENGINE/ R, B, S, EPS, RPM, H, C, THETAS, THETAD,
     &                  EN, PHI, F, P, T, TW, OMEGA, UNOT,
     &                  EMFI, HF, GAMMA
        DATA PI/3.141593/
        RAD = THETA*PI/180.
        VTDC = PI/4.*B**2*S/(R - 1.)
        V = VTDC*(1. + (R - 1.)/2.*(1. - COS(RAD) + 1./EPS*(1. -
     &      SQRT(1. - (EPS*SIN(RAD))**2))))
        XDOT = 0.
        IF(THETA .LE. THETAS) RETURN
        XDOT = OMEGA/GAMMA*((THETA - THETAS)/THETAD)**(EN - 1.)*
     &         EXP(-(THETA - THETAS)/THETAD)/(THETAD*PI/180.)
        RETURN
        END
C
C
        BLOCK DATA
        COMMON /ENGINE/ R, B, S, EPS, RPM, H, C, THETAS, THETAD,
     &                  EN, PHI, F, P, T, TW, OMEGA, UNOT,
     &                  EMFI, HF, GAMMA
        DATA R/15./, B/10./, S/10./, EPS/.15/, RPM/2000./, H/500./,
     &       C/0.8/, THETAS/-20./, THETAD/5./, EN/4./, PHI/0.7/,
     &       F/.05/, P/1.0/, T/325./, TW/400./
        END
```

SOLUTION:

THETA DEG ATDC	VOLUME CM**3	MDOTFI GM/SEC	PRESSURE BARS	TEMP KELVIN	MASS GRAMS	ENERGY JOULES	WORK JOULES	HEAT LOSS JOULES	H-LEAK JOULES
-180.	841.5	.000	1.0	325.	.8979	-153.	.0	.00	.000
-170.	836.4	.000	1.0	327.	.8975	-152.	-.5	-1.01	-.030
-160.	821.3	.000	1.0	331.	.8971	-149.	-2.1	-1.98	-.059
-150.	796.3	.000	1.1	336.	.8967	-146.	-4.7	-2.86	-.087
-140.	761.8	.000	1.2	344.	.8963	-141.	-8.6	-3.65	-.111
-130.	718.6	.000	1.3	353.	.8959	-135.	-13.9	-4.30	-.133
-120.	667.3	.000	1.4	364.	.8955	-128.	-20.7	-4.81	-.150
-110.	609.2	.000	1.6	378.	.8951	-118.	-29.4	-5.15	-.162
-100.	545.7	.000	1.9	394.	.8947	-107.	-40.4	-5.31	-.168
-90.	478.4	.000	2.2	415.	.8943	-94.	-54.1	-5.26	-.167
-80.	409.3	.000	2.8	441.	.8939	-77.	-71.4	-5.01	-.156
-70.	340.6	.000	3.6	472.	.8935	-56.	-93.0	-4.54	-.133
-60.	274.6	.000	4.8	512.	.8931	-29.	-120.3	-3.83	-.096
-50.	213.7	.000	6.8	562.	.8927	5.	-154.9	-2.87	-.060
-40.	160.2	.000	10.0	624.	.8923	47.	-198.9	-1.64	.039
-30.	116.1	.000	15.5	699.	.8919	100.	-253.6	-.11	.147
-20.	83.2	.000	24.2	784.	.8915	162.	-317.0	1.75	.289
-10.	63.0	25.348	48.3	1173.	.8967	207.	-381.5	4.37	.477
	56.1	27.444	92.5	1960.	.9129	195.	-425.4	10.32	.754
10.	63.0	12.535	97.8	2293.	.9235	84.	-357.0	19.18	1.077
20.	83.2	4.021	73.8	2275.	.9273	-112.	-183.9	29.00	1.348

THETA DEG ATDC	VOLUME CM**3	MDOTFI GM/SEC	PRESSURE BARS	TEMP KELVIN	MASS GRAMS	ENERGY JOULES	WORK JOULES	HEAT LOSS JOULES	H-LEAK JOULES
30.	116.1	1.063	49.6	2133.	.9281	-324.	14.5	38.87	1.516
40.	160.2	.249	33.2	1971.	.9280	-513.	193.0	48.59	1.575
50.	213.7	.053	23.0	1825.	.9277	-671.	340.7	58.21	1.538
60.	274.6	.011	16.7	1700.	.9273	-800.	460.0	67.82	1.421
70.	340.6	.002	12.6	1595.	.9269	-905.	555.7	77.50	1.239
80.	409.3	.000	9.9	1508.	.9265	-991.	632.5	87.31	1.003
90.	478.4	.000	8.1	1434.	.9261	-1063.	694.3	97.25	.722
100.	545.7	.000	6.8	1372.	.9257	-1122.	744.0	107.32	.404
110.	609.2	.000	5.8	1319.	.9252	-1172.	783.9	117.50	.055
120.	667.3	.000	5.1	1274.	.9248	-1214.	815.7	127.77	-.321
130.	718.6	.000	4.6	1236.	.9244	-1249.	840.7	138.08	-.718
140.	761.8	.000	4.2	1204.	.9240	-1278.	859.9	148.40	-1.134
150.	796.3	.000	4.0	1178.	.9236	-1302.	874.0	158.70	-1.565
160.	821.3	.000	3.8	1156.	.9232	-1321.	883.7	168.94	-2.009
170.	836.4	.000	3.7	1138.	.9228	-1336.	889.4	179.08	-2.463
180.	841.5	.000	3.6	1125.	.9224	-1348.	891.2	189.10	-2.924

ETA = 4.8916e-01 IMEP = 1.1347e+01 ERROR1 = 7.5888e-03 ERROR2 = -8.3447e-07

Some comments about this program are in order.

Otto Cycle The equivalent fuel–air Otto cycle predicts $\eta = 0.521$, hence $\eta/\eta_{\text{otto}} = 0.94$. The equivalent limited pressure fuel–air cycle predicts $\eta_{1p} = 0.518$, hence $\eta/\eta_{lp} = 0.95$.

Double Check The following errors are computed once the cycle is completely determined

$$\epsilon_1 = 1 - \phi F_s \frac{m_a}{m_f} \tag{4.100}$$

$$\epsilon_2 = 1 + \frac{W}{\Delta(mu) + Q_l + H_l - m_{fi} h_f} \tag{4.101}$$

That these errors are both small instills confidence that the analysis and its programming are correct. The error ϵ_1 is not as small as ϵ_2 because we tacitly assumed that the fuel–air ratio of the residuals is equal to the delivered fuel-air ratio, which is not strictly correct.

IMSL As with the previous example, DVERK was used only because the reader is already familiar with it. Some other routine based on a different numerical method may be more efficient. In any case one has to write a subroutine RATES to incorporate the physics of the model. The remaining portions of the program deal with input/output management.

STATE This subroutine solves Eq. (4.96) through (4.98) for T, P, and h given U, V, ϕ. Reference to Eq. (3.141) through (3.143) will help to understand its methodology.

4.6 REFERENCES

Abramowitz, M. and J. A. Stegun, Ed., (1972), *Handbook of Mathematical Functions*, Dover, New York, p. 257.

Beretta, G. P. and J. C. Keck, (1983), "Energy and Entropy Balances in a Combustion Chamber; Analytical Solution," *Combustion Sci. and Tech.*, **30** pp. 19–29.

Mattavi, J. N. and C. A. Amann, Eds., *Combustion Modeling in Reciprocating Engines*, Plenum, New York, 1980.

Obert, E. F., (1968), *Internal Combustion Engines and Air Pollution*, Harper & Row, New York, p. 81.

Taylor, C. F., (1977), *The Internal Combustion Engine in Theory and Practice*, MIT Press, Cambridge, Massachusetts, p. 81.

4.7 HOMEWORK

1. Show that Eq. (4.7) reduces to Eq. (2.7) when there is only heat transfer instead of combustion.
2. Derive Eq. (4.9).
3. Repeat Example 4.1 for $r = 8.0$ $\phi = 1.0$ $f = 0.15$ $P_1 = 0.4$ bars $T_1 = 310$ K
4. With reference to Fig. 4-2, explain why the heats of combustion at $\phi = 0.2$ and $\phi = 1.2$ are less than those at $\phi = 1.0$.
5. **a.** Explain why there exists a maximum r giving $P_l/P_1 = 50$ in Fig. 4-9.
   b. Explain why there exists a minimum ϕ to give $P_l/P_1 = 100$ in Fig. 4-8.
6. Prepare a subroutine BLWDWN which given:

P5	Pressure (bar)
S5	Entropy (J/g)
PHI	Equivalence ratio

returns:

V5	Specific volume (cm^3/g)
T5	Temperature (K)
H5	Enthalpy (J/g)

A review of Section 3.9 might prove useful in solving this problem.

7. Prepare a subroutine TSTART that uses Eq. (4.11) to find T_1. The routine is given:

H1	Enthalpy (J/g)
PI	Intake pressure (bar)
PHI	Equivalence ratio
F	Residual fraction

and returns:

T1	Temperature (K)

8. Prepare the subroutine FIBURN which given:

P3	Pressure (bar)
H3	Enthalpy (J/g)
PHI	Equivalence ratio

returns

T	Temperature (K)
U	Internal energy (J/g)
V	Specific volume (cm^3/g)
S	Entropy (J/g/K)

9. The notes in Example 4.3 indicate that the subroutine ECP must be modified to accomodate the change to diesel fuel. What lines are affected and what are the changes to be made? (Careful ECP calls FARG for low temperatures.)
10. Derive Eq. (4.17), (4.21), and (4.29).
11. Show that the FORTRAN expressions in the code of Example 4.5 which assign initial values to y_5 and y_6 are correct. Also show that the mass of fuel to be injected is given by:

$$m_{fi} = \phi F_s (1 - f) m_o$$

where m_o is the initial mass in the cylinder.

12. An internal combustion engine for use on spaceships has been proposed by a mad scientist. The heat release is caused by the reaction

$$2O_3 \rightarrow 3O_2$$

The exhaust is then used for an oxygen supply and for space heating. Analyze the engine assuming the following processes:

1 to 2	Isentropic compression of pure ozone
2 to 3	Constant pressure, adiabatic combustion
3 to 4	Isentropic expansion of pure oxygen

Given parameters are:

$T_1 = 298$ K $\quad P_1 = 1$ atm

$P_2 = 14.683$ atm $\quad P_4 = 1.00$ atm

There are two moles of O_3 at state 1.

a. Show that:

$$T_4 = 1721 \text{ K}$$

b. Find the indicated work in kcal.

c. Find the indicated thermal efficiency. Note the following:

$$P_r = \exp\left(\frac{s^o - s^o_{298}}{R}\right)$$

$$v_r = \frac{T}{298}\frac{1}{P_r}$$

$R = 1.9872$ cal/mole/K

$G = H - TS$ (Gibbs' Free Energy)

Thermodynamic properties of O_3 and O_2 are in appendix F.

Five

ACTUAL CYCLES AND THEIR DETERMINATION

To analyze the actual cycle of an engine one needs to connect the engine to a dynamometer for controlling the speed and applying a load. One also needs to instrument the engine to measure such parameters as fuel flow rate, air flow rate, cylinder pressure versus volume, the residual fraction, the coolant temperature, the oil temperature, and the spark or fuel injection timing.

Some of the measurements are rather straightforward and require little, if any, explanation. For example, the oil temperature is easily measured by insertion of a thermocouple into the lubricating circuit at the point one wishes to know the temperature. Some of the measurements require analysis to obtain the desired result. For example, the residual fraction is determined by measuring the composition of the cylinder gases during the compression stroke and using atom balancing to compute the residual fraction.

There are mainly two purposes of this chapter: (1) to introduce the instrumentation and analysis used; (2) to present results typical of both spark ignition and compression ignition engines.

5.1 DYNAMOMETERS

A schematic of an engine connected to a dynamometer is shown in Fig. 5-1. It is intended to reflect the components of an electric dynamometer as opposed to a hydraulic dynamometer, both of which will be discussed. In either type, there is one sensor to indicate speed and torque. The signals from these sensors are fed to indicators and to the controller. Via knobs on the control panel, the operator can set the dynamometer to control either speed or torque.

With the speed control selected, the dynamometer applies whatever load is required to maintain that speed. For example, if the engine being tested were a spark-ignition engine with a throttle body fuel injection system, then the response of the dynamometer to the operator increasing the inlet manifold pressure by opening the throttle would be to increase the load (resistance to turning or applied torque) to maintain the speed.

With torque control selected, the dynamometer maintains a fixed load. For example, the dynamometer's response to opening the throttle of a spark-ignition engine would be of a safeguard character only, the applied torque would stay the same. In this case, the engine speed would increase to a point

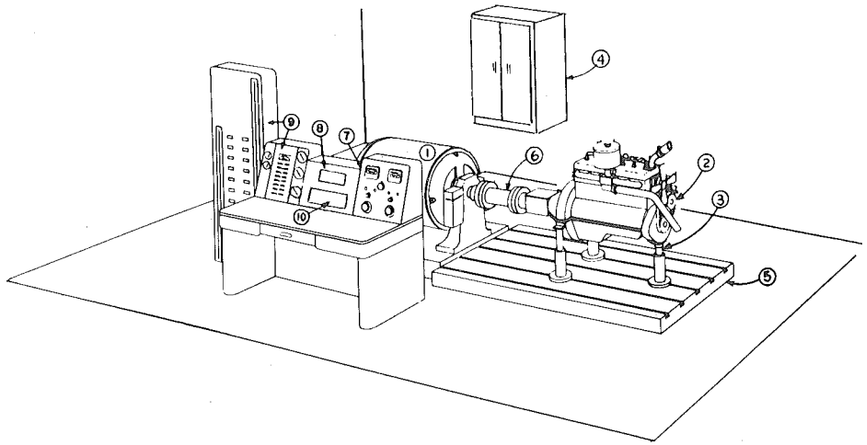

Figure 5-1 Typical engine test stand. (1) Dynamometer (2) test engine (3) engine jacks (4) dynamometer controller (5) "T" slot engine base (6) coupling (7) control panel (8) speed indicator (9) engine panels (10) torque indicator. Courtesy Eaton Corporation—Kenosha Division.

where the friction in the engine would have increased by an amount equal to the increase in the net indicated torque. If the engine speed exceeded an operator set point, chosen to prevent engine damage, the dynamometer controller would trip a switch to shut off the ignition and close the throttle.

In the case of an electric dynamometer, the power absorbed from the engine is converted to electricity which is then dissipated as heat by resistance heating (in direct current or regenerative alternating-current machines, the electricity generated can be used, and transformers are available that allow it to supplement a power system). In the case of a hydraulic dynamometer, the power absorbed is used to pump water through a network that dissipates the energy as heat by fluid friction.

There are a number of different kinds of electric dynamometers. These include: direct current, regenerative alternating current, and eddy current. Historically, direct-current machines offered the greatest flexibility but at the greatest cost. Because the manufacturers of the various systems compete with one another and are always upgrading the technology of their products, it has reached the point where the differences in capabilities of systems are rather small.

Types of dynamometers can further be classified depending upon whether or not they also have the capability to motor an engine, that is, spin an engine not producing power as the starter motor of an automobile engine does. Hydraulic dynamometers cannot motor an engine. Strictly speaking, neither can eddy-current machines, but because they are often configured into a package with an electric motor to run an engine, for practical purposes the distinction is moot.

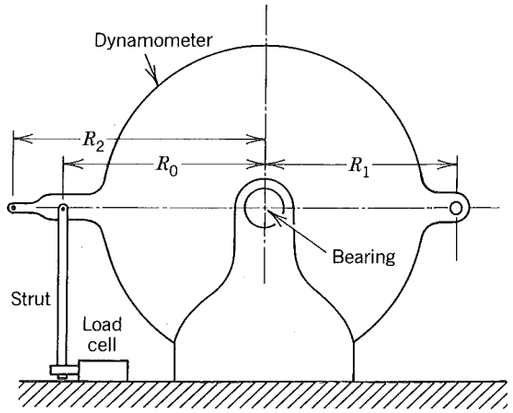

Figure 5-2 Torque measurement using a cradle mounted dynamometer.

The method most commonly employed to measure torque is shown in Fig. 5-2. The dynamometer is supported by bearings and restrained from rotation only by a strut connected to a load cell. Whether the dynamometer is absorbing or providing power, a reaction torque is applied to the dynamometer. Hence, if the force applied by the strut is F, then the torque applied to the engine is

$$\tau = FR_o \tag{5.1}$$

where R_o is defined in Fig. 5-2. The load cell measures the force F. For calibration, lever arms are located at R_1 and R_2 for hanging known weights.

Since the work done in rotating the engine's crankshaft through one revolution, or 2π radians, is $2\pi\tau$, it follows that for two- and four-stroke engines, respectively

$$\text{mep} = \frac{2\pi\tau}{V_d} \qquad \text{(two stroke)} \tag{5.2}$$

$$\text{mep} = \frac{4\pi\tau}{V_d} \qquad \text{(four stroke)} \tag{5.3}$$

If the engine is absorbing energy, then the brake mean effective pressure, bmep, is determined. If the engine is being motored then the motoring mean effective pressure, mmep, is determined (which, as explained in Chapter 6, is a rough measure of the friction losses in an engine).

Fig. 5-3 shows a four-cylinder, 2.30 liter Pontiac engine and a four-speed manual transmission coupled to a regenerative alternating-current dynamometer. Compare this figure with those shown earlier. It also shows the way in which engine speed is commonly measured. Note that at the back of the dynamometer there is a gear attached to the rotating shaft. A magnetic pickup

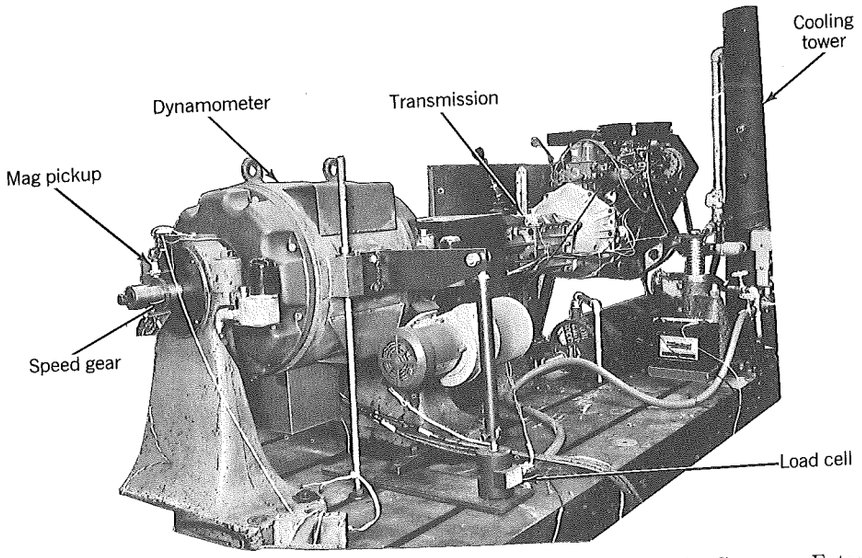

Figure 5-3 Actual components in a particular engine test stand. Courtesy Eaton Corporation—Kenosha Division.

generates a signal with the passing of each gear tooth. This generates a periodic signal, the frequency of which is proportional to engine speed. The readout instrument that displays the signal in the desired units, usually rpm, is called a tachometer.

Note too that there is a cooling tower, which in this case controls the coolant temperature. A complete test stand has, in addition, provisions to control the fuel and air temperature, the atmospheric pressure, and the air humidity.

5.2 FUEL AND AIR FLOW

An old technique to measure fuel flow, that remains particularly valuable today because it can be used to calibrate other methods, weighs a quantity of fuel delivered to an engine in a period of approximately 2 min. The essence of such a system is shown in Fig. 5-4. As fuel is consumed by the engine from a beaker on a scale, eventually, the balance point will be reached (assuming the fuel and beaker weighed more than the setting of the scale weight and that the beaker alone weighs less than the scale weight). When the scale tips, a sensor provides a signal to start a clock. The operator then reduces the scale weight so that the process can be repeated. This time when the scale tips, the clock is stopped. The average mass flow rate of fuel is the difference between the two balance weights divided by the elapsed time recorded on the clock.

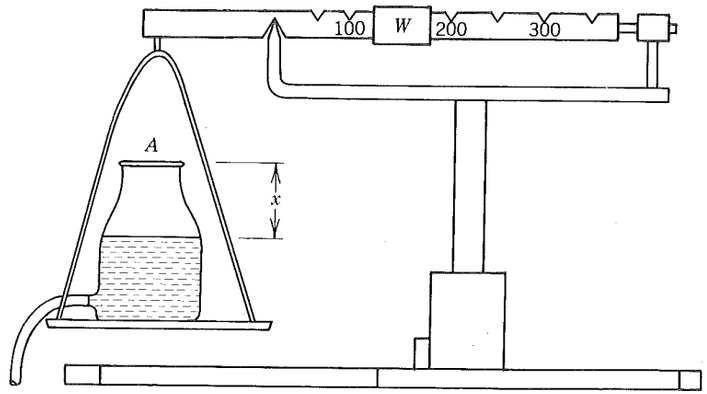

Figure 5-4 An accurate and simple way to measure fuel flow to the engine is to locate the fuel supply on a scale and time the period required to consume a certain weight of fuel.

This method suffers from two significant disadvantages: (1) it does not give an instantaneous readout of fuel flow rate; (2) it is inconvenient to automate for computer controlled testing and/or data logging.

There are some manufacturers that make small, positive displacement turbines designed to be installed in the fuel line as an electronic fuel flow transducer. Basically, the rotational speed of the turbine is proportional to the fuel flow rate. These transducers are also convenient in terms of minimizing bulk in the test cell, maximizing safety, and maintaining a clean fuel system. Unfortunately, they measure a volumetric flow rate instead of a mass flow rate, and the calibration is weakly dependent upon the fuel viscosity. Thus, in practice, calibration curves have to be established as a function of the fuel temperature (and possibly pressure) and new ones generated if the fuel type is varied.

At considerably greater cost than the turbine-type flow meters, there is at least one electronic transducer on the market that directly measures the mass flow rate. Flo-Tron linear mass flow meters are the hydraulic equivalent of the electrical Wheatstone bridge. The bridge comprises four matched orifices (resistors) and a recirculating pump (current source) to generate an internal reference flow. The external fuel flow through the meter and to the engine generates a pressure unbalance, the magnitude of which is proportional to the mass flow rate. The manufacturer claims that the meter is accurate to within $\pm \frac{1}{2}\%$ and reproducible to within $\pm \frac{1}{4}\%$; in other words the meter's performance is outstanding.

Air flow to engines cannot be measured with the same precision as can fuel flow. There are two main reasons for this: (1) the instrumentation available is at best accurate to within about $\pm 1\%$; (2) it is harder to ensure

that all of the air delivered to the engine is metered or retained; air can leak into and out of the cylinder of naturally aspirated engines and supercharged engines, respectively, through the valve guides for example. As a result, it is wise to measure air flow directly and by inference from exhaust gas analysis as a double check. A discussion of air flow meters follows. A discussion of air-flow measurement via exhaust gas analysis is given in Section 5.3.

A common problem in measuring air flow is that the flow is unsteady; although often in testing it is periodic, the meters available are usable only in a steady flow. (A similar problem can be encountered in measuring fuel flow). The severity of the problem decreases with an increasing number of cylinders sharing a common intake manifold and with an increase in the volume between the meter and the intake ports. The volume acts as a fluidic capacitor to damp out fluctuations at the meter. The flow at the meter is smoother with multicylinder engines than with single-cylinder engines because the cylinders are out of phase with one another; thus as the peaks and valleys in the flow rates to individual cylinders are superimposed, the flow at the meter becomes smooth.

A solution for the worst case, that is, for a single cylinder engine, that can be applied to steady-state engine testing (which produces a periodic air flow rate) is illustrated in Fig. 5-5. All of the air to be delivered to the engine is metered by a steady-state air-flow meter located upstream of a surge tank (whose volume is about 100 times the displacement volume) that acts as the atmosphere from which the engine draws its air.

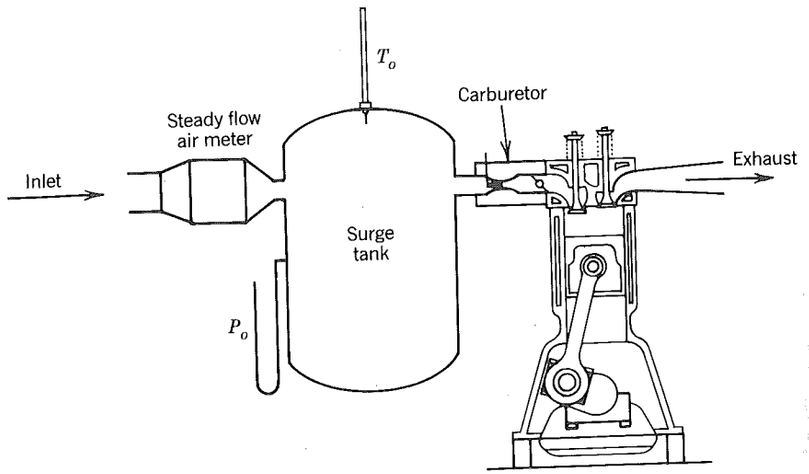

Figure 5-5 Single-cylinder engine equipped with inlet surge tank and steady flow air meter.

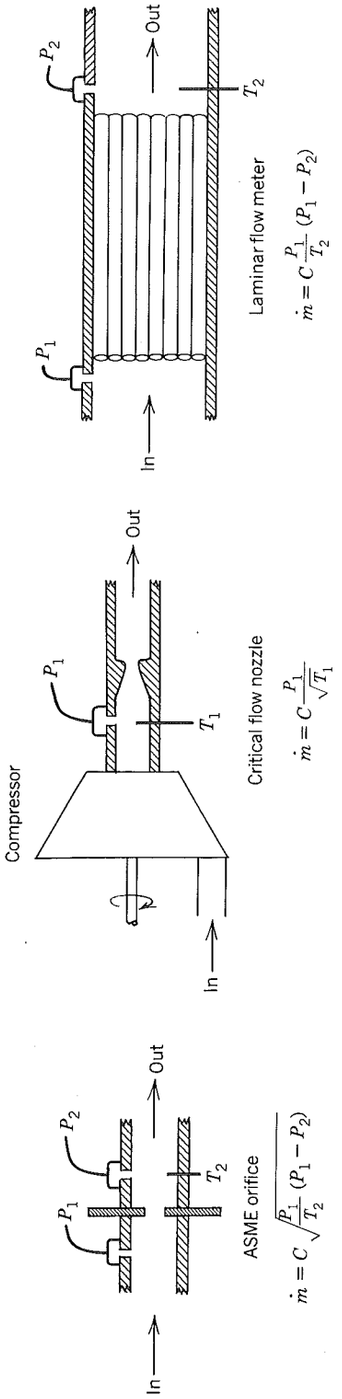

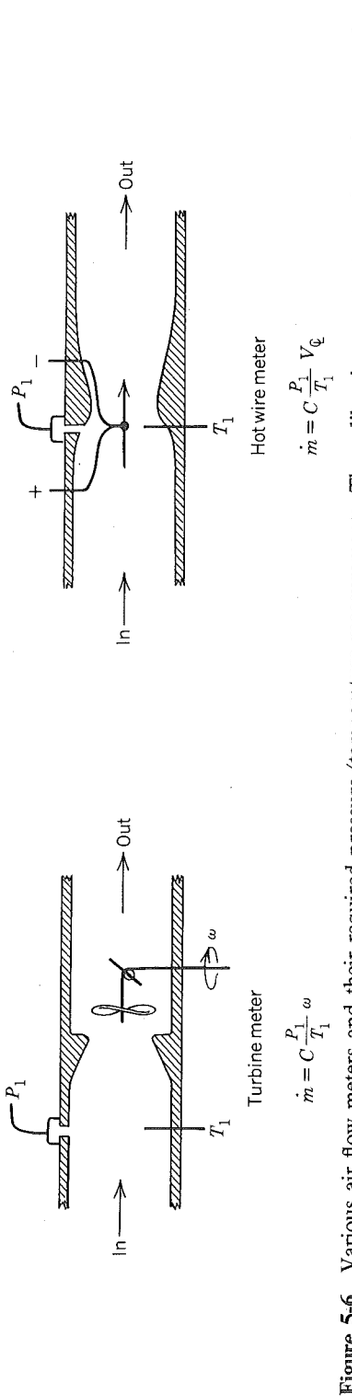

Figure 5-6 Various air flow meters and their required pressure/temperature measurements. The calibration constants are dependent upon the Reynolds number through the meters.

The various types of air-flow meters that can be used include the following:

ASME Orifice Often employed as a secondary standard to calibrate other meters; flow rate depends on the square root of the pressure drop across the orifice.

Laminar Flow Meter A bundle of tubes (not necessarily round in cross section) sized so that the Reynold's number in each is well within the laminar regime; flow rate depends linearly on the pressure drop across the meter.

Critical Flow Nozzle A venturi in which the flow is choked; the flow rate is then linearly dependent upon the delivery pressure (an external compressor is thus required) and independent of the pressure in the surge tank.

Turbine Meter The air flow rate is linearly dependent upon the rotational speed of the turbine.

Hot Wire Meter A hot wire anemometer is inserted into the flow to measure the center-line velocity; the air-flow rate is proportional to center-line velocity.

No matter which of the various methods is used, subsidiary measurements of temperature and pressure have to be made. Key components to systems employed using these various meters are identified in Fig. 5-6.

For transient engine testing, only the hot wire meter can be used, as it can measure the instantaneous mass flow rate; it can also be used in steady-state testing where the required surge tank is viewed as a nuisance. It must, however, be used with care because it is possible that in some engines a flow reversal will occur and the meter does not know whether the flow is going forward or backward.

5.3 EXHAUST GAS ANALYSIS

Electronic instruments that are easy to use and reliable are available for several of the constituents of interest to us including carbon dioxide, carbon monoxide, oxygen, nitric oxides, and hydrocarbons. Many laboratories, especially those studying or testing emissions, have a set of these instruments mounted together with a suitable sample handling system. A document in the SAE Handbook[1] describes recommended practice in building such a system. I will briefly explain how the instruments for the species mentioned operate and then we will look at how experimental data can be used to compute the fuel–air ratio (which with the measured fuel flow rate allows an independent check on the air-flow measurement).

Infrared analyzers are used for carbon dioxide and carbon monoxide. They can also be used for methane, hexane, nitric oxide, sulfur dioxide,

[1] Published annually by the Society of Automotive Engineers, Warrendale, Pennsylvania

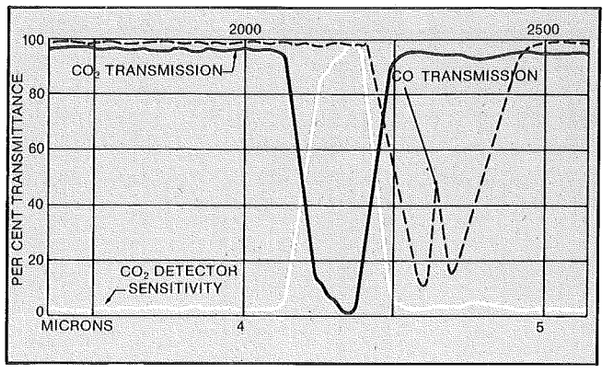

(a)

Figure 5-7(*a*) For the most part gases are transparent to electromagnetic radiation. However, at certain frequencies, the energy associated with a photon coincides with that required to change a molecule from one quantized energy level to another. At those frequencies a gas will absorb radiation. It is found that the fraction of the radiation transmitted by the gas at any wavelength λ obeys Beer's Law, $\tau_\lambda = \exp(-\rho\kappa_\lambda L)$, where ρ is the gas density, κ_λ is its absorption coefficient, and L is the path length of the radiation through the gas.

Combustion products absorb radiation in the infrared portion of the spectrum. (*a*) The transmittance of carbon dioxide and of carbon monoxide over the range of $3.5 < \lambda < 5$ microns. Notice that carbon dioxide absorbs at about 4.2 microns; whereas carbon monoxide absorbs at about 4.6 microns. Thus by using a radiation detector with a sensitivity as shown, one can detect carbon dioxide in a sample without interference from any carbon monoxide that may also be present.

ethylene, and water. Fig. 5-7 describes the principle of operation of a Beckman Instrument and Table 5-1 illustrates the concentration ranges and gases that can be measured.

The preferred technique for hydrocarbon detection is the flame ionization method. Introduction of hydrocarbons into a hydrogen air flame produces, in a complex process, electrons and positive ions. By burning the sample in an electric field it is possible to count these ions which are indicative of the number of carbon atoms introduced into the flame.

An example of such a burner is shown in Fig. 5-8. The sample is mixed with the hydrogen–diluent fuel and burned in a diffusion flame. The combustion products pass between electrodes. An ion current is established and detected to indicate hydrocarbon concentration.

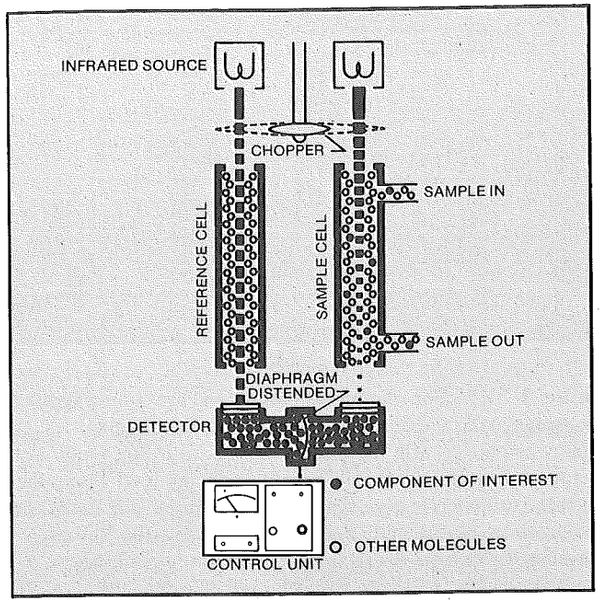

(b)

Figure 5-7(*b*) The Beckman model 865 infrared analyzer passes infrared radiation through two cells, one a reference cell containing a nonabsorbing background gas and the other a sample cell containing a continuous flowing sample. The detector is filled with the component gas of interest to absorb infrared radiation transmitted through the two cells. The detector will absorb less radiation on the right than on the left because of the attenuation in the sample cell causing a diaphragm to deflect in proportion to the difference in the rates of energy absorption. Since the deflection will depend on the component density in the sample stream, the amount of deflection can be sensed and displayed on an electric meter calibrated to read in units of concentration. Notice that by filling the detector with the component of interest one automatically obtains the desired sensitivity so as to eliminate interference from other components. Illustrations Courtesy Beckman Instruments, Inc.

Table 5.1 Preselected Ranges and Their Respective Cell Lengths of Beckman Model 865 Infrared Analyzers

SAMPLE GAS	15 in. (381 mm) CELL	5 in. (127 mm) CELL	0.5 in. (12.7 mm) CELL	0.125 in. (3.17 mm) CELL
CO	0–50 P/10^6[a] 0–500 P/10^6	0–1000 P/10^6 0–5000 P/10^6	0–1% 0–5%	0–10% 0–100%
CO_2	0–100 P/10^6 0–500 P/10^6	0–500 P/10^6 0–2500 P/10^6	0–5000 P/10^6 0–2.5%	0–5% 0–15%
CH_4		0–2000 P/10^6 0–1%	0–2% 0–10%	0–10% 0–50%
N-hexane	0–200 P/10^6 0–1000 P/10^6	0–1000 P/10^6 0–5000 P/10^6	0–1%	
NO	0–500 P/10^6 0–2000 P/10^6	0–2000 P/10^6 0–1%	0–2% 0–10%	0–25% 0–100%
SO_2	0–500 P/10^6 0–2000 P/10^6	0–2000 P/10^6 0–1%	0–1% 0–5%	0–10% 0–30%
Ethylene		0–2% 0–10%		
Water		0–3000 P/10^6 0–1.5%	0–5%	

[a] P/10^6 means parts per million (ppm) 1 ppm = 10^{-4}% = 10^{-6}.

The magnitude of the current depends slightly on the molecular structure of the hydrocarbon being detected. The characteristic response of a given molecular structure normalized by the response to methane is given here.

MOLECULAR STRUCTURE	APPROXIMATE RESPONSE
Methane	1.0
Alkanes	1.0
Aromatics	1.0
Alkenes	0.95
Alkynes	1.30
Carbonyl radical	0.0
Nitrile radical	0.3

The instrument counts carbon; according to this table, the following concentrations would all read approximately 1% on the meter:

1.00% of CH_4, methane
0.1% of $C_{10}H_{22}$, decane
0.132% of C_8H_{16}, octene
0.385% of C_2H_2, acetylene

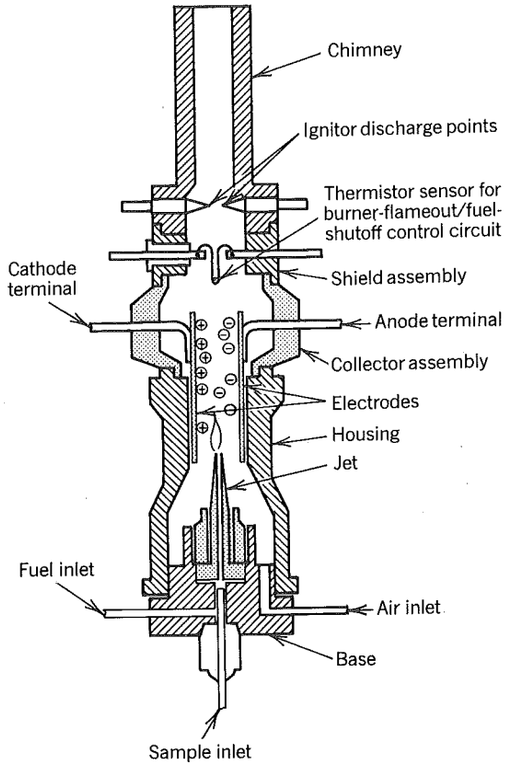

Figure 5-8 Sectional view of a burner in a Beckman flame ionization hydrocarbon detector. Courtesy Beckman Instruments, Inc.

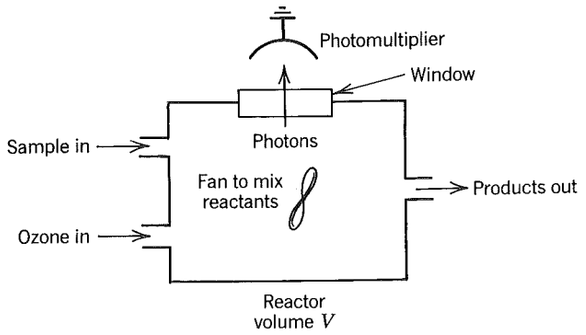

Figure 5-9 Model representation of the reactor in a chemilumenescent nitric oxide analyzer.

The flame ionization detector gives no information about the type of hydrocarbons in the exhaust or their average hydrogen to carbon ratio. In recognition of this latter point it is preferred to report measurements as ppmC (particles per million carbon) rather than as ppm CH_4 or C_3H_8 or $C_\alpha H_\beta$ equivalent. Studies of the hydrocarbon types that appear use gas chromatography, mass spectrometry, or combinations of the two.

Light is emitted when nitric oxide reacts with ozone. This process is called chemiluminescence. An ideal model to illustrate the principle is shown in Fig. 5-9. The reactor is assumed to be perfectly stirred, that is, homogeneous. To measure nitric oxides we calculate the rate at which photons flow out the window for detection by the photomultiplier.

The chemical kinetics involved are

1. $NO + O_3 \rightarrow NO_2^* + O_2$
2. $NO_2^* \rightarrow NO_2 + \text{photon}$
3. $NO_2^* + M \rightarrow NO_2 + M$

The asterisk denotes NO_2 in an electronically excited state and M is a symbol chemists use to denote any molecule in the system.

The nitric oxide reacts with ozone to produce electronically excited nitric dioxide. The excited nitric oxides can be deactivated by emission of a photon or by collision with any other molecule.

When the system is in steady state, the rate of change of concentration of any species in the reactor is zero. In particular, consider excited nitric dioxide

$$\frac{d(NO_2^*)}{dt} = k_1(NO)(O_3) - k_2(NO_2^*) - k_3(NO_2^*)(M) - \dot{V}_f(NO_2^*) = 0 \tag{5.4}$$

This equation says that the rate at which NO_2^* is produced by reaction (1) in the reactor is balanced by the chemical disappearance rates in (2) and (3) and the rate at which it flows out of the reactor. Parentheses denote the concentrations that have units of moles/cm^3, and $\dot{V}_f$ is the volumetric flow rate of products leaving the reactor. We can solve for (NO_2^*).

$$(NO_2^*) = \frac{k_1(NO)(O_3)}{k_2 + k_3(M) + \dot{V}_f} \tag{5.5}$$

The rate at which photons leave the system is equal to the rate at which they are produced in reaction (2). Therefore, the intensity recorded by the photomultiplier is

$$I = k_2(NO_2^*) = \frac{k_2 k_1(NO)(O_3)}{k_2 + k_3(M) + \dot{V}_f} \tag{5.6}$$

Assume that the reactor is large enough that there is plenty of time for the nitric oxide to disappear by reaction (1), since $d(\mathrm{NO})/dt = 0$ we have

$$k_1(\mathrm{NO})(\mathrm{O_3}) = \dot{V}_f(\mathrm{NO})_{\text{sample}} \tag{5.7}$$

$$I = \frac{k_2\dot{V}_f(\mathrm{NO})_{\text{sample}}}{k_2 + k_3(\mathrm{M}) + \dot{V}_f} \tag{5.8}$$

If the reactor is operated such that the ozone flow rate is large compared to the sample flow rate, then

$$\dot{V}_f = \dot{V}_{f,\mathrm{O_3}}$$
$$(\mathrm{M}) = (\mathrm{O_3}) = P/RT \tag{5.9}$$

Fixing the reactor temperature fixes the chemical rate constants, and fixing the pressure fixes the ozone concentration. Therefore, for a given volumetric flow rate of ozone and sample, the intensity is proportional to the concentration of nitric oxide in the entering sample stream.

The notation $\mathrm{NO_x}$ usually denotes the sum of nitric oxide and nitric dioxide concentrations. Commercial instruments measure $\mathrm{NO_x}$ by passing the sample through a catalyst to convert $\mathrm{NO_2} \rightarrow \mathrm{NO}$ prior to delivery to the reactor volume.

Both paramagnetic and polarographic analyzers are in common use for measuring oxygen concentration. In the latter, a teflon membrane separates the sample gas stream from a sensor that consists of a gold cathode and a silver anode immersed in potassium chloride gel.

The rate at which oxygen diffuses through the membrane is proportional to its partial pressure in the same stream. At the cathode, the following reaction takes place

$$\mathrm{O_2} + 2\mathrm{H_2O} + 4\mathrm{e}^- \rightarrow 4\mathrm{OH}^-$$

and at the anode

$$4\mathrm{Ag} + 4\mathrm{Cl}^- \rightarrow 4\mathrm{AgCL} + 4\mathrm{e}^-$$

There is a current flow because electrons are produced at the anode and consumed at the cathode. Because the oxygen concentration in the gel is small, this flow is proportional to the oxygen concentration in the sample.

To solve for the fuel–air equivalence ratio from exhaust gas analysis we essentially invert the analysis that led to Table 3-3 but use a slightly different set of approximations. Let us write the combustion reaction as

$$\epsilon\phi\,\mathrm{C_\alpha H_\beta O_\gamma N_\delta} + (0.21\mathrm{O_2} + 0.79\mathrm{N_2}) \rightarrow \nu_1\mathrm{CO_2} + \nu_2\mathrm{H_2O} + \nu_3\mathrm{N_2} + \nu_4\mathrm{O_2} + \nu_5\mathrm{CO} + \nu_6\mathrm{H_2} + \nu_7\mathrm{CH_z(g)} \tag{5.10}$$

In this equation $\mathrm{CH_z(g)}$ represents the gaseous hydrocarbons that a flame ionization detector records. The parameter z is the average hydrogen to carbon ratio of the hydrocarbons and is unknown. In engines that function properly,

the hydrocarbons contain negligible carbon and hydrogen, as far as atom balancing is concerned. They are included in the analysis because they are important in engines that misfire.

A carbon and oxygen balance on this equation leads to

$$\phi = \frac{2\left(1 + \frac{1}{4}\frac{\beta}{\alpha} - \frac{1}{2}\frac{\gamma}{\alpha}\right)(y_1 + y_5 + y_7)}{2y_1 + y_2 + 2y_4 + y_5} \tag{5.11}$$

Notice that if we had an instrument to measure water (generally we do not) then the equivalence ratio could be determined with no further analysis or approximations.

A complication arises in that most instruments do not function if water condenses in them. A common way to handle this is to condense the water from the sample prior to delivery to the instruments. We then say the concentration is "dry," as opposed to "wet." Denoting a dry concentration with a superscript zero, we can relate the dry concentration of any species i to the wet concentration by

$$y_i^0 = \frac{y_i}{1 - y_2} \tag{5.12}$$

Of course there is no physical significance when $i = 2$ (dry water). It is mathematically convenient, however, to speak of dry water defined by Eq. (5.12). In terms of dry concentrations, the equivalence ratio is

$$\phi = \frac{2\left(1 + \frac{1}{4}\frac{\beta}{\alpha} - \frac{1}{2}\frac{\gamma}{\alpha}\right)(y_1^0 + y_5^0 + y_7^0)}{2y_1^0 + y_2^0 + 2y_4^0 + y_5^0} \tag{5.13}$$

There is no change in the function since $(1 - y_2)$ factors out!

The water concentration is found by introducing the hydrogen balance. However, that does not solve the problem completely because it introduces two new unknowns, the hydrogen concentration and the hydrogen to carbon ratio of the exhaust hydrocarbons.

Spindt (1965) has found by experiment that it is satisfactory to assume

$$z = \frac{\beta}{\alpha} \qquad \mathrm{K} = 3.5 = \frac{y_2 y_5}{y_1 y_6}$$

Substitution of these relationships into the hydrogen balance gives, after much manipulation

$$y_2^0 = \frac{\frac{1}{2}\frac{\beta}{\alpha}(y_1^0 + y_5^0)}{1 + \frac{y_5^0}{3.5y_1^0}} \tag{5.14}$$

In the best of experiments the measured fuel–air ratios and those determined from exhaust gas analysis agree to within $\pm 2\%$.

5.4 RESIDUAL FRACTION

The residual fraction can be determined directly by use of a sampling valve to withdraw gases from the compression stroke for analysis with the same instruments already described. The mole fraction of carbon dioxide in those gases is

$$y_{CO_2} = y_r y''_{CO_2} \tag{5.15}$$

where y_r is the residual mole fraction and y''_{CO_2} is the carbon dioxide mole fraction in the exhaust gases. The residual mass fraction is, by Eq. (5.15) and (3.37)

$$f = \left[1 + \frac{M'}{M''}\left(\frac{y''_{CO_2}}{y_{CO_2}} - 1\right)\right]^{-1} \tag{5.16}$$

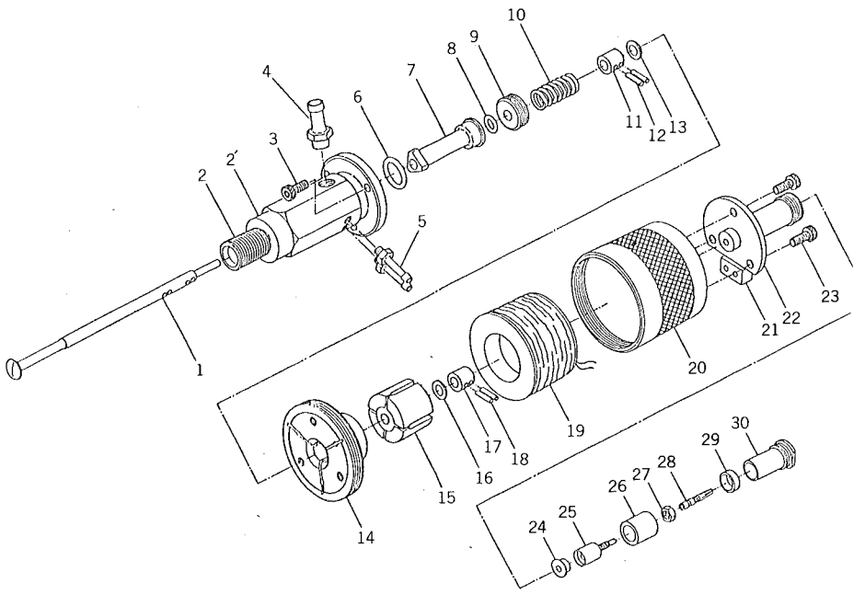

Figure 5-10 A typical sampling valve. The poppet valve (1) is electromagnetically opened by dumping two to five amps of current through a coil (19). A spring (10) closes the valve when the current stops. A capacitance type of valve motion detector (24, 25) is incorporated into the valve; the output connection is the pin (28). The seat (2) has threads that are screwed into a receiving hole that provides access to the combustion chamber. The sampled gases flow out the port (4). Cooling water flows in and out through ports at (5). Courtesy Tsukasa Sokken, Ltd.

The molecular weights of the residual gas M'' and fuel–air mixture M' are known because their compositions are known and Eq. (3.14) can be applied.

An example of a sampling valve is shown in Fig. 5-10. In this application, the valve would be mounted in the cylinder head so that when opened gases in the cylinder are withdrawn. These valves are opened by a trigger signal corresponding to a given crank angle and are open for 1 to 2 ms. By opening the valve at the same angle in successive cycles, it is possible to have a steady flow of gas for delivery to the exhaust gas analyzers.

It is also possible, though certainly more difficult, to determine the residual fraction by measuring the temperature at some angle during the compression stroke and applying the equation of state

$$PV = mRT \tag{5.17}$$

A technique for determining temperature by measuring sound speed is discussed by Taylor (1977).

5.5 PRESSURE–VOLUME MEASUREMENT

A number of ways have been used to measure pressure as a function of cylinder volume. We will restrict our attention to use of piezoelectric transducers since they are now the method preferred by most laboratories. The reader is referred to Chapter 5 of Obert (1973) for a discussion of some other methods. A discussion of the piezoelectric effect is given in Fig. 5-11. Quantitative use of these transducers is nontrivial. Care and methodical procedure is required. The reader who is using these transducers is advised to also consult SAE papers by Brown (1967) and by Lancaster, Krieger, and Lienesch (1975).

A typical system for measuring cylinder pressure as a function of cylinder volume is shown in Fig. 5-12. The transducer measures instantaneous pressure which when displayed on the oscilloscope is recorded as pressure versus time. A flywheel-mounted chopper is used to expose a light detector to a light source and thus generate signals at crank angles corresponding to slot position. For the chopper illustrated in Fig. 5-12, a signal is generated every 20°.[2] The slot at top dead center is made deeper so that more light will fall on the detector at this position and the resultant pulse will be larger. This identifies the top dead-center pulse on the oscilloscope display and thereby establishes the phasing of cylinder pressure to crank angle. To phase with cylinder volume, the theoretical formula derived from the slider crank mechanism is used to transform angle into volume; it is important to accurately measure the clearance volume and compression ratio.

[2] For data logged via computer, resolution of 0.1° is possible.

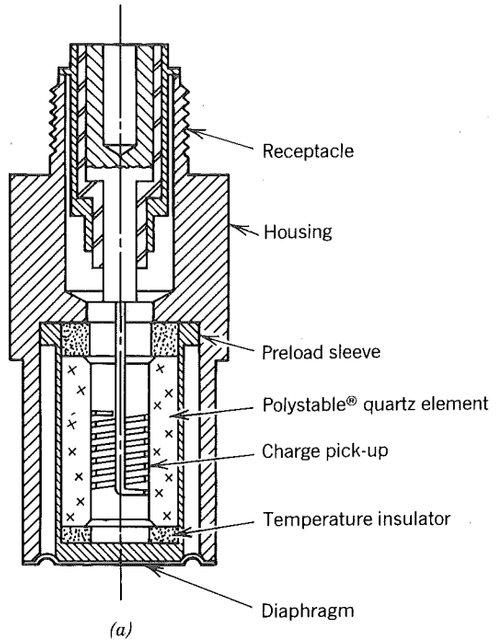

(a)

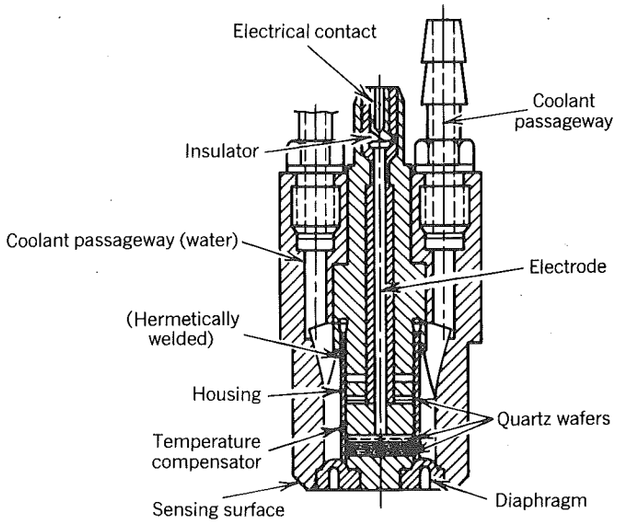

(b)

5.6 SPARK IGNITION ENGINE—ACTUAL CYCLES

Since the efficiency of an actual engine must be less than the efficiency of its equivalent Otto fuel–air cycle, the fuel–air cycle is a convenient standard for comparison. With reference to Fig. 5-13, an equivalent fuel–air cycle is constructed by matching the temperature, pressure, and composition (and thereby entropy) at some reference point after closing of the intake valve and prior to firing of the spark plug. Since the actual process is nearly isentropic, the compression curves of the two cycles nearly coincide. Soon after the spark fires, the pressure of the actual cycle stars rising above that of the fuel–air cycle.

Because the combustion actually is not at constant volume, the peak pressure is considerably less than that predicted by the fuel–air cycle. The

Figure 5-11 (*facing page*) Quartz Piezoelectric Pressure Transducers, (*a*) Courtesy of Kistler Instrument Corp., (*b*) Courtesy of AVL Corp.

Consider that a crystalline solid is made up of positive and negative charges distributed over a space in a lattice structure. If the distribution of charges is nonsymmetrical, stressing the crystal may displace positive charges relative to negative charges (by distortion of the lattice). Thus a surface that was electrically neutral may become positive in charge (or negative) from the displacement. Substances such as table salt (NaCl) have a symmetrical distribution of charges and therefore stresses do not lead to piezoelectricity. The crystal should be cut along a crystalline axis such that the relative charge displacement is maximum. There are two primary piezo effects: (1) The transversal effect: Charges on the x-planes of the crystal from force acting upon the y-plane, and (2) The longitudinal effect: Charges on the x-planes of the crystal from force acting upon the x-plane.

In (*a*) the quartz is cut as a cylinder (with two 180 deg or three 120 deg sectors). The potential difference between outer and inner (curved) surfaces of the cylinder is a measure of the gas pressure (transversal effect). In (*b*) the quartz is cut into a number of wafers electrically connected (not shown) in parallel. The potential difference is measured between the plane surfaces (longitudinal effect).

Note that in both pickups the charge is measured on the x-planes of the crystal; thus a crystal element in (*a*) is 90 deg displaced in (*b*). In (*a*) sufficient charge (sensitivity) is obtained by the height of the cylinder; in (*b*) it is obtained by the number of wafers. As a consequence, both types of pickups have about the same output.

The pressure pickup may be obtained with internal coolant passages and with a temperature compensator. Note that a rise in temperature will cause the housing to expand and thereby relieve the precompressed crystals from load. To compensate, a metal wafer may be added below the quartz, see (*b*), so that it can expand with the housing. Temperature compensation, however, is only necessary when precise measurements are necessary (imep values for example). Pickups can also be obtained with flame shields (to reduce flame impingement errors). Such errors are also reduced by coating the diaphragm with a silicone rubber to act as a heat shield (R. Hatschek, 1965).

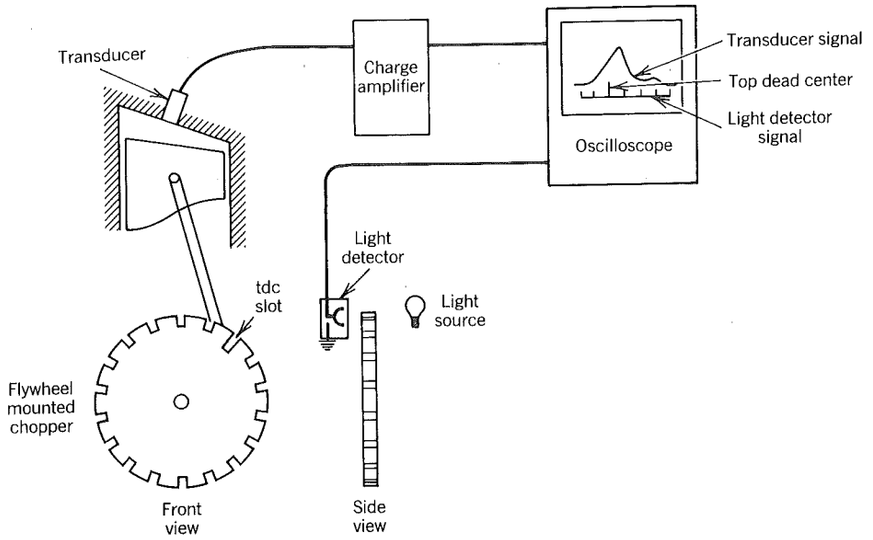

Figure 5-12 Typical pressure measurement system.

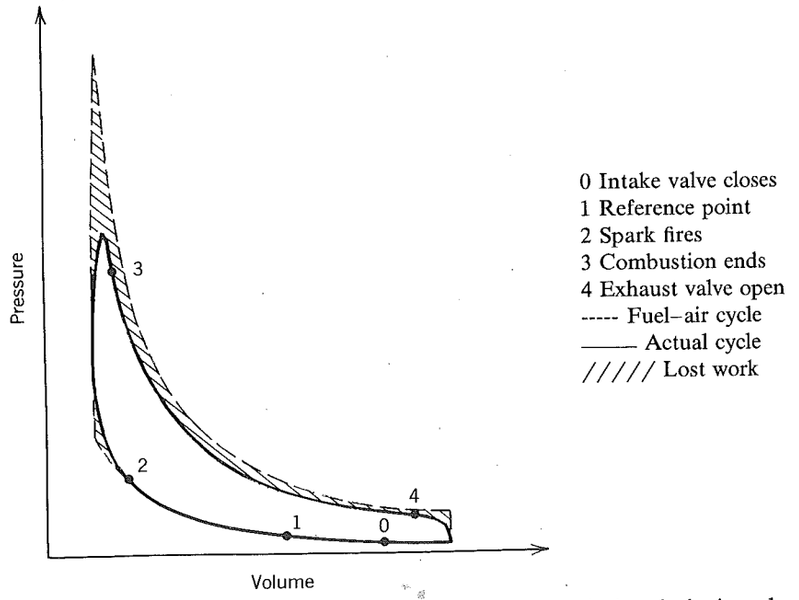

Figure 5-13 Comparison of an actual cycle with its equivalent fuel–air cycle.

expansion curve 3 to 4 is polytropic in character; measurements show that the entropy decreases during expansion. At point 4 the exhaust valve opens, and soon after, the pressure falls rapidly to the exhaust pressure.

The crosshatched area represents "lost work" that can mainly be attributed to the following

- Heat loss
- Mass loss
- Finite burn rate
- Finite blowdown rate

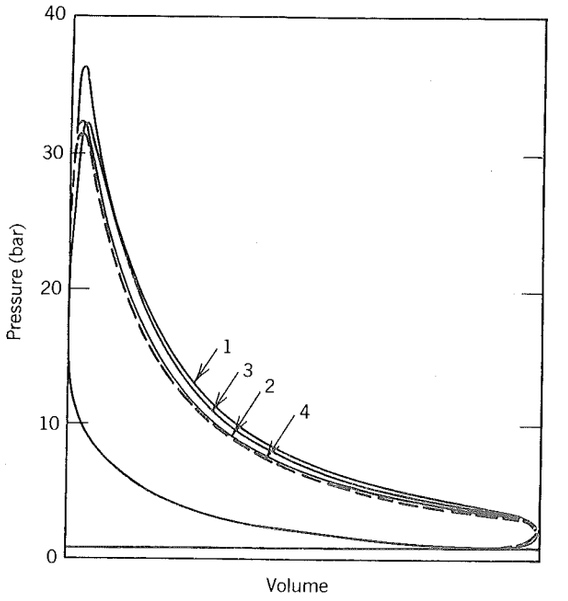

Figure 5-14 Effect of fuel–air equivalence ratio on P–V diagram. Reprinted from *The Internal Combustion Engine in Theory and Practice*, Vol. 1, by C. Fayette Taylor, with permission of MIT Press.

CURVE	ϕ	θ_s (DEG atdc)	θ_b (DEG)	bmep (BAR)	imep (BAR)	η/η_{Otto}
1	1.17	−15	33	—	7.7	0.85
2	0.80	−23	39	—	6.4	0.83
3	1.80	−20	39	—	7.0	0.83
4	0.74	−33	58	—	6.3	0.80

CFR engine, $b = 82.6$ mm, $S = 114.3$ mm, $r = 7$, 1200 rpm, $P_i = 0.95$ bar, $P_e = 1.02$ bar, $T_i = 355$ K.

These losses result in the actual efficiency being less than that of the equivalent fuel–air cycle by a factor ranging from 0.8 to 0.9.

Figures 5-14 through 5-19 show measured pressure–volume diagrams as functions of several engine variables. The results strictly apply only to the engine tested but the trends revealed and orders of magnitude are typical of most engines. With the exception of Fig. 5-15, all the data are obtained using optimum spark timing.

Important points to notice are:

- The ratio η/η_{otto} is on the order of 0.85, and varys little with engine operating variables at most decreasing slightly with increasing compression ratio.
- The combustion duration θ_b is on the order of 35°, decreases with increasing compression ratio or inlet pressure, and is minimum at a slightly rich equivalence ratio.

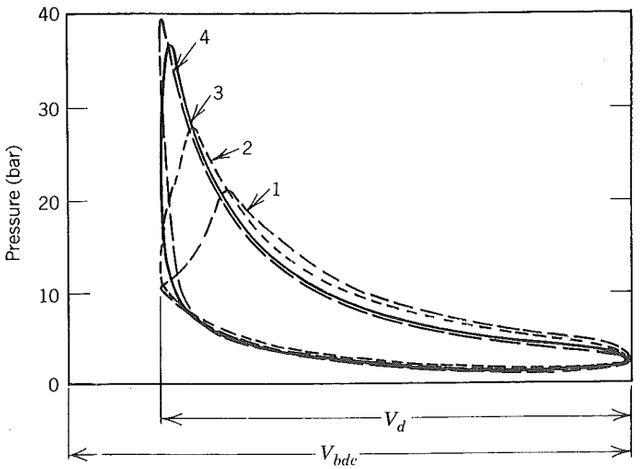

Figure 5-15 Effect of spark advance on P–V diagram. Reprinted from *The Internal Combustion Engine in Theory and Practice*, Vol. 1, by C. Fayette Taylor, with permission of MIT Press.

CURVE	θ_s (DEG atdc)	θ_b (DEG)	bmep (BAR)	imep (BAR)	η/η_{Otto}
1	0	40	5.0	6.0	0.73
2	−13	40	5.7	7.5	0.82
3	−26	38	5.8	7.5	0.82
4	−37	39	5.0	6.9	0.74

CFR engine, $b = 82.6$ mm, $S = 114.3$ mm, $r = 6$, $\phi = 1.13$, $P_i = 0.99$ bar, $P_e = 1.02$ bar, $T_i = 328$ K, 1200 rpm.

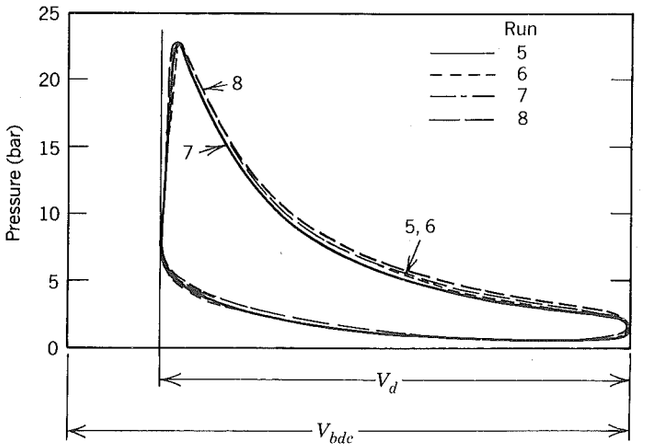

Figure 5-16 Effect of speed on P–V diagram, constant delivery ratio. From *The Internal Combustion Engine in Theory and Practice*, Vol. 1, by C. Fayette Taylor, with permission of MIT Press.

CURVE	P_i (BAR)	RPM	θ_s (DEG atdc)	θ_b (DEG)	bmep (BAR)	imep (BAR)	η/η_{Otto}
5	0.76	900	−18	36	3.90	5.89	0.842
6	0.79	1200	−19	39	3.77	5.94	0.848
7	0.95	1500	−22	40	3.80	6.07	0.865
8	0.98	1800	−18	38	3.59	6.14	0.877

CFR engine, $b = 82.6$ mm, $S = 114.3$ mm, $r = 6$, $T_i = 339$ K, $\phi = 1.13$, $P_e = 1.02$ bar.

- The optimum spark advance θ_s increases with combustion duration and with increased engine speed.
- Whereas imep increases with engine speed, bmep decreases, which, as we will see, is caused by increased friction.

The ratio η/η_{otto} from these data shows a weak dependence on compression ratio and an even weaker dependence on inlet temperature. It is independent of equivalence ratio and the exhaust to inlet pressure ratio. Some of these data are compared with data for other engines in Fig. 5-20. The coincidence in the orders of magnitude among the various engines lends credence to the earlier assertion that the results shown in Fig. 5-14 through 5-19 are typical of most engines. An important implication of these results is that there is slightly greater potential for improving the efficiency of spark-ignition engines by increasing their theoretical efficiency rather than by reducing their losses.

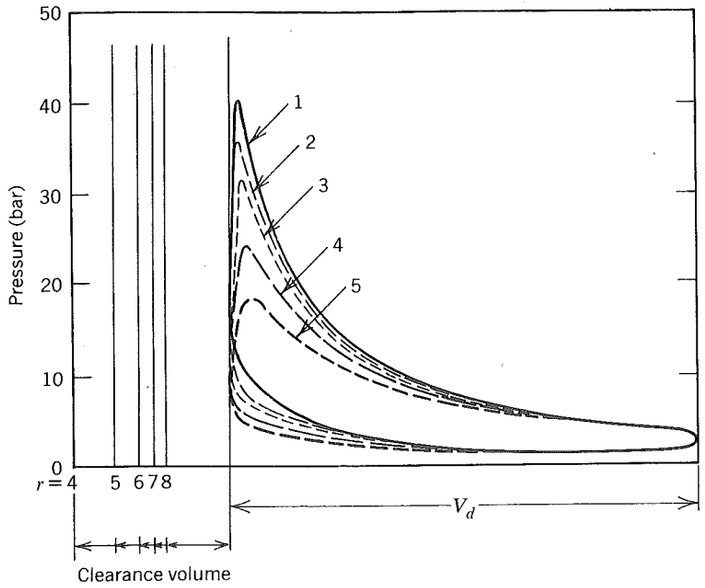

Figure 5-17 Effect of compression ratio on P–V diagram. From *The Internal Combustion Engine in Theory and Practice*, Vol. 1, by C. Fayette Taylor, with permission of MIT Press.

CURVE	r	θ_s (DEG atdc)	θ_b (DEG)	bmep (BAR)	imep (BAR)	η/η_{Otto}
1	8	−13	29	5.5	7.9	0.79
2	7	−14	31	5.3	7.9	0.86
3	6	−15	33	5.2	7.2	0.84
4	5	−16	37	4.8	6.8	0.87
5	4	−17	39	4.1	6.1	0.86

CFR engine, $b = 82.6$ mm, $S = 114.3$ mm, $P_i = 0.95$ bar, $P_e = 1.04$ bar, $T_i = 339$ K, $\phi = 1.13$, 1200 rpm.

To illustrate, suppose that by reducing the heat loss or increasing the burn rate one could increase η/η_{otto} from 0.80 to 0.90. The efficiency might be 0.324 instead of 0.288. On the other hand, suppose that research results showed that the compression ratio could be increased to 20. The fuel–air cycle (theoretical) efficiency would increase to about 0.46 and if η/η_{otto} were still 0.8, the actual efficiency would now be 0.368. There is greater potential to this avenue because the second law of thermodynamics does not limit the choice of

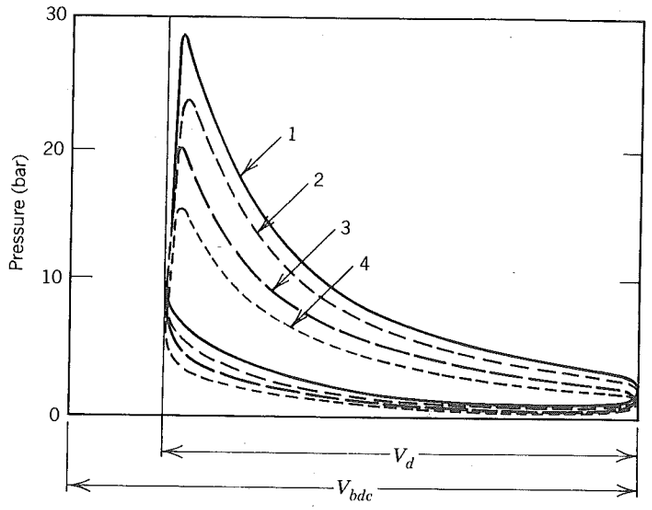

Figure 5-18 Effect of inlet pressure on P–V diagram. From *The Internal Combustion Engine in Theory and Practice*, Vol. 1, by C. Fayette Taylor, with permission of MIT Press.

CURVE	P_i (BAR)	θ_s (DEG atdc)	θ_b (DEG)	bmep (BAR)	imep (BAR)	η/η_{Otto}
1	0.95	−19	36	5.1	7.3	0.86
2	0.81	−20	38	4.0	6.3	0.87
3	0.68	−26	42	2.7	5.0	0.89
4	0.54	−28	44	1.6	3.7	0.82

CFR engine, $b = 82.6$ mm, $S = 114.3$ mm, $r = 6$, $P_e = 1.0$ bar, $T_i = 339$ K, 1200 rpm, $\phi = 1.13$.

variables that fix the theoretical efficiency but it does limit the gains that can be realized once the parameters that specify the fuel–air cycle are fixed.

5.7 COMPRESSION IGNITION ENGINES—ACTUAL CYCLES

Diesel engines are designed to limit the rates of pressure rise and the maximum pressures to satisfy constraints imposed by considerations for durability, noise, and emissions. Therefore, a convenient standard appears to be the equivalent limited pressure fuel–air cycle, and indeed this was the choice of Taylor (1977) in his book. Figures 5-21 and 5-22 compare actual pressure–volume diagrams with their ideal limited-pressure counterparts. As in the spark-ignition engine, the losses are attributed to heat and mass loss, the finite blowdown rate, and combustion occurring at less than the maximum pressure. Note that the ratio

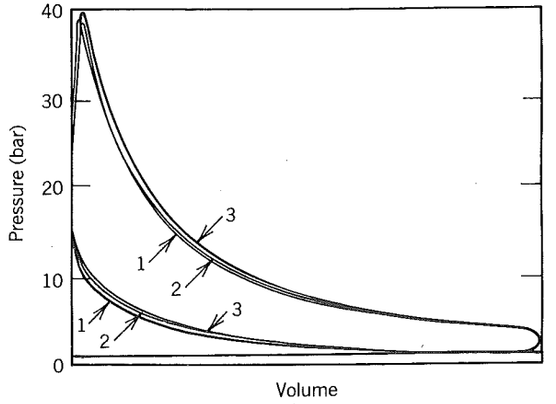

Figure 5-19 Effect of exhaust pressure on P–V diagram with constant mass of fresh mixture inducted. From *The Internal Combustion Engine in Theory and Practice*, Vol. 1, by C. Fayette Taylor, with permission of MIT Press.

CURVE	P_i (BAR)	P_e (BAR)	θ_s (DEG atdc)	θ_b (DEG)	bmep (BAR)	imep (BAR)	η/η_{Otto}
1	0.92	0.51	−18	24	—	7.7	0.83
2	0.95	0.95	−18	25	—	7.7	0.83
3	0.99	1.52	−18	25	—	7.7	0.83

CFR engine, $b = 82.6$ mm, $S = 114.3$ mm, $r = 7$, 1200 rpm, $\dot{m}_a = 4.70$ g/s, $\phi = 1.17$, $T_i = 356$ K.

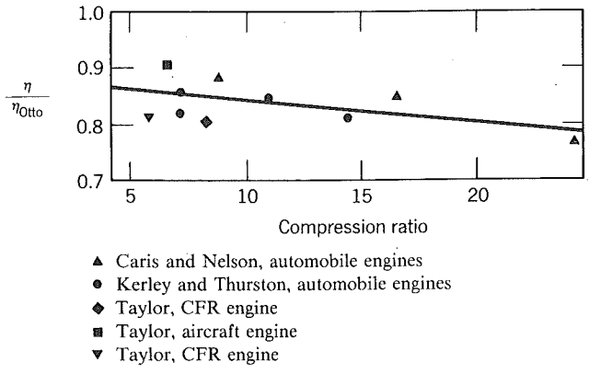

Figure 5-20 Indicated efficiency of some spark-ignition engines at optimum spark advance compared with values for their equivalent constant volume fuel–air cycle. From *The Internal Combustion Engine in Theory and Practice*, Vol. 2, by C. Fayette Taylor, with permission of MIT press.

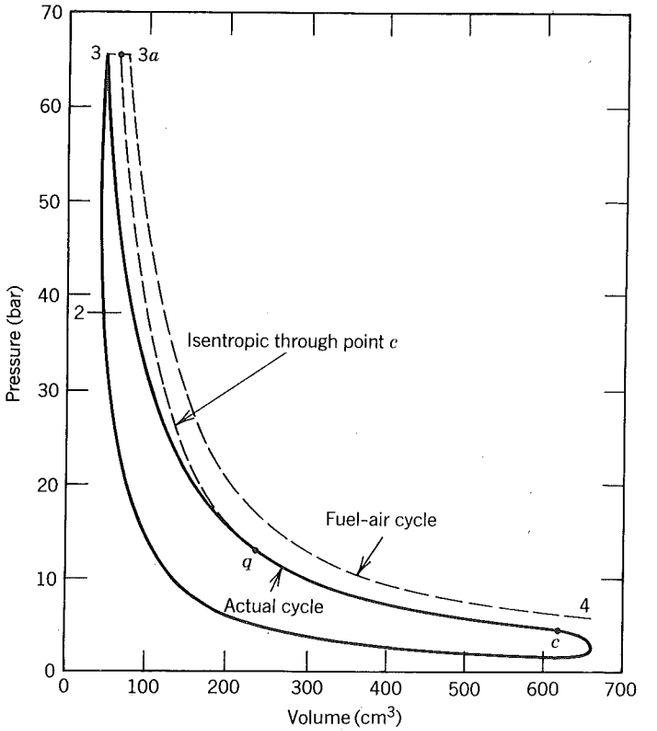

Figure 5-21 Cylinder pressures in a diesel prechamber engine compared with equivalent limited pressure fuel–air cycle: $f = 0.255$, imep = 7.72 bar, $\eta/\eta_{lp} = 0.614$. single-cylinder Waukesha comet-head diesel engine: $r = 14.5$, $b = 82.6$ mm, $S = 114.3$ mm, 1000 rpm, $\phi = 0.9$, optimum injection timing, air consumption = 4.93 g/s, $P_i = 0.99$ bar, $P_e = 1.01$ bar, $T_i = 560$ K. From *The Internal Combustion Engine in Theory and Practice*, Vol. 1, by C. Fayette Taylor, with permission of MIT Press.

η/η_{lp} is less for the prechamber engine than it is for the direct-injection, two-stroke engine.

There are two problems with using the limited-pressure fuel–air cycle as a standard: (1) an engine that can operate at a higher peak pressure and still satisfy the constraints imposed by durability, noise, and emissions considerations is a better engine and ought to be recognized as such and (2) for some engines, it is not possible to construct an equivalent limited-pressure fuel–air cycle because the losses are so great that the peak pressure is less than would be achieved via isentropic compression alone. An example of such a case is provided by the cycle shown in Fig. 5-23.

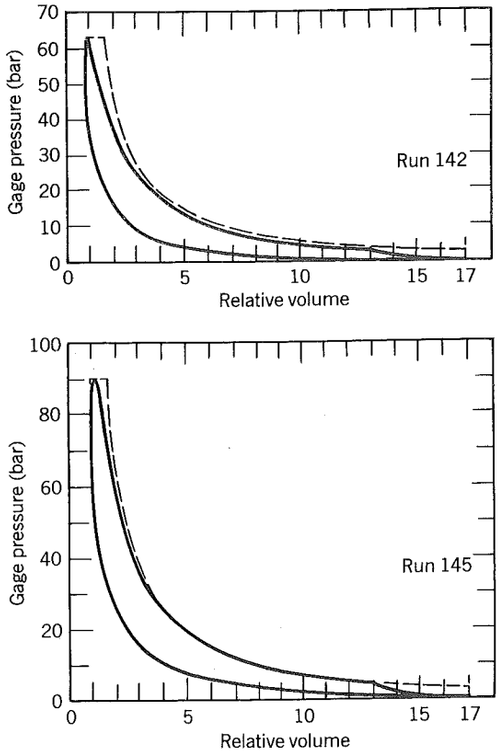

Figure 5-22 Actual open-chamber diesel cycles compared with equivalent limited pressure fuel–air cycles.

	Run Number	
	142	145
ϕ	0.56	0.59
f	0.08	0.06
m'_a, (trapped) g	1.07	1.36
imep, bar	7.10	9.86
η/η_{IP}	0.85	0.84
P_i, bar	1.19	1.66
P_e, bar	1.02	1.02

GM-71, two stroke, $b = 108$ mm, $S = 150$ mm, $r = 17$, 1600 rpm. From *The Internal Combustion Engine in Theory and Practice*, Vol. 1, by C. Fayette Taylor, with permission of MIT Press.

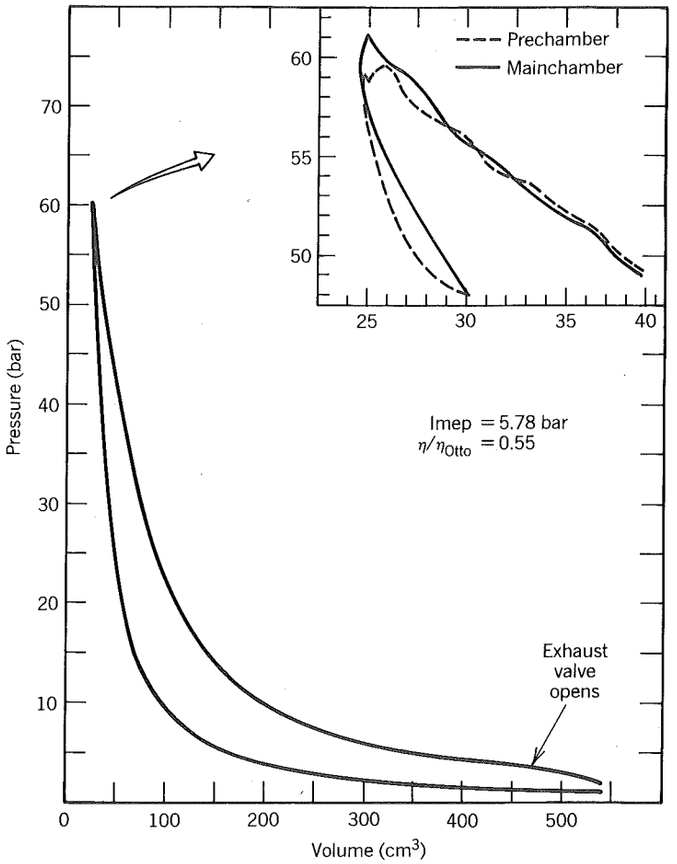

Figure 5-23 Pressure–volume diagram of a high compression ratio diesel prechamber engine. Multicylinder Opel engine with a Ricardo Mark V6 combustion chamber: $b = 88$ mm, $S = 85$ mm, $\epsilon = 0.266$, $r = 22.0$, $R_s = 1600$ rpm, $\phi = 0.57$, $e_v = 0.854$. Data courtesy D. Siegla and R. Talder, General Motors. (See also Fig. 10 of Amann and Siegla, 1982).

The compression ratio of this prechamber engine is considerably higher than that considered earlier in Fig. 5-20. If the mixture in the cylinder at closure of the inlet valve were compressed isentropically to the volume at top center, the resultant pressure would exceed the observed peak pressure. Thus an equivalent limited-pressure fuel–air cycle cannot be constructed.

As indicated in Fig. 5-20, when this engine is compared to an equivalent fuel-injected Otto cycle, the ratio η/η_{otto} is only 0.55; the engine is operating at about one half its potential. That is not to say that the engine is inefficient; recognize that at a compression ratio of 22 its equivalent Otto cycle efficiency

is quite high. The figure also shows that the difference between the pressure in the main chamber and the prechamber is quite small. There are not enough data available in the literature to say that this is typical of prechamber engines; if the cross-sectional area of the passage connecting the two chambers were smaller, the difference in pressure would be greater.

We conclude by noting that if the ratio of η/η_{otto} is a measure of how well an engine of a given compression ratio is developed, it appears that gasoline engines are more highly developed than diesel engines. This suggests that there is more potential for payoff from research and development on losses in diesel engines than there is on losses in spark-ignition engines.

5.8 REFERENCES

Amann, C. A. and D. C. Siegla (1982), "Diesel Particulates What Are They and Why?," *Aerosol Sci. and Tech.*, **1** pp. 73–101.

American Society of Mechanical Engineers Research Committee on Fluid Meters, (1961), *Flowmeter Computational Handbook*, ASME, New York.

Brown, W. L. (1967), "Methods for Evaluating Requirements and Errors in Cylinder Pressure Measurement," SAE paper 670008.

Danieli, G. A. (1977), "Pressure Measuring Technique in I.C.E.," *Meccanica*, **12**(3), p. 159–170.

Hatschek, R. (1965), "Piezoelectric Transducers," Vibrometer Corp.,

Lancaster, D. R., R. B. Krieger, and J. H. Lienesch (1975), "Measurement and Analysis of Engine Pressure Data," SAE paper 750026.

Obert, E. F. (1973), *Internal Combustion Engines and Air Pollution*, Intext, New York.

Spindt, R. S. (1965), "Air–Fuel Ratios from Exhaust Gas Analysis," SAE Trans., Vol. 74, paper 650507.

Taylor, C. F. (1977), *The Internal Combustion Engine in Theory and Practice*," MIT Press, Cambridge, Massachusetts.

5.9 HOMEWORK

1. A particular spark-ignition engine has an actual indicated power of 300 kW fueled with gasoline. For that same engine estimate the actual indicated power when it is operated on
   a. Methanol
   b. Nitromethane,
   In each case, assume $r = 10$, $\phi = 1.0$, $P_i = P_e = 1$ bar, $T_i = 300$ K, rpm = 5000 rpm. You may also assume that the equivalent fuel–air cycles correspond to the cases of $r = 10$ in Table 4-2.
2. In 1970, Ford built an engine with the following specifications:

$$b = 101.6 \text{ mm} \qquad r = 11$$
$$S = 88.9 \text{ mm} \qquad N_c = 8$$

The engine is naturally aspirated and the maximum power is

$$P_b = 225 \text{ kW at } 5400 \text{ rpm}$$

   a. Estimate theoretically the indicated power of that same engine assuming the equivalent fuel–air cycle is such that

$$\text{fuel} = C_7H_{17} \qquad P_1 = 0.9 \text{ bar}$$
$$T_1 = 350 \text{ K} \qquad f = 0.10$$
$$\phi = 1.2 \qquad \eta/\eta_{otto} = 0.85$$

   Because the engine is at wide-open throttle you may assume pmep $\ll$ imep.
   b. The mechanical efficiency of an engine is defined as the ratio of the brake power to the actual net indicated power or

$$\eta_{mech} = \frac{\text{bmep}}{(\text{imep})_{net}}$$

   What would it be in this case if the theoretical calculation is correct?
3. With reference to Section 5.3, the exhaust composition of a test engine is as follows:

$CO_2 = 11.50\%$	$NO = 310$ ppm
$H_2O = 7.11\%$	$NO_2 = 20$ ppm
$N_2 = 77.99\%$	$CH_4 = 350$ ppm
$O_2 = 3.19\%$	$C_3H_8 = 225$ ppm
$CO = 0.06\%$	$C_7H_{17} = 475$ ppm
$H_2 = 0.01\%$	

   Find the following:
   a. Wet concentration in ppm of HC and NO_x as would be indicated by heated flame ionization and chemilumenescence detectors, respectively. (Assume the FID responds to all carbon atoms equally.)
   b. Dry concentrations of CO_2, O_2 in percent and CO in ppm.
   c. Fuel–air equivalence ratio if the hydrogen to carbon ratio of the fuel is 1.3.
4. Explain how Eq. (5.17) could be used to measure the residual fraction.
5. A diesel engine operated on $C_{14}H_{27}$ produced exhaust gas of the following dry composition:

$CO_2 = 6.22\%$	$N_2 = 81.51\%$
$O_2 = 12.20\%$	$NO_x = 400$ ppm
$CO = 0.024\%$	HC = 200 ppm C

   a. Explain how the method of hydrocarbon measurement can yield a situation wherein the sum of the exhaust constituents adds up to slightly greater than 100%.

b. At what equivalence ratio was the engine operated? How would the answer differ if one neglected the carbon monoxide and hydrocarbons?

6. Manufacturers of laminar air–flow meters typically provide a calibration curve of the following form:

$$\dot{V}_{stp} = c_1 \Delta P + c_2 \Delta P^2$$

where

$\dot{V}_{stp}$ = volumetric flow rate at standard temperature and pressure

ΔP = pressure drop across the meter

a. Use dimensional analysis to show how the constants c_1 and c_2 would change for measurements made at conditions other than standard temperature and pressure (stp).

b. How can one determine the mass flow rate in (a) rather than the volumetric flow rate?

7. Assuming one-dimensional, isentropic steady flow of an ideal gas with constant specific heats, derive an expression for the constant C of the critical flow nozzle in Fig. 5-6. The calibration constant depends on the nozzle throat area A, the gas constant R, and the ratio of specific heats γ. You may assume the upstream area is large enough that measured P_1, T_1 are stagnation properties.

8. Replot Fig. 5-23 as $\ln P$ versus $\ln V$. Estimate the polytropic exponent $n \equiv -d \ln V / d \ln P$ in the middle of both expansion and compression. How should these exponents relate to the specific heat ratio?

Six
FRICTION

Friction refers to forces acting between surfaces in relative motion. Engines are lubricated to reduce these forces. The friction forces between sliding or rotating parts in engines arise from the hydrodynamic shear stresses in oil films and metal to metal contact, where, for reasons to be discussed, the lubricant is squeezed out.

In this chapter we will examine friction of the entire engine, the friction caused by various parts, and the nature of friction. To begin, let us first define the friction mean effective pressure, for in that form, it should be easier to generalize about the friction work.

amep = work to power nonessential auxiliaries such an air conditioner

bmep = work done by the engine

cmep = work to power a compressor such as a supercharger

fmep = work to overcome friction internal to the engine and to power essential auxiliaries such as an oil pump

imep = work done by the gas during compression and expansion

mmep = work required to motor an engine

pmep = work done on the gas during intake and exhaust

tmep = work recovered from the exhaust gas by a turbine

By definition it follows that

$$\text{fmep} = \text{imep} - \text{pmep} - \text{bmep} - \text{amep} - \text{cmep} + \text{tmep} \qquad (6.1)$$

For convenience, we will restrict ourselves to the special case in which amep = 0 and cmep = tmep. The latter condition applies to naturally aspirated engines with no exhaust turbine or to turbocharged engines in which all of the turbine work is used by the compressor. In these special cases it follows that

$$\text{fmep} = (\text{imep})_{net} - \text{bmep} \qquad (6.2)$$

Measurements are made of fmep by integrating a pressure–volume diagram to obtain $(\text{imep})_{net}$ and subtracting the bmep determined by a dynamometer reading. Very few measurements of this type have been published partly because, as we shall see, approximate measures can be realized by using

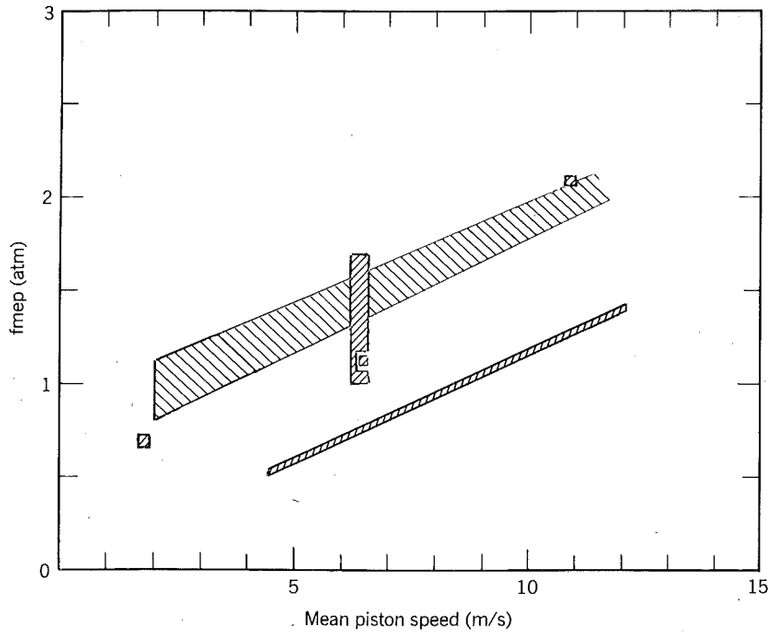

Figure 6-1 Friction mean effective pressure of three engines.

motoring tests. Results available to me are shown in Fig. 6-1. Table 6-1 provides the data key.

It is clear from Fig. 6-1, that, for any given engine, increasing piston speed increases the friction mean effective pressure. It is also apparent that friction depends on more than piston speed since all the data do not fall on the same curve. Brown's single-cylinder diesel data show that friction is reduced by increasing the inlet air temperature. Gish's spark-ignition engine has the

Table 6.1 Data Key for Fig. 6-1

SYMBOL	BORE × STROKE (CM)	REFERENCE
/////	9.53 × 11.4 four cylinder, in line, overhead valve test engine. Load and compression ratio vary.	(Gish, 1957)
\\\\	11.4 × 11.4 Single cylinder, D.I. diesel test engine, Inlet temperature varies.	(Brown, 1973)
//////	13.7 × 16.5 six cylinder, prechamber diesel engine. Load varies.	(Brown, 1973)

characteristic that friction increases with load and/or compression ratio; whereas Brown's six-cylinder diesel engine shows no dependence of friction on load.

6.1 MOTORING MEAN EFFECTIVE PRESSURE

The motoring mean effective pressure is defined as the work per unit displacement volume required to spin an engine operated without combustion. A direct-current electric cradle type dynamometer is the most convenient apparatus for such a measurement. The principle of operation was discussed in Chapter 5. The dynamometer is mounted on bearings and is restrained from rotation by only a strut connected to a load beam. Whether the dynamometer is absorbing or providing power, a torque is applied to the dynamometer. The work done in rotating the crankshaft through 2π radians is $2\pi\tau$. Hence for two- and four-stroke engines, respectively

$$\text{mep} = \frac{2\pi\tau}{V_d} \quad \text{or mep} = \frac{4\pi\tau}{V_d} \tag{6.3}$$

Equation (6.3) is valid whether or not the engine is firing. Recognize that although the sign of τ changes, we think of bmep and mmep as positive numbers.

Practical application comes from the observation that under controlled conditions

$$\text{fmep} \cong \text{mmep} \tag{6.4}$$

Therefore, motoring tests are useful because it is much easier to measure mmep than fmep. Hence most friction studies have been done by application of Eq. (6.4). For any given engine, it can be written that

$$\text{mmep} = -(\text{imep})_m + (\text{pmep})_m + (\text{fmep})_m \tag{6.5}$$

where the subscript m denotes the fact that the engine is motored.

Because there is heat and mass loss during compression and expansion, the indicated work of motoring is not zero, but less than zero (i.e., there is work done on the gas). Figure 6-2 helps to illustrate this point. The pressures are everywhere lower on the expansion curve than on the compression curve, hence $\int P\,dV < 0$. It is generally true that

$$-(\text{imep})_m \ll (\text{fmep})_m \tag{6.6}$$

The controlled conditions under which Eq. (6.4) is assumed to be valid are:

- The motored engine is operated at wide-open throttle.
- The motored engine is operated at the same oil and coolant temperatures as the fired engine for which one wants to estimate fmep.

By operating at wide-open throttle, where ideally the pumping work is zero, the

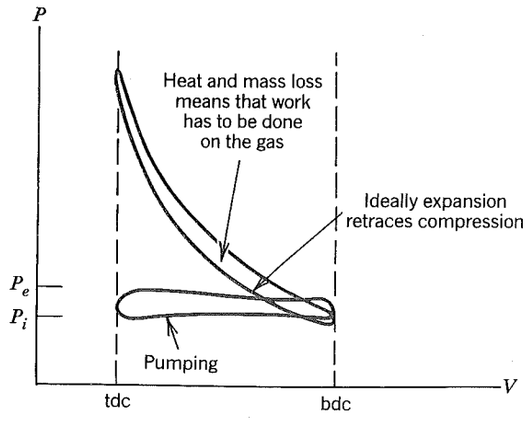

Figure 6-2 Motoring P–V diagram.

pumping loss is minimized and it is generally true that

$$(\text{pmep})_{m,\text{wot}} \ll (\text{fmep})_m \tag{6.7}$$

Finally, by matching oil and coolant temperatures between the motored and fired engines, it turns out that

$$(\text{fmep})_m \approx (\text{fmep})_f \tag{6.8}$$

The friction is not identically equal for a number of reasons including that the pressure–time diagrams are very different and temperature gradients within the engine are much less in the motored engine than in the fired engine.

Comparisons between motoring and firing friction are given in Fig. 6-3*a* for a spark-ignition engine and in Fig. 6-3*b* for a diesel engine. In both cases, motored and fired, the friction is determined by integrating the pressure–volume diagram and using the definition given in Eq. (6.2). Equation (6.8) appears valid for the diesel engine for different piston speeds but is a rather crude approximation at high loads for the gasoline engine. The results illustrate the danger in using motoring tests to measure friction. Whenever possible, the basic definition in Eq. (6.2) should be applied to measure friction. We can conclude that Eq. (6.8) is generally valid only in the limit of no load.

The most important advantage of a motoring test is that the engine can be partially disassembled, which precludes firing, and motored to study the distribution of friction among the various parts. Fig. 6-4 is typical of the results that can be obtained by this method. The first items removed were the manifolds and turbocharger. Brown (1973) showed that this changed only the pumping loss. Next he removed the valves and disconnected the camshafts. The resultant curve C is nearly identical with curve J which is the fmep determined for a motored engine. The small difference is believed to be caused by a change in the gas load which without valves is nonexistent. Curve K is the fmep of the fired engine and, as illustrated, there is a small difference between

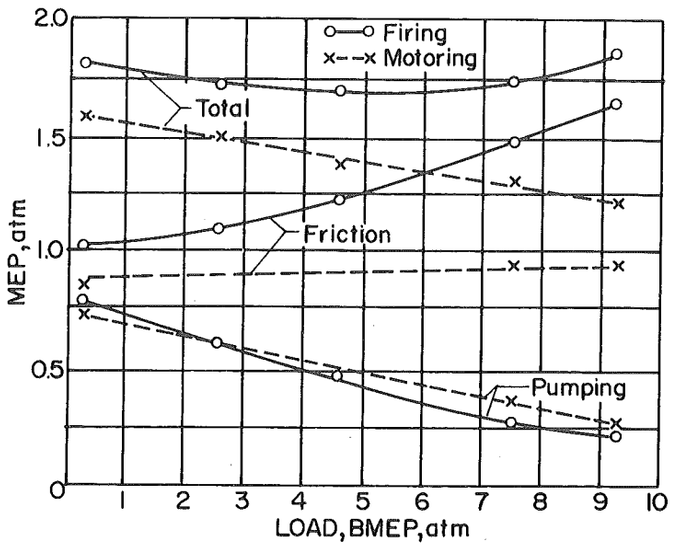

(*a*)

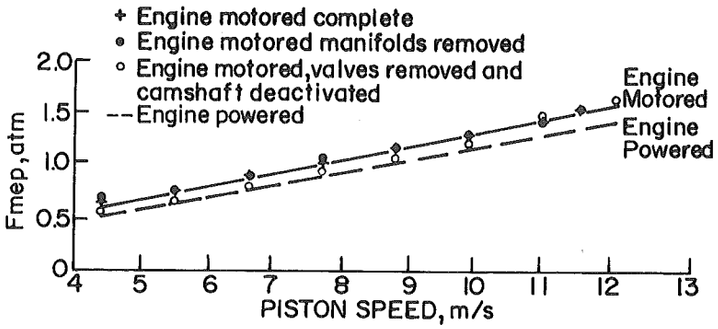

(*b*)

Figure 6-3 (*a*) Friction and pumping work versus load of a gasoline engine, 12/1 compression ratio (Gish, McCullough, Retzloff and Mueller 1957). Reprinted with permission © 1957. Society of Automotive Engineers, Inc. (*b*) Friction of a diesel engine; engine motored versus engine powered. In both cases the friction is measured by application of Eq. (6.2), thus the motored friction is not the motoring mean effective pressure (Brown 1973). Reprinted with permission © 1973. Society of Automotive Engineers, Inc.

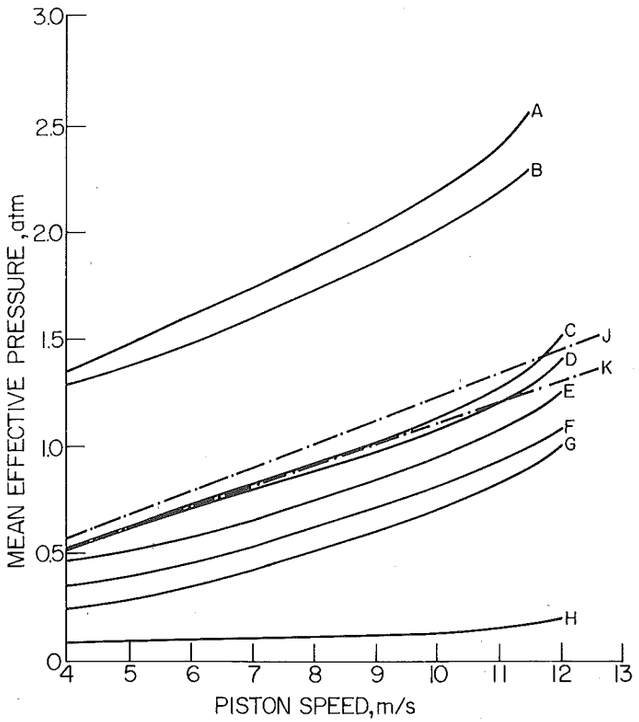

Engine setup

- A Complete engine
- B Complete engine minus intake and exhaust manifolds
- C Setup B minus all valves, camshaft and measured pumping loss
- D Setup C minus water pump
- E Setup D minus oil pump
- F Setup E minus all top and intermediate piston rings
- G Setup E minus all piston rings
- H Crankshaft only
- J Motored engine friction per imep meter measurements on complete engine
- K Idle and load engine friction per imep meter measurements on complete engine

Note—No measurable loss in fuel pump and governor group

Figure 6-4 Motored friction (mmep) during disassembly of a diesel engine. (Brown, 1973). Reprinted with permission © 1973. Society of Automotive Engineers, Inc.

fired and motored friction. It was concluded that the difference between curve A and curve C is due to pumping losses and a nonzero imep during motoring.

As disassembly proceeds it becomes clear that pistons and rings are responsible for about one half to three quarters of the friction, this is consistent with other studies. Since friction due to the piston and rings is the major component, it has received a lot of attention and we will discuss it.

The last curve, H, shows friction due to spinning only the crankshaft. This friction is caused by shear in an oil film between the journal and its bearing, the understanding of which is on a firm theoretical basis (which we will also discuss.)

6.2 DIMENSIONAL ANALYSIS

The previous section showed that friction depends on the piston speed and the load. Other variables that immediately come to mind are the oil viscosity μ_o, oil density ρ_o, the compression ratio, the bore, and other geometrical parameters that specify the bearings, rings, pistons, cams, lifters, and so on. Mathematically

$$\text{fmep} = f\left[\overline{U}_p, \mu_o, \rho_o, r, \text{imep}, b, l_i\ (i=1,2,\ldots), \sigma_j\ (j=1,2,\ldots)\right] \quad (6.9)$$

where the l_i $(i=1,2,\ldots)$ represent all the lengths and σ_j $(j=1,2,\ldots)$ all the material properties necessary to specify the engine on a set of blueprints. In dimensionless groups, it can be written that

$$\frac{\text{fmep}}{\rho_o \overline{U}_p^2} = \tilde{f}_1\left[\frac{\rho_o \overline{U}_p b}{\mu_o}, r, \frac{\text{imep}\, b}{\mu_o \overline{U}_p}, \tilde{l}_i, \tilde{\sigma}_j\right] \quad (6.10)$$

The first dimensionless group in the argument list is a Reynolds number based on the piston speed, the bore, and the oil kinematic viscosity ν_o.

$$R_e = \frac{\overline{U}_p b}{\nu_o} \quad (6.11)$$

All the lengths are normalized by the bore.

In the case of motoring mean effective pressure, the dependence on load is no longer necessary and we conclude that

$$\frac{\text{mmep}}{\rho_o \overline{U}_p^2} = \tilde{f}_2\left(R_e, r, \tilde{l}_i, \tilde{\sigma}_j\right) \quad (6.12)$$

That the Reynolds number based on piston speed is the proper scaling parameter has been demonstrated by Taylor (1977), who did experiments with geometrically similar engines.

Geometrically similar engines refers to any family of engines manufactured from the same materials and the same blueprints but to different sizes or scales. Such engines have different bores, strokes, and so on, but identical compression ratio, stroke to bore ratio, $\tilde{l}_i$, and $\tilde{\sigma}_j$. Results obtained by Taylor

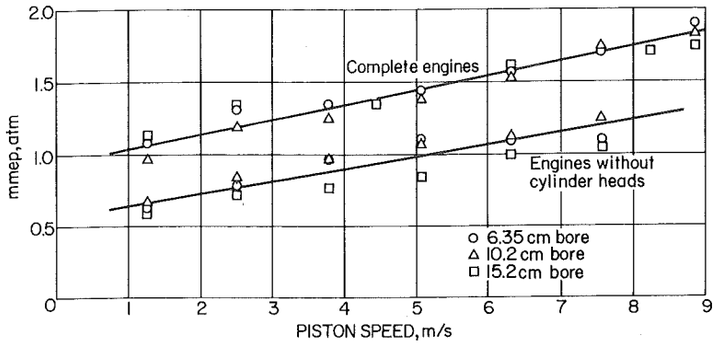

Figure 6-5 Motoring mep of MIT similar engines. Jacket water temperature 339 K in, 356 K out. Oil viscosities at 394 K proportional to bore; thus at a given piston speed all three engines have the same Reynolds number. From *The Internal Combustion Engine in Theory and Practice*, Vol. 1, by C. Fayette Taylor, with permission of MIT Press.

are shown in Fig. 6-5 for three different geometrically similar engines. Since the data all fall on a common curve for the three engines, it follows that

$$\frac{\text{mmep}}{\rho_o \bar{U}_p^2} = \tilde{f}_3(R_e) \text{ (geometric similarity)} \tag{6.13}$$

When one recognizes that to a certain degree all reciprocating piston engines are geometrically similar, then Eq. (6.13) applies in an order of magnitude analysis for any engine.

Finally, as an illustration of application of Eq. (6.13), the correlation of Bishop (1964) when made dimensionless yields:

$$\frac{\text{mmep}}{\rho_o \bar{U}_p^2} = \frac{1.3 \times 10^5}{R_e} + \frac{1.7 \times 10^8}{R_e^2}(r + 15) \tag{6.14}$$

6.3 PISTON AND RING FRICTION

The friction due to the piston and its rings has been directly measured in a fired engine by the apparatus shown in Fig. 6-6. Notice that the combustion cylinder is free to move axially against a stiff spring. By measuring the deflection of the cylinder and applying knowledge of the spring constants, one can one compute the force due to friction.

Typical results are shown in Fig. 6-7. The following features should be noted (Taylor, 1977):

- Friction forces are comparable on the compression-intake and compression-exhaust strokes.
- Friction forces occurring during expansion are about twice as large as those occurring during any other stroke.

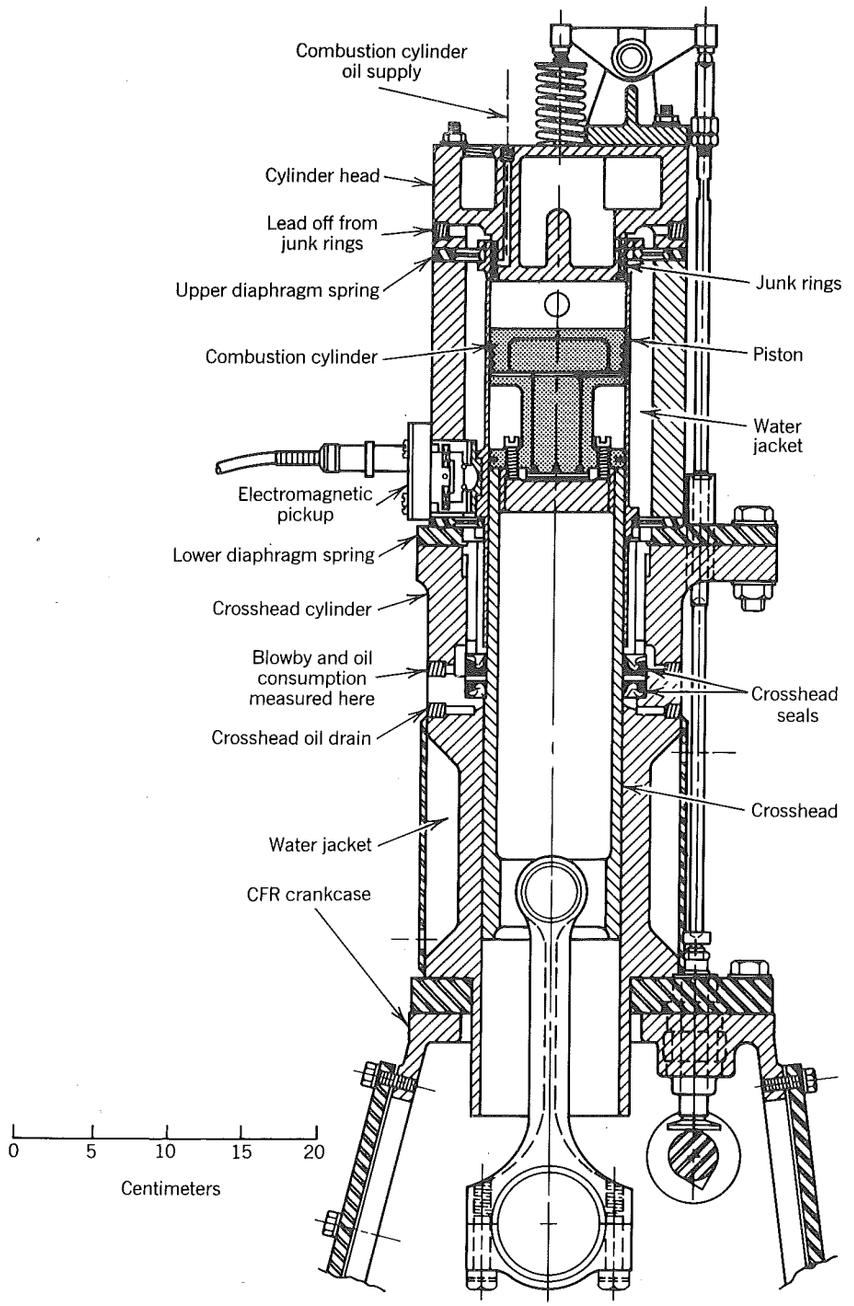

Figure 6-6 Friction research engine with spring mounted barrel: 82.6×114 mm, $r = 5.05$. Can be used with or without cross-head (Livengood and Wallour, 1947).

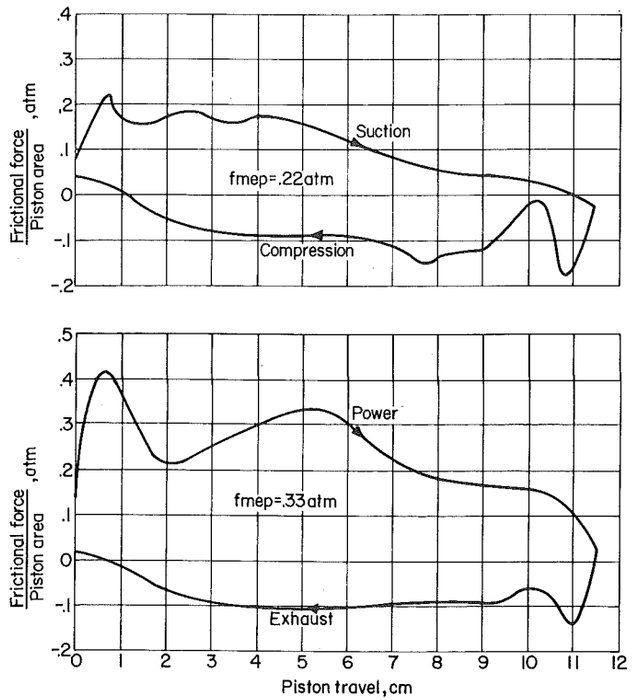

Figure 6-7 Piston and ring friction as a function of piston position measured using the engine of Fig. 6-6. $\overline{U}_p = 4.57$ m/s, bmep = 5.78 atm., $T_c = 356$ K, $T_{oil} = 356$ K (Leary and Jovellanos, 1944).

- Friction forces tend to be high just after top and bottom dead center, probably because there is metallic contact between the rings and the cylinder wall.
- The friction force is nonzero at top and bottom dead centers. This is probably caused by deflection of the engine parts such that the piston velocity is nonzero at top and bottom dead center.
- The fmep due to piston and ring friction is on the order of 0.3 atm in this engine.

The effects of operating parameters on the piston and ring friction as determined using the apparatus in Fig. 6-6 are shown in Fig. 6-8. The results indicate that the piston and ring fmep increase with oil viscosity, piston speed, and imep. For the experimental results shown by dashed lines, the piston was guided by a crosshead so that only the rings came in contact with the cylinder. The friction is reduced 20%, suggesting that most of the friction is caused by the rings.

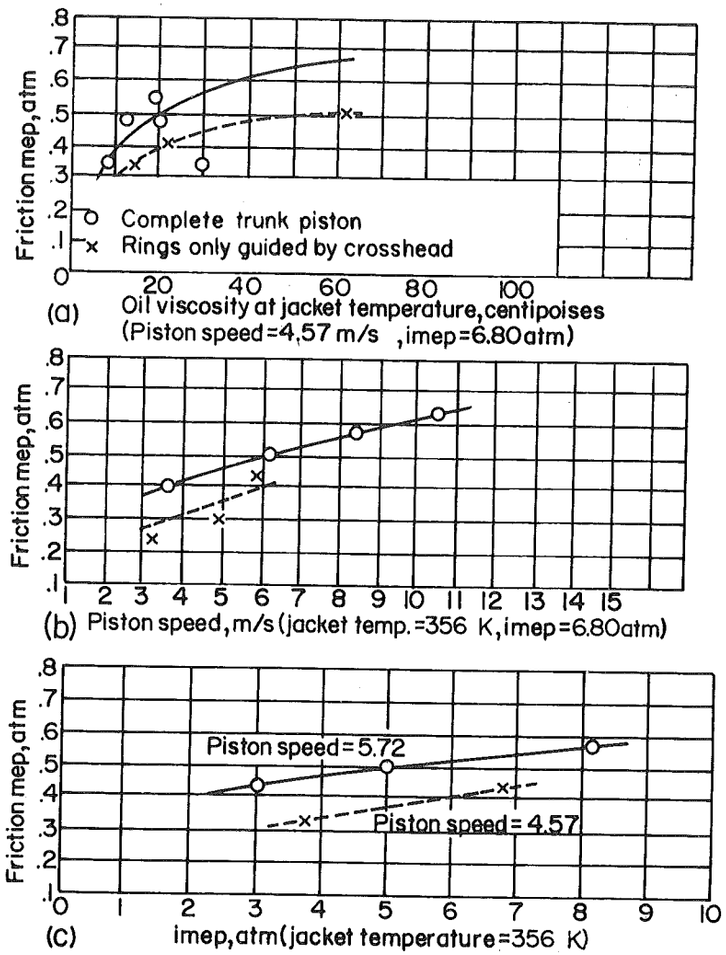

Figure 6-8 The effect of operating variables on piston and ring friction measured using the engine of Fig. 6-6 (Leary and Jovellanos, 1944; Livengood and Wallour, 1947).

The nonlinear dependence of piston and ring friction on oil viscosity is caused by the oil between the sliding surfaces being warmer than the jacket temperature and its temperature varies with crank angle. Since oil viscosity varies considerably for small temperature changes, the oil viscosity distribution along the cylinder wall scales nonlinearly with the viscosity in the oil pan or the viscosity evaluated at the jacket temperature.

Support for Taylor's hypothesis that metallic contact occurs in the vicinity of top dead center comes from observation of the oil film in running

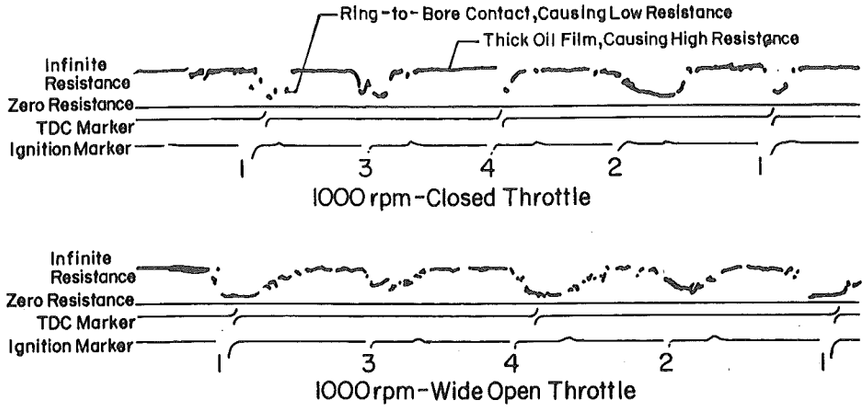

Figure 6-9 Typical oil film electrical resistance result in gasoline engine (McGeehan, 1978). Reprinted with permission © 1978. Society of Automotive Engineers, Inc.

engines. Rhodes (1970) has measured the electrical resistance between a piston ring and the cylinder in a running engine. His results are given in Fig 6-9. They show that resistance is low in the vicinity of top and bottom dead center, as one would expect, if there is metallic contact. The electrical resistance is higher at the middle of each stroke where piston speed is high and hydrodynamic lubrication is expected.

With the ever-increasing prowess of computers, calculation of ring friction from lubrication theory is becoming more and more practical. Current practice introduces some unknown constants of proportionality that are determined by forcing a match between computed and measured results. Like combustion models, friction models are not truly predictive but are useful tools for diagnostic and exploratory exercises.

Fig. 6-10 illustrates some concepts key to theoretical analysis of ring friction. There is an oil layer separating the ring from the cylinder wall whose thickness δ is both time and spatially dependent. The one dimensional situation depicted is not a bad approximation since the bore is so much larger than the oil film thickness. In the situation shown, the coordinate system is defined so that the ring is stationary and the cylinder wall is translating with the instantaneous piston speed U. When the ring is sitting on the bottom of the land as depicted, a force balance on the ring per unit length yields

$$\int_0^L P_o(x,t)\,dx = L\left[P_e + P_t(t) + P_{\text{top}}(t)\right] \tag{6.15}$$

where

$P_o(x,t)$ = spatially and temporally varying oil pressure

P_e = the elastic ring pressure

$P_t(t)$ = time dependent piston side thrust pressure

$P_{\text{top}}(t)$ = time dependent gas pressure on top side of the ring. For the first ring it would be the cylinder pressure.

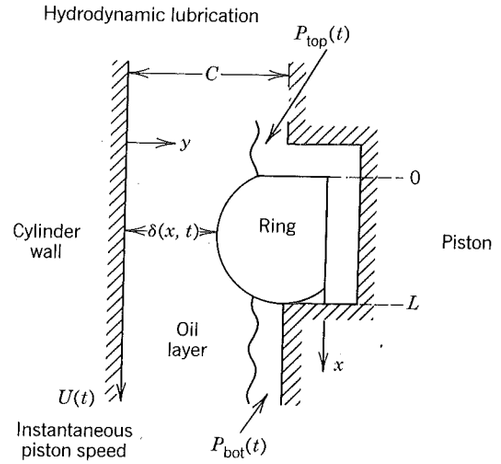

Figure 6-10 Essential features of a hydrodynamic analysis of ring friction. Account can also be taken of ring motion and rough walls.

For the special and practical case in which the oil film is much thinner than the ring width, that is

$$\delta(x,t) \ll L \tag{6.16}$$

the Navier–Stokes equations for the oil motion reduce to a Reynolds equation, which is

$$\frac{\partial}{\partial x}\left(\delta^3 \frac{\partial P_o}{\partial x}\right) = 6\mu U \frac{\partial \delta}{\partial x} + 12\mu \frac{\partial \delta}{\partial t} \tag{6.17}$$

The boundary conditions to be applied to the Reynolds equation in the case illustrated by Fig. 6-10 are

$$P_o(0,t) = P_{\text{top}}(t) \tag{6.18}$$

$$P_o(L,t) = P_{\text{bot}}(t) \tag{6.19}$$

where $P_{\text{top}}(t)$ and $P_{\text{bot}}(t)$ are periodic functions known either from direct measurements or from a combustion model complete with a blowby model (see Chapter 8) that predicts interring gas pressures. Numerical solution of the Reynolds equation yields the oil film thickness $\delta(x,t)$ and oil pressure $P_o(x,t)$ such that the boundary conditions are satisfied.

The friction force on the ring is caused by shear stress in the oil. It is evaluated directly from Newton's law, which in this case is

$$F(t) = \pi b \int_0^L \mu \left(\frac{\partial u}{\partial y}\right)_{y=0} dx \tag{6.20}$$

In the case of the Reynolds equation, this reduces to

$$F(t) = \pi b \int_0^L \left(\frac{\delta}{2}\frac{\partial P}{\partial x} - \mu \frac{U}{\delta}\right) dx \tag{6.21}$$

Recognition that work is force times distance leads to the following expression for the work required to overcome this friction

$$\delta W = F \cdot U\,dt = \frac{FU}{\omega}\,d\theta \tag{6.22}$$

The contribution to the fmep of this ring is then

$$\text{fmep} = \frac{1}{V_d}\int_0^{4\pi}\frac{\delta W}{d\theta}\,d\theta$$

$$= \frac{4}{\pi\omega S b^2}\int_0^{4\pi}\pi b U \int_0^L \left(\frac{\delta}{2}\frac{\partial P}{\partial x} - \mu\frac{U}{\delta}\right) dx\,d\theta \tag{6.23}$$

Let us introduce the mean piston speed $\overline{U}_p = 4\pi\omega S$ and normalize all lengths by the bore b, the oil viscosity by an average value μ_o, and the pressure by $P_o = 2\mu_o \overline{U}_p/b$. The fmep is then given by

$$\frac{\text{fmep}}{\rho_o \overline{U}_p^2} = \frac{16\tilde{C}_1}{R_e} \tag{6.24}$$

where the dimensionless parameter $\tilde{C}_1$ is given by

$$\tilde{C}_1 = \int_0^{4\pi}\tilde{U}\int_0^{\tilde{L}}\left(\tilde{\delta}\frac{\partial \tilde{P}}{\partial \tilde{x}} - \tilde{\mu}\frac{\tilde{U}}{\tilde{\delta}}\right) d\tilde{x}\,d\theta \tag{6.25}$$

Note that $\tilde{C}_1$ is expected to be more or less a constant for geometrically similar engines. The experimental data which are available suggest that $\tilde{C}_1$ increases slightly with compression ratio. For example, the piston and ring friction determined Bishop (1964) can be roughly correlated by the following expression

$$\text{Pistons and rings: } \frac{\text{fmep}}{\rho_o \overline{U}_p^2} = \frac{6.2\times 10^4 r^{0.2}}{R_e} \tag{6.26}$$

Some calculated oil-film thicknesses for a particular engine are shown in Fig. 6-11. In the graph, the minimum oil thickness is plotted for different speeds and loads. The results are similar in shape for all conditions and are fairly insensitive to speed and load. Surface roughness in engines is such that for film thickness less than about a micron, metal to metal contact can be expected to occur. The results in Fig. 6-11 show that metal to metal contact can be expected to occur at top and bottom dead center for all speeds and loads. The results also show that at high load, metal to metal contact can occur for most, if not all, of the power stroke.

A state of the art friction computation for a ring pack deals with surface roughness of the cylinder and the rings, with cavitation in the oil film by requiring $P = \partial P/\partial x = 0$ at the cavitation boundaries, and accounts for the ring tilting in the grooves. Effects of non-Newtonian oils can also be studied. The procedure (Ting, 1980) is:

1. Obtain the P–V or P–θ diagram for the given operating conditions.
2. Use blowby theory (Chapter 8) to calculate interring pressures.

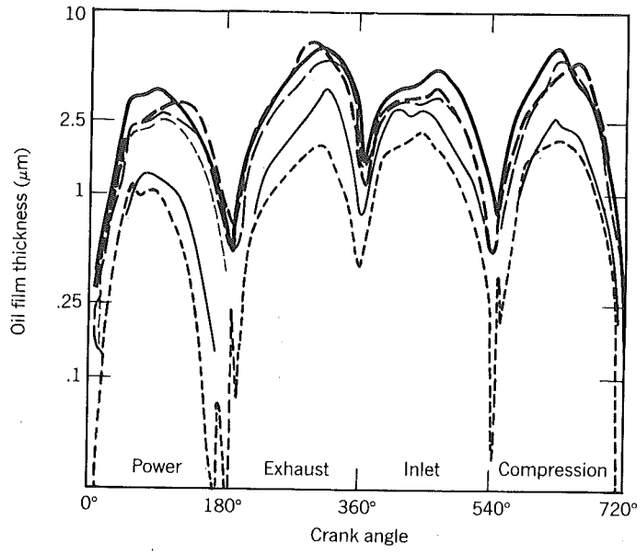

	bmep (bar)	Rs (rpm)
———	0	1500
— — —	2.76	1500
– – – –	1.50	1500
· · · · · ·	0	2200
— — — —	2.76	2200
— – —	9.38	2200

Figure 6-11 Effect of load and speed on the minimum oil film thickness. The calculations were done for a Perkins AT6-354 diesel engine on the major thrust side of the cylinder (Allen, Dudley, Middletown, and Panka 1976).

3. Solve for the oil film thickness $\delta(x, t)$ and pressure $P_o(x, t)$ for each ring.
4. Determine the frictional force of each ring via a coefficient of friction depending upon whether or not metal to metal contact is occurring or the friction is hydrodynamic (in which case Newton's law applies as discussed).
5. Sum up the fmep due to each ring.

McGeehan (1978) discusses the piston and ring design changes that occurred between 1950 and 1975. Piston skirt areas and weights have been significantly reduced. Fig. 6-12 illustrates typical changes. The modern piston design reduces the area of the oil film under shear and the inertia load contribution to the effective pressure. That inertia load (side thrust) has also been lowered with the introduction of offset wrist pins.

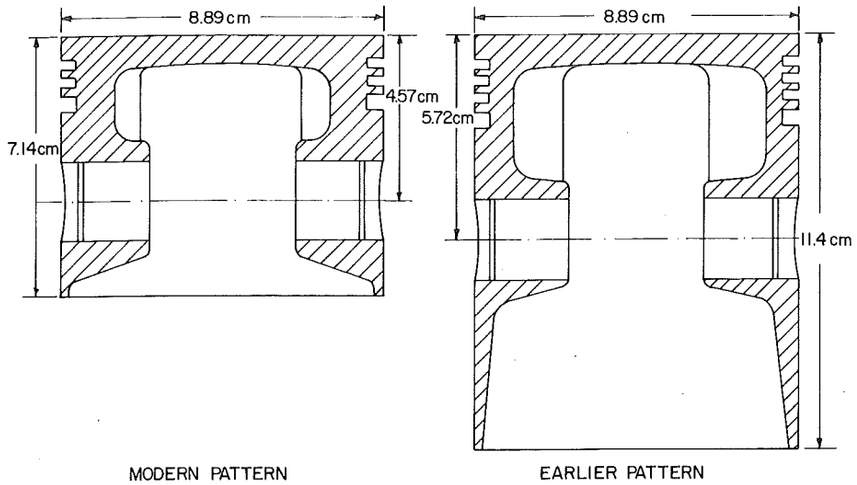

Figure 6-12 Typical changes to piston proportions over 10 years (1960 to 1970). There are now fewer and smaller rings, a smaller skirt, and less weight (McGeehan, 1978). Reprinted with permission © 1978. Society of Automotive Engineers, Inc.

An appreciation of the nature of the side thrust forces is important in understanding why piston designs have changed as they have. Fig. 6-13 illustrates a force balance applied to the piston. In Chapter 1, the instantaneous piston velocity (Homework Problem 1) was derived. The same analysis can yield the piston acceleration. The results in this case are

$$U(\theta) = \frac{\omega S}{2}\left(\sin\theta + \frac{\epsilon \sin 2\theta}{2(1-\epsilon^2 \sin^2\theta)^{1/2}}\right) \tag{6.27}$$

$$\frac{dU}{dt}(\theta) = \frac{\omega^2 S}{2}\left(\cos\theta + \frac{\epsilon(\cos 2\theta + \epsilon^2 \sin^4\theta)}{(1-\epsilon^2 \sin^2\theta)^{3/2}}\right) \tag{6.28}$$

With reference to Fig. 6-13, the reader need not at this point be concerned with the details of the force analysis but rather should recognize that piston acceleration enters Newton's first law ($F = ma$) in the x direction. Those forces are solved for simultaneously with the forces in the y direction. The designer concerned with ring friction is looking for the side thrust force F_t that will be transmitted through the rings that enter the force balance considered earlier. The thrust pressure is the thrust force divided by one half the total ring area. It is only one half the ring area because the load switches from side to side depending upon the piston direction.

Results of calculations for a particular engine are given in Fig. 6-14. The computation requires the P–V diagram, the masses of the piston and connecting rod, as well as the latter's moment of inertia, and the engine speed. The curve shows that side thrust force switches from side to side and that the left

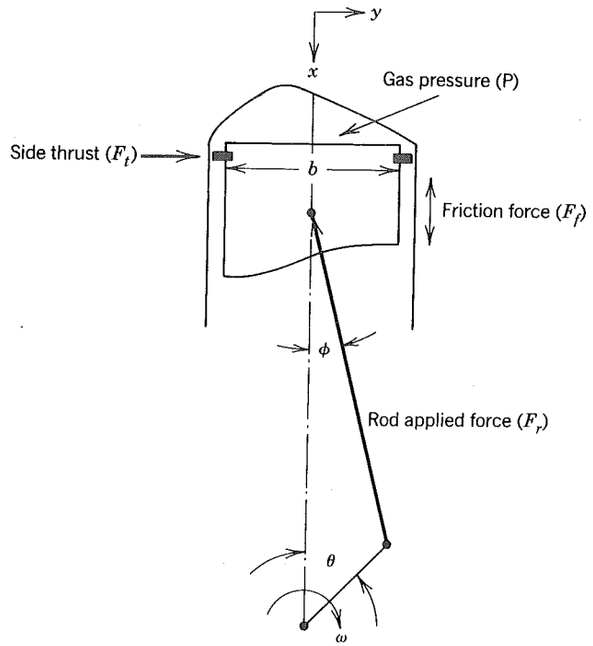

$$\sum F_x = m\frac{dU}{dt} = -F_r\cos\phi + P\frac{\pi}{4}b^2 \pm F_f \qquad \begin{matrix} + \text{ when } \theta \le 0 \\ - \qquad \theta > 0 \end{matrix}$$

$$\sum F_y = 0 = F_t - F_r \sin\phi$$

Therefore

$$F_t = \left(-m\frac{dU}{dt} + P\frac{\pi}{4}b^2 \pm F_f\right)\tan\phi$$

Figure 6-13 Piston force balance. The side thrust force switches sides as the piston passes through top and bottom center. Notice that near top dead center the friction force changes sign. This and the fact that cylinder pressures during expansion are greater than during compression mean that the side thrust on the left during expansion will be greater than on the right during compression. Engines show more upper cylinder wear on the major thrust side than on the minor thrust side as a result.

side of the clockwise rotating engine is subjected to larger forces than the right side. In this case the left side is referred to as the major thrust side whereas the right side is called the minor side. Clearly the friction and attendant wear is larger on the major thrust side.

Other changes have been made to reduce piston and ring friction. The number and width of piston rings has been reduced, see Fig. 6-12. Smoother

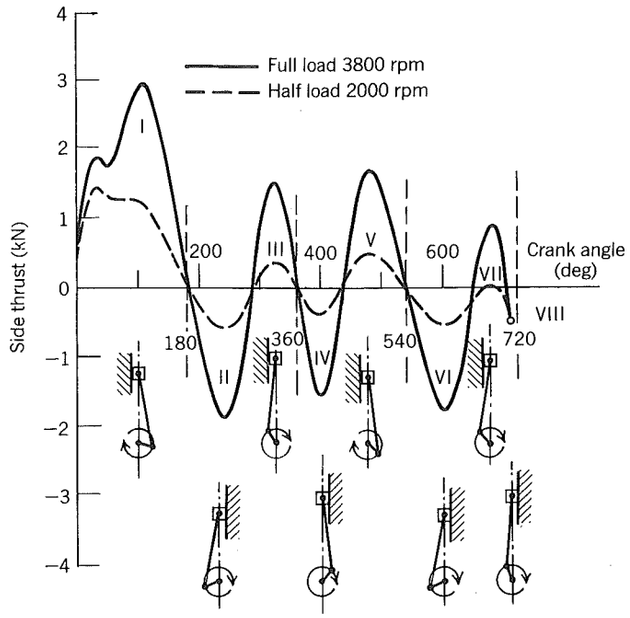

Figure 6-14 Piston side thrust load and the switch of ring-bore contact sides (Ting and Mayer, 1974). Reprinted with permission © 1974. ASME.

finishes have been incorporate on the cylinder wall to reduce regimes of metal to metal contact. Piston ring cross sections have changed from being more or less square to having a barrel face, see Fig. 6-15. Finally, the stroke to bore ratios have been reduced, resulting in a lower piston speed at the same rpm.

6.4 JOURNAL BEARINGS

There are journal bearings on the crank, both ends of the rod, and the camshaft. These can also be analyzed via the Reynold's approximation to the Navier–Stokes equations. In this case the bearings are treated as axisymmetric but two-dimensional to account for their finite length. The situation typically analyzed is shown in Fig. 6-16. In this case, the Reynold's equation that accounts for journal rotation and center precession is written as follows (Lloyd, Horsnell and McCallion 1966–67):

$$\frac{\partial}{\partial x}\left(\frac{\delta^3}{\mu}\frac{\partial P}{\partial x}\right)+\frac{\partial}{\partial z}\left(\frac{\delta^3}{\mu}\frac{\partial P}{\partial z}\right)=6\left[-e\sin\left(\frac{x}{R}\right)\left\{\omega_b-2\frac{d\phi}{dt}\right\}+2\frac{de}{dt}\cos\left(\frac{x}{R}\right)\right] \tag{6.29}$$

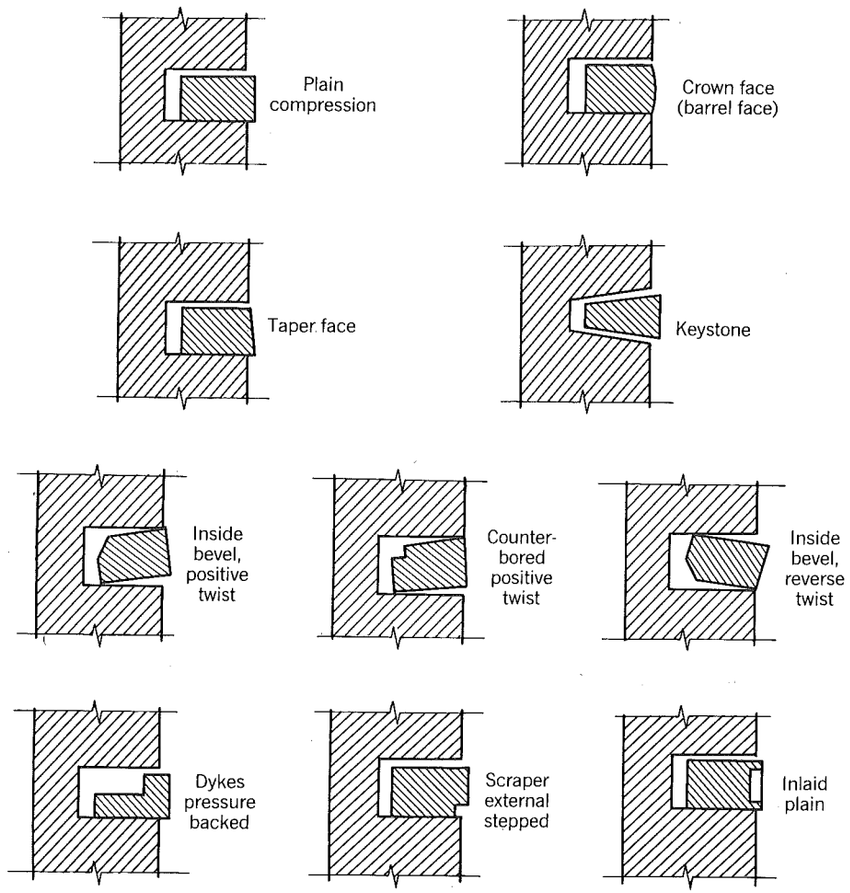

(a)

Figure 6-15 (*a*) Common types of piston rings: compression rings (Peterson and Winer, 1980). Reprinted with permission © 1980. ASME.

where

x = distance around the bearing
z = distance across bearing
δ = oil film thickness
R = bearing radius
ω_b = instantaneous angular velocity of journal relative to bearing
e = eccentricity
ϕ = angle between eccentricity vector and a fixed axis (see Fig. 6-16)

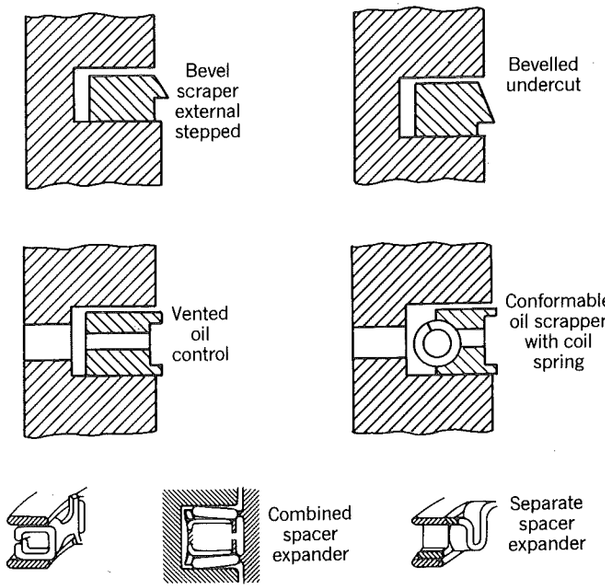

(b)

Figure 6-15 (*b*) Common types of piston rings: oil control rings (Peterson and Winer, 1980). Reprinted with permission © 1980. ASME.

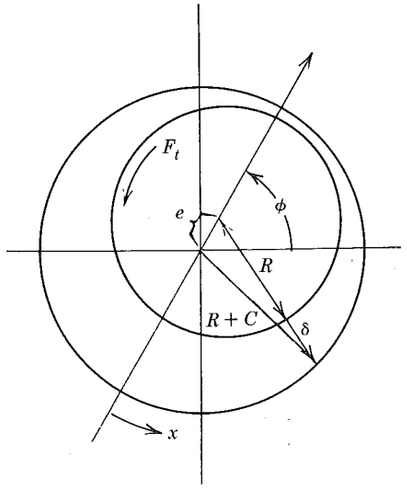

Figure 6-16 Two-dimensional journal bearing geometry (Lloyd, Horsnell, and McCallion, 1966–67). Reprinted with permission © 1967. Council of the Institution of Mechanical Engineers.

In general, ω_b scales with the engine frequency but is not identical to that frequency. For example, the cam rotates at one half the engine speed, the piston pin bearing on the rod oscillates back and forth without completing a revolution, and the big-end rod bearing oscillates in addition to journal rotation. Whatever the case, we can write

$$\omega_b = \omega f(\theta) \tag{6.30}$$

where $f(\theta)$ is a function of crank angle. In the case of the big-end bearing, for example

$$f(\theta) = 1 + \frac{\cos\theta}{\sqrt{\left(\frac{2l}{S}\right)^2 - \sin^2\theta}} \tag{6.31}$$

where, as in Chapter 1, l is the rod length between bearing centers and S is the stroke.

The instantaneous torque to spin any of the journal bearings is

$$\tau = \frac{F_t e}{2} + \frac{2\pi\mu\omega f(\theta) R^3 L}{(c^2 - e^2)^{1/2}} \tag{6.32}$$

where

F_t = tangential force on journal from the oil film

L = bearing length

c = radial clearance

The average torque for one engine cycle is then

$$\bar{\tau} = \frac{1}{4\pi}\int_0^{4\pi} \tau(\theta)\, d\theta \tag{6.33}$$

As in the piston rings analysis, let us normalize all lengths by the bore b, the viscosity by the oil viscosity μ_o in the pan, and, in this case, F_t by $2\mu_o \overline{U}_p b$. The engine frequency will be replaced by the mean piston speed, $\omega = \overline{U}_p/(4\pi S)$. Equations (6.33) and (6.32) then become

$$\bar{\tau} = \frac{1}{4\pi}\left\{\mu_o \overline{U}_p b^2 \int_0^{4\pi} \tilde{F}_t \tilde{e}\, d\theta + \frac{\mu_o \overline{U}_p b^2 \tilde{L}\tilde{\mu}}{2\tilde{S}} \int_0^{4\pi} \frac{f(\theta)\, d\theta}{\left[(\tilde{c})^2 - (\tilde{e})^2\right]^{1/2}}\right\} \tag{6.34}$$

Hence

$$\frac{\text{fmep}}{\rho_o \overline{U}_p^2} = \frac{\tilde{C}_2}{\pi^2 R_e}\left(\frac{b}{S}\right) \tag{6.35}$$

where the parameter $\tilde{C}_2$ is expected to be a weak function of operating conditions and is defined via

$$\tilde{C}_2 = \int_0^{4\pi} \tilde{F}_t \tilde{e}\, d\theta + \frac{L}{S}\tilde{\mu}\int_0^{4\pi} \frac{f(\theta)\, d\theta}{\left[(\tilde{c})^2 - (\tilde{e})^2\right]^{1/2}} \tag{6.36}$$

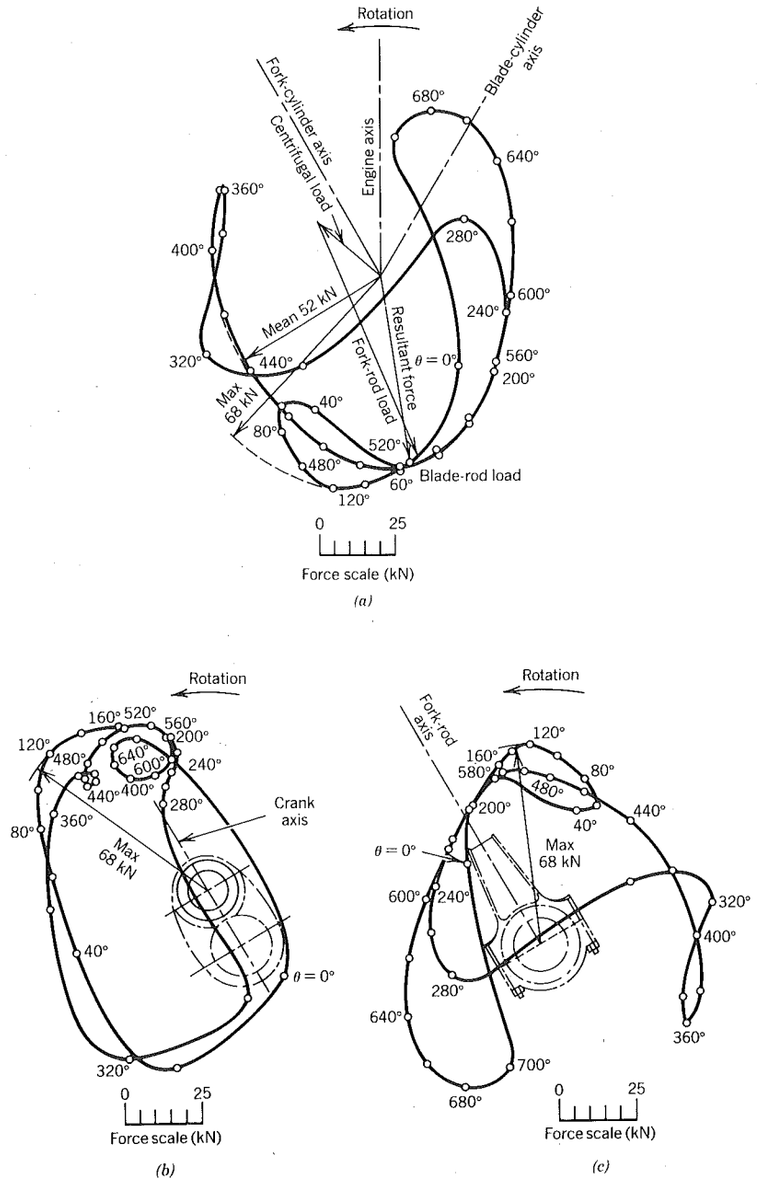

Figure 6-17 Bearing load diagrams. (*a*) Polar diagram showing the magnitude of the resultant force on the crankpin of the Allison V-1710 engine and its direction with respect to the engine axis. Engine speed = 3000 rpm, imep = 16.5 atm. (*b*) Polar diagram showing the magnitude of the resultant force on the crankpin of the Allison V-1710 engine and its direction with respect to the crank axis. Engine speed = 3000 rpm, imep 16.5 atm. (*c*) Polar diagram showing the magnitude of the resultant force on the crankpin bearing of the Allison V-1710 engine and its direction with respect to the fork-rod axis. Engine speed = 3000 rpm, imep = 16.5 atm. (Burwell, 1949).

The parameter $\tilde{C}_2$ is determined by solution of the Reynold's equation for $\tilde{c}$, $\tilde{e}$, and $\tilde{F}_i$. Some solutions are given by Campbell, Love, Martin and Rafique (1967, 1968). These require as an input the forces imposed on the bearing. In the case of the rod's big-end bearing, these are computed along the lines indicated earlier for the piston side thrust. Results for a particular engine are given in Fig. 6-17.

Bishop (1964) gives an empirical expression for the fmep due to all the journal bearings in an engine. Although he gives a detailed formula to account for the different bearing sizes, the similarity that exists among engines leads to the typical result that

$$\text{Journal bearings: } \frac{\text{fmep}}{\rho_o \bar{U}_p^2} = \frac{6.6 \times 10^4}{R_e} K \left(\frac{b}{S} \right) \tag{6.37}$$

where $K = 0.85$ for spark-ignition engines and $K = 1.8$ for diesel engines. The similarity between Eq. (6.35) and (6.37) is not fortuitious.

6.5 OTHER FRICTION

Four different ways in which poppet valves can be opened are shown in Fig. 6-18. The major losses in the valve train occur at the camlifter interface and in the rocker-arm pivot (Rosenberg, 1982). Since the overhead-cam, direct-acting system has only one sliding contact, the torque required to drive the valve train is lowest for this design. Notice that for each design, unlike for friction in the piston and ring pack or journal bearings, the torque decreases with increasing speed. Indeed, computations using the hydrodynamic theory of friction predict oil film thicknesses too small to avoid metal to metal contact (Lim, Evans, and Suidle (1983) and Dyson (1980)). For typical intake to exhaust valve diameter ratios (i.e., $d_i/d_o \approx 1.3$), one exhaust valve per intake valve, and N_i intake valves per cylinder, Bishop's (1964) results for a pushrod design are correlated by

$$\text{Valve train: } \frac{\text{fmep}}{\rho_o \bar{U}_p^2} = \left(\frac{1.5 \times 10^9}{R_e^2} - \frac{1.4 \times 10^4}{R_e} \right) \frac{b}{S} \left(\frac{d_i}{b} \right)^{1.8} N_i \tag{6.38}$$

Valve trains must be able to carry high loads over the entire speed range. At low speeds the spring forces dominates, whereas at high speeds the inertia forces dominate. Under these circumstances, to employ roller bearings is an effective method to reduce friction, as Fig. 6-19 illustrates. In this case there are roller bearings at the cam lifter interface, the rocker pivot, and the interface between the rocker nose and the valve stem. The disadvantages of such a design include the bearings' susceptibility to contact fatigue and the cost of the design (Rosenberg, 1982).

The remaining friction in an engine, after accounting for the piston, rings, journal bearings, and valve train, is primarily caused by the pumps

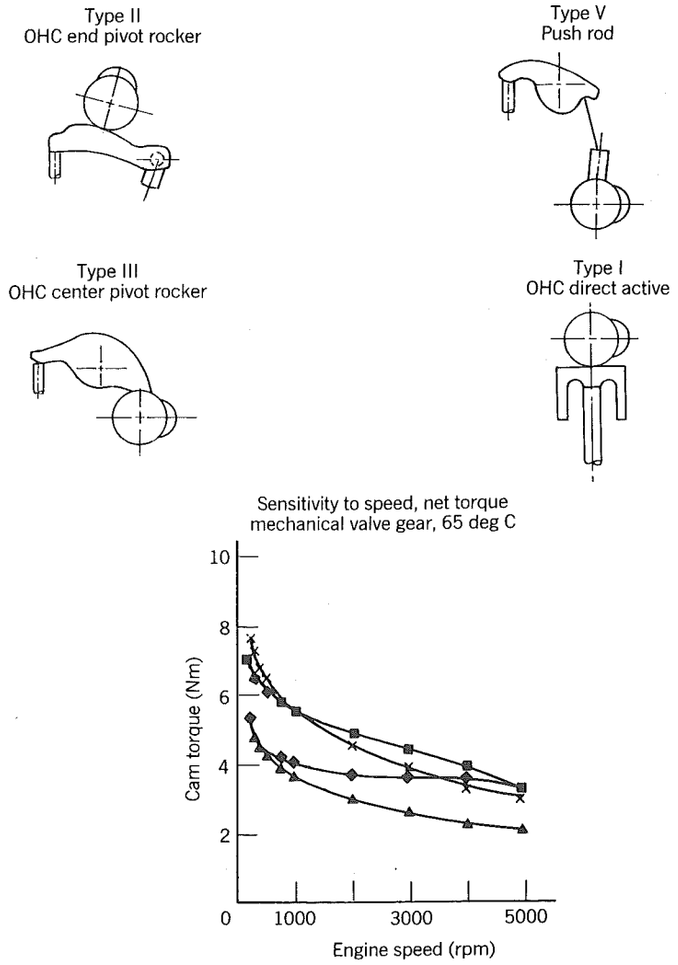

Figure 6-18 Energy losses in various valve train designs. Pushrod and direct acting (OHC) have lowest friction at low speeds. At high speeds direct acting (OHC) has lowest friction. This may be related to elimination of losses in rocker arm pivots (Rosenberg, 1982). Reprinted with permission © 1982. Society of Automotive Engineers, Inc.

employed to circulate the oil, water, and fuel. Bishop (1964) lumped all this remaining fiction into one category and correlated the results. In dimensionless form one obtains:

$$\text{Pumps: } \frac{\text{fmep}}{\rho_o \bar{U}_p^2} = \frac{R_e^{0.5}}{670} \tag{6.39}$$

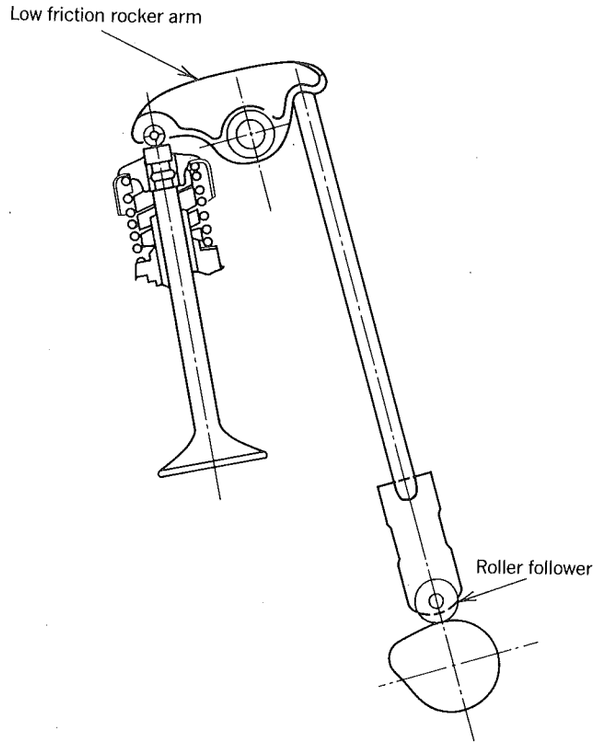

Figure 6-19 Rolling element bearing application. Because of high loads at low speed, rolling element bearings are possible alternatives in the engine valve train. They have been used in racing engines (Rosenberg, 1982). Reprinted with permission © 1982. Society of Automotive Engineers, Inc.

6.6 THE NATURE OF FRICTION

A rather neat piece of instrumentation, easily duplicated for use in an undergraduate engine laboratory, is shown in Fig. 6-20. This was used by McKee and McKee (1929) to develop some friction data for automotive journal bearings of various width L to diameter D ratios and for a number of clearances.

The big ends of connecting rods are used as bearing holders. A nut allows compression of a calibrated spring to load the bearing with a known force W per unit projected bearing area DL. The pressure of the load is $P = W/DL$. Low pressure oil of viscosity μ is fed into the bearing through a hole on the unloaded side. The entire unit is placed in a lathe to control the rotational speed of the shaft R_s. The friction torque is measured by balancing the position of the sliding counterweight.

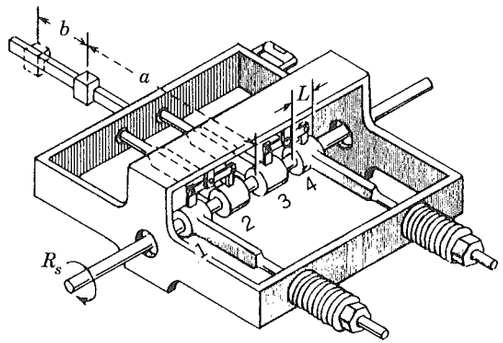

Figure 6-20 Bearing testing machine of McKee and McKee (1929). From Norton (1942), Lubrication, McGraw-Hill.

Results obtained from such apparatus are plotted in a form that has become known as a Stribeck diagram, see Fig. 6-21. The coefficient of friction is generally the ratio of the force to be exerted to overcome friction to the force imposed by the normal load. For a journal bearing in the rig of Fig. 6-20, the coefficient of friction specifically is the tangential force of the friction torque τ divided by the load W. Hence

$$f = \frac{2\tau}{D^2 LP} \tag{6.40}$$

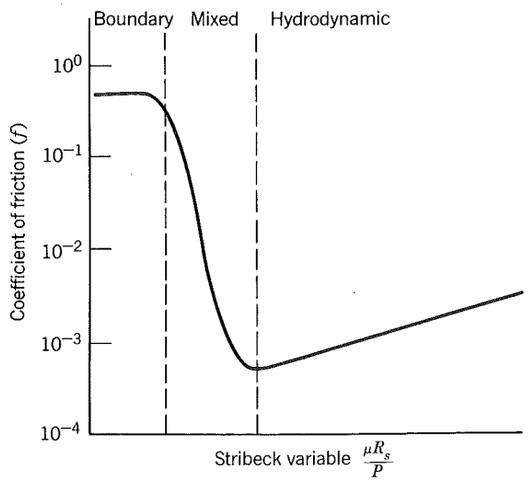

Figure 6-21 Stribeck diagram showing regimes of friction and orders of magnitude of the coefficient of friction.

In the hydrodynamic regime, the friction torque is caused by the force required to overcome shear in the oil film, and solution of the Reynold's equations will accurately predict the friction coefficient, as discussed earlier in connection with engine journal bearings. In the rig mounted bearing the situation is simpler since the load is independent of time.

For rig mounted bearings with L/D greater than 1, a rather simple expression can be derived which is called Petroff's equation. It is useful since the friction of real bearings approaches the Petroff value at high values of the Stribeck variable $\mu R_s/P$. If the bearing radial clearance c is small compared to the bearing diameter D, as is the usual case, the flow is basically a Couette flow, and the velocity gradient in the clearance space is given by

$$\left(\frac{\partial u}{\partial r}\right)_{r=D/2} = \frac{\pi D R_s}{c} \tag{6.41}$$

Thus the friction coefficient is

$$f = \frac{\mu\left(\frac{\partial u}{\partial r}\right)\pi DL}{PDL} = \pi^2 \frac{\mu R_s}{P}\frac{D}{c} \tag{6.42}$$

Notice that in the hydrodynamic regime, the friction coefficient increases linearly with the Stribeck variable and the slope is dependent upon the bearing diameter to clearance ratio.

As the load is increased or the speed decreased, the oil film thins out to the point where it is comparable in size to the surface irregularities of the bearing and shaft. This is the regime of mixed lubrication. In boundary lubrication, the sliding surfaces are separated by oil films here and there where the thickness is just a few molecular diameters of the lubricant.

In boundary lubrication the coefficient of friction depends on properties of the lubricant and of the sliding surfaces. It is important to know how the lubricant can be adsorbed by the surfaces, whether or not the surfaces and the lubricant react to form a metallic soap (as fatty acids do at high temperatures, thus being good lubricants for the boundary regime), how rough the surfaces are, and whether or not the surface molecules themselves are prone to adhering to one another.

In the boundary regime the coefficient of friction is independent of viscosity, speed, and load. However it still depends on oil properties due to the presence of an adsorbed oil film. When two surfaces rub, as in Fig. 6-22, the real area of contact depends primarily on the applied load, the yield strength σ_m, and asperities of the softer material; just enough microscopic areas contact so that the yield pressure of the softer material balances the applied load, Lee and Booser (1967). As the load increases, the real area of contact increases proportionately.

The force required to cause tangential motion is approximately the real area of contact multiplied by the shear strength of the adsorbed oil layer, σ_o. It

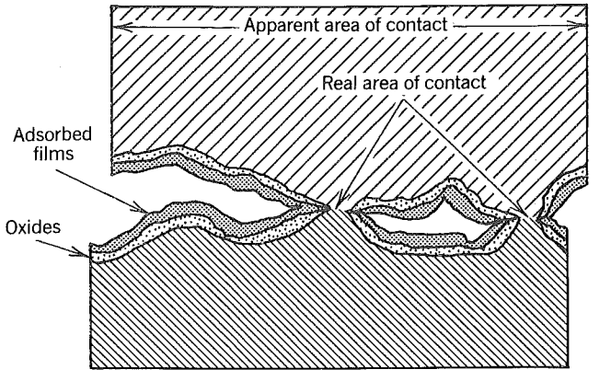

Figure 6-22 In boundary lubrication, metal to metal contact occurs at high points of the surface topography. The asperities, as they are called, yield until the real area of contact balances the applied load (Rosenberg, 1982). Reprinted with permission © 1982. Society of Automotive Engineers, Inc.

follows that the coefficient of friction is

$$f = \frac{\sigma_o}{\sigma_m} \tag{6.43}$$

Minimum friction is obtained by use of a low shear strength oil and hard surfaces. Additives are added to lubricating oils which preferentially adsorb to bearing surfaces and lower the coefficient of friction; these include organic fatty acids and amines, lard oil, high molecular weight organic phosphorus, and phosphoric acid esters, Shilling and Bright (1977).

The properties of lubricating oils are discussed in Chapter 10. The reader interested in boundary lubrication is referred to the two volumes by Bowden and Tabor (1958 and 1964). There too is a discussion of rolling friction. An understanding of this may be important to designers wishing to employ roller or ball bearings in an engine, particularly as Rosenberg (1982) states that one problem yet unsolved with the roller bearings used in valve trains is that they are susceptible to contact fatigue.

6.7 REFERENCES

Allen, D. G., B. R. Dudley, J. Middletown, and D. A. Panka, (1976), "Prediction of Piston Ring-Cylinder Bore Oil Film Thickness in Two Particular Engines and Correlation with Experimental Evidences," *Piston Ring Scuffing*, Mechanical Engineering Pub. Ltd., London, p. 107.

Amstrong, W. B. and B. A. Buuck (1981), "Effect of Various Valve Gear Designs on Valve Gear Energy Consumption," SAE paper 810787.

Bishop, J. N. (1964), "Effects of Design Variables on Friction and Economy," SAE paper 812A.

Bowden, F. P. and D. Tabor, (1958), *The Friction and Lubrication of Solids*, Oxford Univ. Press, London/New York.

Bowden, F. P. and D. Tabor, (1964), *The Friction and Lubrication of Solids Part II*, Oxford Univ. Press, London/New York.

Brown, W. L. (1973), "The Caterpillar imep Meter and Engine Friction," SAE paper 730150.

Burwell (1949), "The Calculated Performance of Dynamically Loaded Sleeve Bearings," *J. Appl. Mech.*, **16** (4), p. 358.

Campbell, J., P. P. Love, F. A. Martin and S. O. Rafique (1967–1968), "Bearings for Reciprocating Machinery: A Review of the Present State of Theoretical, Experimental and Service Knowledge," Proc. IME, **182**, Part 3A.

Dyson, A. (1980), "Kinematics and Wear Patterns of Cam and Finger Follower Automotive Valve Gear," *Tribology*, June, pp. 121–132.

Gish, R. E., S. D. McCullough, J. B. Retzloff, and H. T. Mueller (1957), "Determination of True Engine Friction," SAE paper 117.

Leary, W. A. and J. U. Jovellanos, (1944), "A Study of Piston and Piston-Ring Friction," NACA ARR-4J06.

Lee, R. E. and E. R. Booser, (1967), "Lubrication and Lubricants," *Encyclopedia of Chemical Technology*, Vol. 12, Wiley, New York.

Lim, C. E., H. P. Evans, and R. W. Suidle, (1983), "Kinematics and Lubrication Conditions at Car Contact in a Centrally Pivoted Cam-Finger Follower," SAE paper 380309.

Livengood, J. C. and C. Wallour (1947), "A Study of Piston-Ring Friction," NACA TN 1249.

Lloyd, T., R. Horsnell, and H. McCallion, (1966–1967), "An Investigation into the Performance of Dynamically Loaded Journal Bearings: Theory," *Proc. IME.* **181**, Part 3B, pp. 1–9.

McGeehan, J. A. (1978), "A Literature Review of the Effects of Piston and Ring Friction and Lubricating Oil Viscosity on Fuel Economy," SAE paper 780673.

McKee, S. A. and T. R. McKee (1929), "Friction of Journal Bearings as Influenced by Clearance and Length," *Trans. ASME*, **51**, pp. 161–171.

Norton, A. E., *Lubrication*, McGraw-Hill, New York, 1942.

Rhode, S. M. and H. S. Cheng, Eds. (1980), *Surface Roughness Effects in Hydrodynamic and Mixed Lubrication*, ASME, New York.

Rhode, S. M., D. F. Wilcock, and H. S. Cheng, Eds. (1979), *Energy Conservation through Fluid Film Lubrication Technology: Frontiers in Research and Design*, ASME, New York.

Rhodes, M. L. P. (1970), "Piston Research and Development Techniques," see McGeehan (1978).

Rosenberg, R. C. (1982), "General Friction Considerations for Engine Design," SAE paper 821576.

Schilling, G. J. and G. S. Bright, (1977), "Fuel and Lubricant Additives—II," *Lubrication*, Texaco, Inc., New York.

Taylor, C. F., (1977), *The Internal Combustion Engine—Theory and Practice*, MIT Press, Cambridge, Massachusetts.

Ting, L. L., (1980), "Lubricated Piston Rings and Cylinder Bore Wear," in M. B. Peterson and W. O. Winer, Eds., *Wear Control Handbook*, ASME, New York.

Ting, L. L. and J. E. Mayer, Jr. (1974), "Piston Ring Lubrication and Cylinder Bore Analysis, Part I—Theory and Part II—Theory Verification," *J. Lubr. Tech.*, p. 96.

6.8 HOMEWORK

1. Oil companies are advertising "slippery oils" that if used in your automobile will slightly reduce the fuel consumption. The implication is that when the slippery oil is compared to a conventional oil of equal viscosity, the slippery oil will have a reduced friction coefficient. How is this possible?
2. Racing mechanics often will modify an engine increasing the bearing clearances above the manufacturers specification. This can increase the power of an engine. Discuss why and the trade offs the manufacturer must consider in choosing a clearance.
3. How is the fmep computed from data in Fig. 6-7?
4. In his paper on the oil film, Rhodes (1970) states that the film thickness tends to be greater at lower powers. Relate this observation to curves (c) in Fig. 6-8.
5. How might piston and ring friction depend on the mass of the piston?
6. Explain the zero crossings in Fig. 6-14. Why is there not a zero crossing in the range $0 < \theta < 180$?
7. Use Eqs. (6.14), (6.26), (6.37), (6.38), and (6.39) to construct a graph akin to Fig. 6-4 using the following notation for the various curves:

A	Complete engine
B	setup A minus pumps
C	setup B minus valve train
D	journal bearings only
E	motoring mean effective pressure

Your graph should cover the following range of piston speed $1 < \overline{U}_p < 15$ m/s and use bars as the unit on mep. Data you may take as given are:

Oil	*Spark Ignition Engine*	
$\rho_o = 0.88$ g/cm^3	$r = 10$	N_i = one valve per cylinder
$\nu_o = 15.5 \times 10^{-6}$ m^2/s	$b = 8.26$ cm	$d_i = 4.00$ cm
	$S = 8.00$ cm	

8. Multiply both sides of Eq. (6.14) by $\rho_o \overline{U}_p^2$. Show that the resultant equation is linear in piston speed and is consistent with the trends shown in Fig. 6-1. Now explain why the largest bore engine shows the lowest fmep in Fig. 6-1.

Seven

AIR, FUEL, AND EXHAUST FLOWS

So far we have restricted our attention to the ideal four-stroke model which predicts the volumetric efficiency of an engine and the residual gas fraction. The ideal model is qualitatively useful but quantitatively lacking since no account is made of such important factors as valve timing, lift and size or intake and exhaust manifold geometry. No ideal model was presented for two-stroke engines; rather the delivery ratio and the residual fraction had to be specified to do cycle computations. One of the purposes of this chapter is to show how to account for some of these variables.

Another purpose of this chapter is to provide an introduction to the various means employed to meter the fuel delivered in proportion to the air flow. Thus the basic principles of carburetors and fuel-injection systems are laid out.

7.1 THERMODYNAMIC ANALYSIS—FOUR-STROKE ENGINES

The first law of thermodynamics applied to an open system doing only boundary work says

$$\Delta E = -\int P\,dV + \int (\dot{m}_{\text{in}} h_{\text{in}} - \dot{m}_{\text{out}} h_{\text{out}})\,dt + \int \dot{Q}\,dt \tag{7.1}$$

For an ideal gas with constant specific heats it can be shown that

$$\Delta E = c_v \Delta(mT) = \frac{1}{\gamma - 1}\Delta(PV) \tag{7.2}$$

Let us assume that during overlap, exhaust gas flows into the intake manifold and later an equal amount flows out. The flow into the cylinder is then exhaust gas until the total residuals pushed into the intake manifold return. It follows that for the intake process

$$\int_{io}^{ic} \left[(\dot{m}c_pT)_{\text{in}} - (\dot{m}c_pT)_{\text{out}}\right] dt = \int_{io}^{ec} [\ ] + \int_{ec}^{is} [\ ] + \int_{is}^{ic} [\ ] \tag{7.3}$$

where the integrand is the same in all integrals and is abbreviated on the

right-hand side by brackets to save space. The time notation is:

io = intake valve opens

ic = intake valve closes

ec = exhaust valve closes

is = intake of fresh mixture starts

The first integral on the right-hand side is assumed to be zero arguing that during overlap the enthalpy flow into the cylinder from the exhaust port is balanced by the enthalpy flow from the cylinder to the intake manifold. (We are neglecting the small decrease in temperature that occurs between the exhaust coming in and going out because of heat loss while in the intake port or pipe.)

The second integral is equal to the amount of enthalpy that flowed into the cylinder from the exhaust port during the overlap period; since we assume this gas returns prior to the start of induction. Hence

$$P_{ic}V_{ic} - P_{io}V_{io} = (\gamma - 1)\left[- \int_{io}^{ic} P\,dV + \int_{io}^{ec} (\dot{m} c_p T)_{ov}\,dt + c_p T_i \int_{is}^{ic} \dot{m}_{\text{in}}\,dt + \int_{io}^{ic} \dot{Q}\,dt \right] \tag{7.4}$$

Let us introduce the mass inducted

$$m_i = \int_{is}^{ic} \dot{m}_{\text{in}}\,dt \tag{7.5}$$

and the mass of exhaust that flows into the cylinder from the exhaust system during overlap

$$m_{\text{ov}} = \int_{io}^{ec} \dot{m}_{\text{ov}}\,dt \tag{7.6}$$

We then have for the volumetric efficiency

$$e_v = \frac{1}{\gamma}\frac{P_{ic}V_{ic} - P_{io}V_{io}}{P_i V_d} + \frac{\gamma - 1}{\gamma}\int_{io}^{ic}\frac{P\,dV}{P_i V_d} - \frac{\gamma - 1}{\gamma}\frac{Q}{P_i V_d} - \frac{T_{ov}}{T_i}\frac{m_{ov}}{P_i V_d} \tag{7.7}$$

Notice that heat transfer to the gases and gas exchange during overlap both decrease the volumetric efficiency.

Now let us consider the limiting case in which the engine speed is small, $R_s \to 0$. In this case there should be no pressure drop across the valves at closure, therefore

$$P_{ic} = P_i,\ P_{io} = P_e \qquad (R_s \to 0) \tag{7.8}$$

Equation (7.7) then becomes

$$e_v = \frac{V_{ic} - V_{io}}{V_d} - \frac{1}{\gamma}\left(\frac{P_e}{P_i - 1}\right)\frac{V_{io}}{V_d} - \frac{\gamma - 1}{\gamma}\frac{Q}{P_i V_d} - \frac{T_{ov}}{T_i}\frac{m_{ov}}{\rho_i V_d} \tag{7.9}$$

Recall that for engines with a short stroke to rod ratio ($\epsilon \to 0$), the cylinder

volume is given by

$$\frac{V}{V_o} = 1 + \frac{r - 1}{2}(1 - \cos\theta) \qquad (\epsilon \to 0) \tag{7.10}$$

where θ is the crank angle measured from top dead center. Finally, we can write

$$e_v = \frac{\cos\theta_{io} - \cos\theta_{ic}}{2} - \frac{(P_e/P_i - 1)}{\gamma(r - 1)}\left[1 + \frac{r - 1}{2}(1 - \cos\theta_{io})\right] - \frac{\gamma - 1}{\gamma}\frac{Q}{P_i V_d} - \frac{T_{ov}}{T_i}\frac{m_{ov}}{\rho_i V_d} \tag{7.11}$$

Data are available for three geometrically similar engines in which the valve overlap is small and the cylinders are not much warmer than the inlet air; thus the overlap and heat loss terms are negligible in this case. Figure 7-1 presents the volumetric efficiency of those engines as a function of piston speed. Using the specified valve timings, compression ratio, exhaust to intake pressure ratio, and a specific heat ratio of $\gamma = 1.4$, Eq. (7.11) predicts that $e_v \to 0.78$ as R_s or $\overline{U}_p \to 0$. The prediction is seen to be quite good and similar agreement would be realized for different pressure ratios.

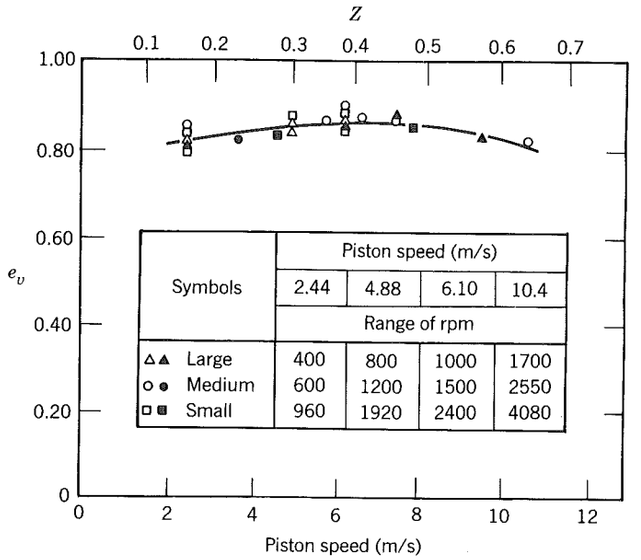

Figure 7-1 Volumetric efficiency versus mean piston speed of the MIT geometrically similar engines under similar operating conditions: $r = 5.74$, $\phi = 1.10$, $P_i = 0.95$ bar, $P_e = 1.08$ bar, $T_i = 339$ K, $T_c = 356$ K, optimum spark advance. From *The Internal Combustion Engine in Theory and Practice*, Vol. 1, by C. Fayette Taylor (1977), with permission of MIT Press.

Our analysis shows that opening and closing valves at angles other than top and bottom center hurts the volumetric efficiency as $R_s \to 0$. Why then are valves opened earlier and closed later than the ideal case? The answer lies in the fact that the analysis is only valid in the limit of $R_s \to 0$.

For a finite R_s, there will be a pressure drop across the valves, the most important of which is at the intake valve at closing. In the limiting case, air is pushed out of the cylinder as the piston moves up during the time from bottom dead center to inlet valve closure. At a finite engine speed, the cylinder pressure at bottom center will be less than the inlet pressure because of the finite pressure drop across the valve as the charge was entering. Hence as the piston begins the compression stroke, mixture can continue to flow into the cylinder until the pressure rises because of the filling and the upward moving piston. The flow will reverse itself when the two pressures are equal and then flow back into the intake system until valve closure. The volumetric efficiency will then increase with speed until a point is reached where the flow reversal starts at intake valve closure. For speeds beyond that point, volumetric efficiency will drop because the valve will close during a time in which mixture is still flowing in the engine. The trend of volumetric efficiency with speed discussed here is shown very clearly in Fig. 7-1.

Now consider the exhaust process. The energy equation can be written as

$$c_v m\dot{T} + c_v \dot{m} T = -P\dot{V} + \dot{m} c_p T - \dot{Q}_l \tag{7.12}$$

Combined with the equation of state and integrated, we have

$$f = \frac{m_{io}}{m_{eo}} = \left(\frac{P_i}{P_{eo}}\right)^{1/\gamma} \frac{V_{io}}{V_{eo}} \exp\left(\int_{eo}^{io} \frac{\dot{Q}_l}{PV}\, dt\right) \tag{7.13}$$

Integration is carried only to the time when the intake valve opens because during overlap it is assumed that the gases are pushed into the intake manifold only to return later. Notice that heat loss increases the residual fraction and is important here because the exhaust gases are considerably hotter than the

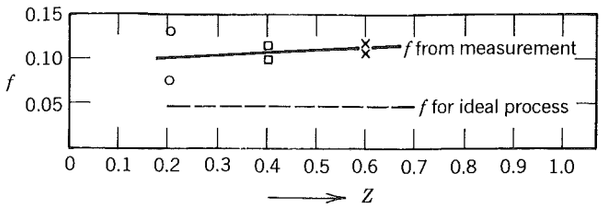

Figure 7-2 Comparison of residual gas fraction for fuel–air cycles with the ideal four-stroke inlet process with measured values. The parameter Z is the mach index based on piston speed, see Eq. (7.21). Livengood, Taylor and Wu, 1958. Reprinted with permission © 1958. Society of Automotive Engineers, Inc.

cylinder walls. This is the main reason for the discrepancy between fuel–air-cycle calculations with ideal intake and exhaust and experiment noted in Fig. 7-2.

7.2 VALVE FLOW

In accounting for the pressure drop across valves considerable success has been realized by modeling flow through valves as one-dimensional and quasi-steady. The symbols we will employ to present the analysis are shown in Fig. 7-3. Recall that in gas dynamics an area A^*, the minimum area normal to the flow, is of interest. In the situation shown in Fig. 7-3 two possibilities are evident; either $A^* = A_1$ or $A^* = A_2$. A graph of A^* versus valve lift is shown in Fig. 7-4. It should be clear that there is little reason to open a valve much beyond $l/d \approx \frac{1}{4}$ since the flow area at such lifts would be limited by the port size. Also shown is a curve of the flow area typically observed from steady flow bench measurements, to be described shortly. The mass flow rate through the valve is given by

$$\dot{m} = \rho_o c_o A^* \sqrt{\frac{2}{\gamma - 1}\left[P_*^{2/\gamma} - P_*^{(\gamma+1)/\gamma}\right]} \tag{7.14}$$

Where

ρ_o = stagnation density

$c_o = \sqrt{\gamma R T_o}$ is the stagnation sound speed

P_* = ratio of pressure at A^* to stagnation pressure

Equation (7.14) assumes isentropic flow from the upstream reservoir to the throat of area A^*. For flow out of the cylinder, the upstream conditions refer

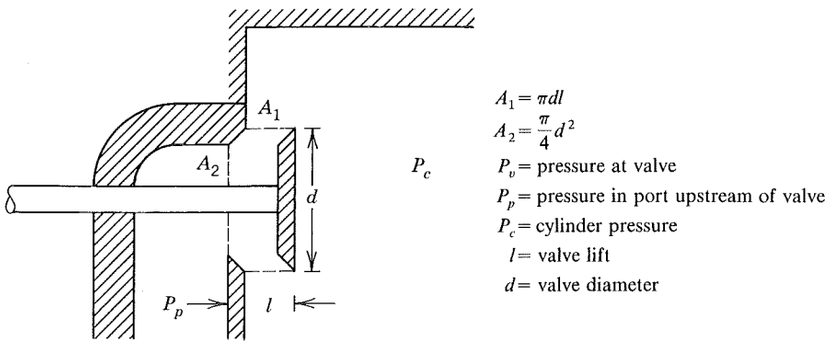

Figure 7-3 Valve flow—symbol definitions. For flow into the cylinder the pressure ratio pulling the flow is $P_* = P_v/P_p$. For flow from the cylinder the pressure ratio $P_* = P_v/P_c$.

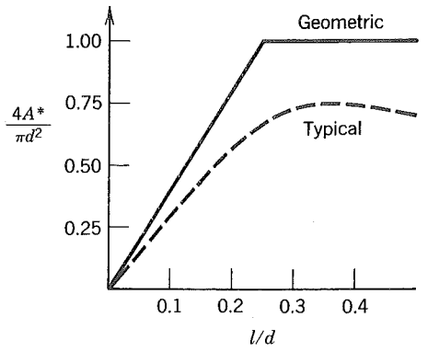

Figure 7-4 Valve flow area versus lift. The actual curve is reduced because of vena-contra, boundary layer effects. The ratio of the actual area to the geometrical or theoretical area is commonly called the discharge coefficient. The discharge coefficient depends on details of the port and valve design and may vary anywhere from 0.4 in the poorest designs to 0.8 in the best designs. For a number of practical design guidelines the book by Annand and Roe (1974) appears to be quite useful.

to gases in the cylinder. For flow into the cylinder, the upstream conditions refer to conditions in the port.

For nonchoked flow into the cylinder, it may generally be assumed that the throat pressure is equal to the cylinder pressure. Since kinetic energy in the cylinder is negligible, one need not distinguish between static and stagnation cylinder pressure. However, for flow from the cylinder in nonchoked situations, one equates the throat pressure to the port static pressure and this may differ significantly from the port stagnation pressure.

Choked flow occurs when the upstream pressure to downstream pressure exceeds a critical value. The criterion is if

$$\frac{P_{\text{up}}}{P_{\text{down}}} > \left(\frac{\gamma+1}{2}\right)^{\gamma/(\gamma-1)}$$

then

$$P_* = \left(\frac{2}{\gamma+1}\right)^{\gamma/(\gamma-1)} \tag{7.15}$$

Note that for choked flow, the throat pressure is independent of the downstream pressure.

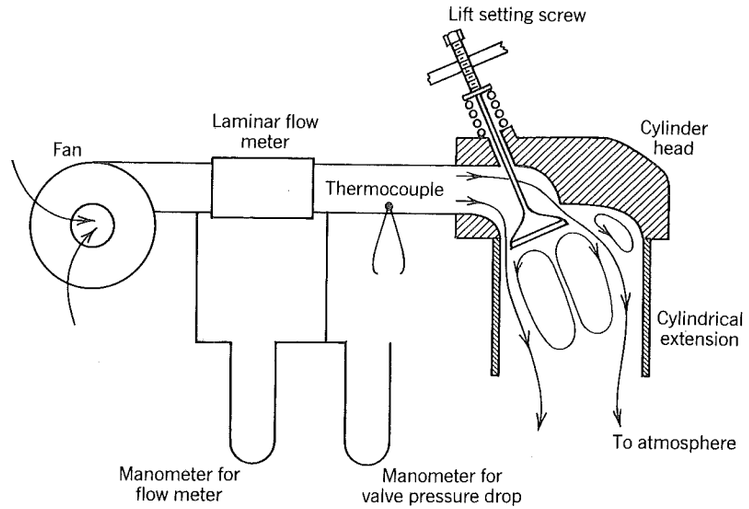

Figure 7-5 Essential features of a steady flow bench to measure flow areas and discharge coefficients of a valve.

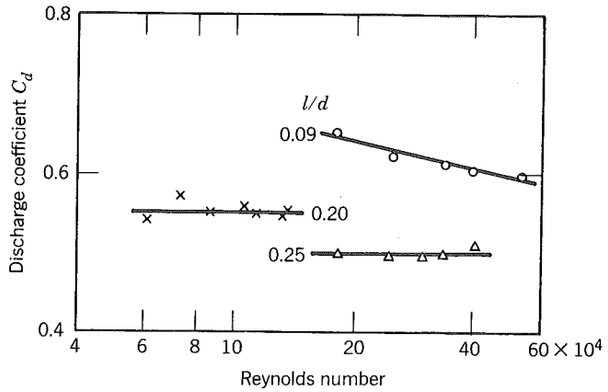

Figure 7-6 The effect of Reynolds number and valve lift on the discharge coefficient of a sharp cornered inlet valve © Annand and Roe, (1974), *Gas Flow in the Internal Combustion Engine*, G. T. Foulis & Co. Ltd, Sparkford, Somerset, England. The Reynolds number is defined in this case as $R_e = \dot{m}D/\mu A^*$.

A valve and its associated port are said to be efficient if there is minimal discrepancy between the effective or actual flow area and the geometrical flow area. This efficiency is quantitated by means of a discharge or flow coefficient defined as the ratio of the actual flow area to the geometrical flow area. The designer of valves and ports strives for as large a discharge coefficient as can be practically obtained.

Discharge coefficients are measured using flow benches like that illustrated in Fig. 7-5. The mass flow rate and pressure drop across the valve are measured for a number of different valve lifts. Equation (7.14) is then solved for flow area A^* and the results plotted as either A^* or as the discharge coefficient.

Some experimental results obtained in this manner are given in Fig. 7-6. They illustrate two general features of flow through valves; the discharge coefficient (1) decreases with increasing lift and (2) is dependent upon the Reynolds number of the flow only at small lifts.

The dependence on Reynolds number can be understood in terms of the flow patterns shown in Fig. 7-7. At high lifts, the fluid inertia prevents the flow from turning the corners and thus breaks away forming a free jet. The flow area of the jet is more or less independent of viscosity, thus the discharge coefficient is independent of Reynold's number.

The jet flow streaming from the valve entrains fluid from the surroundings and establishes zones of recirculation as depicted in Fig. 7-5. The pressure in these zones drops and the jet expands in response. At some intermediate lift the jet will reattach itself to the valve seat. At lower lifts the points of reattachment are closer to the corners around which the flow tried to turn. The more the jet fills the gap, the greater is the discharge coefficient.

We conclude by noting that if the jet is attached, then the discharge coefficient decreases slightly with increasing Reynold's number.

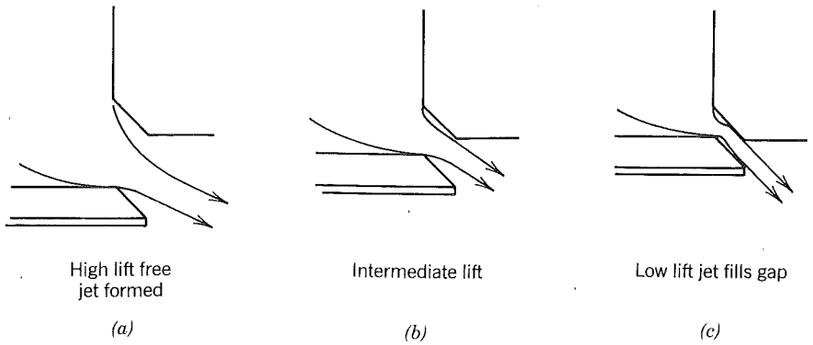

Figure 7-7 Flow patterns through a sharp-cornered inlet valve © Annand and Roe, (1974), *Gas Flow in the Internal Combustion Engine*, G. T. Foulis & Co. Ltd, Sparkford, Somerset, England.

7.3 SHORT PIPES

An arrangement found convenient for laboratory test engines is shown in Fig. 7-8. The intake and exhaust pipes are short and the plenums are large (on the order of 100 times the engine displacement). The pressure in the intake and exhaust ports may be assumed to be equal to the pressure in the intake and exhaust plenums, respectively. The mass inducted is

$$m_i = \frac{1}{\omega}\int_{\theta_{io}}^{\theta_{ic}} A^* \rho c \sqrt{\frac{2}{\gamma - 1}\left[P_*^{2/\gamma} - P_*^{(\gamma+1)/\gamma}\right]}\, d\theta \tag{7.16}$$

where θ_{io} is the crank angle at which the intake valve opens and θ_{ic} is the angle at which it closes. The terms A^*, ρ, c, P_*, and γ depend on whether flow is into the cylinder or out of the cylinder. Following the lead of Taylor, let us normalize Eq. (7.16) by the average flow area

$$\bar{A}_i \equiv \frac{1}{\theta_{ic} - \theta_{io}}\int_{\theta_{io}}^{\theta_{ic}} A^*\, d\theta \tag{7.17}$$

and the intake plenum density and sound speed. We then have for the volumetric efficiency

$$e_v = \frac{m_i}{\rho_i V_d} = \frac{\bar{A}_i c_i}{\omega V_d}\int_{\theta_{io}}^{\theta_{ic}} \frac{A^*}{\bar{A}_i}\frac{\rho}{\rho_i}\frac{c}{c_i}\sqrt{\frac{2}{\gamma - 1}\left(P_*^{2/\gamma} - P_*^{(\gamma+1)/\gamma}\right)}\, d\theta \tag{7.18}$$

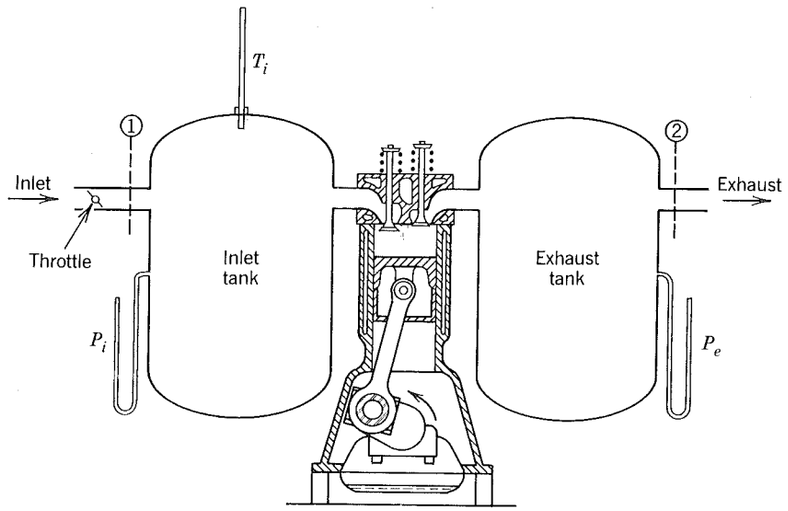

Figure 7-8 Single-cylinder engine equipped with large surge tanks and short inlet and exhaust pipes to ensure time independent port pressures. From *The Internal Combustion Engine in Theory and Practice*, Vol. 1, by C. Fayette Taylor (1977), with permission of MIT Press.

Note that in the absence of reverse flow during induction $\rho/\rho_i = c/c_i = 1.0$; the terms are included as shown to cover the more general case in which reverse flow occurs.

Let us consider the limiting case in which the flow is always choked and into the cylinder. The pressure ratio is independent of time

$$P_* = \left(\frac{2}{\gamma+1}\right)^{\gamma/(\gamma-1)} \tag{7.19}$$

and

$$e_v = \left(\frac{2}{\gamma+1}\right)^{\frac{\gamma+1}{2(\gamma-1)}} \frac{\bar{A}_i c_i}{\omega V_d}(\theta_{ic} - \theta_{io}) \tag{7.20}$$

Introducing $\gamma = 1.4$ and the Mach index defined by Taylor (1977) as

$$Z = \frac{\frac{\pi}{4}b^2}{\bar{A}_i}\frac{\bar{U}_p}{c_i} \tag{7.21}$$

we have

$$e_v = 0.58\left(\frac{\theta_{ic} - \theta_{io}}{\pi}\right)\frac{1}{Z} \tag{7.22}$$

Experimental results are available for an engine in which $(\theta_{ic} - \theta_{io})/\pi = 1.3$ and thus $e_v = 0.75/Z$. They are given in Fig. 7-9. That Eq. (7.18) is an upper bound is evident and it appears to be an asymptotic formula valid for large Z.

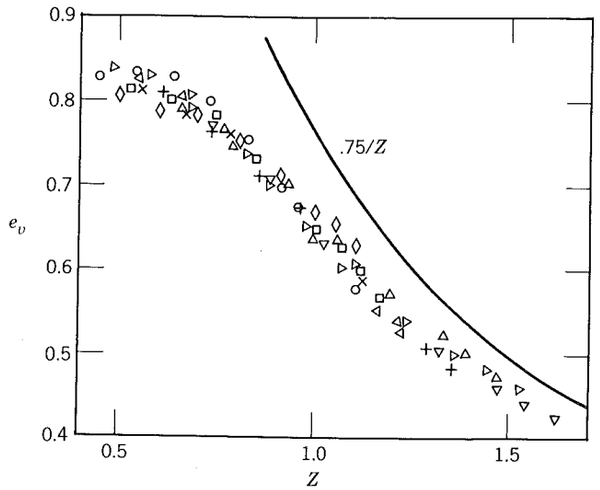

Figure 7-9 Volumetric efficiency versus inlet valve Mach index in the regime where choking occurs at the inlet valve (Livengood and Stanitz, 1943).

It should be noted that the Mach index is not a parameter that characterizes an actual gas speed, rather, it characterizes what the average gas speed through the inlet valve would have to be to realize complete filling of the cylinder at that particular piston speed; the Mach number of that average inlet gas speed would be $Z/0.58$ for $\gamma = 1.4$.

7.4 DIMENSIONAL ANALYSIS

In the limiting cases, several variables were identified as important, including:

$$r, P_e/P_i, Z, \theta_{io}, \theta_{ic}, \theta_{eo}, \theta_{ec}$$

In the more general case, the following variables must be also admitted into the analysis.

α Ratio of exhaust to intake average flow area which affects residuals and the flow during overlap.

T_w/T_i Cylinder wall temperature (normalized by inlet temperature) which influences heat transfer to the incoming charge.

R_{ei} Reynolds number, based on bore, piston speed, and inlet air viscosity (which affects boundary layers along inlet flow paths).

$\tilde{L}_i, \tilde{L}_e$ Intake and exhaust pipe lengths (in a manifold there is more than one characteristic length).

$\tilde{D}_i, \tilde{D}_e$ Intake and exhaust pipe diameters (in a manifold there is more than one characteristic diameter).

ϕ Fuel–air equivalence ratio.

Q_c/P_iV_d Heat of combustion of the fuel normalized by inlet pressure and displacement volume.

Experiments done with geometrically similar engines should obey the following:

$$e_v = e_v(P_e/P_i, Z, T_w/T_i, R_{ei}, \phi, Q_c/P_iV_d) \tag{7.23}$$

since all other variables are held constant. Figure 7-1 shows results obtained in which the only variables changing are Z and R_{ei}. The results lead to the important conclusion that the volumetric efficiency is independent of the Reynolds number.

At first, this appears to be a surprising result for it suggests that the flows during intake are inviscid when in fact they are not. There is, for example, a vena contracta effect at the inlet valve causing the effective flow area to be less than the geometrical area. However, this effect has been accounted for by basing the Mach index on the effective area rather than on the geometrical area. For this reason, the volumetric efficiency is independent of the Reynolds number.

Equation (7.23) has practical application in the programming of microcomputers used for engine control. Differentiation of Eq. (7.23) yields

$$de_v = \sum_{i=1}^{N} \frac{\partial e_v}{\partial x_i} dx_i \tag{7.24}$$

where x_i $(i = 1, 2, \ldots, N)$ are the variables on which e_v depends. For small changes we can write

$$e_v = \sum_{i=1}^{N} \left(\frac{\partial e_v}{\partial x_i} \right) \Delta x_i \tag{7.25}$$

or

$$\frac{e_{v_2}}{e_{v_1}} = 1 + \sum_{i=1}^{N} \left(\frac{\partial \ln e_v}{\partial x_i} \right) \Delta x_i \approx \prod_{i=1}^{N} \left(1 + \frac{\partial \ln e_v}{\partial x_i} \Delta x_i \right) \tag{7.26}$$

Defining correction factors K_i by

$$K_i = 1 + \frac{\partial \ln e_v}{\partial x_i} \Delta x_i \tag{7.27}$$

the volumetric efficiency of an engine can be estimated relative to some baseline using measured curves of K_i versus x_i for that particular engine, in which case

$$e_v = e_{v_b} \prod_{i=1}^{N} K_i \tag{7.28}$$

where e_{v_b} is the baseline volumetric efficiency obtained for the set of operation parameters $x_{i,b}$.

Typical values of K_i are as follows (Taylor, 1977):

x_1 = Exhaust to intake pressure ratio
Baseline: $P_e/P_i = 1.0$

$$K_1 = 1.0 - \frac{1}{1.4} \frac{P_e/P_i - 1}{r - 1}$$

(The similarity between this factor and the first terms in Eq. (7.9) is not fortuitous.)

x_2 Inlet air temperature
Baseline: $T_i = 330$ K

$$K_2 = \sqrt{T_i/330}$$

x_3 Coolant temperature
Baseline: $T_c = 340$ K

$$K_3 = \frac{1450}{T_c + 1110}$$

x_4 Equivalence ratio
Baseline: $\phi = 0.8$

$$K_4 = \begin{cases} 1.0 & \phi \geq 0.8 \\ 1.12 - 0.15\phi & \phi < 0.8 \end{cases}$$

x_5 Mach index
Baseline: $Z = 0$

$$K = 1 + 0.09 \sin(1.4Z\pi) \qquad Z \leq 0.7$$

The methodology outlined evolved as a design tool and in the older literature one can find K's for different design parameters such as valve timing, compression ratio, and pipe lengths. Because computer solutions to conservation equations can now be done routinely and accurately, Eq. (7.28) is of little value as a predictor of volumetric efficiency. Today its greatest uses are as a correlation of experimental data and as an algorithm in microcomputers used for electronic fuel control.

EXAMPLE 7.1

Estimate the volumetric efficiency of a spark-ignition four-stroke engine with the following characteristics:

Compression ratio	$r = 8$	Short inlet pipe	$L_i \approx 0$
Bore	$b = 10$ cm	Short exhaust pipe	$L_e \approx 0$
Stroke	$S = 8$ cm	Engine speed	$R_S = 2000$ rpm
Rod length	$l = 25$ cm	Inlet pressure	$P_i = 0.9$ atm
Number of cylinders	$N_c = 4$	Exhaust pressure	$P_e = 1.05$ atm
Inlet flow area	$A_i = 4$ cm^2	Inlet temperature	$T_i = 320$ K
Exhaust flow area	$A_e = 3$ cm^2	Coolant temperature	$T_c = 390$ K
Inlet opens	$\theta_{io} = 15°$ BTDC	Equivalence ratio	$\phi = 1.0$
Inlet closes	$\theta_{ic} = 50°$ ABDC	Octane fuel	C_8H_{18}
Exhaust opens	$\theta_{eo} = 45°$ BBDC	Oil	SAE 30
Exhaust closes	$\theta_{ec} = 10°$ ATDC	At baseline conditions the volumetric efficiency is 85%.	

SOLUTION:

Estimating the volumetric efficiency according to Eq. (7.28) requires:

$$K_1 = 0.982 \qquad K_2 = 0.985 \qquad K_3 = 0.967 \qquad K_4 = 1.0$$

The mean piston speed is

$$\bar{U}_p = 2R_s S = 533 \text{ cm/s}$$

The sound speed can be computed assuming the gas is air and is a level of

approximation consistent with application of Eq. (7.28). Therefore

$$c_i = \sqrt{\gamma R T_i} = 35{,}900 \text{ cm/s}$$

$$Z = \frac{\frac{\pi}{4} b^2}{\bar{A}_i} \frac{\bar{U}_p}{c_i} = 0.291$$

Finally, $K_s = 1.09$ and $e_v = 0.86$.

7.5 VALVE SIZING

The results in Fig. 7-9 show that for good volumetric efficiency one should keep the Mach index down to less than about $Z = 0.6$. Based on the analyses that led to Eq. 7.22, we can interpret this to mean that the average gas speed through the inlet valve should be less than the sonic velocity. Hence inlet valves can be sized on the basis of the maximum piston speed for which the engine is designed; choose $Z = 0.6$ at this speed and it follows that

$$\bar{A}_i = 1.3 b^2 \frac{\bar{U}_{p,\max}}{c_i} \tag{7.29}$$

Likewise for efficient expulsion of the exhaust gas, exhaust valves should be such that their Mach index is less than about 0.6, in which case

$$\alpha = \frac{\bar{A}_e}{\bar{A}_i} \approx \frac{c_i}{c_e} = \sqrt{\frac{T_i}{T_e}} \tag{7.30}$$

Current practice dictates that the valve area ratio α is on the order of 70 to 80%. A smaller exhaust valve diameter and lift ($l \approx d/4$) can be used because the speed of sound is higher in the exhaust gases than in the inlet charge.

In many situations it turns out that the intake valves are sized as big as possible while being consistent with Eq. (7.30). This is because there is only so much room available for valves and it may not be possible to satisfy Eq. (7.29), thereby compromising the maximum speed of the engine. Herein lies one advantage pent-roof combustion chambers have over cylindrical ones; there is more room for valves. Likewise one can obtain more valve area per unit piston area by employing four valves per cylinder rather than two.

7.6 NUMERICAL MODELING—SHORT PIPES, MIXED PLENUMS

The mixed plenum is defined as being internally homogeneous and in a steady state. This can be approached in practice by constructing the plenum to be large and using an internal fan or the inlet flow to stir the fluid. Consider Fig. 7-10 as a model of an exhaust plenum.

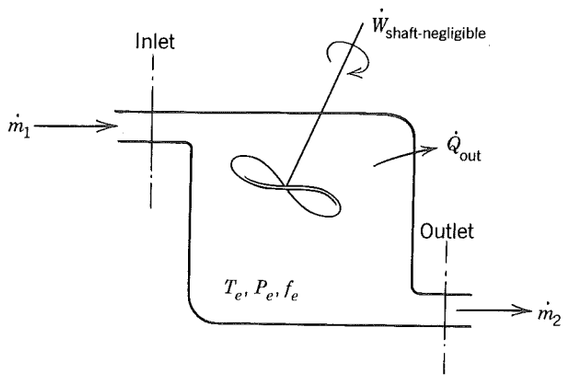

T_e Exhaust temperature
P_e Exhaust pressure
f_e Mass fraction of burned gas in plenum
$\dot{m}_1$ Mass flow rate in from engine
$\dot{m}_2$ Mass flow rate out

$$\frac{dT_e}{dt} = \frac{dP_e}{dt} = \frac{df_e}{dt} = \frac{d\dot{m}_2}{dt} = 0$$

Figure 7-10 Perfectly mixed exhaust plenum.

When the flow is from the engine into the tank, the intensive properties convected into the system at the inlet are those associated with the cylinder gases. When the flow reverses itself, they are those associated with the gases in the plenum. Consider the energy equation applied to the plenum and integrated over one cycle of the engine's operation.

$$\oint \dot{m}_1 h_1 \, dt = h_e m_2 \oint dt + \dot{Q}_e \oint dt \tag{7.31}$$

To handle the flow reversal let us define the following:

$\dot{m}_{1,f,e}$ *Forward flow rate through exhaust valve*
$\dot{m}_{1,r,e}$ *Reverse flow rate through exhaust valve*
h_c *Instantaneous enthalpy of cylinder gases*
h_r *Enthalpy of residual gas*
h_{fa} *Enthalpy of fuel–air mixture with no residuals present*

In these terms the energy equation is

$$\oint \dot{m}_{1,f,e} h_c \, dt - h_e \oint \dot{m}_{1,r,e} \, dt = h_e \dot{m}_2 \oint dt + \dot{Q}_e \oint dt \tag{7.32}$$

This equation can be solved to determine the enthalpy of the gases in the exhaust plenum.

$$h_e = \frac{\oint \dot{m}_{1,f,e} h_c \, dt - \dot{Q}_e \oint dt}{\dot{m}_2 \oint dt + \oint \dot{m}_{1,r,e} \, dt} = \frac{\oint \dot{m}_{1,f,e} h_c \, dt - \dot{Q}_e \oint dt}{\oint \dot{m}_{1,f,e} \, dt} \tag{7.33}$$

By a similar analysis in which the mass of product gas is conserved, it can be shown that the residual mass fraction in the exhaust plenum is

$$f_e = \frac{\oint \dot{m}_{1,f,e} f_c \, dt}{\dot{m}_2 \oint dt + \oint \dot{m}_{1,r,e} \, dt} = \frac{\oint \dot{m}_{1,f,e} f_c \, dt}{\oint \dot{m}_{1,f,e} \, dt} \tag{7.34}$$

Equations (7.33) and (7.34) together with

$$h_e = f_e h_r(T_e) + (1 - f_e) h_{fa}(T_e) \tag{7.35}$$

fix the gas temperature in the plenum.

A similar analysis is required to handle reverse flow at the intake port into the intake plenum. In this case, define the following:

$\dot{m}_{2,f,i}$ *Forward flow through intake valve*
$\dot{m}_{2,r,i}$ *Reverse flow through intake valve*
$\dot{m}_1$ *Air and fuel flow into plenum*

In this case the plenum is characterized by T_i, P_i, f_i, and $d\dot{m}_1/dt = 0$. As heat loss in the intake plenum can generally be neglected, the energy equation gives

$$\dot{m}_1 h_1 \oint dt = h_i \oint \dot{m}_{2,f,i} \, dt - \oint \dot{m}_{2,r,i} h_c \, dt \tag{7.36}$$

which when solved for the plenum enthalpy gives

$$h_i = \frac{\dot{m}_1 h_1 \oint dt + \oint \dot{m}_{2,r,i} h_c \, dt}{\oint \dot{m}_{2,f,i} \, dt} \tag{7.37}$$

Likewise it follows that

$$f_i = \frac{\cancel{\dot{m}_1 f_1 \oint dt}^{\,0} + \oint \dot{m}_{2,r,i} f_c \, dt}{\oint \dot{m}_{2,f,i} \, dt} \tag{7.38}$$

The engine cylinder can also be assumed to be well mixed because of the nature of the flow through the valves. In terms of the quantities defined for the plenums and the energy equation given in Fig. 7-11, the enthalpies flowing in

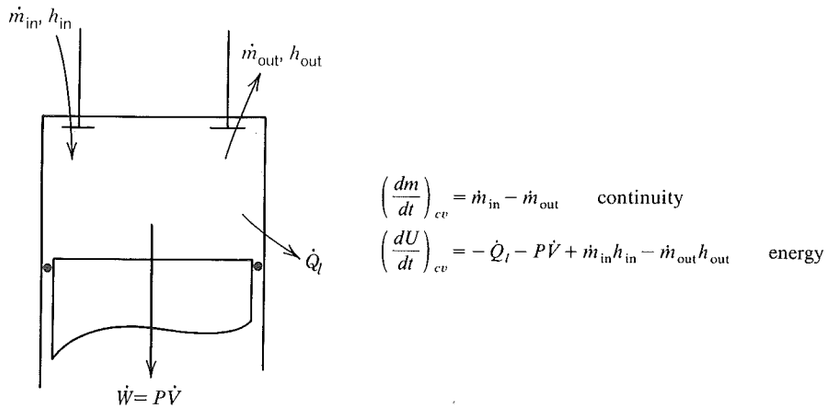

Figure 7-11 Engine model for numerical solution of intake and exhaust processes.

and out are given by

$$\dot{m}_{in} h_{in} = \dot{m}_{1,r,e} h_e + \dot{m}_{2,f,i} h_i \tag{7.39}$$

$$\dot{m}_{out} h_{out} = \dot{m}_{1,f,e} h_c + \dot{m}_{2,r,i} h_c \tag{7.40}$$

The system energy at any time is

$$\frac{U}{m} = f_c u_r(T_c, P_c) + (1 - f_c) u_{fa}(T_c, P_c) \tag{7.41}$$

and the volume is

$$\frac{V}{m} = f_c v_r(T_c, P_c) + (1 - f_c) v_{fa}(T_c, P_c) \tag{7.42}$$

The mass is found by integrating

$$\frac{dm}{dt} = \dot{m}_{2,f,i} - \dot{m}_{2,r,i} - \dot{m}_{1,f,e} + \dot{m}_{1,r,e} \tag{7.43}$$

The problem is completed by writing equations for the heat loss

$$\dot{Q}_l = \mathbf{h} A (T_c - T_w) \tag{7.44}$$

Each of the mass flow rates on the right-hand side of Eq. (7.43) are computed according to Eq. (7.14), the mass flow rate through a valve is assumed quasi-steady and isentropic. The gas is assumed to have constant specific heats over the range of temperature change induced by accelerating the flow. This latter statement does not mean that a constant γ is assumed for gases within the cylinder or either plenum. Rather, γ is evaluated at the instantaneous stagnation temperature for use in Eq. (7.14).

We have a set of algebraic and ordinary differential equations to solve for the volumetric efficiency, residual fraction, pressure and temperature at inlet

Table 7-1 Simultaneous O.D.E. Describing Intake and Exhaust

$$\dot{y}_1 = \dot{m}_{1,f,e} = \dot{m}(A^*_{f,e}, P_c, T_c, \gamma_c, R_c, P_e)$$
$$\dot{y}_2 = \dot{m}_{1,r,e} = \dot{m}(A^*_{r,e}, P_e, T_e, \gamma_e, R_e, P_c)$$
$$\dot{y}_3 = \dot{m}_{2,f,i} = \dot{m}(A^*_{f,i}, P_i, T_i, \gamma_i, R_i, P_c)$$
$$\dot{y}_4 = \dot{m}_{2,r,i} = \dot{m}(A^*_{r,i}, P_c, T_c, \gamma_c, R_c, P_i)$$
$$\dot{y}_5 = \dot{m}_{1,f,e} h_c = \dot{y}_1 h(T_c, f_c)$$
$$\dot{y}_6 = \dot{m}_{1,f,e} f_c = \dot{y}_1 f_c$$
$$\dot{y}_7 = \dot{m}_{2,r,i} h_c = \dot{y}_4 h(T_c, f_c)$$
$$\dot{y}_8 = \dot{m}_{2,r,i} f_c = \dot{y}_f f_c$$
$$\dot{y}_9 = \dot{Q}_l(\mathbf{h}, T_c, T_w, A_c)$$
$$\dot{y}_{10} = P_c \dot{V}$$
$$m(\theta) = m(0) + y_3 - y_4 - y_1 + y_2$$
$$U(\theta) = U(0) - y_9 - y_{10} - y_5 - y_7 + y_3 h_i + y_2 h_e$$
$$f_c(\theta) = (y_3 f_i + y_2 f_e - y_6 - y_8)/m$$

$A^*_{f,e}, A^*_{r,e}, A^*_{f,i}, A^*_{r,i}, A_c, \dot{V}$ are known functions of θ.
γ_c, R_c depend on f_c, T_c.
T_c, P_c depend on $U/m, V/m, f_c$ by Eq. (7.41) and (7.42).
$T_w, f_i, f_e, P_e, P_i, h_e, h_i$ are specified.
Once y_i, $i = 1, 10$ are known, when the inlet valve shuts, f_i, f_e, h_e, h_i are computed and the calculation repeated until it converges.

valve closing, conditions in the intake and exhaust plenums, the pumping work, and the heat loss during intake and exhaust. This is an initial value problem, given the state of the systems at the time the exhaust valve opens. The differential equations cast into the form

$$\frac{d\tilde{y}}{d\theta} = f(\theta, \tilde{y}) \tag{7.45}$$

are presented in Table 7-1.

7.7 LONG PIPES

In practice, long pipes are usually required to duct the exhaust gases to a point of expulsion, often far removed from the engine, and to deliver the inlet charge from some preparation device such as a carburetor or compressor. In multicylinder engines, manifolding is used so that cylinders can share the same carburetor, compressor, muffler, or catalytic convertor. The configuration of the tubing networks employed plays an important role in determining the volumetric efficiency and residual fraction.

Experimental results for the simplest case of a single-inlet pipe on a single-cylinder engine are given in Fig. 7-12 for three different camshafts of varying inlet-valve timings. The pipe length L_i is normalized by the stroke S,

and the pipe diameter D_i by the bore b. The graphs show volumetric efficiency as a function of the inlet Mach index. Note that for $L_i/S = 1.83$, the inlet pipe may be considered short provided $D_i/b \geq 0.326$, as there is little, if any, difference between these configurations and those with no pipe at all.

Note further that associated with longer pipes is a speed that maximizes the volumetric efficiency, and that particular speed depends on valve timing, pipe length, and pipe diameter. To minimize engine size and produce a given torque versus speed curve (with torque proportional to the volumetric efficiency at fixed thermal efficiency), it is clearly desirable to be able to vary valve timing with engine speed. Although development of electronically actuated and controlled valves for this purpose is being pursued, current practice is to use a camshaft with fixed valve timing. Thus one is faced with compromises. An auto manufacturer, for example, might choose a valve timing that maximizes fuel economy on an EPA driving cycle. A manufacturer of truck engines for long distance hauling might design for the most probable engine speed. Similar compromises occur in exhaust-pipe design where one tries to minimize or control the residual fraction.

As mentioned in Chapter 1, regarding Table 1-2, engineers charged with manifold design are using computer simulations to search for optimal configurations. These models involve numerical solution of partial differential equations describing conservation of mass, energy, and momentum. Quasi-one-dimensional models in which fluid friction and heat loss are accounted for do an adequate job. A discussion of the methods employed in these calculations is beyond the scope of this text. The interested reader is referred to recent papers by Chapman, Novak, and Stein (1982 and 1983) which are representive of and reference other papers that contributed to the state of the art.

Nevertheless, it is useful to show the kind of data input into a state of the art computation and compare some of the predictions made with experimental results. It should be mentioned that of all the processes that can be modeled in engines, the gas-exchange computations are probably the most quantitative, that is, have minimal influence of undetermined constants or "fudge factors" of any of the process models. The following information comes from the work of Chapman et al. (1982).

A schematic of the intake manifold on a 2.3 liter engine is shown in Fig. 7-13. The over all engine configuration reduced to a quasi-one-dimensional system, including the exhaust manifold, is shown in Fig. 7-14. The runner lengths and plenum volumes are indicated. The intake runners vary linearly in diameter from 3.2 cm at the plenum to 3.5 cm at the head face. Exhaust runners range from 3.7 to 4.4 cm and the exhaust pipe has a diameter of 4.3 cm. The two-barrel carburetor is treated as a single venturi with equivalent "effective" outer and throat diameters of 4.8 and 3.5 cm.

Figures 7-15 and 7-16 show the predicted mass flow rates through the intake and exhaust valves at 1500 rpm (mass flow out is defined as positive). Notice the backflows that occur during the intake and exhaust processes at this

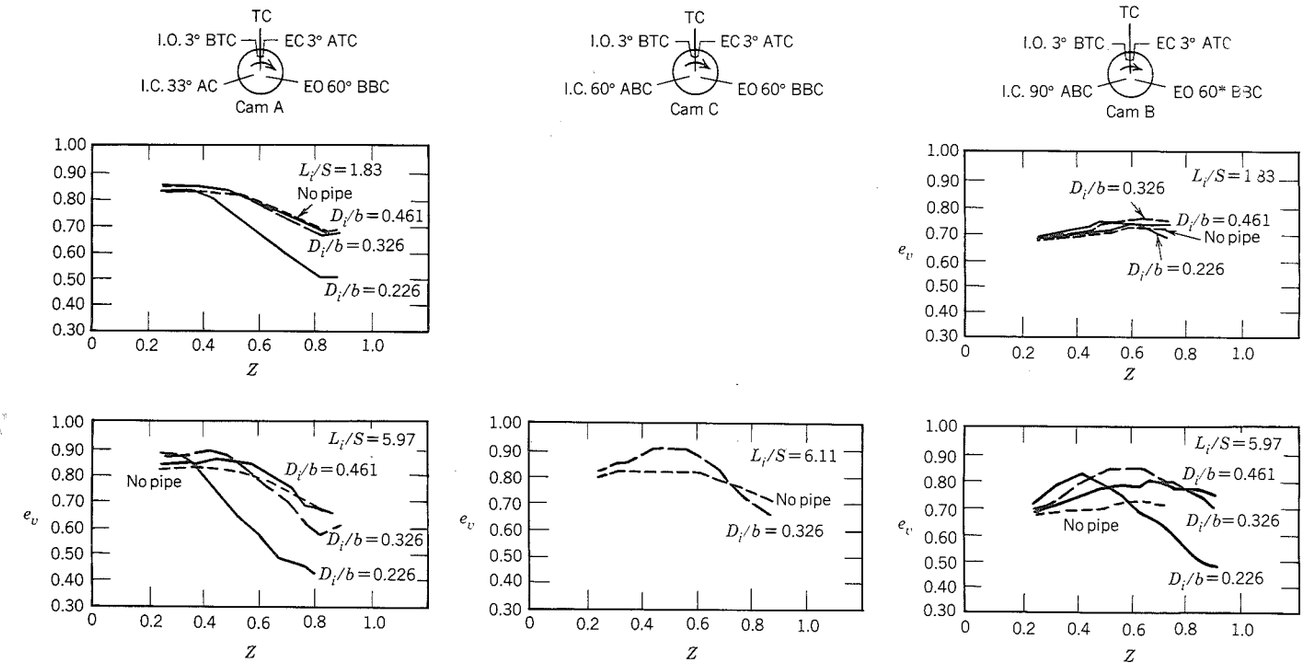

Figure 7-12 Volumetric efficiency as affected by inlet pipe length and diameter and inlet-valve timing: CFR engine, $b = 8.89$ cm, $S = 11.43$ cm, $r = 6$, $P_i = 0.90$ bar, $P_e = 1.04$ bar, $T_i = 311$ K, $\phi = 0.8$, optimum spark timing (Taylor, Livengood, and Tsau, 1955). Reprinted with permission © 1955. ASME.

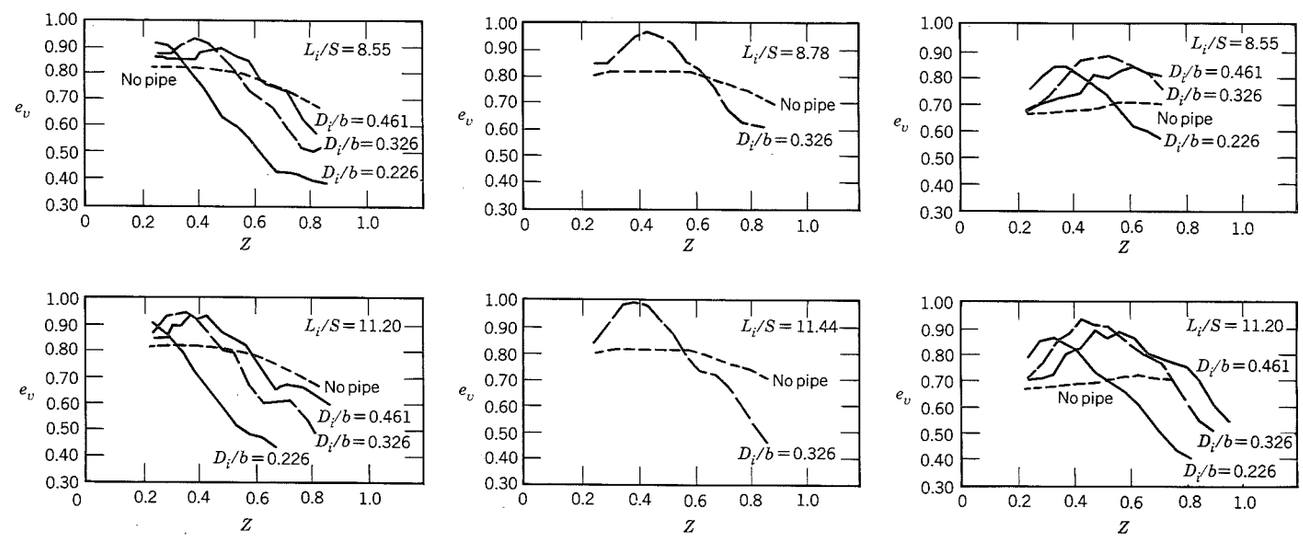

Figure 7-12 *(Continued)*

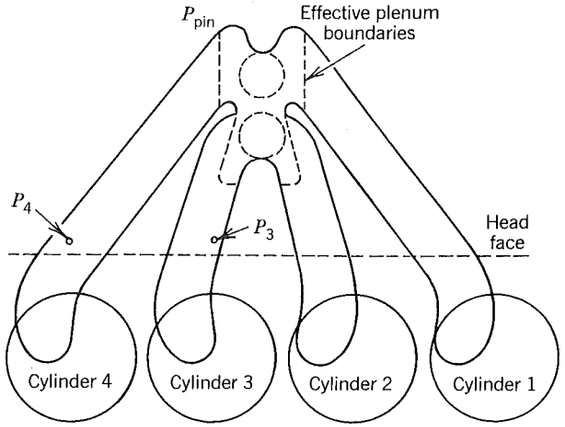

Figure 7-13 Schematic of 2.3 L engine intake manifold (Chapman et al., 1982). Reprinted with permission © 1982. ASME.

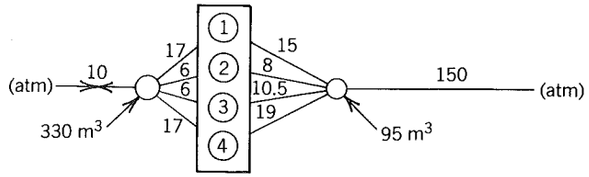

Figure 7-14 Model of overall engine configuration (all lengths in centimeters) (Chapman et al., 1982). Reprinted with permission © 1982. ASME.

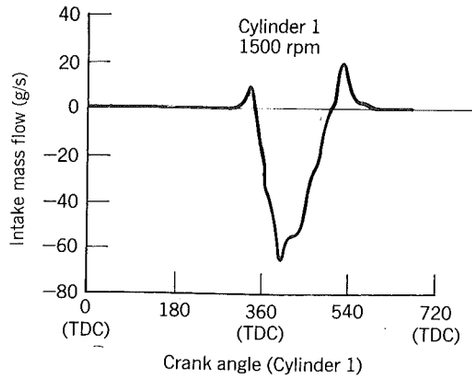

Figure 7-15 Model predictions for flow out of cylinder (1) through the intake valve (Chapman et al., 1982). Reprinted with permission © 1982. ASME.

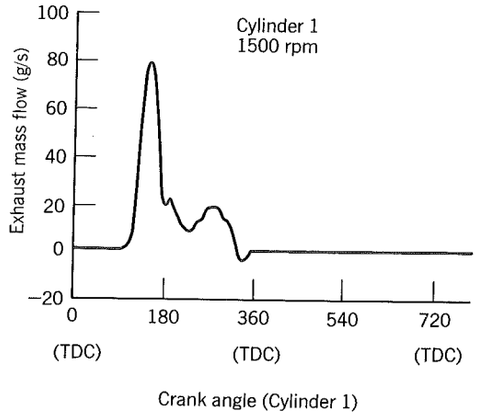

Figure 7-16 Model predictions for flow out of cylinder (1) through the exhaust valve (Chapman et al., 1982). Courtesy ASME.

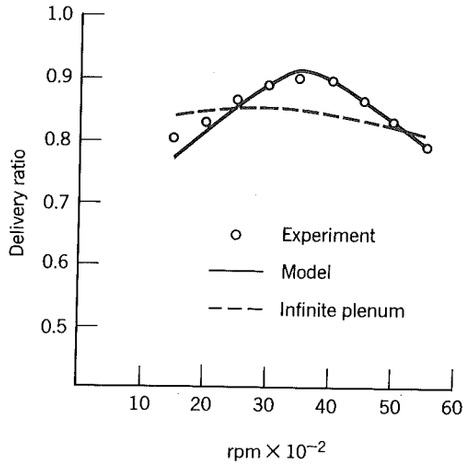

Figure 7-17 Comparison of predicted and experimental delivery ratios at WOT. Also shown are calculated results for the same engine configured with short pipes and large plenums to demonstrate the importance of the manifold configurations (Chapman et al., 1982). Reprinted with permission © 1982. ASME.

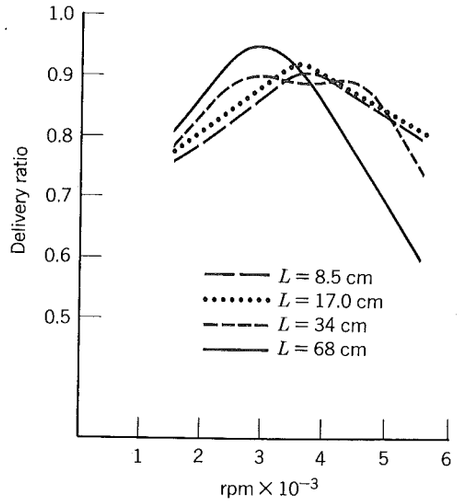

Figure 7-18 Calculated effects of primary intake runner length on delivery ratio (Chapman et al., 1982). Reprinted with permission © 1982. ASME.

low engine speed. Figure 7-17 compares the predicted and experimental delivery ratio for wide-open throttle (WOT) operation (at WOT, delivery ratio and volumetric efficiency are practically the same). Also shown are the results that would be obtained for constant pressure intake and exhaust as occurs with short pipes and large plenums. These results demonstrate the roles the intake and exhaust systems play in determining the air charging characteristic over the engine's entire operating speed range.

To demonstrate the capability of the model as a design tool, Fig. 7-18 shows results obtained by varying the primary intake runner length on the delivery ratio of the 2.3 liter engine. In each case considered, all four runners have the same length. Note that a length of 34 cm produces a desirable delivery ratio curve with increased low-speed and flat mid-speed characteristics relative to the 17 cm case. The 68 cm runner significantly improves the low-speed characteristics but causes poor delivery ratio at high speed.

7.8 TWO-STROKE ENGINES

The scavenging or air-charging characteristics of two-stroke engines can be designed according to a large number of different configurations. In each case the air must be pumped in. A crankcase scavenged engine was discussed in Chapter 1. Air was inducted into the crankcase, subsequently compressed, and pumped into the cylinder. Another class of two-stroke engines is the separately

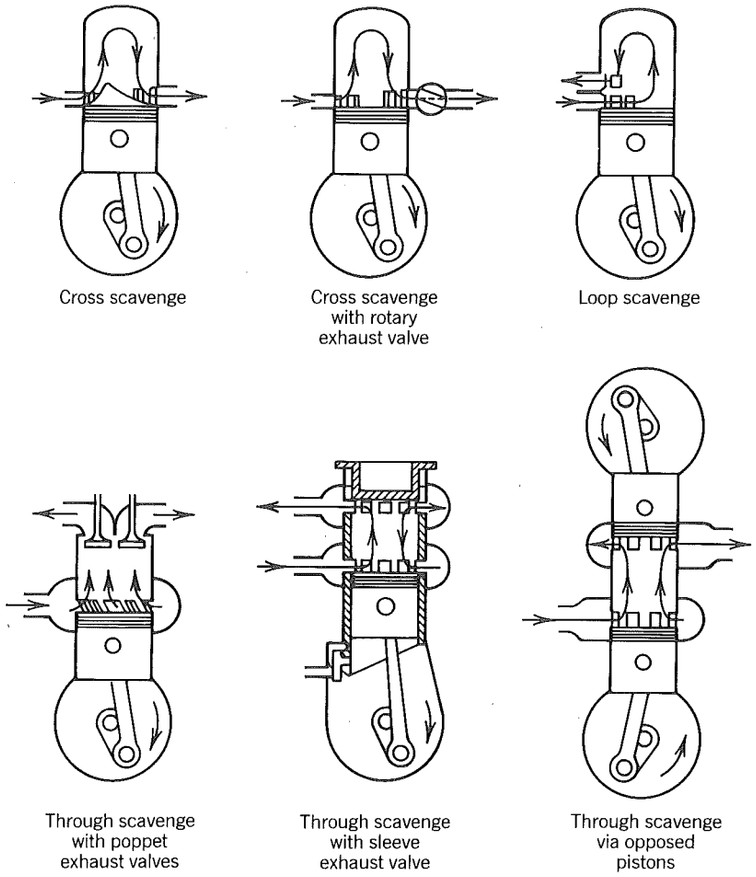

Figure 7-19 Some two-stroke scavenging methods (adapted from Taylor, 1977).

scavenged engine in which a separate compressor, driven by the crank or perhaps an exhaust turbine, delivers the air.

Two-stroke engines are also classified on the basis of what the air path is during the course of scavenging. Figure 7-19 illustrates various ways in which cross, loop, and through scavenging can be realized. Notice the different valve arrangements based on whether the ports open and close by the piston, poppet valves, rotary valves, or sleeve valves. Considering the large number of permutations possible, based on classification of the pumping method, the air path, and the valving arrangement, it is clear why so many different types of two-stroke engines exist.

The best air path is achieved via *through scavenging* in which air is admitted at one end of the cylinder and exhaust gas is discharged at the other

end. Ideally this method could result in perfect scavenging in which the incoming air displaces the exhaust gas without mixing. In *cross scavenging*, care must be taken to avoid what is referred to as *short circuiting*. Notice in Fig. 7-19 that without the hump on the piston top the incoming air would have a tendency to simply go in and out of the cylinder without displacing exhaust gas. This is short circuiting. Insertion of the hump forces the gas to turn and mix with the exhaust gas thus expelling a mixture of air and exhaust. Experimental data tend to suggest that the best scavenging that can be achieved via the cross method occurs when there is perfect mixing in which the fresh air introduced *successively* dilutes the residual exhaust gas. If sufficient air is used, at the end of scavenging an acceptable scavenging efficiency is then achieved.

Some of the terminology applied to two-stroke engines was introduced in Chapter 1. It is reiterated here for convenience and to assign symbols to some of the parameters. Table 7-2 gives performance terminology according to SAE recommended practice. This table as given applies to fuel-injected engines. For fuel-inducted engines, as with a throttle-body injector, the word *mixture* referring to the air–fuel mixture is to be substituted for *air* and *mixture density at ambient pressure and temperature* is to be substituted for *ambient density*.

Scavenging efficiency, charging efficiency, and purity all express a measure of success in clearing the cylinder of residual gases from the preceding cycle and as such can be mathematically related. By definition it follows that

$$e_c = D_r \Gamma \tag{7.46}$$

With excess air, the purity and scavenging efficiency differ because of "left

Table 7.2 Performance Terminology

Delivery ratio	$\dfrac{\text{mass of delivered air}}{\text{displaced volume} \times \text{ambient density}} = D_r$
Delivered air–fuel ratio	$\dfrac{\text{mass of delivered air}}{\text{mass of delivered fuel}}$
Trapped air–fuel ratio	$\dfrac{\text{mass of air retained}}{\text{mass of fuel retained}}$
Trapping efficiency	$\dfrac{\text{mass of delivered air retained}}{\text{mass of delivered air}} = \Gamma$
Scavenging efficiency	$\dfrac{\text{mass of delivered air retained}}{\text{mass of trapped cylinder charge}} = e_s$
Purity	$\dfrac{\text{mass of air in trapped cylinder charge}}{\text{mass of trapped cylinder charge}} = \mathscr{P}$
Relative charge	$\dfrac{\text{mass of trapped cylinder charge}}{\text{displaced volume} \times \text{ambient density}} = R_c$
Charging efficiency	$\dfrac{\text{mass of delivered air retained}}{\text{displaced volume} \times \text{ambient density}} = e_c$
Excess air factor	$\dfrac{\text{trapped air–fuel ratio}}{\text{stoichiometric air–fuel ratio}} = \lambda$

over air" in the residual gas. It can be shown that (Schweitzer 1949):

$$e_s = \mathscr{P} \qquad \text{if } \lambda \le 1$$

$$e_s = \frac{1}{1 + \lambda\left(\dfrac{1}{\mathscr{P}} - 1\right)} \qquad \text{if } \lambda > 1 \tag{7.47}$$

The scavenging efficiency is less than or equal to the purity. However, as the difference is usually small, the two quantities are often confused.

The residual mass fraction required for thermodynamic analysis is

$$f = 1 - e_s \tag{7.48}$$

and the fuel–air equivalence ratio is

$$\phi = \frac{1}{\lambda} \tag{7.49}$$

State of the art models of two-stroke scavenging also solve partial differential conservation equations; see, for example the book edited by Blair et al. (1982). We will limit our analysis to the simplest of cases corresponding to short circuiting, perfect mixing, and perfect scavenging.

Let us consider first the case of perfect scavenging. Recall that no mixing occurs and air simply displaces the exhaust gas to expel it. The trapping and scavenging efficiencies as functions of the delivery ratio are given in Fig. 7-20. At a delivery ratio given by

$$D_r = \frac{V_{bdc}}{V_d} = \frac{r}{r-1} \tag{7.50}$$

the cylinder volume at bottom center is filled with pure air ($\mathscr{P} = e_s = 1.0$), and if any more air is delivered, it is not retained. This occurs at a delivery ratio greater than one and dependent upon the compression ratio because the delivery ratio is defined in terms of the displacement volume rather than the maximum cylinder volume corresponding to bottom center.

In the case of short circuiting, the air initially displaces all the gas within the path of the short circuit and then simply flows into and out of the cylinder along that path. Thus, initially, the scavenging efficiency increases with delivery ratio as if scavenging were perfect; then the scavenging efficiency remains constant once the path has been displaced, see curve B in Fig. 7-20.

For perfect mixing, the first air to come in is instantaneously mixed with the exhaust and the first gas expelled is low in purity, being nearly all residual gas. For large delivery ratios, the gas being expelled is now rather pure and the trapping efficiency is thus low. The scavenging efficiency as a function of the delivery ratio can be expressed via an analysis based on the conservation of delivered air. Let m_a denote delivered air and m'_a denote delivered air retained. It follows that

$$\left(\frac{dm'_a}{dt}\right)_{cv} = \dot{m}_{a,\text{in}} - x\dot{m}_{\text{out}} \tag{7.51}$$

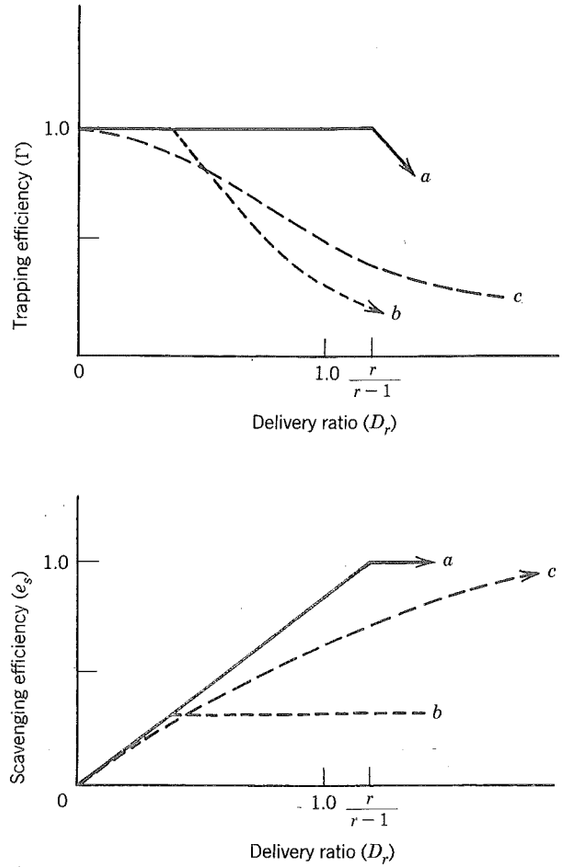

(A)—perfect scavenging
(B)—short circuiting
(C)—perfect mixing

Figure 7-20 Scavenging characteristics of two-stroke engines according to three different idealizations. (*a*) Trapping efficiency versus delivery ratio. (*b*) Scavenging efficiency versus delivery ratio.

where the control volume cv is defined as the cylinder volume and x denotes the mass fraction of retained air to charge in the cylinder at any time.

Since

$$m'_a = xm \tag{7.52}$$

it follows that

$$\frac{dm'_a}{dt} = x\frac{dm}{dt} + \dot{m}\frac{dx}{dt} \tag{7.53}$$

Assuming that the mass flow rates into and out of the cylinder are equal, hence $dm/dt = 0$, one obtains

$$\frac{1}{(1-x)}\frac{dx}{dt} = \frac{\dot{m}_{\text{in}}}{m} \tag{7.54}$$

Integration of Eq. (7.54) over the scavenging event yields

$$e_s = 1 - \exp\left(-\int \frac{\dot{m}_{\text{in}}}{m}\,dt\right) = 1 - \exp\left(\frac{-D_r}{R_c}\right) \tag{7.55}$$

The trapping efficiency is then

$$\Gamma = \frac{R_c}{D_r}\left[1 - \exp\left(\frac{-D_r}{R_c}\right)\right] \tag{7.56}$$

The curves (C) are drawn in Fig. 7-20 accordingly.

Inspection of Fig. 7-19 reveals that more often than not two-stroke engines use piston-controlled ports rather cam actuated valves to admit the fresh charge and expel the exhaust. Numerical modeling of scavenging in the two-stroke engine is not unlike the modeling done for four-stroke equations; that is, differential conservation equations are solved. As in the four-stroke calculations, where one specifies the valve areas as functions of crank angle, in two-stroke calculations, one must specify the effective flow areas of the ports as functions of crank angles.

A steady-flow apparatus for determining flow area of piston controlled ports is shown in Fig. 7-21. Note the similarity with the apparatus in Fig. 7-5. Once again, solution of Eq. (7-14) yields the area A^* from measurements of the mass flow rate and the pressure ratio.

Some measured discharge coefficients for a piston controlled inlet port are shown in Fig. 7-22. Part *b* of the figure shows an important difference

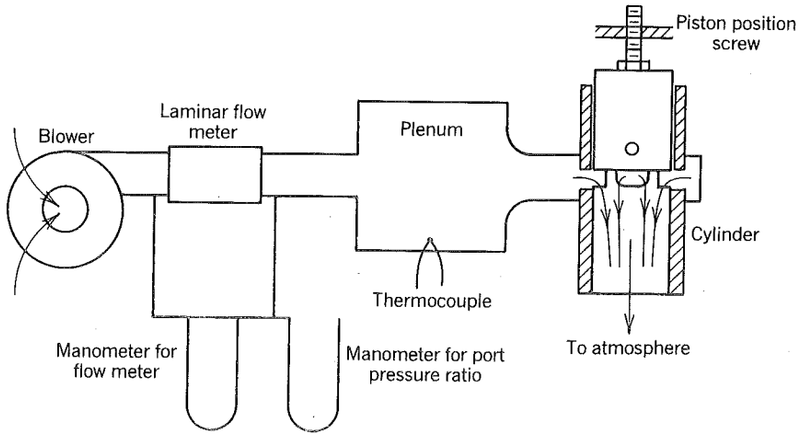

Figure 7-21 Essential features of a steady flow bench to measure flow areas and discharge coefficients of a piston controlled port.

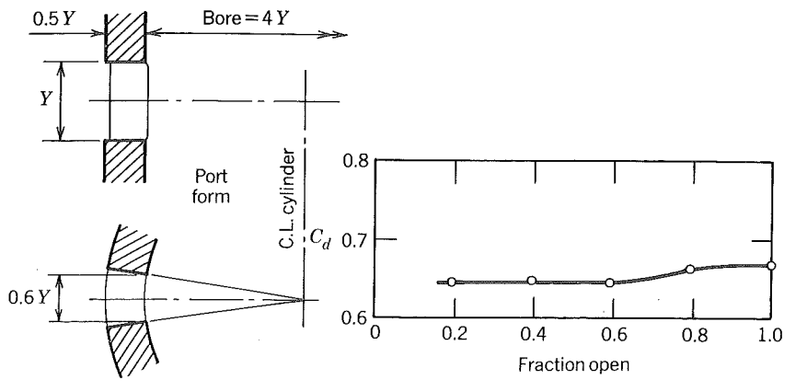

(a)

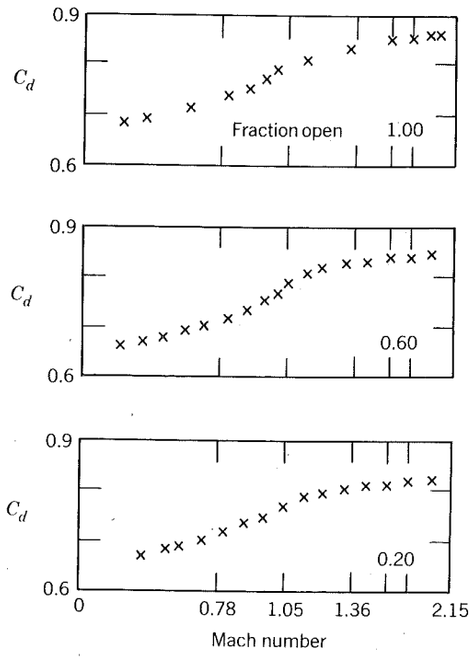

(b)

Figure 7-22 Discharge coefficient of a simple radial port as measured by Benson, see Annand and Roe (1974). (*a*) Variation with port opening at low Mach number. (*b*) Variation with Mach number based on the velocity and sound speed at the throat of area A^*. (The scale is nonlinear because the original data was in terms of the logarithm of the pressure ratio). Copyright Annand and Roe, *Gas Flow in the Internal Combustion Engine*, G. T. Foulis & Co., Ltd, Sparkford, Somerset, England 1974.

between results obtained for poppet valves and those obtained for simple ports. The discharge coefficient increases with Mach number; whereas, with poppet valves, it is nearly independent of Mach number. As the Reynolds number is not constant in Fig. 7-22*b*, the attribution of the observed effects to Mach number tacitly assumes that there is no dependence upon Reynolds number. This assumption seems reasonable; it is mentioned because there has been no rigorous experimentation or analysis done directed at separating Mach number effects from Reynolds number effects (The same can be said of flow through the poppet valves).

7.9 PUMPING AND SCAVENGING WORK

In a four-stroke engine, the pumping work is defined as the work required to shove out the exhaust gas and pull in the fresh charge. It is evaluated from a pressure–volume diagram from bottom center at the start of the exhaust stroke to bottom center at the end of the induction stroke. The ideal model, valid for engines operated at low Mach indices, predicts that the pmep is the difference between the exhaust pressure and the inlet pressure. At higher speeds, the pressure difference across the valves at closing reduces or increases the pumping depending on whether or not the engine is supercharged. Data given by Taylor (1977) for a CFR engine with short pipes are correlated by the following expression.

$$\text{pmep} = (P_e - P_i) - (1.4P_e - 2.6P_i)Z^{1.5} \tag{7.57}$$

This applies to other engines with short pipes only insofar as they are geometrically similar. Brown (1973), for example, used a similar expression for a multicylinder diesel engine and found the exponent on Z to be 1.36. In either case as $Z \to 0$, pmep tends to the ideal case of $P_e - P_i$.

The pumping work of multicylinder engines with long manifolded pipes can be computed employing the quasi-one-dimensional state of the art computer model discussed earlier within the context of volumetric efficiency. In this case, predictions are made of cylinder pressure versus volume during the intake and exhaust stroke; integration of $P\,dV$ divided by the displacement volume yields the pmep.

In the case of a crankcase scavenged two-stroke engine the pumping work is determined by the crankcase pressure as a function of crankcase volume. No major difficulty is encountered when constructing a thermodynamic model of the crankcase. Results obtained by Blair and Ashe (1976) for a 250 cm^3 Husqvarna motorcycle engine are shown in Fig. 7-23. As can be seen, agreement between measurements and predictions is quite good.

For separately scavenged engines, the work done by the compressor is of interest. The adiabatic efficiency η_c of a compressor is defined as the ideal work required to compress the gas over the specified pressure ratio divided by the work actually required to compress the gas over the same pressure ratio. The pressure ratio of compressors used for two-stroke engines is generally

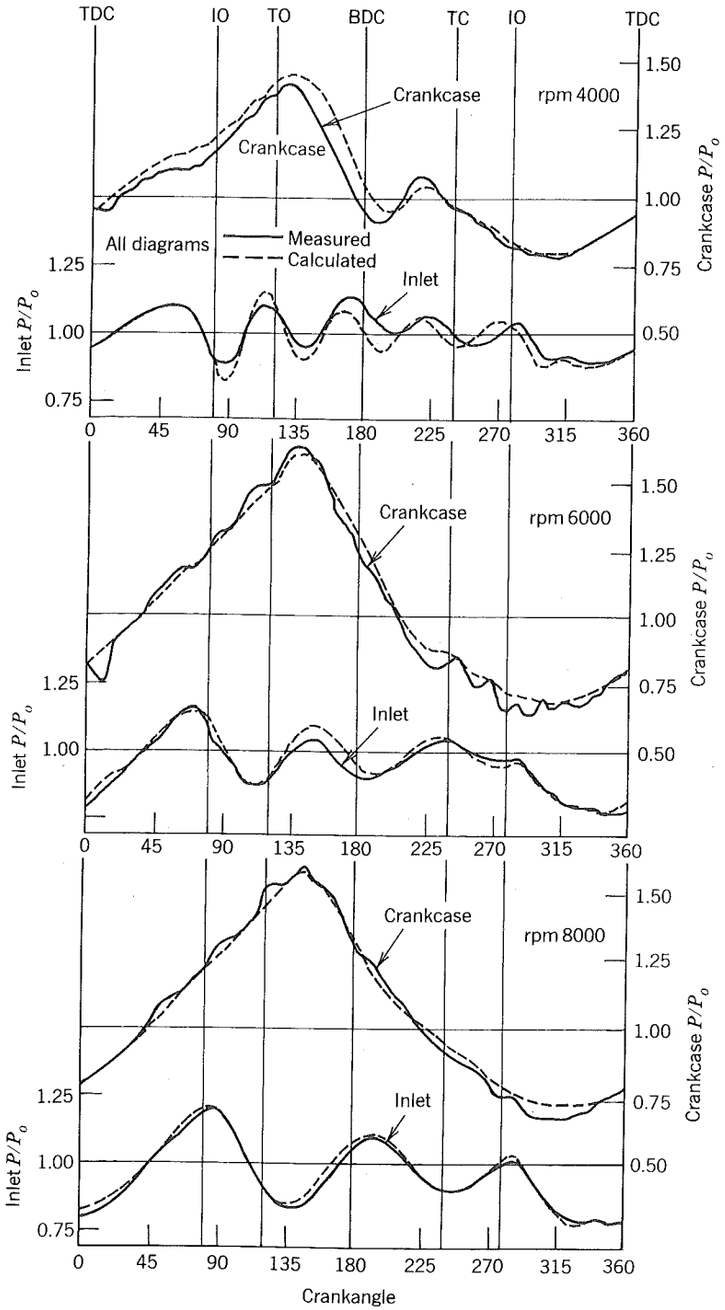

Figure 7-23 Measured and computed crankcase and inlet pressures of a Husqvarna mk-1 motorcycle engine. P_o is ambient pressure (Blair and Ashe, 1976). Reprinted with permission © 1982. Society of Automotive Engineers, Inc.

small enough that the gas may be assumed to have constant specific heats. It follows then that in the ideal case, the work required per unit mass of gas is given by

$$w_{1\to 2} = c_{P1}T_1\left[\left(\frac{P_2}{P_1}\right)^{(\gamma-1)/\gamma} - 1\right] \tag{7.58}$$

The compressor mean effective pressure is therefore

$$\text{cmep} = \rho_a D_r \eta_c c_{P1} T_1\left[\left(\frac{P_2}{P_1}\right)^{(\gamma-1)/\gamma} - 1\right] \tag{7.59}$$

where ρ_a is the ambient density and D_r is the delivery ratio. In deriving Eq. (7.58) and (7.59) it was tacitly assumed that the change in kinetic energy across the compressor was negligible compared to the change in enthalpy, an assumption usually valid in practice.

Experiments with compressors show that the adiabatic efficiency is dependent primarily upon three dimensionless variables:

$\frac{P_2}{P_1}$ Outlet–inlet pressure ratio

$\frac{1}{2}\omega\frac{D}{c}$ Mach number based on wheel tip speed

$\dot{m}/\dot{m}^*$ Mass flow rate over the critical mass flow rate, Eq. (7.14).

Experimental data for a particular compressor are given in Fig. 7-24 as representative of trends observed in practice. It can be seen that compressor efficiencies are on the order of 75%.

The data shown are called a compressor map. The qualitative features shown are common to both axial and radial flow compressors. The surge line represents a boundary between stable and unstable operating points. Compressors cannot be expected to operate to the left of the surge line.

The causes of surge are still debated in the technical community. Watson and Janota (1982) explain that when the mass flow rate is reduced at constant pressure ratio, a point arises where somewhere within the internal boundary layers a flow reversal occurs. If the flow rate is further reduced, then a complete reversal occurs which relieves the adverse pressure gradient. That relief means a flow reversal is no longer needed and the flow then responds toward returning to its initial condition. When this is reached, the process will repeat itself.

To the right of the compressor map is a zone where efficiencies fall rapidly with increasing mass flow rate. The gas speeds are quite high in this zone and the attendant fluid friction losses are increasing with the square of the gas speed.

In this right region there is also a choke limit which occurs at a slightly different value of $\dot{m}/\dot{m}^*$ for each tip speed. Choking occurs when somewhere within the compressor the flow reaches the speed of sound. It occurs at values of $\dot{m}/\dot{m}^*$ less than 1 because $\dot{m}^*$ is based on the compressor wheel diameter

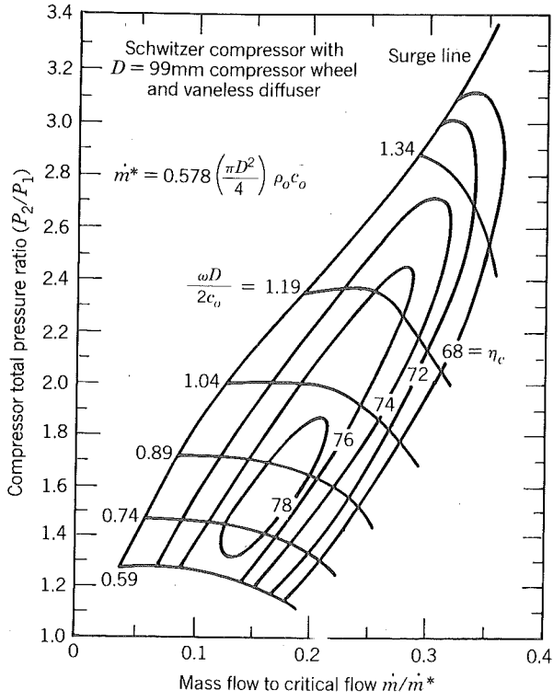

Figure 7-24 Example of a compressor map from which the adiabatic efficiency can be determined. Courtesy R. Hehman of Schwitzer.

rather than on the cross section where choking is occuring. The value of $\dot{m}/\dot{m}^*$ at choking varies with tip speed because the location within the compressor at which choking occurs depends on the structure of the internal boundary layers.

It is tempting at this point to digress into a comprehensive discussion of turbomachinery, as it is clearly relevant to performance predictions of reciprocating engines in turbocharged, supercharged, or turbocompounded configurations. That is a subject unto itself and is treated comprehensively in the book by Watson and Janota (1982).

Instead I will just mention that engineers in this field work with turbine maps which are very much like the maps already discussed for the compressor. Such engineers deal with: coupling compressors and turbines and matching them to the needs of the reciprocating engine; aftercooling of the compressed charge; the fact that even at steady-engine operating conditions the flow through the turbomachinery is periodic, whereas the maps are based on steady-flow bench tests; transient response of the whole engine system; and finally alternative devices that compete with the turbomachines. Examples of such alternatives include an exhaust turbine driven refrigerator compressor to

cool the inlet charge rather than compress it, Helmich (1965), or a device called the Comprex in which air is compressed by means of exhaust pressure waves and momentary direct contact between the exhaust stream and the fresh air (Gaschler, Eib, and Rhode, 1983).

7.10 SWIRL AND SQUISH

Swirl refers to a rotational flow within the cylinder about its axis. Swirl is used in some gasoline engines to promote a fast burn and is one of two principal means to ensure rapid mixing between fuel and air in direct-injected diesel or stratified charge engines. Diesel engines without swirl are said to be quiescent and the intensity of the fuel injection is instead relied upon to mix the fuel and air.

Squish is a radial flow most commonly associated with direct-injection engines in which the combustion chamber is a cup located within the piston. The cup is there to amplify swirl generated during the intake process and squish is a necessary byproduct of using a cup.

The swirl level at the end of the compression process is dependent upon the swirl generated during the intake process and how much it is amplified during the compression process. The induction swirl is generated either by tangentially directing the flow into the cylinder or by preswirling the incoming flow by use of a helical port.

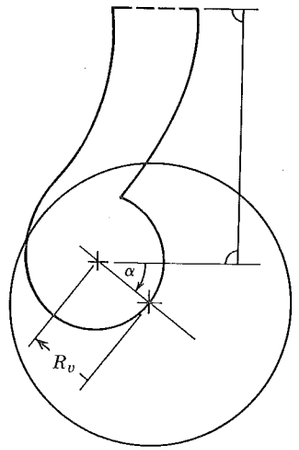

Figure 7-25 Sketch of the intake port in the baseline configuration, showing the definition of the parameters R_v and α (Uzkan, Borgnakke, and Morel 1983). Reprinted with permission © 1983. Society of Automotive Engineers, Inc.

The helical ports are generally more compact than directed ports. They are capable of producing more swirl than directed ports at low lifts but are inferior at higher lifts. Either design creates swirl at the expense of volumetric efficiency. In trying to compromise the port design for both good swirl and volumetric efficiency, current high swirl ports are in part both directed and helical.

Some parameters to consider in the design of a port are shown in Fig. 7-25. These are the radius of the valve offset R_v and the orientation angle α. Development work, like that for maximizing the discharge coefficient, is typically done on a steady-flow bench. One way in which the swirl produced can be measured is shown in Fig. 7-26. A honeycomb structure of low mass, supported by a low-friction air bearing straightens the flow. The change in angular momentum of the flow applies a torque to the honeycomb which is measured by recording the force required to restrain it. The swirl is proportional to that torque.

The efficiency of the port as a swirl producer is characterized by a swirl coefficient defined as

$$C_s = \frac{\tau}{(\dot{m}Ub)/2} \tag{7.60}$$

where

τ = torque applied to honeycomb
$\dot{m}$ = mass flow rate
U = discharge velocity of gas
b = cylinder bore

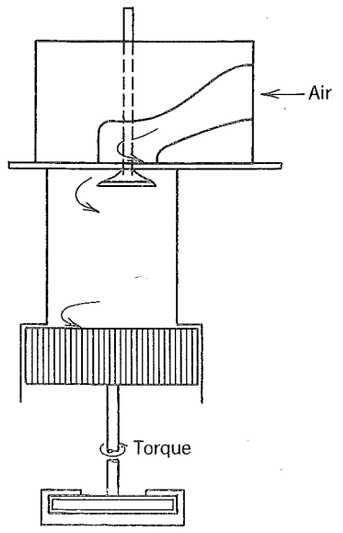

Figure 7-26 Steady-state flow and swirl system (Uzkan et al., 1983).

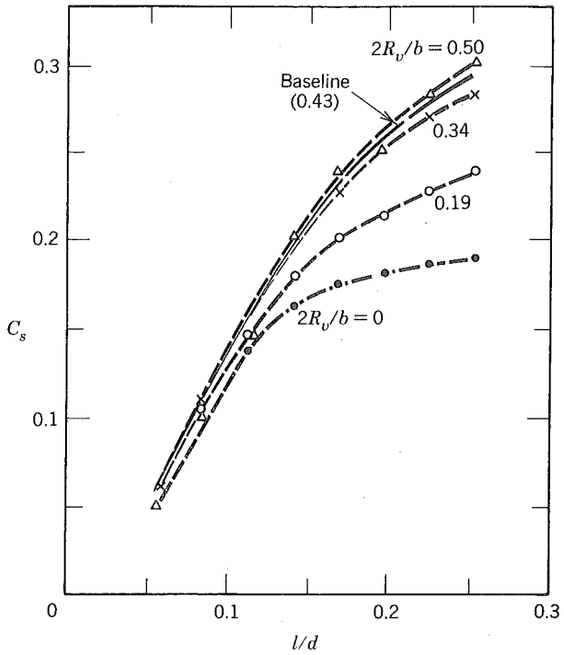

Figure 7-27 Effect of valve offset from the cylinder center line on swirl coefficient. Pressure differential set at 2000 Pa (20 cm H_2O) (Uzkan et al., 1983).

This parameter assigns unity to the case where the inlet flow issues tangentially at the cylinder wall with the discharge velocity.

Some results obtained using prototypical hardware that allowed variation in the valve offset and port orientation are given in Fig. 7-27 and 7-28. They show that the swirl coefficient varies in magnitude from 0 to 0.3, that it increases with the valve lift or offset, and that the port orientation is important only at the larger lifts. Notice too that even at zero offset, the port is producing swirl because of the helical path upstream of the valve.

Although the swirl coefficient characterizes the angular momentum of the flow by a single number, in fact, many different velocity distributions within the cylinder can yield the same angular momentum. Detailed resolution of the flow is a subject of current research that is taking advantage of recent developments in instrumentation and computer science.

With the advent of the laser, it has become possible to measure local and instantaneous velocity, temperature, and some species concentrations within reacting flows without insertion of the instrusive probe required in the familiar examples of thermocouples and pitot tubes. Figure 7-29 shows an arrangement for measuring velocity using a technique called Laser Doppler Velocimetry (LDV).

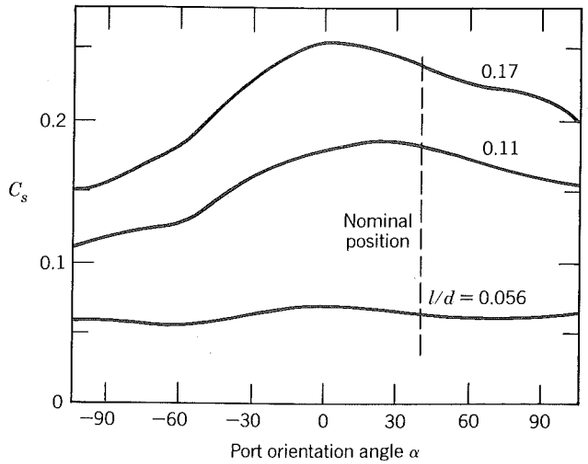

Figure 7-28 Effect of inlet port orientation angle on swirl coefficient at several valve lifts. Pressure differential set at 2500 Pa (25 cm H_2O) (Uzkan et al., 1983).

The beam from an argon ion laser is split into two beams which are then focused to a small volume within the flow. Small particles, about one half micron in diameter, are deliberately added to the flow to track the gas speed. As these particles pass through the probe volume made by the intersecting laser beams, they reflect, or as it is more properly called, scatter, radiation in all directions. In this case the radiation scattered in the forward direction is collected by a lens and focused onto a photomultiplier to measure its intensity.

Since the particles are moving with respect to the photomultiplier, the frequency of the light scattered is altered by the Doppler effect. Electronics filter and process and signal to detect the frequency shift that through a calibration constant is proportional to the particle velocity.

The arrangement shown in Fig. 7-29*a* measures the axial component of velocity. By rotating the laser beams into different planes, the velocity can be resolved into all three components. The shifter is an optical device for discriminating between a forward and backwards velocity. By moving the probe volume, the velocity can be measured at different points within the cylinder. The instrument response is very fast and the system measures the instantaneous velocity. In this steady flow that means the signal can be processed to yield the mean velocity and the velocity fluctuations due to turbulence.

Figure 7-30 shows results obtained for the high swirl port and the low swirl port of Figure 7-29*b*. The flow is three dimensional and finding a means of portraying the results is in itself a challenge. The figures shown are the results of measurements made at 80 points within the cylinder, of doing a three-dimensional nonlinear interpolation to find velocities in between the

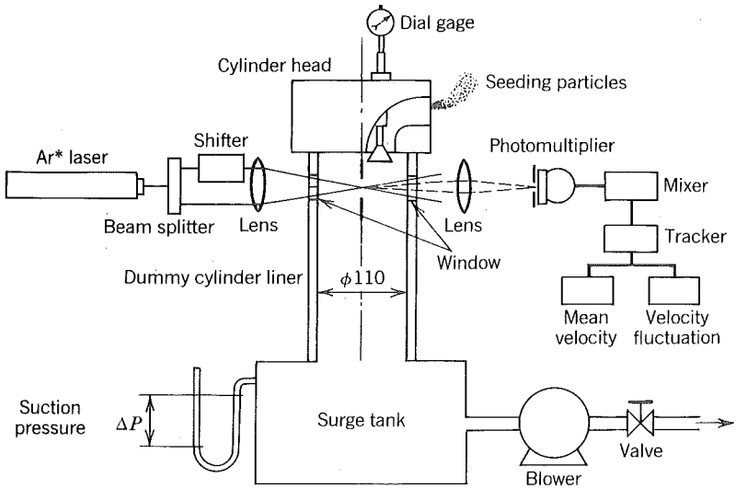

(a)

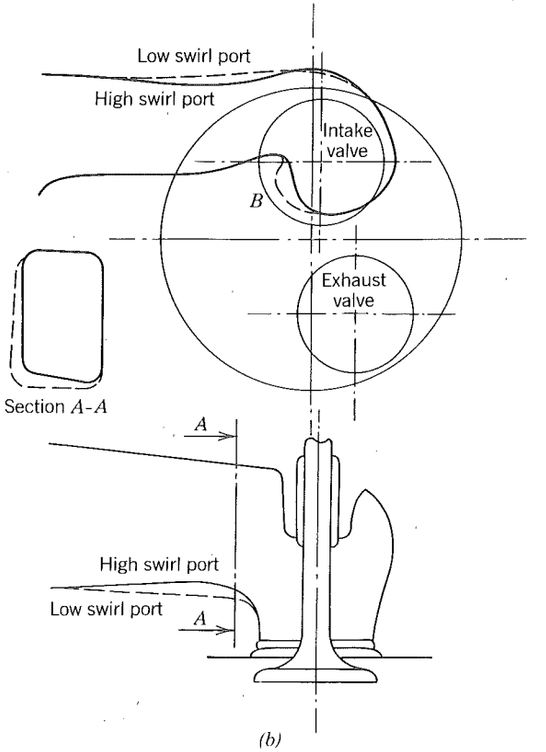

(b)

Figure 7-29 (*a*) Arrangement of steady flow test rig and LDV (Kajiyama, Mishida, Murakami, Arai, and Hiroyasu, 1984). (*b*) Profiles of inlet ports.

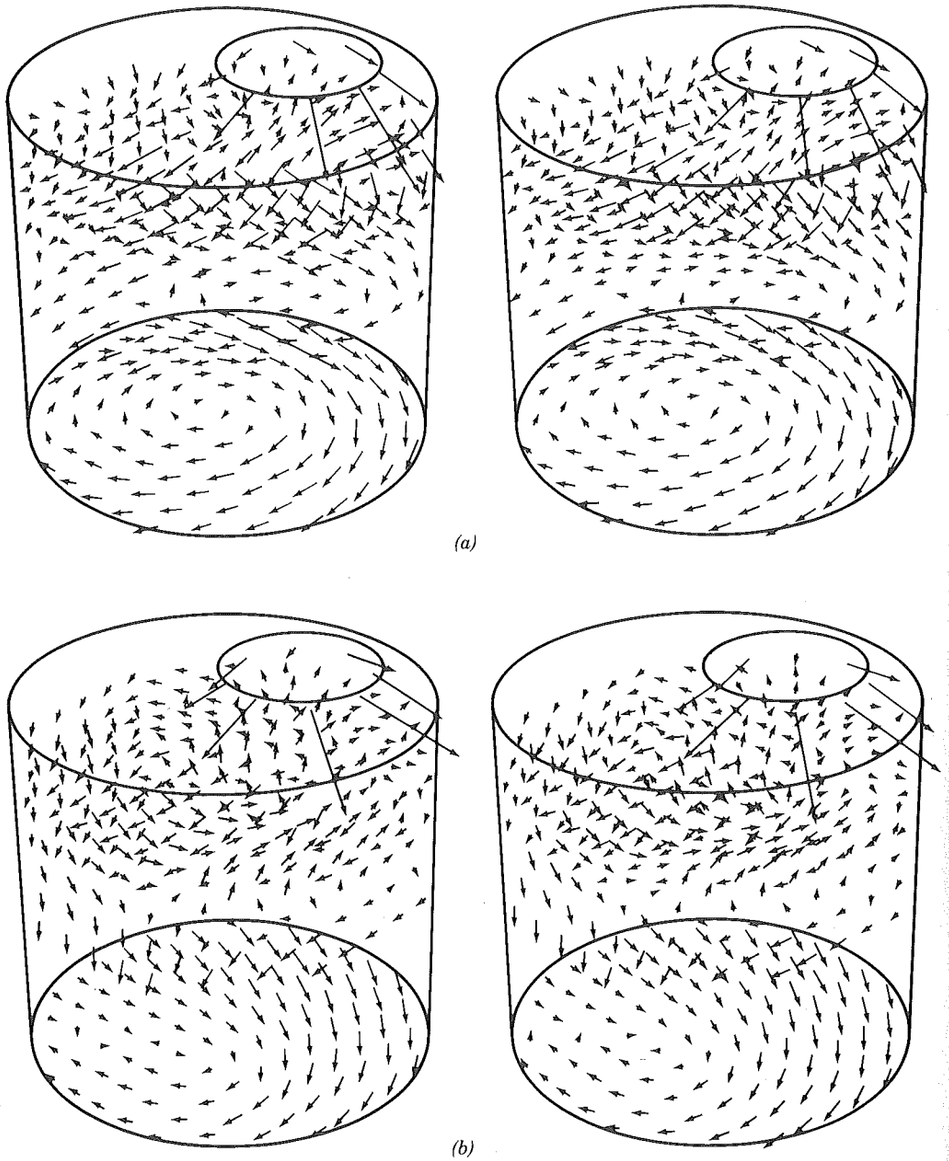

Figure 7-30 Perspective views of air flow through an inlet valve. (*a*) High swirl port. (*b*) Low swirl port (Kajiyama et al., 1984). Reprinted with permission © 1984. Society of Automotive Engineers, Inc.

measurement points, and of designing and executing a computer plotting routine to produce a stereographic display.

These figures are best examined by viewing them through an instrument called a stereoscope, a rather inexpensive device often found in laboratories involved with reading topographical maps. Some people can force their left eye and right eye to focus on the left and right perspectives, respectively, thereby obtaining a stereo-image. Either way, the stereo-image reveals the jet nature of the flow at the valve periphery, the collision of that jet with the cylinder wall, and the establishment of a swirl that is by no means like a solid body rotation or even axisymmetrical.

Measurements like those just described are possible in an operating engine; although to date sacrifices have been made in the engine geometry in order to provide optical access. In fact, research engines are built in which optical access becomes one of the primary design constraints. An example of such an engine is shown in Fig. 7-31. This particular engine is a direct-injection stratified-charge (DISC) engine with a disk-shaped combustion chamber. Optical access is achieved by locating the valves, the fuel injector, and the spark plug circumferentially. This clearly compromises the engine's performance, especially the volumetric efficiency. Furthermore, a direct-injection stratified-charge engine (e.g., Fig. 1-36) will usually have a bowl-in-piston combustion chamber to amplify the swirl during the compression stroke.

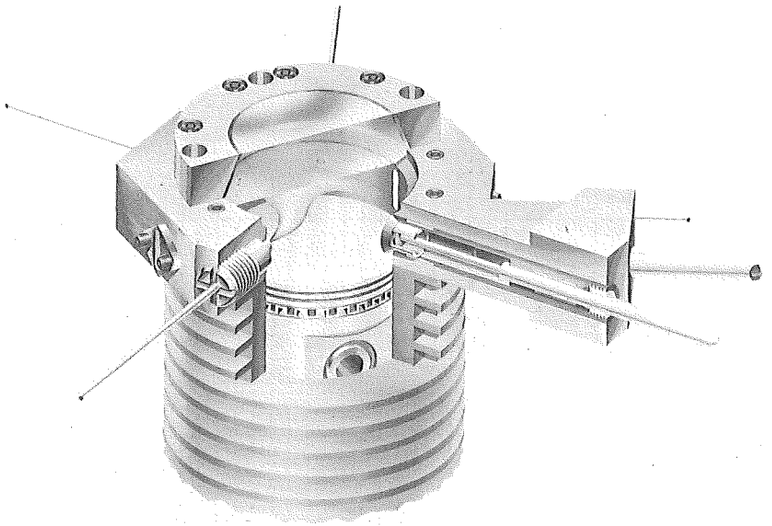

Figure 7-31 Optical direct injection stratified charge engine has a simple combustion chamber shape. Valves, injector, and spark plug are located in the side wall. Three windows provide optical access (Johnston, Robinson, Rorke, Smith, and Witze, 1979).

The reader must be wondering how the results can be applied when the engine geometry is not representative of what would be used in practice. The experiments are justified in that theoretical calculations are being developed to explain engine geometry effects. These computations should be capable of predicting performance in either a specially constructed research engine or a mass-produced production engine.

Consider for example the finite difference grid shown in Fig. 7-32. Using this grid, made to match a specially constructed research engine, numerical solutions to differential conservation equations for mass, momentum, energy, and turbulence parameters are obtained. Since the equations for the turbulence parameters are not rigorous but rather are modeled, the assumptions used in their development need to be checked. They are checked by comparing the

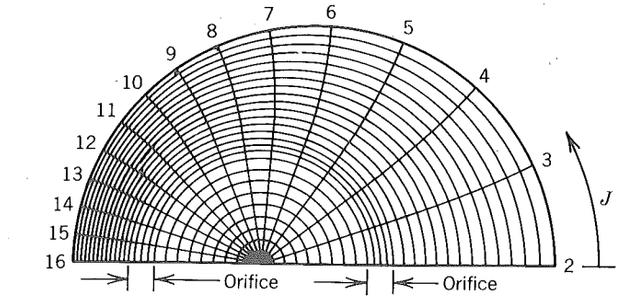

(a)

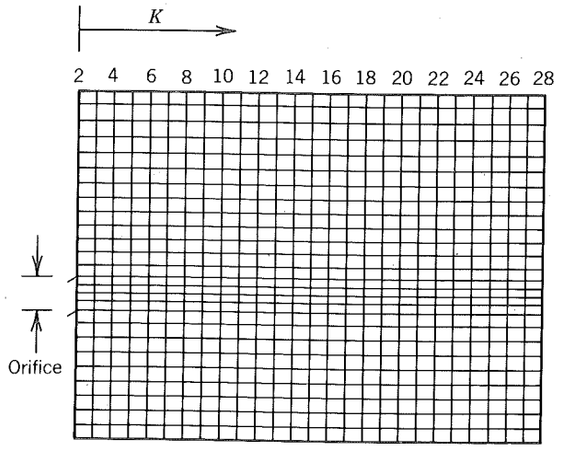

(b)

Figure 7-32 Grid employed for annulus test case. (*a*) Plan view. (*b*) Elevation view, plane J = 2. (Gosman, Tsui, and Watkins 1984).

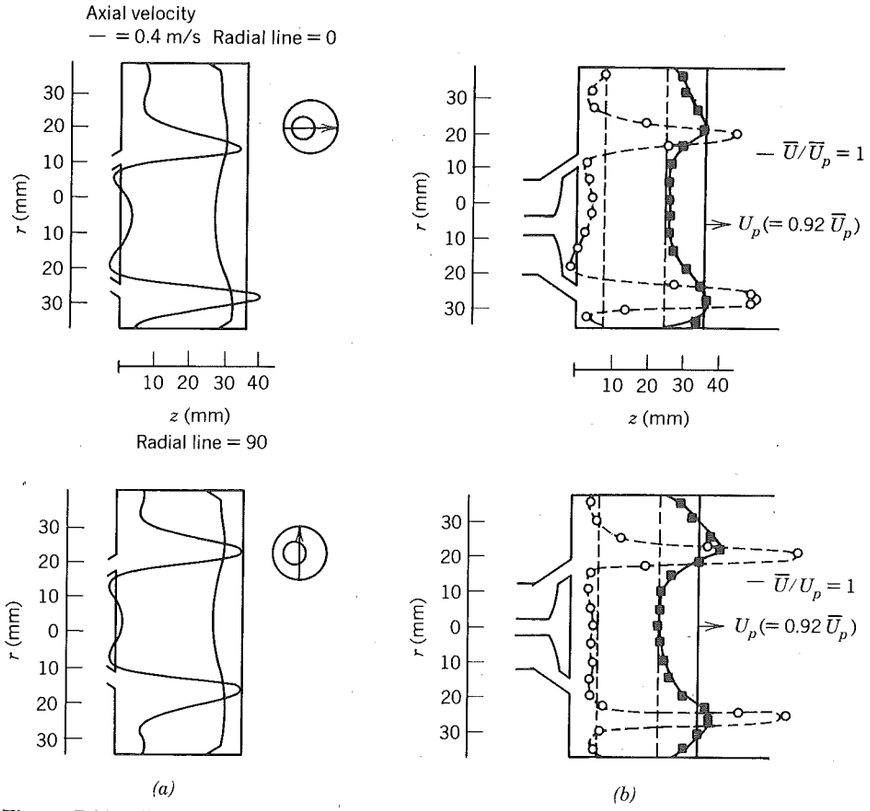

(a) (b)

Figure 7-33 Comparison of predicted axial velocity profiles with experimental data at 36°CA for annulus case. (*a*) Predictions. (*b*) Measurements (Gosman et al., 1984).

numerical predictions of velocity with those that can be measured. Figure 7-33 shows that good agreement can be obtained for the axial velocity profiles. If good agreement can be obtained for all the velocity profiles and at all crank angles, then the turbulence model can be assumed valid and thus applicable to the grid shown in Fig. 7-34. Solution for this grid represents the problem of interest and we assume that since the computations worked for the research engine, they will work here too.

The calculations just described are not yet practical for use as a design tool. The validation process is still going on, the calculations require the largest and fastest computers available, and there are esoteric issues that need to be dealt with, the most important of which deal with specifying initial conditions throughout the flow and boundary conditions at the valve.

To circumvent these problems and provide interim design tools, models have been developed that are directed only at predicting the time-dependent

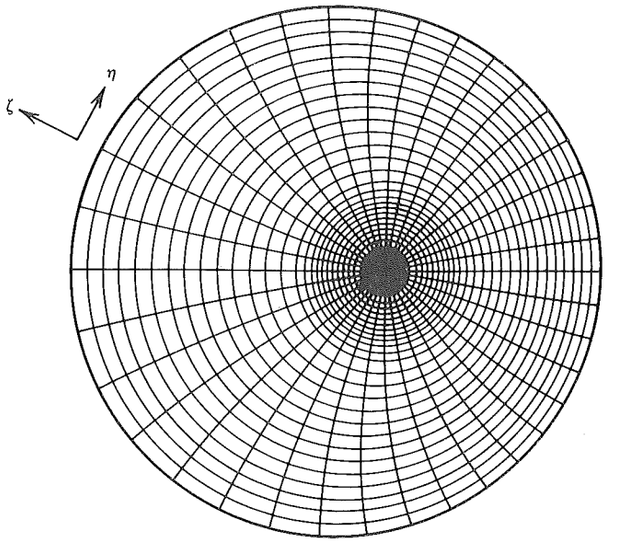

Figure 7-34 Illustration of general grid arrangement. (*a*) Plan view. (*b*) Elevation view (Gosman et al., 1984).

angular momentum of the flow without predicting the details of the velocity distribution. Computationally they are very much like those described earlier for predicting volumetric efficiency.

Ordinary differential equations are solved that now include conservation of angular momentum. A quasi-steady assumption is made that the instantaneous rate at which angular momentum comes into the cylinder is to be

computed using swirl coefficients deduced from steady-state bench tests. Angular momentum within the cylinder is destroyed by fluid friction. The rate expression for that destruction has to be modeled and undetermined constants selected so that results predicted are consistent with experimental data.

Results obtained using such a model are shown in Fig. 7-35 to illustrate how a cup within the piston amplifies swirl during the compression stroke.

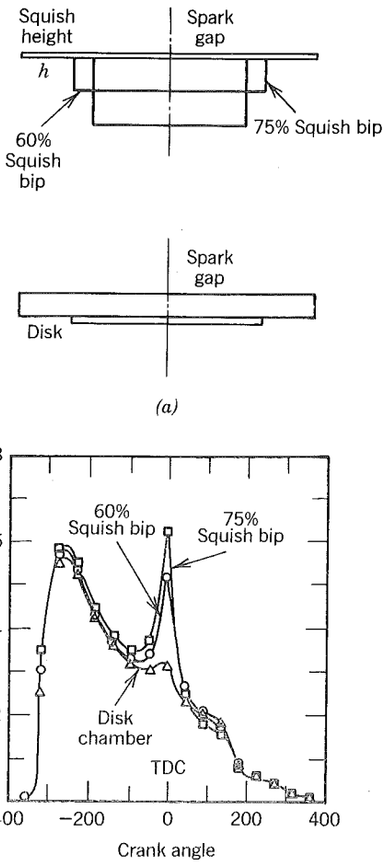

Figure 7-35 (*a*) Combustion chambers investigated: $h = 0.05$ in. (1.27 mm), 10:1 compression ratio. 75% squish bip means that the cross-sectional area of the "bowl in piston" is 25% of the piston area. (*b*) Computed swirl ratio (swirl rpm/engine rpm) versus crank angle: 1500 rpm, WOT, 16:1 A/F ratio, 0% EGR (Belaire, Davis, Kent, and Tabaczynski, 1983).

Here swirl is defined as the solid body rotational speed of the fluid that has the same angular momentum as the actual flow. It is normalized by the engine speed. Notice that in these cases, which are typical, the swirl can be anywhere from zero to six times the engine speed.

The angular momentum of the flow increases only during the intake process because of the angular momentum convected in; otherwise it is always decaying because of fluid friction. Near top center the swirl increases and decreases in a rather short period over which the angular momentum is always decaying. The swirl is proportional to the angular momentum but it is also inversely proportional to the moment of inertia. At top center the moment of inertia goes through a minimum in a manner dependent upon the design of the piston cup. The deeper the bowl (at constant compression ratio), the greater is the change and the greater is the swirl amplification, as shown in Fig. 7-35.

Incorporation of a bowl into the piston induces another fluid motion called squish. This can be appreciated in terms of a rather simple argument based on Fig. 7-36. The density within the cylinder at any time is more or less uniform during the compression stroke. Thus, at any instant, the mass within any of the zones labeled (1), (2), and (3) is proportional to the volume in these zones at any time. During compression, zones (1) and (2) are getting smaller whereas zone (3) remains fixed. Thus, during compression, mass must flow out of zones (1) and (2) into zone (3). The velocity of the gas crossing the control surface between zones (1) and (2) is called the squish velocity and zone (1) is called the squish zone.

When, in fact, the density is always uniform (though time dependent), the squish velocity is dependent only on the engine cylinder geometry and the

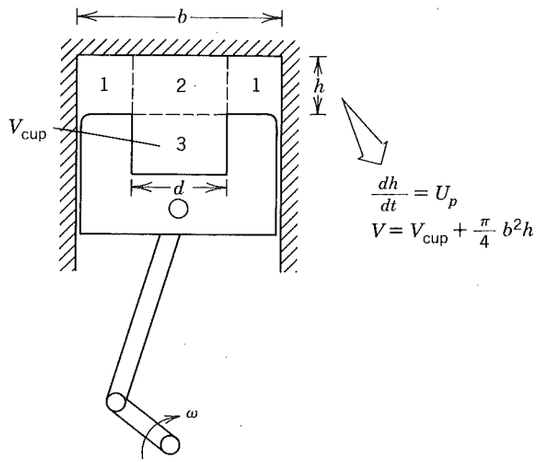

Figure 7-36 The equation of continuity applied to the control volume defined by zone 1 yields the squish velocity.

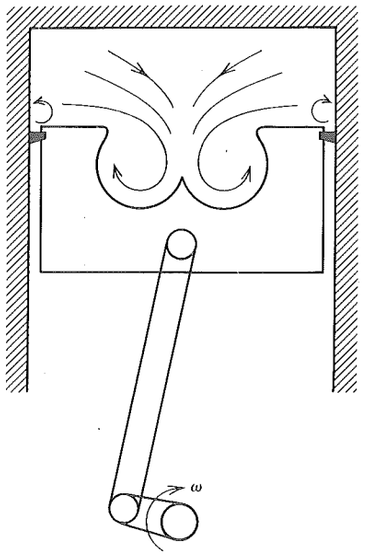

Figure 7-37 Squish also generates a swirl about a circumferential axis in piston bowls.

rotational speed. Application of the equation of continuity to zone (1), assuming a one-dimensional flow across the control surface yields the following expression for the ratio of squish velocity to instantaneous piston speed.

$$\frac{U_s}{U_p} = \frac{b^2 - d^2}{4dh} \frac{V_{cup}}{V} \tag{7.61}$$

The squish, although a byproduct of swirl control, is in itself useful. In the course of spilling into the piston cup, it generates turbulence as well as another rotational flow, see Fig. 7-37. The resultant flow within the cup resembles a rotating torus with an internal swirl about a circumferential axis.

Piston cups within direct injection engines have evolved into different shapes, Fig. 1-28, 1-29, 1-36, 1-38, and 1-41, for purposes of swirl amplification and turbulence generation. It is difficult to draw any further generalizations and that is reflected in that fact the design of the cup shape remains highly empirical.

It is important to reiterate the role of air motion in direct-injected engines. As fuel is injected, the swirl convects it away from the fuel injector making fresh air available for the fuel about to be injected. It has been said, though equivocally, that the period of the swirl ought to equal that of the fuel injection divided by the number of holes in the injection nozzle, thereby avoiding collision of the first and last elements of fuel injected. This mixing by convection is often called large-scale mixing to distinguish it from the smaller

scale mixing caused by turbulence, and because the diameter of the swirling flow is on the order of the combustion chamber diameter whereas the randomly superimposed vortices due to turbulence are much smaller.

It was also mentioned earlier that large-scale mixing and turbulence generation can also be achieved by a high pressure fuel injection into quiescent air. In this case, the fuel rushes into the cylinder dragging air with it, thus creating air motion to ensure that fresh air is available to the fuel about to be injected. In all direct-injected engines, the large-scale mixing is partly achieved by swirl and partly achieved by fuel injection induced air motion. The design employed is a compromise of many conflicting demands. Creation of swirl hinders volumetric efficiency and increases convective heat losses. Reliance on fuel injection induced air motion requires a higher injection pressure and thus a more costly fuel injection system.

On this scale of reliance between swirl and fuel injection induced air motion to effect large-scale mixing, there are limits to the amount of swirl that can be used effectively to minimize demands on the fuel injection system. Herein lies one of the primary reasons for building divided-chamber, or, as they are often called, indirect-injection engines; less reliance on air motion induced by the fuel injection is required to effect large-scale mixing.

Examine Fig. 1-25 through 1-27. In each of these engines combustion occurs in a prechamber or swirl chamber. During the compression stroke air is forced to flow into these chambers establishing three-dimensional air motion and generating turbulence. Because of the geometries involve, it is harder to distinguish large-scale motion from small-scale motion because the many scales between are partly responsible for the better mixing that can be realized. The other reason these designs can effect better mixing is that the pressure rise during combustion creates a flow out of the antechamber and back into the cylinder.

The velocities of that backflow can be rather high, creating turbulence at the expense of an attendant head loss. As can be seen most clearly in Fig. 1-25, passages are often contained within the piston top or organize that flow into the cylinder for large-scale mixing of the combustion products and the cylinder air.

7.11 TURBULENCE

Turbulent flow can be envisioned as mean flow upon which are superimposed vortices of different sizes randomly dispersed in the flow. The vortices have finite lifetimes and appear to be born at random times. The axis of the vortices also assume random orientations. There are even vortices within vortices. It is not until the flow is analyzed statistically that any regularity begins to appear.

Flows that are statistically steady are treated using time averaging. Flows that are statistically periodic, as in the case with intermittent internal combustion engines, are treated using ensemble averaging. For example the ensemble

average velocity is given by

$$\bar{u}_i(x,\theta) = \frac{1}{N}\sum_{j=1}^{N} u_i(x,\theta,j) \tag{7.62}$$

where N is the number of cycles averaged and θ varies from 0 to 4π for a four-stroke engine and from 0 to 2π for a two-stroke engine.

The left-hand side of Eq. (7.62) is read as the ensemble average of the ith velocity component at position x within the flow and at a time corresponding to the crank angle θ. The velocity summed on the right-hand side is the ith component of velocity at position x and angle θ for the jth cycle.

To define the instantaneous turbulence within a cycle, one writes

$$u_i(x,\theta,j) = \bar{u}_i(x,\theta) + u_i'(x,\theta,j) \tag{7.63}$$

where u_i' is the turbulent fluctuation. To quantify the magnitude of the turbulent fluctuations, a root mean square is determined by ensemble averaging

$$u_i'(x,\theta) = \left[\frac{1}{N}\sum_{j=1}^{N} u_i'^2(x,\theta,j)\right]^{1/2} \tag{7.64}$$

Turbulence characteristics of flows in engines have been measured using both hot-wire anemometry and the now-prefered technique of laser doppler velocimetry which was discussed in the previous section. The two techniques are critically compared by Witze (1980). One of the most important conclusions reached to date is that the magnitude of the fluctuating component increases with engine speed.

Figure 7-38 shows results obtained for flows near top center by a number of investigators using motored engines. These results cover a range of engine configurations including engines with and without swirl. It seems that the order of magnitude of the turbulent velocity depends primarily on the piston speed. Of course there are differences from engine to engine at the same piston speed. The differences are caused partly by differences in the engine design and partly because flow cannot be quantitatively characterized by a measurement of just one velocity component at just one point. In the same engine with and without swirl, it can be seen that turbulent velocity is increased by swirling the flow. Liou, Hall, Santavicca, and Bracco (1984) conclude from these results that in the absence of data one can estimate that the order of magnitude of the top center turbulent velocity is one half the mean piston speed

$$u' \approx \tfrac{1}{2}\bar{U}_p \tag{7.65}$$

To fully characterize a turbulent flow, one needs to also specify the average size of the random vortices that make up the turbulence. Researchers in this field deal with three different sizes: (1) the integral scale l that represents the largest possible size that confining geometry of the walls will

Summary of Measurement Conditions for rpm Scaling Studies

RESEARCHERS[b]	YEAR	TECHNIQUE	MOTORED FIRING	CHAMBER CONFIGURATION	VALVED PORTED	SWIRL NO SWIRL
WINSOR and PATTERSON	1973	HW	M	(Simple) pancake	V(2)	NS
LANCASTER	1976	HW	M	(Simple) pancake	V(2)	S NS
WITZE	1977	HW	M	(Complex) L-Head	V(2)	NS
WAKISAKA et al.	1979	HW	M	(Simple) pancake	V(2)	S
MATTAVI et al.	1980	HW	M	(Simple) open (complex) wedge	V(2)	NS
GROFF et al.	1980	HW	M	(Complex) wedge	V(2)	S NS
RASK	1979	LDV	M	(Complex) L-head	V(2)	S
COLE and SWORDS	1978	LDV	M	(Simple) pancake	V(2)	NS
LIOU et al.	1982	LDV	M	(Simple) pancake	Ported	S NS
LIOU et al.	1983	LDV	M	(Simple) open	V(4)	NS

ANISO	Anisotropy	M	Motoring	WOT	Wide-open throttle
F	Firing	NS	No swirl	λ	Integral length scale
HOM	Homogeniety	S	Swirl	λ	Micro length scale
INHOM	Inhomogeniety	T	Integral time scale	τ	Micro time scale
ISO	Isotropy	V(2)	Valved engine with two valves	u^t	Fluctuation intensity

[a] Numbers in brackets refer to number of measurement points used to show rpm scaling.
[b] Complete citations may be found in Liou, Hall, Santavicca, and Bracco (1984)

allow; (2) the Taylor microscale η which is useful in estimating the mean strain rate of the turbulence; (3) the Kolmogorov microscale η which is the smallest size viscous damping will allow.

Dimensional analysis of simple turbulent flows leads to the following relationships between the three scales.

$$\frac{\lambda}{l} = \left(\frac{15}{C_1}\right)^{1/2} R_l^{-1/2} \tag{7.66}$$

$$\frac{\eta}{l} = C_1^{-1/4} R_l^{-3/4} \tag{7.67}$$

where the constant C_1 is number unique to the flow of interest but whose order of magnitude is unity, Tennekes and Lumley (1972). The Reynolds number

RPM	COMPRESSION RATIO	LOAD	MEASUREMENT POINTS[a]	MEASURED PARAMETERS	HOM/ISO OF MEASURED TURBULENCE
500–1500		WOT	6 [1–5]	$\bar{u}$ u^t	HOM ISO
1000–2000	8.84–10.55	0.25 0.50 0.75	1	$\bar{u}u^t$ T τ λ λ	ISO
500–2500	7.25	WOT	5 [1]	$\bar{u}u^t$ T τ λ λ	INHOM
600–1200	4.1	WOT	5 [1]	$\bar{u}u^t$ T τ λ λ	INHOM
1250–2050	8.4	0.43	2 [1]	$\bar{u}$ u^t	ISO(OPEN) ANISO (WEDGE
500–2000	6.85	0.55	3 [1]	$\bar{u}$ u^t	HOM ANISO
270–800	7	WOT	26 [1]	$\bar{u}$ u^t	HOM
400–1200	7	0.25–WOT	9 [2]	$\bar{u}$ u^t	ISO
1200–2400	13.5	1.00	6 [6] 12 [4]	$\bar{u}$ u^t T τ	ISO HOM
300–1800	8.5	WOT	5 [5]	$\bar{u}$ u^t	HOM

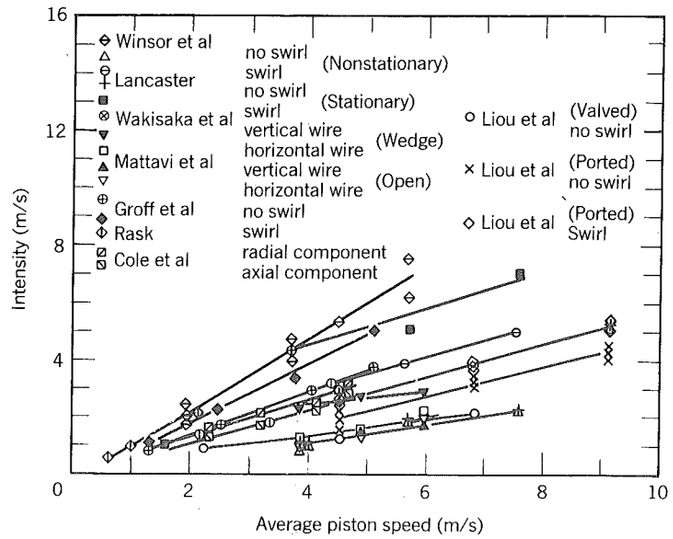

Figure 7-38 A comparison of fluctuation or turbulence intensity versus average piston speed measured by various researchers (Liou et al., 1984).

shown is based on the integral scale and the turbulent velocity

$$R_l = \frac{u'l}{\nu} \tag{7.68}$$

Thus we see that if the integral scale can be determined, so can the other scales. The integral scale is the largest possible turbulent vortex size that the confining geometry allows. Clearly in a pipe no vortices can exist that are larger than the diameter. In simple three-dimensional enclosures, the integral scale is determined by the surface to volume ratio

$$l = \frac{C_2 V}{A} \tag{7.69}$$

Here again, C_2 will be unique to a particular flow but a constant of order unity.

For a cylinder of height h and diameter b, one obtains

$$l = \frac{\frac{1}{2}C_2 b^2 h}{b^2 + 2bh} \tag{7.70}$$

Inspection of this equation reveals that for a cylindrical combustion chamber, one should expect near top center, where $h \ll b$, that the integral scale be roughly equal to the clearance height h; whereas near bottom center, where $h \gg b$, the integral scale should be roughly equal to the bore. With a cylindrical cup in the piston, near top center the integral scale would be roughly the cup diameter.

At this point, perhaps the most pertinent thing the reader should note is that as the turbulent Reynolds number goes up, the smaller microscales go down according to Eq. (7.66) and (7.67). Since the turbulence in an engine increases with piston speed and the integral scale is independent of engine speed, we should expect that as engine speed goes up, the microscales of the turbulence will go down. In examining the results shown in Fig. 7-39, one cannot help but be impressed with this prediction.

Finally, some comments on the utility of these results and their limitations. First the utility: The simplest models of turbulent diffusion for momentum, heat, or mass assume that the effective diffusivities are given in each case, respectively, by

$$\nu_e = C_3 u'l + \nu \tag{7.71}$$

$$\alpha_e = C_4 u'l + \alpha \tag{7.72}$$

$$\mathscr{D}_e = C_5 u'l + \mathscr{D} \tag{7.73}$$

where each of the constants C_3, C_4, and C_5 are constants of order unity. To calculate a flow then, the appropriate conservation equations are solved with effective diffusivities substituted for the molecular or laminar diffusivities.

Now the limitations: the description of turbulent flows is, of necessity, glossed over and stripped to the barest of essentials. A number of constants

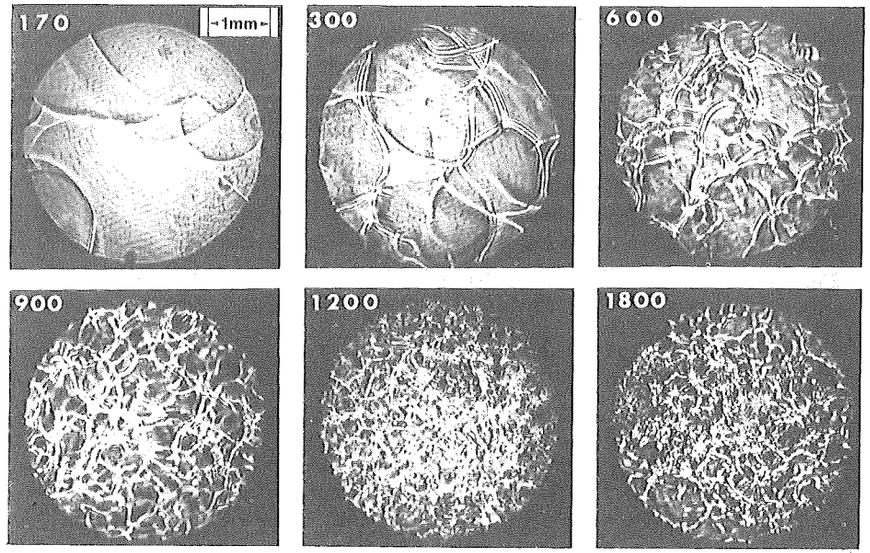

Figure 7-39 Microshadowgraphs of flame propagating toward the viewer showing increased wrinkling as engine speed increases. Engine rpm is indicated in the upper left corner of each photo (Smith, 1982).

(C_i, $i = 1, \ldots, 5$) were introduced that in state of the art models are in fact calculated to be weak functions of flow fields. Turbulence was defined by Eq. (7.64) and it fails to recognize that a part of the fluctuation may be due to cycle to cycle variations in an organized flow that in any one cycle is different from the ensemble mean flow. These more esoteric points are subjects of current research and the reader interested in learning more has no choice but to turn to the current literature. Extensive lists of references can be found in papers by Tabaczynski (1976) and Liou et al. (1984).

7.12 CARBURETION

Carburetors are used on homogeneous-charge engines to meter the fuel flow delivered to an engine in proportion to the air flow. The also serve to mix the fuel with the air and this is done by atomizing the liquid into droplets so that it will evaporate quickly. The basic principle behind a carburetor is shown in Fig. 7-40.

The mass flow between (1) and (4) is determined by the engine speed and throttle position. The pressure at (2) and the fuel to air ratio $\dot{m}_f/\dot{m}_a$ are dependent variables that adjust themselves to match the mass flow $\dot{m}_4 = \dot{m}_f + \dot{m}_a$ that the engine is demanding.

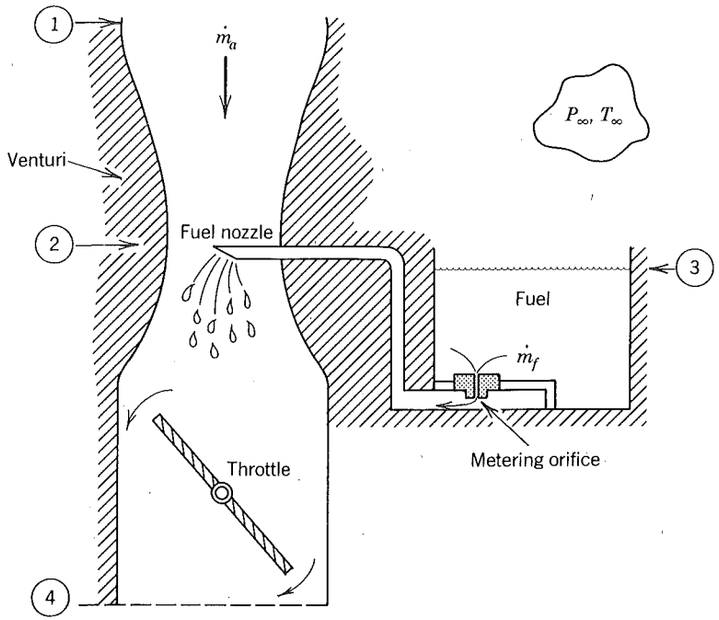

Figure 7-40 The basic principle of a carburetor is that air is accelerated by a venturi. The pressure P_2 is there less than P_1 which is less than the atmospheric pressure P_∞. The pressure difference $P_\infty - P_2$ pushes fuel through the metering orifice in an amount proportional to its effective area A_f^*.

Assuming a steady flow through the carburetor, the air flow is computed assuming that the air is an ideal gas, in which case by Eq. (7.14) one realizes

$$\dot{m}_a = \rho_\infty c_\infty A_a^* \sqrt{\frac{2}{\gamma - 1}\left[\left(\frac{P_2}{P_\infty}\right)^{2/\gamma} - \left(\frac{P_2}{P_\infty}\right)^{(\gamma+1)/\gamma}\right]} \tag{7.74}$$

In Eq. (7.74), c_∞ is the speed of sound in the atmospheric air and A_a^* is the effective flow area at the venturi throat. That flow area is less than that of a circle equal to the venturi throat diameter because of blockage by the fuel nozzle and boundary layers along the venturi walls.

The fuel flow is computed assuming the fuel is incompressible, in which case

$$\dot{m}_f = A_f^* \sqrt{2\rho_f (P_\infty - P_2)} \tag{7.75}$$

where now the area A_f^* is the effective flow area of the metering orifice. According to Obert (1973), the discharge coefficient of metering orifices used in carburetors is typically 0.75; it accounts for boundary layers in the orifice and for the small pressure drop from the orifice to the nozzle.

The maximum flow rate of air that can be flowed through a carburetor occurs when the flow chokes at the venturi nozzle. In this case one has

$$\left(\frac{P_2}{P_\infty}\right)_c = \left(\frac{2}{\gamma + 1}\right)^{\gamma/(\gamma-1)} \tag{7.76}$$

$$\dot{m}_{ac} = \rho_\infty c_\infty A_a^* \sqrt{\left(\frac{2}{\gamma + 1}\right)^{(\gamma+1)/(\gamma-1)}} \tag{7.77}$$

Equation (7.77) follows from (7.74) by substitution of (7.76) for the pressure ratio. This equation is useful in sizing a carburetor venturi; the area A_a^* is solved for in terms of the maximum air flow rate to be encountered.

Let us call the ratio of the air flow to the critical or choked air flow the carburetor demand and give it the symbol $\mathbf{D}_c$; it should be clear that $0 \le \mathbf{D}_c \le 1$. For air, the ratio of specific heats is $\gamma = 1.4$, which when substituted into Eq. (7.74) and (7.77) and solved with (7.75) for the fuel–air ratio yields

$$F = \frac{\dot{m}_f}{\dot{m}_a} = \frac{1.73}{\mathbf{D}_c} \frac{\rho_f}{\rho_\infty} \frac{A_f^*}{A_a^*} \left[\frac{2(P_\infty - P_2)}{\rho_f c_\infty^2}\right]^{1/2} \tag{7.78}$$

By definition, the carburetor demand is then

$$\mathbf{D}_c = 3.86\left[\left(\frac{P_2}{P_\infty}\right)^{1.43} - \left(\frac{P_2}{P_\infty}\right)^{1.71}\right]^{1/2} \tag{7.79}$$

A graph of the fuel–air ratio as a function of carburetor demand is shown in Fig. 7-41 assuming typical values for gasoline properties and different values of the ratio A_f^*/A_a^*. Note that for demands between 20 and 80%, the fuel–air ratio is a weak function of demand and its value is dependent primarily upon the geometric properties of the carburetor through the ratio A_f^*/A_a^*. At demands less than about 20%, the fuel–air ratio would in reality be much less than predicted by Eq. 7.78 because of surface tension effects at the nozzle exit. The simple carburetor just described can be expected then to operate only over the range $0.20 < \mathbf{D}_c < 0.80$.

A complex carburetor uses the simple circuit just described as just one of many circuits used in parallel to achieve a satisfactory fuel–air ratio over a larger range of demands. Since the simple carburetor operates well over most of the demand range it is incorporated into complex carburetors as the main metering system. For low demands, an idle circuit is added; for starting, a choke circuit is used to provide a rich mixture; for high demands, a power circuit is added to deliver a slightly rich fuel–air mixture; and for rapidly changing demands, an accelerating pump is installed.

An example of a carburetor used on small engines is shown in Fig. 7-42. This is called an updraft carburetor because the airflow is up through the venturi, the opposite of that in a downdraft carburetor previously described. Fuel is admitted to the carburetor via a float-controlled needle value. The reservoir or bowl in which the fuel sits is vented to the atmosphere through a

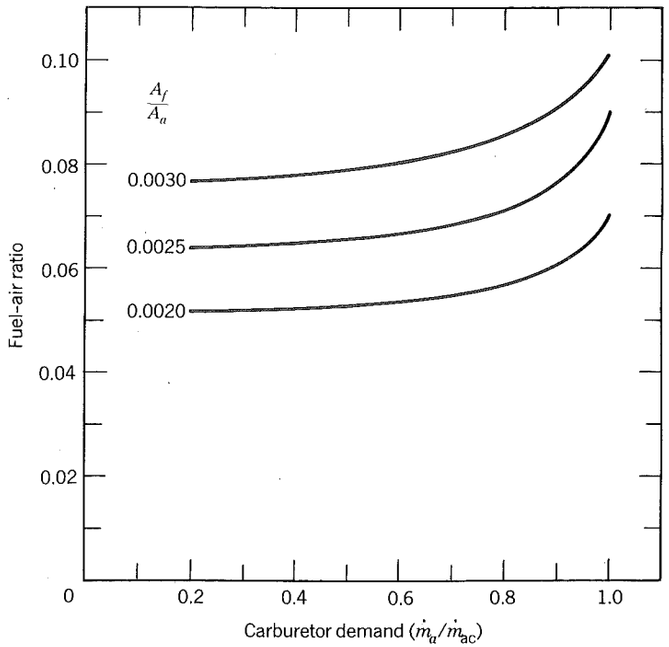

Figure 7-41 The fuel–air ratio as a function of carburetor demand for the system shown in Fig. 7-40. The curves are theoretical based on Eq. (7.78) for $P_\infty = 0.987$ bar, $\rho_f = 749$ kg/m^3, $c_\infty = 346$ m/s, $\rho_\infty = 1.17$ kg/m^3.

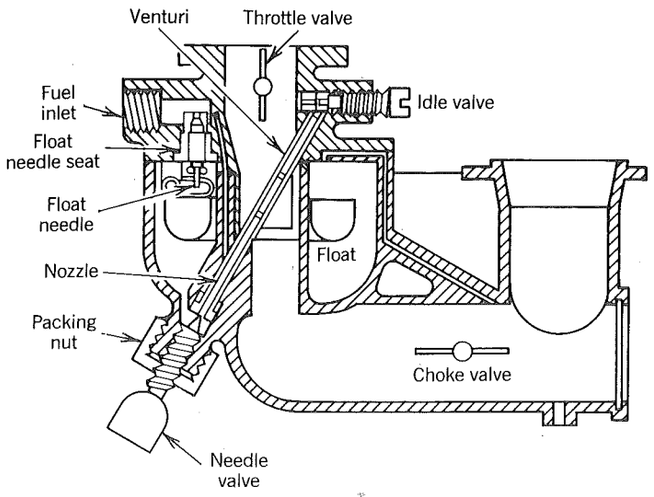

Figure 7-42 An updraft carburetor used on Briggs and Stratton engines. Courtesy Briggs and Stratton.

drilled passage to a point upstream of the choke valve. This ensures that $P_\infty = P_3$ in the context of Fig. 7-40.

Under all demands, the fuel flows through a needle valve that serves as the metering orifice for the main metering system. Use of a needle valve as depicted allows for adjustment of the effective flow area of the orifice. The fuel flows through the nozzle and is admitted to the air stream in part at the venturi through holes drilled normal to the figure and in part at the idle valve. At the wide-open-throttle position shown, the pressure at the idle valve exit will be nearly atmospheric and most of the fuel is admitted to the air at the venturi. At idle, the throttle drops the intake manifold pressure and the idle valve sees a much lower pressure than that at the venturi throat. The result is that the fuel is now admitted at and metered by the idle valve. This idle circuit is in essence the metering system at low demands.

For starting purposes a choke is added. This too is a throttle but it is upstream of the carburetor and can be thought of as acting to lower the P_∞ driving the air into the engine without affecting the P_∞ driving the fuel into the engine.

Automotive carburetors contain these same elements and more. Additional elements to consider include electronic control, accelerating pumps, and power circuits. Aircraft carburetors have, in addition, systems to compensate for the change in barometric pressure because of changes in altitude.

An example of an electronically controlled main metering system is given in Fig. 7-43. The idea is similar to that of the adjustable needle valve used in

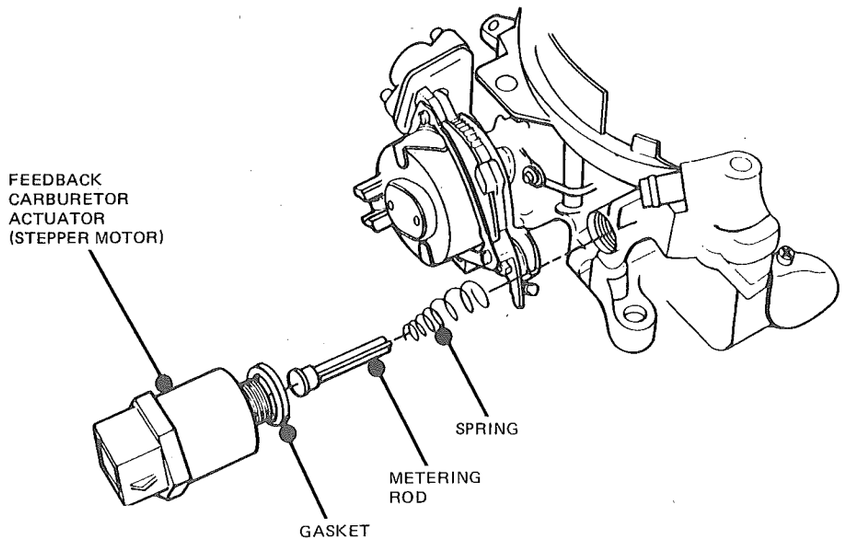

Figure 7-43 A Ford system for electronic control of the fuel–air ratio. In this system the metering rod acts as a valve in an air passage to vary the P_∞ acting on the fuel to a value between P_∞ and P_2. Courtesy Ford Motor Co.

the carburetor of Fig. 7-42 except that a stepper motor adjusts the effective flow area in response to a computer command. That computer is programmed to fix the fuel–air equivalence ratio to a predetermined value dependent upon such parameters as engine speed, inlet pressure, coolant temperature, or exhaust oxygen concentration.

Electronic control of the main metering orifice is an important step toward simplifying carburetors. No longer needed are additional circuits that mechanically respond to engine vacuum or barometric pressure to enrich mixtures during power or provide for altitude compensation. Look at the number of parts in the exploded view of a mechanical carburetor in Fig. 7-44. This carburetor is called a four-barrel carburetor because there are four independent air passages. At light loads, only two, the so called primaries, are used. At high loads, secondary throttles open, allowing use of all four. In addition there is, in the main metering system of each of the primary venturis,

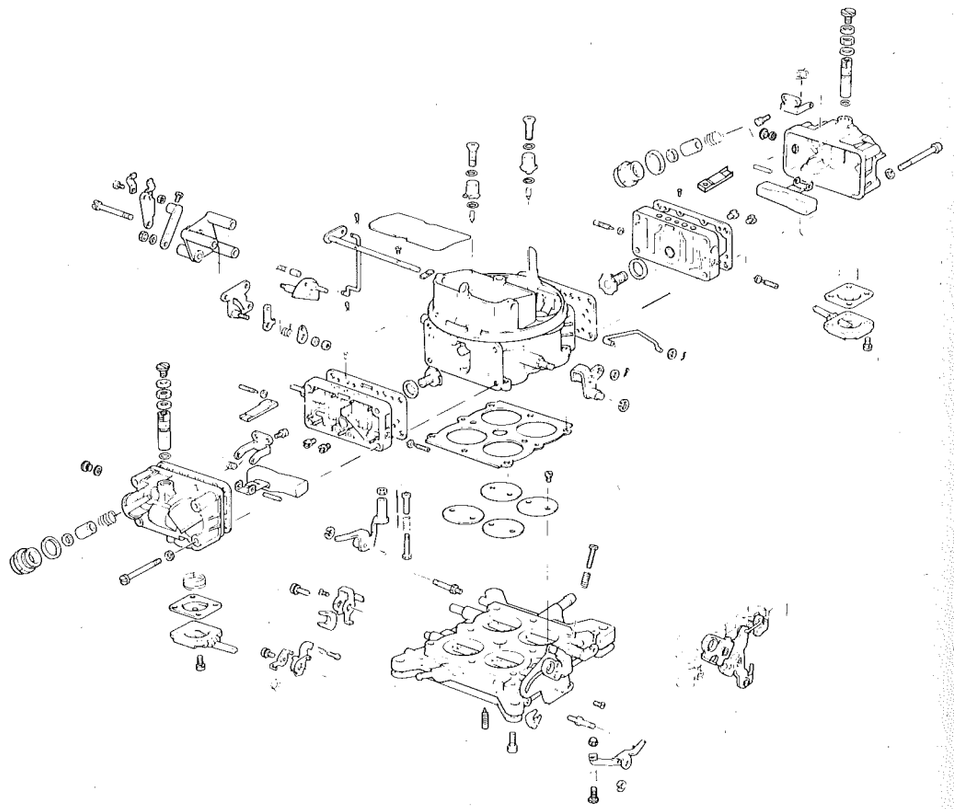

Figure 7-44 Exploded view of a Holley 4150 four-barrel carburetor. Courtesy Colt Industries.

a power valve that opens another metering orifice in parallel with the main metering orifice when the engine vacuum is low. There are even venturis within venturis. All these circuits tailor the shape of the fuel–air ratio versus delivery curve to broaden it out or move it up and down. The accelerator pump, however, serves a different purpose.

Because the fuel is more dense, its inertia is greater than that of the air. During transient operation, the fuel flow lags behind the air flow enough that it has to be compensated for. Accelerator pumps are the means by which this is achieved.

Figure 7-45 depicts the operation of the accelerator pump used in a Holley carburetor. The pump diaphragm is displaced in response to a change in throttle position by a cam actuation. If the diaphragm moves slowly, the drag of the flowing fuel around the sphere used as a check valve is not sufficient to seat it and the fuel simply returns to the reservoir. But if the diaphragm moves quickly, then the inlet check valve will seat, the discharge valve will lift off its seat, and fuel will be injected into the air stream to compensate for the lag in the fuel of the main metering system.

So far, our discussion of carburetors has been limited to the means by which metering is achieved. It is also important that the fuel mostly evaporate before delivery to the engine. If the fuel in the air were to exist as large droplets, then these would collide with walls in the usually tortuous path to the cylinder. Accumulation of liquid fuel on the walls alters in an uncontrolled

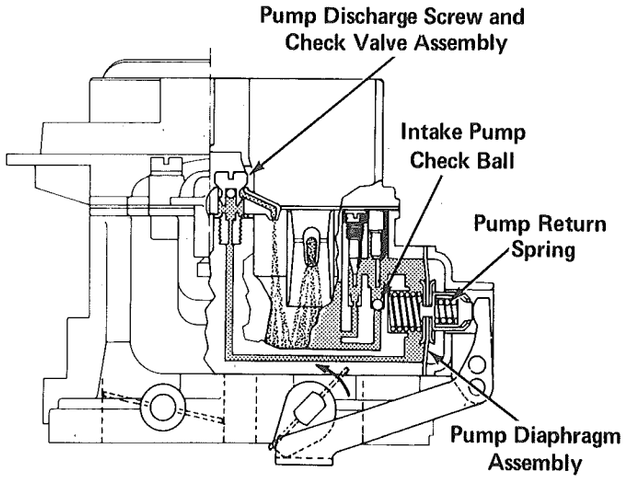

Figure 7-45 Accelerator pump used on a Holley Model 5200 carburetor. Actuation of the pump diaphragm by the accelerator linkage causes fuel to close the intake check valve and open the discharge check valve. Fuel is injected into the air flow as shown. Courtesy Colt Industries.

manner the fuel–air ratio of the fuel delivered to the cylinders. It causes lags and overshoots in the fuel flow with respect to the air flow delivered and it causes variations in the fuel–air ratio from cylinder to cylinder.

Prandtl (1952) argues that the maximum drop diameter than can stably exist in an air stream is

$$d_{\max} = 7.7 \frac{\sigma_f}{\frac{1}{2}\rho_a U_a^2} \tag{7.80}$$

where σ_f is the surface tension of the fuel and U_a is the relative velocity of the air and fuel droplet. Herein lies one reason for the use of booster venturis within venturis: they increase the relative velocity of the air and fuel at the nozzle discharge and thus reduce the maximum size droplet that can be formed.

A boost venturi is illustrated in Fig. 7-46. Also shown is an emulsion tube that with an air bleed mixes some air with the fuel prior to delivery to the discharge nozzle. This reduces the effective surface tension of the droplets thereby reducing further the maximum size of the fuel droplets that will be formed. The effective viscosity of the fuel is also altered, thereby reducing the small flow resistance from the metering orifice to the nozzle, and therefore the

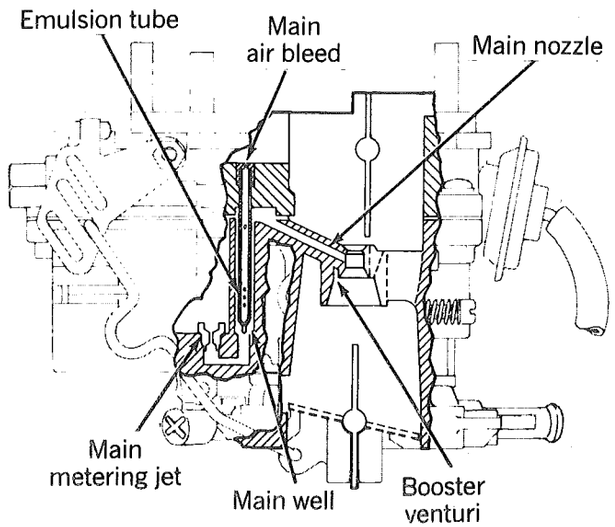

Figure 7-46 Main metering system used on a Holley Model 2210 carburetor. The features shown are typical of most carburetors. Fuel from the float bowl flows through the main metering jet into the main well where it is premixed with a small amount of air. That premixed fuel and air is discharged into the main air flow at the booster venturi. Courtesy Colt Industries.

fuel–air ratio demand curve is altered slightly. This latter effect is especially important at low demands.

7.13 FUEL INJECTION

Carburetors atomize the fuel by processes relying on the air speed being greater than the fuel speed at the fuel nozzle. They also meter the fuel using the air flow as the independent variable. Fuel injection differs in both respects. The fuel speed at the point of delivery is greater than the air speed to atomize the fuel and the fuel is metered proportionally to air flow but not by the air flow itself; rather a pump is used to generate the pressure difference necessary to flow the fuel.

Fuel injection systems can be classified according to the following characteristics:

- ***Single Point***—One fuel injector serves more than one cylinder. Throttle body fuel injection is an example. These systems are used only on homogeneous charge engines.
- ***Multipoint***—One fuel injector per cylinder. These systems are always used on diesel engines and direct-injection stratified-charge engines.
- ***Electronic***—The metering of the fuel by solenoid actuation.
- ***Mechanical***—The metering of the fuel by cam actuation.
- ***Port***—The fuel injector sprays into the air stream at the inlet port.
- ***In-cylinder***—The fuel injector spray is directly into the cylinder.
- ***Low Pressure***—Fuel is injected into gas at a pressure level on the order of the intake pressure.
- ***High Pressure***—Fuel is injected into the cylinder near the end of the compression stroke and therefore into gas at a pressure level on the order of the compression pressure.
- ***Timed or Pulse***—Each injection has a finite duration; controlling the duration's width is the dominant part of the metering scheme. The injection is then timed to begin and end at specific times in the cycle. All in-cylinder injection systems and some port fuel injection systems are timed.
- ***Continuous or Steady***—The fuel is flowing through the injector through all times in the engine cycle. In these systems the fuel is metered by controlling the pressure upstream of the fuel injectors.

With respect to carburetion, fuel injection offers many advantages that design engineers have to evaluate for their cost effectiveness. Foremost among these are the following:

- Increased volumetric efficiency and therefore increased power and torque. This occurs because: A venturi and its attendant head loss are not required; lower gas velocities in the intake manifold are required since the fuel

droplets are smaller; and the intake manifold need not be heated to promote vaporation because the fuel droplets are smaller.

- Better thermal efficiency. This occurs because of the improvements realized in mixture control. With a carburetor, engineers deal with tolerance stack-ups, the shape of fuel–air ratio versus demand curve, and cylinder to cylinder or cycle to cycle variations in fuel–air ratio by ensuring that the leanest cylinder at the leanest demand with the leanest tolerance stackup is still rich enough to burn reliably. This means that on average the engines are running richer than would be realized with no tolerance stackups, a perfectly tailored fuel–air ratio versus demand curve, and no cylinder to cylinder or cycle to cycle variations in fuel–air ratio.
- Lower exhaust emissions for the same reasons better thermal efficiency can be realized but also because during starting, atomization does not depend on cranking speed and during deceleration, the fuel flow may be cut off.
- More fuel tolerant. This is because distribution can be independent of vaporization and therefore of the fuel volatility. Likewise, with improved mixture distribution, the probability that one cylinder is more prone to knock than the others is reduced so a lower octane fuel or higher compression ratio can be used.
- Charge stratification. With timed fuel injection late in the intake process or during the compression stroke, it is possible to stratify the charge, that is, to create a charge in which the fuel–air ratio varies with position in the cylinder. The later in the cycle (with respect to the opening of the intake valve) injection occurs, the more stratification is realized. A rich mixture near the spark plug ensures easy ignition, a lean end gas reduces the tendency to knock, and a lean overall charge has favorable emission characteristics. Less throttling may be required because overall leaner mixtures can be spark ignited.
- Elimination of short circuited fuel in turbo or supercharged four-stroke engines and in all two-stroke engines since the injection can be timed to begin once the exhaust valve or port is closed.

The more one exploits the advantages offered by fuel injection, the greater will be the cost of the engine. A number of fuel injection systems are now discussed in an order that roughly reflects their cost. Carburetors are by far the cheapest of fuel meters, next are single-point systems, followed by port multipoint systems, low-pressure-in cylinder systems, and finally, the high-pressure-in cylinder systems used on diesel engines.

In Chapter 1, Fig. 1-15, an example of a single-point fuel injection system employing a throttle body fuel injector, was briefly discussed. Reexamine that figure paying particular attention to the fuel path. The injector itself is shown more clearly in Fig. 7-47.

At an appropriate time in the engine cycle, a computer issues a command to open and close the pintle nozzle. The pintle is lifted off its seat by a solenoid

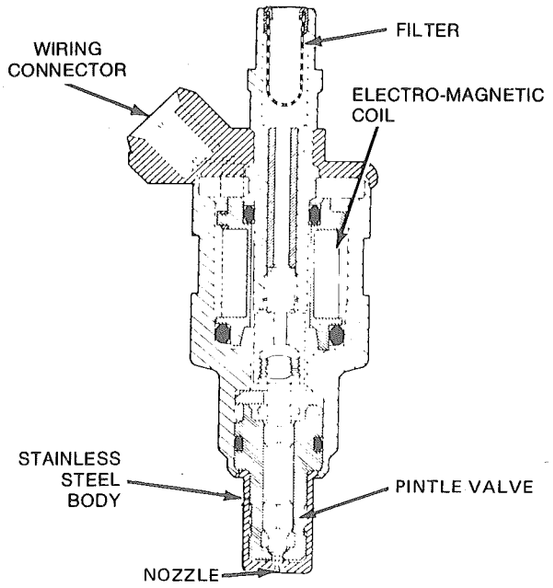

Figure 7-47 A Throttle body fuel injector; the quantity of fuel injected is controlled by the open duration. Courtesy Ford Motor Co.

and the quantity of fuel injected increases more or less linearly with the duration of the open period. Assuming quasi-steady flow through the fuel nozzle, one obtains for the mass of fuel injected in one period the following expression

$$m_f = \int_0^{\Delta t} \dot{m}_f \, dt = \sqrt{2\rho_f \Delta P} \int_0^{\Delta t} A_f^* \, dt \tag{7.81}$$

where ΔP is the difference between the fuel delivery pressure and the air pressure upstream of the throttle. In terms then of an average flow area of the injector nozzle

$$\bar{A}_f = \frac{1}{\Delta t} \int_0^{\Delta t} A_f^* \, dt \tag{7.82}$$

one has

$$m_f = \sqrt{2\rho_f \Delta P}\, \bar{A}_f \Delta t \tag{7.83}$$

and Δt is the open duration of the injection.

The prediction that the mass of fuel injected is linearly proportional to the open duration is borne out by experiment as evidenced by the results shown in Fig. 7-48.

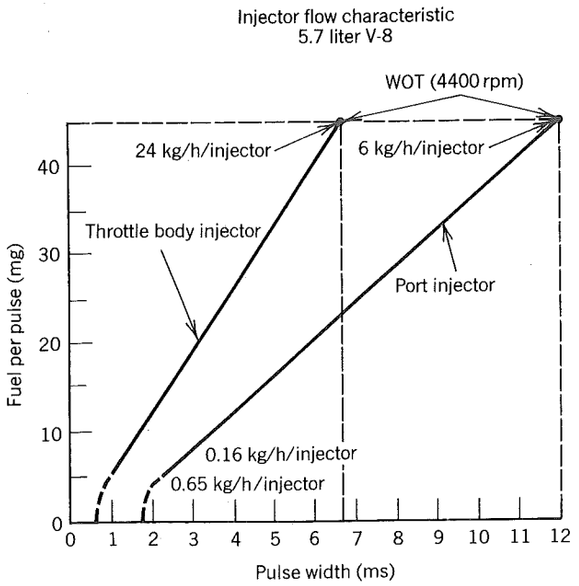

Figure 7-48 Mass of fuel injected as a function of injector pulse duration. One reason the curves are not strictly linear is that the effective flow area depends on the pulse width. The throttle body injector serves four cylinders; whereas the port injector is serving an individual cylinder. With the multiple-point fuel injection system a larger range of pulse widths can be employed and thus a larger range of engine speeds is possible (Bowler 1980). Reprinted with permission © 1980. Society of Automotive Engineers, Inc.

In order for the computer to specify Δt, it must know the desired fuel–air ratio and the mass of air that will flow into a cylinder with the fuel. one way in which this can be done is to program Eq. (7.28) into the computer. Then by sensing inlet temperature, coolant temperature, intake manifold pressure, and so on, it can calculate the volumetric efficiency. The mass of air per intake stroke is then computed.

$$m_a = \frac{e_v \rho_i \frac{\pi}{4} b^2 S}{1+F} \tag{7.84}$$

Based on information given to it about the engine operating condition, the computer chooses from a table a value for the fuel–air ratio needed in Eq. (7.84) and then solves for Δt

$$\Delta t = \frac{F m_a}{\sqrt{2\rho_f \Delta P}\, A_f} \tag{7.85}$$

Another way in which Δt can be specified is to install a sensor on the engine to measure the instantaneous air-flow rate $\dot{m}_a$. With the exception of the critical-flow nozzle, sensors based on any of the principles illustrated in Fig. 5-6 can be employed. In these cases, the duration for a four-stroke engine would be

$$\Delta t = \frac{2F\dot{m}_a}{\frac{1}{2}N_c R_s \sqrt{2\rho_f \Delta P}\, A_f} \tag{7.86}$$

The number of cylinders enters this equation because the injector is actuated once per intake stroke per cylinder. The factor of $\frac{1}{2}$ is there because, in the example case, there are two injectors serving all the engine cylinders.

The principles underlying metering with multipoint systems are no different; one simply needs now to take into account that there is an injector associated with each cylinder. Equation (7.85) is still valid and one drops $\frac{1}{2}N_c$ from Eq. (7.86). Figure 7-49 shows an example of a system using multipoint, timed port-fuel injection.

With continuous fuel injection, Eq. (7.81) is replaced with

$$\dot{m}_f = \sqrt{2\rho_f (P_f - P_a)}\, A_f \tag{7.87}$$

and the pressure of the fuel is used to meter the fuel. An example of a single-point continuous system is shown in Fig. 7-50.

Again the air flow can be either calculated or measured. The calculated air flow of a four-stroke engine is

$$\dot{m}_a = \frac{R_s}{2} \frac{e_v \rho_i V_d}{(1+F)} \tag{7.88}$$

Using either a measured or a calculated air flow rate the computer than calculates a fuel pressure that will produce the correct fuel–air ratio for the particular operating condition.

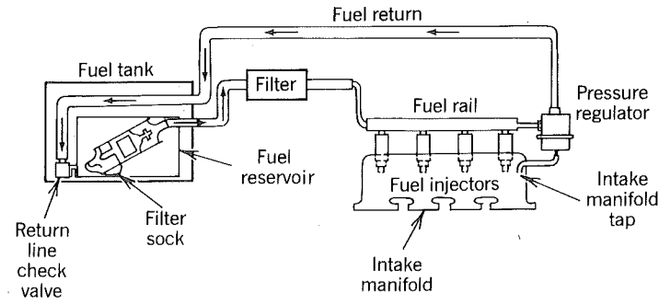

Figure 7-49 Multipoint fuel injection system used on Chrysler's 2.2-liter four-cylinder engine (Allen and Rinschler, 1984). Reprinted with permission © 1984. Society of Automotive Engineers, Inc.

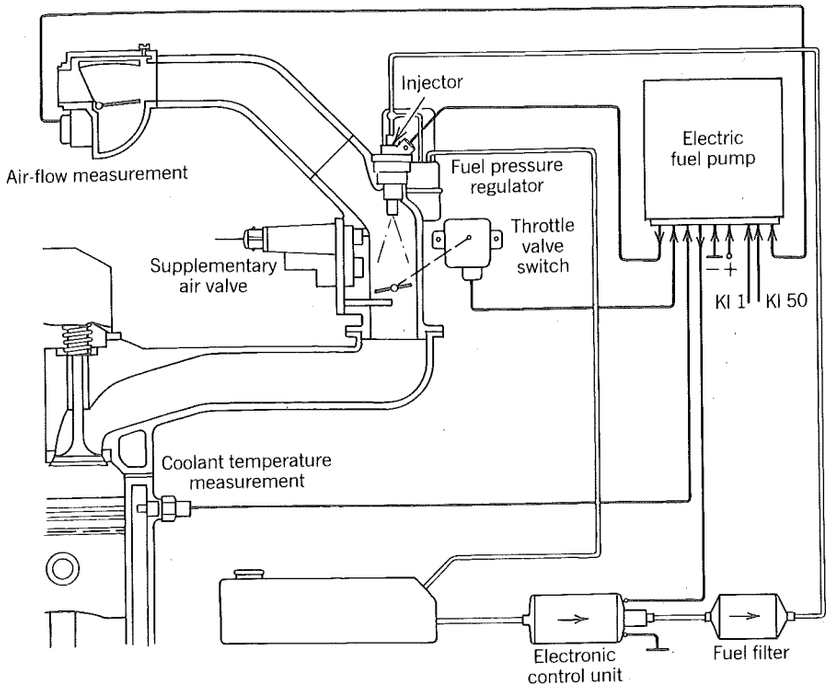

Figure 7-50 Bosch Mono-Jetronic, single point, continuous fuel injection system. Illustration only, courtesy of Robert Bosch Corporation.

Not all injection systems for spark-ignition engines are electronically calculated and metered. The Bosch K-Jetronic system, Fig. 7-51, is a mechanical system that uses multipoint, continuous flow. The incoming air acting on a pressure-sensing flap suspended on a counterbalanced lever deflects that lever in direct proportion to the mass flow rate. The lever in turn acts on a metering piston to vary the fuel flow rate.

Mechanical systems have been around for as long as the carburetor. Norbye (1981) reviews the history of fuel injection and discusses many mechanical systems. The metering of the fuel is typically done by limiting the displacement of a pump used to deliver the fuel. Most of the systems are spin-offs of diesel engine fuel injection systems.

Diesel fuel injection systems are high pressure for two reasons: (1) the fuel pressure must be greater than the compression pressure in order to inject the fuel into the cylinder at the time combustion is to commence; (2) to impart a high fuel velocity relative to the air so that the maximum stable size of the droplets will be small enough that the fuel can evaporate quickly so as not to impede the ignition delay.

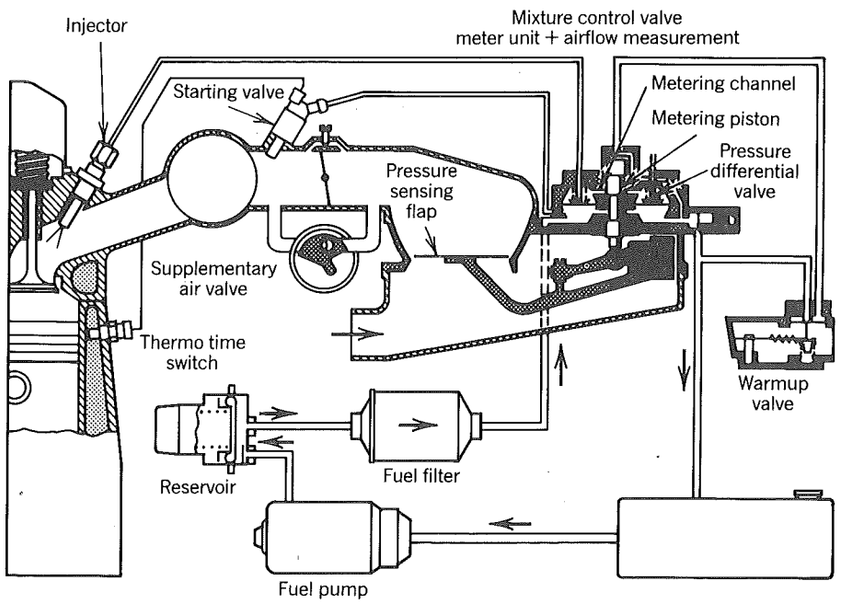

Figure 7-51 Bosch K-Jetronic mechanical fuel injection system. Unlike most mechanical systems, this one is not a spin-off of diesel technology. Illustration only, courtesy of Robert Bosch Corporation.

In Chapter 1, Fig. 1-23, the system used by the Cummins Engine Company was briefly described to illustrate that with diesel engines, fuel is sprayed directly into the cylinders at the time combustion is intended to occur. This system is an example of a low-pressure common-rail system.

It is called common rail because one pump delivers the fuel to each injector, see Fig. 7-52. When the cam allows the injector plunger to rise, fuel enters the orifice at (A). Most of the fuel (80% or so) passes through the drain at (C) and returns to the tank. This bypass flow serves to cool the injector. Some of the fuel enters the cavity ahead of the plunger through the metering orifice (B). The greater the fuel pressure is, the greater is the mass of fuel that enters the cavity. When the fuel is to be injected, the cam pushes down on the plunger, closing the metering orifice and compressing the fuel, causing it to discharge into the engine cylinder. Note that the only high pressure in the system is in the injector at this time; metering and distribution takes place at the low pressure in the common rail.

There are also fuel injection systems that employ a high pressure common rail. Figure 7-53 illustrates the differences with respect to a low-pressure system. In this case the plunger is called a needle valve and it is lifted rather than forced down. This opens a flow path through the nozzle, and the fuel

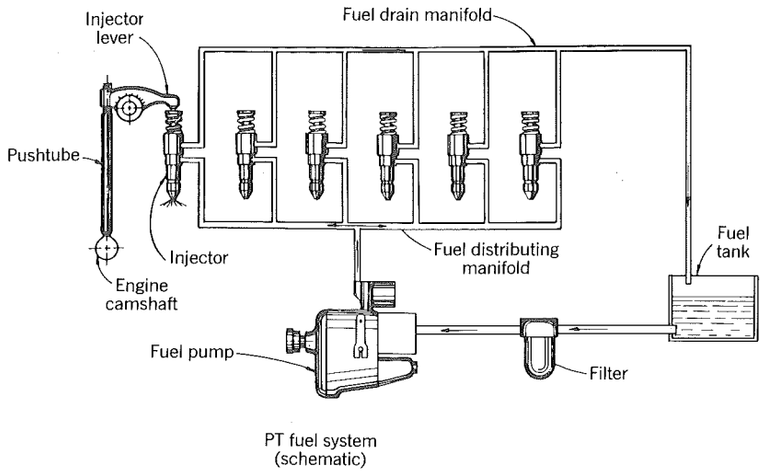

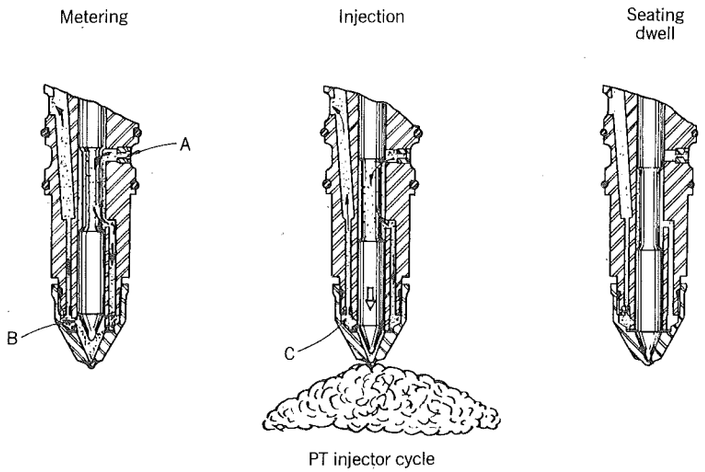

Figure 7-52 A common rail injection system used on Cummins diesel engines (Reiners et al., 1960). Reprinted with permission © 1960. Society of Automotive Engineers, Inc.

which is already at a high pressure discharges into the engine cylinder. Assuming quasi-steady flow of an incompressible[1] fluid one finds that mass of fuel injected is

$$m_f = \sqrt{2\rho \Delta P}\, \bar{A}_f \frac{\Delta\theta}{2\pi} \frac{1}{R_s} \tag{7.89}$$

[1]A quantitative analysis would have to assume the fuel is compressible to be generally applicable.

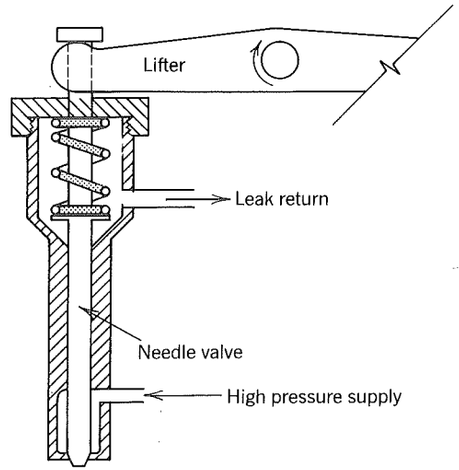

Figure 7-53 A common rail injector wherein the fuel pump generates the high pressure instead of the injector plunger doing so as in Fig. 7-52.

Note that this expression is identical to Eq. (7.84) except that Δt is expressed in terms of the crank angle change during the injection duration. It is clear, in this form, that in order to hold $\Delta\theta$ constant as engine speed varies, one must increase or decrease the fuel pressure to hold m_f constant. In fact, since typically the fuel injection pressure is large compared to the cylinder pressure, one must vary the fuel injection pressure with the square of engine speed.

$$P_f \approx \Delta P \propto R_s^2 \quad \text{if } m_f,\ \Delta\theta \text{ are constant} \tag{7.90}$$

Herein lies one basic problem with trying to build a diesel engine that will operate over a large speed range: if $R_{s,\max}/R_{s,\min} = 5$, then $P_{f,\max}/P_{f,\min} = 25$; furthermore, if at low speeds $P_{f,\min} = 50$ bar is needed to ensure good atomization and penetration into the combustion chamber, then $P_{f,\max} = 1250$ bar. Pressures significantly higher than this can be dealt with but at great expense. Electronically controlled fuel injectors offer promise in terms of solving this problem by altering the effective flow area $\bar{A}_f$ with engine speed. Recall that

$$\bar{A}_f = \frac{1}{\Delta\theta} \int_0^{\Delta\theta} A_f\, d\theta \tag{7.91}$$

By altering the shape of $A_f(\theta)$, through varying needle lift profiles with engine speeds, $\bar{A}_f$ can be made to increase with engine speed.

An example of an electronically controlled fuel injector is shown in Fig. 7-54. Metering is initiated by actuation of a solenoid operated three-way valve. The rail pressure is then applied to the low pressure piston which is directly connected to the high pressure plunger. The cross-sectional area of the low

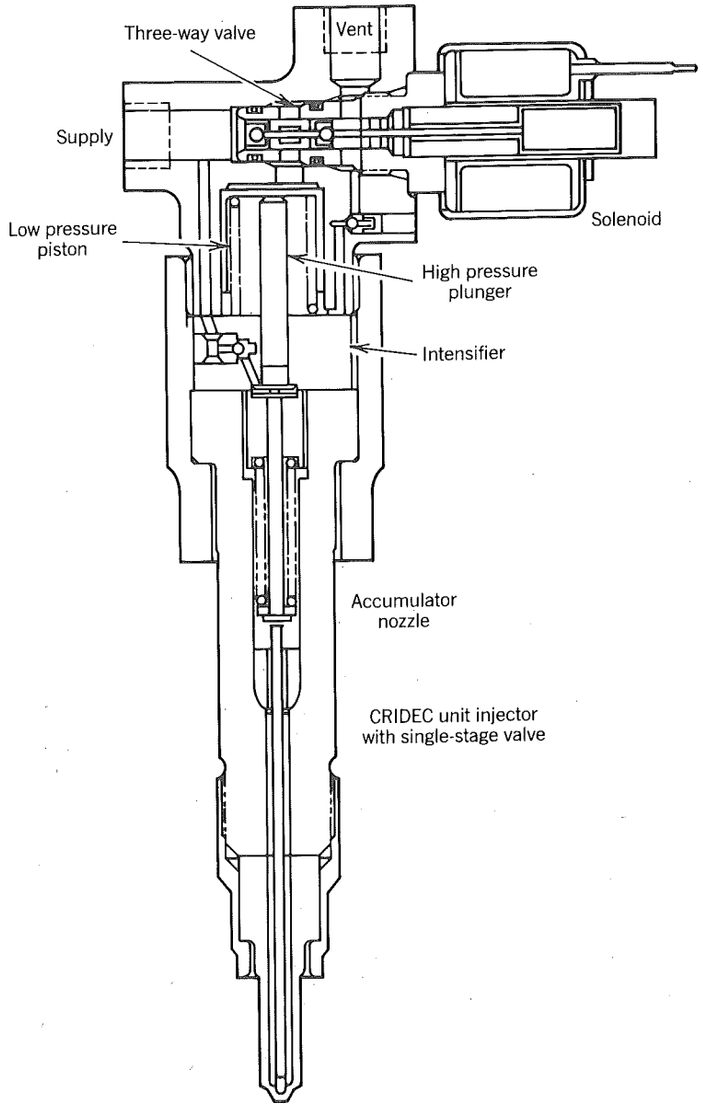

Figure 7-54 An electronically controlled diesel fuel injector (Beck, Barkhimer, Calkins, Johnson, and Wesdoh, 1984).

pressure piston is 15 times that of the high pressure piston. Since the force transmitted is the same, the pressure on the fuel that will be compressed by the high pressure plunger will be 15 times the common rail pressure. These pistons and their bores form a unit appropriately called an intensifier.

The high pressure plunger compresses fuel into the accumulator nozzle. Injection is initiated by deenergizing the solenoid that vents the low-pressure side of the intensifier. This creates a pressure imbalance on the needle, allowing it to lift and fuel to be discharged into the engine cylinder. In this design, the fuel is metered by varying the common rail pressure, but it is clear that with more development the venting process can be controlled to vary the needle lift profile, effecting a low value of $\bar{A}_f$ at low engine speeds and high value at high engine speeds.

In all the diesel systems described so far, the pressure is the independent variable and the mass injected is the dependent variable. There are also systems that use a positive displacement pump so that the mass injected is the independent variable and the fuel pressure adjusts itself accordingly.

These so called jerk-pump systems utilize the principle depicted in Fig. 7-55. A low pressure transfer pump fills the cavity ahead of a pumping plunger. A cam is configured to displace the plunger at the time injection is to occur. The plunger moves up, shuts off the inlet port, and, because the fuel is nearly incompressible, it rapidly increases the fuel pressure. The rise in fuel pressure creates a pressure imbalance on the needle in the injector nozzle, causing it to open and allowing fuel to discharge into the engine cylinder through the

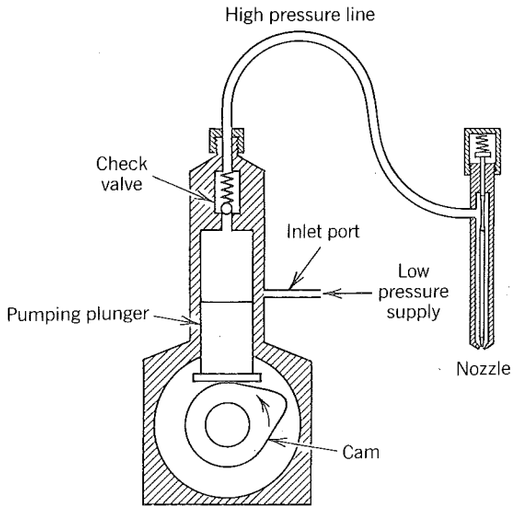

Figure 7-55 Essential features of a jerk-pump fuel injection system.

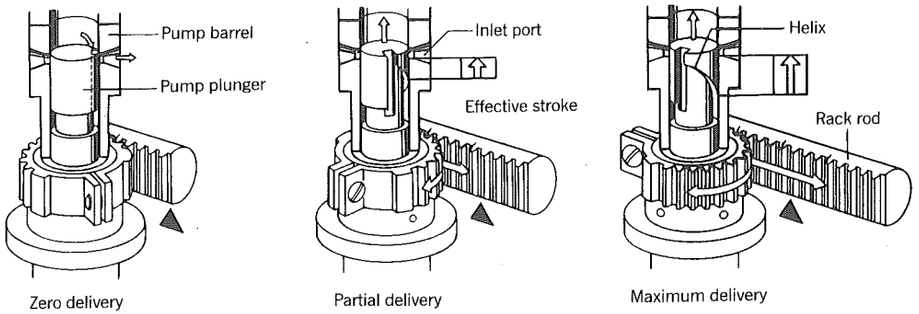

Figure 7-56 Use of a helix cut into the pumping plunger of a jerk-pump to vary the effective stroke. The rack rotates the helix with respect to the inlet ports to meter the fuel injected. Illustration only, courtesy of Robert Bosch Corporation.

nozzle. Once the fuel pressure falls to some predetermined value, a spring forces the needle down shutting off the injector.

The mass of fuel injected is controlled by varying the displacement of the pumping plunger. One way in which this is done is shown in Fig. 7-56. A helix is cut into the pumping plunger that reopens the inlet port at some intermediate position in the plunger's stroke. A rack and pinion arrangement varies the effective stroke by rotating the plunger and thus the position at which the

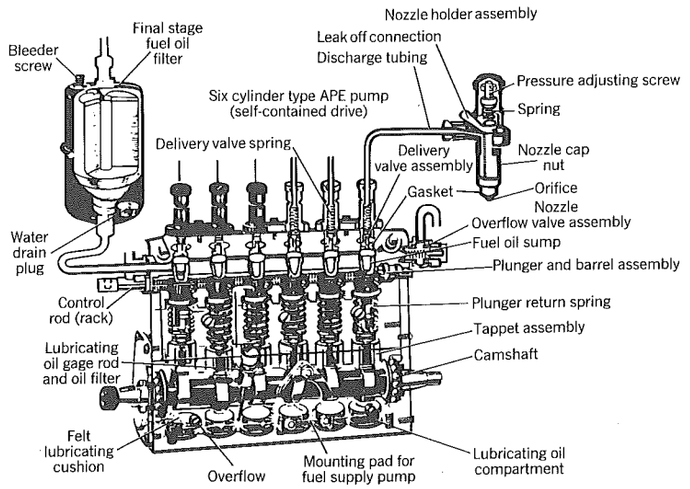

Figure 7-57 A six-cylinder diesel jerk-pump fuel injection system. Courtesy United Technologies Diesel Systems.

port will reopen and thus drops the fuel pressure. Fig. 7-57 is a cross-sectional view of a diesel fuel pump that operates on this principle.

7.14 REFERENCES

Andersson, J., A. Bengtsson, and S. Eriksson (1984), "The Turbocharged and Intercooled 2.3 Liter Engine for the Volvo 760," SAE paper 840253.

Annand, W. J. D. and G. E. Roe (1974), *Gas Flow in the Internal Combustion Engine*, G. T. Foulis, Somerset, England.

Beck, N. J., R. L. Barkhimer, M. A. Calkins, W. P. Johnson, and W. E. Weseloh (1984), "Direct Digital Control of Electronic Unit Injectors," SAE paper 840273.

Belaire, R. C., R. G. Davis, J. C. Kent, and R. J. Tabaczynski, (1983), "Combustion Chamber Effects on Burn Rates in a High Swirl Spark Ignition Engine," SAE paper 830335.

Blair, G. P. and M. C. Ashe, (1976), "The Unsteady Gas Exchange Characteristics of a Two-Cycle Engine," SAE paper 760644.

Blair, G. P., R. R. Booy, and B. L. Sheaffer, Eds., (1982) "Two-Stroke Cycle Spark Ignition Engines," SAE Progress in Technology Series, No. 26.

Bowler, L. (1980), "Throttle Body Fuel Injection (TBI)—An Integrated Engine Control System," SAE paper 800164.

Brown, W. L. (1973), "The Caterpillar imep Meter and Engine Friction," SAE paper 73550.

Campbell, C., (1971), *The Sports Car Engine: Its Tuning and Modification*, Robert Bentley, Cambridge, Massachusetts.

Chapman, M., J. M. Novak, and R. A. Stein (1983), "Numerical Modeling of Inlet and Exhaust Flows in Multi-Cylinder Internal Combustion Engine," presented at the Winter Annual Meeting of the American Society of Mechanical Engineers, Phoenix, Arizona, November 14 to 19, 1982, in T. Uzkan, Ed. *Flows in Internal Combustion Engines*, ASME.

Chapman, M., J. M. Novak, and R. A. Stein, (1983), "A Nonlinear Acoustic Model of Inlet and Exhaust Flow in Multicylinder Internal Combustion Engines," ASME paper 83-WA/DSC-14.

Dempsey, P. (1976), *How to Repair Small Gasoline Engines*, Tab Books, Blue Ridge Summit, Pennsylvania.

Engelman, H. W. (1973), "Design of a Tuned Intake Manifold," ASME paper 73-WA/DGP-2.

Gaschler, E., W. Eib, and W. Rhode, (1983), "Comparison of the 3-Cylinder DI-Diesel with Turbocharger or Comprex-Supercharger," SAE paper 830143.

Gosman, A. D., Y. Y. Tsui, and A. P. Watkins, (1984), "Calculation of Three Dimensional Air Motion in Model Engines," SAE paper 840229.

Helmich, M. J. (1965), "Development of Combustion Air Refrigeration System Enabling Reliable Operation at 220 PSI BMEP for a Large Four-Cycle Spark Ignited Gas Engine," CIMAC 65, B-2.

Johnston, S. C., C. W. Robinson, W. S. Rorke, J. R. Smith, and P. O. Witze (1979), "Application of Laser Diagnostics to an Injected Engine," SAE paper 790092.

Kajiyama, K., K. Nishida, A. Murakami, M. Arai, and H. Hiroyasu (1984), "An Analysis of Swirling Flow in Cylinder for Predicting D. I. Diesel Engine Performance," SAE paper 840518.

Liou, T. M., M. Hall, D. A. Santavicca, and F. N. Bracco (1984), "Laser Doppler Velocimetry Measurements in Valved and Ported Engines," SAE paper 840375.

Livengood, J. C. and J. B. Stanitz (1943), "The Effect of Inlet Valve Design, Size and Lift on the Air Capacity and Output of a Four-Stroke Engine," NACA TN 915.

Livengood, J. C., C. F. Taylor, and P. C. Wu (1958), "Measurements of Gas Temperatures by the Velocity of Sound Method," SAE Trans. Vol. 66, p. 683.

Norbye, J. P. (1981), *Automotive Fuel Injection Systems: A Technical Guide*, Motorbooks Int., Osceola, Wisconsin.

Obert, E. F. (1973), *Internal Combustion Engines and Air Pollution*, Harper & Row, New York p. 388–389.

Prandtl, L. (1952), *Essentials of Fluid Dynamics*, Hafner, New York, p. 328.

Reiners, N., R. Schmidt, and J. Perr (1960), "Cummins New PT Fuel Pump," SAE paper 258B.

Schweitzer, P. H. (1949), *Scavenging of Two-Stroke Diesel Engines*, Macmillan, New York.

Smith, J. R. (1982), "Turbulent Flame Structure in a Homogeneous-Change Engine," SAE paper 820043.

Smith, P. H. and P. A. Millington (1971), *The Design and Tuning of Competition Engines*, Robert Bentley, Cambridge, Massachusetts.

Sorenson, S. C. (1984), "Simulation of a Positive Displacement Supercharger," SAE paper 840244.

Tabaczynski, R. J. (1976), "Turbulence and Turbulent Combustion in Spark Ignition Engines," *Prog. Energy Combust. Sci.*, **2**, pp. 143–165.

Tabaczynski, R. J. (1982), "Effects of Inlet and Exhaust System Design on Engine Performance," SAE paper 821577.

Taylor, C. F. (1977), *The Internal Combustion Engine in Theory and Practice*, MIT Press, Cambridge, Massachusetts.

Taylor, C. F., J. Livengood, and D. Tsai (1955), "Dynamics of the Inlet System of a Four-Stroke Single-Cylinder Engine," ASME Trans., Vol. 77, p. 1133.

Tennekes, H. and J. L. Lumley (1972), *A First Course in Turbulence*, MIT Press, Cambridge, Massachusetts. p. 68.

Urich, M. (1980), *Holley 4150 & 60 Handbook*, H. P. Books, Tuscon, Arizona.

Uzkan, T., C. Borgnakke, and T. Morel (1983), "Characterization of Flow Produced by a High-Swirl Inlet Port," SAE paper 830266.

Watson, N. and M. S. Janota (1982), *Turbocharging the Internal Combustion Engine*, Wiley, New York.

Witze, P. O. (1980), "A Critical Comparison of Hot-Wire Anemometry and Laser Doppler Velocimetry for I. C. Engine Application," SAE paper 800132.

Zinner, K. (1978), *Supercharging of Internal Combustion Engines*, Springer–Verlag, New York.

7.15 HOMEWORK

1. Derive an expression for the volumetric efficiency of a supercharged engine.
2. Based on the intake-valve size, what is the maximum speed at which the engine in Example 7.1 was intended to be operated?
3. Equation (7.34) shows how to compute the residual mass fraction in an exhaust plenum. What is the order of magnitude of f_e? Explain how unburned fuel can appear in the exhaust during the intake and exhaust strokes.
4. A constant-volume cylinder contains air at $P_o = 50$ atm, $T_o = 298$ K. At time $t = 0$, a valve opens and closes 20 ms later. When the valve is open, its effective flow area is given by

$$\frac{A^*}{A^*_{\max}} = \left[\sin\left(\frac{\pi t}{\tau}\right)\right]^{1/4}$$

where $A^*_{\max} = 1.0$ cm^2 and $\tau = 20 \times 10^{-3}$ s. Assuming the heat transfer coefficient between the gas and the vessel walls is $\mathbf{h} = 100$ w/m^{2}K, find the pressure and temperature as a function of time during the valve-open period. How much mass escapes the cylinder? The air may be assumed to have constant specific heats with $\gamma = 1.4$ and $M = 29.0$.

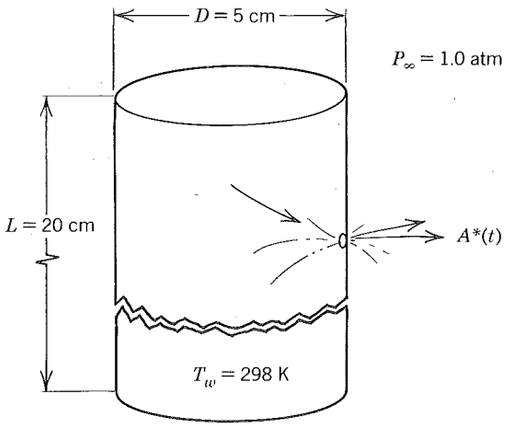

5. It was explained in Section 7.1 that because of the pressure drop across a valve, it is advantageous to close the intake valve after bottom dead center. Use the same logic to explain why exhaust valves are closed after top dead center and what the effect of engine speed is on the residual fraction.

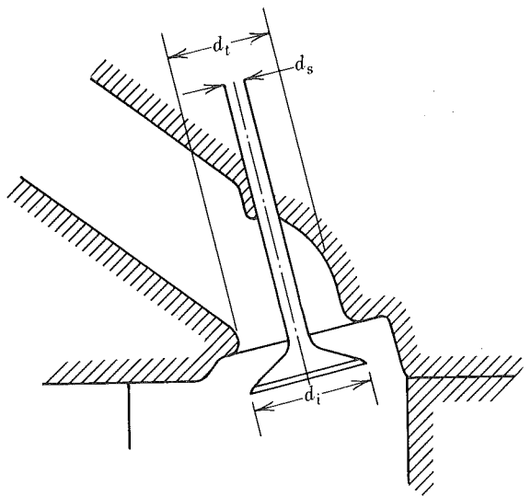

Figure 7-58 Valve throat and stem dimensions. The effect of throat shape, valve fillets, and so on are discussed in detail by Campbell (1971).

6. Suppose an engine were constructed with variable valve timing, thus ensuring optimum timing at all speeds. Explain how the volumetric efficiency would depend on speed for wide-open throttle operation with short pipes and $Z < 0.6$.
7. Figure 7-58 shows an inlet valve opened to $l/d_i = 0.25$. If the stem is chosen to be $d_s = 0.15d_i$ and the throat of the port is $d_t = 0.85d_i$, what would be the discharge coefficient based purely on the geometrical blockage?
8. **a.** Calculate the ratios of valve area to piston area for the following three configurations, recommended by Taylor (1977) as being the maximum feasible for a flat cylinder head.
   b. If the inlet Mach index in each case is held to $Z_i = 0.6$ and $c_i = 400$ m/s, $\bar{A}_i = 0.35N_i(\pi/4)d_i^2$ (N_i = number of intake valves), then what is the maximum piston speed in each case?
9. Engleman (1973) in modeling a single-cylinder four-stroke engine as a Helmholtz resonator with an effective volume of

$$V_e = \frac{V_d}{2}\frac{r+1}{r-1}$$

predicts that the resonant tuning rpm of an inlet pipe of length L_i and diameter D_i is

$$R_s = 77c_\infty \left(\frac{\frac{1}{4}\pi D_i^2}{L_i V_e}\right)^{1/2}$$

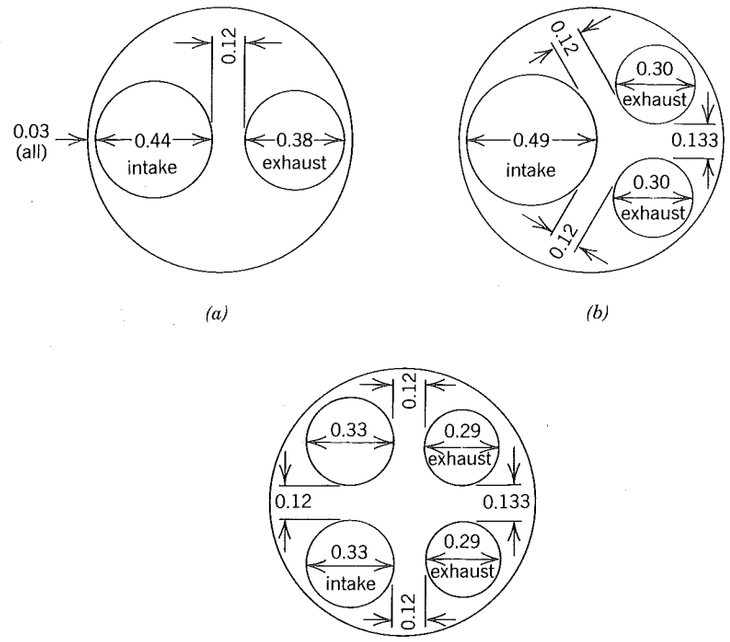

Figure 7-59 Illustration for Homework Problem 8. The use of multiple valves increases the valve area per unit piston area and hence the piston speed at which the engine power becomes flow limited. Heads are often wedge shaped or domed to increase the valve area. Intake valve area to piston area ratios of one half can be attained.

where all quantities have to have the following units:

R_s	rpm	L_i	in.
c_∞	ft/s	V_e	in.^{3}
D_i	in.	r	compression ratio

Campbell (1971), on the other hand, says he finds the following formula useful:

$$R_s = \frac{90c_\infty}{L_i}$$

In both cases, L_i is an effective length from the inlet valve to the atmosphere and D_i is an effective diameter that with L_i matches the actual inlet system volume. Shown in Fig. 7-60 are volumetric efficiency curves of a Jaguar D-type racing engine in which each cylinder was fitted with a intake pipe. This engine has the following specifications:

$b = 3.27$ in. $\quad r = 9$ (assumed) $\quad S = 4.18$ in.

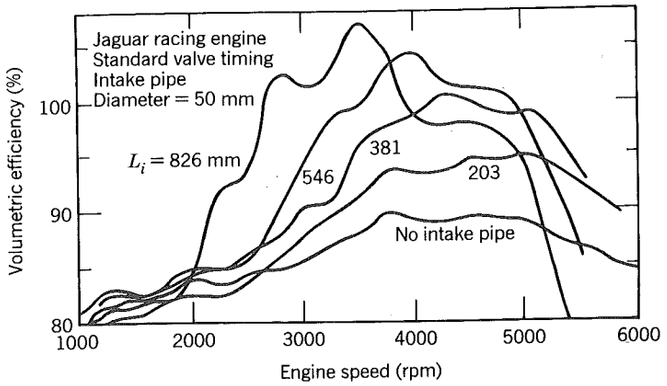

Figure 7-60 The effect of inlet pipe length on volumetric efficiency of multicylinder engine using individual intake pipes. Tabaczynski (1982). Reprinted with permission © (1982). Society of Automotive Engineers, Inc.

Make a table of the tuning rpm versus inlet pipe length normalized by the stroke. Compare with predictions using the formulas of Engleman and Campbell.

A number of cam shafts are available for the Jaguar D-type engine. These include

CAM	TIMING (DEG) IO BTC	IC ABC	EO BBC	EC ATC	LIFT in
Factory	30	60	60	30	0.375
Racer Brown 460-A	26	66	66	26	0.450
Isky XM-3	22	62	62	22	0.404

Compare the results of Fig. 7-60 with those in Fig. 7-12 and discuss the effects these different cams might have.

10. The carburetion analysis presented assumed that a steady flow existed. This is approximately true in carburetors serving four or more cylinders as at any point in the cycle there is an intake process occurring, Obert (1973). If there are less than four cylinders served by a carburetor, then the fraction of time an intake flow exists is given approximately by

$$t_f \approx \tfrac{1}{4} N_c / N \qquad (7.92)$$

where N_c is the number of cylinders served by N carburetors. The average quasi-steady air flow rate through a carburetor when an intake flow is occurring is then

$$\dot{m}_a \approx \frac{1}{t_f} \frac{R_s}{2} e_v \rho_i V_d$$

where V_d is the total displacement volume of the engine and $t_f \leq 1$. Carburetor venturis are sized assuming the maximum quasi-steady flow is twice the average.

a. Assuming $\rho_i = \rho_\infty$, $F = 0$, solve Eq. (7.74) for the effective flow area of the air based on a demand of $\mathbf{D}_c = 1.0$.

b. Assume that there are N identical single-barrel carburetors so that

$$A_a^* = N C_d \frac{\pi}{4} d_v^2$$

and that the discharge coefficient is $C_d = 0.75$. Derive an expression for the venturi throat diameter d_v for an engine with N_c cylinders.

c. Campbell (1971) offers the following practical hint in sizing carburetor venturis.

$$d_v, \text{mm} = 20 \sqrt{\frac{V_d^1}{1000} \times \frac{R_s}{1000}}$$

where

d_v = venturi diameter

V_d^1 = the displacement volume of one cylinder cm^3

R_s = the maximum engine speed, rpm

He points out that this is based on a mean gas speed through the venturi of 360 ft/s and that the venturi size is independent of the number of cylinders and the number of carburetors.

Compare Campbell's equation with your result assuming $P_\infty = 1$ atm, $T_\infty = 298$ K and show that venturi size is independent of the number of cylinders and independent of the number of carburetors if and only if Eq. 7.92 is applicable.

11. Volvo (Andersson et al., 1984), builds a naturally aspirated four-cylinder, four-stroke gasoline engine with the following specifications.

V_d	2316 cm^3
b	96 mm
S	80 mm
r	9.5
$\mathbf{P}_b$	83 kW at $R_s = 90$ rps
τ_b	184 N-m at $R_s = 46$ rps

Volvo also builds a turbocharged version of the engine that utilizes the compressor mapped in Fig. 7-61. Estimate the brake power of the turbocharged engine at $R_s = 90$ rps if the compressor ratio is $P_2/P_1 = 1.5$. What is the cmep and the bmep at this speed? Is the tmep greater than, less than, or equal to the cmep?

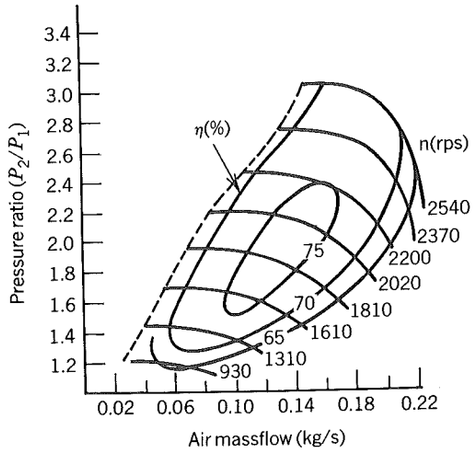

Figure 7-61 Compressor map for a turbocharged Volvo engine showing adiabatic efficiency as a function of pressure ratio, mass flow rate, and compressor speed (Anderson, Bengtsson, and Eriksson, 1984). Reprinted with permission © 1984. Society of Automotive Engineers, Inc.

Make the following assumptions.

- For the NA engine

  Inlet manifold conditions: $T_i = 310$ K, $P_i = 1.0$ bar, $\phi = 1.0$.

  Volumetric efficiency: $e_v = 0.84$.

  Mechanical efficiency: $\eta_M = \text{bmep}/(\text{imep})_{\text{net}} = 0.90$.

- For the TC engine

  Aftercooled gas temperature: $T_i = 340$ K.

  Volumetric efficiency: Correct using K_1 and K_2 in Eq. (7.28);

  Mechanical efficiency: $\eta_M = 0.88$.

- Net indicated power is proportional to airflow rate

$$\frac{(\text{imep})_{\text{net,TC}}}{(\text{imep})_{\text{net,NA}}} = \frac{\left(\dfrac{e_v P_i}{T_i}\right)_{\text{TC}}}{\left(\dfrac{e_v P_i}{T_i}\right)_{\text{NA}}}$$

In practice, the compression ratio was lowered to 8.7 to avoid knock and the engine produced 117 kW at 88 rps.

12. Sorenson (1984) has developed a computer simulation for positive displacement superchargers. A calculated compressor map is given in Fig.

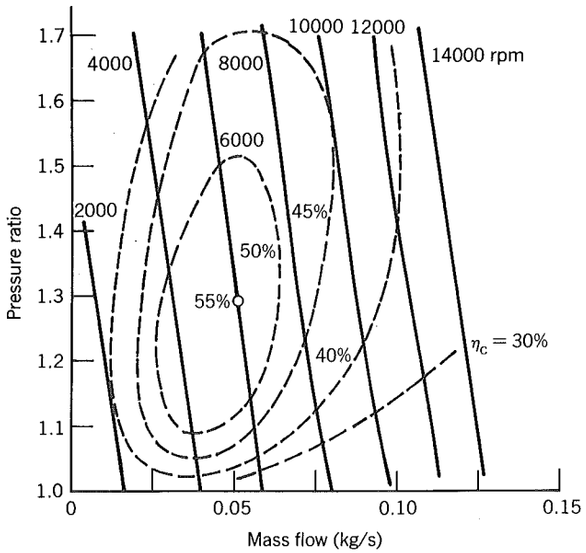

Figure 7-62 Simulated supercharger performance (Sorenson, 1984).

7-62. Match (i.e., find the resultant pressure ratio) this supercharger to a 2.0 liter, 4-stroke engine with the following volumetric efficiencies.

R_s (rpm)	e_v (%)
1000	68
2000	72
3000	75
4000	76
5000	73
6000	70

Find the power required to drive the supercharger at each condition as well as the outlet temperature. Choose a compressor speed equal to twice the engine speed. The procedure is as follows:

a. Assume a pressure ratio.
b. Read the compressor efficiency and mass flow rate.
c. Solve for the temperature and density after compression (adiabatic values but not isentropic values).
d. Calculate the engine mass flow rate with the density found in c and the known volumetric efficiency.
e. Iterate until the engine mass flow rate and compressor flow rate are equal.
f. Calculate the compressor power.

Eight

HEAT AND MASS LOSS

8.1 CONDUCTION HEAT TRANSFER

Before considering conduction heat transfer in engines, it will facilitate the discussion to first consider heat transfer within an infinite slab. A problem that mocks the engine case can be constructed in which at $x = 0$ a heat flux with a periodic component is imposed and at $x = L$ the surface temperature is held constant. The problem posed requires solution of the heat conduction equation

$$\frac{\partial T}{\partial t} = \alpha \frac{\partial^2 T}{\partial x^2} \tag{8.1}$$

subject to the following boundary conditions

$$-\lambda \frac{\partial T}{\partial x} = q_0'' + q_1'' \sin(\omega t) \qquad \text{at } x = 0 \tag{8.2}$$

$$T = T_L \qquad \text{at } x = L \tag{8.3}$$

as well as an initial condition

$$T = T_i(x) \qquad \text{at } t = 0 \tag{8.4}$$

An exact solution can be written in closed form but it is quite cumbersome and as a result no more illustrative than a computer solution. Fortunately, an approximate solution can be derived for the practical case where

$$\omega t \gg 1 \quad \text{and} \quad \frac{\omega L^2}{2\alpha} \gg 1 \tag{8.5}$$

In this case the temperature field is given by

$$T = T_L + \frac{q_0''}{\lambda}\left(1 - \frac{x}{L}\right) + \frac{q_1''}{\sqrt{2}\,\lambda} \exp\left(-\sqrt{\frac{\omega}{2\alpha}}\, x\right) \sin\left(\omega t - \sqrt{\frac{\omega}{2\alpha}}\, x - \frac{\pi}{4}\right) \tag{8.6}$$

Inspection of this solution shows that: (1) the surface temperature at $x = 0$ oscillates with the same frequency as the imposed heat flux but with a phase difference of $\pi/4$; (2) the amplitude of the oscillations decays exponentially with the distance x from the surface; the amplitude is reduced to 10% of that

at the surface at a distance given by

$$l = -\ln(0.10)\sqrt{\frac{2\alpha}{\omega}} = 2.3\sqrt{\frac{2\alpha}{\omega}} \tag{8.7}$$

For an engine operating at 2000 rpm ($\omega = 209\ s^{-1}$) and made of cast iron ($\alpha = 21 \times 10^{-6}\ m^2/s$) this length is rather small, $l = 1.0$ mm. For aluminum $l = 2.2$ mm and for partially stabilized zirconia (a ceramic used in prototype insulated engines) $l = 0.7$ mm.

The length l is a measure of how far into the material fluctuations about the mean heat flux penetrate. For distances x greater than l, the temperature distribution is more or less steady and driven only by the time average heat flux. Since the length l is rather small compared to the dimensions (wall thickness, bore, etc.) over which conduction heat transfer occurs, two simplifications can be made: (1) conduction heat transfer in the various parts can be assumed steady and driven by the average flux; (2) heat transfer from the gas can be coupled to the conduction analysis accounting for capacitance only in a penetration layer of thickness l in series with a resistance computed or measured for a steady state (an electrical analog for a one dimensional case is given in Fig. 8-1). The penetration layer can be complicated by the presence of

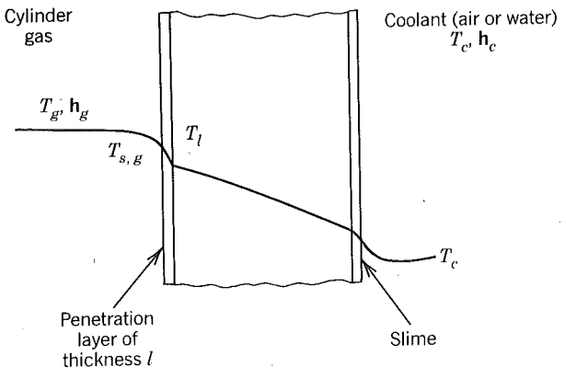

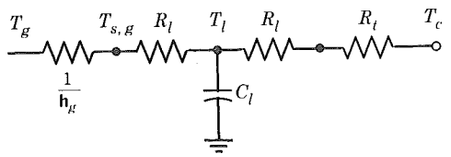

$R_l = \frac{1}{2}\frac{l}{k}$ $\qquad C_l = \rho c l$

R_t = conduction path resistance to coolant

Figure 8-1 A one-dimensional representation of the heat loss from the cylinder gas.

an oil film or deposits. Fortunately an accurate model is not required as the fluctuations in the mean about $\bar{T}_l$ tend to be small compared to temperature difference $T_g - \bar{T}_l$.

For an engine operated at a steady state, the penetration layer is thin because the engine frequency, which dictates the frequency components of the heat flux imposed on the gas–solid interfaces, is rather high. On the other hand, in the case of an engine being accelerated or decelerated, the penetration layer is thicker because lower frequency components are added to the heat flux that are characteristic of the rates of change of engine speed. For example, one could define a characteristic time τ by

$$\tau^{-1} = \frac{1}{\omega}\frac{d\omega}{dt} \tag{8.8}$$

In the case where $\tau = 5$ s, the penetration layer would be

$$l = 2.3\sqrt{2\alpha\tau} \tag{8.9}$$

which is $l = 33$ mm for cast iron and no longer small compared to the typical dimensions over which the heat is transferred. To correctly analyze heat transfer in engines operated on transient cycles, the three-dimensional and unsteady features must all be accounted for and is, as of this writing, beyond the state of the art.

Nevertheless the state of the art is rapidly developing and studies of heat transfer in the steady state can be effective. As an illustration, a case study of heat transfer in a piston will be presented (Li, 1982). Figure 8-2 shows how a piston can be divided into a number of control volumes or finite elements for analysis. Only one quadrant of the piston in the x–y plane needs to be considered as the piston is, in this case, symmetrical. As mentioned earlier, the piston can be treated as steady and driven by an average heat flux since the penetration layers are small. The boundary conditions employed are illustrated in Fig. 8-3 which shows a distribution of 20 overall heat transfer coefficients at various positions along the surfaces and convection temperatures corresponding to a mean gas temperature $\bar{T}_g$, a mean coolant temperature T_c (the overall heat transfer coefficient accounts for the thermal resistance across the cylinder wall), and a mean oil temperature T_{oil}.

The mean cylinder gas temperature is computed using a cycle simulation to predict instantaneous gas temperatures and then integrated according to

$$\bar{T}_g = \frac{1}{4\pi\mathbf{h}_g}\int_0^{4\pi}\mathbf{h}_g T_g\, d\theta \tag{8.10}$$

where $\mathbf{h}_g$ is the instantaneous heat transfer coefficient (the computation of which is the subject of the next section). Likewise an average heat transfer coefficient

$$\bar{\mathbf{h}}_g = \frac{1}{4\pi}\int_0^{4\pi}\mathbf{h}_g\, d\theta \tag{8.11}$$

is used in estimating the heat transfer coefficients 2 through 6. Results obtained

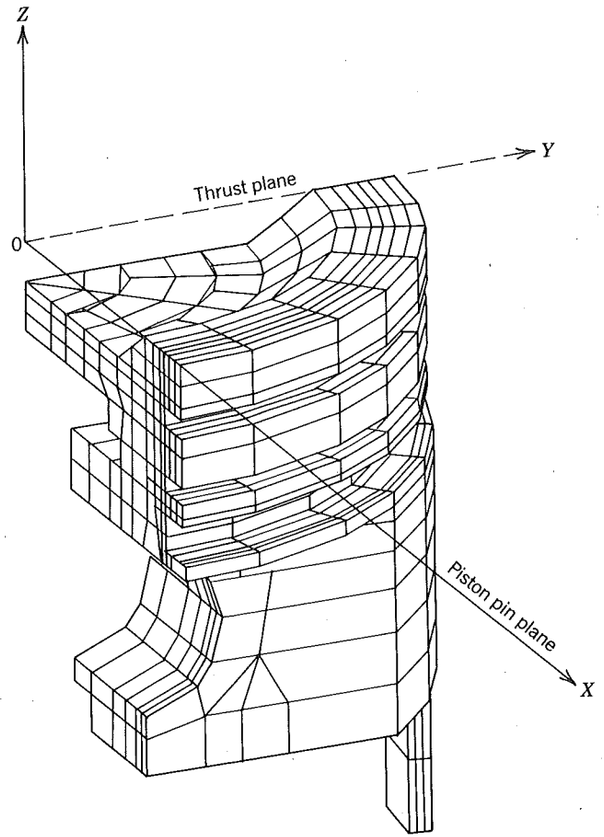

Figure 8-2 Grid structure for a finite element calculation of conduction heat transfer in a piston (Li, 1982). Reprinted with permission © 1982. Society of Automotive Engineers, Inc.

for a 2.5 liter, four-cylinder engine at WOT are given in Table 8-1. Notice that both the mean gas temperature and the mean heat transfer coefficient (HTC) increase with engine speed. The former increases because there is less time for the gases to lose heat as engine speed increases (despite the latter); whereas the latter increases because of increased gas motion at higher speeds.

The remaining heat transfer coefficients, including the underside of the dome, pin boss surfaces, ring land area, and skirt surfaces are determined by order of magnitude engineering analysis and adjusted by less than one order of magnitude so that measured and predicted surface temperatures are matched. Thus, as in friction or combustion modeling, the results are correlative rather than predictive. They are used to explain phenomena and look for trends by parametric variation rather than by experiment.

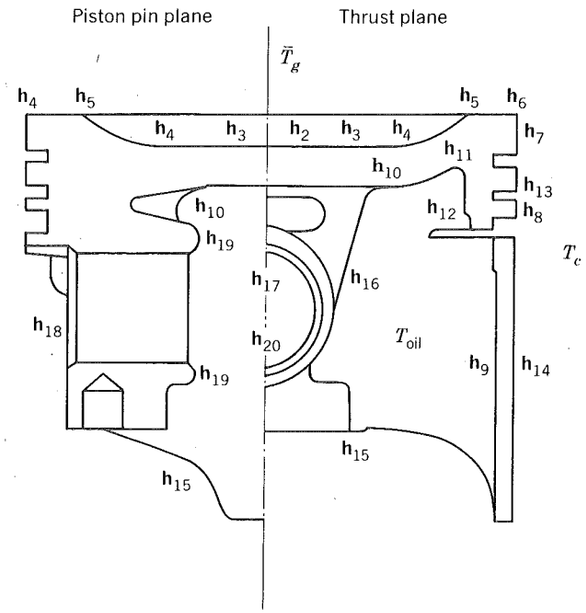

Figure 8-3 Distribution of heat transfer coefficients on piston surfaces used in finite element calculation of conduction heat transfer in a piston (Li, 1982). Reprinted with permission © 1982. Society of Automotive Engineers, Inc.

Results obtained for a dished and slotted piston run in a 2.5 liter four-cylinder engine at 4600 rpm and wide-open throttle are given in Fig. 8-4. The values associated with the dots are measured temperatures (deduced from a change in the material hardness), and the isotherms shown are the results of computations. The agreement obtained is reasonable except in the skirt area where the computed temperatures are too low. If the coefficient $\mathbf{h}_{14}$ is arbitrarily reduced by two orders of magnitude, the computed skirt temperature increases to the values given in the parentheses.

Table 8.1 Variation of Ambient Temperature and Heat Transfer Coefficient at the Top of the Piston with Engine Speed[a].

ENGINE SPEED rpm	MEAN GAS TEMPERATURE (°C)	MEAN HTC $\times 10^{-4}$ (W/mm^2 · K)
2400	990	1.82
3600	1037	2.43
4600	1062	2.80

Source: Li (1982).

[a]A dished piston running in a 2.5 l engine WOT.

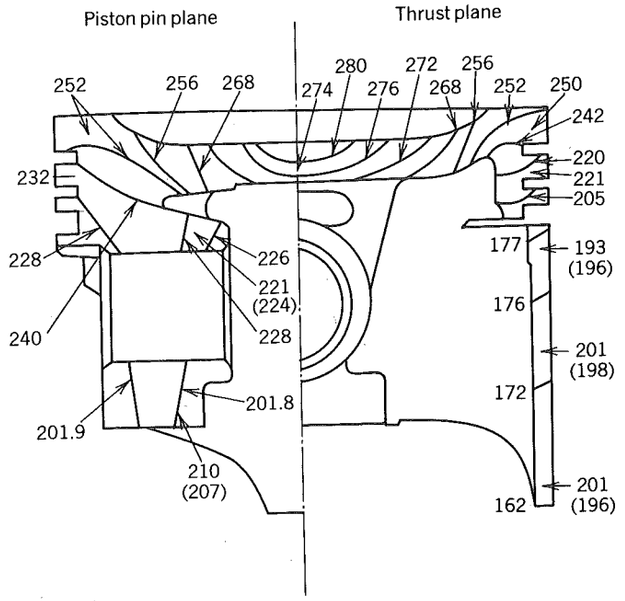

Figure 8-4 Calculated and measured temperature distributions in piston pin and thrust planes (deg C). Measured values indicated by dots (Li, 1982). Reprinted with permission © 1982. Society of Automotive Engineers, Inc.

The value of $\mathbf{h}_{14}$ was estimated to be 2.5×10^{-4} W/mm^2/K, assuming that normal heat transfer occurs between the skirt and the cylinder bore. The fact that $\mathbf{h}_{14}$ would have to be reduced by two orders of magnitude to match measured skirt temperatures implies that heat transfer is poor. This fact led the engineer doing the work, Li (1982), to suspect that significant amounts of heat are generated in the oil film between the skirt and bore by viscous dissipation. He also performed computations using finite elements of the strains in the piston and found that when the engine is operated at WOT and high speed, the skirt expansion is restrained by the bore, causing pressure buildup in the oil film which leads to increased viscous dissipation.

The calculated results show that three areas are particularly important in dissipating the piston heat input: (1) the ring groove surfaces, (2) the underside of the dome and (3) the upper portion of the pin bearing surface. From the ring groves, heat flows into the rings, through the bore, and is eventually absorbed by the coolant. From the underside of the dome and the surface of the pin bearing, the heat is convected into an air–oil mist and is eventually absorbed by the oil in the sump.

The results of similar calculations are summarized in Fig. 8-5 to show the effect of engine speed at WOT on piston temperature. Temperatures in the

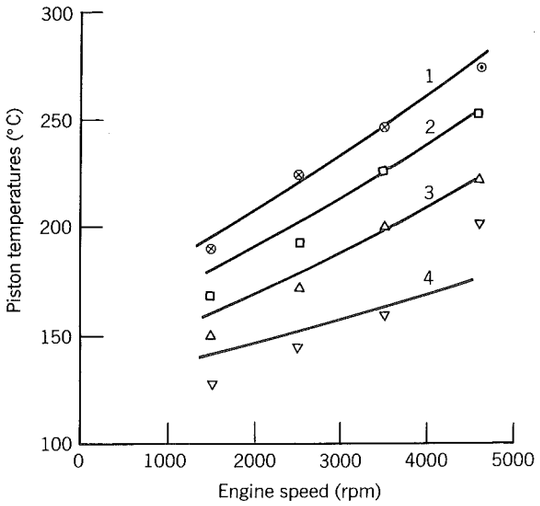

	Measured	Finite Element Computations
Center of crown	○	1
Top ring land	□	2
Second ring land	△	3
Middle of skirt	▽	4

× by Tasa and Furuhama
· by Madizar

Figure 8-5 Piston temperatures versus engine speed at full load (Li, 1982). Reprinted with permission © 1982. Society of Automotive Engineers, Inc.

piston are determined by the average heat flow in and the effectiveness with which the heat can be dissipated to the oil and the coolant. As speed increases, the heat flow increases, whereas the overall heat transfer coefficients to the coolant and oil change little; thus piston temperature increases.

8.2 CONVECTIVE HEAT LOSS

A correlation for an average heat transfer coefficient, similiar to that defined earlier in Eq. (8.11), particularly useful in conceptualizing effects of engine speed on the thermal efficiency of engines, is that of Taylor (1977). It states that for either two- or four-stroke engines, compression or spark ignited,

$$N_u = \frac{\bar{\mathbf{h}}_g b}{\lambda_g} = 10.4 R_e^{0.75} \tag{8.12}$$

where the Nusselt number and the Reynolds number are based on the bore. The velocity needed to define the Reynolds number is based on the mass flow

rate into the engine per unit piston area

$$R_e = \frac{(\dot{m}_a + \dot{m}_f)b}{A_P \mu_g} \tag{8.13}$$

Eq. (8.13) is a little easier to deal with in terms of the delivery ratio, in which case

$$R_e = \begin{cases} \dfrac{D_r}{4}\dfrac{\rho_\infty \bar{U}_p b}{\mu_g}(1+F) & \text{(four-stroke)} \\ \dfrac{D_r}{2}\dfrac{\rho_\infty \bar{U}_p b}{\mu_g}(1+F) & \text{(two-stroke)} \end{cases} \tag{8.14}$$

With the exception of ρ_∞ (ambient air density), gas properties are evaluated at the appropriate mean effective gas temperature.

The heat loss by convection is then given by

$$\dot{Q}_l = \bar{\mathbf{h}}_g A_p (\bar{T}_g - T_w) \tag{8.15}$$

where $A_p = \frac{1}{4}\pi b^2$ is the piston area. It is of interest to normalize this heat loss by the maximum available power that could be realized by burning the fuel

$$\frac{\dot{Q}_l}{\dot{m}_f a_o} = 10.4 \frac{1+F}{F} \frac{\lambda_g (\bar{T}_g - T_w)}{a_o \mu_g} R_e^{-0.25} \tag{8.16}$$

In this form one can see that the fraction of the available energy lost by the gases by convection will drop slightly as either the delivery ratio or the engine speed increase thereby increasing the Reynolds number. Notice too that large engines will lose slightly less available energy than small engines. All these effects, speed, delivery ratio, and engine size manifest themselves through the Reynolds number. The fuel–air ratio affects the mean gas temperature and the gas properties.

The gases in the cylinder of an engine lose heat to the containing walls during compression, combustion, expansion, and exhaustion. During intake, naturally aspirated engines generally gain heat and in turbo or supercharged engines, whether heat is lost or gained is dependent upon the degree, if any, of aftercooling employed.

The heat transfer coefficient varies with position in the cylinder and is time dependent. The state of the art does not deal with the spatial variation since it would require solution of three-dimensional, unsteady Navier–Stokes equations coupled to the energy equation, atom conservation equations, a turbulence model, equations of state, and chemical kinetic rate equations. As stated in Chapter 4, this is an area of current research.

Instead, the state of the art employs a dimensionless correlation that yields the spatial average heat transfer coefficient as a function of time. One such correlation that is widely used is (Woschni, 1967):

$$N_u = 0.035 R_e^{0.8} \tag{8.17}$$

where N_u is a Nusselt number and R_e is a Reynolds number. The characteristic length on which both numbers are based was arbitrarily chosen to be the cylinder bore on the premise that whatever the length really is, it ought to get bigger as engine size increases. Woschni could have chosen intake valve lift or stroke, both of which can be varied independently of the bore. The fact that there are lengths that can be varied independently of the bore results in a less than perfect correlation. Fortunately the resultant heat transfer coefficient is a weak function ($\mathbf{h} \propto b^{-0.2}$) of the length, so its choice is not critical.

Finally we need a gas speed $U_{m,g}$ for use in evaluating the Reynolds number. Annand (1963) proposed a correlation similar to Eq. (8.17) in which the appropriate speed was assumed to be proportional to the mean piston speed. Woschni's correlation also uses piston speed but introduces a factor to account for gas motion induced by combustion. The gas velocity induced by combustion is assumed to be proportional to the pressure rise due to combustion. Accordingly

$$U_{m,g}(m/s) = 2.28\bar{U}_p + 0.00324 \frac{T_o V}{V_o} \frac{\Delta P_c}{P_o} \tag{8.18}$$

where

$\bar{U}_p = \omega S/\pi$ = mean piston speed

T_o = temperature (K) at intake valve closing

V_o = cylinder volume at intake valve closing

V = instantaneous cylinder volume

ΔP_c = instantaneous pressure rise due to combustion

P_o = pressure at intake valve closing

The pressure rise due to combustion is the cylinder pressure in the firing engine minus the cylinder pressure in the motored engine at the same crank angle. The latter can be estimated accurately enough by use of the isentropic relation $PV^\gamma = P_o V_o^\gamma$ = constant.

Equation (8.18) is applicable when the valves are shut. When the valves are open, the gases are accelerated because of the flow in or out. In this case Woschni uses

$$U_{m,g} = 6.18\bar{U}_p \tag{8.19}$$

The constants in Woschni's correlation were determined by matching experimental results obtained using a particular diesel engine. When applied to any other engine, the constants are estimates at best and it is not uncommon to find engineers adjusting them to better suit their own engine.

Recent work by Borgnake, Arpaci, and Tabaczynski (1980) directed at modeling turbulence characteristics during compression and expansion in homogeneous charge engines has predicted that the Nusselt number depends on a Reynolds number and a function of a dimensionless boundary layer

thickness; accordingly

$$N_u = \left(\frac{u' l_\infty}{\nu}\right)^{2/3} f\left(\frac{\delta}{l_\infty}\right) \tag{8.20}$$

where u' is the fluctuating turbulent velocity and l_∞ is the turbulent eddy or vortex size. The parameter δ is a boundary layer thickness that like u' and l_∞ is computed by solving a modeled ordinary differential equation simultaneously with those used to model the combustion. The initial conditions (time zero is inlet valve closure) relate u' to the average gas speed through the intake valve and l_∞ to the intake valve lift. The boundary layer thickness in unburned gas is assumed to be zero when the inlet valve shuts and equal to the quench layer thickness[1] at the time burned gas first appears at the walls. The equations, which model the rates of change of u', l_∞ and, δ, depend on the thermodynamic state, the transport properties, and a length characteristic of the cylinder volume such as $V^{1/3}$, V/A, or V/A_p.

Delineating the rate equations and attempting to pin down which length best characterizes the cylinder is beyond the scope of this text. The models used are the subject of current research and are likely to change as new developments are reported. The point in introducing the model of Borgnake et al. (1980) is that it represents the beginning of a new class of models which can account for variations in stroke or valve lift at fixed bore and thus offer promise of a more universal approach to the problem than the simpler correlations developed by Annand (1963) or Woschni (1967).

Convective heat loss is an important consideration in exhaust port design especially for engines with exhaust turbines or catalytic convertors. Hires and Pochmara (1976) have addressed this problem for a number of different ports. They correlated their results and deduced for instantaneous heat loss that

$$N_u = 0.158 R_e^{0.8} \tag{8.21}$$

where their Reynolds number is defined as

$$R_e = \left(\frac{\dot{m} d}{\mu A}\right) \tag{8.22}$$

and $\dot{m}$ is the instantaneous flow rate, d is the throat diameter, A is the exit cross section, and μ is the exhaust gas viscosity. Some of the ports studied are shown in Fig. 8-6.

Malchow, Sorenson, and Buckius (1979) obtained the following correlation for time and spatially average heat loss in a straight circular exhaust pipe.

$$N_u = 0.0483 R_e^{0.783} \qquad D_e/L_e = 0.3 \tag{8.23}$$

Their data are compared in Fig. 8-7 to computations based on the steady-state correlation for turbulent flow in a smooth pipe (Holman, 1963):

$$N_u = 0.023 R_e^{0.8} P_r^{0.33} (1 + D/L)^{0.7} \tag{8.24}$$

[1]This is the small but finite distance away from a wall over which the flame is extinguished.

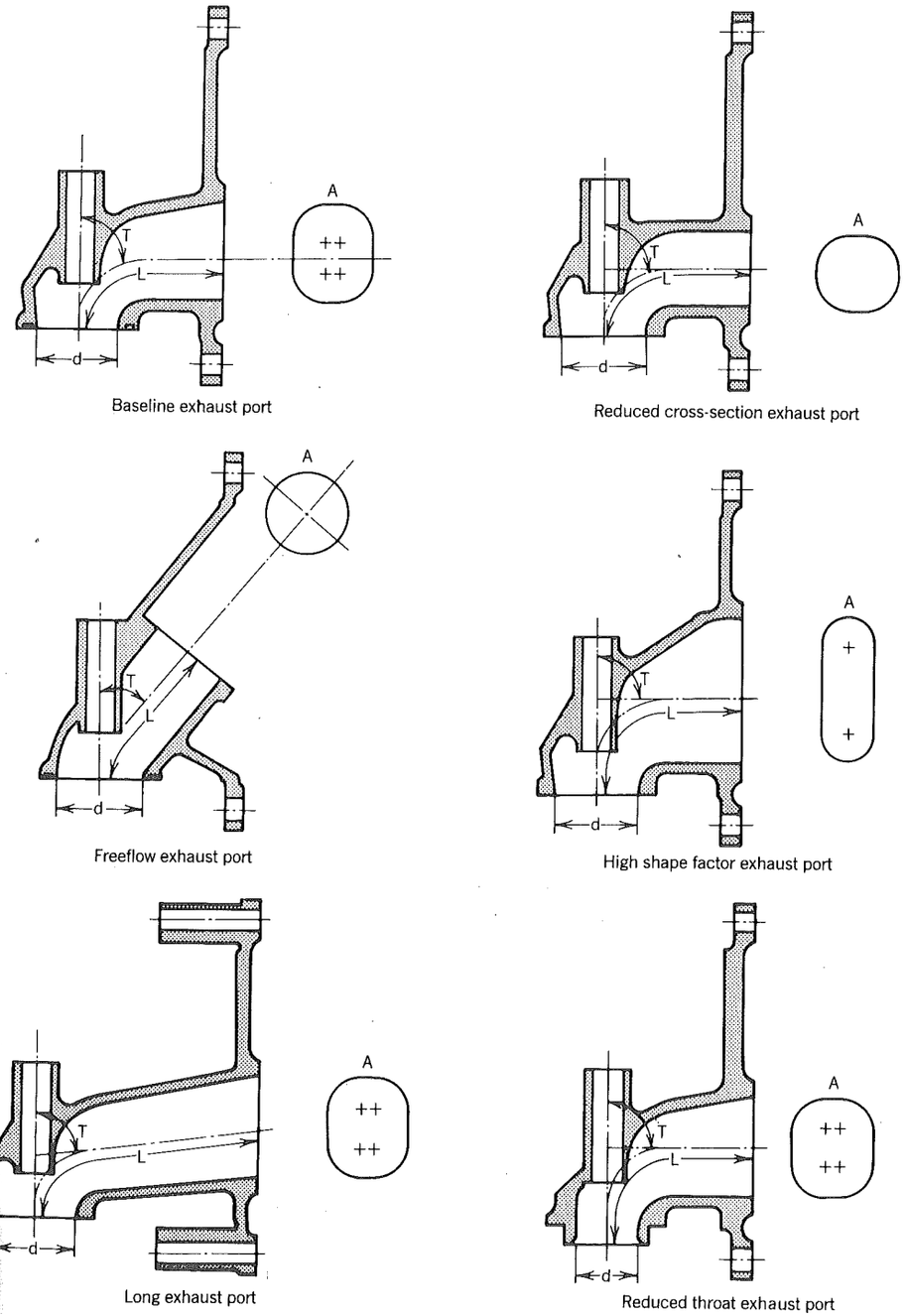

Figure 8-6 A number of exhaust ports the heat transfer coefficients of which can be determined from Eq. (8.21) and (8.22) (Hires and Pochmara, 1976). Reprinted with permission © 1976. Society of Automotive Engineers, Inc.

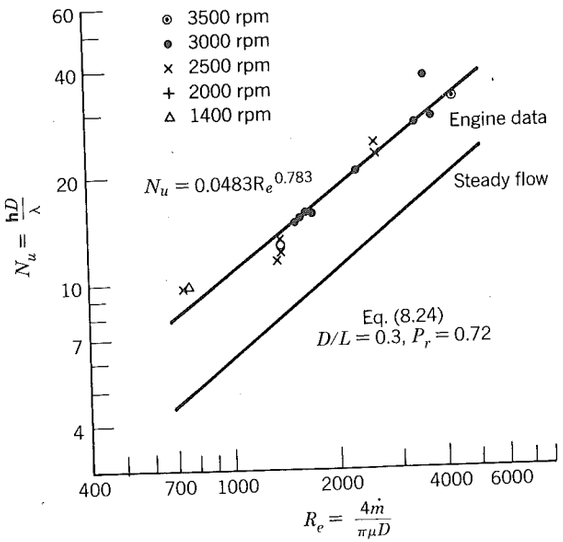

Figure 8-7 Spatial average Nusselt number for heat transfer in an exhaust pipe (Malchow et al., 1979). Reprinted with permission © 1979. Society of Automotive Engineers, Inc.

In Eq. (8.24), P_r is the Prandtl number and L is the pipe length. Notice that the heat transfer in the exhaust pipe is about 50% greater than would exist in a truly steady flow in the same pipe. In an exhaust port, Eq. (8.21) applies; it appears that the heat transfer coefficient is about eight times what it would be in a steady flow in the same port. This is believed to be caused by turbulence generated by flow separation at the valve. In that neither Eq. (8.21) nor (8.23) include information about the valve, such as lift or valve seat angle, they are applicable to other engines only in so far as they are geometrically similar. Recent work by Caton and Heywood (1981) has started to address the problems in incorporating the valve geometry into a heat transfer correlation.

8.3 TRANSPORT PROPERTIES OF GAS MIXTURES

The kinetic theory of gases is developed sufficiently enough that the thermal conductivity and viscosity of gases can be computed accurately (Hirschfelder, Curtiss, and Bird, 1954). For example, the viscosity of a pure component is given by

$$\mu = 26.693 \times 10^{-6} \frac{\sqrt{MT}}{\sigma^2 \Omega} \tag{8.25}$$

where the units are g $cm^{-1}s^{-1}$ or poise, σ is the molecular diameter in

Table 8-2 Collision Parameters

SPECIES (i)		σ (Å)	ϵ/k (K)
1	CO_2	3.941	195.2
2	H_2O	2.641	809.1
3	N_2	3.798	71.4
4	O_2	3.467	106.7
5	CO	3.690	91.7
6	H_2	2.827	59.7
7	H	2.708	37.0
8	O	3.050	106.7
9	OH	3.147	79.8
10	NO	3.492	116.7

Source: Svehla (1962).

angstroms, and Ω is a dimensionless integral of order unity dependent on the details of the force interaction during a collision. For Lennard–Jones[2] interaction, the integral is given by (Hattikudur and Thodos, 1970)

$$\Omega = 1.155(T^*)^{-0.1462} + 0.3945e^{-0.6672T^*} + 2.05e^{-2.168T^*} \tag{8.26}$$

where T^* is a dimensionless temperature defined

$$T^* = \frac{kT}{\epsilon} \tag{8.27}$$

k is Boltzmann's constant, and ϵ is the maximum energy of attraction during the collision. Table 8-2 lists values of the interaction parameters for the species of interest here. The thermal conductivity in a gas is split to account for transport of translational energy λ' and internal energy λ''. By definition

$$\lambda = \lambda' + \lambda'' \tag{8.28}$$

The translational contribution is given by

$$\lambda' = \frac{15}{4}\frac{R_u}{M}\mu \tag{8.29}$$

and the internal contribution is approximately given by

$$\lambda'' \approx 0.88\left(\frac{2}{5}\frac{c_p}{R} - 1\right)\lambda' \tag{8.30}$$

The viscosity of a mixture of the 10 species listed in Table 8-2 is approximately

$$\mu_{\text{mix}} \approx \sum_{i=1}^{10} \frac{\mu_i}{1 + \sum_{\substack{j=1 \\ j\neq i}}^{10} \Phi_{ij}\frac{y_j}{y_i}} \tag{8.31}$$

[2]The potential energy ϕ as a function of the distance r separating two molecules is given by $\phi = 4\epsilon[(\sigma/r)^{12} - (\sigma/r)^6]$.

where Φ_{ij} is a coefficient given by

$$\Phi_{ij} = \frac{\left[1 + \left(\frac{\mu_i}{\mu_j}\right)^{1/2}\left(\frac{M_j}{M_i}\right)^{1/4}\right]^2}{2\sqrt{2}\left(1 + \frac{M_i}{M_j}\right)^{1/2}} \tag{8.32}$$

and, as in Chapter 3, y denotes a mole fraction. The approximate formula for the translational contribution to the thermal conductivity is

$$\lambda'_{\text{mix}} \approx \sum_{i=1}^{10} \frac{\lambda'_i}{1 + \sum\limits_{\substack{j=1 \\ j\neq i}}^{10} \Psi_{ij}\frac{y_j}{y_i}} \tag{8.33}$$

and the coefficient is

$$\Psi_{ij} = \Phi_{ij}\left[1 + 2.41\frac{(M_i - M_j)(M_i - 0.142M_j)}{(M_i + M_j)^2}\right] \tag{8.34}$$

Finally, the internal contribution to the thermal conductivity is approximately

$$\lambda''_{\text{mix}} \approx \sum_{i=1}^{10} \frac{\lambda''_i}{1 + \sum\limits_{\substack{j=1 \\ j\neq i}}^{10} \Phi_{ij}\frac{y_j}{y_i}} \tag{8.35}$$

The approximations (8.30), (8.31), (8.33), and (8.35) are derived from rigorous kinetic theory by Brokaw (1961).

In the case of reacting mixtures, that is mixtures in which, the composition shifts with temperature and pressure, as opposed to frozen mixtures, there is also a contribution to the thermal conductivity caused by dissociation and recombination as molecules fluctuate back and forth in the temperature gradient driving the heat flux. For practical application, the following approximation will suffice to account for this effect

$$\lambda_{\text{mix}} \approx \left(\lambda'_{\text{mix}} + \lambda''_{\text{mix}}\right)\frac{c_p}{c_{p,f}} \tag{8.36}$$

where c_p is the equilibrium specific heat and $c_{p,f}$ is the frozen specific heat (refer to Homework problem 3-7).

A subroutine for computing the transport properties according to Eq. (8.25) through (8.36) follows.


```
C*****************************************************************
C
      SUBROUTINE TRANSP ( T, Y, CP, MU, LAMBDA )
C
C     PURPOSE:
C        COMPUTE THE TRANSPORT PROPERTIES OF EQUILIBRIUM COMBUSTION
C        PRODUCTS
C
C     GIVEN:
C        T       - TEMPERATURE (K)
C        Y       - A TEN DIMENSIONAL COMPOSITION VECTOR OF
C                  MOLE FRACTIONS
C                  1=CO2, 2=H2O, 3=N2, 4=O2, 5=CO, 6=H2,
C                  7=H, 8=O, 9=OH, 10=NO
C        CP      - SPECIFIC HEAT AT CONSTANT PRESSURE (J/G/K)
C
C     RETURNS:
C        MU      - VISCOSITY (G/CM/SEC OR POISE)
C        LAMBDA  - THERMAL CONDUCTIVITY (W/CM/K)
C
C     REMARKS:
C        1. VALID FOR 300 < T < 4000
C        2. TREATS WATER (A POLAR MOLECULE) THE SAME AS NON-POLAR
C           MOLECULES: REFER TO DANON AND AMDUR (1969)
C        3. FUEL AIR RESIDUAL GAS TRANSPORT PROPERTIES CAN BE
C           COMPUTED BY MODELING THE FUEL AS CARBON DIOXIDE.
C           IN THIS CASE INPUT FOR Y(1) : Y(1) + YFUEL
C        4. IF A FROZEN THERMAL CONDUCTIVITY IS THE DESIRED OUTPUT,
C           THEN INPUT CP = 0.
C
C
C*****************************************************************
C
      REAL LAMBDA, LMMIX1, LMMIX2, LMBDA1, LMBDA2, M, MJ, MI, MU, MU1,
     &     MU1I, MU1J, MW
      DIMENSION A0(7,10), A(7,6), M(10), SIGMA(10), EPS(10), MU1(10),
     &          CP0(10), Y(10)
C
C
C     SPECIFIC HEAT DATA FROM GORDON AND MCBRIDE (1971)
C
C     HIGH TEMPERATURE SET
C
      DATA A0/
     1  .44608041E+01,  .30981719E-02, -.12392571E-05,  .22741325E-09,
     1 -.15525954E-13, -.48961442E+05, -.98635982E+00,
     2  .27167633E+01,  .29451374E-02, -.80224374E-06,  .10226682E-09,
     2 -.48472145E-14, -.29905826E+05,  .66305671E+01,
     3  .28963194E+01,  .15154866E-02, -.57235277E-06,  .99807393E-10,
     3 -.65223555E-14, -.90586184E+03,  .61615148E+01,
     4  .36219535E+01,  .73618264E-03, -.19652228E-06,  .36201558E-10,
     4 -.28945627E-14, -.12019825E+04,  .36150960E+01,
     5  .29840696E+01,  .14891390E-02, -.57899684E-06,  .10364577E-09,
     5 -.69353550E-14, -.14245228E+05,  .63479156E+01,
     6  .31001901E+01,  .51119464E-03,  .52644210E-07, -.34909973E-10,
     6  .36945345E-14, -.87738042E+03, -.19629421E+01,
     7  .25000000E+01, 0., 0., 0., 0.,  .25471627E+05, -.46011763E+00,
     8  .25420596E+01, -.27550619E-04, -.31028033E-08,  .45510674E-11,
     8 -.43680515E-15,  .29230803E+05,  .49203080E+01,
     9  .29106427E+01,  .95931650E-03, -.19441702E-06,  .13756646E-10,
```

```
     9  .14224542E-15,  .39353815E+04,  .54423445E+01,
     #  .31890000E+01,  .13382281E-02, -.52899318E-06,  .95919332E-10,
     # -.64847932E-14,  .98283290E+04,  .67458126E+01/
C
C
C      LOW TEMPERATURE SET
C
       DATA A/
     1 .24007797E+01, .87350957E-02, -.6607878E-05, .20021861E-08,
     1 .63274039E-15, -.48377527E+05, .96951457e+01,
     2 .40701275E+01, -.11084499E-02, .41521180E-05, -.29637404E-08,
     2 .80702103E-12, -.30279722E+05, -.32270046E+00,
     3 .36748261E+01, -.12081500E-02, .23240102E-05, -.63217559E-09,
     3 -.22577253E-12, -.10611588E+04, .23580424E+01,
     4 .36255985E+01, -.18782184E-02, .70554544E-05, -.67635137E-08,
     4 .21555993E-11, -.10475226E+04, .43052778E+01,
     5 .37100928E+01, -.16190964E-02, .36923594E-05, -.20319674E-08,
     5 .23953344E-12, -.14356310E+05, .29555535E+01,
     6 .30574451E+01, .26765200E-02, -.58099162E-05, .55210391E-08,
     6 -.18122739E-11, -.98890474E+03, -.22997056E+01/
C
C      MOLECULAR COLLISION PARAMETERS FROM SVHELA (1962)
C      (LENNARD JONES 6-12)
C
       DATA SIGMA/3.941, 2.641, 3.798, 3.467, 3.690, 2.827, 2.708,
     &            3.050, 3.147, 3.492/
       DATA EPS/195.2, 809.1, 71.4, 106.7, 91.7, 59.7, 37.0, 106.7,
     &          79.8, 116.7/
C
C      MOLECULAR WEIGHTS
C
       DATA M/44.01, 18.02, 28.008, 32.000, 28.01, 2.018, 1.009, 16.,
     &        17.009, 30.004/
C
C      GAS CONSTANT
C
       DATA RU/8.3143/
C
C      STATMENT FUNCTION FOR COLLISION INTEGRAL, HATTIKUDUR AND
C      THODOS (1970)
C
       OMEGA(TSTAR) = 1.155*TSTAR**(-.1462) + .3945*EXP(-.6672*TSTAR)
     &              + 2.05*EXP(-2.168*TSTAR)
C
C
C      STATEMENT FUNCTIONS FOR AUXILARY COEFFICIENTS, BROKAW(1961)
C
       PHI(MU1I,MU1J,MI,MJ) = (1. + (MU1I/MU1J)**0.5*(MJ/MI)**0.25)**2
     &                      /(2.*SQRT(2.*(1. + MI/MJ)))
       PSI(PHIIJ,MI,MJ) = PHIIJ*(1. + 2.41*(MI - MJ)*(MI - 0.142*MJ)
     &                  /(MI + MJ)**2)
C
C      COMPUTE THE NORMALIZED SPECIFIC HEAT OF INDIVIDUAL COMPONENTS
C
       IF( T .GT. 1000.) GO TO 10
       N = 6
       DO 20 I = 1,6
20     CPO(I) = A(1,I) + A(2,I)*T + A(3,I)*T**2 + A(4,I)*T**3 +
     &          A(5,I)*T**4
       GO TO 25
C
```



```
10     N = 10
       DO 30 I = 1,10
       CPO(I) = AO(1,I) + AO(2,I)*T + AO(3,I)*T*T + AO(4,I)*T**3
     &        + AO(5,I)*T**4
30     CONTINUE
C
C      COMPUTE THE VISCOSITY AND THERMAL CONDUCTIVITY OF THE
C      INDIVIDUAL COMPONENTS
C
25     DO 40 I = 1, N
       TSTAR = T/EPS(I)
       MU1(I) = 26.693E-06*SQRT(M(I)*T)/SIGMA(I)**2/OMEGA(TSTAR)
       LMBDA1(I) = 3.75*RU*MU1(I)/M(I)
       LMBDA2(I) = 0.88*(0.4*CPO(I) - 1.)*LMBDA1(I)
40     CONTINUE
C
C      COMPUTE THE VISCOSITY, FROZEN SPECIFIC HEAT AND FROZEN THERMAL
C      CONDUCTIVITY OF THE MIXTURE; BROKAW(1961)
C
       CPFROZ = 0.
       MW = 0.
       MU = 0.
       LMMIX1 = 0.
       LMMIX2 = 0.
       DO 50 I = 1,N
          IF(Y(I) .EQ. 0.) GO TO 50
          DEN1 = 1.0
          DEN2 = 1.0
          DO 60 J = 1,N
          IF( J .EQ. I .OR. Y(J) .EQ. 0. ) GO TO 60
          DUMMY = PHI(MU1(I),MU1(J),M(I),M(J))
          DEN1 = DEN1 + DUMMY*Y(J)/Y(I)
          DEN2 = DEN2 + PSI(DUMMY,M(I),M(J))*Y(J)/Y(I)
60        CONTINUE
       CPFROZ = CPFROZ + CPO(I)*Y(I)
       MW = MW + Y(I)*M(I)
       MU = MU + MU1(I)/DEN1
       LMMIX1 = LMMIX1 + LMBDA1(I)/DEN2
       LMMIX2 = LMMIX2 + LMBDA2(I)/DEN1
50     CONTINUE
C
       LAMBDA = LMMIX1 + LMMIX2
C
C      COMPUTE EQUILIBRIUM THERMAL CONDUCTIVITY ASSUMING UNITY
C      REACTION LEWIS NUMBER AS DEFINED BY SVHELA & MCBRIDE (1973)
C
       CPFROZ = CPFROZ*RU/MW
       CP = AMAX1(CP,CPFROZ)
       LAMBDA = LAMBDA*CP/CPFROZ
       RETURN
       END
```

8.4 RADIATION HEAT TRANSFER

In homogeneous charge engines, water and carbon dioxide radiate energy to the walls. Computations show that this heat loss is less than 10% of the convective heat loss. This is not significant enough to include in the dimen-

sional analysis although it is accounted for implicitly in any constants determined from experimental data.

To illustrate the latter point, let us suppose that

$$\frac{\dot{Q}}{A} = \mathbf{h}(T - T_w) + \epsilon\sigma(T^4 - T_w^4) \tag{8.37}$$

where ϵ is an emissivity and σ is the Stefan–Boltzmann constant. This equation can be rewritten as

$$\frac{\dot{Q}}{A} = (\mathbf{h} + \mathbf{h}_r)(T - T_w) \tag{8.38}$$

where $\mathbf{h}_r$ is a radiation heat transfer coefficient defined as

$$\mathbf{h}_r = \epsilon\sigma(T + T_w)(T^2 + T_w^2) \tag{8.39}$$

Suppose experimental data are to be correlated over the temperature range $T_1 < T < T_2$. It is possible to expand Eq. (8.39) into a Taylor Series about $\overline{T} = \frac{1}{2}(T_1 + T_2)$ as follows:

$$\mathbf{h}_r = \mathbf{h}_r\Big|_{T=\overline{T}} + \frac{d\,\mathbf{h}_r}{dT}\Big|_{T=\overline{T}}(T - \overline{T}) + \cdots \tag{8.40}$$

$$\mathbf{h}_r = c_0 + c_1(T - \overline{T}) + \cdots \tag{8.41}$$

where c_0 and c_1 are constants. If experimental data are correlated by

$$\frac{\dot{Q}}{A} = \mathbf{h}_{\text{exp}}(T - T_w) \tag{8.42}$$

when in fact Eq. (8.38) applies, then the best fit is achieved by choosing

$$\mathbf{h}_{\text{exp}} = \mathbf{h} + c_0 \tag{8.43}$$

which means the higher order terms in Eq. (8.39), such as $c_1(T - \overline{T})$, have been neglected. This is justified as long as

$$c_1(T - \overline{T}) \ll \mathbf{h} + c_0 \tag{8.44}$$

Since radiation heat transfer is small compared to convective heat transfer in homogeneous charge engines, Eq. 8.44 is the case. The heat transfer coefficient deducted from experimental accounts for the small amount of radiation present through the term c_0 even though it was never accounted for explicitly through the choice of correlating formula (8.42) rather than (8.37).

With diesel engines, radiation heat transfer is important during the combustion phase because of the presence of soot particles. Water and carbon dioxide radiate over narrow bands in the wavelength spectrum but soot particles radiate over the entire spectrum and are thus more significant. Annand (1963) accounts for radiation by Eq. (8.37) with $\epsilon = 0.58$ for diesel engines. Such an approach is a crude approximation at best.

A more accurate reflection of the physical processes involved in the diesel radiation heat transfer requires many more analyses, some of which cannot yet be done unequivocally. Papers by Dent and Suliaman (1977), Kamel and Watson (1979) and Chapman, Friedman, and Aghan (1983) are representative of the state of the art.

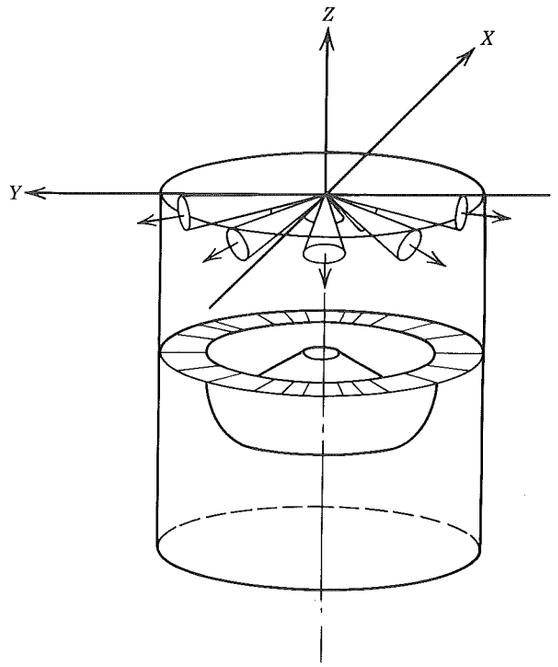

Figure 8-8 Isometric view of three-dimensional geometry used for computations of radiation heat transfer in a diesel engine (Chapman et al., 1983). Reprinted with permission © 1983. Society of Automotive Engineers, Inc.

An appreciation for the computational complexities involved can be gained by inspection of Fig. 8-8. Chapman et al. (1983), with knowledge of the plume shapes, their emissivities, and temperatures as functions of time, compute radiation view factors for all possible combinations of elemental surfaces on the plumes, the head, the cylinder wall, and the piston. Taking advantage of the symmetry present, the cylinder is divided into a pie shape with an included angle of 11.5 deg; even so there are nearly 600 surfaces treated in the computation.

8.5 HEAT TRANSFER MEASUREMENTS

Figure 8-9 depicts an engine instrumented to determine the quantities of heat rejected to the oil, the water, and to ambient. Flow meters are installed in the water and oil circuits and thermocouples measure the inlet and outlet temperatures. The first law applied to the water coolant and the oil flowing through the

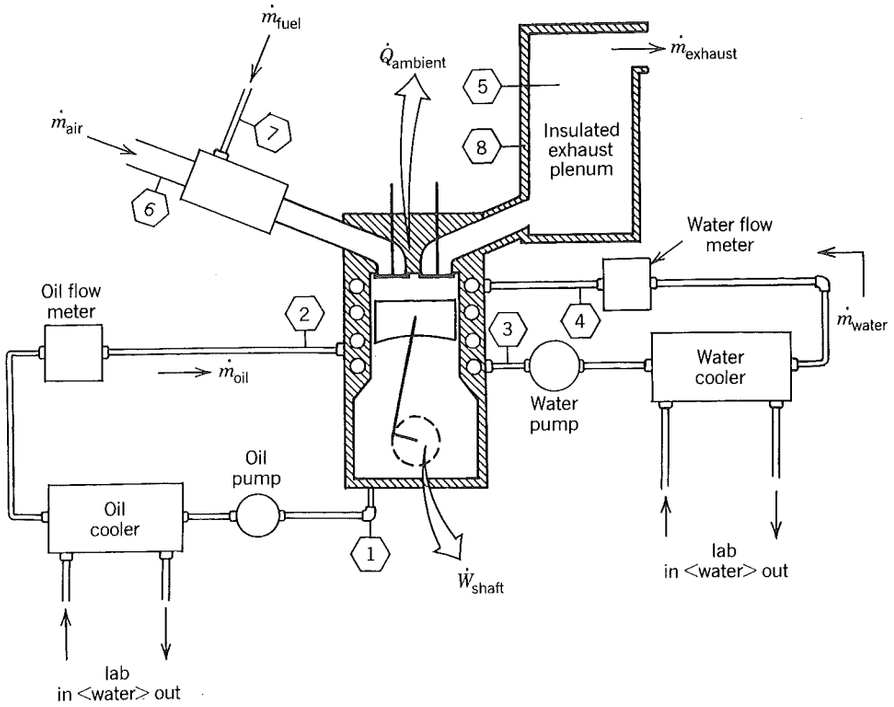

Figure 8-9 Engine equipped with instrumented oil and water circuits for doing energy balance experiments. The hexagons denote points of temperature measurement. An insulated exhaust plenum is used to determine the mass average exhaust temperature. The exhaust thermocouple must be shielded or a correction applied using equation (8.49).

engines yields

$$\dot{Q}_{water} = (\dot{m}c_p)_{water}(T_3 - T_4) \tag{8.45}$$

$$\dot{Q}_{oil} = (\dot{m}c_p)_{oil}(T_1 - T_2) \tag{8.46}$$

Determining the heat loss to ambient air is more involved. The first law is applied to the engine system from which one obtains

$$\dot{Q}_{ambient} = (\dot{m}h)_{air} + (\dot{m}h)_{fuel} - (\dot{m}h)_{exhaust} - \dot{Q}_{water} - \dot{Q}_{oil} - \dot{W}_{shaft} \tag{8.47}$$

The mass flow rate of the exhaust is known in terms of the measured mass flow rates of air and fuel since

$$\dot{m}_{exhaust} = \dot{m}_{air} + \dot{m}_{fuel} \tag{8.48}$$

The enthalpies of the fuel, the air, and the exhaust are based on the measured temperatures T_7, T_6, and T_5, respectively. The exhaust composition can be calculated theoretically from the known fuel–air equivalence ratio or it may be

measured. In either case it is important that the temperature T_5 correspond to the mass average temperature of the exhaust; for this reason there is an insulated plenum that serves to mix the hot exhaust gas emitted early in the cycle with the cooler exhaust gas emitted later in the cycle. A further complication is that the thermocouple radiates and thus reads too low and must be corrected to obtain the true gas temperature. An energy balance on the thermocouple tip yields

$$T_{exhaust} = T_5 + \frac{\epsilon\sigma}{\mathbf{h}}(T_5^4 - T_8^4) \tag{8.49}$$

where ϵ is the emissivity of the thermocouple tip, σ is the Stefan–Boltzmann constant, $\mathbf{h}$ is the heat transfer coefficient at the tip, T_5 is the tip temperature, and T_8 is the exhaust plenum inner wall temperature.

In doing these energy balances, it is common practice to evaluate the maximum heat that can be recovered from the exhaust gas. This is computed from an energy balance on the exhaust where it is cooled to ambient temperature

$$\dot{Q}_{exhaust} = \dot{m}_{ex}[h_{ex}(T_{exhaust}) - h_{ex}(T_{ambient})] \tag{8.50}$$

In evaluating the exhaust enthalpy at ambient temperature, equilibrium water quality should be used, as discussed at length in Chapter 4.

If Eq. (8.50) is substituted into Eq. (8.47), one obtains

$$\dot{Q}_{ambient} = \dot{Q}_{in} - \dot{Q}_{exhaust} - \dot{Q}_{water} - \dot{Q}_{oil} - \dot{W}_{shaft} \tag{8.51}$$

where, by definition

$$\dot{Q}_{in} = (\dot{m}h)_{air} + (\dot{m}h)_{fuel} - \dot{m}_{ex}h_{ex}(T_{ambient}) \tag{8.52}$$

Finally, if the fuel and air are at the ambient temperature, if the engine runs lean or stoichiometric, and if the ambient temperature and pressure are coincident with the reference temperature and pressure, then the heat in is the product of the fuel flow rate and the fuel's stoichiometric heat of combustion.

Some results obtained by Whitehouse (1970–1971) for a medium speed diesel engine are given in Table 8-3. The table also gives heat equivalence of

Table 8.3 Energy Balance on a Medium Speed, Four-Stroke, Direct-Injection,Shallow-Bowl, Turbocharged Diesel Engine[a]

R_s (rpm)	bmep (bar)	$\dot{Q}_{exhaust}$	$\dot{Q}_{water}$	$\dot{Q}_{oil}$	$\dot{Q}_{ambient}$	$\dot{W}_{shaft}$	$\dot{Q}_{friction}$	$\dot{Q}_{loss}$
500	9.90	0.459	0.118	0.037	0.069	0.317	0.100	0.124
500	3.52	0.437	0.108	0.065	0.092	0.298	0.178	0.087
400	3.50	0.432	0.151	0.074	0.026	0.315	0.092	0.159

Source: Whitehouse (1970–71).

[a]Engine: $b = 304.8$ mm, $S = 381$ mm, $r = 12.85$.

Ambient: $T = 293$ K, $P = 1.01$ bar.

$\dot{Q}_{loss} = \dot{Q}_{water} + \dot{Q}_{oil} + \dot{Q}_{ambient} - \dot{W}_{friction}$

All energy rates are normalized by the fuel rate, $\dot{Q}_{in}$.

This engine is a single cylinder version of the Mirrlees–National F4A multicylinder engine.

the friction so that one can ascertain how much of the heat lost to the ambient air, to the oil, and to the water is from the working fluid and how much is from friction.

Inspection of this table reveals that the engine to which it refers has a brake thermal efficiency of about 30%. About 45% of the energy is rejected in the exhaust, 10 to 15% is dissipated by friction, and 10 to 15% is dissipated by heat loss. It is interesting to compare these results with similar results for an automotive engine.

Figure 8-10 shows the results of an energy balance on a small, spark-ignition automobile engine. This engine has an internal oil pump and the heat rejected to the oil is carried away partly by the coolant and partly by the heat lost to ambient air.

As the load varies from $P_i = 0.4$ bar to $P_i = 0.8$ bar, the energy converted to shaft work varies from about 20 to 30%, the coolant load varies from about 40 to 30%, the exhaust energy varies from about 30 to 35%, and the heat lost to

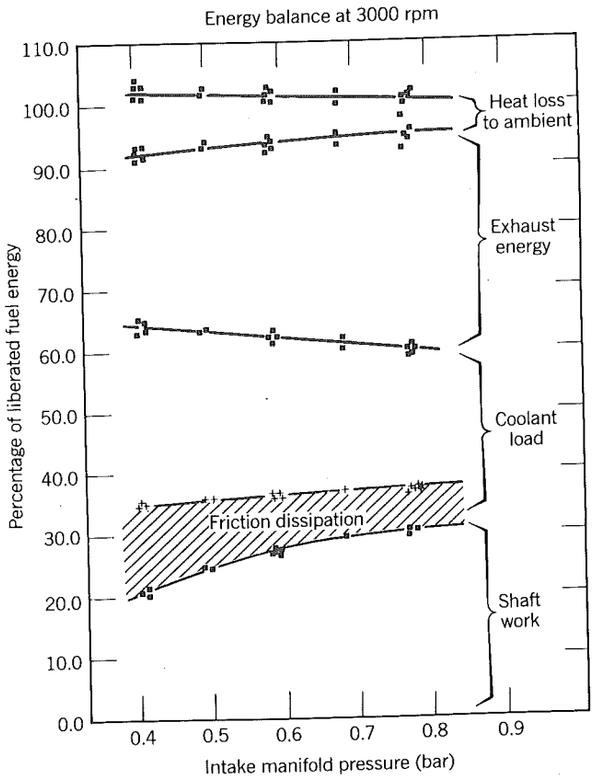

Figure 8-10 Energy balance on an automotive engine (Brigham, 1985). Courtesy Ford Motor Co.

ambient air varies from about 10 to 5%. The energy dissipated by friction varies from about 14 to 7% for the same loads; the total heat loss by the gas during the cycle must therefore be about 36 to 28%.

The diesel engine loses only about one half as much heat as the gasoline engine, yet their shaft efficiencies are about equal.[3] Experiments with insulated engines show that a reduction in heat loss has a small impact on the shaft efficiency and that the heat no longer lost mostly appears in the exhaust energy. That the diesel engine of Table 8-3 has more exhaust energy than the gasoline engine of Fig. 8-10 is consistent with this observation.

There are two reasons why reducing the heat loss has little impact on the engine efficiency: (1) the engine utilizes only about 30% of the heat added in the vicinity of top center; therefore it could use no more than 30% of the heat saved by reducing the heat loss; (2) the heat saved is not added at top center; rather it is distributed throughout the expansion stroke. Therefore the efficiency with which it can be used is much less than 30%.

Not all engines are water cooled. Air cooling offers several advantages, Mackerle (1961). One is elimination of the water cooling system, failure in which is a major cause of down time in engine systems. Furthermore there is no coolant to freeze at low temperatures. Foremost among the disadvantages are an increased noise level because of the absence of the water and water jackets that act as sound dampers and the need for a directed air flow. Aircraft engines are, for the most part, air cooled; supplying the required air flow is not a problem since the engine need not be enclosed and is usually located right behind a propeller. Figure 8-11 shows one cylinder used on a Pratt and Whitney Mark R-2800 air cooled aircraft engine. (This 28-cylinder engine is an example of a piston engine that was displaced by the gas turbine.) Notice that fins were used to enhance the heat transfer from the engine. Results of an energy balance obtained on a single-cylinder version of this engine are given in Table 8-4.

Under cruise conditions the engine runs at $R_s = 1800$ rpm, bmep = 8.75 bar, $\phi = 0.90$. During takeoff, $R_s = 2700$ rpm, bmep = 13.72 bar, $\phi = 1.65$, the engine is fueled extremely rich, and only about one half of the fuel's energy is released. This is done to utilize the liquid fuel's latent heat for cooling and to avoid knock limiting the power. Because the fuel consumed during takeoff is small compared to that used in the entire trip, the fact that fuel is wasted is of secondary concern. Notice that during takeoff 35% of the heat released is used but that the brake thermal efficiency of the engine is only $0.45 \times 35\% = 16.1\%$.

When an engine is running at a steady state, the heat transfer throughout most of the engine structure is steady. As we have seen, unsteady periodic effects are limited to a penetration layer about 1 to 5 mm thick at the gas–wall interface. Resolution of the instantaneous heat transfer at that interface can be achieved by inserting a surface thermocouple into the engine structure, con-

[3] The diesel engine is a single cylinder research engine. Its friction is a little higher than representative of a production multicylinder engine.

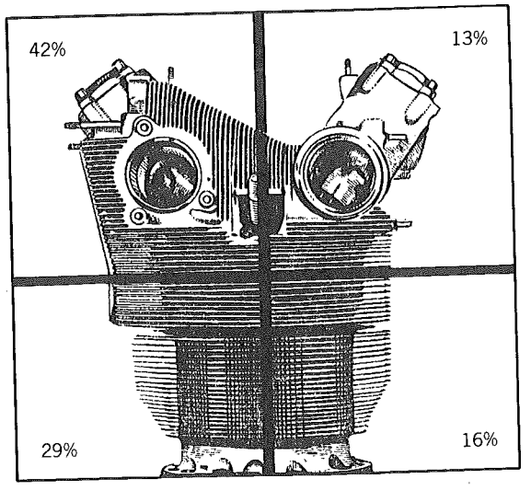

Figure 8-11 Distribution of heat loss from the fins of an air-cooled aircraft engine. Note that 42% of the heat loss is dissipated by fins in the vicinity of the exhaust valve (Ryder, 1950). Reprinted with permission © 1950. Society of Automotive Engineers, Inc.

Table 8.4 Energy Balance on an Air-Cooled, Spark Ignition Aircraft Engine[a]

		Normalized by $\dot{Q}_{in}$					
R_s (RPM)	bmep (BAR)	$\dot{Q}_{exhaust}$	$\dot{Q}_{oil}$	$\dot{Q}_{ambient}$	$\dot{W}_{shaft}$	ϕ	$\dot{Q}_{in}/\dot{m}_f q_c$
1800	8.75	0.44	0.09	0.18	0.29	0.90	0.98
2700	13.72	0.44	0.08	0.12	0.35	1.65	0.46

Source: Ryder (1950).

Engine: $b = 146.1$ mm, $S = 152.4$ mm.

[a]This engine is a single cylinder version of the Pratt and Whitney R-2800 multicylinder engine.

figured in a design by Bendersky (1953). The essential features of a surface thermocouple used for this purpose are shown in Fig. 8-12.

Within the plug are two thermocouple junctions, one at the surface and one at a depth Δx from the surface. The basic idea is that according to Fourier's law for small Δx, one could realize

$$q'' \approx -\lambda \frac{\Delta T}{\Delta x} \tag{8.53}$$

Unfortunately, the criterion for small Δx is that it be small compared to the penetration layer l. It is just not practical to build a plug with $\Delta x \ll l$. Therefore, instead, one solves the heat conduction equation between the two thermocouples assuming that it is one dimensional.

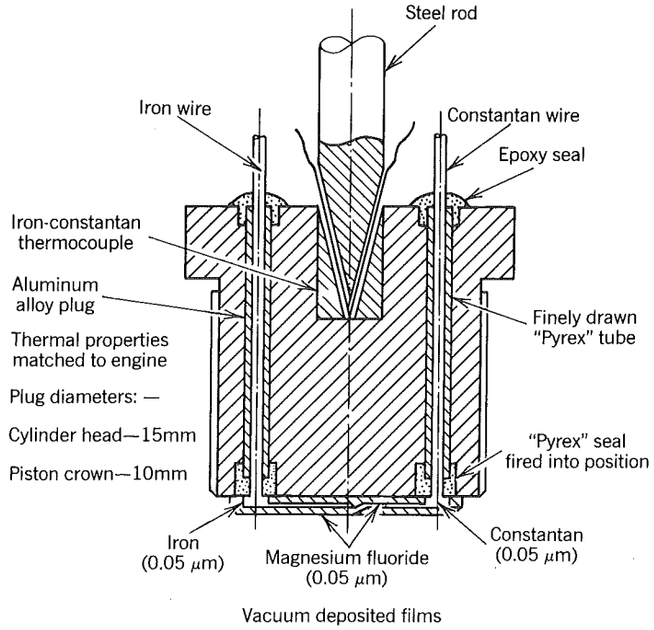

Figure 8-12 Essential features of a surface thermocouple plug used to measure local, instantaneous heat loss, (Dent and Suliaman, 1977). Reprinted with permission © 1977. Society of Automotive Engineers, Inc.

The measured surface temperature variation in time is fitted by a Fourier series

$$T(0,t) = \bar{T}(0) + \sum_{i=1}^{N} \left[A_i \cos(i\omega t) + B_i \sin(i\omega t) \right] \tag{8.54}$$

to determine the coefficients A_i and B_i. The heat flux is then

$$q'' = -\lambda \left\{ \frac{\Delta \bar{T}}{\Delta x} + \sum_{i=1}^{N} \sqrt{\frac{i\omega}{2\alpha}} \left[(B_i - A_i) \sin(i\omega t) + (B_i + A_i) \cos(i\omega t) \right] \right\} \tag{8.55}$$

The term ω is one half the engine frequency for a four-stroke engine and equal to the engine frequency for a two-stroke engine. The curve fit, Eq. (8.54) is applied to one engine cycle.

A surface thermocouple gives a measurement of the local heat flux. In order to determine the total heat loss from the gas, one must evaluate the heat transfer at every point in the combustion chamber and integrate.

$$\dot{Q}(t) = \int_{A(t)} q''(t)\, dA \tag{8.56}$$

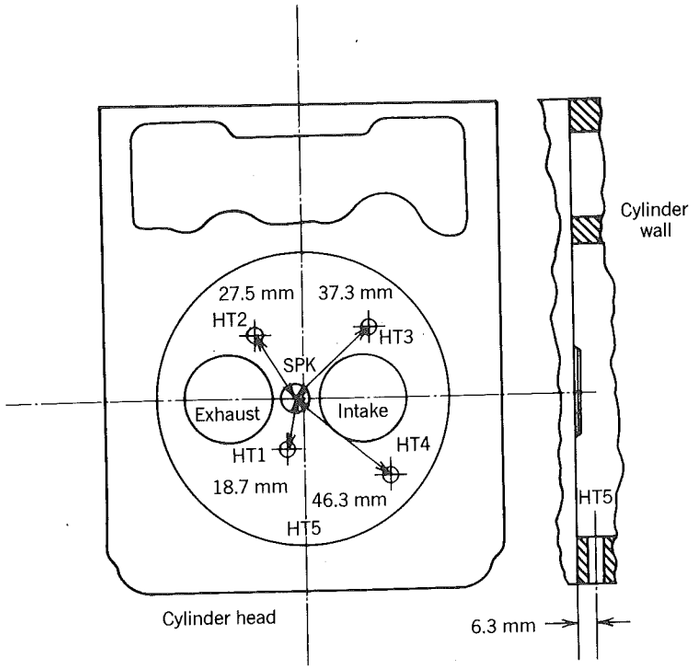

Figure 8-13 Five locations (HT1, HT2,...) of surface thermocouples in a spark-ignition engine studied by Alkidas and Myers (1982): $b = 104.7$ mm, $S = 95.3$ mm, $r = 8.56$. Reprinted with permission © 1982. ASME.

For this reason a number of surface thermocouple should be installed into the engine.

Figure 8-13 shows the location of five surface thermocouples in a four-stroke, spark-ignition engine used by Alkidas and Myers (1982). There are four in the head and one on the major thrust side of the cylinder. The combustion chamber is disk shaped and has a centrally located spark plug.

Results obtained at the location HT1 are given in Fig. 8-14 for five consecutive cycles. Notice that most of the heat transfer occurs early in the expansion stroke $360 < \theta < 420$. The gas temperatures are highest at this time but so is the heat transfer coefficient. Results obtained for other thermocouple locations are shown in Fig. 8-15. That the flame arrives at position HT5 later than at the other positions is clearly indicated. The cycle to cycle variations noted in Fig. 8-14 are caused by cycle to cycle variations in arrival times of the turbulent flame at the position HT1.

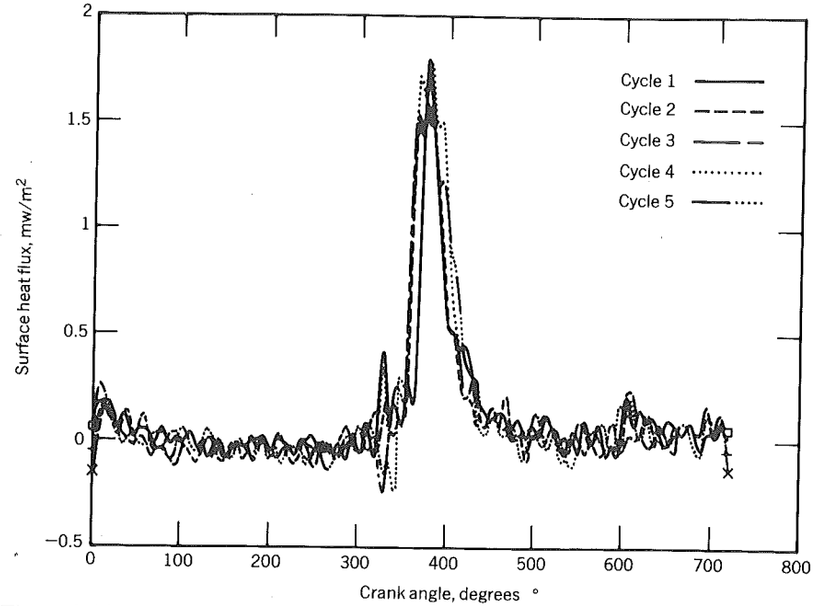

Figure 8-14 Heat flux histories of five consecutive cycles at location HT1 defined in Fig. 8-13: $R_s = 1500$ rpm, $\phi = 0.87$, $D_r = 0.40$, MBT (Alkidas and Myers, 1982). Reprinted with permission © 1982. ASME.

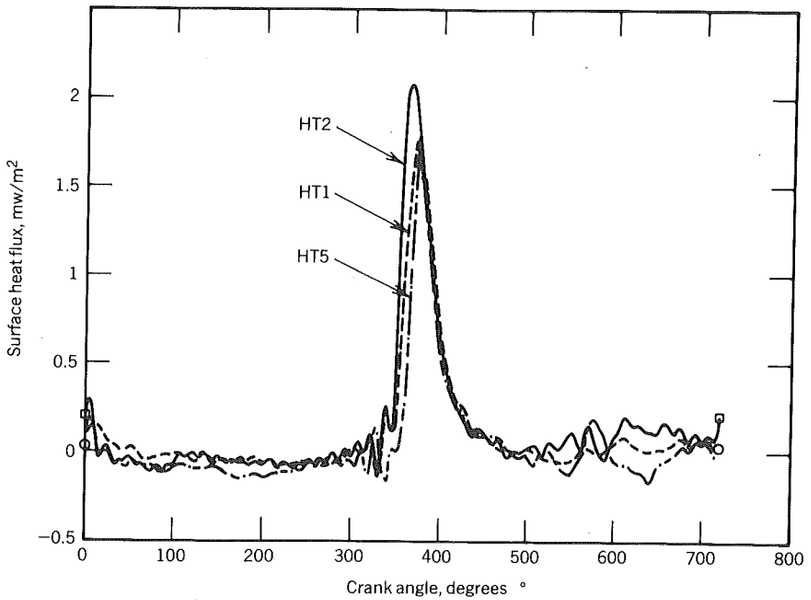

Figure 8-15 Heat flux histories for three different locations: HT1, HT2, and HT5 defined in Fig. 8-13 and operating conditions of Fig. 8-14 (Alkidas and Myers, 1982). Reprinted with permission © 1982. ASME.

8.6 MASS LOSS OR BLOWBY

There are three primary reasons for an interest in blowby. It influences (1) the gas pressure acting on the rings which influences the friction and wear characteristics; (2) the indicated performance; (3) the hydrocarbon emissions.

Typically a ring pack consists of two compression rings and an oil ring. The pressure drop across the oil ring is generally neglible. Such a ring pack is represented in Fig. 8-16. A one-dimensional representation of the ring pack is also shown; it consists of three plenums in series through passages whose sizes are dependent upon the ring gaps, the piston to cylinder wall clearance, and any ring tilt present. The volumes are all time dependent: V_0 changes because of piston motion; V_1 changes because of ring motion; and V_2 changes because of piston motion (including those of the other cylinders in a multicylinder engine).

Figure 8-17 shows the results of measurements made for the ring gas pressures in a two-stroke diesel engine. Notice that at about 70 deg after top dead center, the pressure between the rings is greater than the cylinder pressure which, if the flows are quasi-steady, means the flow has reversed itself. The figure also shows pressures computed assuming the flows are one-dimensional, quasi-steady, and isentropic as they pass from one plenum to another. The mass flow from one plenum to another is governed by Eq. (7.14). The requisite stagnation properties and the specific heat ratio are based on current values in the upstream plenum. The throat area is proportional to the ring gap and the

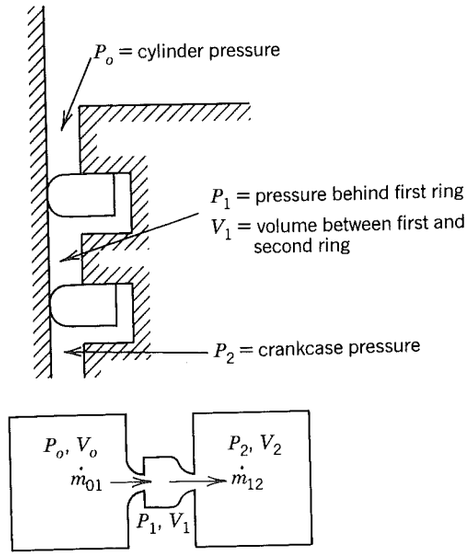

Figure 8-16 Ring pack and 1-D flow model of blowby.

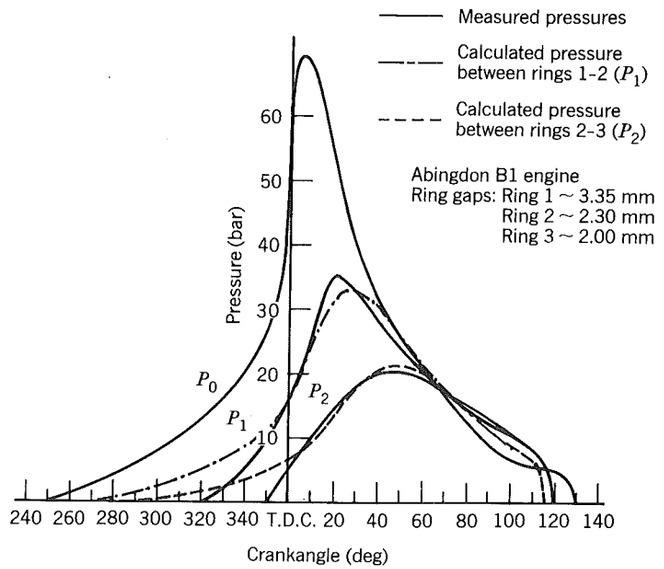

Figure 8-17 Abingdon B1. Measured and predicted interring pressure (Ruddy, 1979).

bore to cylinder clearance. The constant of proportionality, which depends at least on the Reynolds number of the flow and probably on whether or not the ring is tilted, is not known with certainty. It is of order unity and its magnitude is fixed by forcing a match between some measured and predicted data (such as the average blowby rate and the interring pressure distribution).

It is typical in such computations to assume that the gas between rings is at a temperature equal to the average of the piston temperature and the cylinder liner temperature. In so doing, there is no need to solve the energy equation for each plenum. The equation of continuity for mass conservation is applied to each plenum where the mass flows in and out are determined as just described. By simultaneously integrating the resultant ordinary differential equations, one obtains the mass within each plenum. These are coupled to equations of motion for each ring, thereby obtaining the plenum volumes. With the plenum volumes and the mass contained therein, one then uses an equation of state to compute the pressure in each plenum.

It was mentioned that blowby influences the hydrocarbon emissions. During compression and the early stages of combustion, unburned fuel and air is being compressed into the plenums between the rings. As mentioned, the gases rapidly equilibrate thermally to the environment and are thus at the average of the piston and liner temperature. In fact, the heat transfer is so effective that the flame propagating in the cylinder is extinguished when it tries to propagate into the spaces between the rings. The unburned fuel and air

pushed into the ring pack remains unburned. Soon after the blowby flow reverses itself, unburned fuel and air emerges from the ring pack back into the cylinder. Since this occurs late in the expansion stroke, the burned gases in the cylinder are relatively cold, and thus a large part of this reemerging fuel and air will not be oxidized as it mixed with the in-cylinder combustion products. Thus unburned fuel or hydrocarbons will be expelled from the engine during the exhaust process, Namazian and Heywood (1982).

Figure 8-18 shows a sampling valve mounted in the piston of a Nissan 1.3 liter, four-cylinder, gasoline engine by Furuhama and Tateishi (1972). This valve can be opened for 1.25 ms at the same angle in consecutive cycles. Thus gases can be withdrawn for analysis from the space between the top land and

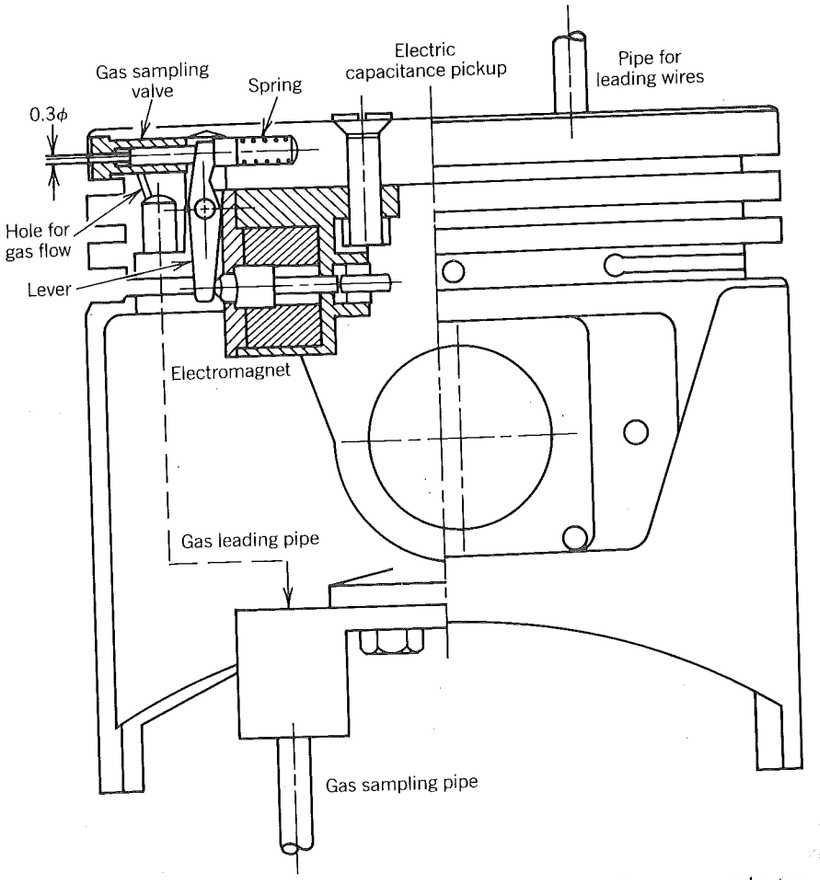

Figure 8-18 Gas sampling valve installed in a piston for sampling gases at the top land (Furuhama and Tateishi, 1972).

the cylinder at different angles during the cycle. Results obtained at wide-open throttle and 2000 rpm are given in Fig. 8-19.

During the compression stroke concentrations of oxygen and hydrocarbons (as *n*-Hexane equivalent) are high because fuel and air is entering the ring pack. Likewise carbon dioxide and carbon monoxide are low in concentrations attributable to the residual gas content. About 15 deg before top dead center, there is a sudden drop in oxygen and hydrocarbon concentrations as now burned gases are beginning to enter the ring pack. About 30 deg after top dead center, it appears that the unburned gases that entered earlier reemerge though diluted somewhat by the burned products that entered the ring pack.

By writing conservation equations for each species in the burned and unburned gases, Furuhama and Tateishi (1972) were able to formulate and integrate a set of ordinary differential equations for the gas composition in the top land as a function of time. The computed results, shown in Fig. 8-19, agree well with the experimental values. In the case of the hydrocarbons, the agreement is not as good and only the trend appears reliable. The discrepancy is attributable in part to the computation and in part to the instrumentation, both of which assume there is only one type of hydrocarbon present when in fact there are 10 to 20 different species of significance. This is often ignored as a problem in practice only; that is, in principle we understand the nature of the blowby. At the light loads the computations and experiments show no corre-

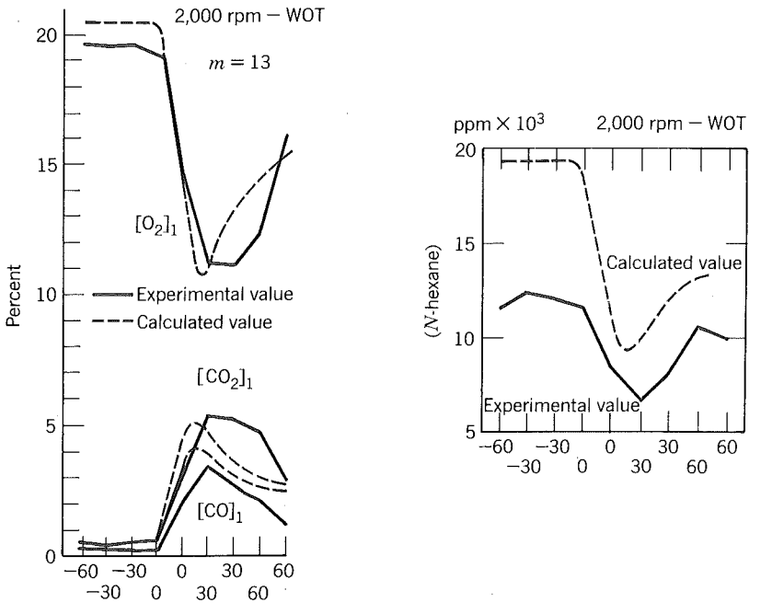

Figure 8-19 Measured and calculated gas composition at top land of a gasoline engine at WOT (Furuhama and Teteishi, 1972).

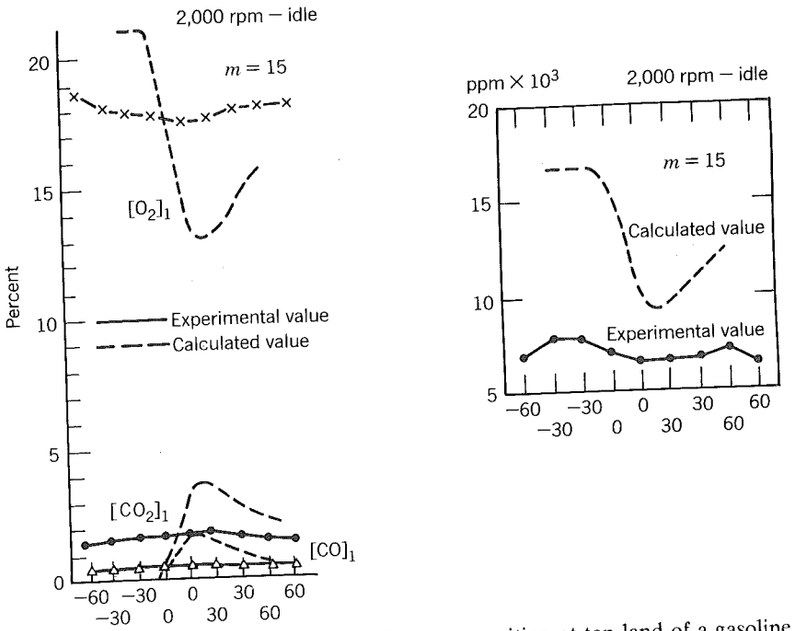

Figure 8-20 Measured and calculated gas composition at top land of a gasoline engine at idle (Furuhama and Teteishi, 1972).

spondence whatsoever (Fig. 8-20). This fundamental problem awaits resolution.

In Chapters 2 and 4 we investigated the influence of blowby on indicated performance. It was assumed that the flow was always out of the cylinder and that the rate was proportional to the mass of the cylinder contents. The constant of proportionality was selected so that about 2.5% of the charge leaked out, consistent with observation. The results showed blowby had little influence on indicated performance; yet it is known that blowby can be a significant loss.

The computations were deliberately simple for illustration purposes. They ignore the fact that a flow reversal occurs during the expansion stroke. Thus they underestimate the mass of unburned gas that is pushed into the ring pack during compression. As already mentioned, when this gas reemerges, much of it fails to oxidize and thus fuel is wasted. Namazian and Heywood (1982), in doing the computations, more correctly estimate that anywhere from 2 to 7% of the fuel is wasted this way. Herein lies another advantage of diesel engines since in them mostly air will be compressed into the ring pack.

There are better methods than using the butt joint for controlling blowby. Figure 8-21 shows some different types of ring joints that can be employed. The butt joint is the most common because it is cheapest and more forgiving when bore distortion is present.

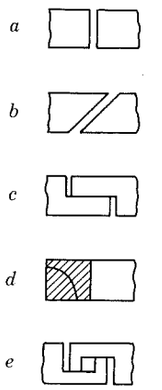

Figure 8-21 Types of ring joints (*a*) Butt joint. (*b*) Angle joint. (*c*) Overlapped joint. (*d*) Gas tight joint. (*e*) Interlocked joint. (Duck, Beyer, and Mierbach, 1977).

8.7 REFERENCES

Alkidas, A. C. and J. P. Myers (1982), "Transient Heat-Flux Measurements in the Combustion Chamber of a Spark Ignition Engine," *J. Heat Transfer*, ASME Trans., Vol. 104, pp. 62–67.

Annand, W. J. D. (1963), "Heat Transfer in the Cylinders of a Reciprocating Internal Combustion Engine," *Proc. IME*, **177**, p. 973.

Bendersky, D. (1953), "A Special Thermocouple for Measuring Transient Temperature," *Mech. Eng.*, **75**, p. 117.

Borgnake, C., V. S. Arpaci, and R. J. Tabaczynski (1980), "A Model for the Instantaneous Heat Transfer and Turbulence in a Spark Ignition Engine," SAE paper 800287.

Brigham, D. R. (1985), Ford Motor Co., SAE publication pending.

Brokaw, R. S. (1961), "Alignment Charts for Transport Properties Viscosity, Thermal Conductivity and Diffusion Coefficients for Nonpolar Gases and Gas Mixtures at Low Density," NASA TR-R-81. See also W. M. Rohsenow and J. P. Hartnett, *Handbook of Heat Transfer*, McGraw-Hill, New York, (1973) pp. 2–109 through 2–129.

Caton, J. A. and J. B. Heywood (1981), "An Experimental and Analytical Study of Heat Transfer in an Engine Exhaust Port," *Int. J. Heat Mass Trans.*, **24** (4), pp. 581–595.

Chapman, M., M. C. Friedman, and A. Aghan (1983), "Radiation Heat Transfer From Soot in D.I. Diesel Engine," SAE paper 831725.

Dent, J. C. and S. J. Suliaman (1977), "Convective and Radiative Heat Transfer in a High Swirl Direct Injection Diesel Engine," SAE paper 770407.

Duck, G. E., H. Beyer and A. Mierbach (1977), *Piston Ring Manual*, GOETZE-AG, Germany.

Furuhama, S. and Y. Tateishi (1972), "Gases in Piston Top-Land Space of Gasoline Engine," *Trans. Soc. Automotive Eng. of Japan*, **4**, pp. 30–39.

Hattikudur, V. R. and G. Thodos (1979), "Equations for the Collision Integrals," *J. Chemical Phys.*, **52** (8), p. 4313.

Hires, S. D. and G. L. Pochmara (1976), "An Analytical Study of Exhaust Gas Heat Loss in a Piston Engine Exhaust Port," SAE paper 760767.

Hirschfelder, J. P., C. F. Curtiss, and R. B. Bird (1954), *Molecular Theory of Gases and Liquids*, Wiley, New York.

Holman, J. P., 1963, *Heat Transfer*, McGraw-Hill, New York.

Kamel, M. and N. Watson (1979), "Heat Transfer in the Indirect Injection Diesel Engine," SAE paper 790826.

Li, C. H. (1982), "Piston Thermal Deformation and Friction Considerations," SAE paper 820086.

Mackerle, J. (1961), *Air Cooled Motor Engines*, Cleaver–Hume Press Ltd., London.

Malchow, G. L., S. C. Sorenson, and R. O. Buckius (1979), "Heat Transfer in the Straight Section of an Exhaust Port of a Spark Ignition Engine," SAE paper 790309.

Namazian, M. and J. B. Heywood (1982), "Flow in the Piston-Cylinder-Ring Crevices of a Spark-Ignition Engine: Effect on Hydrocarbon Emissions, Efficiency and Power," SAE paper 820088.

Ruddy, B. (1979), "Calculated Inter-Ring Gas Pressures and their Effect upon Ring Pack Lubrication," *DAROS Information*, **6**, pp. 2–6, Sweden.

Ryder, E. A. (1950), "Recent Developments in the R-4360 Engine," *SAE Quart. Trans.*, **4**(4), p. 559.

Svehla, R. A. (1962), "Estimated Viscosities and Thermal Conductivities of Gases at High Temperatures," NASA TR R-132.

Taylor, C. F. (1977), *The Internal Combustion Engine in Theory and Practice*, MIT Press, Cambridge, Massachusetts.

Whitehouse, N. D. (1970–1971), "Heat Transfer in a Quiescent Chamber Diesel Engine" *Proc. IME*, **185**, p. 963.

Woschni, G. (1967), "A Universally Applicable Equation for the Instantaneous Heat Transfer Coefficient in the Internal Combustion Engine," SAE paper 670931.

8.8 HOMEWORK

1. The heat transfer coefficient increases with engine speed; whereas the time available to lose heat decreases. Explain what the net effect will be in terms of engine efficiency.
2. How would you expect the number 6.18 in Eq. (8.19) to change if Woschni had varied the diameter of his intake valve?
3. Equation (8.16) predicts that as far as engine speed is concerned, the indicated efficiency should show the following dependence

$$(1 - \eta/\eta_{\text{otto}}) \propto R_s^{-0.25}$$

since the ratio η/η_{otto} is dominated by heat loss. Show that this is consistent with the results given in Fig. 5-16 by plotting them on log–log paper and observing that the slope is nearly equal to $\frac{1}{4}$. Assume that $\eta_{\text{otto}} = 0.34$ and is independent of engine speed.

4. Derive various forms of Eq. (8.17) assuming that $\mu \propto T^{0.7}$, $\lambda \propto T^{0.8}$, and $P_r = 0.7$. In the discussion of Fig. 8-14 it was mentioned that the heat transfer is a maximum in the early part of the expansion stroke. Explain the various ways in which the high temperature and pressure are manifested here.
5. Crudely estimate the maximum rate in kilowatts at which an automobile radiator would have to dissipate heat if the engine produces a maximum brake power of 75 kW. What would be the temperature change in the water as it passes through the radiator if the water flow rate is 100 *l*/min? What would it be as it passes through the engine?
6. Practical application of Eq. (8.51) is limited because the heat loss to ambient air is determined by the small differences between much bigger numbers. Suppose each term on the right-hand side can be determined to within $\pm 5\%$. What tolerances could then be attached to $\dot{Q}_{\text{ambient}}$? For nominal values use the results given in Table 8-3.

Nine

COMBUSTION AND EMISSIONS

9.1 FLOW VISUALIZATION

In the late 1930s, Rassweiler and Withrow (1938) at General Motors modified an L-head cylinder so that a quartz window could be installed allowing an unobstructed view of the entire combustion space. Using high-speed motion photography they were able to record the combustion process. Figure 9-1 shows a typical sequence obtained illustrating flame propagation in a homogeneous-charge spark-ignition engine.

Ignition occurs at $\theta = -25$ deg. Notice that no flame is visible until $\theta = -16$ deg which is 9 deg later. That 9 deg period is called the ignition delay $\Delta\theta_{id}$. Once formed, the flame spreads like a spherical wave into the unburned gas with a ragged surface because of turbulence. The end of combustion is discerned from simultaneously recorded cylinder pressure. The combustion duration $\Delta\theta_c$, from $\theta = -16$ to $\theta = +21$, is 37 deg. Notice that the burned gases remain luminous even after combustion is complete.

Movies can be made in overhead valve engines using a quartz piston engine as illustrated in Fig. 9-2. In this case, the camera looks through a fixed tube at a mirror to view the combustion from the underside of the piston. Results obtained are similar to those already mentioned.

Shadow photography is a method of flow visualization that shows contrasts due to differences in density of the flow. It does not record light emitted by the flame; rather it records light transmitted through and refracted by the gases. Figure 9-3 shows shadowgraph sequences for lean and slightly rich combustion. Again, a ragged edge wave is seen propagating into the unburned mixture. Ignition delay is on the order of 10 deg for the rich case and 20 deg for the lean case.

At 20 and 25 deg after ignition in the rich case the width of the flame front is clearly discernible, one of the advantages shadow photography offers over ordinary photography. The width is more difficult to discern in the lean case because it is two or three times thicker. Thus a completely burned region does not appear until approximately 40 deg after ignition. At this time the whitest region is burned gas, the greyish region in front of the flame is

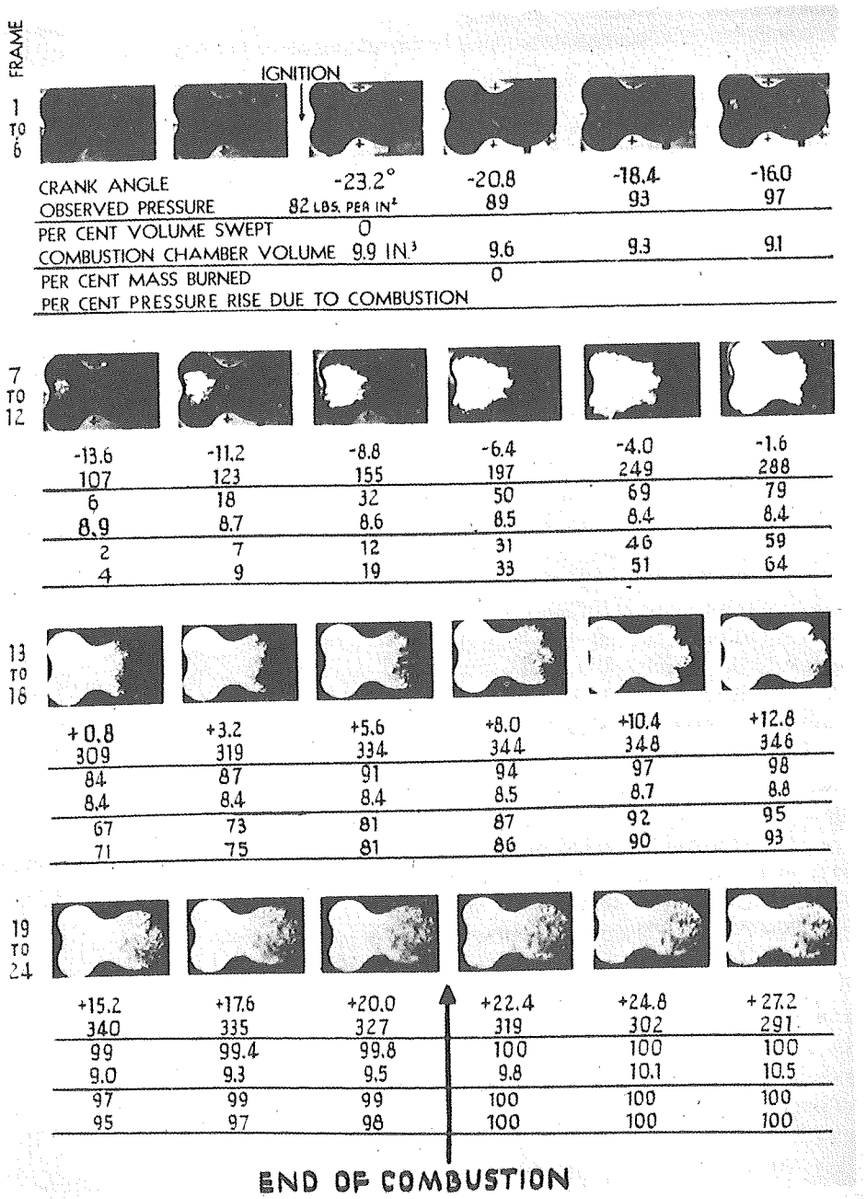

Figure 9-1 Rassweiler and Withrow (1938). Reprinted with permission © 1938. Society of Automotive Engineers, Inc.

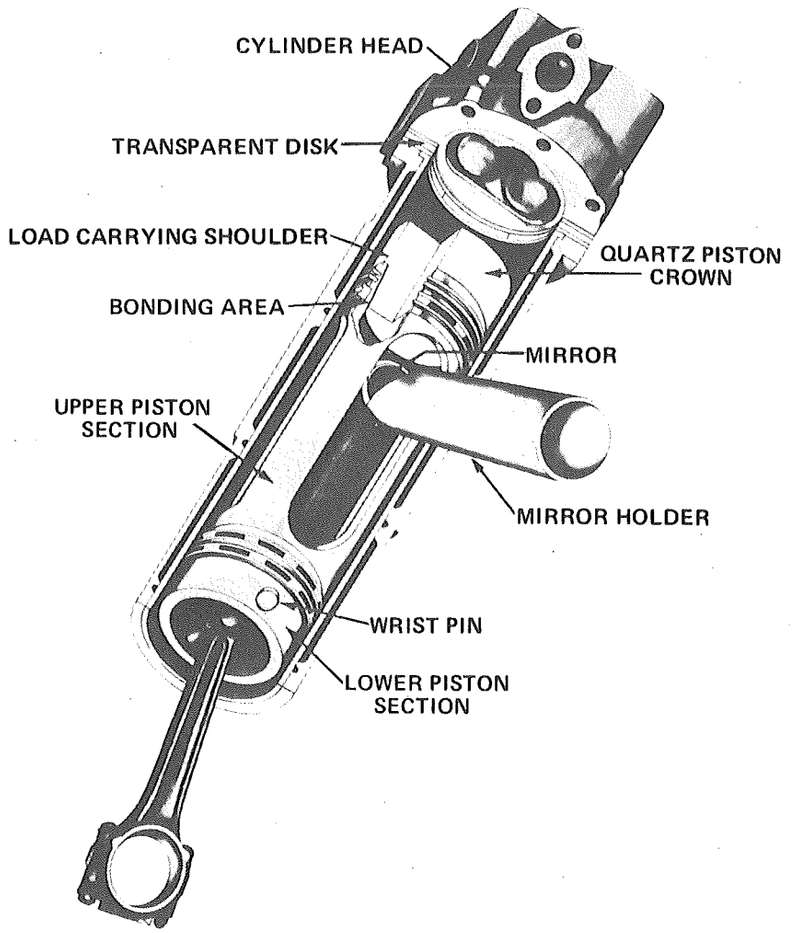

Figure 9-2 Quartz piston engine cylinder; piston and head assembly (Bowditch, 1961). Reprinted with permission © 1961. Society of Automotive Engineers, Inc.

unburned gas, and the highly convoluted dark and white region is mixture of burned, burning, and unburned gas.

A convenient way to conceptualize the flame propagation is in terms of ink rollers. The ink roller model is shown in Fig. 9-4. Imagine a bunch of cylindrical rolls as depicted to represent vortices in the turbulent flow field. Now consider ignition as being analogous to continuously depositing a stream of ink at the periphery of one roll. The rollers are rotating and as a result the ink spreads. A ragged edge wave emerges from the initial deposition site.

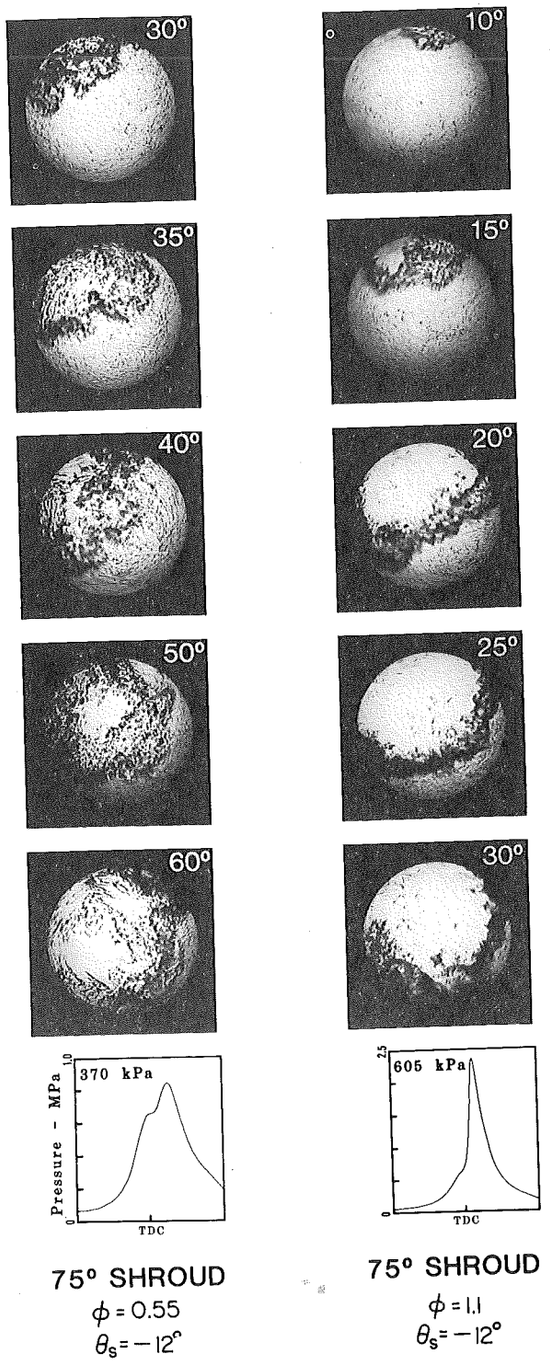

In the flow field, the turbulent vortices spread ignition sites via a ragged-edge wave emerging from the spark plug. The speed of the propagation is proportional to the velocity at the edge of the vortices.

Now further imagine that the ink rolls are porous so that ink will begin to seep into their centers. In the flow field this is analogous to laminar spreading of the flame within the vortices.

If the surface of each roll generates new ink as a result of contacting old ink, then ink will never thin out as it spreads. When it is far removed from the initial deposition site, a definite front will appear separating rolls without ink from rolls in which the ink has seeped all the way through. The front itself will contain rolls that are mostly ink free at the leading edge and mostly ink saturated at the trailing edge of the front. Thus the front will take on a thickness determined by the speed of the rollers, their size, and the rate at which ink seeps into the rolls. In the flow field the flame thickness will depend on the vorticity, the eddy sizes, and the laminar flame spreading rate. The leading edge of the flame will be mostly unburned gas and the trailing edge mostly burned gas. Since it is known that laminar flames spread slower at $\phi = 0.55$ than at $\phi = 1.1$, this model explains why the flame front appears thicker in the lean case.

The vortex tubes in the flow field are more likely to resemble a mesh of spaghetti than perfectly aligned ink rollers. Furthermore they will disappear and new ones will appear with some frequency characteristic of their vorticity. They will not appear and disappear with a definite frequency because of a randomness superimposed upon whatever order exists. Finally, the whole mess may be rotating about the cylinder axis, in which case the flow is said to be swirling.

There are cycle-to-cycle variations in the flame propagation caused by the random features of the flow field. Figure 9-5 shows flames from four different cycles in an engine under identical operating conditions. It is not difficult to imagine that the leftmost picture coincided with the spark igniting a region of high shear near the perimeter of a vortex so that turbulent spreading began immediately, whereas in the rightmost picture the spark ignited the center of a vortex so that laminar spreading had to precede turbulent spreading.

Combustion has also been photographed in diesel engines. Figure 9-6 show a sequence taken in a Cummins engine modified along the lines shown in

Figure 9-3 (*facing page*) Laser shadowgraph photographs of combustion in a homogeneous-charge spark-ignition engine. Optical access was obtained using the configuration shown in Fig. 7-31 with a mirror attached to the piston. Experiments were done with a shrouded inlet valve at various orientations to vary the swirl rate. At an orientation of 75 deg, used for the photographs shown here, the swirl is small. The spark plug is in the upper right, crank degrees shown are from the time of ignition, and on each pressure trace the imep is given (Witze and Vilchis, 1981). Reprinted with permission © 1981. Society of Automotive Engineers, Inc.

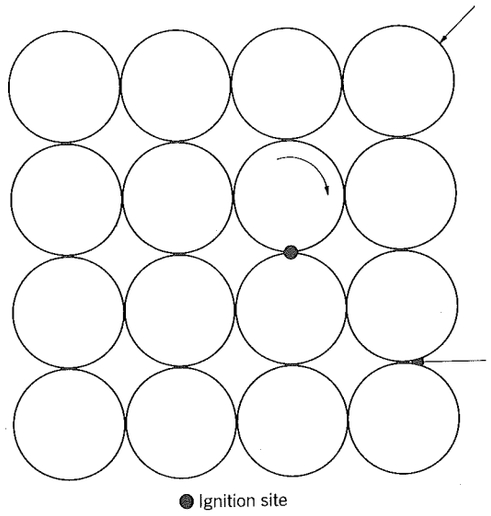

Figure 9-4 Ink roller model of turbulent combustion. (*a*) time $t = 0$ (ignition). (*b*) One half eddy revolution.

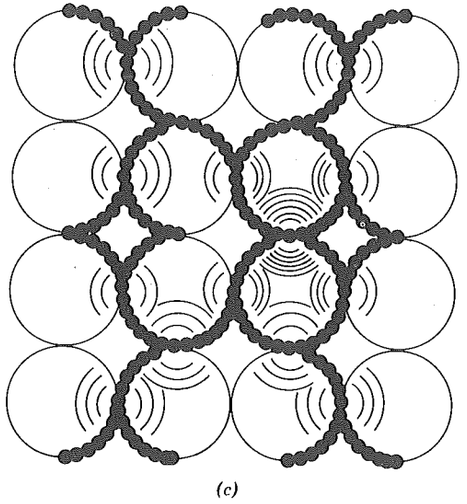

Figure 9-4 *(Continued)* (*c*) One eddy revolution since ignition.

Fig. 9-2. The period between the start of injection and the start of combustion is called the ignition delay. During this time fuel is evaporating, mixing with air, and decomposing into new chemical species called precursors which at high enough concentration will lead to autoignition. Once autoignition occurs, a flame rapidly spreads among all the fuel already mixed with enough air to burn via some of the same mechanisms responsible for flame propagation in the spark ignition engine, that is turbulence and laminar flame spread. This period of the combustion is called the premixed phase or the period of rapid combustion. Following the premixed phase, combustion occurs at a rate limited by the rate at which the remaining fuel to be burned can be mixed with air.

The quantity of fuel burned in each of the three phases is strongly influenced by the engine and injector design as well as by the fuel type. For

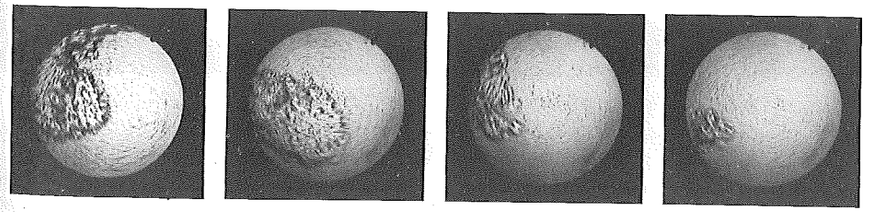

Figure 9-5 Examples of cyclic variation in the combustion process. The flames shown are for identical conditions of shroud angle $\Gamma = 45$ deg and $\phi = 0.55$ at 30 deg after ignition at 12 deg btdc (Witze, 1981). Reprinted with permission © 1981. Society of Automotive Engineers, Inc.

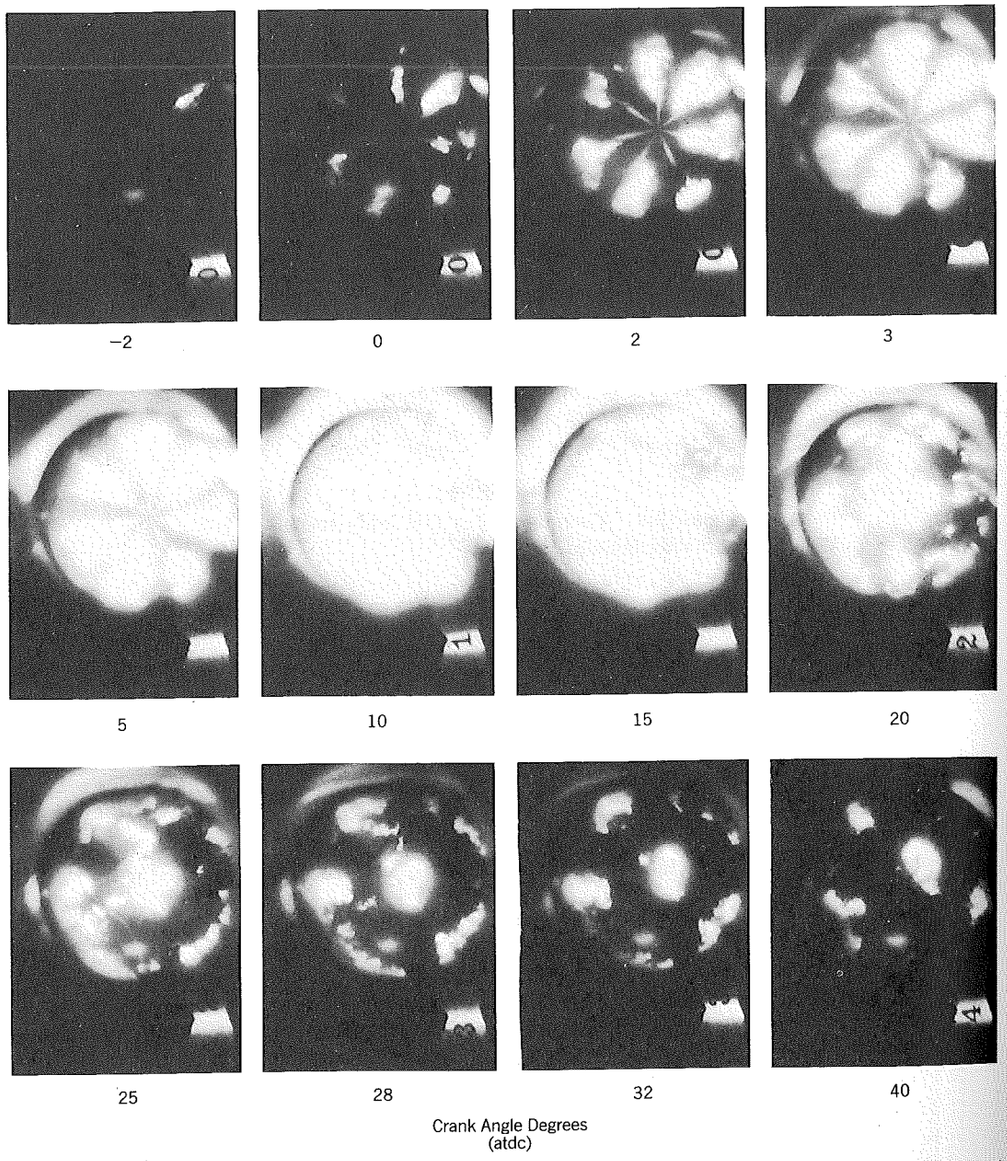

Figure 9-6 Diesel combustion as viewed through the piston in a modified Cummins engine. Reprinted with permission. Cummins Engine Co.

example, aromatic hydrocarbons have chemical bonds that are difficult to break and result in a long ignition delay. If this fuel is injected quickly so that it mixes completely with air before autoignition occurs, it will all burn rapidly when ignition occurs in the premixed phase, producing a large rate of change of pressure and a high peak pressure.

On the other hand, the chemical bonds of some fuels are easily broken. Ignition delay is then short, and with a slow injection most of the fuel to be burned is injected after autoignition occurs. Little fuel burns in the premixed phase and most burns at a rate limited by the rate of fuel injection.

Thus the ratio of the ignition delay period to the injection period is seen to be an important parameter in controlling the rate of pressure rise and the peak pressure.

9.2 THERMODYNAMIC ANALYSIS

In Chapter 4 predictions of cylinder pressure from a specified burning law relating the mass fraction burned to crank angle were discussed for the homogeneous-charge engine. Now measurements of the cylinder pressure versus crank angle are taken as given and the same analysis will be applied to compute the mass fraction burned.

Recall that the analysis assumed the charge could be split into a burned and an unburned zone. That unburned zone includes gas ahead of the flame and within the flame. The burned zone includes gas behind the flame and within the flame. Thus the highly convoluted flame structure observed via flow visualization is accounted for and the analysis is limited in principle only by the assumption that the mass of gas actually reacting is small. In practice the analysis is limited further by imprecise estimates of the heat and mass loss as well as experimental error in the pressure measurement.

Typical results obtained by this method are shown in Fig. 9-7. For conditions near stoichiometric, the ignition delay is seen to be approximately 10 deg and the combustion duration is approximately 40 deg. Consistent with observations made via flame photography, the ignition delay and combustion duration both increase as the mixture is leaned out from stoichiometric.

For the particular engine and fuel in Fig. 9-7, the lean flammability limit is near $\phi = 0.68$. Under these conditions, the ignition delay and combustion duration are quite long, about 20 and 70 deg, respectively.

That the mass-fraction-burned curves so deduced do not go to one and remain constant is caused by imprecision in the model and the experimental measurements. Results are usually deemed satisfactory if the curves level off at $x = 1.00 \pm 0.05$. To achieve this one has to account for blowby, heat loss, and incomplete combustion.

Researchers at the Ford Motor Company have developed a model to predict mass-fraction-burned curves from fundamental quantities such as the laminar flame speed of the fuel and the turbulence intensity of the flow. Key to the analysis are assumptions that ignition sites are spread by turbulence and

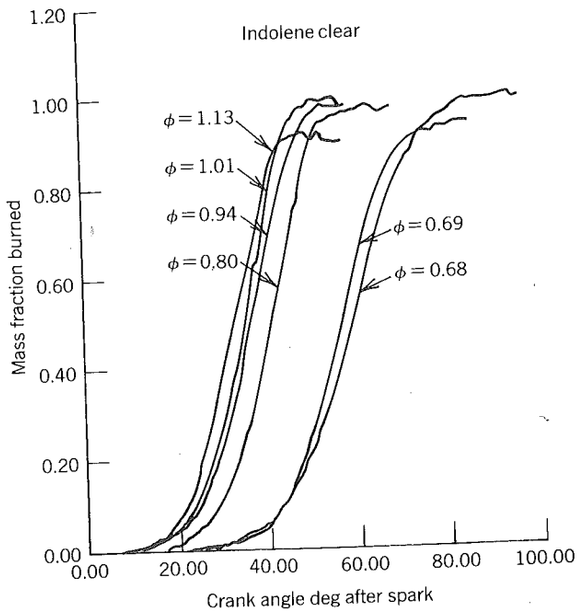

Figure 9-7 Mass fraction burned (x) versus crank angle degrees (θ) and equivalence ratio (ϕ) for indolene: CFR engine, 1600 rpm, $r = 6.9$, $T_i = 355$ K, imep = 3.7 bar (inlet pressure varies) (LaRusso, 1976).

the laminar burnup of material between sheer layers occurs. Figure 9-8 shows comparisons of measured and predicted mass-fraction-burned curves for varying equivalence ratios and amounts of exhaust gas recirculation. The good agreement realized is also obtained for variations in spark advance, engine speed, and load (imep).

The laminar flame speed is a well-defined characteristic of a fuel–air mixture. It represents the speed at which a one-dimensional laminar flame propagates into the unburned gas under adiabatic conditions. It depends on the pressure, temperature, and composition of the unburned gas. Some of these dependencies are illustrated in Fig. 9-9. The laminar flame speed, or burning velocity, shows a maximum for slightly rich mixtures, is a strong function of unburned gas temperature, and is a weak function of pressure. It also decreases linearly with the residual fraction (see homework problem 9-1).

Two aspects of mass-fraction-burned curves that are used to characterize the combustion are the ignition delay and the combustion duration. Figure 9-10 shows results obtained by Young (1980) for ignition delay, defined as the angle between the time of spark firing and the time at which 1% of the mass fraction is burned. The ignition delay varies mainly with spark timing, residual fraction, and equivalence ratio. The ignition delay increases with spark ad-

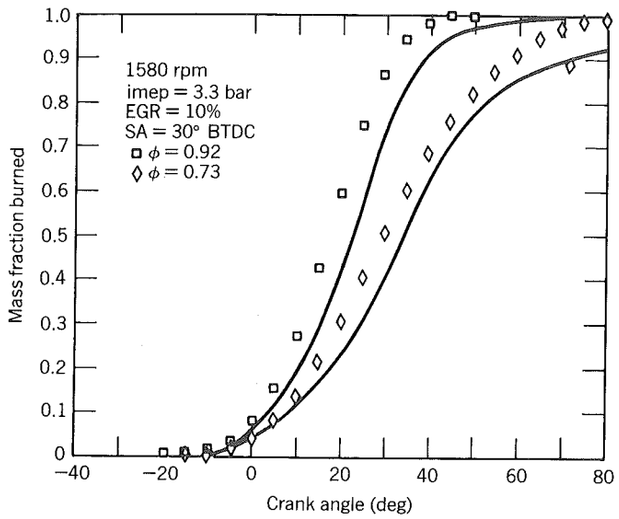

(a)

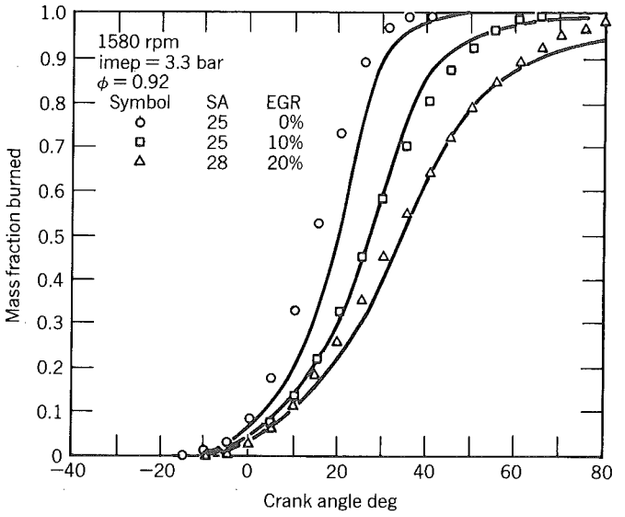

(b)

Figure 9-8 Comparison of predicted and experimental mass fraction burned curves. Ford engine: $b = 83$ mm, $S = 74$ mm, $r = 9.9$ (Tabaczynski, Trinker, and Shannon, 1980). *Comb. & Flame*, Vol. 39, #2, pp. 111–122. (a) For varying equivalence ratio, 1580 rpm, imep = 3.3 bar, and 10% egr. (b) For varying egr, 1580 rpm, imep = 3.3 bar, and $\phi = 0.92$.

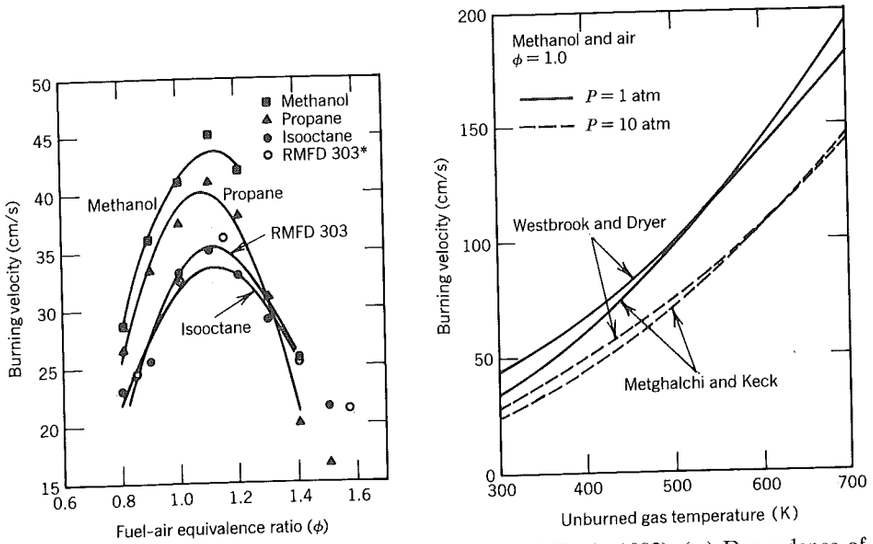

Figure 9-9 Laminar flame speed data (Metghalchi and Keck, 1982). (*a*) Dependence of the burning velocity of mixtures of methanol, propane, isooctane, and partially vaporized RMFD303 with air on the fuel–air equivalence ratios determined from the vapor pressure of the fuel. RMFD303 is indolene, a research grade gasoline. (*b*) Comparison of the burning velocities of stoichiometric methanol–air mixtures calculated by Westbrook and Dryer with those measured in this study at 1 and 10 atm as a function of unburned gas temperature. For methanol the chemical kinetics are known with enough accuracy that Westbrook and Dryer (1980) could theoretically predict the laminar flame speed.

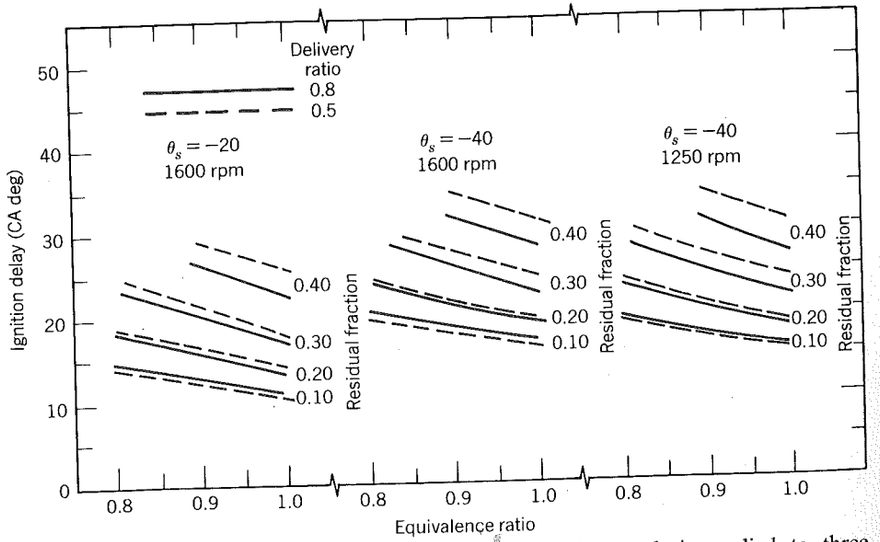

Figure 9-10 Ignition delay as determined by a regression analysis applied to three differently shaped combustion chambers on an automotive engine. Adapted from Young (1980).

vance because the laminar flame speed drops because of lower temperatures at the time of spark, but it is not the sole effect for the turbulent field is also different. Likewise it increases as the mixture is diluted either by leaning the charge or recirculating the exhaust. The change is proportionately less than the laminar flame speed changes and the combustion models indicate that this is because the combustion influences the turbulence as the flame grows.

The combustion duration, defined as the angle change from 1 to 90% burned fraction, for an automotive engine is shown in Fig. 9-11. Like ignition delay, the burn duration depends on the equivalence ratio, the residual fraction, and the spark timing. However, it shows a stronger dependence on engine speed and delivery ratio.

The combustion duration depends on (in addition to the laminar flame speed) the turbulence intensity of the flow and the combustion chamber geometry. The rate at which mass is entrained or engulfed by the flame is governed by the spreading of the ignition sites. The entrainment theory of turbulent combustion assumes that the entrainment rate is

$$\frac{dm_e}{dt} = \rho_u A_f \left(u' + S_L \right) \tag{9.1}$$

where A_f is the area of the flame front, ρ_u is the density of the unburned gas

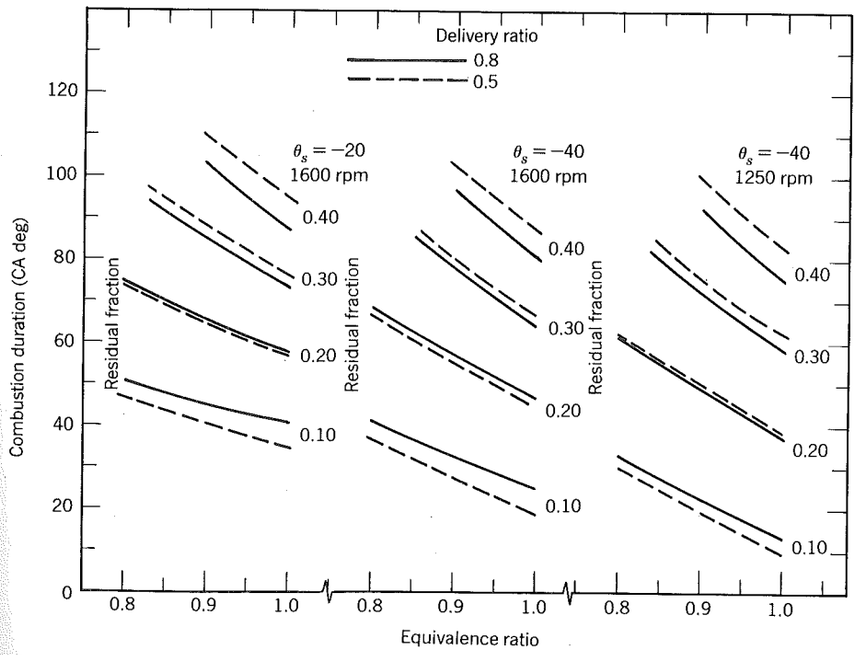

Figure 9-11 Burn duration as determined by a regression analysis applied to a low squish, open-chamber automobile engine. Adapted from Young (1980).

ahead of the flame, and u' is the turbulence intensity (essentially the rim speed in the ink roller model).

To illustrate the effect of combustion chamber geometry, consider the limiting cases of combustion in a sphere centrally ignited and in a tube ignited at one end. Assume that the sphere and the tube have the same volume. In each case the flame will propagate as a ragged spherical front of radius r_f from the spark plug. In the sphere the area of the front grows as r_f^2. Thus the entrainment rate gets faster and faster as the flame grows. One the other hand, in the tube, the flame front will initially grow as r_f^2 but it will soon hit the walls and be constrained to be more or less constant from then on. Thus combustion in a sphere can be expected to burn faster; that is, it will take less time to burn the charge.

To minimize the burn duration in an engine requires a high turbulence intensity (which is often achieved at the expense of volumetric efficiency), a flame area that increases with distance from the spark plug, and a centrally located plug to minimize flame travel. As one expects, minimizing the burn duration maximizes the work done, but, as will be discussed later, it also minimizes the octane requirement. Figure 9-12 shows experimental results that confirm these expectations.

With diesel engines it is usual to express the thermodynamic analysis in terms of rate equations so that the parameters used in the correlation for the equivalent rate of fuel injection, that is an equation akin to Eq. (4.88), can be determined. The reader is reminded that the equivalent rate of fuel injection is based on an assumption that the charge within the cylinder is homogeneous and thus it is not known a priori whether or not it will reflect the actual rate of fuel injection.[1] As will be shown, there is a resemblance.

The energy equation applied to a diesel engine is

$$\frac{dU}{dt} = -\dot{Q}_l - P\dot{V} + \dot{m}_{fi}h_{fi} - \dot{m}_l h_l \tag{9.2}$$

where conservation of mass is

$$\frac{dm}{dt} = \dot{m}_{fi} - \dot{m}_l \tag{9.3}$$

In Eqs. (9.2) and (9.3), $\dot{m}_{fi}$ is the fuel injection rate and h_{fi} is the enthalpy of the injected fuel. Assuming the system is homogeneous and at the thermodynamic equilibrium specified by the energy u and volume v per unit mass, the internal energy is a function of temperature, pressure, and equivalence ratio.

$$u = u(T, P, \phi) \tag{9.4}$$

[1]Some models skirt this issue by introducing a new variable called the fraction of the fuel injected that has burned.

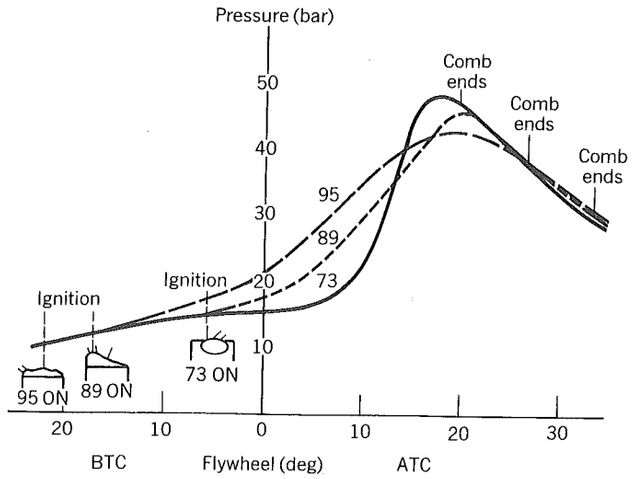

Figure 9-12 Effect of volume distribution on burning time and octane requirement: $r = 9$, 1000 rpm, maximum torque (Caris, Mitchell, McDuffie, and Wyczalek, 1956). Reprinted with permission © 1956. Society of Automotive Engineers, Inc.

Differentiation of Eq. (9.4) with respect to time gives

$$\dot{u} = \frac{\partial u}{\partial T}\dot{T} + \frac{\partial u}{\partial P}\dot{P} + \frac{\partial u}{\partial \phi}\dot{\phi} \tag{9.5}$$

To eliminate the temperature derivative note that

$$\frac{\dot{P}}{P} + \frac{\dot{V}}{V} = \frac{\dot{m}}{m} - \frac{\dot{M}}{M} + \frac{\dot{T}}{T} \tag{9.6}$$

Since $M = M(T, P, \phi)$, it follows that

$$\frac{\dot{M}}{M} = \left(\frac{\partial \ln M}{\partial \ln T}\right)\frac{\dot{T}}{T} + \left(\frac{\partial \ln M}{\partial \ln P}\right)\frac{\dot{P}}{P} + \left(\frac{\partial \ln M}{\partial \ln \phi}\right)\frac{\dot{\phi}}{\phi} \tag{9.7}$$

Combining Eq. (9.3) with (9.6) and (9.7) gives

$$\frac{\dot{T}}{T} = \frac{\dfrac{\dot{P}}{P}\left(1 + \dfrac{\partial \ln M}{\partial \ln P}\right) + \dfrac{\dot{V}}{V} + \dfrac{\dot{m}_l}{m} - \dfrac{\dot{m}_{fi}}{m} + \dfrac{\partial \ln M}{\partial \ln \phi}\dfrac{\dot{\phi}}{\phi}}{\left(1 - \dfrac{\partial \ln M}{\partial \ln T}\right)} \tag{9.8}$$

The equivalence ratio changes because of fuel injection and is related by

$$\frac{\dot{\phi}}{\phi} = \frac{\dot{m}_{fi}}{m_{fi}} \tag{9.9}$$

Finally combining Eqs. (9.2) through (9.9) leads to

$$\dot{m}_{fi} = \frac{-P\dot{V} - \dot{Q}_l - PV\frac{\dot{m}_l}{m} - \frac{\left(P\dot{V} + V\dot{P}\left(1 + \frac{\partial \ln M}{\partial \ln P}\right) + PV\frac{\dot{m}_l}{m}\right)}{(\gamma - 1)\left(1 - \frac{\partial \ln M}{\partial \ln T}\right)} - m\frac{\partial u}{\partial P}\dot{P}}{u - h_{fi} - \frac{c_v T\left(1 - \frac{m}{m_{fi}}\frac{\partial \ln M}{\partial \ln \phi}\right)}{\left(1 - \frac{\partial \ln M}{\partial \ln T}\right)} + \frac{m}{m_{fi}}\frac{\partial u}{\partial \phi}} \tag{9.10}$$

Equations (9.8), (9.9), and (9.10) are a set of ordinary differential equations that when integrated simultaneously using measured values for P, $\dot{P}$, V, and $\dot{V}$ yield $\dot{T}$, T, $\dot{\phi}$, ϕ, $\dot{m}_{fi}$, and m_{fi} as functions of time. At each instant an equilibrium combustion product subroutine[2] gives the required partial derivatives and the internal energy. The heat and mass loss are computed at each instant of time from an appropriate model. The answer is thus model dependent, though the uncertainty introduced is no worse than that caused by assuming the system is homogeneous.

Results obtained by Kreiger and Borman (1966) using this method are given in Fig. 9-13. The area under the curve is approximately equal to the actual mass of fuel injected. By judicious choice of the parameters n and θ_d in Eq. (4.88), repeated here for convenience

$$\dot{m}_{fi} = \frac{m_{fi}\omega}{\Gamma(n)}\left(\frac{\theta - \theta_s}{\theta_d}\right)^{n-1} \exp\left(\frac{-(\theta - \theta_s)}{\theta_d}\right)$$

one hopes to curve fit data such as shown in Figure 9.13. By doing experiments, one tries to relate the parameters n and θ_d to parameters of the fuel injector and engine operation via empirical correlation. The correlation obtained on last year's engine is used in designing this year's engine for the first analysis. In the final analysis, experiments are again performed since the procedure described is an extrapolation based on a model of convenience rather than of reality.

[2]The routine ECP presented in Chapter 3 would have to be extended to give derivatives with respect to ϕ.

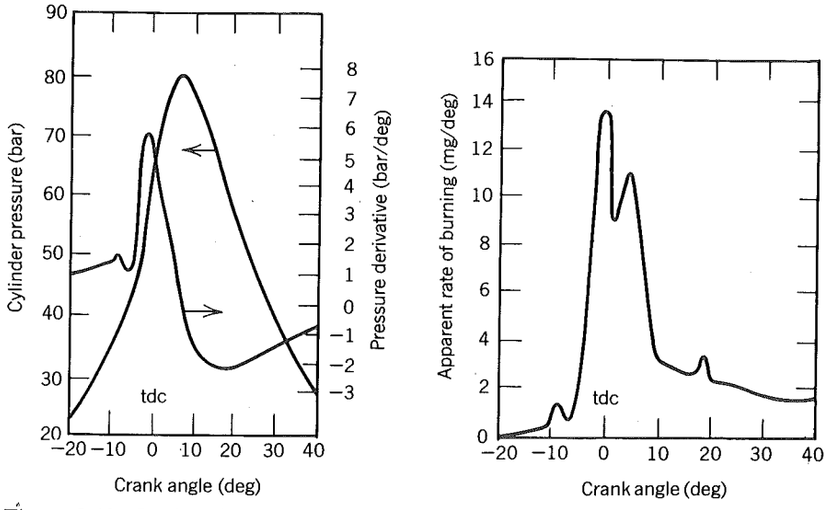

Figure 9-13 Engine data and the deduced burning rate via Eq. 9-10 (Krieger and Borman, 1966). Reprinted with permission © 1966. ASME.

9.3 AUTOIGNITION

Knock in homogeneous-charge, spark-ignition engines is caused by autoignition of the unburned gas ahead of the flame. High speed movies (see Fig. 9-14) reveal that the subsequent flame spread occurs much faster than normal. This is because the unburned gas involved is at an elevated temperature, thus the laminar flame speed is substantially increased. More important, however, several autoignition sites appear almost simultaneously. The attendant rapid rise in pressure can be a serious problem if a significant portion of the charge burns via autoignition.

Using a single-cylinder research engine as depicted in Fig. (7.31), the end gas in a high-swirl, homogeneous-charge engine has been isolated in the center of the combustion chamber by simultaneous ignition at four equally spaced spark plugs mounted in the cylinder wall. Figure 9-14 shows the dramatic change in the Schlieren pattern just before and just after ignition. It took about 2 ms for the flames to spread from the spark plugs to the positions shown in the photograph just before knock; whereas it took only 0.1 ms to propagate through the end gas once autoignition occurred. Neither shock nor detonation waves were observed.

In these experiments, temperature measurements have been made of the end gas using a laser based technique. For temperatures less than 1100 K coherent antistokes Raman spectroscopy (CARS) is used and at the higher temperatures spontaneous Raman scattering is used. The principles underlying

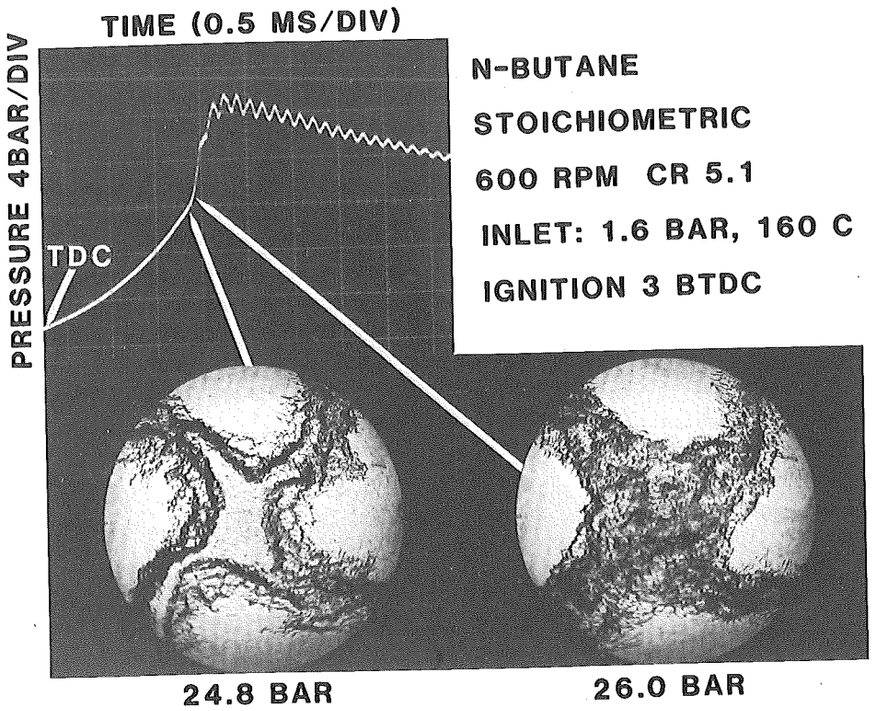

Figure 9-14 Schlieren photographs of knock process (Smith, Green, Westbrook, and Pitz, 1984). Reprinted with permission. Sandia National Laboratories.

these techniques are discussed at length by Eckbreth (1980). The results, Fig. 9-15, show that the temperature, like the pressure, undergoes an abrupt change in the rate of change at the knock point. They also show that the temperature continues to rise even after the 0.1 ms required for the homogeneous ignition sites and attendant flame spread to have consumed the end gas. Clearly oxidation is not complete in the after-knock photograph of Fig. 9-14.

Whether or not an engine will knock depends on the engine design, the engine operating parameters, and the fuel type. The chemistry of autoignition is poorly understood and the coupling to the engine design is complicated. To provide a standard measure of a fuel's knock characteristics, a scale has been devised in which fuels are assigned an octane number. Different engines are then compared in terms of their octane requirement.

To measure its octane number a fuel is burned in a standardized engine operated under standardized operating conditions. The engine employed is a Cooperative Fuel Research (CFR) engine that features a variable compression ratio. Two sets of operating conditions are employed: the motor and the

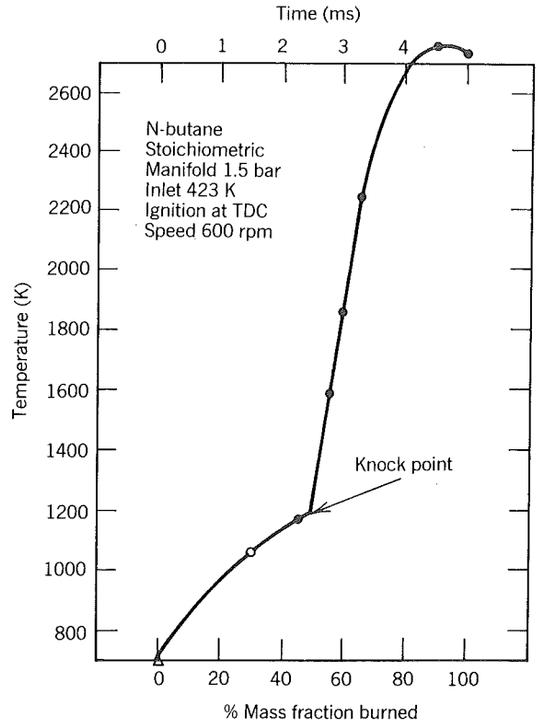

Figure 9-15 Temperature history of the end gas in Fig. 9-14 as determined by CARS and spontaneous Raman scattering (Smith and Green, 1984). Courtesy Sandia National Laboratory.

research method. They are as follows:

	MOTOR	RESEARCH
Inlet temperature (K)	422	325
Jacket temperature (K)	373	373
Speed (rpm)	900	600
Humidity (mass fraction)	0.0036 to 0.0072	0.0036 to 0.0072

The octane number referred to on gasoline pumps as $(R + M)/2$ is the average of the research and motor method octane numbers. It is also called the antiknock index.

The procedure to measure the octane number of a test fuel is as follows:

- Run CFR engine on the test fuel at either the motor or research operating conditions.

- Slowly increase the compression ratio until the standard amount of knock occurs.
- At that compression ratio, run the engine on blends of the reference fuels isooctane and *n*-heptane.
- The octane number is the percentage of isooctane in the blend that produces the standardized knock at that compression ratio.

To measure knock, an American Society for Testing Materials (ASTM) knock meter which responds to rate of pressure rise is used.

The occurrence of knock puts a constraint on engine design such that the compression ratio is less than optimum for maximum efficiency. Knock avoidance can also be dealt with by altering the fuel structure via additives or chemical processing. The octane number of the fuels in the marketplace is the result of an evolutionary process iterating on the tradeoffs involved. Treating of the fuel is covered in Chapter 10.

One measure of an engine's octane requirement is its knock limited indicated mean effective pressure (klimep). The greater the klimep is, the smaller the octane requirement is. Knock limited imep is measured by increasing the inlet pressure P_i until knock occurs; the imep at that condition is the klimep.

Figure 9-16 shows experimental results obtained that show klimep decreases with increasing coolant temperature. Similar results are obtained with increasing inlet air temperature. Both results are to be expected since chemical reaction rates are accelerated strongly by increases in temperature. Figure 9-16 also illustrates two problems with the octane number scale: (1) at low coolant temperatures diisobutylene performs better than isooctane (implying the octane number is greater than 100); (2) the relative ranking of isooctane and diisobutylene depends on coolant temperatures; whereas if the octane scale were perfect (i.e., completely decoupled from engine design, thereby making the assigned number a fuel property), the fuel with the greater octane number would always yield the largest klimep.

The former problem is dealt with by extrapolation. A performance number defined as the ratio of klimep for the fuel in question to klimep of isooctane is used for this purpose. The latter problem is dealt with by using two standard operating conditions (research and motor) and reporting an average number. These shortcomings should be kept in mind; they are easy to forget because of the great utility of the octane number scale.

Typical results obtained for varying fuel–air ratio are shown in Fig. 9-17. Notice that near-stoichiometric mixtures have the lowest klimep (therefore the highest octane requirement). Notice too that maximum klimep is attained with very rich ($\phi \approx 1.6$) mixtures. To obtain maximum power from an engine, one should run near $\phi = 1.6$ with a compression ratio and inlet pressure such that imep = klimep.

Knock occurs if there is enough time for sufficient autoignition precursors to form. Thus at high engine speeds one might not expect knock to be a

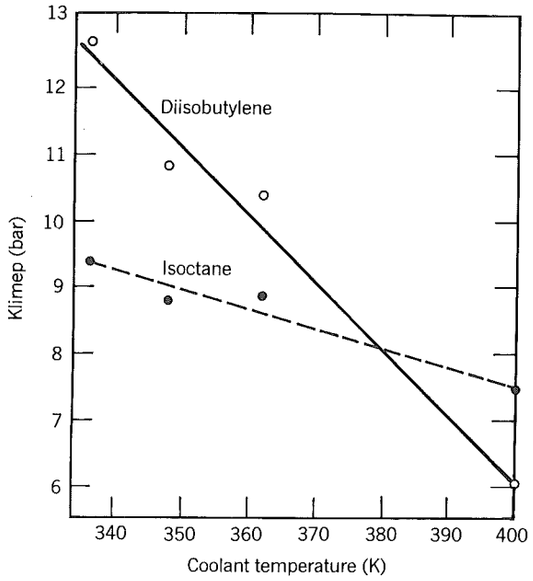

Figure 9-16 Effect of coolant temperature on knock-limited imep: T_c, deg K is temperature entering coolant (Hesselberg and Lovell, 1951). Reprinted with permission © 1951. Society of Automotive Engineers, Inc.

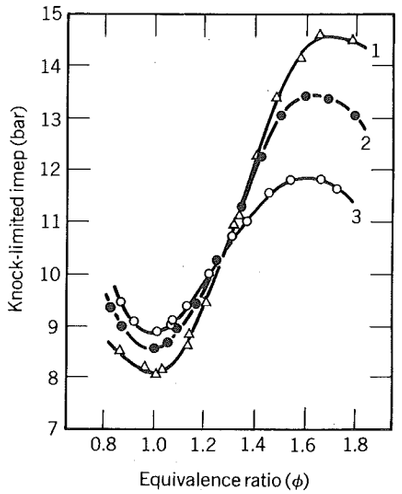

Figure 9-17 Effect of fuel–air ratio on knock limited imep for three aircraft fuels (Cook, Vandeman, and Livengood, 1944).

problem since there is less time available for the precursors to form. On the other hand, as engine speed increases, there is less heat loss from the gases so that gas temperatures will be higher. This accelerates the precursor formation rate so that less time is required to form a concentration high enough for autoignition to occur. As a result of these and other competing effects, some engines show a klimep increasing with speed, others show a decrease.

One way to model engine knock is to suppose that there exists a critical mass fraction of precursors that if attained anywhere within the charge will cause autoignition. Let x_p denote the mass fraction of precursors and x_c denote the critical value. The rate of formation of precursors is often assumed to be governed by an equation of the following form

$$\frac{1}{x_c}\frac{dx_p}{dt} = A\left(1 + B(\phi - 1.1)^2\right)P^n \exp\left(\frac{-E}{RT}\right) \tag{9.11}$$

where the constants A, B, n, and E are chosen later by forcing the predicted answer to match a set of experimental results. Like constants in algebraic burning laws, these constants will vary from engine to engine and fuel to fuel. The model is used as a tool for exploration, not as a tool capable of absolute prediction.

Knock occurs when prior to the end of normal combustion

$$\int_0^t \frac{dx_p}{dt}\,dt = x_c \tag{9.12}$$

Taylor (1977). Time zero has been chosen to coincide with the closing of the intake valve, thus ignoring precursor formation in the carburetor or intake manifold.

It is instructive to consider the dependence of the rate on temperature. For isooctane at $\phi = 1.0$, $P = 10$ atm, the following results are obtained using the constants A, B, n, and E of Douaud and Eyzat (1978):

$\frac{1}{x_c}\frac{dx_p}{dt}$ (s^{-1})	T (K)
2.8×10^{-5}	300
5.9×10^{-1}	500
4.2×10	700
4.5×10^{2}	900
2.0×10^{3}	1100

Notice that the reaction rate is an extremely strong function of the temperature. Indeed, at temperatures characteristic of the intake manifold, the rate of formation of precursors is negligible. Since the combustion occurs over times of order 10^{-2} s, not until the rates approach 10^2 s^{-1} or $T \approx 900$ K will knock occur with isooctane.

To incorporate Eq. (9.12) into an arbitrary heat release model of combustion one defines a parameter ξ called the extent of reaction as the ratio of the precursor mass fraction to the critical mass fraction. By its definition

$$\frac{d\xi}{dt} = \frac{1}{x_c}\frac{dx_p}{dt} \tag{9.13}$$

Equation (9.13) is integrated simultaneously with the energy and continuity equations discussed in Chapter 4. If at any time prior to the end of combustion ξ reaches 1, knock is said to occur and the remaining unburned gas burns instantaneously.

Autoignition in a diesel engine is more complicated than in a homogeneous-charge engine because not only are the temperature and pressure experienced by fluid elements time dependent but so are the equivalence ratios. In fact, many persons in the field break the ignition delay into two parts: (1) a physical delay—the time required for injected fuel to evaporate and mix with enough air to be flammable; (2) a chemical delay—the time required for precursors to form in the flammable mixture. Although convenient, this description is an approximation at best since precursors are forming in the gas phase at all times and mixing continues even after flammable mixtures have been formed.

Different diesel fuels are compared according to their cetane number. The cetane number of a fuel is measured using a standard CFR prechamber engine that features a variable compression ratio. It is operated under the following standard operating conditions.

Inlet temperature	339 K
Jacket temperature	373 K
Speed	900 rpm
Injection timing	13 deg btdc

The compression ratio is adjusted until the ignition delay is 13 deg with the test fuel. At that compression ratio, reference fuels are blended to again produce an ignition delay of 13 deg. Then

$$\text{cetane number} = (\text{percentage of hexadecane}) + 0.15\,(\text{percentage of heptamethylnonane})$$

The name *cetane* is derived from the fact that many persons refer to hexadecane as *n*-cetane. Originally, the cetane scale assigned a number of zero to alpha-methylnaphthalene as a reference fuel. Later the poor reference fuel was changed to heptamethylnonane, probably because it is cheaper, and assigned a cetane number of 15, so that results obtained in the past were still valid.

The chemical processes occurring during ignition delay in a diesel engine are related to those leading to knock in the homogeneous charge engine. In fact, the octane number and the cetane number of a fuel are inversely correlated. Gasoline is a poor diesel fuel and vice versa.

9.4 NITRIC OXIDES

The mechanisms that produce nitric oxides are generally understood. The following chemical reactions are of greatest importance.

$$N + NO \leftrightharpoons N_2 + O \tag{9.14}$$

$$N + O_2 \leftrightharpoons NO + O \tag{9.15}$$

$$N + OH \leftrightharpoons NO + H \tag{9.16}$$

The forward rate constants for these reactions are as follows:

$$k_1 = 2.7 \times 10^{-11}$$

$$k_2 = 1.1 \times 10^{-14} T \exp(-3150/T)$$

$$k_3 = 7 \times 10^{-11}$$

where the units are cm^3 molecule^{-1} s^{-1} (Heywood, 1976).

Using the chemical reactions given, one can write the following expression for the rate of change of nitric oxide concentration in a fluid element of volume V:

$$\frac{1}{V}\frac{d}{dt}[NO]V = -k_1[NO][N] + k_{1r}[N_2][O] + k_2[N][O_2] - k_{2r}[NO][O] + k_3[N][OH] - k_{3r}[NO][H] \tag{9.17}$$

where the brackets denote concentrations in units of molecules/cm^3 and the additional subscript r on the rate constants denotes the reverse rate constant.

To apply Eq. (9.17) two approximations are introduced.

- The C-O-H system is in equilibrium and is not perturbed by N_2 dissociation.
- N atoms change concentration by a quasi-steady process.

The first approximation means simply that given the pressure, temperature, equivalence ratio, and residual fraction of a fluid element, one simply computes the equilibrium composition to determine the concentrations of N_2, O_2, O, OH, and H.

The second approximation means that one writes an expression for the rate of change of N atoms and sets it to zero to solve for the N atom concentration

$$0 = -k_1[N][NO] + k_{1r}[N_2][O] - k_2[N][O_2] + k_2[NO][O] - k_3[N][OH] + k_{3r}[NO][H] \tag{9.18}$$

With these two approximations it can be shown that

$$\frac{dx_{NO}}{dt} = \frac{60}{\rho}(1-\alpha^2)\frac{R_1}{1+\alpha K} \tag{9.19}$$

where x_{NO} is the nitric oxide mass fraction, ρ is the gas density, α is the ratio of the nitric oxide mass fraction to its equilibrium value $x_{NO}/x_{NO,e}$, $K = R_1/(R_2 + R_3)$, and R_i $(i = 1, 2, 3)$ is the forward rate of reaction i at equilibrium (e.g., $R_1 = k_1[N]_e[NO]_e$).

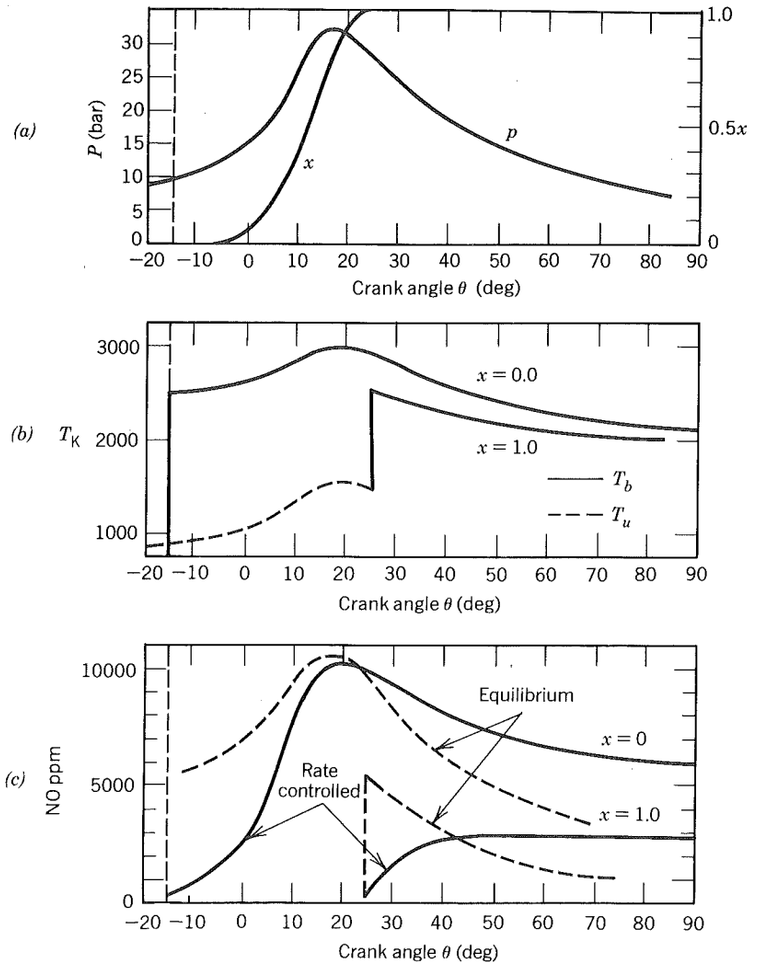

Figure 9-18 (*a*) Measured pressure P and calculated mass fraction burned, x as function of crank angle. (*b*) Calculated temperature of burned gas T_b and unburned gas T_u as function of crank angle for two elements that burn at different times. (*c*) NO mass fractions as function of crank angle for two elements that burn at different times (Komiyama and Heywood, 1973). Reprinted with permission © 1973. Society of Automotive Engineers, Inc.

Figure 9-18 illustrates application of Eq. (9.19) to a homogeneous-charge, spark-ignition engine. The curves in *a* show the cylinder pressure and mass fraction burned at different crank angles. The curves in *b* show temperature time histories (time is proportional to crank angle) of the first element to burn

($x = 0$) and the last element to burn ($x = 1$). The computation assumes that fluid elements retain their identity, that is to say, no mixing among the fluid elements occurs.

Each element burns to its adiabatic flame temperature based on the unburned gas temperature at the time it burned. Once burned, an element's temperature tracks the pressure as it is more or less isentropically compressed or expanded. Notice that the first element to burn is compressed considerably; each subsequent element to burn is compressed less, and the last element to burn undergoes no compression. As a result the first element to burn is hotter than all the rest, and the last element to burn is the coolest.

The curves in *c* illustrate how the nitric oxides vary with time in the different fluid elements. The dashed curves correspond to the equilibrium concentration based on the local temperature, pressure, equivalence ratio, and residual mass fraction. The solid curves are computed by integrating Eq. (9.19).

At the time an element burns its nitric oxide concentration is close to zero but finite because of the residual gas present. Once burned, the equilibrium concentration is high, whereas the actual concentration is low since the chemistry is not fast enough to assume the process is quasi-static; it is rate controlled. Notice that each element tries to equilibrate in that if the equilibrium concentration is higher than the actual concentration then nitric oxides are forming, whereas they decompose if the equilibrium concentrations are less than the actual concentrations.

The chemical reaction rates increase strongly with temperature. As a result there are large differences between the nitric oxide concentration in the first and last elements to burn. Furthermore it can be seen that when the temperatures drop to about 2000 K, the decomposition rate becomes very slow and for practical purposes it may be said that the nitric oxides freeze at a concentration greater than the equilibrium values. The amount of nitric oxides that appears in the exhaust is computed by summing the frozen concentrations for all the fluid elements.

$$\bar{x}_{NO} = \int_0^1 x_{NO,f}\, dx \tag{9.20}$$

Comparisons between some measured exhaust concentrations with predictions made using the procedure described are given in Fig. 9-19. The figure shows the agreement is quite good. It also shows a result typical of all engines, nitric oxides are maximum for mixtures slightly lean of stoichiometric.

Recall that the increased temperatures favor nitric oxide formation and that burned gas temperatures are maximum in mixtures that are slightly rich. On the other hand, there is little excess oxygen in rich mixtures to dissociate and attach to nitrogen atoms to form nitric oxide. The competition among these two effects results in maximum nitric oxides occurring in slightly lean mixtures.

At this point it is useful to discuss the mixing of the burned gases. Fluid elements are mixed with one another via turbulence. If the rate of mixing is

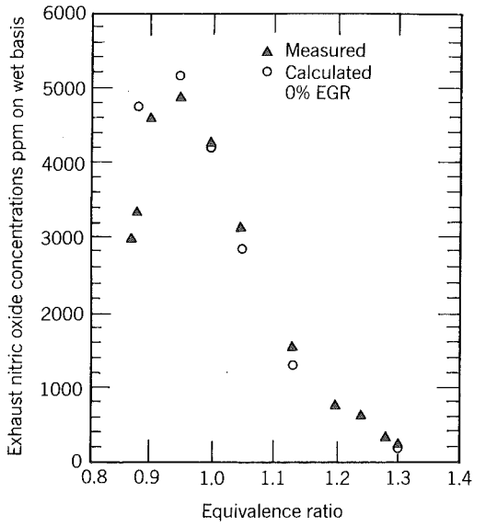

Figure 9-19 Measured and calculated exhaust NO concentration as function of equivalence ratio with no EGR (Komiyama and Heywood, 1973). Reprinted with permission © 1973. Society of Automotive Engineers, Inc.

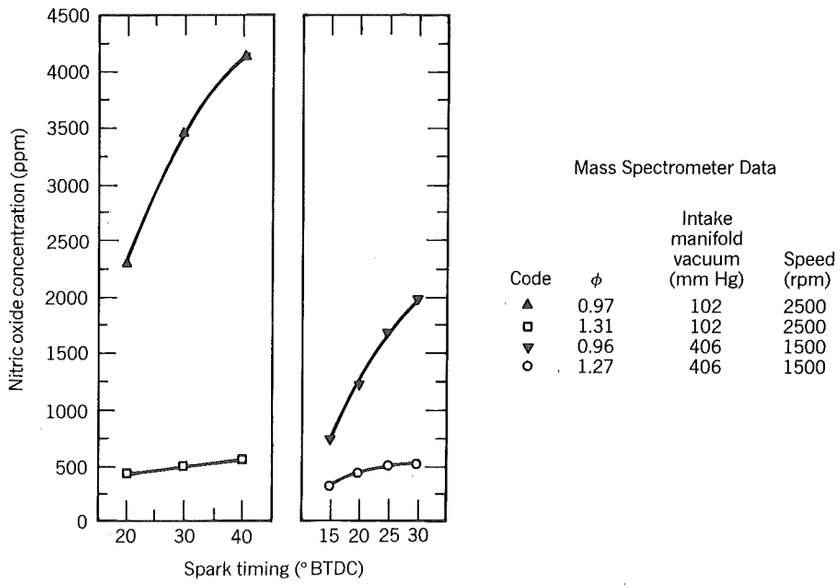

Figure 9-20 Advancing timing increases NO (Huls and Nickol, 1967). Reprinted with permission © 1967. Society of Automotive Engineers, Inc.

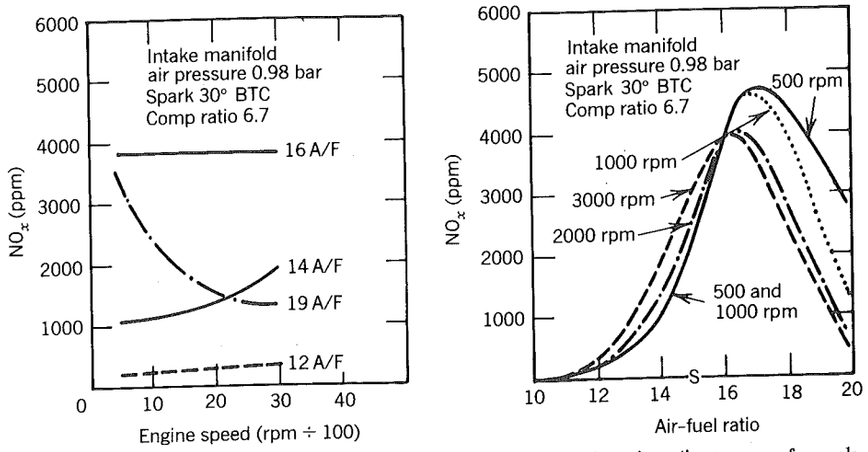

Figure 9-21 Speed effects are complicated as combustion duration (in terms of crank angle) increases slightly with speed and heat loss per unit mass decreases slightly with speed (Nebel and Jackson, 1958). Reprinted with permission © 1958. Society of Automotive Engineers, Inc.

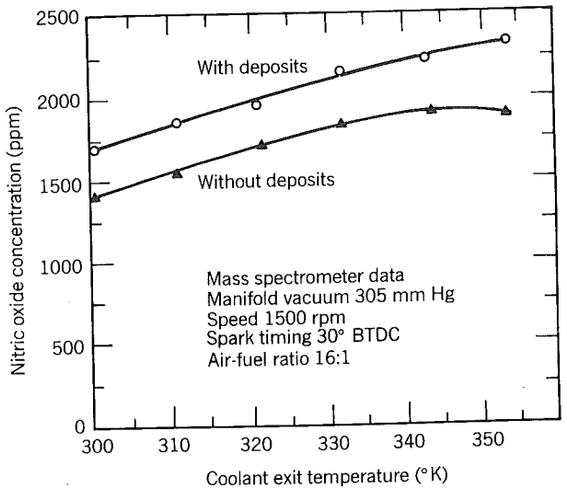

Figure 9-22 Increased coolant temperature or presence of deposits reduce heat losses, both of which increase NO (Huls and Nickol, 1967). Reprinted with permission © 1967. Society of Automotive Engineers, Inc.

faster than the rate at which burned gas is produced, then the burned gas can be assumed homogeneous and characterized by a single temperature. If the mixing is slow, then the burned gas must be treated as an ensemble of fluid elements at different temperatures. Experimentally it is observed that there are different temperature fluid elements in the burned gases but that the differences are smaller than predicted, as in Fig. 9-18. Thus it can be stated that mixing occurs but it is not complete during the combustion.

It was shown in Chapter 4 that regardless of the degree of mixing, for computing cylinder pressure, one can assume perfect mixing since the energy of the gas is a nearly linear function of temperature (i.e., the specific heat varies little over the range of temperatures encountered in the burned gas). The same cannot be said of nitric oxides since the chemical rates are nonlinear functions of temperature. Since the computations done for Fig. 9-19 did not admit to any mixing and ignored the temperature gradients due to wall boundary layers, the good agreement shown is somewhat fortuitous. The state of the art requires

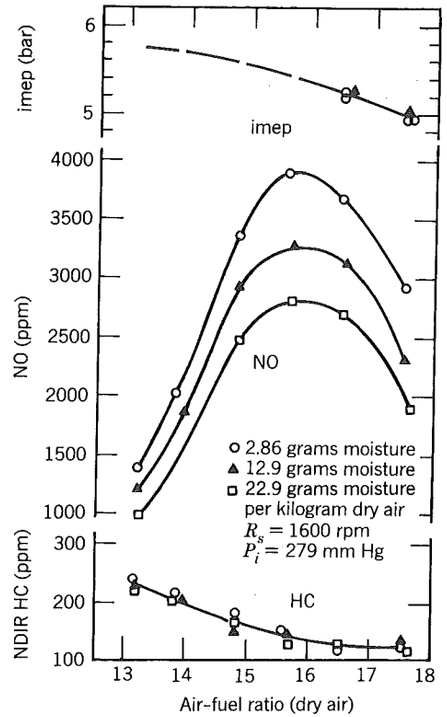

Figure 9-23 Humidity reduces burned gas temperatures and consequently NO emissions (Robinson, 1970). Reprinted with permission © 1970. Society of Automotive Engineers, Inc.

one to account for these effects to realize good agreement under all circumstances. With diesel engines, one has to further account for variations in equivalence ratio from fluid element to fluid element.

In conclusion, some experimental results are presented to illustrate how nitric oxides in the exhaust depend on various engine parameters. The trends although typical are by no means universal; especially for diesel engines. Figures 9-20 to 9-23 for homogeneous-charge, spark-ignition engines lead to the following observations:

- The dependence on spark timing and inlet pressure is strong for lean mixtures and weak for rich mixtures.
- Nitric oxides are maximum for slightly lean mixtures.
- The dependence on engine speed cannot be stated simply; factors to consider are the variation in the combustion duration and heat loss with engine speed.
- Increased coolant temperature or the presence of deposits each reduce heat loss and increase the nitric oxides.
- Dilution of the charge by residual gas (either explicitly via exhaust gas recirculation or implicitly via throttling) or by moisture in the inlet air reduces the nitric oxides.

The last four observations just cited also apply to diesel engines. Figure 9-24

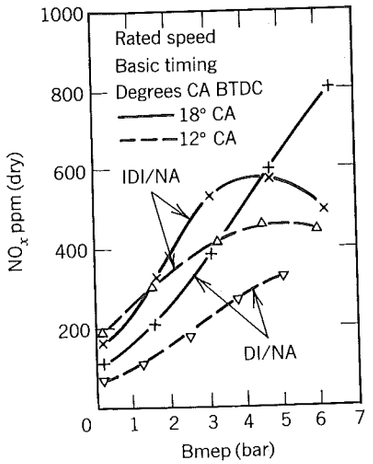

Figure 9-24 Nitric oxide emissions as a function of load for a naturally aspirated direct-injection and an indirect-injection engine (Pischinger and Cartellieri, 1972). Reprinted with permission © 1972. Society of Automotive Engineers, Inc.

illustrates the effects of injection timing and fuel–air equivalence ratio. The results show

- The nitric oxides are a strong function of injection timing.
- For direct injection engine (DI), nitric oxides increase with load (bmep).
- For indirect injection engines (IDI), nitric oxides are maximum at loads slightly less than full.

9.5 CARBON MONOXIDE

In rich-running engines why carbon monoxide appears in the exhaust should be clear: There is insufficient oxygen to convert all the carbon in the fuel to carbon dioxide. Table 3-3 could be used with confidence to predict carbon monoxide emissions from engines running rich if the exhaust gases were in complete thermochemical equilibrium. It has already been mentioned that the C-O-H system is more or less in equilibrium during combustion and expansion to the point where the nitric oxide chemistry freezes. Thus, whether it is a lean- or rich-running engine, one should be able to compute the carbon monoxide concentration during these times using an equilibrium subroutine.

Late in the expansion stroke, with temperatures down to around 1800 K, the chemistry in C-O-H systems starts to become rate limited and is generally frozen by the time blowdown finishes. The rate controlling reactions are three-body recombination reactions such as

$$H + H + M \leftrightharpoons H_2 + M \tag{9.21}$$

$$H + OH + M \leftrightharpoons H_2O + M \tag{9.22}$$

$$H + O_2 + M \leftrightharpoons HO_2 + M \tag{9.23}$$

In addition, the unusually slow bimolecular reaction is thought to be important

$$CO + OH \leftrightharpoons CO_2 + H \tag{9.24}$$

Results obtained by using an unmixed model for the burned gas and accounting for these rate limiting reactions are illustrated in Fig. 9-25. In these plots x is the fraction of the total charge burned when each element is burned and z is the mass fraction that has left the cylinder at the time each element leaves the cylinder. Because that time is unknown, results are given for several values of z for each element. Gas that leaves early ($z \ll 1$) cools more rapidly than gas that leaves last ($z \approx 1$). The results show that gases that burn early carry more CO into the exhaust than gases that burn later. They also show the fortuitous fact that the frozen concentrations are close to the equilibrium concentrations that exist in the cylinder at the time the exhaust valve opens. This suggests an approximation that is often used in practice: to assume that the C-O-H system is in equilibrium until the exhaust valve opens at which time it freezes instantaneously.

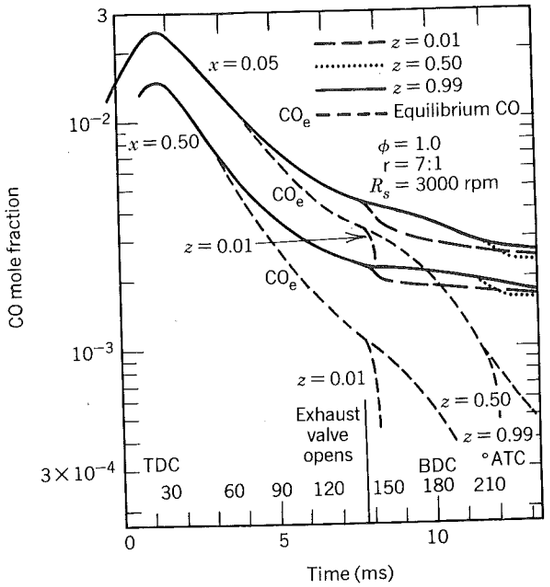

Figure 9-25 CO concentration in two elements of the charge that burned at different times during the expansion and exhaust processes; x is the mass fraction burned when element burned, z is fraction of gas that has left the cylinder during exhaust process (Heywood, 1976). Courtesy of Pergamon Press Ltd.

In lean-running engines there appears to be an additional source of CO caused by the flame–fuel interaction with the walls, the oil films, and the deposits. Under these circumstances the exhaust concentrations are so low they are not a practical problem and thus details of these interactions remain largely unexplored.

The most important engine parameter influencing carbon monoxide emissions is the fuel–air equivalence ratio. All other variables cause second-order effects. Thus results obtained when varying fuel–air ratio are more or less universal. Typical results are shown in Fig. 9-26.

Notice that near stoichiometric conditions emission is a highly nonlinear function of equivalence ratio. Under these circumstances, in multicylinder engines, it becomes important to ensure that each cylinder is delivered the same fuel–air ratio. If half the cylinders run lean and the other half run rich, then the lean cylinder produces much less CO than the rich cylinders. The average CO emission of such an engine would correspond not to the average equivalence ratio but to an equivalence ratio richer than average, producing more CO than is necessary.

Thus the key to minimizing CO emissions is to minimize the times the engine must run rich (such as during start-up) and to develop an induction

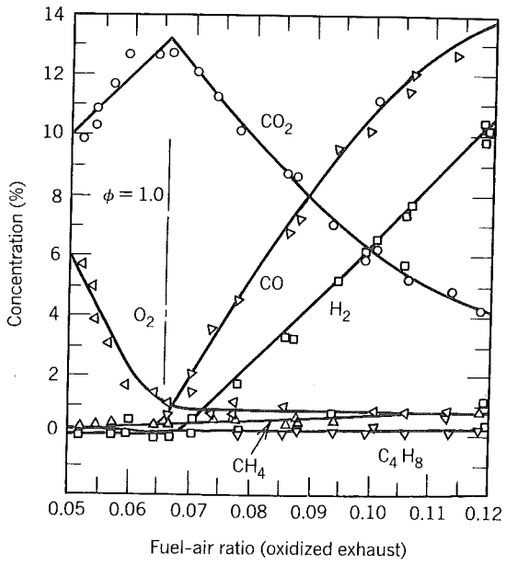

Figure 9-26 Exhaust gas composition versus oxidized or measured fuel–air ratio for supercharged engine with valve overlap; fuel C_8H_{18} (Gerrish and Meem, 1943).

system that minimizes variance in fuel–air ratio from cylinder to cylinder (and perhaps cycle to cycle).

Finally, since diesel engines run lean overall, their emissions of carbon monoxide are low and generally not considered a problem. It does appear that direct-injection engines emit more CO than indirect-injection engines.

9.6 HYDROCARBONS

By hydrocarbon emission one generally means unburned fuel. The fuel is composed of 10 to 20 major species and some 100 to 200 minor species. Most of these same species are found in the exhaust. However, some of the exhaust hydrocarbons are not found in the parent fuel and have to be attributed to some other source. These emissions are still hydrocarbons derived from the fuel but whose structure was altered within the cylinder by chemical reactions which did not go to completion. These could be anywhere from 20 to 80% of the total hydrocarbons emitted. Hydrocarbons can also originate from the oil, but this is unusual in engines in good condition.

Three principal mechanisms are believed to be responsible for hydrocarbons appearing in the exhaust of homogeneous charge engines: (1) misfire; (2) storage and release of fuel by deposits and/or oil layers; (3) flame quenching within crevices.

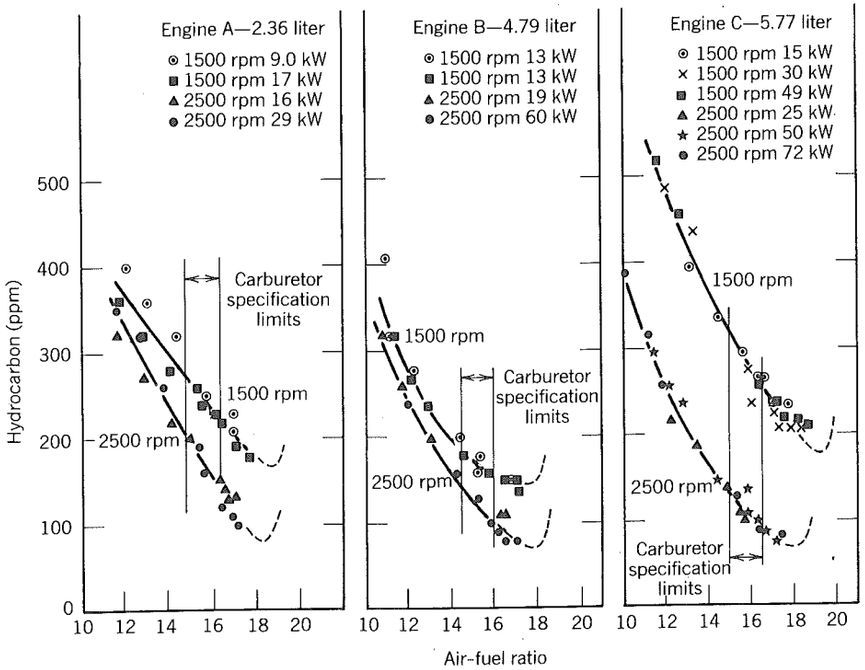

Figure 9-27 Exhaust hydrocarbons as a function of air–fuel ratio for three different engines. At the onset of misfire, because of a lean flammability limit, the curves are expected to show a sudden increase as depicted. Also shown is the range of air–fuel ratios delivered by mechanical carburetors built to normal tolerances (Hagen and Holiday, 1964). Reprinted with permission © 1964. Society of Automotive Engineers, Inc.

The emission index of hydrocarbons is on the order of 1 g/kg of fuel. Thus if only one cycle out of a thousand misfires, it results in hydrocarbon emission of this magnitude. Misfire, whether total lack of combustion or a partial burn, is a problem in engines operated with a dilute charge, either lean or with EGR, near the flammability limit. Hydrocarbons as a function of air–fuel ratio generally exhibit the behavior shown in Fig. 9-27. The sharp turnup occurring near an air–fuel ratio of 18 is caused by the onset of misfire.

Figure 9-28 is a plot of the change in hydrocarbon emission from an engine as it ages. Initially the engine is clean but as time goes on deposits accumulate in the cylinder. As a result of using leaded fuel, the hydrocarbons increase by about 375 ppmC_6 (which on a flame ionization detector reads 2250 ppmC). When an additive is used, this increase is cut in half, and when unleaded fuel is used the increase is less than 10 ppmC_6 after 75 hours.

The researchers doing this experiment examined the deposits under an electron microscope. They found that when leaded fuel was used the deposits

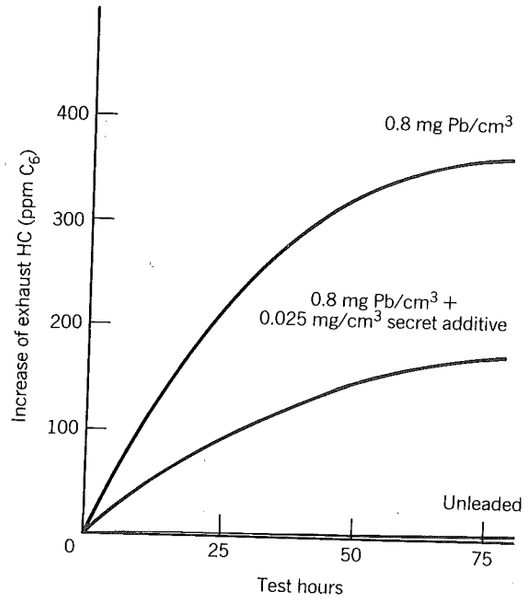

Figure 9-28 The effect of deposit structure as influenced by fuel additives on exhaust hydrocarbon emissions: 1500 rpm, $\phi = 1.1$, base fuel is unleaded gasoline, spark timing = 15°btc. (Doelling, Gerber, Kerschner, Rakow, and Robinson, 1972). Reprinted with permission © 1972. Society of Automotive Engineers, Inc.

were very rough and full of caves; the additive smoothed the surface somewhat and produced smaller caves; whereas unleaded fuel produced a rather smooth surface with no caves; Doelling, Gerber, Kerschner, and Rakow and Robinson (1972).

When a flame tries to propagate into a narrow channel, it may or may not be successful depending upon the size of the channel and a characteristic of fuel–air mixtures called the quenching distance. The sizes of most of the caves or pores in the deposits are smaller than the quenching distance, and as a result the flame cannot burn the fuel–air–residual gas mixture compressed into the pores. This mixture comes out of the pores during expansion and blowdown. Although some of it will burn up when mixed with the hotter gases within the cylinder, eventually cylinder gas temperatures will have dropped to the point where those reactions fail to complete, resulting in hydrocarbons being emitted from the engine.

Oil layers within an engine can also trap some of the fuel and later release it during expansion. Kaiser, LoRusso, Lavoie, and Adamczyk (1982) added oil to the engine cylinder and found that the exhaust hydrocarbons

increased in proportion to the amount of oil added when the engine was fueled on isooctane. They verified that the increased emissions were unburned fuel and fuel oxidation species and not unburned oil and oil oxidation species. They also did experiments in which the engine was fueled with propane and found no increase in the exhaust hydrocarbons when oil was added. Since propane is not soluble in the oil, they concluded that the increase observed is caused by fuel having been dissolved in the oil layer during compression later being released into the cooling burned gas during the expansion stroke. Thus one can conclude that hydrocarbon emissions from engines will depend on the amount of oil in the cylinder and the solubility of the fuel in the oil.

The volume between the top ring, the piston, and the cylinder wall is called the crevice volume. The clearance between the piston and cylinder is smaller than the quenching distance. As a result the flame cannot propagate into the fuel–air-residual gas mixture that is compressed into the volume during the compression stroke. This unreacted fuel escapes during expansion but remains in the vicinity of the cylinder wall. Because of its proximity to the

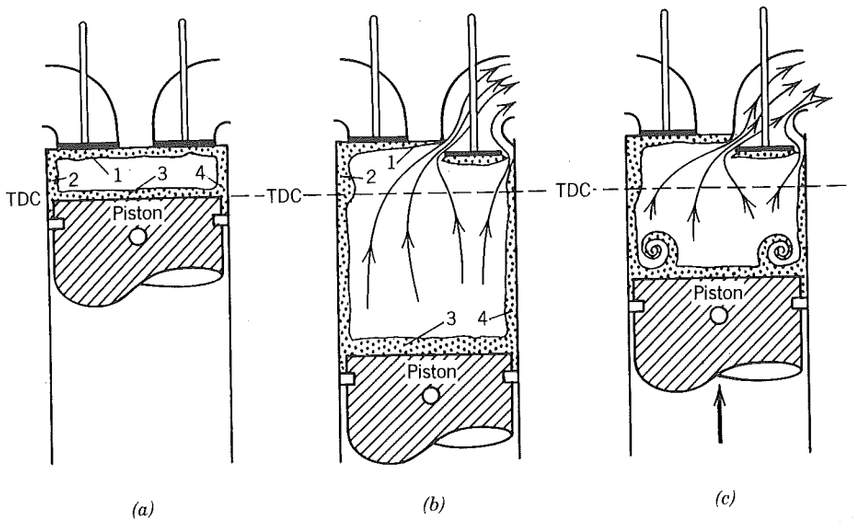

Figure 9-29 Schematic summarizing processes important in hydrocarbon emissions. (*a*) After the charge is burned, unburned fuel is in the vicinity of the walls at (1), (2), and (3) because of flame quenching and absorption by oil layers. In the crevice volume (4), the flame is quenched by the cool walls. (*b*) During the expansion process, hydrocarbons are desorbed by the oil layers and gas in the crevice volume expands and is laid along the cylinder walls. When the exhaust valve opens, hydrocarbons from regions (1) and (2) are entrained by the flow and exit the cylinder. (*c*) Roll-up of hydrocarbon rich cylinder wall boundary layer into a vortex as piston moves up cylinder during exhaust stroke (Tabaczynski et al., 1972). Reprinted with permission © 1972. Society of Automotive Engineers, Inc.

wall oxidation after it escapes the crevice is impeded and results in hydrocarbons being emitted from the engine.

Figure 9-29 is a schematic depicting how hydrocarbons are exhausted from the engine. At the end of combustion there are hydrocarbons all along the walls trapped in deposits, oil layers, or the crevice volume. During expansion hydrocarbons leave the crevice volume and are distributed along the cylinder wall. When the exhaust valve opens, the large rush of gas escaping drags with it some of the hydrocarbons released from oil layers and deposits. During the exhaust stroke, the piston rolls the crevice volume hydrocarbons that were distributed along the walls into a vortex that ultimately becomes large enough that a portion of it is exhausted.

Tabaczynski et al. (1972) have verified in a water analog experiment that a piston rolls the wall layer into a vortex. They have also measured the hydrocarbon emission mass flow rate as a function of time during the exhaust stroke. Their results, illustrated in Fig. 9-30, show that roughly one half the hydrocarbons in their engine are exhausted during blowdown and one half are exhausted during the latter portion of the exhaust stroke. The concentration profile shown with a peak during blowdown and a sudden increase at about

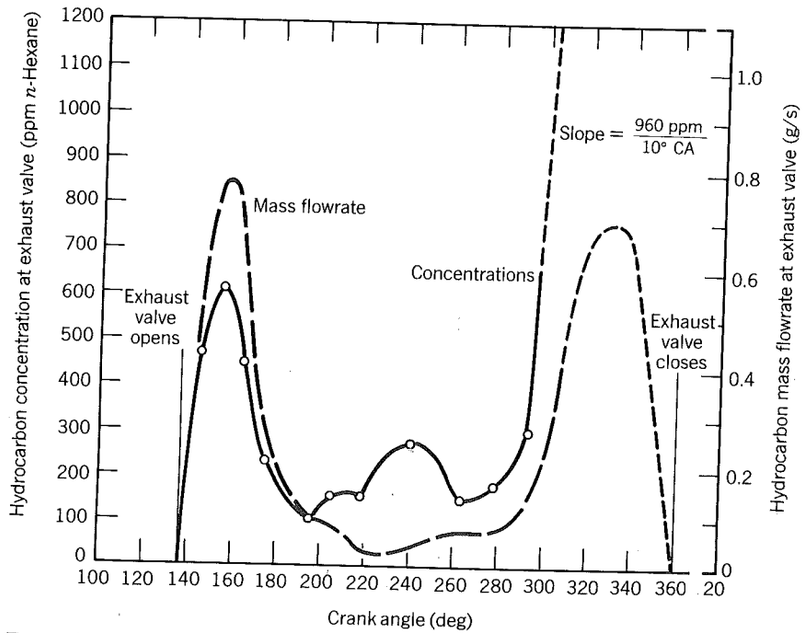

Figure 9-30 Variation of HC concentration and HC mass flow rate at the exhaust valve during the exhaust process (Tabaczynski, Heywood and Keck, 1972). Reprinted with permission © 1972. Society of Automotive Engineers, Inc.

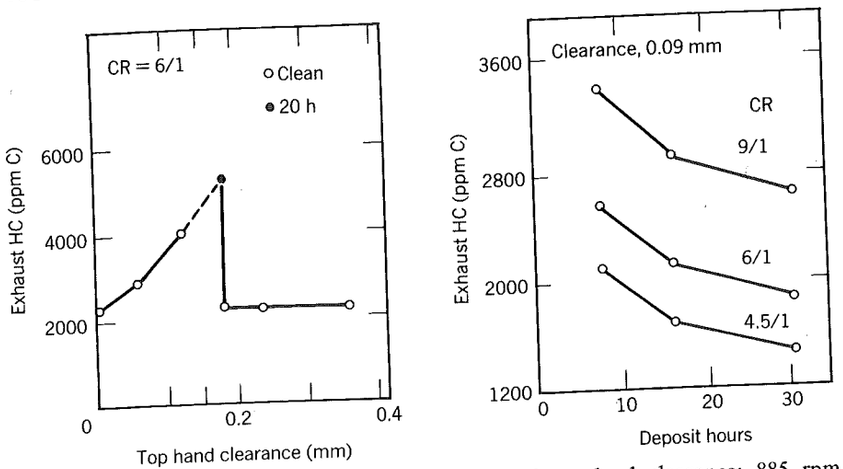

Figure 9-31 Exhaust hydrocarbons as a function of top land clearance: 885 rpm, $\phi = 1.09$, MBT spark (Haskell and Legate, 1972). Reprinted with permission © 1972. Society of Automotive Engineers, Inc.

290 deg (evidently the vortex starts to come out at 290 deg) is consistent with the process description given.

Haskell and Legate (1972) experimented with varying the top land clearance. They installed a piston with a clearance close to zero and measured the exhaust hydrocarbons. Then they took the piston out, chucked it in a lathe, and turned it to reduce its diameter and increase the clearance. By repeating this procedure they obtained the results shown in Fig. 9-31. The hydrocarbons increase until the clearance is about 0.2 mm, then they suddenly drop and then remain constant. The explanation offered is that for clearances less than 0.2 mm the flame quenches; whereas for large clearances it does not.

Haskell and Legate (1972), using a one to one mixture of isooctane and benzene as fuel, which is unleaded, also did experiments as a function of time. The hydrocarbons decreased. Deposits started to fill up the crevice volume and reduce the hydrocarbon emitted. These results do not necessarily contradict those of Doelling et al. (1972) discussed earlier. We can presume that had Haskell and Legate used a leaded fuel they would have observed an increase in hydrocarbons with time.

Wentworth (1971) was one of the first to recognize the importance of the crevice volume. He designed a special ring package to eliminate it, shown in Fig. 9-32. So far it has found application only in research engines where it allows one to make crevice hydrocarbons a negligible source. This allows study of the effects of engine variables on the remaining sources. For example, Wentworth has shown that hydrocarbon from the remaining sources are strongly dependent on the wall temperature.

At this point it should be mentioned that not all persons in the field believe that absorption–desorption of fuel by the oil layers is the remaining

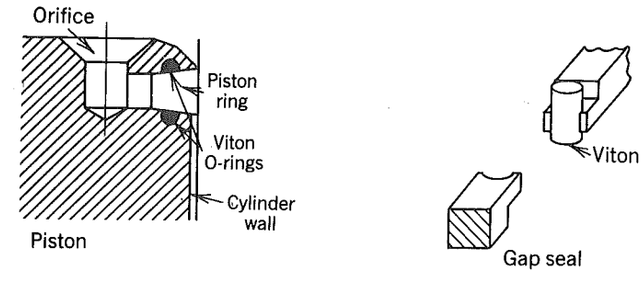

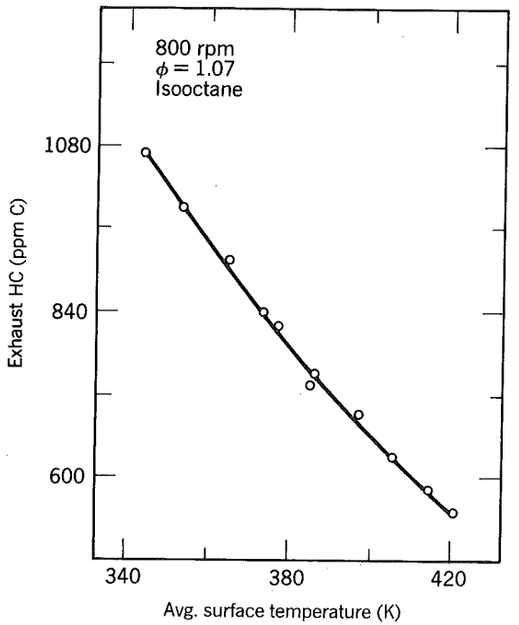

Figure 9-32 Exhaust hydrocarbons as a function of wall temperature: spark timing = 22°btc, intake pressure = 0.60 atm, compression ratio = 8.51 (Wentworth, 1971). Reprinted with permission © 1971. Society of Automotive Engineers, Inc.

source in a deposit-free engine. Although the experiments of Kaiser et al. (1982) are convincing in that added oil increases hydrocarbons, it is an assumption that there are sufficient oil layers in the engine to absorb–desorb the hydrocarbons that appear in the exhaust because of sources other than the crevice volume. Indeed Wentworth (1972) has done experiments with an engine lubricated with water and equipped with his orifice sealed ring pack. That the hydrocarbons from that engine were the same whether it was lubricated with oil or water casts doubt on the role of oil layers. I am of the opinion that

Wentworth's ring pack eliminates the conventional crevice volume and creates a new one, namely the clearance space behind the ring into which gases flow through the sealing orifice. The dependence upon surface temperature shown in Fig. 9-32 can be explained by assuming differential thermal expansion shrinks that new crevice volume as the surface temperatures are increased, Haskell and Legate (1972).

Researchers who doubt the role of oil layers, believe, that flame quenching along the surfaces is an important mechanism. Daniel (1957) showed that as the flame propagates toward the walls in an engine, it is extinguished at a small but finite distance away from the wall. Flame photographs revealed a dark region near the wall of thickness about one half the quench distance. For a long time this was thought to be an important source of hydrocarbons for if one multiplied that thickness by the surface area of the combustion chamber and an unburned gas density at the time of quench, one obtained a mass of hydrocarbons the same order of magnitude as those emitted by the engine. More recent measurements have shown that these hydrocarbons are subsequently oxidized with a high efficiency as they diffuse into the burned gases during expansion (LoRusso, Kaiser, and Lavoie 1981).

The hydrocarbons story does not end once they escape the cylinder. There is considerable burnup in the exhaust port. Some emission control techniques pump air into the exhaust manifold to further oxidize the hydrocarbons.

Hydrocarbons from diesel engines come primarily from fuel trapped in the injector at the end of injection that later diffuses out, fuel mixed into air surrounding the burning spray so lean that it cannot burn, and fuel trapped along the walls by crevices, deposits, or oil due to impingement by the spray (Greeves, Khan, Wang, and Fenne 1979; and Yu, Wong, and Shahed 1980).

A typical sac volume is illustrated in Fig. 9-33. However, not all diesel engines employ injectors that have a sac volume; the poppet injector in Fig. 9-34 shows an example of sacless injector.

The combustion process relies on mixing fuel and air at the time they are intended to burn. As already mentioned a characteristic time is required for

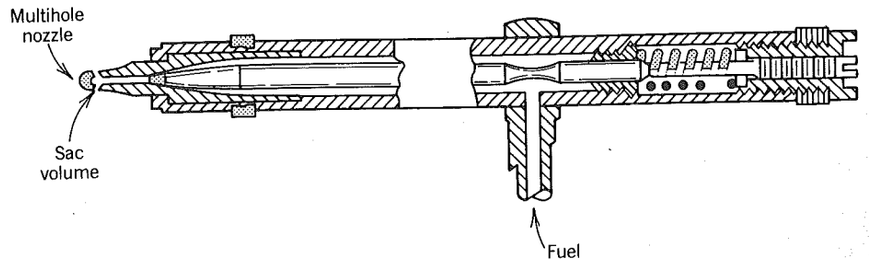

Figure 9-33 Roosa master diesel fuel injector (Roosa, Hess, and Walker, 1964). Reprinted with permission © 1964. Society of Automotive Engineers, Inc.

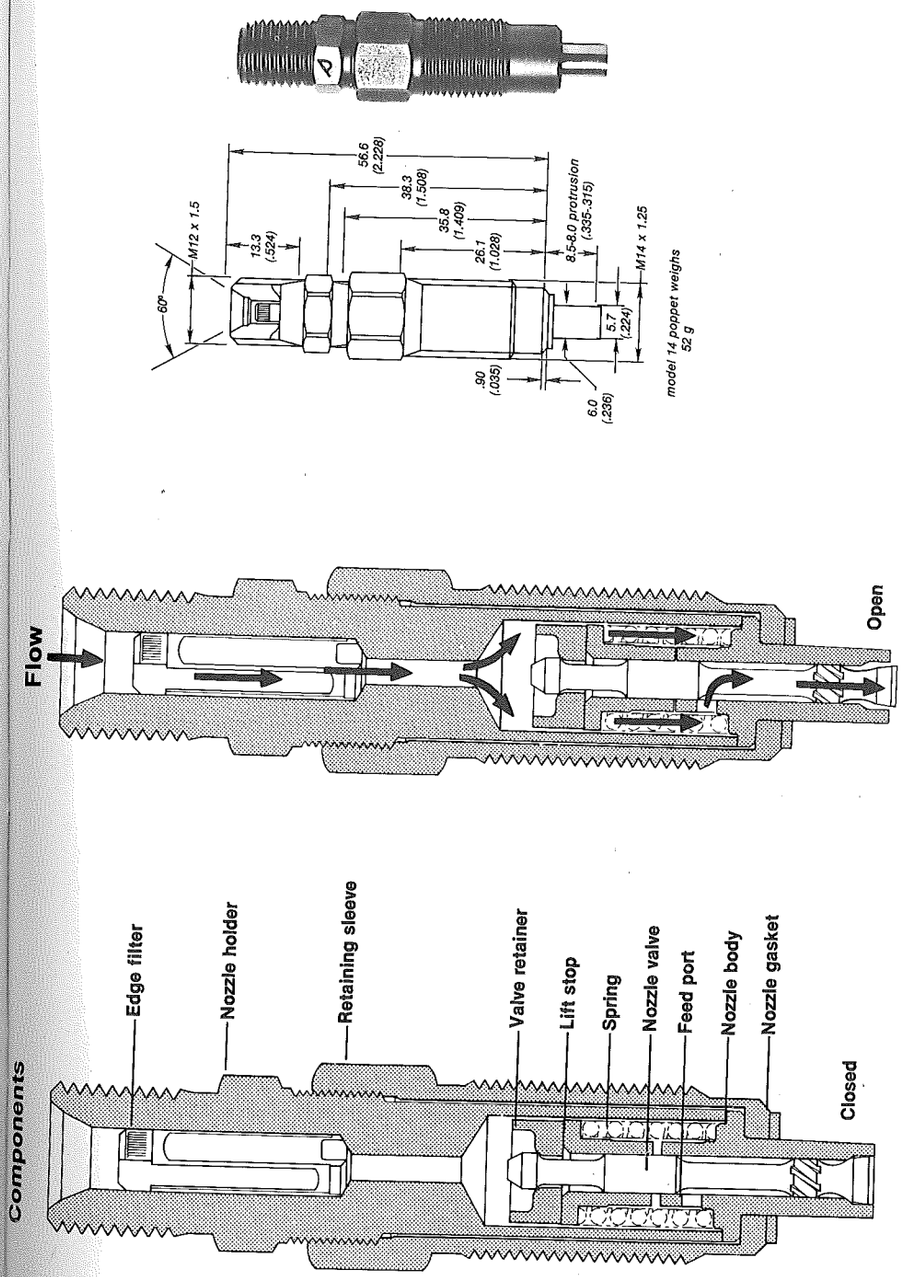

Figure 9-34 Stanadyne poppet injector, Courtesy Stanadyne Inc.

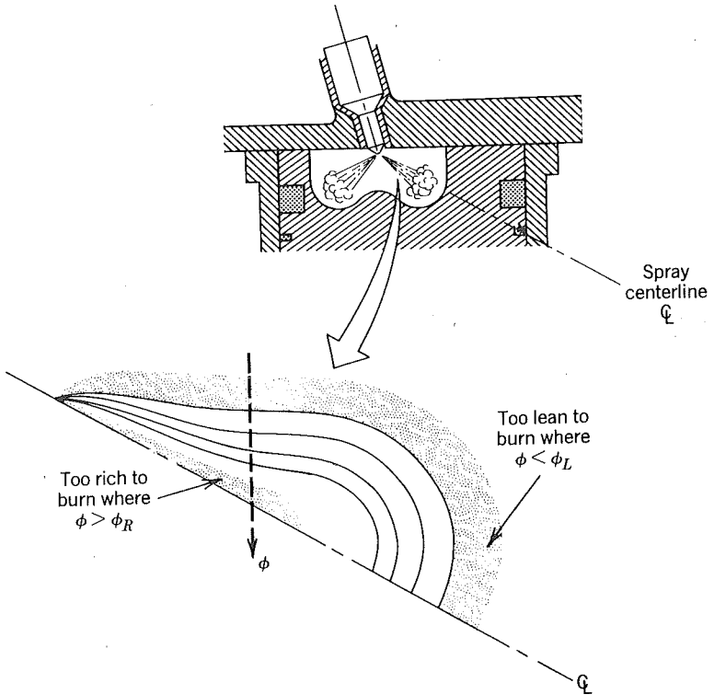

Figure 9-35 Axisymmetric idealization of a diesel fuel spray. The lower portion of the figure depicts lines of constant equivalence ratio with respect to the spray center line. Autoignition is most likely to occur at points in the neighborhood of $\phi = 1.0$. A premixed flame then rapidly burns all the fuel within the contours of the rich and lean flammability limits, ϕ_R and ϕ_L. From then on combustion occurs at rate at which fuel at $\phi > \phi_R$ is leaned out by mixing.

enough precursors to form in order for autoignition to occur. That time is a strong function of equivalence ratio and minimum near stoichiometric proportions of fuel and air. As a result when ignition occurs, it is in pockets where the fuel and air are mixed into nearly stoichiometric proportions. A schematic of equivalence ratio contours at the time ignition is to take place is shown in Fig. 9-35. Recognize that if the characteristic time to form precursors was zero for stoichiometric mixtures, then no fuel could be mixed leaner than stoichiometric without first burning. In this case there would be no hydrocarbons due to mixing fuel and air to equivalence ratios less than the lean limit. However since that time is finite, a fuel–air pocket can be mixed to stoichiometric proportions and then diluted by more air before autoignition occurs in that element. As a result there are contours for lean equivalence ratios and when autoignition

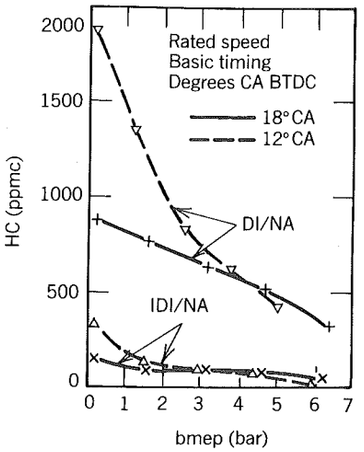

Figure 9-36 HC concentrations, naturally-aspirated direct-injection and prechamber engines (Pischinger and Cartellieri, 1972). Reprinted with permission © 1972. Society of Automotive Engineers, Inc.

occurs there is fuel and air mixed locally to proportions less than the lean flammability limit. Thus this fuel does not burn and contributes to the hydrocarbon emission.

There is also fuel mixed too rich to burn at the time of autoignition. However, it will burn later when it finds air, provided the gases are hot enough. Some hydrocarbons are also produced because some of this fuel does not find enough air to burn until late in the expansion stroke.

Figure 9-36 shows hydrocarbon emissions from both a naturally aspirated direct injection (DI/NA) engine and a naturally aspirated indirect injection engine (IDI/NA). The results, although unique to the engines in question, illustrate what is generally regarded as true, that direct injection engines emit more hydrocarbons than indirect injection engines.

Notice that for the direct injection engine the hydrocarbons are worst at light load. Thus hydrocarbons at idle have been the focus of a lot of attention. Figure 9-37 shows how they can be influenced considerably by rather small changes in engine or injector geometry. Nozzles (A) and (B) were manufactured by different companies from the same specifications. This illustrates the need for precise control in manufacturing to achieve low emissions. The other variable shown is the influence of the bowl (in piston) diameter which had negligible influence on the bsfc, a slight change in NO_x, but a dramatic change in the hydrocarbons.

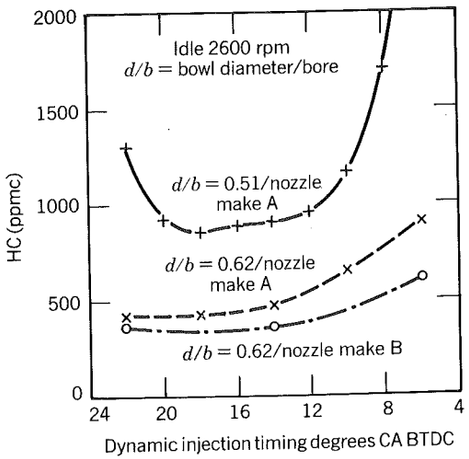

Figure 9-37 Effect of combustion bowl diameter and make of nozzle (identical nozzle specification) on high-idle HC emissions (AVL research engine) (Pischinger and Cartellieri, 1972). Reprinted with permission © 1972. Society of Automotive Engineers, Inc.

.7 PARTICULATES

Basically, particulates are any substance other than water that can be collected by filtering the exhaust. With the use of unleaded fuel they are not a problem in homogeneous-charge engines.

Particulates are a problem for diesel engines. The material collected on a filter is generally classified into two parts: a solid carbon material or soot and an organic fraction that is hydrocarbons and their partial oxidation products condensed onto the filter or adsorbed to the soot.

The organic fraction is influenced by the processes that dilute the exhaust with air upon expulsion from the engine. For this reason and others the United States Environmental Protection Agency defines particulates as any substance other than water that can be collected by filtering diluted exhaust at or below 325 K.

One means to collect particulates is shown in Fig. 9-38. By flowing dilution air through a converging–diverging nozzle, the venturi effect is used to withdraw exhaust gas from the engine. Downstream of the nozzle the exhaust is well mixed with the air and the diluted gas is filtered. The particulate concentration is measured as the mass of particulate collected on the filter per unit mass of gas filtered. Carbon dioxide concentration is measured in both the engine exhaust and the diluted sample in order to compute the dilution ratio

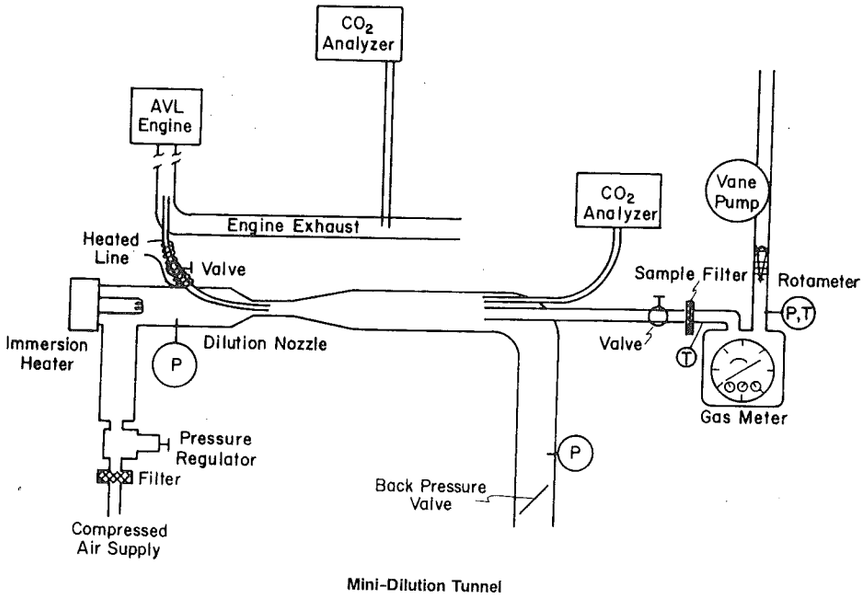

Figure 9-38 Minidilution tunnel for collecting diesel particulate emission (MacDonald, Plee, D'Arcy, and Shreck, 1980). Reprinted with permission © 1980. Society of Automotive Engineers, Inc.

(ratio of dilute mixture flow rate to exhaust gas flow rate) and thereby to express the particulates as mass of particulate per unit mass of exhaust gas.

Results obtained using a direct-injection diesel are shown in Fig. 9-39 and 9-40. The amount of particulates is extremely dependent on equivalence ratio. The soot fraction is believed to form in regions of the fuel spray that do not lean out until the gases have cooled considerably by the expansion process. It is reasonable to expect that the more fuel one injects, the more likely this is to happen.

The organic fraction results from all the processes that result in hydrocarbons and their partial oxidation products. During the dilution process some of them cool enough to condense or adsorb to the soot. In addition, some species originating from the lubricating oil are found in the particulate and may be anywhere from 25 to 75% of the organic fraction (Mayer, Lechman, and Hilders, 1980). How these species become part of the particulate is not known.

The dependence on speed is complicated. For the condition in Fig. 9-39, particulates are minimum at 1500 rpm. A mass spectrum of the organic fraction for particulates collected at these same conditions and a dilution ratio of 30 is given in Fig. 9-41. Notice that the spectrum changes with speed

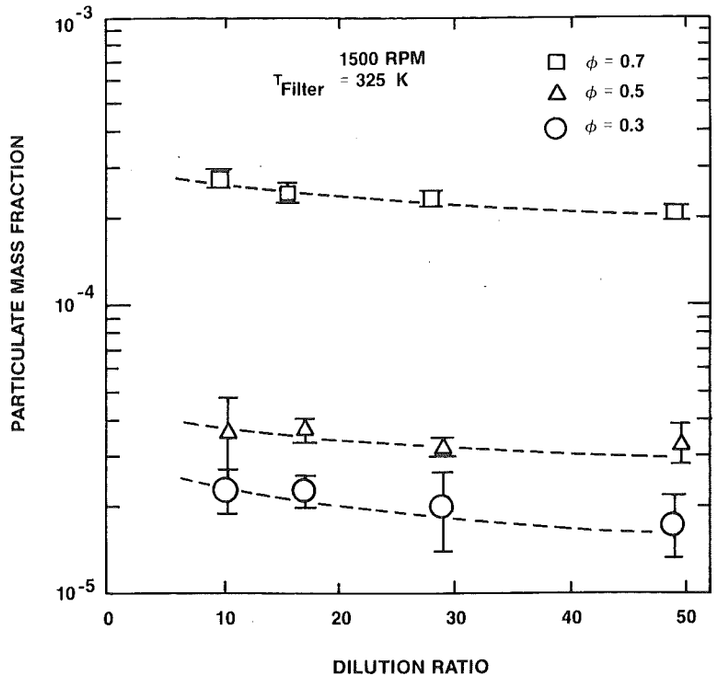

Figure 9-39 Log particulate mass fraction versus dilution ratio, 1500 rpm (Gillette and Ferguson, 1983). Particulate Science and Technology, Vol. 1, #1, p. 77–90. Reprinted with permission of the Hemisphere Publishing Corporation.

particularly for molecular weights greater than 300. The mean molecular weight of the organic fraction is on the order of 200.

Inspection of the soot fraction under an electron microscope reveals it to be agglomerates of spherical soot particles approximately 200 Å in diameter. The agglomerates can resemble a bunch of grapes in a more or less spherical configuration or be branched and chainlike in character. The characteristic dimensions of the agglomerates, on the order of 0.1 micron, pose a health hazard because they are too small to be trapped by the nose and large enough that some deposition in the lungs occurs.

A considerable body of information concerning particulates in the recent literature has been compiled into a book by Johnson, Somer, and Rosebrock (1979) and other books by SAE with prefaces written by Uyehara (1980), Hilden (1981) and Dunteman et al. (1982).

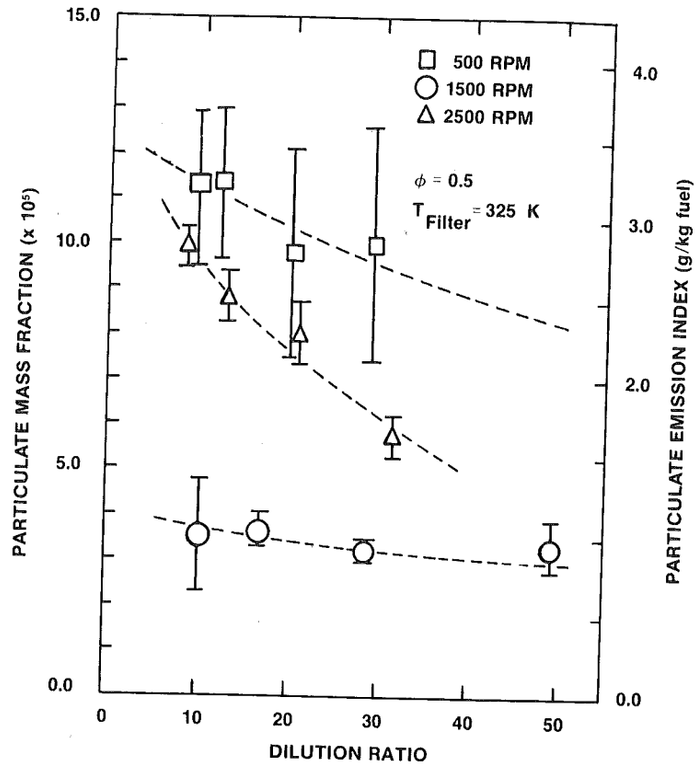

Figure 9-40 Particulate mass fraction and emission index versus dilution ratio, $\phi = 0.5$ (Gillette and Ferguson, 1983). Particulate Science and Technology, Vol. 1, #1, p. 77–90. Reprinted with permission of the Hemisphere Publishing Corporation.

9.8 EMISSION CONTROL

There are three basic methods by which engine emissions are controlled: by the design of the combustion process, by optimizing choice of the operating parameters, and by using aftertreatment devices in the exhaust system. It should be emphasized that whatever measures are taken, they are meant to maximize fuel economy subject to constraints that the emissions are low enough to be acceptable. Changes made by Nissan engineers to an existing engine are listed in Table 9-1 and are typical (if not somewhat more liberal) of what may be done from time to time as an engine continually evolves. Previous sections discussed how various parameters of engine design and operation influence the emissions characteristics. In Chapter 1 there is a discussion of

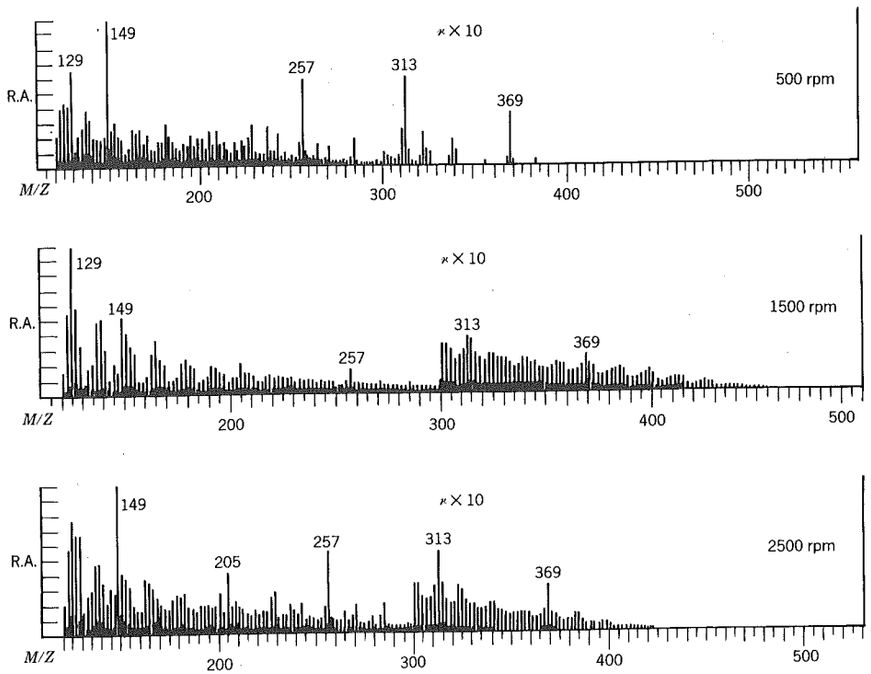

Figure 9-41 Comparison of the Chemical Ionization Mass spectra of diesel particulates collected at three different engine speeds: 500 rpm, 1500 rpm, and 2500 rpm; R. A. denotes relative abundance (Wood, Ciupek, Cooks, and Ferguson, 1982). Reprinted with permission © 1982. Society of Automotive Engineers, Inc.

stratified charge engines including how they offer the engine designer more degrees of freedom. In this sense they offer promise for emission control by design of the combustion process. They also offer more degrees of freedom in the way the engine can be operated to produce a given result and thus offer promise for better emission characteristics via optimization of control of the operating parameters.

Currently the most important aftertreatment device is the three-way catalyst. It derives its name from the fact that it works on all three of the gaseous pollutants of concern: nitric oxides, carbon monoxide, and hydrocarbons. Figure 9-42 is a schematic of a three-way catalyst. All catalytic convertors are built to expose the exhaust gases to a larger surface made of one or more of the noble metals. In the converter shown, a thin layer of the metal covers a honeycomb foundation.

A three-way catalyst will function correctly only if the exhaust gas composition corresponds to nearly stoichiometric combustion. If the exhaust is too lean, nitric oxides are not destroyed and if it is too rich, carbon monoxide and hydrocarbons are not destroyed, see Fig. 9-43. Herein lies one constraint

Table 9-1 Details of Improvements Adopted for NAPS-Z Engine, Harada et al (1981).

IMPROVEMENT ON BASIC CHARACTERISTICS			
IMPROVED COMBUSTION PERFORMANCE		MODIFICATIONS FOR OPTIMIZATION	
IMPROVED COMBUSTION ITSELF	UNIFORM COMBUSTION AMONG CYLINDERS	REDUCED MECHANICAL LOSS	ITEM	CONCRETE MEASURES TAKEN
Improved manifold heating using hot water for better mixture atomization	Improved manifold heating using hot water for better mixture atomization	Use of EAI (frictional losses are reduced through elimination of air pump)	Efficient reduction of NO_x (EGR with priority given to heavy-load operation)	Use of VVT type EGR control (venturi vacuum transducer)
Semispherical combustion chamber that produces good swirl	Tournament manifold to improve mixture distribution			
Tangential type intake port advantageous for producing swirl	Mixture heater for better mixture atomization		Optimized matching of mixture ratio, EGR, and ignition timing	
Swirl blade added to intake value	EGR gas outlet port that assures uniform EGR distribution			
Two spark plugs per cylinder to effect fast-burn combustion			Reduction of fuel consumption during deceleration	Fuel cutoff
			Reduction in fuel consumption during idling	Adoption of vacuum advance type for idling
			Improvement in fuel efficiency during engine warming	Adoption of auto-return fast idle

Source: From Harada, Kodota, and Sugiyama (1981). Reprinted with permission © 1981. Society of Automotive Engineers, Inc.

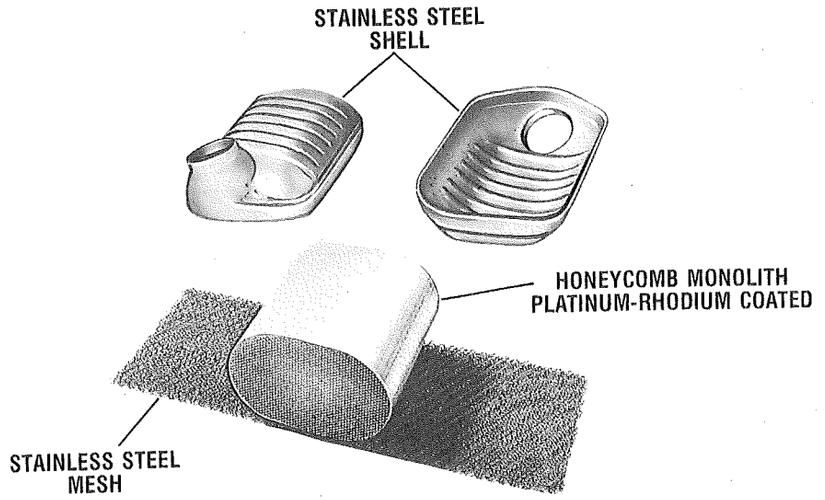

Figure 9-42 Three-way catalytic converter. Reprinted with permission. Chrysler Corp.

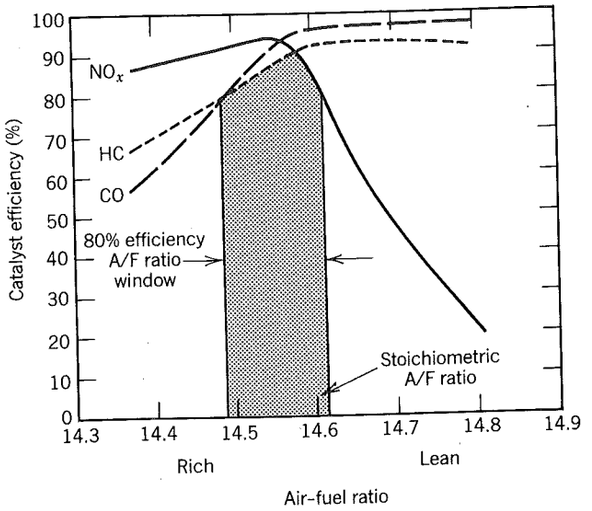

Figure 9-43 Conversion efficiency of a three-way catalyst as a function of the air–fuel ratio. Only in the vicinity of a stoichiometric air–fuel ratio is the efficiency high for all three pollutants (Kummer, 1980). Courtesy Pergamon Press, Ltd.

that emission control imposes upon the engine design: To use a three-way catalyst, the engine must operate in a narrow window about stoichiometric fuel–air ratios. This constraint is of little consequence for spark-ignition engines, but since diesel engines must run lean they cannot use a three-way convertor.

Analysis of fuel–air cycles showed that lean operation was beneficial to the thermal efficiency of the engine and at first it appears that preclusion of lean operation is a rather severe constraint. However, if one realizes that the excess air in lean combustion is acting as nothing more than a dilutant, then one can appreciate that exhaust gas recirculation can be used to achieve the same effect. Indeed the fuel–air cycle computations showed that efficiency increased with increasing residual fraction.

When a spark-ignition engine is expected to produce maximum power, it should be operated slightly rich to maximize the imep. This will produce intolerable carbon monoxide and hydrocarbon emissions. However, there is a clever way to remove these pollutants with a three-way catalyst even though the engine is fueled rich.

Figure 9-44 shows a system of secondary air management developed by Volvo. When the engine is fueled rich, an air pump is activated that pumps air into the exhaust, thereby leaning the exhaust out. An oxygen sensor measures the exhaust oxygen concentration and is used as a feedback signal for controlling the flow rate required of the air pump. The oxygen sensor is also used to ensure that when the engine is supposed to receive a stoichiometric fuel–air mixture that it in fact does.

With diesel engines, catalytic conversion of the exhaust nitric oxides is not possible because the engine runs lean. Thus this pollutant has to be controlled by design of the combustion process and/or the choice of operating

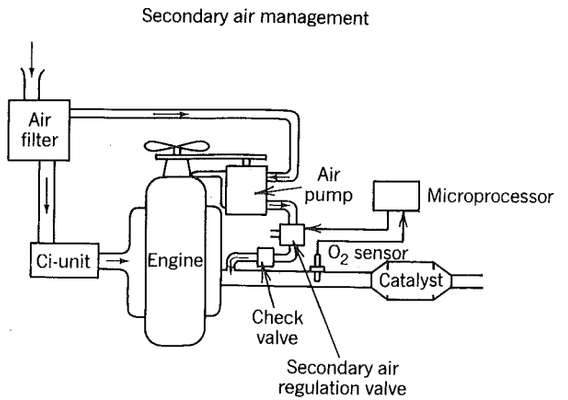

Figure 9-44 When $\phi > 1$, air injection into the exhaust maintains $\phi = 1$ at the catalyst (Engh and Wallman, 1977). Reprinted with permission © 1977. Society of Automotive Engineers, Inc.

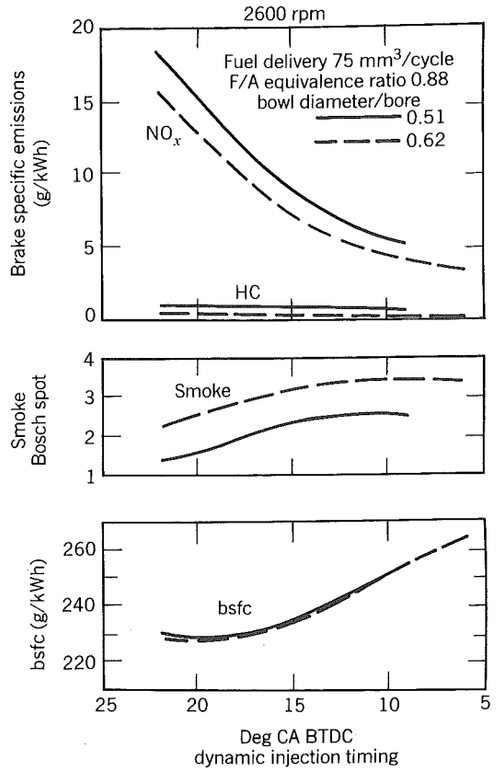

Figure 9-45 Effect of enlarged combustion bowl diameter on performance and emissions (AVL research engine) (Pischinger and Cartellieri, 1972). Reprinted with permission © 1972. Society of Automotive Engineers, Inc.

conditions. Consider Fig. 9-45 which shows experimental results for a direct injection engine. Notice that as the injection timing is retarded from 22 to 15 deg before top dead center, the nitric oxides drop by about a factor of 2, whereas the fuel consumption increases only about 3%. For this reason, diesel engines are usually operated at injection timings slightly retarded from that which produces best fuel economy.

Notice too that the diameter of the bowl or cup in the piston has been varied. The larger cup yields lower nitric oxides and yet nets virtually the same brake specific fuel consumption. If it were not for the attendant increased smoke, it could be stated unequivocally that the larger bowl is the better of the two.

It is frustrating to engine designers that generally when a reduction in nitric oxides has been achieved it is at the expense of an increase in smoke.

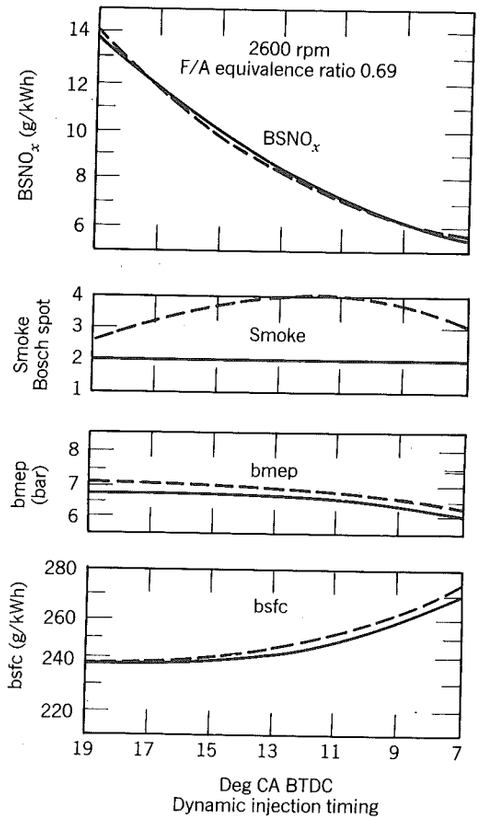

Figure 9-46 Effect of new intake system design on smoke and performance (AVL research engine). Pischinger and Cartellieri (1972). Reprinted with permission © 1972. Society of Automotive Engineers, Inc.

Figure 9-45 showed that this was true as bowl diameter varied and as injection timing varied. The engineer who obtained the results shown in Fig. 9-46 must have been very happy, for a change in the intake system realized a significant reduction in the smoke (and thus very likely in the particulates too) without increasing the nitric oxides. The only penalty paid was a slight decrease in the bmep.

Catalytic conversion of the hydrocarbons and carbon monoxide emissions is possible though not always practical. In practice, convertors seem to be used in stationary applications only. Emissions from automotive diesels (which recall is a reference to size that does not preclude trucks) are controlled by design of the combustion process and control of the engine operation.

9.9 REFERENCES

Bowditch, F. W. (1961), "A New Tool for Combustion Research: A Quartz Piston Engine," SAE Trans. Vol. 69, p. 17.

Caris, D., B. Mitchell, A. McDuffie, and F. Wyczalek (1956), "Mechanical Octanes for Higher Efficiency," SAE Trans., Vol. 64, pp. 76–100.

Cook, H. A., J. B. Vandeman, and J. C. Livengood (1944), "Effect of Several Methods of Increasing Knock-Limited Power on Cylinder Temperatures," NACA ARR E4115 E-36.

Daniel, W. A. (1957), "Flame Quenching at the Walls of an Internal Combustion Engine" Sixth Symposium (International) on Combustion, p. 886, Reinhold, New York.

Doelling, R. P., A. F. Gerber, P. N. Kerschner, M. S. Rakow, and F. H. Robinson (1972), "Additives Can Control Combustion Chamber Deposit Induced Hydrocarbons Emissions," SAE paper 720500.

Douaud, A. M. and P. Eyzat (1978), "Four-Octane-Number Method for Predicting the Anti-Knock Behavior of Fuels," SAE Trans., Vol. 87, paper 780080.

Dunteman, N. R., R. C. Strahman, and O. A. Uyehara (eds) (1982), *Diesel Engine Combustion, Emissions and Particulates*, SAE P-107, SAE, Warrendale, Pennsylvania.

Eckbreth, A. C., (1980), "Recent Advances in Laser Diagnostics for Temperature and Species Concentration in Combustion" Eighteenth Symposium (International) on Combustion, The Combustion Institute, Pittsburgh, 1981.

Engh, G. T. and S. Wallman (1977), "Development of the Volvo Lambda-Sond System," SAE Trans., Vol. 86, pp. 1393–1408, paper 770295.

Gerrish, H. C. and J. L. Meem (1943), "The Measurement of Fuel Air Ratio by Analysis of the Oxidized Exhaust Gas," NACA report 757.

Gillette, A. D. and C. R. Ferguson (1983), "Measurement and Analysis of the Particulate Emission from a Direct Injection Diesel," *Particulate Sci. and Tech.*, vol. 1, no. 1, pp. 77–90.

Greeves, G., I. M. Khan, C. H. T. Wang, and I. Fenne (1977), "Origins of Hydrocarbons Emissions from Diesel Engines," SAE Trans., Vol. 86, paper 770259.

Hagen, D. F. and G. W. Holiday (1964), "The Effects of Engine Operating and Design Variables on Exhaust Emissions," SAE TP-6, p. 206.

Harada, M., T. Kodota, and Y. Sugiyama (1981), "Nissan NAPS-Z Engine Realizes Better Fuel Economy and Low NOX Emission," SAE Trans., Vol. 90, paper 810010.

Haskell, H. H. and C. E. Legate (1972), "Exhaust Hydrocarbons Emissions from Gasoline Engines—Surface Phenomena," SAE paper 720255.

Hesselberg, H. E. and W. G. Lovell (1951), "What Fuel Antiknock Quality Means in Engine Performance," *J. SAE*, **59**, (April) p. 32.

Heywood, J. B. (1976), "Pollutant Formation and Control in Spark Ignition Engines," *Prog. Energy Combust. Sci.*, Vol. 1, pp. 135–164.

Hilden, D. L. (ed) (1982), *Fuel and Combustion Effects on Particulate Emissions*, SAE SP-502, SAE, Warrendale, Pennsylvania.

Huls, T. A. and H. A. Nickol (1967), "Influence of Engine Variables on Exhaust Oxides of Nitrogen Concentrations from a Multi-Cylinder Engines," SAE paper 670482.

Johnson, J. H., J. H. Somers and T. Rosebrock (eds) (1979), *The Measurement and Control of Diesel Particulate Emissions*, SAE PT-17, SAE, Warrendale, Pennsylvania.

Kaiser, E. W., J. A. LoRusso, G. A. Lavoie, and A. A. Adamczyk (1982), "The Effect of Oil Layers on the Hydrocarbon Emissions from Spark Ignited Engines," *Combust. Sci. and Tech.*, Vol. 28, pp. 69–73.

Komiyama, K. and J. B. Heywood (1973), "Predicting NO_x Emissions and Effects of Exhaust Gas Recirculation in Spark Ignition Engine," SAE Trans., Vol. 82, paper 730475.

Krieger, R. and G. Borman (1966), "The Computation of Apparent Heat Release for Internal Combustion Engines," ASME paper 66-WA-DGP-4.

Kummer, J. T. (1980), "Catalysts for Automobile Emission Control," *Prog. Energy Combust. Sci.*, Vol. 6, pp. 177–199.

LoRusso, J. A. (1976), "Combustion and Emissions Characteristics of Methanol, Methanol-Water and Gasoline-Methanol Blends in a Spark Ignition Engine," MS thesis, MIT, Cambridge.

LoRusso, J. A., E. W. Kaiser, and G. A. Lavoie (1981), "Quench Layer Contributions to Exhaust Hydrocarbons from a Spark Ignition Engine," *Combustion Sci. and Tech.*, **25**, p. 121.

MacDonald, J. S., S. L. Plee, J. B. D'Arcy, and R. M. Shreck (1980), "Experimental Measurements of the Independent Effects of Dilution Ratio and Filter Temperature on Diesel Exhaust Particulate Samples," SAE Trans., Vol. 89, paper 800185.

Mayer, W. J., D. C. Lechman, and D. L. Hildens (1980), The Contribution of Engine Oil to Diesel Exhaust Particulate Emissions," SAE Trans., Vol. 89, paper 800256.

Metghalchi, M. and J. C. Keck (1982), "Burning Velocities of Mixtures of Air with Methanol, Isooctane and Indolene at High Pressure and Temperature," *Combustion and Flame*, **48**(2), pp. 191–120.

Nebel, G. J. and N. W. Jackson (1958), "Some Factors Affecting the Concentration of Oxides of Nitrogen in Exhaust Gases from Spark Ignition Engines," *J. APCA*, **8**(3), p. 213.

Obert, E. F., *Internal Combustion Engines and Air Pollution*, Intext, New York, (1973).

Pischinger, R. and W. Cartellieri (1972), "Combustion System Parameters and Their Effect upon Diesel Engine Exhaust Emissions," SAE Trans., Vol. 81, paper 720756.

Rassweiler, G. M. and L. Withrow (1938), "Motion Pictures of Engine Flames Correlated with Pressure Cards," *A Landmark Reprint Paper Commemorating SAE's 75th Anniversary*, SAE paper 800131.

Robinson, J. A. (1970), "Humidity Effects on Engine Nitric Oxide Emissions at Steady-State Conditions," SAE Trans., Vol. 79, paper 700467.

Roosa, V., T. Hess, and J. Walker (1964), "The Roosa Master Nozzle," SAE paper 907B.

Smith, J. R., R. M. Green, C. K. Westbrook and W. J. Pitz (1984), "An Experimental and Modeling Study of Engine Knock", *Twentieth Symposium (International) on Combustion*, The Combustion Institute, Pittsburgh PA.

Tabaczynski, R. J., J. B. Heywood and J. C. Keck (1972) "Time-Resolved Measurements of Hydrocarbon Mass Flowrate in the Exhaust of a Spark Ignition Engine," SAE Trans., Vol. 83, paper 72112.

Tabaczynski, R. J., F. H. Trinker, and B. A. S. Shannon (1980), "Further Refinement and Validation of a Turbulent Flame Propagation Model for Spark Ignition Engines," *Combustion and Flame*, **39**(2), pp. 111–122.

Taylor, C. F., *The Internal Combustion Engine in Theory and Practice*, Vol. 1, MIT Press, Cambridge, Massachusetts, (1977).

Uyehara, O. A. (ed) (1980), *Diesel Combustion and Emissions*, SAE P-86, SAE Warrendale, Pennsylvania.

Wentworth, J. T. (1971), "Effect of Combustion Chamber Surface Temperature on Exhaust Hydrocarbon Concentration," SAE Trans., Vol. 80, paper 710587.

Wentworth, J. T. (1972), "More on Origins of Exhaust Hydrocarbons—Effects of Zero Oil Consumption, Deposit Location, and Surface Roughness," SAE Trans., Vol. 81, paper 720939.

Westbrook, C. K. and F. L. Dryer (1980), "Prediction of Laminar Flame Properties of Methanol–Air Mixtures," *Combustion and Flame*, **37**(2), pp. 171–192.

Withrow, L. and G. M. Rassweiler (1936), "Slow Motion Shows Knocking and Nonknocking Explosions," *Journal SAE*, **39**, p. 297.

Witze, P. O. and F. R. Vilchis (1981), "Stroboscopic Laser Shadowgraph Study of the Effect of Swirl on Homogeneous Combustion in a Spark Ignition Engine," SAE paper 810226.

Wood, K. V., J. D. Ciupek, R. G. Cooks, and C. R. Ferguson (1982), "Characterization of Diesel Particulates by Mass Spectrometry Including MS-MS," SAE paper 821217.

Young, M. B. (1980), "Cyclic Dispersion—Some Quantitative Cause-and-Effect Relationships," SAE paper 800459.

Yu, R. C., V. W. Wong, and S. M. Shahed (1980), "Sources of Hydrocarbon Emissions from Direct Injection Diesel Engines," SAE Trans., Vol. 89, paper 800049.

9.10 HOMEWORK

1. For stoichiometric gasoline–air mixtures it has been found that

$$S_L = 25.25P^{-0.13}\left(\frac{T_u}{298}\right)^{2.19}(1-2.1f)$$

where S_L is cm/s, P is bars, T_u is K, and f is the residual mass fraction. Assume for a given engine that the pressure and temperature at the time of ignition are given by

$$T_{u,s} = 350\left(\frac{V_{\text{BDC}}}{V_s}\right)^{(\gamma-1)/\gamma} \qquad \text{where } \gamma = 1.3$$

$$P_s = 0.5\left(\frac{V_{\text{BDC}}}{V_s}\right)^{\gamma}$$

Assume further that for the engine design $\Delta\theta_{\text{id}} = 25$ deg for $r = 8$ and $\theta_s = -25$ deg. The residual fraction is given by $f = 0.10(8/r)$ and the kinematic viscosity is given by

$$\nu \approx \nu_{\text{air}} = \frac{9.47 \times 10^{-6} T_u^{1.7}}{P} \quad (\text{cm}^2/\text{s})$$

If the bore and stroke of the engine are 10 and 8 cm, respectively, using the cosine relationship (valid for $\epsilon \to 0$) for relating cylinder volume to crank angle, compute the laminar flame speed at ignition as a function of compression ratio and spark timing. Assuming the delay is inversely proportional to the laminar flame speed at the time of ignition. Plot the ignition delay versus θ_s for $-50 < \theta_s < 0$ and show lines of constant compression ratio for $r = 8$ and $r = 10$.

2. A combustion model predicted the following data for an engine operated at wide-open throttle on isooctane:

θ (DEG ATC)	x	P (ATM)	T_u (K)	T_b (K)
−40	0.000	5.6	600	2500
−30	0.001	7.5	650	2572
−20	0.062	12.6	745	2652
−10	0.383	31.6	900	2700
0	0.843	57.8	950	2750
10	0.994	58.6	1000	2800
20	1.000	45.2	975	2747

If the precursor formation rate is (Douaud and Eyzat, 1978)

$$\frac{1}{x_c}\frac{dx_p}{dt} = 50.5P^{1.7}\exp\left(\frac{-3800}{T}\right)$$

a. Determine the minimum engine speed for which knock-free operation occurs assuming the table is speed independent. Plot the extent of reaction versus crank angle at that speed. Comment on assumptions implicit or explicit in the analysis.

b. Assume that throttling the engine reduces all pressure 25% and all temperatures 5%, repeat part (a).

3. The existence of a temperature gradient in the burned gas can be explained fairly simply using an ideal gas model in which the fluid is broken into an ensemble of elements. The average pressures and specific volumes of an Otto cycle are represented in Fig. 9-47 by the diagram 1-2-3-4. All the gas is compressed isentropically from 1 to 2; hence at point 2 the gas is at a uniform temperature T_2.

The first element (infinitesimal) to burn will not influence the cylinder pressure and thus burns at constant pressure to 2′. Thus

$$T_{2'} = T_2 + \frac{q}{c_p}$$

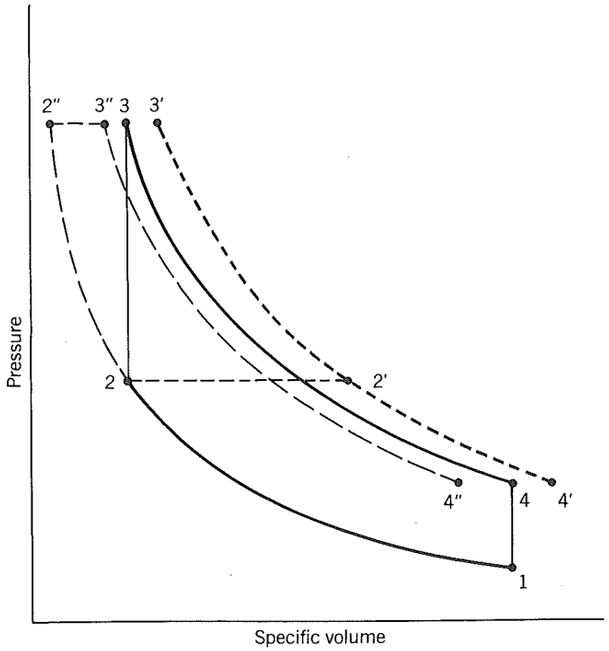

Figure 9-47 Because of progressive burning, the first element to burn ends up hotter at the end of all combustion than the last element to burn; that is, $T_{3'} > T_{3''}$.

where q is the heat release per unit mass. That gas is then compressed isentropically to the peak pressure P_3, hence

$$\frac{T_{3'}}{T_{2'}} = \left(\frac{P_3}{P_2}\right)^{\gamma-1/\gamma}$$

The last element to burn is compressed isentropically as unburned gas to the peak pressure at 2″.

$$\frac{T_{2''}}{T_2} = \left(\frac{P_3}{P_2}\right)^{(\gamma-1)/\gamma}$$

The last element then also burns at constant pressure so that

$$T_{3''} = T_{2''} + \frac{q}{c_p}$$

All the elements expand isentropically after the last element burns.

Taking as the average cycle the conditions used in Figure 2.1 of Chapter 2, find

a. The ratio $T_{3'}/T_{3''}$
b. The ratio $v_{4'}/v_{4''}$

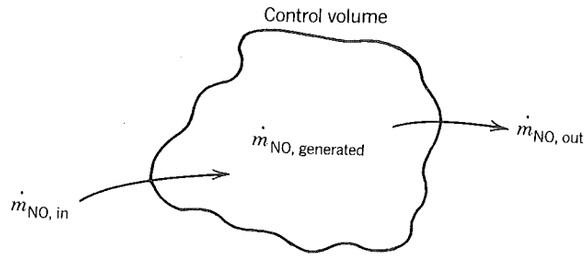

Figure 9-48 Illustration for Homework Problem 4.

4. The rate of change of nitric oxide mass fraction for a fluid element because of chemical reaction is given by Eq. (9.19). The mass fraction can also change because of NO convected in and out of the fluid element. Consider this control volume. Write an expression for the rate of change of nitric oxide mass fraction for this element where the fluid entering is devoid of nitric oxides, the fluid leaving has the same properties as fluid in the element, and the generation of NO within the control volume is given by Eq. (9.19).
5. Emissions data are often presented as the mass flow rate of the pollutant emitted divided by the engine's power. Brake specific nitric oxides for a single cylinder research engine are given in Fig. 9-49 that follows. These results indicate that to minimize the pollutant emission in grams per hour at a given power level one should operate at as high a bmep as possible. Since the experiments are done at constant fuel–air ratio, they illustrate an advantage of turbocharging as far as nitric oxides are concerned. Present the same data in the different forms found in practice:

- Emission index—Grams of nitric oxides per kilogram of fuel versus bmep.
- Mass fraction—Grams of nitric oxide per kilogram of exhaust versus bmep.
- Concentration—Ppm versus bmep (assume the molecular weight of exhaust is that of air).

6. Use Table 3-2 to compute the exhaust CO concentration for an engine fueled with C_7H_{17}. Plot CO versus ϕ for two different gas temperatures at the time of exhaust valve opening, $T = 1800$ K and $T = 1500$ K.
7. Reaction of hydrocarbons in the exhaust port of an engine is an important process used in determining emissions from either a gasoline or a diesel engine. The rate of change of the mass fraction due to chemical reaction is given by:

$$-\frac{dx_{HC}}{dt} = Ax_{HC}x_{O_2}\exp\left(\frac{-E}{RT}\right)$$

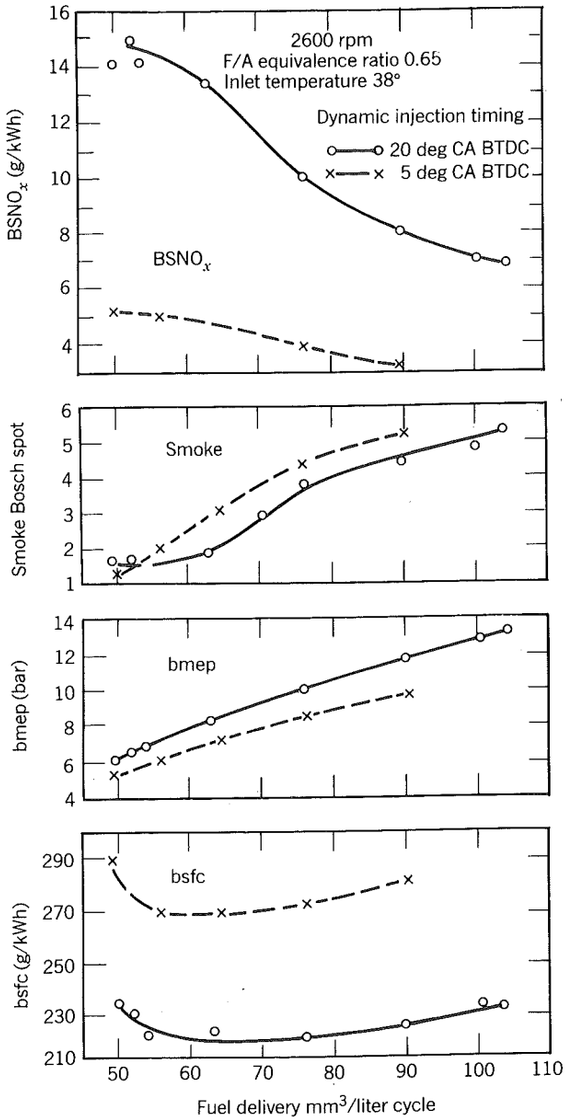

Figure 9-49 Effect of timing on emissions and performance, supercharged standard AVL research engine, not modified, at constant fuel–air ratio and constant air inlet temperature (Pischinger and Cartellieri, 1972). Reprinted with permission © 1972. Society of Automotive Engineers, Inc.

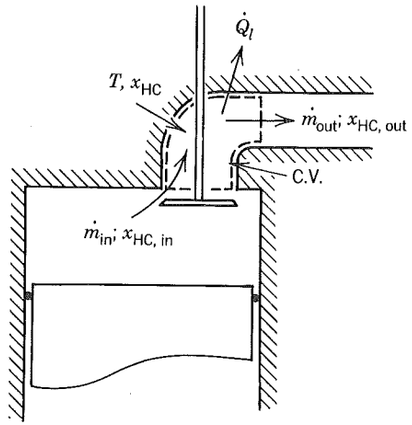

Figure 9-50 Illustration for Homework Problem 7.

Assuming that gases in the port are well mixed, show that

$$\left(\frac{dx_{HC}}{dt}\right)_{c.v.} = \frac{\dot{m}_{in}}{m}(x_{HC,in} - x_{HC}) - Ax_{HC}x_{O_2}\exp\left(\frac{-E}{RT}\right)$$

8. As an engine warms up, clearance between various parts change because of differing amounts of thermal expansion. Explain how this can affect hydrocarbon emissions from a spark-ignition, homogeneous-charge engine.
9. Explain how blowby can affect hydrocarbon exhaust emissions (not crankcase emissions which are no longer a problem). Specifically discuss the influence of engine speed.

Ten
FUELS AND LUBRICANTS

So far our attention has been on fuels composed of only one chemical species. A typical gasoline or diesel fuel may consist of 100 hydrocarbons and another 100 to 200 trace species. This chapter explains why fuels are so complex, how they are manufactured, and how to estimate their thermodynamic properties required for performance analysis. This chapter also discusses some of the properties of lubricating oils.

10.1 CRUDE OIL

There are four significant sources of crude oil: (1) petroleum; (2) coal liquefaction; (3) shale oil; and (4) tar sands. Most of the crude oil used to date has been petroleum derived since what is found in the ground requires little processing before delivery to a refinery. Coal, on the other hand, must be treated to increase its hydrogen content and remove undesirable elements such as nitrogen, sulfur, arsenic, mercury, cadmium, or phosphorous. Shale oil is difficult to get out of the ground since it is soaked up in rocks. Tar sands contain hydrocarbons mixed with sand and are more difficult to remove from the ground than petroleum. Like coal derivatives and shale oil, oils from tar sands require hydrogenation and removal of undesirable chemicals from the crude before it is delivered to the refinery. As petroleum supplies dwindle, more and more crude oil will be made from alternative sources.

Regardless of the source, crude oil contains a large number of different hydrocarbons. For example, 25,000 different compounds have been found in one sample of petroleum derived crude oil subjected to an extraordinarily thorough analysis. The compounds range from gases to viscous liquids and waxes.

The purpose of a refinery is to physically separate crude oil into various fractions and then chemically process the fractions into fuels and other products.

10.2 REFINING

The separation process is called distillation and the device employed is often called a still. The generic features of a still are illustrated in Fig. 10-1. The sample is heated preferentially boiling off the lighter components. The classifi-

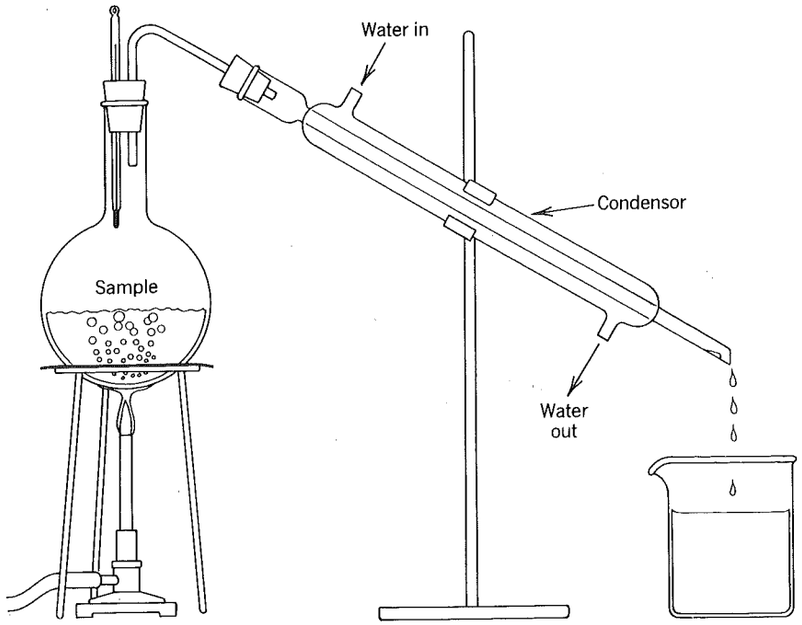

Figure 10-1 Distillation separates crude oil into "fractions."

cation of the various fractions is arbitrary. In the order in which they leave the still the various fractions are commonly referred to as: naphtha, distillate, gas oil, and residual oil. Further subdivision uses the adjectives *light*, *middle*, or *heavy*. The adjectives *virgin* or *straight run* are often used to signify that no chemical processing has been done to the fraction. For example, since light virgin naphtha can be used as gasoline, it is often called straight run gasoline. The physical properties of any fraction are controlled by the distillation temperatures of the products collected in the beaker.

A broad cut fraction is collected over a large range of distillation temperatures, a narrow cut over a small range, a light fraction over a low temperature range, and a heavy fraction over a high temperature range.

Chemical processing is required to convert one fraction into another. For example a crude might yield, on an energy basis, 25% straight run gasoline but the product demand could be 50%. In this situation the other 25% would be picked up by chemical processing of some other fraction into gasoline. Chemical processing is often required to upgrade a given fraction. For example straight-run gasoline might have an octane number of 70; whereas the product demand could be 90. In this case chemical processing would be used to increase the octane number from 70 to 90.

An example illustrating refinery processing paths is shown in Fig. 10-2. The chemical processes shown are alkylation, reforming, catalytic cracking,

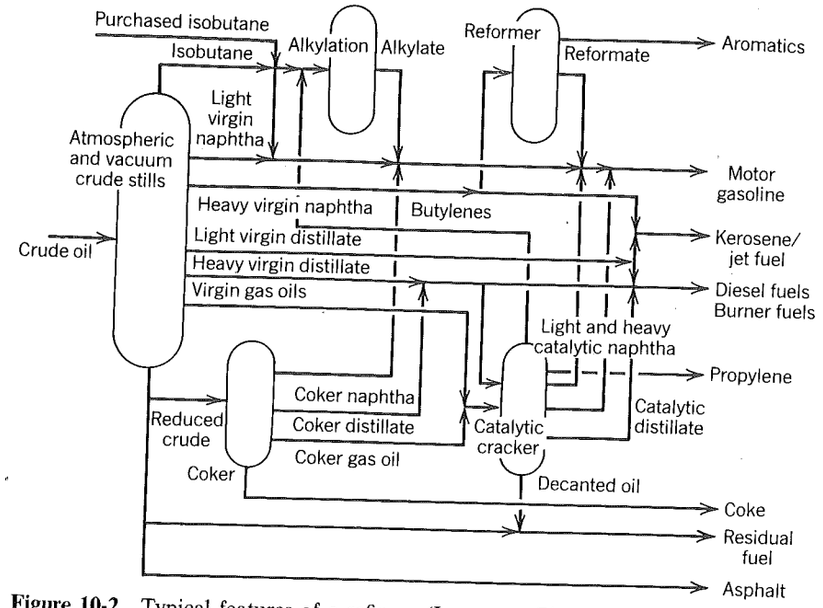

Figure 10-2 Typical features of a refinery (Lawrence, Plantz, Keller, and Wagner, 1980). Reprinted with permission © 1980. Society of Automotive Engineers, Inc.

and coking. An actual refinery uses many more processes but we will limit our study to these most important ones. Likewise a refinery will produce more products than those shown. The refinery illustrated produces fuels for engines (gasoline, diesel, jet), fuels for heating (burner, coke, kerosene, residual), chemical feedstock (aromatics, propylene), and asphalt. We will limit our attention to gasoline and diesel fuel.

The section following describes pure hydrocarbons and is prerequisite to later sections that discuss chemical processing and the thermophysical properties of gasoline and diesel fuel.

10.3 HYDROCARBONS

Paraffins (alkanes) are molecules in which carbon atoms are chained together by single bonds. The remaining bonds are with hydrogen. They are called saturated hydrocarbons because there are no double or triple bonds. The number of carbon atoms are specified by a prefix:

1—meth	4—but	7—hept	10—dec
2—eth	5—pent	8—oct	11—undec
3—prop	6—hex	9—non	12—dodec

The paraffin hydrocarbon is designated as an alkane by the suffix *ane*. The general formula for the family is C_nH_{2n+2}.

Examples of straight chain paraffins are

methane, CH_4

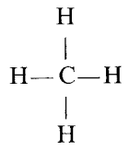

octane, C_8H_{18}

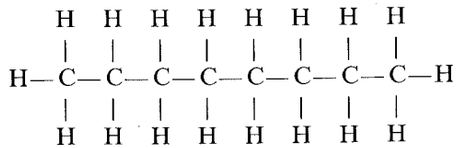

Isooctane is an example of an isomer of octane. That is, it has the same number of carbon atoms as octane but not in a straight chain. For this reason octane is sometimes called normal octane or n-octane. The structure of isooctane follows.

isooctane, C_8H_{18} or 2,2,4 trimethylpentane

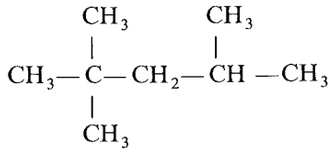

The group CH_3 attached to the second and fourth carbons from the right is called a methyl radical, *meth* because it has one carbon atom and *yl* because it is of the alkyl radical family C_nH_{2n+1}.

Isooctane is more properly called 2,2,4 trimethylpentane, *2,2,4* because methyl groups are attached to the second and fourth carbon atoms, *trimethyl* because three methyl radicals are attached, and *pentane* because the straight chain has five carbon atoms.

Thermophysical properties of some hydrocarbons were given in Chapter 3. The octane numbers of some pure fuels are tabulated in Table 10-1. In general it has been found that the octane number is improved by reducing the straight-chain length. This can be accomplished by reducing the total number of carbon atoms or by rearranging them in to a branch chain structure. These generalizations are illustrated in Fig. 10-3. The critical compression ratio is determined by increasing the compression ratio of an engine until incipient knocks occurs. That it correlates with octane number should be clear.

Olefins (alkenes) are molecules with one or more carbon–carbon double bonds. Monoolefins have one double bond, the general formula C_nH_{2n}, and

Table 10-1 Knock Characteristics of Single Component Fuels

FORMULA	NAME	CRITICAL COMPRESSION RATIO[a]	OCTANE NUMBER[b]	
			RESEARCH	MOTOR
CH_4	Methane	12.6	120	120
C_2H_6	Ethane	12.4	115	99
C_3H_8	Propane	12.2	112	97
C_4H_{10}	Butane	5.5	94	90
C_4H_{10}	Isobutane	8.0	102	98
C_5H_{12}	Pentane	4.0	62	63
C_5H_{12}	Isopentane	5.7	93	90
C_0H_{14}	Hexane	8.3	25	26
C_6H_{14}	Isohexane	9.0	104	94
C_7H_{16}	Heptane	3.0	0	0
C_7H_{16}	Triptane	14.4	112	101
C_8H_{18}	Octane	2.9	−20	−17
C_8H_{18}	Isooctane	7.3	100	100
$C_{10}H_{12}$	Isodecane	—	113	92
C_4H_8	Methylcyclopropane	—	102	81
C_5H_{10}	Cyclopentane	12.4	101	95
C_6H_{12}	Cyclohexane	4.9	84	78
C_6H_{12}	1,1,2-trimethylcyclopropane	12.2	111	88
C_7H_{14}	Cycloheptane	3.4	39	41
C_8H_{16}	Cyclooctane	—	71	58
C_6H_6	Benzene	—	—	115
C_7H_8	Toluene	15	120	109
C_8H_{10}	Ethyl benzene	13.5	111	98
C_8H_{10}	Xylene-m	15.5	118	115
C_3H_6	Propylene	10.6	102	85
C_4H_8	Butene-l	7.1	99	80
C_5H_{10}	Pentene-l	5.6	91	77
C_0H_{12}	Hexene-l	4.4	76	63
C_5H_8	Isoprene	7.6	99	81
C_6H_{10}	1,5-hexadiene	4.6	71	38
C_5H_8	Cyclopentene	7.2	93	70
CH_4O	Methanol	—	106	92
C_2H_6O	Ethanol	—	107	89

Source: An Abridgement of Tables 8-6 and 8-7 from *Internal Combustion engines and air pollution*. Based on *Internal Combustion engines*, 3rd Ed. by Edward F. Obert (Intext) Copyright 1944, 1950, c 1968, 1973 by Harper and Row, Publishers, Inc. Reprinted by permission of the publisher.

[a] The critical compression ratio is for audible knock at 600 rpm, inlet temperature at 311 K, coolant at 373 K, spark advance and fuel–air ratio set for best power (GM tests).

[b] Octane ratings above 100 are obtained by matching against leaded isooctane.

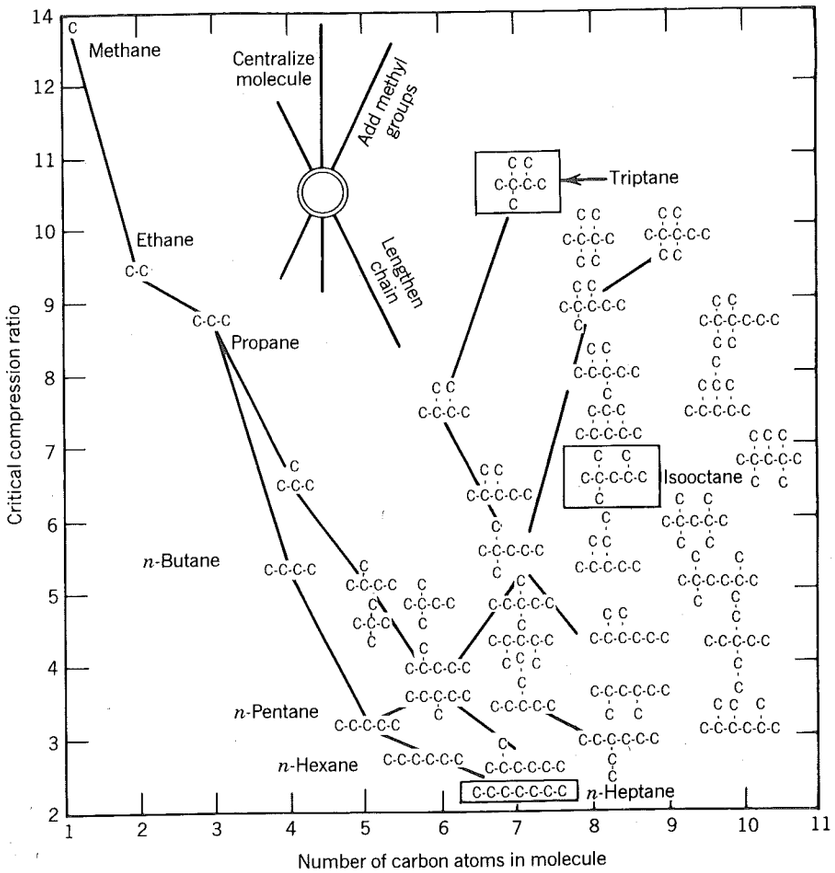

Figure 10-3 Effect of fuel structure on detonation tendency of paraffinic Hydrocarbons: CFR engine, 600 rpm, inlet temperature 450 K (Lovell, 1948).

their names end with *ene*. For example

C_8H_{16}, l-octene

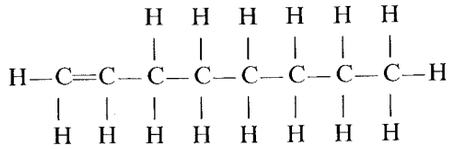

Isomers are possible not only by branching the chain with the addition of a methyl radical but also by shifting the position of the double bond without changing the carbon skeleton.

Olefins with more than one carbon–carbon double bond are undesirable components of fuel that lead to storage problems. Consequently they are refined out and the only olefins of significance in diesel fuel or gasoline fuel are monoolefins.

Naphthenes (cycloalkanes) have the same general formula as olefins, C_nH_{2n}, but there are no double bonds. They are called cyclo because the carbon atoms are in a ring structure. Two examples are

cyclopropane

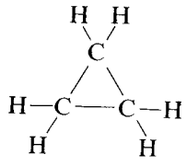

cyclobutane

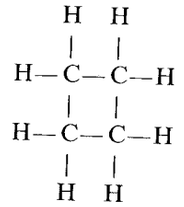

Rings having more than six carbon atoms are not as common.

Aromatics are hydrocarbons with carbon–carbon double bonds internal to a ring structure. The most common aromatic is benzene.

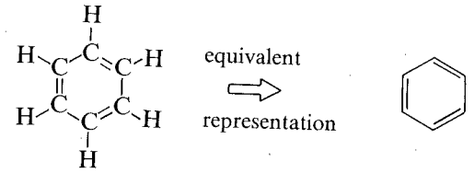

Some common aromatics have groups substituted for hydrogen atoms.

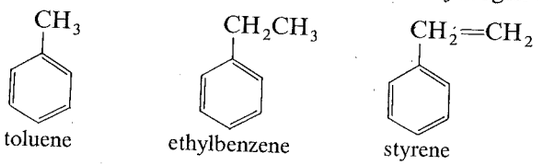

Others have more than one ring.

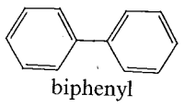

Finally there are aromatics with two carbon atoms shared between more than one ring.

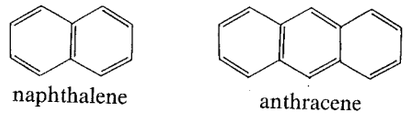

Notice that the double bonds alternate in position between the carbon atoms. This makes the molecule hard to break and, as a result, aromatics are desirable in gasoline since they increase the octane number. Aromatics are undesirable components of diesel fuels.

10.4 ALCOHOLS, PHENOLS, AND ETHERS

Alcohols are derived from hydrocarbons by replacing a hydrogen atom by the hydroxyl radical OH. If the hydrogen atom attached to an aromatic ring is replaced by the hydroxyl radical, the molecule is called a phenol. Ethers are isomers of alcohols with the same number of carbon atoms. Some examples are

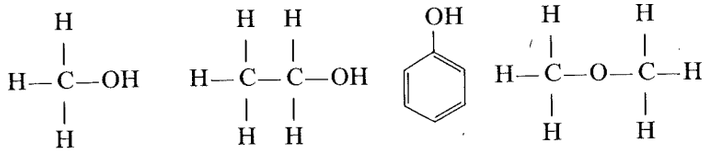

methanol ethanol phenol methyl ether

Alcohols, especially methanol, are of interest because they are high octane fuels and can be made from gasified coal. Ethers such as methyl-tert-butyl ether are used in gasoline to increase the octane number.

10.5 CHEMICAL PROCESSING

It has already been mentioned that chemical processing is used to upgrade a given fraction and to convert one fraction to another. The chemical processes in the simplified refinery are now discussed as representative of what is done in practice.

Alkylation is used to increase the octane number of gasoline by adding alkyl radicals to a molecule. Light olefin gases are reacted with isobutane in the presence of a catalyst. Isooctane results from reacting butene with isobutane. The process is low temperature (275 K) and pressure (3 atm) and therefore consumes much less energy than other chemical processes.

Catalytic cracking breaks molecules and its major function is to convert distillates into naphthas for use as gasoline. The naphtha products of catalytic cracking are high octane gasolines. The reactions are at high temperature (700 to 800 K) and at low to moderate pressure (2 to 8 atm). Considerable energy is consumed in the process.

Reforming refers to reactions designed to alter molecular structure to yield higher octane gasoline (e.g., conversion of paraffins into aromatic hydrocarbons). This is often done in a hydrogen atmosphere at high temperature (800 K), at high pressure (30 atm), and in the presence of a catalyst. Considerable hydrogen is produced as a result of the "reaction"

$$C_nH_{2n+2} \rightarrow C_nH_{2n-6} + 4H_2$$

Coking is used to convert the heavy reduced crude fraction to the more usable naphtha and distillate fractions. It is done by heating the reduced crude in an oven. Upon heating, the molecules undergo pyrolytic decomposition and recombination. The average molecular weight of the fraction remains the same but a greater spectrum of components is produced. The heaviest component, called coke, is a solid material not unlike charcoal.

10.6 GASOLINE

The properties of gasolines sold through service stations in the United States are reported each year in accordance with a cooperative arrangement between the American Petroleum Institute and the federal government. About 2000 samples are analyzed each summer and winter representing the products of nearly 50 companies, large and small, that manufacture and supply gasoline.

Trends in octane number are shown in Fig. 10-4 for regular gasoline and for premium gasoline. In each case the octane number shows an increase from 1920 to about 1963. The increase of octane number with time prior to 1963 started in the early 1920s when chemical processing started to emerge in refineries. As that technology developed, the octane number increased and the compression ratio of engines followed.

The octane number pretty much stagnated throughout the 1960s and into the early 1970s. Since about 1972 it has dropped as the additive tetraethyl lead began to be phased out so that catalytic reactors could be used on automobiles for emission control.

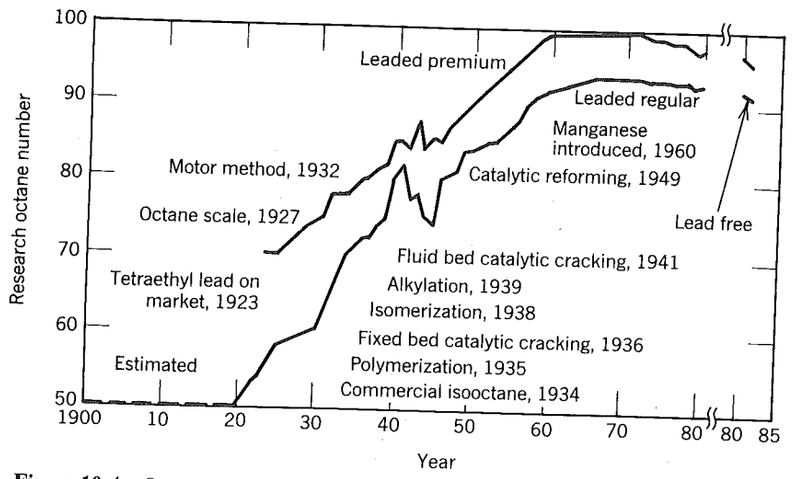

Figure 10-4 Octane number of U.S. motor fuels and some important events that contributed to change (Gibson, 1982). Reprinted with permission © 1982. Society of Automotive Engineers, Inc.

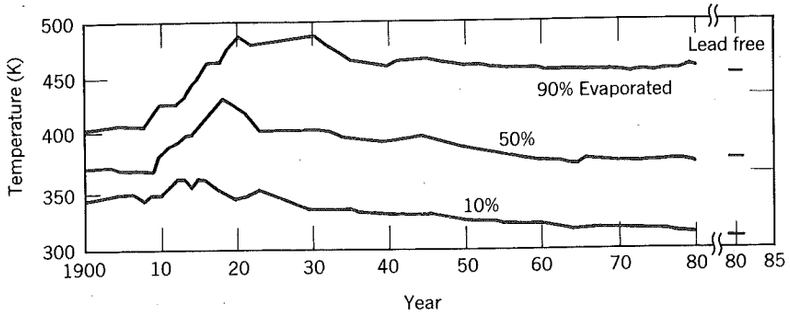

Figure 10-5 Motor gasoline volatility average, summer regular and premium (Gibson, 1982). Reprinted with permission © 1982. Society of Automotive Engineers, Inc.

Figure 10-5 illustrates the trends in volatility for summer gasolines. The distillation temperature for "90% evap" refers to the temperature recorded in a still, like that illustrated in Fig. 10-1, when 90% of the sample has evaporated. The most significant change occurred between 1910 and 1930 as refiners took a larger cut of the crude to be gasoline. The difference in distillation temperatures between summer and winter gasoline is on the order of 5 K and that difference is slightly larger at 10% evap than 90% evap. The data reflect that with colder ambient air it is harder to evaporate the fuel prior to delivery to an engine. The trends with time for both winter and summer gasoline indicate that the volatility of gasoline (ease with which it evaporates) has increased with time. Some other properties of gasoline reported annually are illustrated in Table 10-2. Sulfur or sulfur compounds are undesirable components in fuels because they are corrosive to fuel delivery systems, they can lead to formation of sulfuric acid in the crankcase and in the atmosphere, and they can reduce the octane number.

Gum is a product of oxidation reactions with certain molecules often found in fuels. Use of gasoline with a high gum component can lead to sticking of valves and piston rings, carbon deposits, and clogging of fuel metering orifices.

The test developed by the American Society of Testing of Materials (ASTM method D381) involves evaporating 50 ml of gasoline in a glass dish at approximately 430 K by passing heated air over the sample for a period of about 10 min. The difference in weight of the dish before and after the test is called the existant gum content. Inhibitors are often added to gasoline to reduce the gum formed in such a test under an assumption they will also reduce gum formation in service.

Benzene is an aromatic hydrocarbon and a known carcinogen. Lead is an additive for improving the octane number, it was not measured for the unleaded fuels even though some lead (0.0005 g/l is typical) may be present due to contamination in the distribution system. The antiknock index is the

Table 10-2 Summary of Properties from Gasoline Survey, Summer 1980

		GRADES OF GASOLINE			
PROPERTY	ASTM METHOD	UNLEADED (R + M)/2 BELOW 90	AVERAGE (R + M)/2 90.0 AND ABOVE	REGULAR AVERAGE	PREMIUM AVERAGE
Specific gravity at 289 K	D287	0.744	0.752	0.738	0.737
Sulfur, Wt%	D1266	0.028	0.019	0.049	0.034
Gum, mg/100 ml	D381	1	1	1	2
Benzene, volume %	D3606	1.11	1.02	1.14	1.08
Lead, g/l	—	—	—	0.32	0.37
Octane, research	D2699	92.1	96.7	92.6	97.0
Octane, motor	D2700	83.4	86.4	85.2	88.1
Antiknock index, (R + M)/2		87.8	91.6	88.9	92.8
Reid vapor pressure, N	D323	44	44	44	45
Vapor-liquid ratio of 20, K	D439	331	331	329	329
Distillation, K	D86				
IBP		305	305	306	305
5%		314	315	314	313
10%		322	322	321	321
20%		336	337	332	334
30%		351	351	344	348
50%		378	378	370	373
70%		403	401	402	399
90%		442	436	446	441
95%		461	454	466	461
End point		484	478	487	483
Residue, volume %		1.6	1.8	1.5	1.7
Loss, volume %		1.7	1.8	1.5	1.8

average of the research and motor octane numbers and is the number displayed on pumps at service stations.

The Reid vapor pressure, vapor–liquid ratio of 20, and the distillation curve are all in principle redundant measures of fuel volatility. Theoretically, it is possible to predict the Reid vapor pressure and the vapor–liquid ratio of 20 given the distillation curve. However in practice, some limiting assumptions have to be made and the ASTM tests D323 and D439 are so easily performed that the theory is rarely exercised. Knowledge of a fuel's volatility is important not only in designing fuel delivery and metering systems but also in controlling evaporative emissions. The residue and loss refer to uncertainties in the test which will be discussed later.

For performance computations the data included in the survey are incomplete. Required are the hydrogen to carbon ratio, the molecular weight, the heat of combustion, the temperature dependent specific heat of the vapor, and the available energy of combustion. The first three can be easily measured,

Table 10-3 Some Properties of Unleaded Gasoline and Naphtha

	UNLEADED GASOLINE			NAPHTHA	
Distillation (K, ASTM D86)					
IBP	303	299	300	408	434
10%	322	319	319	421	441
20%	341	332	332	426	443
50%	377	377	381	436	447
70%	386	401	416	439	452
90%	406	437	451	443	485
EP	480	492	481	466	485
Viscosity, CST (313 K)	0.55				
Specific gravity (285 K)	0.690	0.732	0.738	0.771	0.783
Hydrocarbons ASTM D1319					
% Aromatics	0.6	20.4	27.1	8.7	14.2
% Olefins	0.8	7.4	5.3	1.9	2.2
% Saturates	98.6	72.2	67.6	89.4	83.6
Higher heat of combustion (cal/g)	11545	11043	11043	11006	10989
Hydrogen: carbon (moles)	2.46	[a]	[a]	—	1.93
Molecular weight	(100 to 105 average[b])			—	—
Octane number					
Research	92.4	92.1	91.6	48.5	43.6
Motor	88.4	84.6	88.2	37.6	32.4
Cetane number	17.2			39.9	54.8
AL label	7927G	8166G	8668G	8073F	7986F

Source: from B. K. Bailey and J. A. Russell, SAE paper 810444.

[a] These numbers were not reported but from Table 2 of the source we can infer that $1.6 < H{:}C < 2.1$ is typical of gasolines.

[b] P. Dorn and A. M. Mourau (1984) report that $M = 111$ (C_8H_{15}) is typical of gasoline.

whereas the latter two cannot. Fortunately, an approximation to the specific heat is all that is required and this can be done from knowledge of the fractions of paraffins, olefins, aromatics, and naphthenes from which the gasoline is composed. Measurements of these fractions is routine and the information can also lead to an approximation for the available energy.

Example data for three unleaded gasolines, medium naphtha, and a heavy naphtha are given in Table 10-3. Notice that even though the three gasolines have significantly different compositions, their distillation curves, octane numbers, molecular weights, and heats of combustion are nearly the same. Notice too that the naphthas have significantly lower octane numbers, which we can expect since these are narrow cuts of straight run gasoline.

10.7 DIESEL FUEL

Given the complexity of gasoline, it is incredible how little the properties vary from sample to sample. Results of the gasoline survey previously discussed showed that for winter unleaded gasolines, where $(R + M)/2 > 90$, geographical differences in the initial boiling point are on the order of 5 K, at the end point the difference is around 10 K. Differences in the distillation curves between summer and winter vary by about 10 K. Differences between grades (high versus low octane) are only a few degrees Kelvin. The same cannot be said for diesel fuels.

Diesel fuels show significant variations with time, geographic location, and intended service. The government, in cooperation with the American Petroleum Institute also surveys diesel fuels. The four groups of service for which diesel fuels are classified are as follows:

Type C–B	City bus
Type T–T	Trucks, tractors
Type R–R	Railroad
Type S–M	Stationary and marine

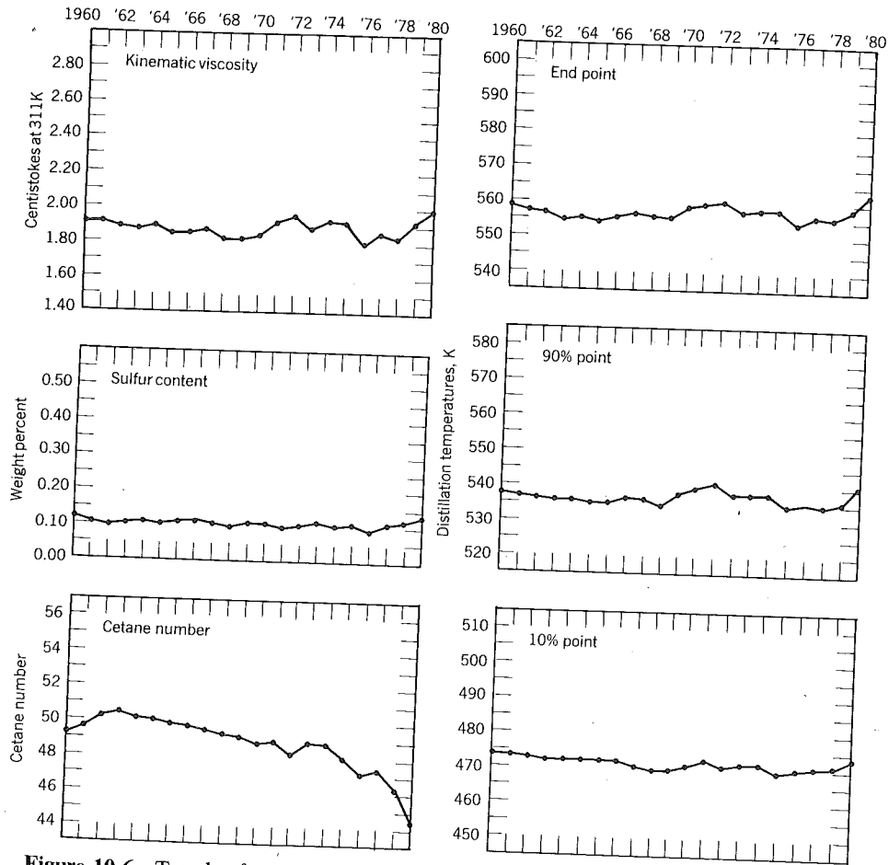

Figure 10-6 Trends of some properties of type C–B diesel fuel oils (Shelton, 1982).

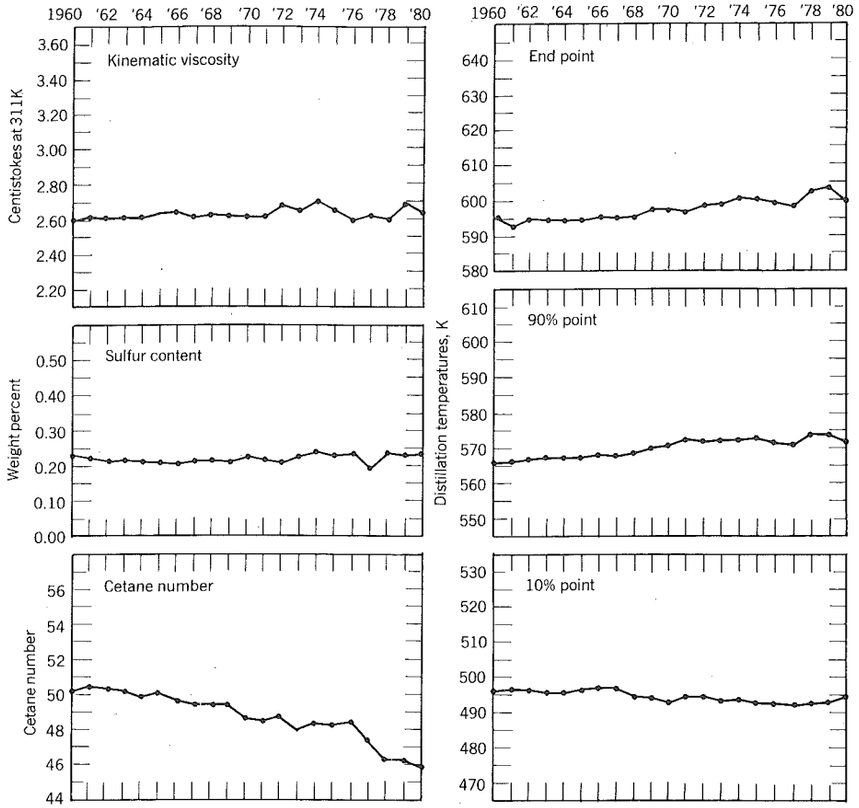

Figure 10-7 Trends of some properties of type T–T diesel fuel oils (Shelton, 1982).

Figures 10-6 through 10-9 illustrate recent trends with time of certain average properties. The following points are particularly significant:

- In the past two decades cetane numbers have dropped.
- S–M fuel properties fluctuate considerably.
- Viscosity, sulfur, and distillation temperatures increase in the order C–B, T–T, R–R, S–M.

It should be clear that stationary and marine engines are designed to accept wide variations in fuel properties. This is easier to do for these engines than for, say, city bus diesel engines since their mode of operation is more predictable. Since bus engines are expected to operate under wide variations in

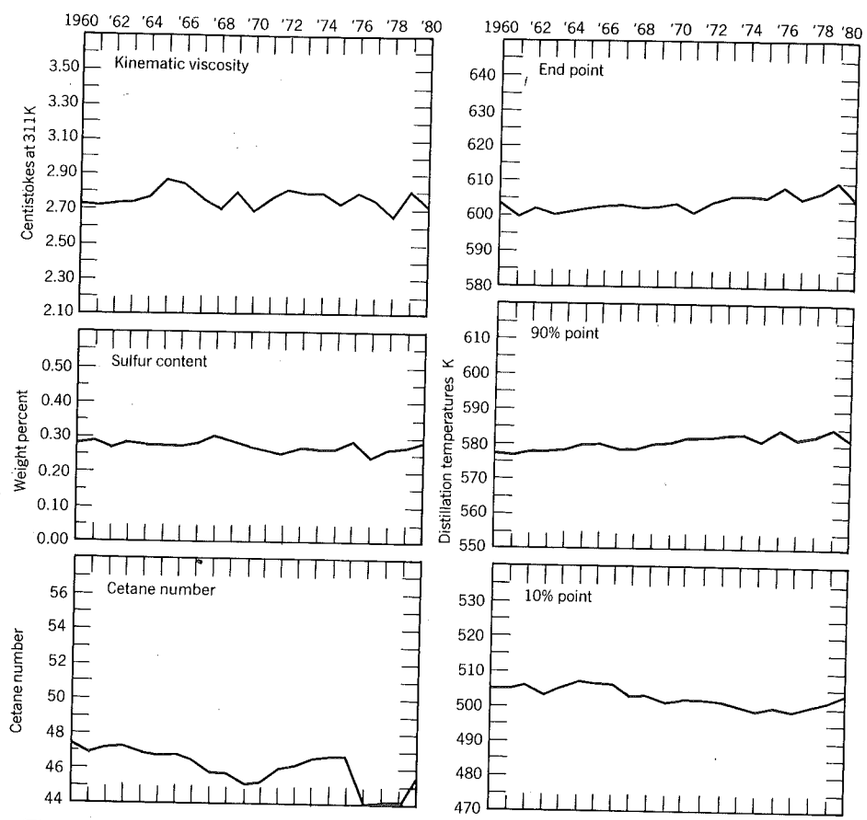

Figure 10-8 Trends of some properties of type R–R diesel fuel oils (Shelton, 1982).

speed and load, more compromises need to be made in their design. One of the compromises is to allow there to be less tolerance to fuel property variations.

Other information surveyed about diesel fuels and an indication of how the properties vary is given in Table 10-4 for fuels in the eastern United States. It can be seen that for a given type of diesel fuel there is significant variation within a region, that cetane numbers are largest for C–B fuels and smallest for S–M fuels, and that variations are greatest for S–M fuels.

The API gravity is a measure of the fuel's density. It is related to the specific gravity of the fuel at 289 K by

$$\text{API}_{\text{gravity}} = \frac{141.5}{\text{SP}_{\text{gravity}}} - 131.5$$

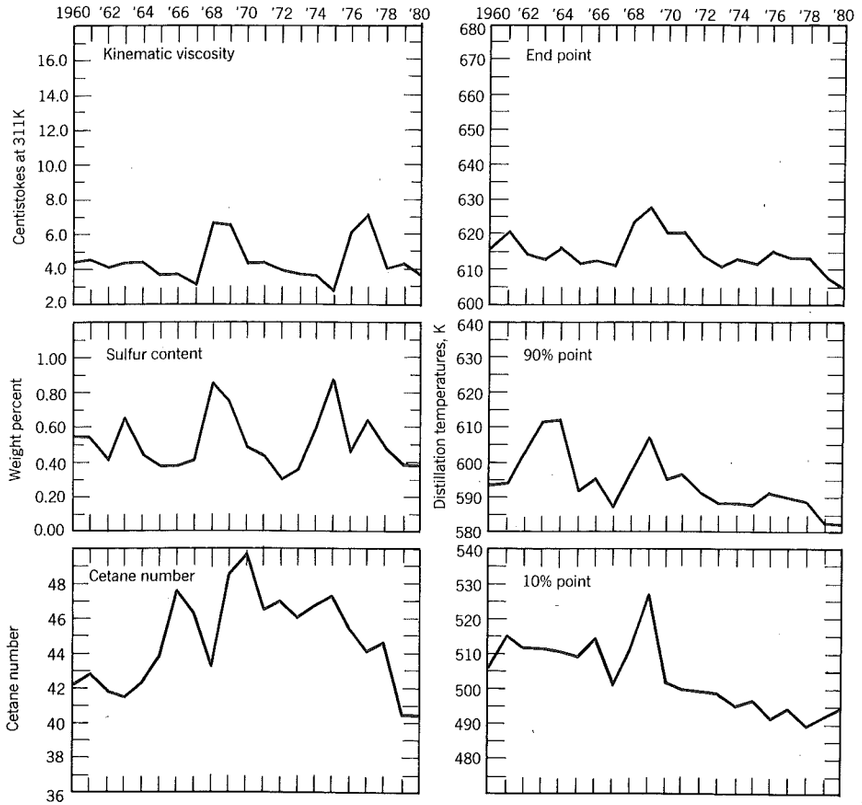

Figure 10-9 Trends of some properties of type S–M diesel fuel oils (Shelton, 1982).

The cetane index is an approximation to the cetane number computed from the following ASTM (D976) empirical correlation for petroleum derived diesel fuels:

$$\text{Cetane Index} = -420.34 + 0.016G^2 + 0.192G \log M + 65.01(\log M)^2 - 0.0001809M^2$$

where

G = API gravity

M = Mid-boiling temperature, °F

The index is useful because it is cheaper to obtain than a measurement of the

Table 10-4 Diesel Fuel Survey, Eastern United States, 1980

PROPERTY	ASTM METHOD	C–B			T–T			R–R			S–M		
		MINIMUM	AVERAGE	MAXIMUM	MINIMUM	AVERAGE	MAXIMUM	MINIMUM	AVERAGE	MAXIMUM	MINIMUM	AVERAGE	MAXIMUM
Gravity °API	D287	33.9	41.0	46.8	29.8	35.7	46.9	28.4	34.2	46.1	28.4	33.3	41.5
Flash point (K)	D93	324	—	354	324	—	367	331	—	359	333	—	348
Viscosity at 311 K, CS	D445	1.36	1.93	3.27	1.55	2.56	4.59	1.67	2.68	3.26	1.85	2.60	3.00
Cloud point (K)	D2500	228	—	268	< 233	—	273	238	—	262	< 236	—	262
Pour point (K)	D97	217	—	253	233	—	269	236	—	258	< 236	—	273
Sulfur, Wt%	D129	0.000	0.095	0.300	0.010	0.205	0.500	0.049	0.233	0.590	0.100	0.210	0.320
Carbon residue, Wt%	D524	0.000	0.056	0.210	0.000	0.095	0.270	0.016	0.114	0.220	0.040	0.133	0.220
Ash, Wt%	D482	0.0000	0.0003	0.0010	0.0000	0.0043	0.0900	0.0000	0.0093	0.0900	0.0000	0.0033	0.010
Cetane number	D613	41.3	46.2	49.9	39.0	44.0	47.4	35.0	41.2	47.4	35.0	41.4	46.7
Cetane index	D975	44.0	47.5	54.0	37.7	46.2	55.7	42.8	48.2	64.2	43.5	—	43.5
Distillation (K)	D86												
IBP		436	456	477	423	466	521	446	467	480	452	463	478
10%		458	477	503	458	494	546	481	497	512	481	499	514
50%		474	502	540	482	529	568	513	536	551	500	534	552
90%		507	534	589	506	572	606	540	579	594	518	576	593
EP		532	558	617	521	598	643	554	604	619	538	599	617

Table 10-5 Example Diesel Fuels

	PETROLEUM				TAR	SHALE
	T–T		JET A	SM	SANDS	MARINE
Distillation (K)						
IBP	462	485	441	442	454	483
10%	493	518	462	467	503	552
50%	536	547	489	542	563	586
90%	571	591	525	596	606	620
EP	589	636	564	620	621	634
Viscosity, cst (313 K)	2.67	3.13	1.47	2.63	4.35	5.58
Specific gravity (285 K)	0.850	0.854	0.809	0.877	0.882	0.861
Hydrocarbons						
% Aromatics	30.5	32.8	18.9	40.1	43.6	33.7
% Olefins	—	2.7	1.0	2.0	0.0	—
% Saturates	—	64.5	80.1	57.9	56.4[a]	—
Higher heat of combustion (cal/g)	10926	10660	11078	10525	10072[b]	10135[b]
Hydrogen: carbon, moles	1.73	1.83	—	1.70	1.71	1.77
Molecular weight	198	—	—	—	—	—
Cetane index	47.8	51.1	461.1	46.0	36.8	52.2
References	1	2	3	4	5	5

Source: 1. Tests by Phillips Petroleum and Southwest Research Institute on EPA Emissions Test fuel in use at Purdue University, June, 1981.

2. SAE 810444, AL-7799-F

3. SAE 810444, AL-7926-F

4. SAE 810444, AL-8007-F

5. SAE 800331

[a] Naphthenes = 43.7, paraffins = 12.7

[b] Lower or net

actual cetane number. More important, it illustrates that not all diesel fuel properties can be specified independently of one another.

For thermodynamic analysis of the diesel engine performance, we need to know the molecular weight, the hydrogen to carbon ratio, the heat of combustion, and the available energy of combustion. The latter has to be estimated from knowledge of the composition, whereas the other three can easily be measured. Some example diesel fuels are given in Table 10-5. Also shown for comparison are jet fuels, the demand for which competes with diesel fuels in decision making at the refinery.

An important and widely used classification scheme for diesel fuels has been developed by the ASTM. Their specifications chart contained in ASTM D975 is shown here as Table 10-6. No. 1-D and 2-D are basically highway transportation fuels, the former being reserved for low-temperature applications. No. 4-D is basically for stationary applications where the engine speed is low and more or less constant.

Table 10-6 ASTM D 975 Diesel fuel oil specifications[a, b, c]

GRADE OF DIESEL FUEL OIL	FLASH POINT, °C (°F)		CLOUD POINT, °C (°F)	WATER AND SEDIMENT, VOLUME (%)	CARBON RESIDUE ON 10% PERCENT RESIDUUM, (%)	ASH, WEIGHT (%)	DISTILLATION TEMPERATURES, C(°F) 90% POINT		VISCOSITY KINEMATIC cSt OR mm^2/s[d] AT 40° C		SAYBOLT, SUS AT 100°F		SULFUR,[e] WEIGHT (%)	COPPER STRIP CORROSION	CETANE NUMBER[f]
	MIN	MAX	MAX	MAX	MAX	MAX	MIN	MAX	MIN	MAX	MIN	MAX	MAX	MAX	MIN
No. 1-D A volatile distillate fuel oil for engines in service requiring frequent speed and load changes	38 (100)	[f]		0.05	0.15	0.01	—	288 (550)	1.3	2.4	—	34.4	0.50	No. 3	40[g]
No. 2-D A distillate fuel oil of lower volatility for engines in industrial and heavy mobile service	52 (125)	[f]		0.05	0.35	0.01	282[h] (540)	338 (640)	1.0	4.1	32.6	40.1	0.50	No. 3	40[g]
No. 4-D A fuel oil for low and medium speed engines	55 (130)	[f]		0.50	—	0.10	—	—	5.5	24.0	45.0	125.0	2.0	—	30[g]

Source: (From SAE Handbook, 1983).

[a] To meet special operating conditions, modifications of individual limiting requirements may be agreed upon between purchaser, seller, and manufacturer.

[b] The values in SI units are to be regarded as the standard. The values in U.S. customary units are for information only.

[c] Nothing in this specification shall preclude observance of federal, state, or local regulations which may be more restrictive.

[d] Millimeter squared per second (official SI unit) (Note: 1 cST = 1 mm^2/s).

[e] In countries outside the U.S.A., other sulfur limits may apply.

[f] It is unrealistic to specify low-temperature properties that will ensure satisfactory operation on a broad basis. Satisfactory operation should be achieved in most cases if the cloud point (or wax appearance point) is specified at 6°C (10°F) above the tenth percentile minimum ambient temperature for the area in which the fuel will be used. The tenth percentile minimum ambient temperatures for the months of October, November, December, January, February, and March are given in ASTM D 975 in maps for the 48 contiguous states and Alaska. This guidance is of a general nature: some equipment designs, use of flow improver additives, fuel properties, and/or operations may allow higher or require lower cloud point fuels. Appropriate low temperature operability properties should be agreed on between the fuel supplier and purchaser for the intended use and expected ambient temperatures.

[g] Low-atmospheric temperatures as well as engine operation at high altitudes may require use of fuels with higher cetane ratings.

[h] When cloud point less than −12°C (10°F) is specified, the minimum viscosity shall be 1.7 cSt and the 90% point shall be waived.

[i] Where cetane number by Method D 613, is not available, ASTM Method D 976, Calculated Cetane Index of Distillate Fuels may be used as an approximation. Where there is disagreement, Method D 613 shall be the referee method.

10.8 IDEAL GAS ENTHALPY AND ENTROPY ESTIMATES

The following information is assumed to be known from laboratory analysis: heat of combustion, the mass fractions of aromatics, olefins and saturates, molecular weight, and hydrogen to carbon ratio.

The equivalent chemical formula of the fuel $C_\alpha H_\beta$ can be determined from the molecular weight M and the hydrogen to carbon ratio HC. It can be shown that

$$\alpha = \frac{M}{12.01 + 1.008HC} \qquad \beta = \alpha(HC) \tag{10.1}$$

The enthalpy of formation can be determined from the heat of combustion. Equation (3.140) yields

$$h_{f,298,C_\alpha H_\beta} = \alpha h_{f,298,CO_2} + \frac{\beta}{2}\left(h_{f,298,H_2O} - (1-\chi)h_{fg,298,H_2O}\right) + q_{c,298} \tag{10.2}$$

where χ is the quality of the water in the products. (If the fuel is liquid, subtract h_{fg} of the fuel from q_c.) The lower or net heat assumes $\chi = 1.0$; whereas the higher or gross heat assumes $\chi = 0$.

Figures 10-10 and 10-11 show the ideal gas constant pressure specific heats of hydrocarbons found in motor fuels. They show that per unit mass the specific heat is a weak function of carbon number and shows a dependence on

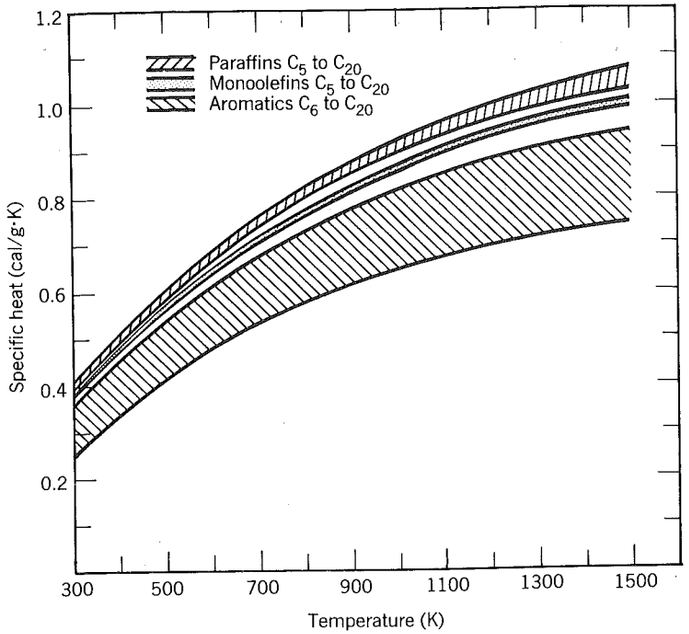

Figure 10-10 Constant pressure specific heat of hydrocarbons found in motor fuels.

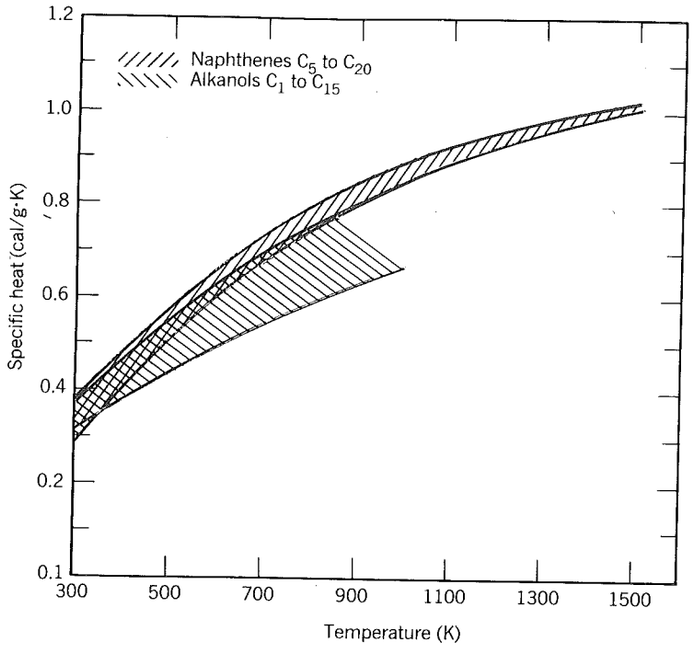

Figure 10-11 Specific heat of naphthenes and alcohols used in motor fuels.

hydrocarbon type. This is not unexpected since the specific heat of a molecule depends on the number and type of bonds. Assuming the specific heat per bond is constant, one expects the specific heat to increase with the number of bonds, and on a molar intensive basis this is true. Since both the number of bonds and the mass of the molecule increase with the numbers of carbon atoms on a mass intensive basis, the specific is nearly constant.

The results shown are correlated by the following equation:

$$c_P = a + bt + ct^2 \qquad \text{cal/g/K} \tag{10.3}$$

where $t = T/1000$ and $300 < T < 1500$ K.

TYPE	a	b	c	INDEX, i
Paraffins	0.08	1.2	−0.37	1
Monoolefins	0.08	1.1	−0.32	2
Aromatics[a]	0.05	1.0	−0.32	3
Naphthenes	0.01	1.2	−0.35	4
Alkanols[b]	0.12	0.8	−0.17	5

[a] C_nH_{2n-6}

[b] $300 < T < 1000$ K

The specific heat of a motor fuel is then

$$c_P \approx \sum_{i=1}^{5} x_i c_{Pi} \tag{10.4}$$

where x_i = mass fraction of component i.

When the fuel is free of any alcohols and only the mass fraction of saturates is known the naphthenes may be neglected.

In order to properly measure the efficiency of an engine we need to compute the available energy of combustion. This computation requires knowledge of the fuel's absolute entropy. A correlation for liquid fuels that is useful in this regard is (Ikumi and Wen, 1981):

$$s(\text{J/mole/K}) = 4.69\alpha + 18.41\beta + 44.55\gamma + 85.97\delta \tag{10.5}$$

10.9 FUEL ADDITIVES

Thousands of compounds have been tested for use as octane improvers in gasoline. Tetraethyl lead emerged in the 1920s and remained the dominant additive until 1970 when lead began to be phased out because it had been

Table 10-7 Antiknock and Proknock Additives

COMPOUND	FORMULA	RELATIVE EFFECTIVENESS[a]
Aniline	$C_6H_5NH_2$	33.9
Benzene	C_6H_6	332
Toluene	$C_6H_5CH_3$	298
Xylene	$C_6H_4(CH_3)_2$	271
Ethanol	C_2H_5OH	161
Ethyl iodide	C_2H_5I	52.5
Diethyl selenide	$(C_2H_5)_2S_e$	7.25
Diethyl telluride	$(C_2H_5)_2T_e$	2.54
Tetraethyl tin	$(C_2H_5)_4Sn$	22.4
Tetraethyl lead	$(C_2H_5)_4Pb$	1.00
Nickel carbonyl	$Ni(CO)_4$	1.80
Dimethyl cadmium	$(CH_3)_2Cd$	41.7
Titanium tetrachloride	$TiCl_4$	21.7
Monomethylaniline	$C_6H_5NHCH_3$	27.8
Triphenylamine	$(C_6H_5)_3N$	1020.
MMT[b]	$CH_3(C_5H_4MnCO_3$	1.30
Ammonia	NH_3	−67.8
Isopropyl nitrite	$C_3H_7NO_2$	−2.88

Source: Boyd (1927) and Obert (1973).

[a]Amount in grams required to give an antiknock effect equivalent to 1 g of tetraethyl lead.

[b]Methylcyclopentadienyl maganese tricarbonyl.

polluting the environment in non-catalyst-equipped cars and because it poisons the catalysts used for emission control.

Some of the additives tested are listed in Table 10-7 along with measures of their effectiveness. Methylcyclopertadienyl manganese tricarbonyl (MMT) is an additive introduced about 1960. It has since been banned in the United States. The ban on metallic antiknock additives has intensified research on chemical processing and searches for nonmetallic additives.

Alcohols and ethers are of interest as high octane blending stock because they can be made from coal or natural gas. About 10% methyl-terbutyl ether added to gasoline increases the octane number by about 2 units. Currently, alcohols and ethers made from coal are too expensive.

Other reasons for putting additives in gasoline are to suppress deposit formation, to reduce gum formation, to lubricate valve guides and upper cylinder regions, to deal with ever-present water to prevent rust or freezing, and to color gasolines for identification purposes.

10.10 LUBRICATING OILS

In addition to lubricating, oil is expected to act as a coolant, to enhance the rings' combustion seal, and to control wear or corrosion. Additives to either petroleum or synthetic base stocks include: antifoam agents, antirust agents, antiwear agents, corrosion inhibitors, detergents, dispersants, extreme pressure agents, friction reducers, oxidation inhibitors, pour point depressants, and viscosity index improvers. We will restrict our attention to the rheological characteristics. The reader interested in the broader picture is referred to the books by Schilling (1972), or Gruse (1967), or to the SAE Handbook and the paper by Sieloff and Musser (1982).

The SAE classifies oils by their viscosity. Two series of grades are defined in Table 10.8 from the recommended practice SAE J300. Grades with the letter W are based on a maximum low-temperature viscosity, a maximum borderline pumping temperature, and a minimum viscosity at 100 deg C. Grades without the letter W are based on a minimum and a maximum viscosity at 100 deg C. A multiviscosity graded oil is one that satisfies one of each of the two grades. The borderline pumping temperature is measured via a standard test, ASTM D3829, and is a measure of an oils' ability to flow to an engine oil pump inlet and provide adequate oil pressure during warm-up.

The portion of the crude oil refiners use to make lubricants is on the order of 1% and comes from the higher-boiling fraction and undistilled residues which possess the necessary viscosity. In terms of carbon content, Gruse (1967) offers the following guidelines.

	RANGE	AVERAGE
SAE 10	C_{25} to C_{35}	C_{28}
SAE 30	C_{30} to C_{80}	C_{38}
SAE 50	C_{40} to C_{100}	C_{41}

Table 10-8 SAE Viscosity Grades for Engine Oils[a]

SAE VISCOSITY GRADE	VISCOSITY[b] (cP) AT TEMPERATURE (°C) MAXIMUM	BORDERLINE PUMPING TEMPERATURE[c] (°C) MAXIMUM	VISCOSITY[d] (cSt) AT 100°C	
			MINIMUM	MAXIMUM
0W	3250 at −30	−35	3.8	—
5W	3500 at −25	−30	3.8	—
10W	3500 at −20	−25	4.1	—
15W	3500 at −15	−20	5.6	—
20W	4500 at −10	−15	5.6	—
25W	6000 at −5	−10	9.3	—
20	—	—	5.6	Less than 9.3
30	—	—	9.3	Less than 12.5
40	—	—	12.5	Less than 16.3
50	—	—	16.3	Less than 21.9

Source: From SAE Handbook, 1983.

[a]1 cP = 1 mPa; 1 cSt = 1 mm^2/s.

[b]SAE J300

[c]ASTM D 3829

[d]ASTM D 445

Refiners use chemical processing and additives to produce oils with desirable characteristics. Straight-run base stock from petroleum crude oil is referred to as a petroleum oil; whereas those base stocks produced by chemical processing are called synthetic oils. Some synthetic base stocks are compatible with petroleum base stocks and the two types may be blended, in which case the stock is referred to as a blend. Additives range in concentration from several parts per million to on the order of 10%.

In any case, the viscosity of an oil decreases with increasing temperature. Trends typical of the Newtonian regime for oils and some other fluids are given in Fig. 10-12. A Newtonian oil is one in which the viscosity is independent of the shear rate. Shear rates in engines are sometimes high enough that the viscosity decreases, and some oils are deliberately made non-Newtonian via the introduction of wax particles. The viscosity of oils increase with pressure. At some times during hydrodynamic lubrication, the loads increase the oil pressure, which is turn increases the viscosity, which in turn increases the load capacity. It has been suggested that this stabilizing effect is a part of the reason for effects attributed to the "property" oiliness.

The kinematic viscosity as a function of temperature and pressure of many oils is correlated by

$$\nu = C_1 \exp\left(\frac{C_2}{T - C_3} + \frac{P}{C_4}\right) \tag{10.6}$$

Values of the constants typical of engine oils are given in Table 10-9.

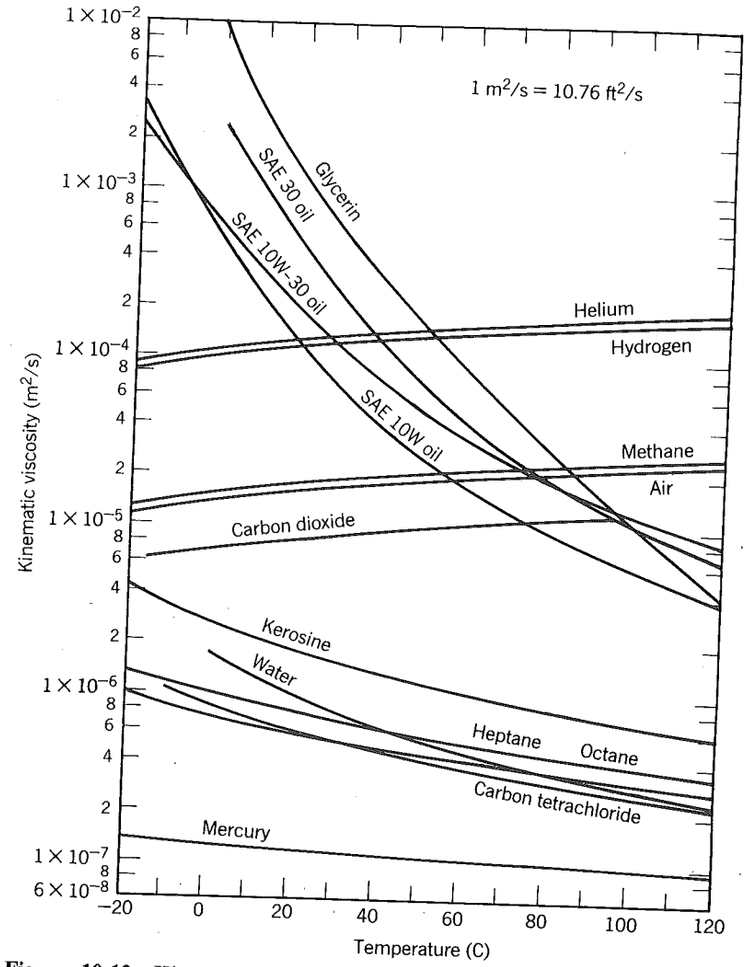

Figure 10-12 Kinematic viscosity of common fluids (at atmospheric pressure) as a function of temperature (Fox and McDonald, 1978). Reprinted with permission © 1978. John Wiley & Sons, Inc.

Finally, it should be mentioned that some two-stroke engines, especially small ones, achieve upper cylinder lubrication by mixing oil with the gasoline. In these cases additional control of the oil (and the fuel) is required to prevent spark fouling, to assure miscibility with the fuel, and to provide for a hydrodynamic film of the proper viscosity. The fuel–oil mixture that contacts the cold walls separates during compression and combustion leaving mostly oil on the wall.

Table 10-9 Typical Properties of Engine Oils at 298 K, P = 1 bar, and Constants for Eq. (10.6)

SAE GRADE	ρ (gm/cm^3)	c_p (J/g K)	ν (cst)	C_1 (st)	C_2 (K)	C_3 (K)	C_4 (bar)
5W	0.860	1.99	48.2	6.44	900	162	433
10W	0.877	1.96	86.9	4.53	1066	157	296
15W	0.879	1.95	102	7.49	902	173	181
20W	0.886	1.94	259	2.63	1361	150	105
20	0.880	1.95	129	5.67	1028	165	153
30	0.886	1.94	259	4.70	1361	140	105
40	0.891	1.92	361	2.17	1396	151	91.7
50	0.899	1.91	639	2.24	1518	150	75.2

Source: Cameron (1981).

10.11 ALTERNATIVE FUELS

Rather than being derived from petroleum, gasoline or diesel fuel can be derived from coal, shale oil, tar sands, or vegetable oils. Since we are more concerned with the end use of a fuel rather than how it is made or where it originates we will consider "alternative fuels" to be those alternative to liquid hydrocarbons. Important alternative fuels are then hydrogen, methane or natural gas, propane or LPG, and alcohols. Feasible fuels but of little promise for internal combustion engines include ammonia, aceteylene, hydrazine, and coal slurries (powdered coal mixed in water, alcohol, or a liquid hydrocarbon). Boron compounds are used in military application and nitroparaffins find application in racing engines.

The technical problems associated with use of an alternative fuel are more often than not associated with the cost of storing the fuel and delivering it to the engine. Hydrogen, methane, propane, and alcohol are all good spark-ignition engine fuels and poor diesel fuels. With the exception of hydrogen, all are in use today in some application where the fuel can be produced cheaply enough relative to conventional fuels to offset the increased storage and fuel system costs.

Hydrogen is of long-term interest since it can be produced by solar or nuclear methods and because its combustion does not add carbon dioxide to the atmosphere (relevant to debates about the greenhouse effect).

The gaseous hydrocarbons are already in widespread use, especially in stationary applications where the increased bulk of the fuel storage system is of minor concern.

Ethanol is used extensively in Brazil, a country without sources of crudes or coal from which conventional fuels can be manufactured. In Brazil the ethanol is made from sugar cane, one of the most efficient crops that can be grown for ethanol production. It has been suggested that the crops that can be grown in the United States to produce ethanol consume more energy in the plowing, planting, harvesting, fermenting, and delivering processes than is contained in the resultant ethanol.

Methanol is of interest because it can be made from coal, which exists in large supplies. Furthermore, spark-ignition engines can be designed with a higher compression ratio to accommodate methanol than that used to operate on gasoline. Thus the increased efficiency of the engine is one factor working to offset the increased fuel cost.

In conclusion, the important issues concerning alternative fuels are economical and, to a certain extent, political. They are not technical; engines can be designed to use them and the principles laid out in this text are applicable.

10.12 REFERENCES

Bailey, B. K. and J. A. Russell (1981), "Emergency Transportation Fuels: Properties and Performance," SAE paper 810444.

Cameron, A., *Basic Lubrication Theory*, Ellis Horwood Ltd., Chichester, England, 1981.

Dorn, P. and A. M. Mourao (1984), "The Properties and Performance of Modern Automotive Fuels," SAE paper 841210.

Fox, R. W. and A. T. McDonald, *Introduction to Fluid Mechanics*, Wiley, New York, 1978.

Gibson, H. J. (1982), "Fuels and Lubricants for Internal Combustion Engines—An Historical Perspective," SAE paper 821570.

Gruse, W. A., *Motor Oils: Performance and Evaluation*, Van Nos Reinhold, New York, 1967.

Ikumi, S. and C. Y. Wen (1981), "Entropies of Coals and Reference States in Coal Gasification Availability Analysis," West Virginia University Internal Report.

Lawrence, D. K., D. A. Plantz, B. D. Keller, and T. D. Wagner (1980), "Automotive Fuels—Refinery Energy and Economics," SAE paper 800225.

Lovell, W. (1948), "Knocking Characteristics of Hydrocarbons," *Ind. Eng. Chem.* **40**, pp. 2388–2438.

Obert, E. I. F., *Internal Combustion Engines and Air Pollution*, Harper & Row, New York, 1973.

SAE Handbook *13—Fuels and Lubricants*, SAE, Warrendale, Pennsylvania, 1983.

Schilling, A., *Automobile Engine Lubrication*, Scholium Intl., New York, 1972.

Shelton, E. M. (1982), "Department of Energy Surveys on Gasoline and Diesel Fuels," available annually from DOE.

Sieloff, F. and J. L. Musser (1982), "What does the Engine Designer Need to Know about Engine Oils," SAE paper 821571.

Taylor, C. F., *The Internal Combustion Engine in Theory and Practice*, Vol. 2, MIT Press, Cambridge, Massachusetts, 1977.

10.13 HOMEWORK

1. In the chemical processing used to convert gasoline to diesel fuel the process efficiency is not necessarily constant. Let us assume the process efficiency η_p changes as the fraction of gasoline converted to diesel fuel goes up according to

$$\eta_p = \eta_0(1-x) + \eta_1 x$$

where

x = fraction of gasoline converted

$\eta_0 = \eta_p$ in the limit $x \to 0$

$\eta_1 = \eta_p$ when $x = 1$

Suppose that a supply of gasoline is available in the amount $\dot{m}_g$ and that you are free to use any proportion of diesel engines versus gasoline engines to burn that fuel to produce power. Defining

w_d = work per unit mass of fuel done by a diesel engine

w_g = work per unit mass of fuel done by a gasoline engine

a. In these terms show that the power which can be produced is

$$\dot{W} = \dot{m}_g(1-x)w_g + x\eta_p\dot{m}_g w_d$$

b. Derive an expression for the value of x which maximizes the power produced.

c. What factors are involved in estimating the ratio w_g/w_d?

2. Calculate the Cetane Index for three unleaded gasolines and the two naphthas in Table 10.3.
3. Estimate the enthalpy of formation of the T–T diesel fuel in Table 10.5 for which the Cetane Index is 47.8.

Eleven
ENGINE PERFORMANCE

11.1 ENGINE SIZE

The torque an engine will produce, by definition of the mean effective pressure, is

$$\tau_b = \begin{cases} \dfrac{1}{4\pi}\,\text{bmep}\,V_d & \text{(four-stroke)} \\ \dfrac{1}{2\pi}\,\text{bmep}\,V_d & \text{(two-stroke)} \end{cases} \tag{11.1}$$

The power can also be expressed in terms of the mean effective pressure

$$\mathbf{P}_b = \begin{cases} \frac{1}{4}\,\text{bmep}\,A_p\bar{U}_p & \text{(four-stroke)} \\ \frac{1}{2}\,\text{bmep}\,A_p\bar{U}_p & \text{(two-stroke)} \end{cases} \tag{11.2}$$

In these expressions the most important effects of engine size have been factored out, for a given stress level (bmep, $\bar{U}_p$) torque is proportional to the displacement volume, and power is proportional to the piston area.

$$V_d = N_c\frac{\pi}{4}b^2S$$

$$A_p = N_c\frac{\pi}{4}b^2 \tag{11.3}$$

Finally, we can also write for either four- or two-stroke engines

$$\text{bsfc} = \frac{F}{1+F}\frac{e_v\rho_i}{\text{bmep}} \tag{11.4}$$

Where, as before, F is the fuel–air ratio, e_v is the volumetric efficiency, and ρ_i is the mixture density in the intake manifold. Notice that Eq. (11.4) has no direct measure of engine size, thus the efficiency of engines is expected to be a weak function of size for a given stress.

The state of the art for current diesel engines is shown in Fig. 11-1. This figure is based on the best of two- and four-stroke designs with bores from 62 to 900 mm. The ratio of the maximum bore to minimum bore is about 15, corresponding to a 3400 to 1 displacement volume ratio; whereas the brake

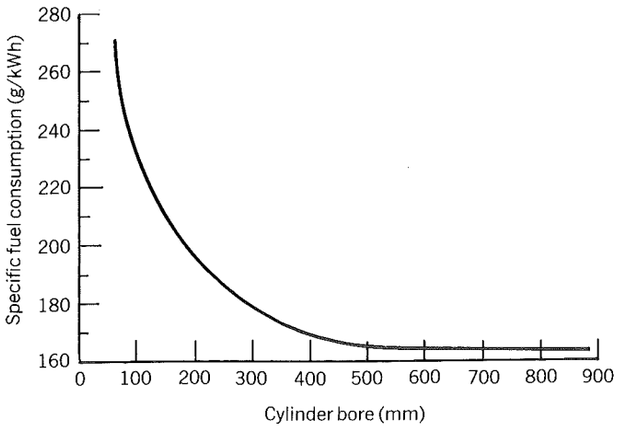

Figure 11-1 Brake specific fuel consumption of the best two- and four-stroke engines on the market. For bores greater than 500 mm, the thermal efficiency is about 50% (Thomas, Ahluwaba, Shamah, and Van der Horst, 1984). Reprinted with permission © 1984. ASME.

specific fuel consumption varies over a range of only 1.6. Although it is indeed a weak function, the change in specific fuel consumption is significant.

An important factor underlying the trend shown in Fig. 11-1 is that the surface to volume ratio of the cylinder is decreasing with increasing bore $[(A/V) \propto b^{-1}]$. This means that there will be less and less heat lost as the bore increases. Another factor working in the favor of large engines is that the rotational speed is decreasing with the bore size ($R_s \propto b^{-1}$) so that there is more time near top center for fuel injection and combustion. This means that there will be less of a volume change during combustion and thus the limit of constant volume combustion will be approached.

Von Schnurbein (1981) has reported that the friction mean effective pressure decreases as engine size increases. To appreciate why, reexamine Eq. (6-14) which, reiterated here, is:

$$\frac{\text{mmep}}{\rho_o \overline{U}_p^2} = \frac{1.3 \times 10^5}{R_e} + \frac{1.7 \times 10^8}{R_e^2}(r + 15) \tag{11.5}$$

In dimensional form this equation is

$$\text{mmep} = 1.3 \times 10^5 \rho_o^2 \overline{U}_p \frac{\mu_o}{b} + \frac{1.7 \times 10^8 (r + 15)}{\rho_o} \frac{\mu_o^2}{b^2} \tag{11.6}$$

In this form it is easy to see that mmep increases linearly with piston speed and that if the oil viscosity is held proportional to the bore then geometrically similiar engines will fall on the same curve (Fig. 6-5). However, the viscosity of oils used in commercial engines is more or less the same for all sizes of engines, therefore the friction can be expected to be less in large engines than in small engines. Millington and Hartles (1968), using a statistical analysis, reached the same conclusion and give a corelation very much like Eq. (11.6). Note that at constant oil properties mmep scales with engine speed and not piston speed since $\overline{U}_p/b = 2R_s(S/b)$.

The brake thermal efficiency of state of the art diesel engines where $b > 500$ mm is about 50%. Surely they are among the most efficient engines in the world. Their low losses due to heat transfer, combustion, and friction have already been mentioned. They also use late closing intake valves to realize a longer expansion stroke than compression stroke, see HW 2.14.

The generalizations just drawn ought to hold true for spark ignition engines too, although the point is academic for they are not practical unless care is taken to stratify the charge. Large homogeneous-charge, spark-ignition engines are not practical because their octane requirements are too high. In Chapter 9 it was pointed that the flame speed is in part controlled by the magnitude of the turbulent velocity fluctuations. It was shown in Chapter 7 that they are proportional to the piston speed. It follows that the combustion duration in crank angle is constant but in time is inversely proportional to the engine's rotational speed. There is consequently more time for knock precursors to form in large engines. Likewise to build small high speed diesel engines becomes a challenge. There is little time for autoignition to occur and/or inject the fuel at reasonable pressures.

11.2 COMPRESSION RATIO AND ENGINE SPEED

The effects of engine speed for three different compression ratios on the power and coolant load of an automotive spark ignition engine at full load, that is, wide-open throttle, are shown in Fig. 11-2. The results shown are, of course, unique to the particular engine design tested. The trends depicted and their underlying causes, however, are typical to all engines, compression or spark ignited, two or four stroke.

First, note that the indicated specific fuel consumption decreases with increasing engine speed and then levels out. This is mainly because the percentage heat loss to the coolant is decreasing with increasing engine speed. On the other hand, the brake specific fuel consumption is flatter at low speeds and is increasing at the higher speeds. This difference is the friction and pumping losses (which though small are still present in an unthrottled engine) increasing with engine speed. The increase in the coolant loads at 3000 rpm can be attributed to the increasing friction.

Second, note that increasing the compression ratio decreases both the indicated and the brake specific fuel consumption. The coolant load drops with increasing compression ratio because the increased thermal efficiency results in lower temperatures in the latter part of the expansion stroke thereby reducing the heat loss.

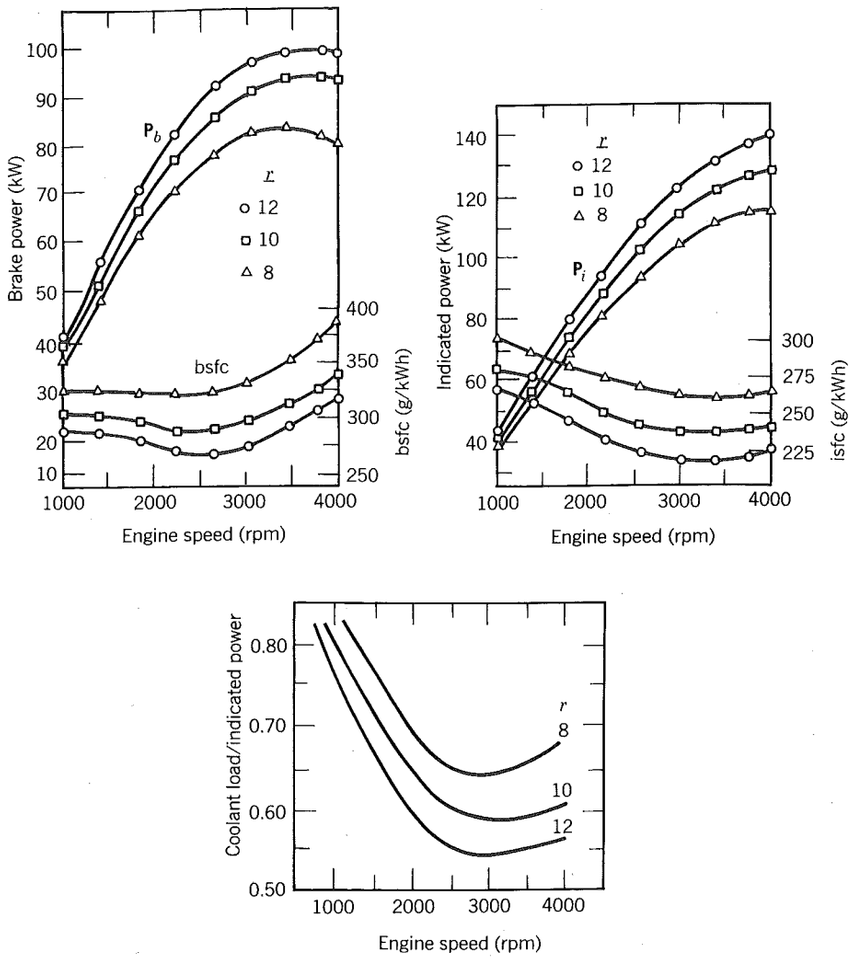

Figure 11-2 Performance of a modified Oldsmobile V-8 at three compression ratios: $b = 95.2$ mm, $S = 8.6$ m, $V_d = 4.70$ liters (Roensch, 1949). The coolant load is the rate at which heat is dissipated (kW) by the engine's cooling system; in this plot it is normalized by the indicated power. Reprinted with permission © 1949. Society of Automotive Engineers, Inc.

The indicated specific fuel consumption improves at a faster rate with increasing compression ratio than the brake specific fuel consumption because both friction and heat losses are increasing with compression ratio. In fact there is an optimum compression ratio due to these effects, see Fig. 11-3. An optimum compression ratio of 12 to 18 is typical and is the underlying reason why direct-injection diesel engines have compression ratios in the same range.

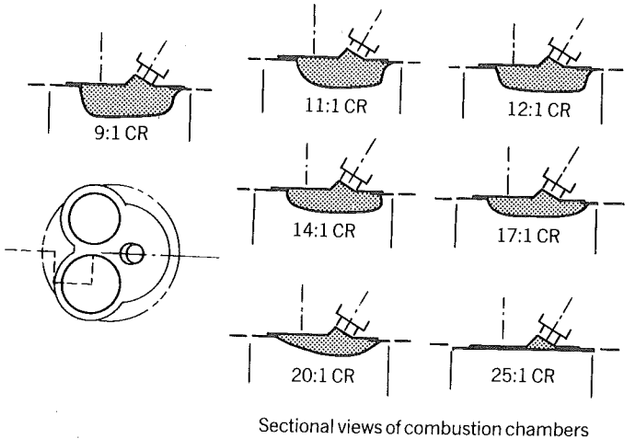

Sectional views of combustion chambers

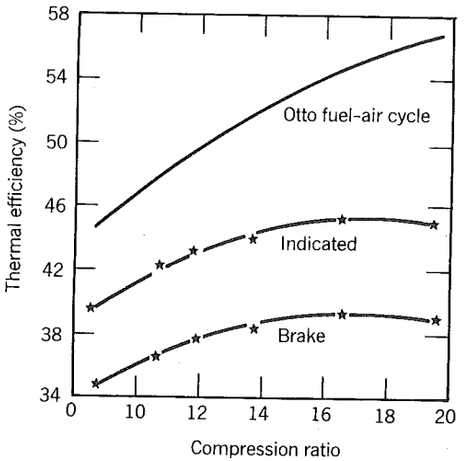

Figure 11-3 Thermal efficiencies of a gasoline engine at the nominal compression ratios shown. The spark advance is set for best efficiency as is the fuel–air equivalence ratio at $\phi = 0.91$. The optimum compression ratio in these and other tests by Caris and Nelson (1959) proved to be independent of load. Knock was avoided by using isooctane doped with additives. Computer simulations of diesel engines show similar results (McAulay, Wu, Chen, Borman, Myers, and Uyehara, 1965). Reprinted with permission © 1965. Society of Automotive Engineers, Inc.

The compression ratios of gasoline-fueled, spark-ignition engines are less than optimum to avoid knock. The compression ratios of indirect-injection diesel engines are greater than optimum to assist in cold starting, which is harder than with direct injection engines because of the high heat loss in the antechamber.

The power curves in Fig. 11-2 are conveniently explained in terms of an expression relating the power of an engine to the delivery ratio, the net indicated thermal efficiency, and the mechanical efficiency. The derivation is as follows.

$$\mathbf{P}_b = \frac{\dot{m}_f}{\text{bsfc}} = \frac{F\dot{m}_a}{\text{bsfc}} \tag{11.7}$$

$$\mathbf{P}_b = \begin{cases} \dfrac{\dfrac{\Gamma}{2} F D_r \rho_\infty V_d R_s a_o \eta_{\text{net}} \eta_{\text{mech}}}{1+F} & \text{(four-stroke)} \\ \dfrac{\Gamma F D_r \rho_\infty V_d R_s a_o \eta_{\text{net}} \eta_{\text{mech}}}{1+F} & \text{(two-stroke)} \end{cases} \tag{11.8}$$

Figure 11-2 gives the indicated power as a function of engine speed. Because the engine is unthrottled, we can assume for qualitative purposes that the curve is the net indicated power versus engine speed. All the terms multiplying the mechanical efficiency in Eq. (11.8) constitute the net indicated power. If the indicated torque was constant then the indicated power would increase linearly with engine speed. Torque as a function of engine speed usually reflects the variation in volumetric efficiency with engine speed, which in an unthrottled engine is more or less equal to the delivery ratio. The falling off of the indicated power at high engine speeds is caused by a falling off in delivery ratio at the higher speeds. Recall that the speed at which the delivery ratio peaks is dependent upon the valve timing. The indicated power is not decreasing as fast as it would if delivery ratio were the only parameter changing with speed. The indicated efficiency is increasing slightly with speed.

The brake power is the product of the net indicated power and the mechanical efficiency. Friction power increases with the square of engine speed since the friction torque (proportional to bmep) increases linearly with engine speed. The mechanical efficiency therefore decreases linearly with engine speed, causing the brake power to exhibit a maximum even though the indicated power is still increasing. It was stated earlier that these generalizations are expected to apply to all engines. That statement needs qualification in the case of two-stroke engines, especially carbureted ones. Recall that in two-stroke engines there is a significant difference between the delivered mass and the trapped mass because of short circuiting. Any fuel that is short circuited is wasted and represents a loss not discussed in the context of Fig. 11-2, since this effect is usually neglible in four-stroke engines. As trapping efficiency generally increases with engine speed, the amount of fuel short circuited will decrease with engine speed.

11.3 PART-LOAD PERFORMANCE

The effect of load, defined as being proportional to the brake mean effective pressure, on the brake specific fuel consumption is qualitatively the same for both compression-ignited and spark-ignited engines, even though they vary the load in different ways; see, for example, Fig. 11-4 and 11-5. In both cases the bsfc will be infinite at idle since the engine is producing no useful work but is consuming fuel. As the load increases, the brake specific fuel consumption drops, goes through a minimum, and may or may not increase depending on how the load is increased at this point.

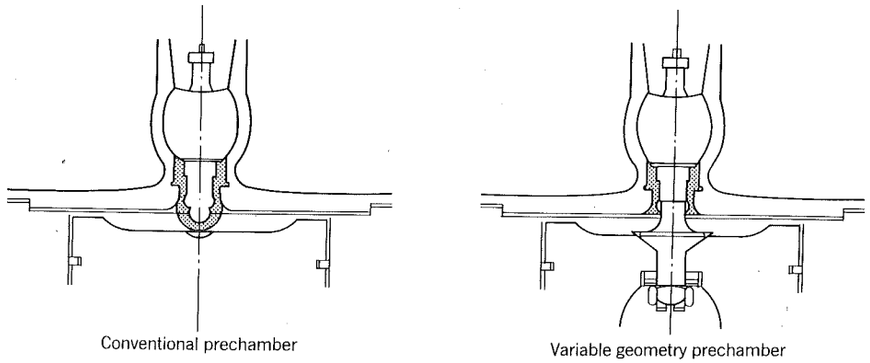

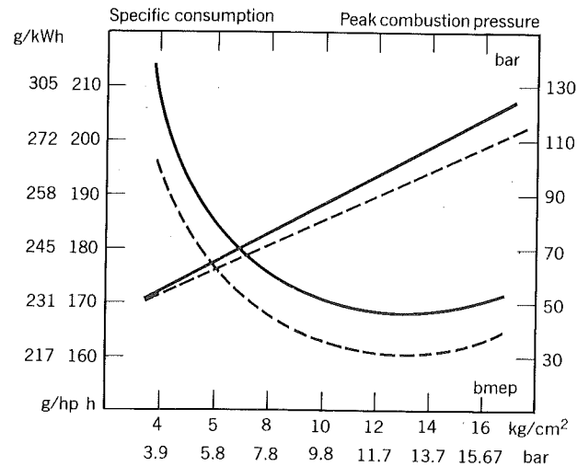

Figure 11-4 Brake specific fuel consumption of a marine diesel engine as a function of load (Hermann 1980). Reprinted with permission © 1980. ASME.

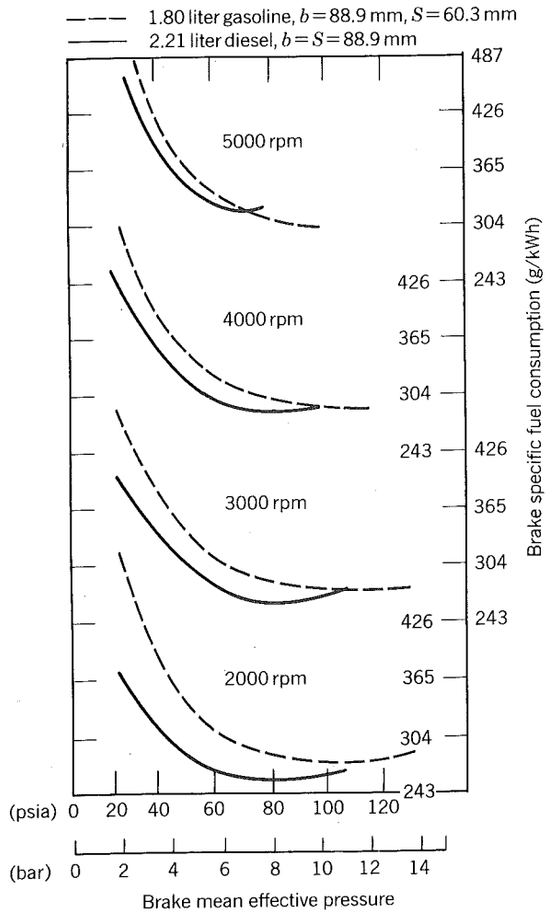

Figure 11-5 Comparison of a SI engine with an IDI-CI engine design to produce equal torque–speed characteristics in an automotive application (Walder, 1965). Reprinted with permission © 1965. Society of Automotive Engineers, Inc.

In the case of compression-ignition engines, the load is increased by increasing the fuel–air ratio, although this slightly drops the indicated efficiency and slightly increases the friction, the increase in mechanical efficiency is so great that it improves the specific fuel consumption. Just before the load is about to become smoke limited, the brake specific fuel consumption begins to increase because significant quantities of fuel begin to be only partially oxidized and thus are wasted.

In the case of spark-ignition engines, the load is increased by increasing the delivery ratio. This has little effect on the indicated efficiency, slightly increases the friction, and significantly reduces the pumping losses. Again, the dominant factor is the increase in mechanical efficiency. At constant fuel–air ratio, the brake specific fuel consumption drops with increasing load all the way to the point of maximum load so long as the imep increases faster than the fmep. In engines running at a fuel–air ratio less than that corresponding to maximum power (about $\phi = 1.1$, as we saw in our studies with fuel–air cycles), the load can be increased further by increasing the fuel–air ratio. This causes the brake specific fuel consumption to begin increasing with load once the engine is running rich.

The effect of fuel–air ratio on brake specific fuel consumption at constant load is shown in Fig. 11-6 and 11-7. The homogeneous charge spark ignition engine is most efficient when running stoichiometric or slightly lean. At very lean fuel–air ratios, the engine wastes fuel because of misfire, and at rich fuel–air ratios it wastes fuel since there is not enough oxygen present to liberate all of the fuel's energy.

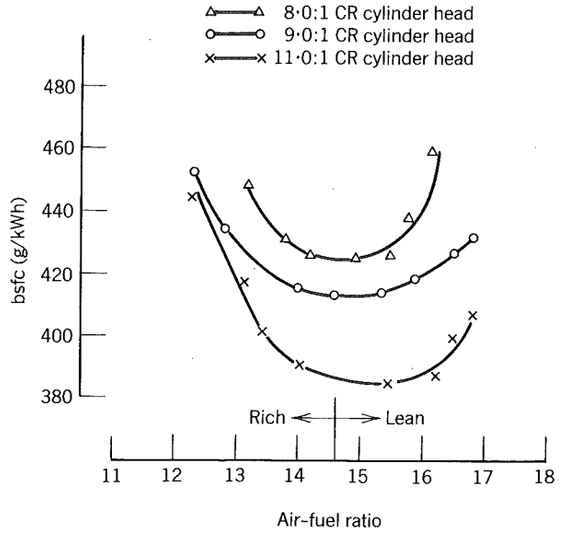

Figure 11-6 Fuel consumption of a single-cylinder research engine at three compression ratios and part load: $R_s = 40$ rps, bmep = 2.5 bar, $b = 80.26$ mm, $S = 88.9$ mm (French, 1983). The best fuel economy is realized at near stoichiometric fuel–air ratios. Reprinted with permission © 1983. Society of Automotive Engineers, Inc.

	COMBUSTION SYSTEM							
	Y.P.C.			SWIRL CHAMBER		D.I.		
Symbol	●	◎	○	▲	△	■	⊡	□
N-bore × stroke (MM)	1–80 × 75	1–95 × 106	1–102 × 106	4–93.7 × 85.6	2–90 × 85	2–92 × 98	1–95 × 106	2–88.9 × 90
Comp. ratio	21.6	19.4	20.1	22.0	21.3	16.5	16.4	16.1
Volume ratio (%)	42.6	56.6	53.1	53.1	53.9	—	—	—
Engine speed	2400	2200	2400	2200	2160	2200	2200	2500

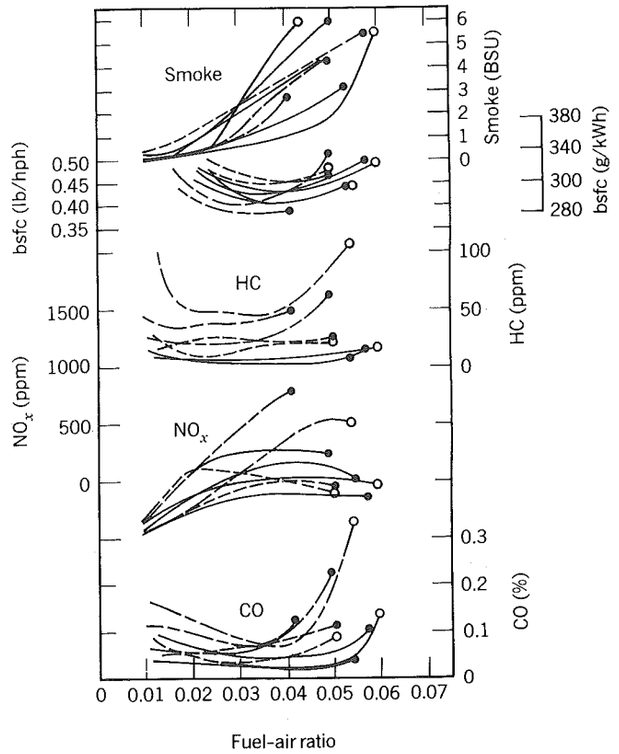

Figure 11-7 The effect of fuel–air ratio on the brake specific fuel consumption and exhaust emissions of a number of diesel engines. The YPC engines are prechamber engines designed by Yanmar. The smoke readings are in Bosch units, a scale that measures the reflectivity of a piece of filter paper through which some of the exhaust gas is passed (Motoushi, Yamada, and Mori, 1976). Reprinted with permission © 1976. Society of Automotive Engineers, Inc.

11.4 AMBIENT PRESSURE AND TEMPERATURE

Aircraft engines need to be designed to operate over large ranges of ambient temperature, pressure, and humidity. Properties of the standard atmosphere are given in Table 11-1. The performance of a number of aircraft engines with changes in altitude is shown in Fig. 11-8.

If the brake thermal efficiency and fuel–air ratio of an engine are constant, then by Eq. (11.4)

$$\text{bmep} \propto e_v \rho_i \approx D_r \rho_\infty \tag{11.9}$$

The delivery ratio of unthrottled engines depends on the square root of temperature, a scaling found empirically (see K_2 in Section 7.4). Hence, we can

Table 11-1 U.S. Standard Atmosphere[a]

ALTITUDE (KM)	TEMPERATURE (K)	PRESSURE, (BAR)	DENSITY (g/cm^3)	VISCOSITY (POISES)	SPEED OF SOUND (m/s)
−5	320.68	1.7776 + 0	1.9311 − 3	1.9422 − 4	358.986
−4	314.17	1.5960	1.7697	1.9123	355.324
−3	307.66	1.4297	1.6189	1.8820	351.625
−2	301.15	1.2778	1.4782	1.8515	347.888
−1	294.65	1.1393	1.3470	1.8206	344.111
0	288.15	1.0132	1.2250	1.7894	340.294
1	281.65	8.9876 − 1	1.1117	1.7579	336.435
2	275.15	7.9501	1.0066	1.7260	332.532
3	268.66	7.0121	9.0925 − 4	1.6938	328.583
4	262.17	6.1660	8.1935	1.6612	324.589
5	255.68	5.4048	7.3643	1.6282	320.545
6	249.19	4.7218	6.6011	1.5949	316.452
7	242.70	4.1105	5.9002	1.5612	312.306
8	236.22	3.5652	5.2579	1.5271	308.105
9	229.73	3.0801	4.6706	1.4926	303.848
10	223.25	2.6500	4.1351	1.4577	299.532
11	216.77	2.2700	3.6480	1.4223	295.154
12	216.65	1.9399	3.1194	1.4216	295.069
13	216.65	1.6580	2.6660	1.4216	295.069
14	216.65	1.4170	2.2786	1.4216	295.069
15	216.65	1.2112	1.9475	1.4216	295.069
16	216.65	1.0353	1.6647	1.4216	295.069
17	216.65	8.8497 − 2	1.4230	1.4216	295.069
18	216.65	7.5652	1.2165	1.4216	295.069
19	216.65	6.4675	1.0400	1.4216	295.069
20	216.65	5.5293	8.8910 − 5	1.4216	295.069

Source From "U.S. Standard Atmosphere, 1962," NASA, USAF, USWB, Washington, D.C., December, 1962.

[a]Below 80 km, the molecular weight is 28.964.

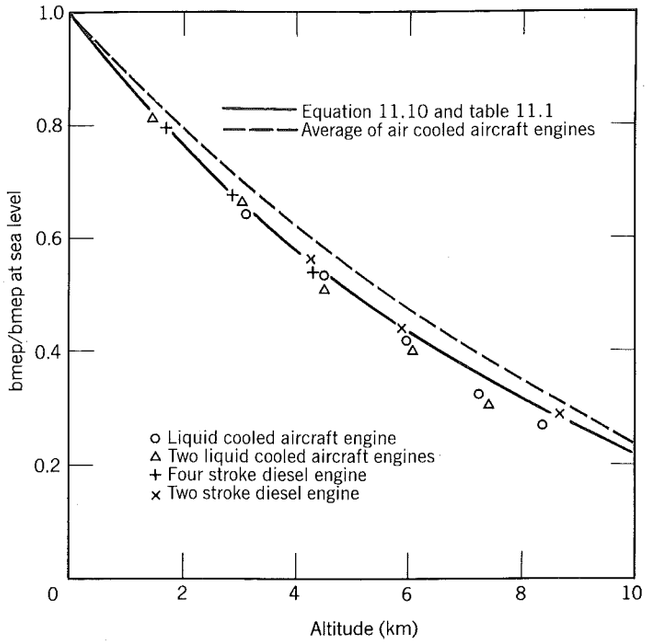

Figure 11-8 Effect of altitude on unthrottled engine performance at constant fuel–air ratio and coolant temperature. Data references are in Fig. 12-9 of Taylor (1977).

write

$$\frac{(\text{bmep})_a}{(\text{bmep})_o} = \frac{P_a}{P_o}\sqrt{\frac{T_o}{T_a}} \tag{11.10}$$

where the subscript a denotes conditions at altitude and the subscript o denotes conditions at sea level. This curve correlates the experimental data very well, as shown in Fig. 11-8; thus there is reason to believe that the effect of altitude through the attendant changes in temperature and pressure on brake specific fuel consumption is small.

Equation (11-10) is valid if and only if the fuel–air ratio is constant. It can thus be applied only to engines with fuel metering systems that respond to changes in altitude to hold the fuel–air ratio fixed. In the SAE Handbook, the engine power test code (SAE J1349 DEC80) gives an equation to replace Eq. (11.10) in the case of a constant fuel rate.

11.5 HEAT RELEASE TIMING

For homogeneous-charge gasoline engines, the parameter of interest is the spark timing. Figure 11-9 shows the effect of spark timing on the brake mean effective pressure for a number of automotive engines at different speeds and

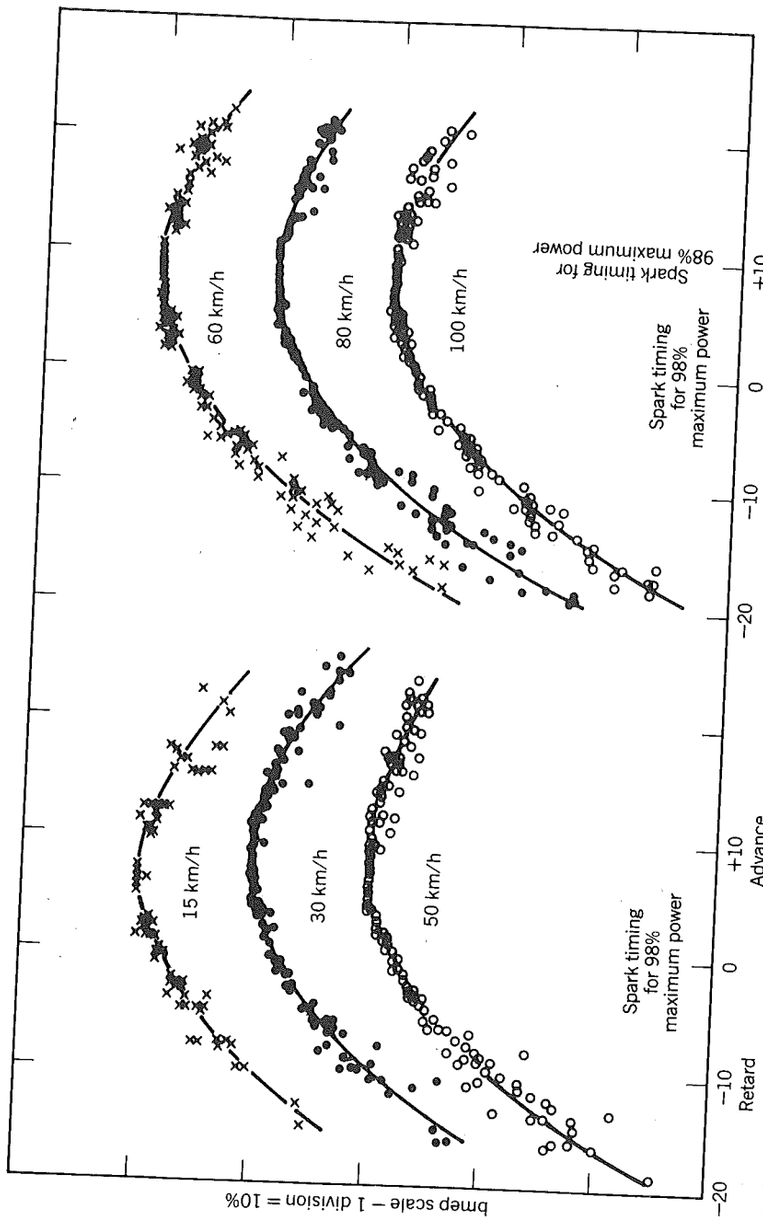

Figure 11-9 The effect of spark timing on bmep at a number of road loads for a number of U.S. passenger car engines (Barber, 1948). Reprinted with permission © 1948. Society of Automotive Engineers, Inc. Because the drag coefficients and frontal areas on automobiles today are less than they were in 1948, the speeds shown are low compared to what the same engines would yield today; however, the shapes of the curves shown are still representative of current engines.

loads. The variations in spark timing have the same percentage effect at all speeds and loads. In fact the data are well correlated by

$$\frac{\text{bmep}}{(\text{bmep})_{\max}} = 1 - \left(\frac{\Delta\theta}{53}\right)^2 \tag{11.11}$$

Where $\Delta\theta$ is the change in degrees of crank angle from the angle of maximum bmep. Although the data correlated are rather old, they are still representative of today's engines; in fact, Eq. (11.11) agrees well with a curve drawn by Amann (1980) as representative of today's engines.

Engines today are usually timed to an angle referred to as MBT (*minimum advance for best torque*). Examine Fig. 11-9 and notice how flat the bmep curve is in the vicinity of the maximum. Now, reexamine Fig. 9-20 and notice how sensitive the nitric oxide emissions are to variations in spark timing. Clearly, if the timing is slightly retarded, say 5 deg from that of maximum bmep, then the engine power will hardly suffer; yet under some operating conditions the nitric oxides will be greatly reduced. Retarded timing also somewhat reduces the engine's octane requirement.

The term *MBT spark timing* is widely accepted yet there is no quantitative definition in terms of how far the spark should be retarded from the point of maximum torque. The fraction of the maximum torque realized for various spark retards, each of which could be a candidate for defining MBT timing, is as follows.

$\frac{\text{bmep}}{(\text{bmep})_{\max}}$ (%)	$\Delta\theta_{\text{retard}}$
98	7.5
99	5.3
99.5	3.8

We will define MBT timing as a spark retard of 4 deg from the angle of maximum torque. This definition should agree with values reported in the literative to a tolerance of about ± 2 deg.

Figure 11-10 shows how the MBT timing can be expected to vary with engine speed, equivalence ratio, and residual mass fraction. Because the charge is diluted by either air (in which case it is lean) or exhaust gas, the combustion duration and ignition delay both increase, thereby requiring a greater spark advance to more or less center the combustion about top center. Likewise, as engine speed increases, ignition delay and the MBT spark advance increases.

In diesel engines the parameter of interest is the fuel injection timing. There are similarities in how diesel engines respond to changes in timing with how, already discussed, gasoline engines respond. The brake mean effective pressure and brake specific fuel consumption are rather insensitive to changes in timing near the optimum for best torque, see Fig. 9-46, for example, Retarding the timing is still an effective means of controlling the nitric oxide

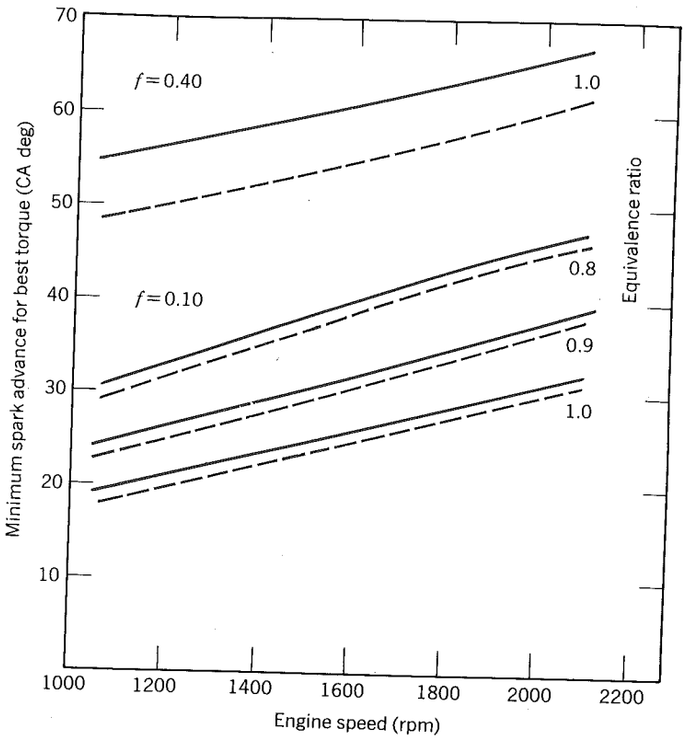

Figure 11-10 Minimum spark advance for best torque as determined by a regression analysis applied to a low squish, open-chamber automotive engine. Adapted from Young (1980).

emissions but with diesel engines it is usually at the expense of there being an increase in the particulate or smoke emissions. Furthermore, retarding the timing does not always reduce the nitric oxides.

One way to illustrate the trade offs involved in controlling nitric oxides by retarding the fuel injection timing is to plot the brake specific nitric oxides versus the brake specific fuel consumption as in Fig. 11-11. The graph shows the response of five different engines to changes in timing at full load and rated speed (which is the maximum power for continuous operation warranted by the manufacturer). For each of the direct-injection engines, a significant reduction in the nitric oxide emissions can be realized at the expense of there being a slight increase in the brake specific fuel consumption. With indirect engines there is no appreciable change in the nitric oxides; whereas, at part loads these same engines show response curves more like those shown for the direct injection engines.

The results discussed point out that it is more difficult to generalize about diesel engines than about gasoline engines. This is because, as discussed in

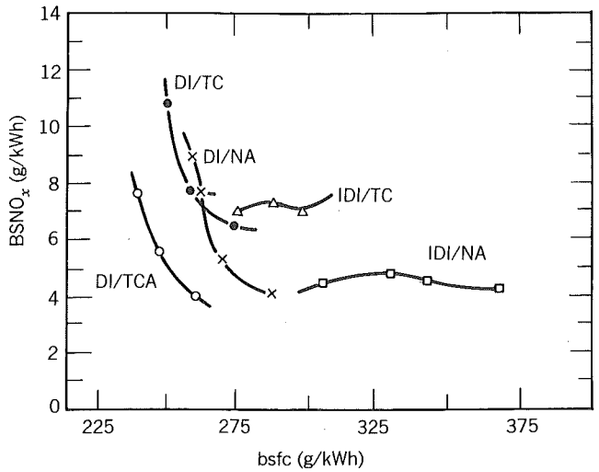

DI—direct injection, $r = 17$
IDI—indirect injection, $r = 16.7$
TC—turbocharged
TCA—turbocharged and aftercooled
NA—naturally aspirated

All engines are production, in-line six-cylinder, four-stroke engines with $V_d = 5.90$ liter. All tests are at $R_s = 2800$ rpm except for IDI/TC which is at $R_s = 3000$ rpm (Pischinger and Cartelleri, 1972). Reprinted with permission © 1972 Society of Automotive Engineers, Inc.

Figure 11-11 Brake specific nitric oxide emissions versus brake specific fuel consumption at full load as fuel injection timing is varied.

Chapter 1, there are so many more degrees of freedom available in the design of a diesel engine. The performance of an engine is the integrated result of processes that are nearly quasi-static in character. The nonequilibrium effects are perturbations highly dependent upon details of the engine design. They assume little significance in drawing generalizations but can be the key to building an engine that is competitive in the marketplace or to emission control.

To put that last statement in perspective, let us reexamine Fig. 11-4. The variable geometry prechamber improved the fuel economy of the PA4-185 engine by about 10 g/kWh or about 5%. The 5% improvement is small and does not affect the trend shown for brake specific fuel consumption with load. Nevertheless, that 5% improvement is very significant since the cost of fuel saved by a ship on a job, although small compared to the total fuel cost, will be comparable to the job's profit.

11.6 PERFORMANCE MAPS

Automotive engines are expected to operate well over a wide range of speeds and loads. Figure 11-12 shows two driving cycles defined by the United States Environmental Protection Agency for regulatory purposes. In each case, vehicle speed as a function of time is specified. From knowledge of the vehicle's characteristics, such as frontal area, drag coefficient, weight and gear ratios, the

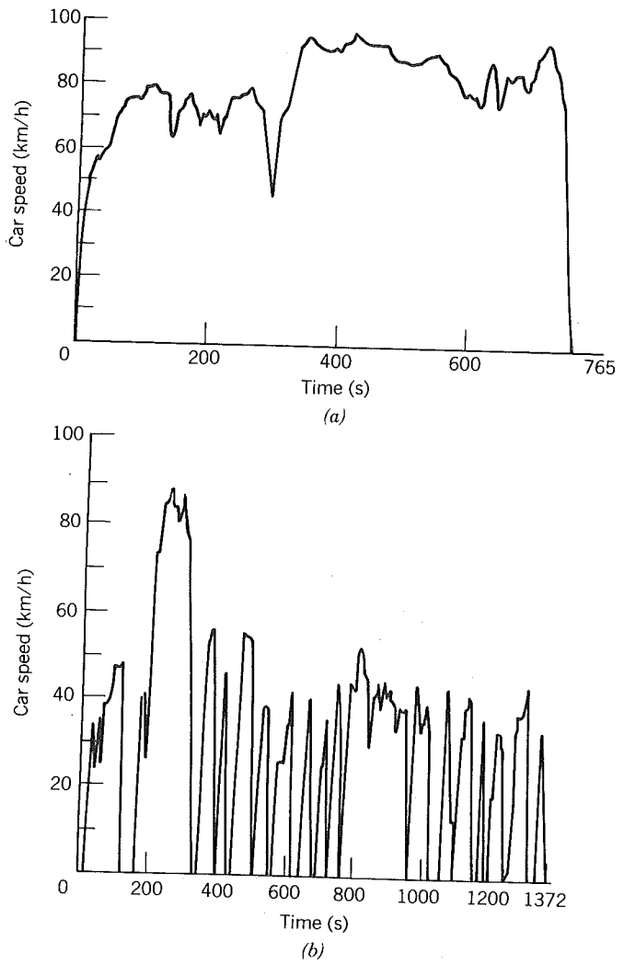

Figure 11-12 EPA driving cycles that with known vehicle characteristics will define an engine's duty cycle. Similar concepts apply in defining duty cycles for marine, truck, locomotive and other engines. (*a*) Federal highway driving schedule. (*b*) Federal urban driving schedule.

driving cycle can be transformed into a specification of the engine's torque and speed as a function of time. The fuel consumed by the vehicle during the trip will be

$$\Delta m_f = \int_0^{\Delta t} \dot{m}_f \, dt = \frac{A_p}{4} \int_0^{\Delta t} \text{bsfc bmep } \overline{U}_p \, dt \qquad (11.12)$$

For a two-stroke engine, the factor of 4 would instead be a factor of 2. In order to do the integration on the right of Eq. 11-12, one needs bsfc, bmep, and $\overline{U}_p$ as functions of time. The latter two are known since engine torque and speed are known through the driving cycle and the vehicle characteristics. The brake specific fuel consumption can be estimated for each load, speed point by running the engine on a dynamometer and measuring the fuel consumption when the engine is at a steady state at that same load and speed. A common way of presenting the data so obtained is shown in Fig. 11-13. This is a contour plot showing lines of constant fuel consumption in the load, speed plane. The graph itself is referred to as an engine or performance map. It contains the necessary information to estimate the fuel consumed by an engine according to Eq. (11-12) given its duty cycle, that is, the load and speed as a function of time.

The upper envelope on this map is the wide-open throttle performance curve. Its shape reflects variations in volumetric efficiency with engine speed though small changes in fuel–air ratio and inlet air density are also involved.

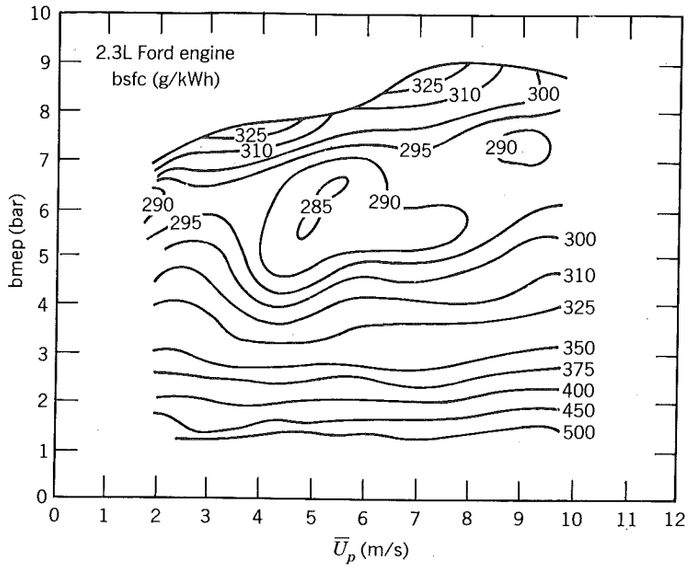

Figure 11-13 Performance map of a four-cylinder carbureted gasoline automotive engine: $b = 93.5$ mm, $S = 84$ mm, $r = 9.00$. Courtesy Ford Motor Co.

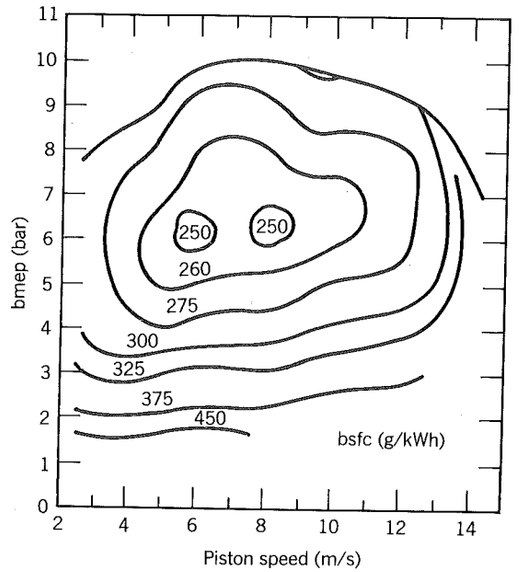

Figure 11-14 Performance map of a high compression ratio spark-ignition engine: $b = 92$ mm, $S = 80$ mm, $r = 13.1$. At part load the engine runs at about $\phi = 0.90$ and at full throttle the engine runs at $\phi = 1.2$ (Sutton, 1983). Reprinted with permission © 1983. Society of Automotive Engineers, Inc.

The brake specific fuel consumption is minimum at about 60% of the maximum bmep and about 60% of the maximum piston speed.

Starting at the minimum, if one increases the piston speed, the fuel consumption increases because of an increase in the friction loss. If one decreases the piston speed, the fuel consumption increases because of an increase in the heat loss. If one increases the load, the fuel consumption increases because the mixture must be enriched beyond stoichiometric. If one decreases the load, the fuel consumption increases because the friction is becoming a larger proportion of the indicated work.

It is amazing how similiar performance maps are from engine to engine. Figure 11-14 shows a performance map for a high compression ratio, spark-ignition engine that on the whole runs leaner than the engine in Fig. 11-13. Minimum fuel consumption still occurs at 60% of the maximum load and 60% of the maximum speed. The higher compression ratio results in a lower value for the minimum fuel consumption as one should expect, but it did not perturb the general shape of the contours.

Maps for a two-stroke gasoline engine in both port fuel injected and carburetted form are given in Fig. 11-15. The advantage to fuel injection in this

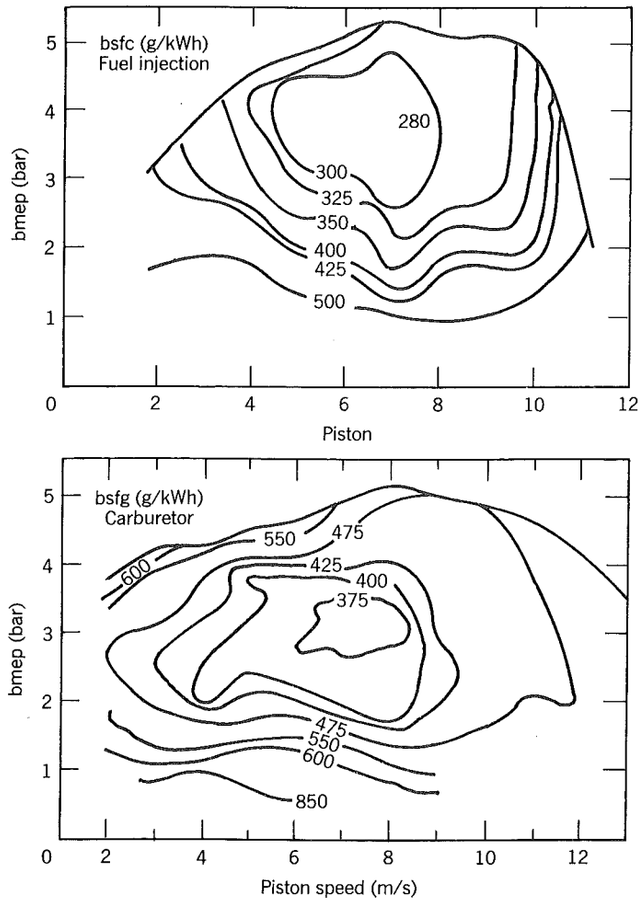

Figure 11-15 Performance maps of a cross-scavenged two-stroke engine: $b = 61.5$ mm, $S = 59.9$ mm, $N_c = 2$, trapped compression ratio = 6.2. The fuel injected version is more efficient than the carbureted version because of a reduction in the short circuited fuel. Its hydrocarbon emissions are a factor of about ten less (Yamagishi, Sato, and Iwasa 1972). Reprinted with permission © 1972. Society of Automotive Engineers, Inc.

application is clearly evident yet in each case minimum fuel consumption still occurs near the 60–60 point and explanations given for Fig. 11-13 apply in either case.

The maps discusses so far have been for homogeneous-charge engines. Results for a direct-injection, stratified-charge engine are given in Fig. 11-16. The point of minimum fuel consumption has moved up closer to the maximum

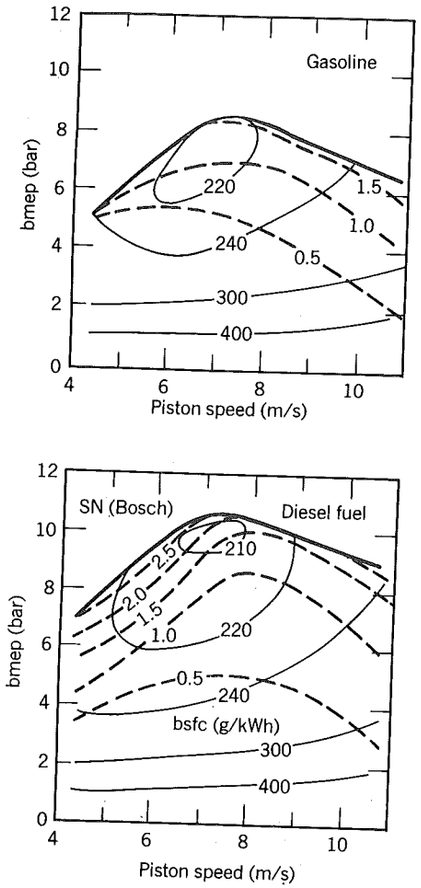

Figure 11-16 Performance and smoke number maps of a direct-injection stratified-charge engine, intercooled and turbocharged: $b = 125$ mm, $S = 130$ mm, $r = 20.1$, $N_c = 10$. The engine produces more power on diesel fuel than on gasoline because the injection system is a jerk pump. Since diesel fuel is denser than gasoline, more diesel fuel by mass is injected at full load (Hardenberg and Buhl, 1982). Reprinted with permission © 1982. Society of Automotive Engineers, Inc.

load and now occurs near 90% of the maximum bmep but still near 60% of the maximum piston speed.

For a homogeneous-charge engine at the point of minimum fuel consumption, the load is increased by increasing simultaneously the fuel–air ratio and the delivery ratio. For an engine in which the fuel is injected at the time combustion is to occur, the load is increased solely by increasing the fuel–air ratio; as the engine is unthrottled the delivery ratio remains nearly constant. Since the torque or bmep will depend on the product of the fuel–air ratio and the delivery ratio, when the two variables are increased simultaneously there is a larger change in torque. That is one reason why the point of minimum fuel consumption in Fig. 11-16 has moved up relative to the points in Figs. 11-13, 11-14, and 11-15. Another reason relates to the fact that power in heterogeneous-charge engines is smoke limited.

In a homogeneous-charge engine, the minimum fuel consumption occurs at about $\phi = 1.0$, as we have seen. In a diesel engine it occurs at a smaller equivalence ratio because the engine will smoke intolerably at $\phi = 1.0$. If ϕ_m is the equivalence ratio where the fuel consumption is minimum, then at $\phi_s = \phi_m + \Delta\phi$, the manufacturer will say the engine smokes intolerably and will set up the fuel injection system so that $\phi < \phi_s$ always. Typically, $\Delta\phi$ is set rather small for emission control and satisfactory engine life, the mixture being enrichened by only 5 to 10% beyond ϕ_m for maximum power. In the homogeneous charge engines, on the other hand, the mixture is usually enriched some 10 to 20% beyond stoichiometric.

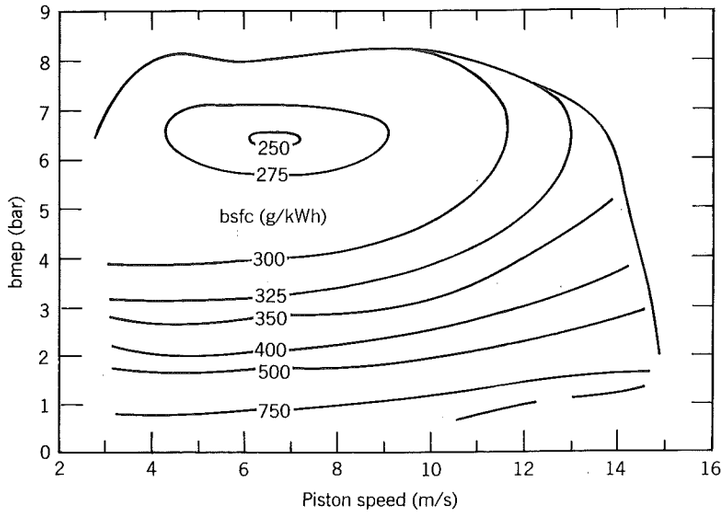

Figure 11-17 Performance map of a NA IDI diesel engine (see Fig. 1-24 and 1-25): $b = 76.5$ mm, $S = 80$ mm, $r = 23$, $N = 4$ (Hofbauer and Sator, 1977). Reprinted with permission © 1977. Society of Automotive Engineers, Inc.

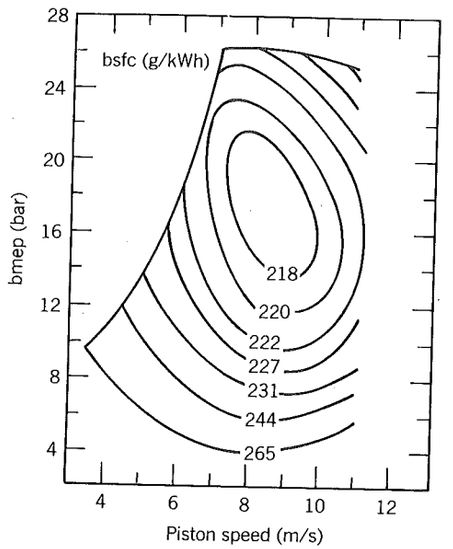

Figure 11-18 Performance map of variable geometry diesel prechamber engine: See also Fig. 11-4. $b = 200$ mm, $S = 210$ mm, $r = 13.7$, intercooled, two-stage turbocharger. Courtesy Societe d'Etudes de Machines Thermiques, SEMT.

Figures 11-17 and 11-18 show maps for two different diesel engines. They reinforce several of the points made earlier and demonstrate that the relative position of the point of minimum fuel consumption can be moved up or down depending on the degree of mixture enrichment the manufacturer will allow by his choice of $\Delta\phi$.

11.7 REFERENCES

Amann, C. A. (1980), "Control of the Homogeneous-Charge Passenger-Car Engine—Defining the Problem," SAE Trans., Vol. 89, paper 801440.

Barber, E. M. (1948), "Knock Limited Performance of Several Automobile Engines," SAE Trans., Vol. 2, p. 401.

Caris, D. F. and E. E. Nelson (1959), "A New Look at High Compression Engines," SAE Trans., Vol. 67, p. 112.

French, C. C. J. (1983), "A Universal Test Engine for Combustion Research," SAE paper 830453.

Hardenberg, H. O. and H. W. Buhl (1982), "The MERCEDES-BENZ OM 403 VA—A Standard Production, Compression-Ignition, Direct-Injection Multifuel Engine," SAE paper 820028.

Hermann, R. (1980), "PA4-200 Engines with Variable Geometry Precombustion Chamber and Two Stage Turbocharging System," ASME paper 80-DGP-22.

Hofbauer, P. and Sator, K. (1977), "Advanced Automotive Power Systems, Part 2: A Diesel for a Subcompact Car" SAE Trans., Vol. 86, paper 770113.

McAulay, K., T. Wu, S. Chen, G. Borman, P. Myers, and O. Uyehara (1965), "Development and Evaluation of the Simulation of the CI Engine," SAE paper 650451.

Millington, B. W. and E. R. Hartles, (1968), "Frictional Losses in Diesel Engines," SAE Trans., Vol. 77, paper 680590.

Motoyoshi, E., T. Yamada, and M. Mori (1976), "The Combustion and Exhaust Emission Characteristics and Starting Ability of Y.P.C. Combustion System," SAE paper 760215.

Pischinger, R. and W. Cartellieri (1972), "Combustion System Parameters and Their Effect upon Diesel Engine Exhaust Emissions," SAE paper 720756.

Roensch, M. (1949), "Thermal Efficiency and Mechanical Losses of Automotive Engines," SAE J., Vol. 51, pp. 17–30.

Sutton, D. L. (1983), "Combustion Chamber Design for Improved Performance and Economy with High Compression Lean Burn Operation," SAE paper 830336.

Taylor, C. F., (1977), *The Internal Combustion Engine in Theory and Practice*, Vol. 1, MIT Press, Cambridge, Massachusetts.

Thomas, F. J., J. S. Ahluwalia, E. Shamah, and G. W. Van der Horst (1984), "Medium-Speed Diesel Engines Part I: Design Trends and the Use of Residual/Blended Fuels," ASME paper 84-DGP-15.

Von Schnorbein, E., and J. Bucher (1981), "Experience with the Rating and Operation of Medium-Speed, Four-Stroke Engines under Extreme Site Conditions," CIMAC paper D64.

Walder, C. J. (1965), "Problems in the Design and Development of High Speed Diesel Engines," SAE paper 978A.

Yamagishi, G., T. Sato, and H. Iwasa (1972), "A Study of Two-Stroke Cycle Fuel Injection Engines for Exhaust Gas Purification," SAE paper 720195.

Young, M. B. (1980), "Cyclic Dispersion—Some Quantitative Cause-and-Effect Relationships", SAE paper 800459

1.8 HOMEWORK

1. A particular car traveling steadily on a level road at 100 km/h requires about 15 kW of power from the engine. For each of the engines in Figs. 11-14, 11-17, and 11.18 determine the fuel economy of the vehicle (km/g), the bore required of a four cylinder engine, and the maximum power the engine will produce. Assume in each case that the engine is operating at its best fuel economy point when the vehicle is cruising at 100 km/h, that engine controls limit the piston speed to 10 m/s, and that the maps are size independent.

2. The price of large diesel engines is roughly proportional to their rated power. Let

$$c_1 = \text{engine price per kilowatt per year}$$

$$c_2 = \text{fuel price per kilogram}$$

At low values of c_1 it pays to buy an engine bigger than required and operate it at its best fuel economy point. For low values of c_2 it pays to buy a smaller engine and run it at its rated power. For the engine characteristics in Fig. 11-18 at what ratio c_1/c_2 will the two different sized engines yield the same total annual cost? Assume the engines are run 20 h/day and their rated power is at $U_p = 11$ m/s, bmep = 25 bars.

3. Write an expression resembling Eq. (11.12) for the mass of pollutant species i (given its emission index at any load, speed point) emitted by an engine operated over a duty cycle from $0 < t < \Delta t$.

Appendix A
IMSL ROUTINES

This appendix describes the subroutines employed from the international mathematical and statistical libraries package. The documentation is from the IMSL reference manual. The routines described here are:

DVERK—differential equation solution, Runge Kutta–Verner fifth and sixth order method
LEQIF—linear equation solution, full matrices (virtual memory version)

The subroutines described and others are available from:

IMSL
Customer Relations
Sixth Floor, NBC Building
7500 Bellaire Boulevard
Houston, Texas 77036-5085

IMSL ROUTINE NAME

DVERK

PURPOSE

Differential equation solver—Runge–Kutta–Verner fifth and sixth order method

USAGE

```
CALL DVERK (N,FCN,X,Y,XEND,TOL,IND,C,NW,W,IER)
```

ARGUMENTS

N Number of equations. (Input.)

FCN Name of subroutine for evaluating functions. (Input.)
The subroutine itself must also be provided by the user and it should be of the following form:

```
SUBROUTINE FCN(N,X,Y,YPRIME)
REAL Y(N), YPRIME(N)
:
```

FCN should evaluate YPRIME(1),...,YPRIME(N) given N,X, and Y(1),...,Y(N). YPRIME(I) is the first derivative of Y(I) with respect to X.
FCN must appear in an EXTERNAL statement in the calling program and N,X,Y(1),...,Y(N) must not be altered by FCN.

X INDEPENDENT VARIABLE. (Input and output.)
On input, X supplies the initial value.
On output, X is replaced with XEND unless error conditions arise. See the description of parameter IND.

Y DEPENDENT VARIABLES, vector of length N. (Input and output.)
On input, Y(1),...,Y(N) supply initial values.
On output, Y(1),...,Y(N) are replaced with an approximate solution at XEND unless error conditions arise. See the description of parameter IND.

XEND VALUE OF X AT WHICH SOLUTION IS DESIRED. (Input.)
XEND may be less than the initial value of X.

TOL TOLERANCE FOR ERROR CONTROL. (Input.)
The subroutine attempts to control a norm of the local error in such a way that the global error is proportional to TOL. Making TOL smaller improves accuracy and more than one run, with different values of TOL, can be used in an attempt to estimate the global error.
In the default case (IND=1), the global error is

```
MAX(ABS(E(1)),...,ABS(E(N)))
```

where E(K) = (Y(K) - YT(K)) / MAX(1,ABS(Y(K))), YT(K) is the true solution, and Y(K) is the computed solution at XEND, for K=1,2,...,N. Other error control options are available. See the description of parameters IND and C below.

IND INDICATOR. (Input and output.)
On initial entry IND must be set equal to either 1 or 2.
IND=1 causes all default options to be used and eliminates the need to set specific values in the communications vector C.

IND=2 allows options to be selected. In this case, the first 9 components of C must be initialized to select options as described below.
The subroutine will normally return with IND=3, having replaced the initial values of X and Y with, respectively, the value XEND and an approximation to Y at XEND.
The subroutine can be called repeatedly with new values of XEND without changing any of the other parameters.
Three error returns are also possible, in which case X and Y will be the most recently accepted values.
IND=-3 indicates that the subroutine was unable to satisfy the error requirement. This may mean that TOL is too small.
IND=-2 indicates that the value of HMIN (minimum step-size) is greater than HMAX (maximum step-size), which probably means that the requested TOL (which is used in the calculation of HMIN) is too small.
IND=-1 indicates that the allowed maximum number of FCN evaluations has been exceeded. This can only occur if option C(7), as described below, has been used.

C COMMUNICATIONS VECTOR OF LENGTH 24. (Input IF IND.NE.1, and output).
C is used to select options and to retain information between calls. The user need not be concerned with the following description of the elements of C when default options are used (IND=1). However, when it is desired to use IND=2 and select options, a basic understanding of DVERK is required. The following paragraph describes, briefly, the basic terms. For more details, see the document reference.
DVERK advances the independent variable X one step at a time until XEND is reached. The solution is computed at XTRIAL=X+HTRIAL along with an error estimate EST. If EST is less than or equal to TOL (successful step), the step is accepted and X is advanced to XTRIAL. If EST is greater than TOL (failure) HTRIAL is adjusted and the solution is recomputed. HMAG=ABS(HTRIAL) is never allowed to exceed HMAX nor is it allowed to become smaller than HMIN. The first trial step is HSTART. During the computation, a counter (C(23)) is incremented each time a trial step fails to provide a solution satisfying the error tolerance. Another counter (C(22)) is used to record the number of successful steps. After a successful step, C(23) is set to zero.
OPTIONS. If the subroutine is entered with IND=2, the first 9 components of the communications vector must be initialized by

the user. Normally this is done by first setting them all to zero, and then those corresponding to particular options are made non-zero.

C(1) ERROR CONTROL INDICATOR.
The subroutine attempts to control a norm of the local error in such a way that the global error is proportional to TOL. The definition of global error for the default case (IND=1) is given in the description of parameter TOL. The default weights are 1/MAX(1,ABS(Y(K))). When IND=2 is used, the weights are determined according to the value of C(1).

If C(1) = 1 The weights are 1
(absolute error control)

If C(1) = 2 The weights are 1/ABS(Y(K)) for K=1,2,...,N.
(relative error control)

If C(1) = 3 The weights are
1/MAX(ABS(C(2)),ABS(Y(K)))
for K=1,2,...,N.
(relative error control, unless
ABS(Y(K)) is less than the floor
value, ABS(C(2)))

If C(1) = 4 The weights are
1/MAX(ABS(C(K+30)),ABS(Y(K)))
for K=1,2,...,N.
(here individual floor values are used.)
In this case, the dimension of C
must be greater than or equal to
N+30 and C(31),C(32),...,C(N+30)
must be initialized by the user.

If C(1) = 5 The weights are 1/ABS(C(K+30))
for K=1,2,...,N.
In this case, the dimension of C
must be greater than or equal to
N+30 and C(31),C(32),...,C(N+30)
must be initialized by the user.

For all other values of C(1) including C(1)=0, the default values of the weights are taken to be 1/MAX(1,ABS(Y(K))) for K=1,2,...,N.

C(2) FLOOR VALUE. used when the indicator C(1) has the value 3.

C(3) HMIN specification. If not zero, the subroutine chooses HMIN to be ABS(C(3)). Otherwise it uses the default value 10*MAX(DWARF,RREB*MAX(NORM(Y)/TOL,ABS(X))) where

DWARF is a very small positive machine number and RREB is the relative roundoff error bound.

C(4) HSTART specification. If not zero, the subroutine will use an initial HMAG equal to ABS(C(4)), except of course for the restrictions imposed by HMIN and HMAX. Otherwise it uses the default value HMAX*(TOL)**(1/6).

C(5) SCALE SPECIFICATION. This is intended to be a measure of the scale of the problem. Larger values of scale tend to make the method more reliable, first by possibly restricting HMAX (as described below) and second, by tightening the acceptance requirement. If C(5) is zero, a default value of 1 is used. For linear homogeneous problems with constant coefficients, an appropriate value for scale is a norm of the associated matrix. For other problems, an approximation to an average value of a norm of the jacobian along the trajectory may be appropriate.

C(6) HMAX SPECIFICATION. Four cases are possible,

If C(6).NE.0 and C(5).NE.0, HMAX is taken to be MIN(ABS(C(6)),2/ABS(C(5))).

If C(6).NE.0 and C(5).EQ.0, HMAX is taken to be ABS(C(6)).

If C(6).EQ.0 and C(5).NE.0, HMAX is taken to be 2/ABS(C(5)).

If C(6).EQ.0 and C(5).EQ.0, HMAX is given a default value of 2.

C(7) MAXIMUM NUMBER OF FUNCTION EVALUATIONS. If not zero, an error return with IND=-1 will be caused when the number of function evaluations exceeds ABS(C(7)).

C(8) INTERRUPT NUMBER 1. If not zero, the subroutine will interrupt the calculations after it has chosen its preliminary value of HMAG, and just before choosing HTRIAL and XTRIAL in preparation for taking a step (HTRIAL may differ from HMAG in sign, and may require adjustment if XEND is near). The subroutine returns with IND=4, and will resume calculation at the point of interruption if re-entered with IND=4.

C(9) INTERRUPT NUMBER 2. If not zero, the subroutine will interrupt the calculations immediately after it has decided whether or not to accept the result of the most recent trial step, with IND=5 if it plans to accept, or IND=6 if it plans to reject. Y(*) is the

previously accepted result, while W(*,9) is the newly computed trial value, and W(*,2) is the unweighted error estimate vector. The subroutine will resume calculations at the point of interruption on re-entry with IND=5 or 6. IND may be changed by the user in order to force acceptance of a step (by changing IND from 6 to 5) that would otherwise be rejected, or vice versa.

NW ROW DIMENSION OF THE MATRIX W EXACTLY AS SPECIFIED IN THE DIMENSION STATEMENT IN THE CALLING PROGRAM. (Input) NW must be greater than or equal to N.

W WORKSPACE MATRIX.
The first dimension of W must be NW and the second must be greater than or equal to 9. W must remain unchanged between successive calls during integration.

IER ERROR PARAMETER. (Output.)
Terminal error
IER=129, NW is less than N or TOL is less than or equal to zero.
IER=130, IND is not in the range 1 to 6.
IER=131, XEND has not been changed from previous call or X is not set to the previous XEND value.
IER=132, the relative error control option (C(1)=2) was selected and one of the solution components is zero.

PRECISION/HARDWARE

SINGLE AND DOUBLE/H32; SINGLE/H36, H48, H60

REQD. IMSL ROUTINES

UERTST,UGETIO

NOTATION

Information on special notation and conventions is available in the manual introduction or through IMSL routine UHELP.

REMARKS

1. In a typical situation, DVERK is called repeatedly with a sequence of values for XEND. After each such call, the user should interrogate IND and IER.

Error conditions are signaled when IND is less than zero and/or IER is greater than zero. Corrective action (such as changing certain parameter values) must be taken prior to re-entry.

2. When error conditions arise, it is often helpful to examine components of the communications vector C. A summary follows:

PRESCRIBED AT THE OPTION OF THE USER

C(1) ERROR CONTROL INDICATOR
C(2) FLOOR VALUE
C(3) HMIN SPECIFICATION
C(4) HSTART SPECIFICATION
C(5) SCALE SPECIFICATION
C(6) HMAX SPECIFICATION
C(7) MAXIMUM NUMBER OF FCN EVALUATIONS
C(8) INTERRUPT NUMBER 1
C(9) INTERRUPT NUMBER 2

DETERMINED BY THE PROGRAM

C(10) RREB (RELATIVE ROUNDOFF ERROR BOUND)
C(11) DWARF (VERY SMALL MACHINE NUMBER)
C(12) WEIGHTED NORM OF Y
C(13) HMIN
C(14) HMAG
C(15) SCALE
C(16) HMAX
C(17) XTRIAL
C(18) HTRIAL
C(19) EST
C(20) PREVIOUS XEND
C(21) FLAG FOR XEND
C(22) NUMBER OF SUCCESSFUL STEPS
C(23) NUMBER OF SUCCESSIVE FAILURES
C(24) NUMBER OF FCN EVALUATIONS

If C(1)=4 OR 5, C(31),C(32),...,C(N+30) are floor values.

3. Parameter NW gives the row dimension of W exactly as it appears in the dimension statement in the calling program. If only one system of equations is being solved, NW normally will have the same value as N. However, if more than one system is being handled, and they are to use a common workspace, W, one after the other, the value of NW (and hence, the row dimension of W in the calling program) must be as large as the maximum value of the individual N values.

ALGORITHM

DVERK finds approximations to the solution of a system of first order ordinary differential equations of the form $y' = f(x, y)$ with initial conditions. It is designed to be easy to use. By setting parameter IND to 1, the user need only provide parameters to describe the problem; everything else is done automatically by the subroutine. Alternatively, the user may set IND to 2 and then select any one of several options, including different kinds of error control, restrictions on step sizes, and interrupts which permit the user to examine the state of the calculations (and perhaps make modifications) during intermediate stages. DVERK attempts to keep the global error proportional to a tolerance specified by the user. The proportionality depends on the kind of error control that is used as well as the differential equation and the range of integration.

DVERK is efficient for non-stiff systems where derivative evaluations are not expensive and where solutions are not required at a large number of finely spaced points (as might be the case for example with graphical output). See the Chapter D prelude for general guidelines.

The subroutine is based on a code designed by T. E. Hull, W. H. Enright, and K. R. Jackson. It uses Runge-Kutta formulas of orders 5 and 6 that were developed by J. H. Verner.

REFERENCES

1. T. E. Hull, W. H. Enright, and K. R. Jackson, "User's Guide for DVERK—A Subroutine for Solving Non-Stiff ODE's", TR No. 100, Department of Computer Science, University of Toronto, October, 1976.
2. K. R. Jackson, W. H. Enright, and T. E. Hull, "A Theoretical Criterion for Comparing Runge–Kutta Formulas TR101", January, 1977.

EXAMPLE 1

This example illustrates the basic usage (all default options) of DVERK. A table of solution values for $x = 1.0, 2.0, \ldots, 10.0$ is obtained for the predator–prey problem:

$$y_1' = 2y_1(1 - y_2) \quad y_1 = 1$$
$$\text{at } x = 0$$
$$y_2' = y_2(y_1 - 1) \quad y_2 = 3$$

```
      INTEGER   N,IND,NW,IER,K
      REAL      Y(2),C(24)W(2,9),X,TOL,XEND
      EXTERNAL  FCN1
      NW  =2
      N   =2
      X   =0.0
      Y(1)=1.0
      Y(2)=3.0
      TOL =.0001
      IND =1
      DO 10 K=1,10
        XEND=FLOAT(K)
        CALL DVERK (N,FCN1,X,Y,XEND,TOL,IND,C,NW,W,IER)
        IF(IND.LT.0.OR.IER.GT.0) GO TO 20
C                       Y(1) AND Y(2) ARE CURRENT SOLU-
C                       TION VALUES AT X.
C                       INSERT WRITE STATEMENT HERE.
 10   CONTINUE
      STOP
 20   CONTINUE
C                       HANDLE IND.LT.0 OR IER.GT.0
C                       ITEMS THAT MAY HELP DIAGNOSE THE
C                       PROBLEM SHOULD BE OUTPUT HERE.
C                       IND,TOL,N,W,Y(1),...,Y(N),XEND,
                        AND C(1),...,C(24).
      STOP
      END
      SUBROUTINE        FCN1(N,X,Y,YPRIME)
      INTEGER           N
      REAL              Y(N),YPRIME(N),X
      YPRIME(1)=2.0*Y(1)*(1.0-Y(2))
      YPRIME(2)=Y(2)*(Y(1)-1.0)
      RETURN
      END
```

Output:

```
IER=0
          X       Y(1)        Y(2)
          1.      0.08        1.46
          2.      0.09        0.58
          3.      0.29        0.25
          4.      1.45        0.19
          5.      4.05        1.44
          6.      0.18        2.26
          7.      0.07        0.91
          8.      0.15        0.37
          9.      0.65        0.19
         10.      3.15        0.35
```

EXAMPLE 2

This example shows how IND=2 is used to select specific options, while using default values for others. The differential equation

$$y' = y, \qquad y = 1 \text{ at } x = 0,$$

is solved for $x = .1, .2, \ldots, 1.0$, using the absolute error control option (C(1)=1).

```
      INTEGER   N,IND,NW,IER,I,K
      REAL      Y(1),C(24),W(1,9),X,TOL,XEND
      EXTERNAL  FCN2
      NW  =1
      N   =1
      X   =0.0
      Y(1)=1.0
      TOL =0.0005
      IND =2
C                       SELECT ALL DEFAULT OPTIONS, FIRST
      DO 5 I=1,9
 5    C(I)=0.0
C                       THEN SPECIFY C(1)=1.0 TO SELECT
C                       THE ABSOLUTE ERROR
C                       CONTROL OPTION.
      C(1)=1.0
      DO 10 K=1,10
        XEND=FLOAT(K)*0.1
        CALL DVERK(N,FCN2,X,Y,XEND,TOL,IND,C,NW,W,IER)
        IF(IND.LT.0.OR.IER.GT.0) GO TO 20
C                       Y(1) IS THE CURRENT SOLUTION
C                       VALUE AT X. INSERT WRITE
C                       STATEMENT HERE.
 10 CONTINUE
      STOP
 20 CONTINUE
C                       HANDLE IND.LT.0 OR IER.GT.0
C                       ITEMS THAT MAY HELP DIAGNOSE THE
C                       PROBLEM SHOULD BE OUTPUT HERE.
C                       IND,TOL,N,X,Y(1),...,Y(N),XEND,
C                       AND C(1),...,C(24).
      STOP
      END
      SUBROUTINE        FCN2(N,X,Y,YPRIME)
      INTEGER           N
      REAL              Y(N),YPRIME(N),X
      YPRIME(1)=Y(1)
      RETURN
      END
```

OUTPUT:

```
IER=0
          X        Y(1)
         .1       1.105
         .2       1.221
         .3       1.350
         .4       1.492
         .5       1.649
         .6       1.822
         .7       2.014
         .8       2.226
         .9       2.460
        1.0       2.718
```


IMSL ROUTINE NAME

LEQIF

PURPOSE

LINEAR EQUATION SOLUTION—FULL MATRICES (VIRTUAL MEMORY VERSION)

USAGE

```
CALL LEQIF(A,IA,N,MA,B,IB,M,IJOB,WK,IER)
```

ARGUMENTS

A — INPUT N BY N MATRIX CONTAINING THE COEFFICIENT MATRIX OF THE EQUATION AX=B. On output, A is replaced by the LU decomposition of a rowwise permutation of A. (Input/output.)

IA — ROW DIMENSION OF A EXACTLY AS SPECIFIED IN THE DIMENSION STATEMENT OF THE CALLING PROGRAM. (Input.)

N — ORDER OF MATRIX A. (Input.)

MA NUMBER OF COLUMNS PER BLOCK (Input). The choice of MA will affect the solution speed as follows. As MA is increased, the algorithm will run faster, until a point is reached beyond which 2*MA*IA working precision words cannot be held in main memory, without paging. MA must be less than or equal to N.

B INPUT N BY M MATRIX CONTAINING THE M RIGHT HAND SIDES OF THE EQUATION AX=B. On output, the solution matrix X replaces B. (Input/output.)

IB ROW DIMENSION OF B EXACTLY AS SPECIFIED IN THE DIMENSION STATEMENT OF THE CALLING PROGRAM. (Input.)

M NUMBER OF RIGHT HAND SIDES (COLUMNS IN B). (Input.)

IJOB OPTION PARAMETER. (Input) IJOB=I implies when
I=0, factor the matrix and solve the equation AX=B.
I=1, solve the equation AX=B. This option implies that LEQIF has already been called using IJOB=0 so that the matrix A has already been factored, and that WK has not been altered since that call.

WK REAL WORK AREA OF LENGTH 3*N.

IER ERROR PARAMETER. (Output.)
Terminal error IER=129 indicates that matrix A is algorithmically singular. (See the chapter L prelude.)

PRECISION/HARDWARE

SINGLE AND DOUBLE/H32; SINGLE/H36,H48,H60

REQD. IMSL ROUTINES

SINGLE/VBLA=SAXPY,UERTST,UGETIO

DOUBLE/VBLA=DAXPY,UERTST,UGETIO

NOTATION

Information on special notation and conventions is available in the manual introduction or through IMSL routine UHELP.

ALGORITHM

LEQIF uses a version of Gaussian elimination which operates on blocks of MA columns, two at a time. The first block is decomposed by Gaussian elimination and then blocks 2, 3... are processed one at a time with multiples of appropriate rows added to others, using the row multipliers saved in the first block. At the end of this cycle, the second block is decomposed and then blocks 3, 4... are processed, using the multipliers saved in the second block. The process continues in this manner until all blocks have been decomposed.

After the elimination stage is complete, the blocks are processed in reverse order, with all superdiagonal elements zeroed in each block before continuing to the next block.

REFERENCES

McKellar, A. C. and Coffman, E. G. Jr., "Organizing Matrices and Matrix Operations for Paged Memory Systems", *Commun. ACM 12*, 3 (March 1969), p. 153ff.

PROGRAMMING NOTES

1. MA should be the largest integer such that if the IA by N matrix were replaced by an IA by 2*MA matrix, the resulting program could be executed in main memory, without paging. Greatest efficiency will be achieved when IA=N.
2. It is assumed that M is small, i.e., less than MA. Otherwise, to avoid excessive page faults, the problem should be broken into parts and solved with MA right hand sides at a time, with IJOB=1 on all but the first part.

EXAMPLE

A 5 by 5 linear system is solved with two right-hand sides.

Input:

```
INTEGER        N,MA,IA,IB,M,IJOB,IER
REAL           A(5,5),B(5,2),WK(15)
```

$$A = \begin{bmatrix} 0. & 1. & 0. & 0. & 0. \\ 2. & 0.5 & 0. & 0. & 0. \\ 1. & 0.5 & 3. & 0. & 0. \\ 1. & 0.5 & 0. & 0. & 4. \\ 1. & 0.5 & 0. & 5. & 0. \end{bmatrix}$$

$$B = \begin{bmatrix} 2. & 3. \\ 2. & 3. \\ 2. & 3. \\ 2. & 3. \\ 2. & 3. \end{bmatrix}$$

```
N=5
MA=2
IB=5
IA=5
IJOB=0
M=2
CALL LEQIF(A,IA,N,MA,B,IB,M,IJOB,WK,IER)
.
.
.
END
```

Output:

$$B=\begin{bmatrix} 0.5 & 0.75 \\ 2.0 & 3.0 \\ 0.166667 & 0.25 \\ 0.1 & 0.15 \\ 0.125 & 0.1875 \end{bmatrix}$$

Appendix B

UNITS AND CONVERSION FACTORS

(Derived from M. B. Peterson and W. O. Winer, Eds., (1980), *Wear Control Handbook*, ASME, New York.)

Table B.1 Names of International Units

PHYSICAL QUANTITY	NAME OF UNIT	SYMBOL	FORMULA
	BASIC UNITS		
Length	meter	m	
Mass	kilogram	kg	
Time	seconds	s	
Electric current	ampere	A	
Temperature	kelvin	K	
Luminous intensity	candela	cd	
	DERIVED UNITS		
Area	square meter	m^2	
Volume	cubic meter	m^3	
Frequency	hertz	Hz	(s^{-1})
Density	kilogram per cubic meter	kg/m^3	
Velocity	meter per second	m/s	
Angular velocity	radian per second	rad/s	
Acceleration	meter per second squared	m/s^2	
Angular acceleration	radian per second squared	rad/s^2	
Force	newton	N	$(kg \cdot m/s^2)$
Pressure and stress	pascal	Pa	(N/m^2)
Kinematic viscosity	square meter per second	m^2/s	
Dynamic viscosity	pascal-second	$Pa \cdot s$	$(N \cdot s/m^2)$
Work, energy, quantity of heat	joule	J	$(N \cdot m)$
Power	watt	W	(J/s)
Electric charge	coulomb	C	$(A \cdot s)$
Voltage, potential difference, electromotive force	volt	V	(W/A)
Electric field strength	volt per meter	V/m	
Electric resistance	ohm	Ω	(V/A)
Electric capacitance	farad	F	$(A \cdot s/V)$
Magnetic flux	weber	Wb	$(V \cdot s)$
Inductance	henry	H	$(V \cdot s/A)$
Wave number	1 per meter	m^{-1}	
Entropy	joule per kelvin	J/K	
Specific heat	joule per kilogram kelvin	$J\,kg^{-1}\,K^{-1}$	
Thermal conductivity	watt per meter kelvin	$W/m^{-1}\,K^{-1}$	
Radiant intensity	watt per steradian	W/sr	
	SUPPLEMENTARY UNITS		
Plane angle	radian	rad	
Solid angle	steradian	sr	

Table B.2 Names of Multiples and Submultiples Of SI Units May Be Formed by Application of Prefixes

FACTOR BY WHICH UNIT IS MULTIPLIED	PREFIX	SYMBOL
10^{12}	tera	T
10^9	giga	G
10^6	mega	M
10^3	kilo	k
10^2	hecto	h
10	deka	da
10^{-1}	deci	d
10^{-2}	centi	c
10^{-3}	milli	m
10^{-6}	micro	μ
10^{-9}	nano	n
10^{-12}	pico	p
10^{-15}	femto	f
10^{-18}	atto	a

Table B.3 Physical constants

QUANTITY	SYMBOL	VALUE	ERROR (ppm)	UNIT
Speed of light in vacuum	c	$2.997\,925 \times 10^8$	0.33	$m \cdot s^{-1}$
Gravitational constant	G	$6.673\,2 \times 10^{-11}$	460	$N \cdot m^2 \cdot kg^{-2}$
Avogadro constant	N_A	$6.022\,169 \times 10^{26}$	6.6	$kmole^{-1}$
Boltzmann constant	k	$1.380\,622 \times 10^{-23}$	43	$J \cdot K^{-1}$
Gas constant	R	$8.314\,34 \times 10^3$	42	$J \cdot kmole^{-1} \cdot K^{-1}$
Volume of ideal gas, standard conditions	V_O	$2.241\,36 \times 10^1$	—	$m^3 \cdot kmole^{-1}$
Planck constant	h	$6.626\,196 \times 10^{-34}$	7.6	$J \cdot s$
	$h/2\pi$	$1.054\,5919 \times 10^{-34}$	7.6	$J \cdot s$
Electron charge	e	$1.602\,1917 \times 10^{-19}$	4.4	C
Electron rest mass	m_e	$9.109\,558 \times 10^{-31}$	6.0	kg
		$5.485\,930 \times 10^{-4}$	6.2	[a]
Stefan–Boltzmann constant	σ	$5.669\,61 \times 10^{-8}$	170	$W \cdot m^{-2} \cdot K^{-4}$

[a] The unified atomic mass unit (u) is equal to the fraction $\frac{1}{12}$ of the mass of an atom of the nuclide ^{12}C.

Table B.4 Conversion To SI Units[a]

MULTIPLY THIS UNIT	BY	TO OBTAIN THIS SI UNIT
	ACCELERATION	
ft/s^2	3.048 * E − 01	$meter/second^2$
free fall (standard gravity)	9.806 65 * E + 00	$meter/second^2$
$in./s^2$	2.54 * E − 02	$meter/second^2$
	AREA	
ft^2	9.290 304 * E − 02	$meter^2$
$in.^2$	6.4516 * E − 04	$meter^2$
	DENSITY	
$gram/cm^3$	1.00 * E + 03	$kilogram/meter^3$
$lbm/in.^3$	2.767 990E + 04	$kilogram/meter^3$
lbm/ft^3	1.601 846E + 01	$kilogram/meter^3$
$slug/ft^3$	5.153 788E + 02	$kilogram/meter^3$
	ENERGY	
British thermal unit (mean)	1.055 87E + 03	joule
British thermal unit (International Steam Tables)	1.055 06E + 03	joule
British thermal unit (Thermochemical)	1.054 35E + 03	joule
calorie (mean)	4.190 * E + 00	joule
calorie (International Steam Tables)	4.1868E + 00	joule
calorie (Thermochemical)	4.184E + 00	joule
electron volt	1.602 19E − 19	joule
erg	1.00 * E − 07	joule
ft lbf	1.355 82E + 00	joule
joule (International of 1948)	1.000 165E + 00	joule
watt h	3.60 * E + 03	joule
kW h	3.60 * E + 06	joule
	ENERGY/AREA · TIME	
Btu (thermochemical)/ft^2 s	1.134E + 04	$watt/meter^2$
Btu (thermochemical)/ft^2 min	1.891E + 02	$watt/meter^2$
Btu (thermochemical)/ft^2 h	3.152E + 00	$watt/meter^2$
Btu (thermochemical)/$in.^2$ s	1.634E + 06	$watt/meter^2$
calorie (thermochemical)/cm^2 min	6.973E + 02	$watt/meter^2$
erg/cm^2 · s	1.00 * E − 03	$watt/meter^2$
watt/cm^2	1.00 * E + 04	$watt/meter^2$
	FORCE	
dyne	1.00 * E − 05	newton
kilogram force (kgf)	9.806 65 * E + 00	newton
kilopond force	9.806E + 00	newton
kip	4.448E + 03	newton
lbf (pound force, avoirdupois)	4.448E + 00	newton
poundal	1.382E − 01	newton

[a] Factors with asterisk are exact.

Table B.4 Conversion To SI Units[a]

MULTIPLY THIS UNIT	BY	TO OBTAIN THIS SI UNIT
	LENGTH	
angstrom	1.00 * E − 10	meter
ft	3.048 * E − 01	meter
in.	2.54 * E − 02	meter
micron	1.00 * E − 06	meter
mil	2.54 * E − 05	meter
	MASS	
kgf s^2/meter (mass)	9.806 65 * E + 00	kilogram
kilogram · mass	1.00 * E + 00	kilogram
lbm (pound mass, avoirdupois)	4.535 924E − 01	kilogram
slug	1.459 390E + 01	kilogram
	POWER	
Btu (thermochemical)/s	1.054E + 03	watt
Btu (thermochemical)/min	1.757E + 01	watt
calorie (thermochemical)/s	4.184 * E + 00	watt
calorie (thermochemical)/min	6.973E − 02	watt
ft lbf/h	3.766E − 04	watt
ft lbf/min	2.259E − 02	watt
ft lbf/s	1.355E + 00	watt
hp (550 ft lbf/s)	7.456E + 02	watt
kilocalorie (thermochemical)/min	6.973E + 01	watt
kilocalorie (thermochemical)/s	4.184 * E + 03	watt
	PRESSURE	
atmosphere	1.013 25 * E + 05	pascal
bar	1.00 * E + 05	pascal
dyne/cm^2	1.00 * E − 01	pascal
in. of mercury (60°F)	3.376 85E + 03	pascal
in. of water (60°F)	2.4884E + 02	pascal
kgf/cm^2	9.806 65 * E + 04	pascal
lbf/ft^2	4.788 026E + 01	pascal
$lbf/in.^2$ (psi)	6.894 757 2E + 03	pascal
mm of mercury (0°C)	1.333 224E + 02	pascal
torr (0°C)	1.333 224E + 02	pascal
N/m^2	1.00 * E + 00	pascal
	SPEED	
miles/h	4.4704E − 01	meter/s
ft/min	5.08E − 03	meter/s
in./s	2.54 * E − 02	meter/s
	TEMPERATURE	
Celsius	$T_K = T_C + 273.15$	kelvin
Fahrenheit	$T_K = (5/9)(T_F + 459.67)$	kelvin
Fahrenheit	$T_C = (5/9)(T_F - 32)$	celsius
Rankine	$T_K = (5/9)T_R$	kelvin

Table B.4 Conversion To SI Units[a] (*Continued*)

MULTIPLY THIS UNIT	BY	TO OBTAIN THIS SI UNIT
	THERMAL CONDUCTIVITY	
Btu/h ft °F	1.731E + 00	watt/meter kelvin
Btu/s in. °F	7.478E + 04	watt/meter kelvin
	VISCOSITY	
centistoke	1.00 * E − 06	meter^2/second
ft^2/s	9.290 304 * E − 02	meter^2/second
in.^{2}/s	6.4516 * E − 04	meter^2/second
centipoise	1.00 * E − 03	pascal-second
lbf s/ft^2	4.788 026E + 01	pascal-second
poise	1.00 * E − 01	pascal-second
lbf s/in.^{2} (reyn)	6.894 757E + 03	pascal-second
rhe (1/pascal s)	1.00 * E + 01	meter^2/newton second
Saybolt Sec Universal[b]		
	VOLUME	
fluid ounce (U.S. fluid)	2.957 353E − 05	meter^3
ft^3	2.831 685E − 02	meter^3
gallon (U.K. liquid)	4.546 092E − 03	meter
gallon (U.S. dry)	4.404 884E − 03	meter^3
gallon (U.S. liquid)	3.785 412E − 03	meter^3
in.^{3}	1.638 706E − 05	meter^3
litre	1.00 * E − 03	meter^3
	TORQUE	
ft lbf	1.355 82E + 00	N-m
	SPECIFIC FUEL CONSUMPTION	
lbm/hp h	6.083 6E − 01	kg/kw · h

[a] Factors with asterisk are exact.
[b] Saybold Sec Universal and other units see Table B.5.

Table B.5 Kinematic and Saybolt Viscosity Equivalents

EQUIVALENT SAYBOLT UNIVERSAL VISCOSITY (s)			EQUIVALENT SAYBOLT UNIVERSAL VISCOSITY (s)		
KINEMATIC VISCOSITY (mm^2/s)	AT 100°F (37.78°C)	AT 210°F (98.9°C)	KINEMATIC VISCOSITY (mm^2/s)	AT 100°F (37.78°C)	AT 210°F (98.9°C)
2	32.6	32.8	28	132.6	133.5
2.5	34.3	34.5	29	137.0	138.0
3	36.0	36.2	30	141.5	142.5
3.5	37.6	37.8	31	146.0	147.0
4	39.2	39.5	32	150.5	151.5
4.5	40.8	41.1	33	155.0	156.0
5	42.4	42.7	34	159.5	160.6
6	45.6	45.9	35	164.0	165.1
7	48.8	49.1	36	168.6	169.7
8	52.1	52.4	37	173.1	174.3
9	55.4	55.8	38	177.6	178.8
10	58.8	59.2	39	182.2	183.4
11	62.4	62.8	40	186.8	188.0
12	66.0	66.4	41	191.3	192.6
13	69.7	70.2	42	195.9	197.2
14	73.5	74.0	43	200.0	201.0
15	77.4	77.9	44	205.0	206.0
16	81.4	81.9	45	210.0	211.0
17	85.4	86.0	46	214.0	215.0
18	89.5	90.1	47	219.0	220.0
19	93.6	94.3	48	223.0	224.0
20	97.8	98.5	49	228.0	229.0
21	102.1	102.7	50	233.0	234.0
22	106.3	107.0	55	256.0	257.0
23	110.6	111.4	60	279.0	280.0
24	115.0	115.8	65	302.0	303.0
25	119.4	120.2	70	325.0	326.0
26	123.7	124.6	Over 75	SUS = mm^2/s ×4.632	SUS = mm^2/s ×4.664
27	128.2	129.0			

Source ASTM Standards on Petroleum Products and Lubricants, D-2161.

Appendix C

THERMODYNAMIC DERIVATIVES

The subroutines FARG and ECP return three partial derivatives, namely c_P, $(\partial \ln v/\partial \ln P)_T$, and $(\partial \ln v/\partial \ln T)_P$. Any other derivative that may be required can be determined from these. Adopting the notation

$$\left(\frac{\partial y}{\partial x}\right)_z = \frac{(\partial y)_z}{(\partial x)_z}$$

the following list can be used to construct any required derivative:[1]

$$(\partial T)_P = -(\partial P)_T = 1$$

$$(\partial v)_P = -(\partial P)_v = \frac{v}{T}\left(\frac{\partial \ln v}{\partial \ln T}\right)_P$$

$$(\partial s)_P = -(\partial P)_s = \frac{c_P}{T}$$

$$(\partial u)_P = -(\partial P)_u = c_P - \frac{Pv}{T}\left(\frac{\partial \ln v}{\partial \ln T}\right)_P$$

$$(\partial h)_P = -(\partial P)_h = c_P$$

$$(\partial v)_T = -(\partial T)_v = -\frac{v}{P}\left(\frac{\partial \ln v}{\partial \ln P}\right)_T$$

$$(\partial s)_T = -(\partial T)_s = \frac{v}{T}\left(\frac{\partial \ln v}{\partial \ln T}\right)_P$$

$$(\partial u)_T = -(\partial T)_u = v\left[\left(\frac{\partial \ln v}{\partial \ln T}\right)_P + \left(\frac{\partial \ln v}{\partial \ln P}\right)_T\right]$$

$$(\partial h)_T = -(\partial T)_h = -v\left[1 - \left(\frac{\partial \ln v}{\partial \ln T}\right)_P\right]$$

$$(\partial s)_v = -(\partial v)_s = \frac{v}{T}\left[\frac{c_P}{P}\left(\frac{\partial \ln v}{\partial \ln P}\right)_T + \frac{v}{T}\left(\frac{\partial \ln v}{\partial \ln T}\right)_P^2\right]$$

[1] *Source* G. N. Lewis and M. Randall, *Thermodynamics*, McGraw–Hill, New York, 1961, p. 667–668 (consult for derivatives involving either the Gibb's or Helmholtz's free energies).

$$(\partial u)_v = -(\partial v)_u = v\left[\frac{c_P}{P}\left(\frac{\partial \ln v}{\partial \ln P}\right)_T + \frac{v}{T}\left(\frac{\partial \ln v}{\partial \ln T}\right)_P^2\right]$$

$$(\partial h)_v = -(\partial v)_h = v\left[\frac{c_P}{P}\left(\frac{\partial \ln v}{\partial \ln P}\right)_T + \frac{v}{T}\left(\frac{\partial \ln v}{\partial \ln T}\right)_P^2 - \frac{v}{T}\left(\frac{\partial \ln v}{\partial \ln T}\right)_P\right]$$

$$(\partial u)_s = -(\partial s)_u = \frac{Pv}{T}\left[\frac{c_P}{P}\left(\frac{\partial \ln v}{\partial \ln P}\right)_T + \frac{v}{T}\left(\frac{\partial \ln v}{\partial \ln T}\right)_P^2\right]$$

$$(\partial h)_v = -(\partial v)_h = v\left[\frac{c_P}{P}\left(\frac{\partial \ln v}{\partial \ln P}\right)_T + \frac{v}{T}\left(\frac{\partial \ln v}{\partial \ln T}\right)^2 - \frac{v}{T}\left(\frac{\partial \ln v}{\partial \ln T}\right)\right]$$

$$(\partial u)_s = -(\partial s)_u = \frac{Pv}{T}\left[\frac{c_P}{P}\left(\frac{\partial \ln v}{\partial \ln P}\right)_T + \frac{v}{T}\left(\frac{\partial \ln v}{\partial \ln T}\right)_P^2\right]$$

$$(\partial h)_s = -(\partial s)_h = -\frac{vc_P}{T}$$

$$(\partial h)_u = -(\partial u)_h = -v\left[c_P - \frac{Pv}{T}\left(\frac{\partial \ln v}{\partial \ln T}\right)_P\right] - Pv\left[\frac{c_P}{P}\left(\frac{\partial \ln v}{\partial \ln P}\right)_T + \frac{v}{T}\left(\frac{\partial \ln v}{\partial \ln T}\right)^2\right]$$

Appendix D

IDEAL GAS PROPERTIES OF AIR

T (K)	γ	h (J/g)	u (J/g)	P_r[a]	v_r	$\nu \cdot 10^6$ (m^2/s)	$\lambda \cdot 10^3$ (W/m·k)
298	1.400	0.00	−85.54	1.000 + 00	1.000 + 00	15.71	26.1
300	1.400	1.98	−84.13	1.012 + 00	9.916 − 01	15.89	26.3
350	1.397	51.89	−48.58	1.740 + 00	6.727 − 01	20.92	30.0
400	1.394	102.34	−12.47	2.795 + 00	4.784 − 01	26.41	33.8
450	1.390	153.34	24.18	4.262 + 00	3.530 − 01	32.39	37.3
500	1.386	204.89	61.37	6.239 + 00	2.678 − 01	38.79	40.7
550	1.381	256.97	99.10	8.836 + 00	2.082 − 01	45.57	43.9
600	1.376	309.58	137.36	1.217 + 01	1.649 − 01	52.69	46.9
650	1.370	362.73	176.15	1.638 + 01	1.327 − 01	60.21	49.7
700	1.365	416.39	215.47	2.162 + 01	1.082 − 01	68.10	52.4
750	1.360	470.58	235.30	2.804 + 01	8.942 − 02	76.37	54.9
800	1.355	525.29	295.66	3.587 + 01	7.454 − 02	84.93	57.3
850	1.350	580.51	336.52	4.528 + 01	6.276 − 02	93.80	59.6
900	1.345	636.23	377.90	5.648 + 01	5.327 − 02	102.9	62.0
950	1.340	692.46	419.78	6.981 + 01	4.553 − 02	112.2	64.3
1000	1.336	749.17	462.15	8.544 + 01	3.915 − 02	121.9	66.7
1100	1.328	864.17	548.39	1.248 + 02	2.947 − 02	141.8	71.5
1200	1.321	981.07	636.58	1.777 + 02	2.259 − 02	162.9	76.3
1300	1.314	1099.9	726.67	2.469 + 02	1.761 − 02	185.1	82
1400	1.309	1220.5	818.67	3.366 + 02	1.391 − 02	213	91
1500	1.303	1343.1	912.47	4.512 + 02	1.112 − 02	240	100
1600	1.298	1467.4	1008.1	5.957 + 02	8.983 − 03	268	106
1700	1.293	1593.5	1105.6	7.765 + 02	7.326 − 03	298	113
1800	1.288	1721.4	1204.7	1.000 + 03	6.016 − 03	329	120
1900	1.281	1851.0	1305.6	1.276 + 03	4.980 − 03	362	128
2000	1.273	1982.2	1408.1	1.613 + 03	4.147 − 03	396	137

Other Properties at Atmospheric Conditions (T = 298 K, P = 1 atm)		
$R = 0.28704$ J/g-K	$\mu = 1.836 \times 10^{-5}$ N·s/m^2	$\mathscr{D}^c = 5.68 \times 10^{-6}$ m^2/s
$\rho = 1.1707$ kg/m^3	$\alpha = 2.22 \times 10^{-5}$ m^2/s	$P_r^b = 0.707$
$c_P = 1.007$ J/g-K	$c = 345.94$ m/s	$S_c^c = 2.77$
$M = 28.966$ g/mole	$v = 0.8542$ m^3/kg	$L_e^c = 3.91$

[a]Relative pressure for isentropic process.
[b]Prandtl number.
[c]Binary diffusion with octane.
Source: R. B. Bird, W. E. Stewart, and E. N. Lightfoot, *Transport Phenomena*, Wiley, New York, 1960; F. P. Incropera and D. P. DeWitt, *Fundamentals of Heat Transfer*, Wiley, New York, 1981; T. F. Irvine, Jr. and P. E. Liley, *Tables and Computer Equations for Steam and Gases*, Academic, New York, 1984.

Appendix E

FUEL–AIR CYCLES VIA CHARTS

This section is intended to serve those users of the text who do not have access to a computer or who are convinced that learning by using tables and charts ensures a greater familiarity with the characteristics of the state and process relationships being employed. It is particularly appropriate for use in an undergraduate course.

To minimize the number of tables and charts required some simplifying assumptions are made that require introduction of the concepts of sensible and chemical enthalpy. First note the following identity

$$h(T) = h(T) - h(298) + h(298) \tag{E.1}$$

The sensible enthalpy is defined as the difference between the enthalpy at temperature T and the enthalpy at 298 kelvin. The chemical enthalpy is defined as the enthalpy of the substance at 298 kelvin.

The sensible enthalpy is evaluated by

$$h(T) - h(298) = \int_{298}^{T} c_P \, dT \tag{E.2}$$

Since the fuel concentration is only a few percent, the fuel contributes little to the specific heat. The predominant species is nitrogen in both the fuel–air mixture and the resultant combustion products, of which the residual gas is composed. The specific heat is therefore a weak function of both the residual mass fraction and the equivalence ratio.

In essence, the sensible enthalpy depends only on temperature and may be evaluated from an air table (Appendix D) which is the special case of $\phi = f = 0$. This approach will typically overestimate the temperature at the end of the compression process by about 50 kelvin. It is important that the student recognize that although a more accurate calculation can be done, exactly the same principles about to be illustrated are employed.

The chemical enthalpy, on the other hand, is independent of temperature (since it is the enthalpy at 298 K) and depends on equivalence ratio and

residual fraction. The chemical enthalpy of a mixture of N species is given by

$$h(298) = \sum_{i=1}^{N} y_i h^0_{f,i,298} \tag{E.3}$$

where $h^0_{f,i,298}$ is the enthalpy of formation at 298 K of species i. Table E.1 lists the enthalpy of formation of some species important in combustion analysis. Notice that the enthalpies of formation of nitrogen and oxygen are zero. Thus air contributes nothing to the chemical enthalpy of a fuel–air mixture. In a fuel–air–residual gas mixture the enthalpy is predominantly determined by the fuel and partly by species such as water and carbon dioxide in the residuals.

For a given residual fraction f, the enthalpy of a fuel–air–residual gas mixture is

$$h = (1-f)h_{fa} + fh_r \tag{E.4}$$

where h_{fa} is the enthalpy of the fuel–air alone and h_r is the enthalpy of the residuals alone. Since the residual mass fraction and residual mole fraction are nearly equal, a good approximation for the molecular weight of a fuel–air–residual gas mixture is

$$M \approx (1-f)M_{fa} + fM_r \tag{E.5}$$

Table E.2 gives the chemical enthalpies and molecular weights of fuel–air mixtures and residual gases for isooctane fuel. Using the process relationships developed in Chapter 4, five example calculations now follow using tables and charts for the equations of state.

Table E.1 Enthalpies of Formation and Molecular Weights of Some Species

SPECIES	SYMBOL (STATE)	$h^o_{f,298}$ (kcal/mol)	M (g/mole)
Carbon	C(s)	0.000	12.01
Carbon monoxide	CO(g)	−26.417	28.01
Carbon dioxide	CO_2(g)	−94.054	44.01
Hydrogen	H_2(g)	0.000	2.018
Water	H_2O(g)	−57.798	18.02
Nitrogen	N_2(g)	0.000	28.008
Oxygen	O_2(g)	0.000	32.00
Methane	CH_4(g)	−17.89	16.04
Propane	C_3H_8(g)	−24.82	44.09
Isooctane	C_8H_{18}(l)	−61.97	114.22
	C_8H_{18}(g)	−53.57	
Cetane	$C_{16}H_{34}$(l)	−108.62	226.47

Table E.2 Chemical Enthalpy and Molecular Weight of Isooctane $C_8H_{18}(g)$ Air Mixtures and Their Residual Products

$\phi = F/F_s$	0.8	1.0	1.2
h_{fa} (cal/g)	−23.70	−29.25	−34.66
h_r (cal/g)	−563.0	−695.1	−649.5
M_{fa} (g/mole)	29.98	30.26	30.54
M_r (g/mole)	28.65	28.60	27.50

EXAMPLE E.1

Find the enthalpy (cal/g) and specific volume (cm^3/g) of an isooctane fuel–air–residual gas mixture at $T = 500$ K, $P = 10$ bar, $\phi = 1.0$ and $f = 0.10$.

SOLUTION:

The chemical enthalpy is

$$h(298) = (1-0.10)(-29.25) + 0.10(-695.1) = -95.80 \text{ cal/g}$$

From Appendix D the sensible enthalpy is

$$h(500) - h(298) = 204.89 - 0 = 204.89 \text{ J/g} = 48.97 \text{ cal/g}$$

Therefore the enthalpy is

$$h(500) = 48.97 - 95.80 = -46.83 \text{ cal/g}$$

The specific volume will be calculated from the ideal gas law where the molecular weight is

$$M = (1-0.10)(30.26) + 0.10(28.60) = 39.09 \text{ g/mole}$$

Hence

$$v = \frac{\left(8.314 \frac{\text{J}}{\text{mole K}}\right)(500 \text{ K})\left(\frac{\text{N-m}}{\text{J}}\right)\left(\frac{10^6 \text{cm}^3}{\text{m}^3}\right)}{\left(30.09 \frac{\text{g}}{\text{mole}}\right)(10 \text{ bar})\left(\frac{10^5 \text{ N/m}^2}{\text{bar}}\right)} = 138.2 \frac{\text{cm}^3}{\text{g}}$$

For isentropic processes involving fuel–air–residual gas mixtures, recall from thermodynamics the concepts of a relative pressure P_r and a relative volume v_r. For any isentropic process, by definition

$$\frac{v_2}{v_1} = \frac{v_{r2}}{v_{r1}} \quad \text{and} \quad \frac{P_2}{P_1} = \frac{P_{r2}}{P_{r1}} \tag{E.6}$$

The relative volume and pressure depend upon the specific heat of the mixture

$$P_r = \exp\left(\int_{298}^{T} \frac{c_p}{R}\frac{dT}{T}\right) \tag{E.7}$$

$$v_r = \frac{T}{298}\frac{1}{P_r} \tag{E.8}$$

Since the specific heat is weakly dependent upon the equivalence ratio and residual fraction, an air table may be used to approximately evaluate the relative volume and pressure of a fuel–air–residual gas mixture.

EXAMPLE E.2

Fuel–air–residual gas initially at $T = 300$ K, $P = 1$ bar is isentropically compressed by a volume ratio $v_2/v_1 = 0.125$. Find the final temperature (K) and the work done (cal/g) if $\phi = 0.8$ and $f = 0.05$.

SOLUTION:

From Appendix D, $v_{r1} = 0.9916$. Therefore

$$v_{r2} = (0.9916)(0.125) = 0.1239$$

By interpolation, it follows that

$$T_2 = 668 \text{ K}$$

The work done on the gas is given by

$$w_{1\to 2} = u_2 - u_1$$
$$= (h_2 - h_1) - R(T_2 - T_1)$$

Notice that the chemical enthalpy need not be evaluated since it is a constant added to the sensible enthalpies at states 1 and 2. Since only sensible changes are required, u_1 and u_2 may be read directly from Appendix D; hence

$$w_{1\to 2} = 190.27 - (-84.139) = 274.40 \text{ J/g} = 65.58 \text{ cal/g}$$

EXAMPLE E.3

Figures E-1 through E-3 give the thermodynamic properties of equilibrium combustion products corresponding to any fuel with a hydrogen to carbon ratio of 2.25 that is burned with air. The charts are for a lean, a stoichiometric, and a rich case; $\phi = 0.8$, 1.0, and 1.2, respectively.

Find the indicated mean effective pressure and efficiency of an Otto fuel–air cycle given the following data:

$r = 10$	$P_1 = 1$ bar	$T_1 = 350$ K
$f = 0.10$	$\phi = 1.0$	fuel = isooctane, $C_8H_{18}(l)$

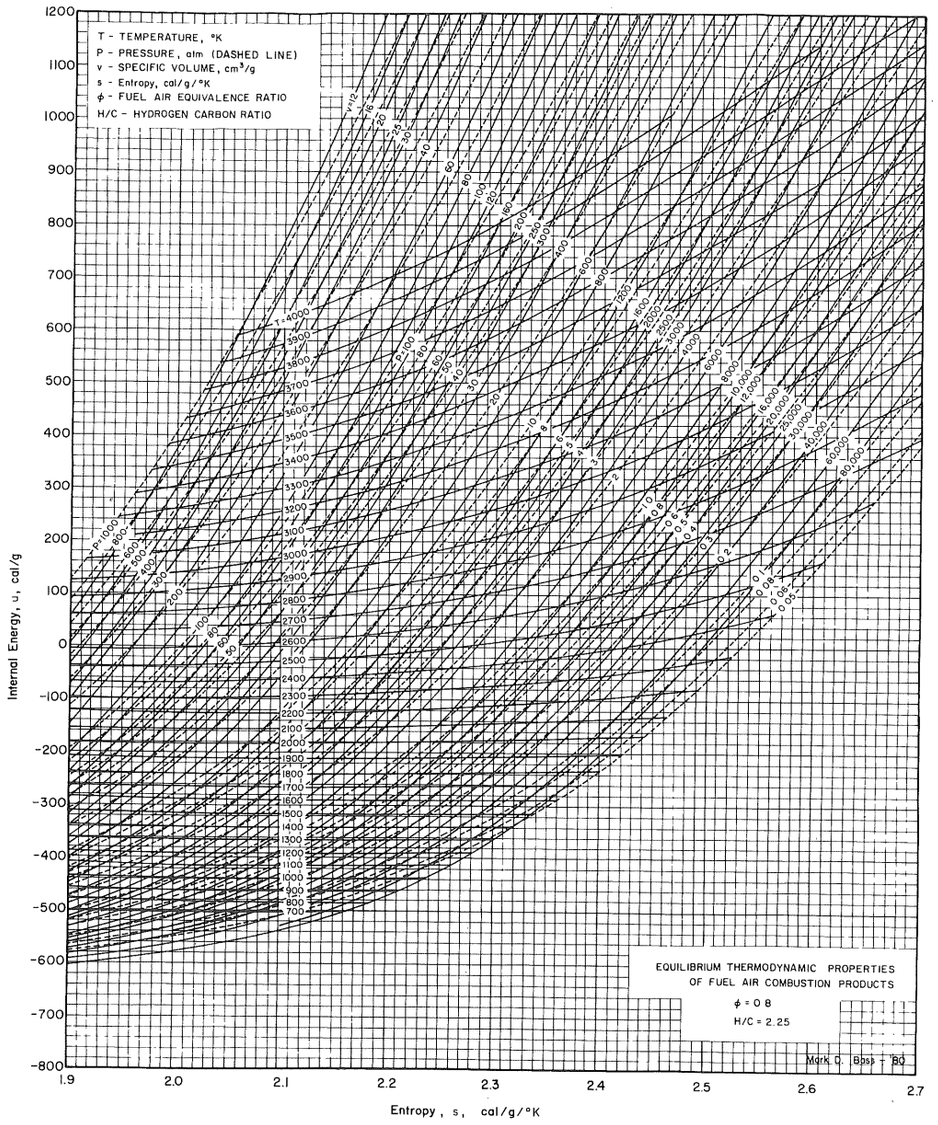

Figure E.1

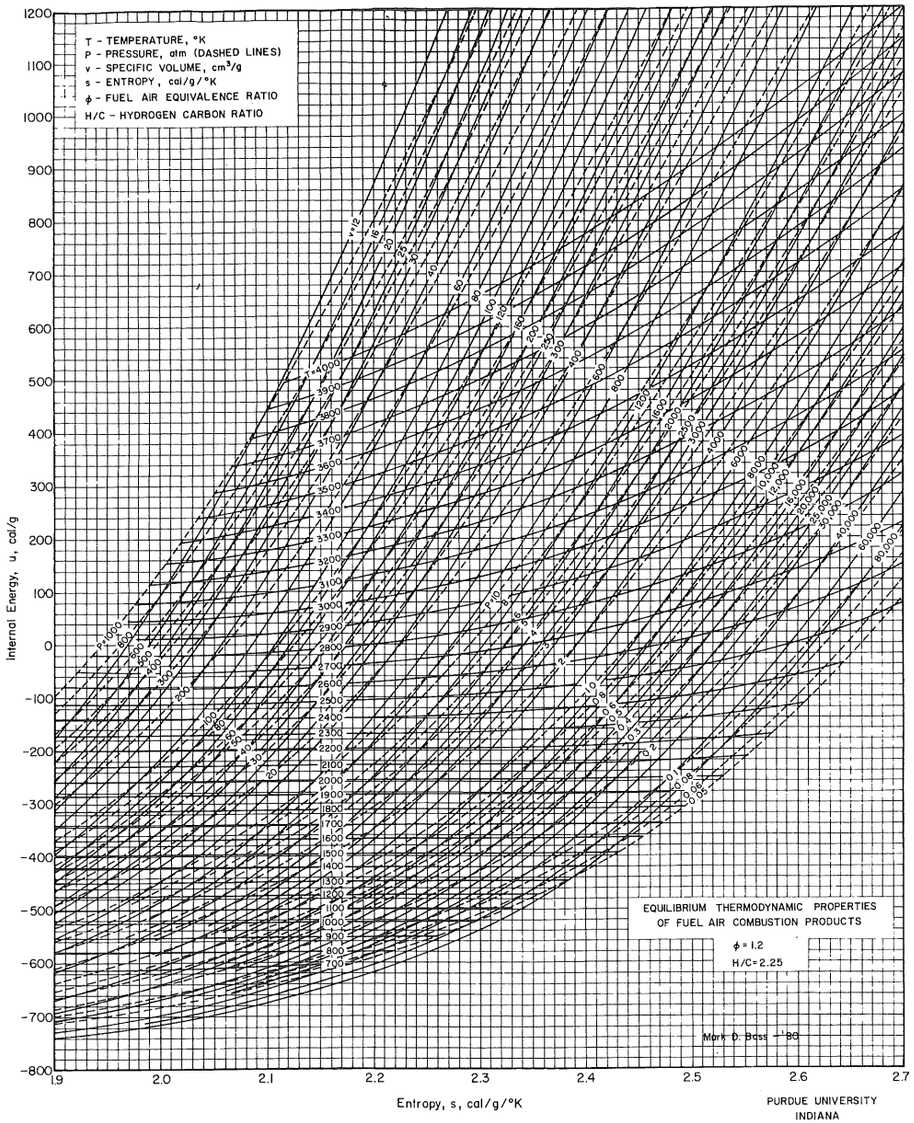

Figure E.2

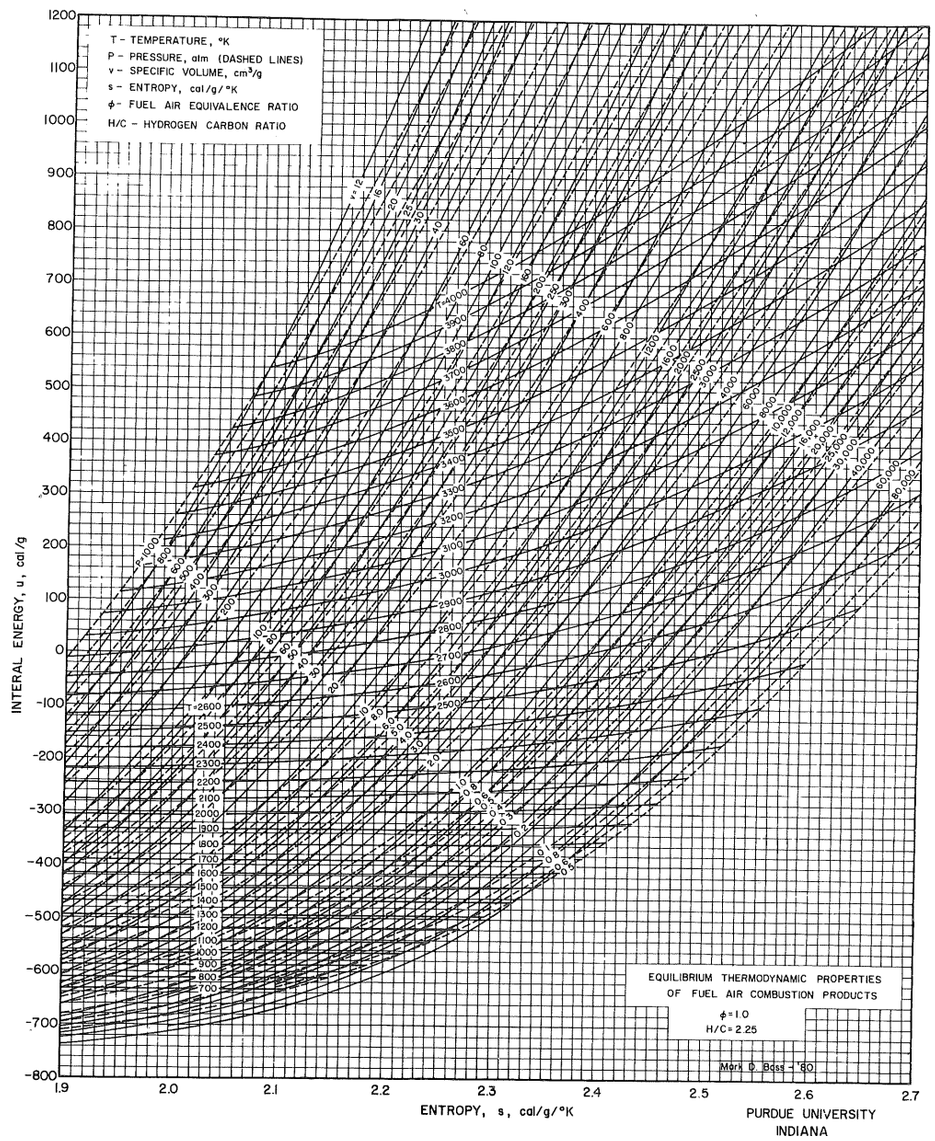

Figure E.3

SOLUTION:

Assume at state 1 that the fuel is entirely evaporated. From $1 \rightarrow 2$, the fuel–air–residual gas is isentropically compressed. As in Example E.2

$$v_{r1} = 0.6727$$
$$v_{r2} = (0.6727)/10 = 0.06727$$
$$T_2 = 831 \text{ K}$$
$$w_{1\rightarrow 2} = 320.88 - (-48.58) = 369.46 \text{ J/g}$$
$$= 88.30 \text{ cal/g}$$

Combustion occurs at constant volume and constant energy, $v_3 = v_2$ and $u_3 = u_2$. Thus v_2 and u_2 need to be evaluated. From Example E.1, the molecular weight and chemical enthalpy of the fuel–air residual gas are 30.09 g/mole and -95.80 cal/g. Hence

$$v_1 = \frac{(8.314)(350)(10^6)}{(30.09)(1)(10)^5} = 967 \text{ cm}^3/\text{g}$$

$$v_2 = v_1/10 = 96.7 \text{ cm}^3/\text{g}$$

The sensible energy at the end of the compression was already found to be 320.88 J/g = 76.69 cal/g. Hence

$$u_2 = 76.69 - 95.80 = -19.11 \text{ cal/g}$$

State 3 is found on the chart E.2 which is for stoichiometric equilibrium combustion products. At $u_3 = -19.11$ cal/g and $v_3 = 96.7$ cm^3 = g, read

$$T_3 = 2790 \text{ K} \qquad P_3 = 85 \text{ atm} \qquad s_3 = 2.068 \text{ cal/g/K}$$

The equilibrium products are expanded isentropically to $v_4 = 10\, v_3 = 967$ cm^3/g. At v_4, s_4 read from the chart

$$T_4 = 1740 \text{ K} \qquad P_4 = 54 \text{ atm} \qquad u_4 = -380 \text{ cal/g}$$

The work done by expanding the gases is

$$w_{3-4} = u_3 - u_4 = -19.1 - (-380) = 360.9 \text{ cal/g}$$

The work of the cycle and the imep are therefore

$$w = 360.9 - 88.3 = 272.6 \text{ cal/g} = 1140 \text{ J/g}$$

$$\text{imep} = \frac{w}{v_1 - v_2} = \frac{(1140)(10)}{967 - 96.7} = 13.1 \text{ bar}$$

Finally the efficiency is

$$\eta = \frac{w(1 + \phi F_s)}{\phi F_s (1 - f) a_o} = \frac{1140(1 + 0.0665)}{0.0665(0.9)(47670)} = 0.426$$

EXAMPLE E.4

Find the net indicated mean effective pressure and efficiency of an Otto fuel–air cycle with the ideal four-stroke and intake process. The following data are given

$r = 10$ $\qquad P_i = 0.5$ atm $\qquad T_i = 350$ K
$\phi = 1.0$ $\qquad$ fuel = isooctane, $C_8H_{18}(l)$

SOLUTION:

As in Example 2.4, iteration is required. To begin, guess that

$$f = 0.10 \qquad T_1 = 350 \text{ K}$$

Following the methodology in Example E.3, one obtains

$v_{r1} = 0.6727$	$v_{r2} = 0.06727$	$T_2 = 831$ K
$v_1 = 1934$ cm^3/g	$v_2 = 193.4$ cm^3/g	$u_2 = -19.11$ cal/g
$T_3 = 2770$ K	$P_3 = 42$ atm	$s_3 = 2.118$ cal/g/k
$T_4 = 1740$ K	$P_4 = 2.5$ atm	$u_4 = -380$ cal/g

From 4 to 5, the gases expand isentropically to the exhaust pressure. Hence at $P_5 = 1$ atm, $s_5 = 2.120$ cal/g/K, read from Chart E.2

$$T_5 = 1430 \text{ K} \qquad v_5 = 4050 \text{ cm}^3/\text{g} \qquad u_5 = -460 \text{ cal/g}$$

The residual fraction is

$$f = \frac{1}{r}\frac{v_4}{v_5} = \frac{1}{10}\frac{1934}{4050} = 0.0478$$

At the end of induction, the enthalpy of the fuel–air–residual gas is

$$h_1 = f\left[h_5 + (P_i - P_e)v_5\right] + (1 - f)h_i$$

where the enthalpy of the inducted fuel–air mixture is

$$h_i = \frac{51.89}{4.184} + (-29.25) = -16.81 \text{ cal/g}$$

The enthalpy at state 5 is

$$h_5 = u_5 + P_5 v_5 = -460 + \frac{(1)(1.013 \times 10^5)(4050)}{(10^6)(4.184)} = -361.9 \text{ cal/g}$$

It follows then that

$$h_1 = 0.0478\left[-361.9 + \frac{(0.5 - 1.0)(1.013 \times 10^5)(4050)}{(10^6)(4.184)}\right] + 0.952(-16.81)$$
$$= -35.6 \text{ cal/g}$$

The chemical enthalpy at state 1, with $f = 0.0478$, is

$$h_{c1} = (0.0478)(-695.1) + 0.952(-29.21) = -61.0 \text{ cal/g}$$

So the sensible enthalpy at state 1 is

$$h_{s1} = -35.6 - (-61.0) = 25.4 \text{ cal/g} = 106 \text{ J/g}$$

From Appendix D, at $h = 106$ J/g, interpolation yields

$$T_1 = 404 \text{ K}$$

The computation is now repeated with $f = 0.05$ and $T_1 = 400$ K. (The numbers are rounded off since they are still approximate and rounding minimizes interpolation.) An iteration table follows.

		ITERATION		
SYMBOL	UNITS	1	22	3
f	—	0.10	0.05	0.051
T_1	K	350	400	416
v_{r1}	—	0.6727	0.4784	0.4383
v_{r2}	—	0.0673	0.0478	0.0438
T_2	K	831	935	964
M_2	g/mole	30.09	30.18	30.18
h_{c2}	cal/g	−95.80	−62.50	−63.2
v_2	cm³/g	193.4	220.3	229.2
u_2	cal/g	−19.1	30.8	40.7
T_3	K	2770	2860	2875
P_3	atm	42	38	38
s_3	cal/g/K	2.118	2.145	2.151
v_4	cm³/g	1934	2204	2292
T_4	K	1740	1850	1875
P_4	atm	2.5	2.4	2.5
u_4	cal/g	−380	−345	−340
T_5	K	1430	1550	1590
v_5	cm³/g	4050	4300	4400
u_5	cal/g	−460	−420	−420
f	—	0.0478	0.051	0.052
h_i	cal/g	−16.81	−16.81	−16.81
h_5	cal/g	−361.9	−315.9	−313.4
h_1	cal/g	−35.6	−34.7	−35.0
h_{c1}	cal/g	−61.0	−63.2	−63.8
h_{s1}	J/g	160	119	121
T_1	K	404	416	418

Three iterations in this type of calculation usually brings one to convergence as best as can be obtained within the accuracy for which the charts can be read. Once convergence is realized for both f and T_1, the indicated work, mean effective pressure, and thermal efficiency may be determined.

$$w = u_1 - u_4 = [(-7.4/4.184) - 63.8] - (-340) = 274 \text{ cal/g}$$

$$\text{imep} = \frac{(274)(10^6)(4.184)}{(2292 - 229)(10^5)} = 5.56 \text{ bar}$$

$$\eta = \frac{(274)(4.184)(1.0665)}{(0.0665)(0.949)(47670)} = 0.406$$

Account of the pumping work yields

$$(\text{imep})_{\text{net}} = 5.56 - 0.05 = 5.06 \text{ bar}$$

$$\eta_{\text{net}} = 0.406(1 - 0.5/5.56) = 0.370$$

In both Example E.3 and E.4 the maximum available energy used in the efficiency computation is based on the fuel in its liquid state since that is its natural state at atmospheric conditions.

EXAMPLE E.5

Find the indicated mean effective pressure and thermal efficiency of a fuel-injected limited pressure fuel–air cycle given the following

$r = 15$ $\quad P_1 = 2.0$ bar $\quad T_1 = 400$ K
$\phi = 0.8$ $\quad P_{\text{limit}} = 100$ bar $\quad P_f = 150$ bar
$T_f = 298$ K $\quad f = 0.05$ $\quad$ Fuel = octane, $C_8H_{18}(l)$

SOLUTION:

The compression of the air–residual gas mixture is isentropic and evaluated using Appendix D. Hence

$v_{r1} = 0.4784$ $\quad u_{s1} = -12.47$ J/g
$v_{r2} = 0.4784/15 = 0.0319$ $\quad T_2 = 1075$ K
$P_2 = P_1 \dfrac{T_2}{T_1}\dfrac{v_1}{v_2} = 2\dfrac{1075}{400}15 = 80.6 < P_{\text{limit}}$ $\quad u_{s2} = 526.8$ J/g

The enthalpy of the fuel to be injected is evaluated from Eq. (3.106) and Table 3.5

$$h_f = (-20845 - 41510)/114.22 + (150 - 1.01)(1.423)10^5/10^6 = -2167 \text{ J/g}$$

The enthalpy at state 3, is given by Eq. (4.22). Since

$$u_2 = 526.8 + (0.05)(-563.0)(4.184) = 408.2 \text{ J/g}$$
$$M_2 = (0.95)(28.84) + (0.05)(28.65) = 28.83 \text{ g/mole}$$
$$v_2 = \frac{(8.314)(1075)(10^6)}{(28.83)(80.6)(10^5)} = 38.46 \text{ cm}^3/\text{g}$$

It follows then that

$$h_3 = \frac{408.2 + (100)(38.46)/10 + (0.95)(0.8)(0.0665)(-2167)}{1 + (0.95)(0.8)(0.0665)}$$
$$= 650.4 \text{ J/g} = 155.5 \text{ cal/g}$$

Also

$$P_3 = 100 \text{ bar} = 98.7 \text{ atm}$$

Chart E.1 applies since $\phi = 0.8$. However, enthalpy is not plotted. Thus we must iterate to locate state 3. We know that

$$u_3 < h_3$$

So let us start by assuming $u_3 = -100$ cal/g. Then on the chart at $P_3 = 98.7$ atm read

$$v_3 = 69 \text{ cm}^3/\text{g}$$

Now compute

$$h_3 = u_3 + P_3 v_3 = (-100)(4.184) + \frac{(100)(69)}{10} = 271.6$$

(The reader should verify the factor of 10 used for units conversion.) This is too small since h_3 is known to be 650.4, therefore a larger value of u_3 should be assumed. A summary of iterations follows.

u_3	v_3	h_3
−100	69	217.6
0	75	750
−20	74	656

The temperature and entropy at $u_3 = -20$, $P_3 = 98.7$ atm are

$$T_3 = 2550 \text{ K} \qquad s_3 = 1.996 \text{ cal/g/K}$$

The gases are expanded isentropically to $v_4 = 14.3$, $v_2 = 549$ cm^3/g; see Eq. (4.25). Read

$$T_4 = 1590 \text{ K} \qquad u_4 = -290 \text{ cal/g} = -1210 \text{ J/g} \qquad P_4 = 9.5 \text{ atm}$$

To compute the indicated work, find by Eq. (4.26) through (4.28)

$$w_{12} = \frac{(u_{s1} - u_{s2})}{1 + \phi F_s(1-f)} = \frac{-12.5 - 526.8}{1 + 0.8(0.0665)(0.95)} = -513 \text{ J/g}$$

$$w_{23} = 100\left(74 - \frac{38.5}{1 + 0.8(0.0665)(0.95)}\right)\Big/10 = 374 \text{ J/g}$$

$$w_{34} = u_3 - u_4 = -83.7 - (-1210) = 1126 \text{ J/g}$$
$$w_{cv} = -513 + 374 + 1126 = 987 \text{ J/g}$$

Also

$$\text{imep} = \frac{w_{cv}[1 + \phi F_s(1-f)]}{v_1 - v_2} = \frac{987[1 + 0.8(0.0665)(0.95)]10}{(576.9 - 38.5)}$$
$$= 19.3 \text{ bar}$$
$$\eta = \frac{(987)[1 + 0.8(0.0665)(0.95)]}{(0.8)(0.0665)(0.95)(47670)} = 0.430$$

Charts for other fuels, analogous to those given for $C_nH_{2.25n}$, can be found in the literature. Those employing the same datum used here include the charts of Newhall and Starkman (some of which can be found only in the archives of the University of California, College of Engineering, Berkeley) for:

nitroethane	hydrogen	CH_{4n}
nitromethane	ammonia	$C_nH_{2.67n}$
methanol	methanol	C_nH_{2n}

Charts may also be found in Taylor (1977) for octene (or any other hydrocarbon of the form C_nH_{2n}). Taylor's charts are based on a different datum, however; and that difference has to be accounted for in employing the methodology described here.

REFERENCES

Newhall, H. K. and E. S. Starkman (1964), "Thermodynamic Properties of Octane and Air for Engine Performance Calculation," SAE Technical Progress Series, Vol. 7.

Starkman, E. S., H. K. Newhall, and R. D. Sutton (1964), "Comparative Performance of Alcohol and Hydrocarbon Fuels," SAE Special Publications 254.

Taylor, D. F., (1977), *The Internal Combustion Engine in Theory and Practice*, Vol. 1, MIT, Cambridge, Massachusetts.

Appendix F

THERMODYNAMIC DATA FOR IDEAL GASES

TABLE	SPECIES	SYMBOL
1	Carbon dioxide	$-CO_2$
2	Water	$-H_2O$
3	Nitrogen	$-N_2$
4	Oxygen	$-O_2$
5	Carbon monoxide	$-CO$
6	Hydrogen	$-H_2$
7	Hydrogen atom	$-H$
8	Oxygen atom	$-O$
9	Hydroxyl	$-OH$
10	Nitric oxide	$-NO$
11	Nitrogen atom	$-N$
12	Carbon	$-C$
13	Ozone	$-O_3$
14	Octane	$-C_8H_{18}$
	2,2,4-trimethylpentane	$-C_8H_{18}$

Tables Courtesy Dow Chemical Co.

Table F.1. Carbon Dioxide (CO_2); Molecular Weight = 44.00995.

	cal/(mol K)			kcal/mol			
T/K	Cp°	S°	$-(G°-H°_{298})/T$	$H°-H°_{298}$	ΔHf°	ΔGf°	Log K
0	0.000	0.000	INFINITE	-2.238	-93.965	-93.965	INFINITE
100	6.981	42.758	58.188	-1.543	-93.997	-94.100	205.645
200	7.734	47.769	51.849	-0.816	-94.028	-94.191	102.922
298.15	8.874	51.072	51.072	0.000	-94.054	-94.265	69.095
300	8.896	51.127	51.072	0.016	-94.055	-94.267	68.670
400	9.877	53.830	51.434	0.958	-94.070	-94.335	51.540
500	10.666	56.122	52.148	1.987	-94.091	-94.399	41.260
600	11.310	58.126	52.981	3.087	-94.124	-94.458	34.405
700	11.846	59.910	53.845	4.245	-94.169	-94.510	29.506
800	12.293	61.522	54.706	5.453	-94.218	-94.556	25.830
900	12.667	62.992	55.546	6.702	-94.270	-94.596	22.970
1000	12.980	64.344	56.359	7.984	-94.321	-94.628	20.680
1100	13.243	65.594	57.143	9.296	-94.371	-94.658	18.806
1200	13.466	66.756	57.896	10.632	-94.419	-94.681	17.243
1300	13.656	67.841	58.620	11.988	-94.469	-94.701	15.920
1400	13.815	68.859	59.315	13.362	-94.515	-94.716	14.785
1500	13.953	69.817	59.984	14.750	-94.562	-94.728	13.801
1600	14.074	70.722	60.627	16.152	-94.607	-94.739	12.940
1700	14.177	71.578	61.246	17.565	-94.650	-94.746	12.180
1800	14.269	72.391	61.843	18.987	-94.696	-94.750	11.504
1900	14.352	73.165	62.418	20.418	-94.742	-94.751	10.898
2000	14.424	73.903	62.974	21.857	-94.788	-94.752	10.353
2100	14.489	74.608	63.512	23.303	-94.834	-94.746	9.860
2200	14.547	75.284	64.031	24.755	-94.885	-94.744	9.411
2300	14.600	75.931	64.535	26.212	-94.936	-94.735	9.001
2400	14.648	76.554	65.023	27.674	-94.991	-94.724	8.625
2500	14.692	77.153	65.496	29.141	-95.048	-94.714	8.280
2600	14.734	77.730	65.956	30.613	-95.107	-94.698	7.960
2700	14.771	78.286	66.402	32.088	-95.170	-94.683	7.664
2800	14.807	78.824	66.836	33.567	-95.235	-94.662	7.388
2900	14.841	79.344	67.259	35.049	-95.305	-94.639	7.132
3000	14.873	79.848	67.670	36.535	-95.377	-94.615	6.892
3100	14.902	80.336	68.071	38.024	-95.451	-94.587	6.668
3200	14.930	80.810	68.461	39.515	-95.530	-94.560	6.458
3300	14.956	81.270	68.843	41.010	-95.611	-94.531	6.260
3400	14.982	81.717	69.215	42.507	-95.696	-94.495	6.074
3500	15.006	82.151	69.578	44.006	-95.784	-94.462	5.898
3600	15.030	82.574	69.933	45.508	-95.874	-94.421	5.732
3700	15.053	82.986	70.280	47.012	-95.968	-94.379	5.574
3800	15.075	83.388	70.620	48.518	-96.064	-94.331	5.425
3900	15.097	83.780	70.953	50.027	-96.162	-94.286	5.283
4000	15.119	84.162	71.278	51.538	-96.263	-94.237	5.149
4100	15.139	84.536	71.597	53.051	-96.367	-94.186	5.020
4200	15.159	84.901	71.909	54.566	-96.473	-94.130	4.898
4300	15.179	85.258	72.216	56.082	-96.583	-94.072	4.781
4400	15.197	85.607	72.516	57.601	-96.694	-94.015	4.670
4500	15.216	85.949	72.811	59.122	-96.807	-93.954	4.563
4600	15.234	86.284	73.100	60.644	-96.923	-93.885	4.460
4700	15.254	86.611	73.384	62.169	-97.040	-93.818	4.362
4800	15.272	86.933	73.663	63.695	-97.160	-93.746	4.268
4900	15.290	87.248	73.937	65.223	-97.281	-93.678	4.178
5000	15.306	87.557	74.206	66.753	-97.404	-93.603	4.091
5100	15.327	87.860	74.471	68.285	-97.530	-93.528	4.008
5200	15.349	88.158	74.731	69.819	-97.656	-93.450	3.927
5300	15.371	88.451	74.988	71.355	-97.783	-93.361	3.850
5400	15.393	88.738	75.239	72.893	-97.912	-93.280	3.775
5500	15.415	89.021	75.488	74.433	-98.042	-93.190	3.703
5600	15.437	89.299	75.732	75.976	-98.173	-93.104	3.633
5700	15.459	89.572	75.972	77.521	-98.305	-93.017	3.566
5800	15.481	89.841	76.209	79.068	-98.438	-92.918	3.501
5900	15.503	90.106	76.442	80.617	-98.572	-92.820	3.438
6000	15.525	90.367	76.672	82.168	-98.707	-92.724	3.377

Table F.2. Water (H_2O); Molecular Weight = 18.016.

	cal/(mol K)			kcal/mol			
T/K	Cp°	S°	$-(G°-H°_{298})/T$	$H°-H°_{298}$	ΔHf°	ΔGf°	Log K
0	0.000	0. 00	INFINITE	-2.367	-57.101	-57.101	INFINITE
100	7.959	36.396	52.205	-1.581	-57.378	-56.543	123.574
200	7.971	41.916	45.838	-0.784	-57.574	-55.632	60.791
298.15	8.028	45.106	45.106	0.000	-57.795	-54.634	40.047
300	8.030	45.156	45.106	0.015	-57.800	-54.614	39.786
400	8.189	47.485	45.423	0.825	-58.038	-53.516	29.239
500	8.419	49.337	46.027	1.655	-58.273	-52.358	22.885
600	8.682	50.895	46.711	2.510	-58.496	-51.154	18.633
700	8.962	52.254	47.408	3.392	-58.704	-49.914	15.584
800	9.255	53.469	48.091	4.303	-58.899	-48.645	13.289
900	9.557	54.577	48.751	5.243	-59.076	-47.352	11.499
1000	9.863	55.600	49.385	6.214	-59.237	-46.041	10.062
1100	10.166	56.554	49.994	7.216	-59.381	-44.714	8.884
1200	10.461	57.451	50.579	8.247	-59.509	-43.375	7.900
1300	10.742	58.300	51.140	9.307	-59.623	-42.026	7.065
1400	11.007	59.106	51.681	10.395	-59.723	-40.668	6.349
1500	11.255	59.874	52.201	11.508	-59.812	-39.304	5.727
1600	11.484	60.607	52.704	12.645	-59.890	-37.935	5.182
1700	11.696	61.310	53.190	13.805	-59.959	-36.560	4.700
1800	11.890	61.984	53.660	14.984	-60.021	-35.182	4.272
1900	12.069	62.632	54.115	16.182	-60.076	-33.800	3.888
2000	12.232	63.255	54.556	17.397	-60.125	-32.416	3.542
2100	12.386	63.856	54.985	18.628	-60.170	-31.029	3.229
2200	12.526	64.435	55.402	19.874	-60.211	-29.641	2.944
2300	12.655	64.995	55.807	21.133	-60.249	-28.250	2.684
2400	12.773	65.536	56.201	22.405	-60.284	-26.858	2.446
2500	12.883	66.060	56.585	23.688	-60.317	-25.464	2.226
2600	12.985	66.567	56.959	24.981	-60.349	-24.069	2.023
2700	13.079	67.059	57.324	26.284	-60.380	-22.673	1.835
2800	13.167	67.536	57.680	27.597	-60.411	-21.277	1.661
2900	13.248	68.000	58.028	28.917	-60.441	-19.879	1.498
3000	13.324	68.450	58.368	30.246	-60.471	-18.479	1.346
3100	13.395	68.888	58.700	31.582	-60.501	-17.079	1.204
3200	13.461	69.314	59.025	32.925	-60.533	-15.678	1.071
3300	13.524	69.730	59.343	34.274	-60.564	-14.275	0.945
3400	13.582	70.134	59.655	35.629	-60.598	-12.873	0.827
3500	13.637	70.529	59.960	36.990	-60.631	-11.468	0.716
3600	13.689	70.914	60.259	38.357	-60.667	-10.063	0.611
3700	13.738	71.289	60.552	39.728	-60.704	-8.657	0.511
3800	13.785	71.656	60.839	41.104	-60.743	-7.250	0.417
3900	13.829	72.015	61.121	42.485	-60.782	-5.842	0.327
4000	13.870	72.366	61.398	43.870	-60.824	-4.432	0.242
4100	13.910	72.709	61.670	45.259	-60.868	-3.022	0.161
4200	13.948	73.044	61.937	46.652	-60.914	-1.610	0.084
4300	13.983	73.373	62.199	48.048	-60.962	-0.198	0.010
4400	14.018	73.695	62.456	49.449	-61.012	1.216	-0.060
4500	14.050	74.010	62.710	50.852	-61.065	2.630	-0.128
4600	14.082	74.319	62.959	52.259	-61.120	4.047	-0.192
4700	14.112	74.622	63.204	53.668	-61.178	5.464	-0.254
4800	14.141	74.920	63.445	55.081	-61.237	6.883	-0.313
4900	14.167	75.212	63.682	56.496	-61.299	8.303	-0.370
5000	14.194	75.498	63.915	57.914	-61.365	9.724	-0.425
5100	14.223	75.780	64.145	59.335	-61.432	11.146	-0.478
5200	14.252	76.056	64.372	60.759	-61.502	12.570	-0.528
5300	14.280	76.328	64.595	62.186	-61.574	13.995	-0.577
5400	14.308	76.595	64.814	63.615	-61.648	15.421	-0.624
5500	14.336	76.858	65.031	65.047	-61.724	16.849	-0.670
5600	14.364	77.116	65.244	66.482	-61.802	18.279	-0.713
5700	14.392	77.371	65.455	67.920	-61.882	19.709	-0.756
5800	14.421	77.621	65.663	69.361	-61.964	21.141	-0.797
5900	14.449	77.868	65.867	70.804	-62.047	22.576	-0.836
6000	14.477	78.111	66.069	72.250	-62.133	24.010	-0.875

Table F.3. Diatomic Nitrogen (N_2); Molecular Weight 28.0134.

	cal/(mol K)			kcal/mol			
T/K	Cp°	S°	$-(G°-H°_{298})/T$	$H°-H°_{298}$	ΔHf°	ΔGf°	Log K
0	0.000	0.000	INFINITE	-2.072	0.000	0.000	0.000
100	6.956	38.170	51.955	-1.379	0.000	0.000	0.000
200	6.957	42.991	46.406	-0.683	0.000	0.000	0.000
298.15	6.961	45.770	45.770	0.000	0.000	0.000	0.000
300	6.961	45.813	45.770	0.013	0.000	0.000	0.000
400	6.991	47.818	46.043	0.710	0.000	0.000	0.000
500	7.070	49.386	46.560	1.413	0.000	0.000	0.000
600	7.196	50.685	47.142	2.126	0.000	0.000	0.000
700	7.350	51.806	47.730	2.853	0.000	0.000	0.000
800	7.513	52.798	48.303	3.596	0.000	0.000	0.000
900	7.670	53.692	48.853	4.355	0.000	0.000	0.000
1000	7.815	54.508	49.378	5.130	0.000	0.000	0.000
1100	7.945	55.259	49.879	5.918	0.000	0.000	0.000
1200	8.060	55.955	50.357	6.718	0.000	0.000	0.000
1300	8.161	56.605	50.813	7.529	0.000	0.000	0.000
1400	8.250	57.213	51.248	8.350	0.000	0.000	0.000
1500	8.328	57.785	51.665	9.179	0.000	0.000	0.000
1600	8.396	58.324	52.065	10.015	0.000	0.000	0.000
1700	8.456	58.835	52.448	10.858	0.000	0.000	0.000
1800	8.508	59.320	52.816	11.706	0.000	0.000	0.000
1900	8.555	59.781	53.171	12.559	0.000	0.000	0.000
2000	8.597	60.221	53.513	13.417	0.000	0.000	0.000
2100	8.634	60.641	53.842	14.279	0.000	0.000	0.000
2200	8.668	61.044	54.160	15.144	0.000	0.000	0.000
2300	8.699	61.430	54.468	16.012	0.000	0.000	0.000
2400	8.726	61.801	54.766	16.883	0.000	0.000	0.000
2500	8.751	62.157	55.055	17.757	0.000	0.000	0.000
2600	8.775	62.501	55.334	18.634	0.000	0.000	0.000
2700	8.796	62.833	55.606	19.512	0.000	0.000	0.000
2800	8.815	63.153	55.870	20.393	0.000	0.000	0.000
2900	8.833	63.463	56.126	21.275	0.000	0.000	0.000
3000	8.850	63.762	56.376	22.159	0.000	0.000	0.000
3100	8.866	64.053	56.619	23.045	0.000	0.000	0.000
3200	8.881	64.335	56.856	23.933	0.000	0.000	0.000
3300	8.895	64.608	57.086	24.821	0.000	0.000	0.000
3400	8.908	64.874	57.312	25.711	0.000	0.000	0.000
3500	8.920	65.132	57.531	26.603	0.000	0.000	0.000
3600	8.932	65.384	57.746	27.496	0.000	0.000	0.000
3700	8.944	65.629	57.956	28.389	0.000	0.000	0.000
3800	8.954	65.867	58.161	29.284	0.000	0.000	0.000
3900	8.965	66.100	58.361	30.180	0.000	0.000	0.000
4000	8.975	66.327	58.558	31.077	0.000	0.000	0.000
4100	8.984	66.549	58.750	31.975	0.000	0.000	0.000
4200	8.993	66.765	58.938	32.874	0.000	0.000	0.000
4300	9.002	66.977	59.123	33.774	0.000	0.000	0.000
4400	9.011	67.184	59.304	34.674	0.000	0.000	0.000
4500	9.020	67.387	59.481	35.576	0.000	0.000	0.000
4600	9.028	67.585	59.655	36.478	0.000	0.000	0.000
4700	9.036	67.779	59.826	37.382	0.000	0.000	0.000
4800	9.045	67.970	59.993	38.286	0.000	0.000	0.000
4900	9.053	68.156	60.158	39.191	0.000	0.000	0.000
5000	9.061	68.339	60.320	40.096	0.000	0.000	0.000
5100	9.070	68.519	60.479	41.003	0.000	0.000	0.000
5200	9.078	68.695	60.635	41.910	0.000	0.000	0.000
5300	9.085	68.868	60.789	42.818	0.000	0.000	0.000
5400	9.093	69.038	60.940	43.727	0.000	0.000	0.000
5500	9.101	69.205	61.089	44.637	0.000	0.000	0.000
5600	9.110	69.369	61.235	45.547	0.000	0.000	0.000
5700	9.119	69.530	61.379	46.459	0.000	0.000	0.000
5800	9.128	69.689	61.521	47.371	0.000	0.000	0.000
5900	9.138	69.845	61.661	48.285	0.000	0.000	0.000
6000	9.148	69.999	61.799	49.199	0.000	0.000	0.000

Table F.4. Diatomic Oxygen (O_2); Molecular Weight = 31.9988.

	cal/(mol K)			kcal/mol			
T/K	Cp°	S°	$-(G°-H°_{298})/T$	$H°-H°_{298}$	ΔHf°	ΔGf°	Log K
0	0.000	0.000	INFINITE	-2.075	0.000	0.000	0.000
100	6.956	41.395	55.206	-1.381	0.000	0.000	0.000
200	6.961	46.218	49.645	-0.685	0.000	0.000	0.000
298.15	7.021	49.005	49.005	0.000	0.000	0.000	0.000
300	7.023	49.049	49.005	0.013	0.000	0.000	0.000
400	7.196	51.090	49.283	0.723	0.000	0.000	0.000
500	7.431	52.721	49.812	1.454	0.000	0.000	0.000
600	7.670	54.097	50.415	2.209	0.000	0.000	0.000
700	7.883	55.296	51.028	2.987	0.000	0.000	0.000
800	8.062	56.360	51.629	3.785	0.000	0.000	0.000
900	8.211	57.319	52.209	4.599	0.000	0.000	0.000
1000	8.334	58.190	52.764	5.426	0.000	0.000	0.000
1100	8.437	58.990	53.294	6.265	0.000	0.000	0.000
1200	8.525	59.728	53.800	7.113	0.000	0.000	0.000
1300	8.601	60.413	54.283	7.969	0.000	0.000	0.000
1400	8.670	61.053	54.744	8.833	0.000	0.000	0.000
1500	8.734	61.653	55.185	9.703	0.000	0.000	0.000
1600	8.795	62.219	55.607	10.580	0.000	0.000	0.000
1700	8.853	62.754	56.012	11.462	0.000	0.000	0.000
1800	8.909	63.262	56.400	12.350	0.000	0.000	0.000
1900	8.965	63.745	56.774	13.244	0.000	0.000	0.000
2000	9.020	64.206	57.134	14.143	0.000	0.000	0.000
2100	9.075	64.648	57.482	15.048	0.000	0.000	0.000
2200	9.129	65.071	57.817	15.958	0.000	0.000	0.000
2300	9.182	65.478	58.141	16.874	0.000	0.000	0.000
2400	9.235	65.870	58.455	17.795	0.000	0.000	0.000
2500	9.287	66.248	58.760	18.721	0.000	0.000	0.000
2600	9.337	66.613	59.055	19.652	0.000	0.000	0.000
2700	9.387	66.966	59.341	20.588	0.000	0.000	0.000
2800	9.435	67.309	59.620	21.529	0.000	0.000	0.000
2900	9.482	67.641	59.891	22.475	0.000	0.000	0.000
3000	9.528	67.963	60.154	23.426	0.000	0.000	0.000
3100	9.572	68.276	60.411	24.381	0.000	0.000	0.000
3200	9.614	68.581	60.662	25.340	0.000	0.000	0.000
3300	9.655	68.877	60.906	26.303	0.000	0.000	0.000
3400	9.694	69.166	61.145	27.271	0.000	0.000	0.000
3500	9.731	69.447	61.378	28.242	0.000	0.000	0.000
3600	9.768	69.722	61.606	29.217	0.000	0.000	0.000
3700	9.802	69.990	61.829	30.196	0.000	0.000	0.000
3800	9.836	70.252	62.047	31.178	0.000	0.000	0.000
3900	9.868	70.508	62.261	32.163	0.000	0.000	0.000
4000	9.900	70.758	62.470	33.151	0.000	0.000	0.000
4100	9.930	71.003	62.675	34.143	0.000	0.000	0.000
4200	9.960	71.243	62.877	35.137	0.000	0.000	0.000
4300	9.990	71.477	63.074	36.135	0.000	0.000	0.000
4400	10.019	71.707	63.267	37.135	0.000	0.000	0.000
4500	10.048	71.933	63.458	38.138	0.000	0.000	0.000
4600	10.077	72.154	63.644	39.145	0.000	0.000	0.000
4700	10.107	72.371	63.828	40.154	0.000	0.000	0.000
4800	10.137	72.584	64.008	41.166	0.000	0.000	0.000
4900	10.168	72.793	64.185	42.181	0.000	0.000	0.000
5000	10.200	72.999	64.359	43.200	0.000	0.000	0.000
5100	10.232	73.201	64.531	44.221	0.000	0.000	0.000
5200	10.267	73.401	64.699	45.246	0.000	0.000	0.000
5300	10.302	73.596	64.865	46.275	0.000	0.000	0.000
5400	10.340	73.789	65.029	47.307	0.000	0.000	0.000
5500	10.379	73.979	65.190	48.343	0.000	0.000	0.000
5600	10.420	74.167	65.348	49.383	0.000	0.000	0.000
5700	10.464	74.352	65.505	50.427	0.000	0.000	0.000
5800	10.510	74.534	65.659	51.476	0.000	0.000	0.000
5900	10.558	74.714	65.811	52.529	0.000	0.000	0.000
6000	10.609	74.892	65.961	53.587	0.000	0.000	0.000

Table F.5. Carbon Monoxide (CO); Molecular Weight = 28.01055.

	cal/(mol K)			kcal/mol			
T/K	Cp°	S°	$-(G°-H°_{298})/T$	$H°-H°_{298}$	ΔHf°	ΔGf°	Log K
0	0.000	0.000	INFINITE	-2.072	-27.200	-27.200	INFINITE
100	6.956	39.613	53.401	-1.379	-26.876	-28.741	62.809
200	6.957	44.435	47.851	-0.683	-26.599	-30.718	33.566
298.15	6.965	47.214	47.214	0.000	-26.417	-32.783	24.029
300	6.965	47.257	47.214	0.013	-26.414	-32.823	23.910
400	7.013	49.265	47.488	0.711	-26.318	-34.975	19.109
500	7.121	50.841	48.006	1.417	-26.296	-37.144	16.235
600	7.276	52.152	48.591	2.137	-26.332	-39.311	14.318
700	7.450	53.287	49.182	2.873	-26.409	-41.468	12.946
800	7.624	54.293	49.759	3.627	-26.514	-43.612	11.914
900	7.786	55.200	50.314	4.397	-26.637	-45.744	11.108
1000	7.931	56.028	50.845	5.183	-26.771	-47.859	10.459
1100	8.057	56.790	51.351	5.983	-26.914	-49.962	9.926
1200	8.168	57.496	51.834	6.794	-27.062	-52.049	9.479
1300	8.263	58.154	52.295	7.616	-27.218	-54.126	9.099
1400	8.346	58.769	52.736	8.446	-27.376	-56.189	8.771
1500	8.417	59.348	53.158	9.285	-27.537	-58.241	8.485
1600	8.480	59.893	53.562	10.130	-27.700	-60.284	8.234
1700	8.535	60.409	53.950	10.980	-27.865	-62.315	8.011
1800	8.583	60.898	54.322	11.836	-28.032	-64.337	7.811
1900	8.626	61.363	54.681	12.697	-28.201	-66.349	7.631
2000	8.664	61.807	55.026	13.561	-28.372	-68.353	7.469
2100	8.698	62.230	55.359	14.430	-28.543	-70.346	7.321
2200	8.728	62.635	55.680	15.301	-28.719	-72.335	7.185
2300	8.756	63.024	55.991	16.175	-28.894	-74.311	7.061
2400	8.781	63.397	56.292	17.052	-29.074	-76.282	6.946
2500	8.804	63.756	56.584	17.931	-29.254	-78.247	6.840
2600	8.825	64.102	56.866	18.813	-29.438	-80.202	6.741
2700	8.844	64.435	57.140	19.696	-29.623	-82.153	6.649
2800	8.863	64.757	57.407	20.582	-29.810	-84.093	6.563
2900	8.879	65.069	57.666	21.469	-30.001	-86.028	6.483
3000	8.895	65.370	57.917	22.357	-30.194	-87.957	6.407
3100	8.910	65.662	58.163	23.248	-30.388	-89.878	6.336
3200	8.924	65.945	58.401	24.139	-30.586	-91.795	6.269
3300	8.937	66.220	58.634	25.032	-30.786	-93.707	6.206
3400	8.949	66.487	58.861	25.927	-30.988	-95.609	6.145
3500	8.961	66.746	59.083	26.822	-31.192	-97.509	6.088
3600	8.973	66.999	59.299	27.719	-31.399	-99.400	6.034
3700	8.984	67.245	59.511	28.617	-31.608	-101.286	5.982
3800	8.994	67.485	59.717	29.516	-31.818	-103.164	5.933
3900	9.004	67.718	59.919	30.416	-32.031	-105.039	5.886
4000	9.014	67.946	60.117	31.316	-32.247	-106.908	5.841
4100	9.024	68.169	60.311	32.218	-32.464	-108.774	5.798
4200	9.033	68.387	60.501	33.121	-32.684	-110.630	5.756
4300	9.042	68.599	60.687	34.025	-32.906	-112.483	5.717
4400	9.051	68.807	60.869	34.930	-33.130	-114.333	5.679
4500	9.059	69.011	61.047	35.835	-33.356	-116.177	5.642
4600	9.068	69.210	61.223	36.741	-33.584	-118.012	5.607
4700	9.076	69.405	61.395	37.649	-33.814	-119.845	5.573
4800	9.084	69.596	61.564	38.557	-34.046	-121.672	5.540
4900	9.092	69.784	61.729	39.465	-34.280	-123.497	5.508
5000	9.100	69.967	61.892	40.375	-34.516	-125.315	5.477
5100	9.107	70.148	62.052	41.285	-34.755	-127.132	5.448
5200	9.115	70.325	62.210	42.196	-34.995	-128.941	5.419
5300	9.123	70.498	62.365	43.108	-35.237	-130.741	5.391
5400	9.130	70.669	62.517	44.021	-35.480	-132.542	5.364
5500	9.138	70.836	62.667	44.934	-35.727	-134.336	5.338
5600	9.145	71.001	62.814	45.849	-35.974	-136.129	5.312
5700	9.153	71.163	62.959	46.763	-36.225	-137.919	5.288
5800	9.160	71.322	63.102	47.679	-36.476	-139.698	5.264
5900	9.167	71.479	63.242	48.595	-36.730	-141.473	5.240
6000	9.175	71.633	63.381	49.513	-36.985	-143.249	5.218

Table F.6. Diatomic Hydrogen (H_2); Molecular Weight = 2.016.

	cal/(mol K)			kcal/mol			
T/K	Cp°	S°	$-(G°-H°_{298})/T$	$H°-H°_{298}$	ΔHf°	ΔGf°	Log K
0	0.000	0.000	INFINITE	-2.024	0.000	0.000	0.000
100	6.729	24.048	37.117	-1.307	0.000	0.000	0.000
200	6.560	28.514	31.829	-0.663	0.000	0.000	0.000
298.15	6.892	31.207	31.207	0.000	0.000	0.000	0.000
300	6.895	31.250	31.207	0.013	0.000	0.000	0.000
400	6.974	33.247	31.479	0.707	0.000	0.000	0.000
500	6.993	34.806	31.994	1.406	0.000	0.000	0.000
600	7.009	36.082	32.572	2.106	0.000	0.000	0.000
700	7.036	37.164	33.153	2.808	0.000	0.000	0.000
800	7.080	38.107	33.714	3.514	0.000	0.000	0.000
900	7.142	38.944	34.250	4.225	0.000	0.000	0.000
1000	7.219	39.700	34.758	4.943	0.000	0.000	0.000
1100	7.309	40.392	35.239	5.669	0.000	0.000	0.000
1200	7.407	41.033	35.695	6.405	0.000	0.000	0.000
1300	7.510	41.630	36.129	7.151	0.000	0.000	0.000
1400	7.615	42.190	36.542	7.907	0.000	0.000	0.000
1500	7.719	42.719	36.936	8.674	0.000	0.000	0.000
1600	7.821	43.220	37.314	9.451	0.000	0.000	0.000
1700	7.920	43.698	37.675	10.238	0.000	0.000	0.000
1800	8.016	44.153	38.023	11.035	0.000	0.000	0.000
1900	8.106	44.589	38.357	11.841	0.000	0.000	0.000
2000	8.193	45.007	38.679	12.656	0.000	0.000	0.000
2100	8.275	45.409	38.990	13.479	0.000	0.000	0.000
2200	8.354	45.795	39.290	14.311	0.000	0.000	0.000
2300	8.428	46.168	39.581	15.150	0.000	0.000	0.000
2400	8.499	46.529	39.863	15.996	0.000	0.000	0.000
2500	8.566	46.877	40.137	16.849	0.000	0.000	0.000
2600	8.631	47.214	40.403	17.709	0.000	0.000	0.000
2700	8.692	47.541	40.661	18.575	0.000	0.000	0.000
2800	8.752	47.858	40.913	19.448	0.000	0.000	0.000
2900	8.809	48.166	41.157	20.326	0.000	0.000	0.000
3000	8.864	48.466	41.396	21.209	0.000	0.000	0.000
3100	8.917	48.757	41.629	22.098	0.000	0.000	0.000
3200	8.969	49.041	41.856	22.993	0.000	0.000	0.000
3300	9.020	49.318	42.078	23.892	0.000	0.000	0.000
3400	9.069	49.588	42.295	24.797	0.000	0.000	0.000
3500	9.118	49.852	42.507	25.706	0.000	0.000	0.000
3600	9.165	50.109	42.715	26.620	0.000	0.000	0.000
3700	9.212	50.361	42.918	27.539	0.000	0.000	0.000
3800	9.258	50.607	43.117	28.463	0.000	0.000	0.000
3900	9.304	50.848	43.312	29.391	0.000	0.000	0.000
4000	9.349	51.085	43.504	30.324	0.000	0.000	0.000
4100	9.393	51.316	43.691	31.261	0.000	0.000	0.000
4200	9.437	51.543	43.876	32.202	0.000	0.000	0.000
4300	9.480	51.765	44.056	33.148	0.000	0.000	0.000
4400	9.523	51.984	44.234	34.098	0.000	0.000	0.000
4500	9.564	52.198	44.409	35.053	0.000	0.000	0.000
4600	9.605	52.409	44.580	36.011	0.000	0.000	0.000
4700	9.645	52.616	44.749	36.974	0.000	0.000	0.000
4800	9.684	52.819	44.915	37.940	0.000	0.000	0.000
4900	9.722	53.019	45.079	38.910	0.000	0.000	0.000
5000	9.758	53.216	45.239	39.884	0.000	0.000	0.000
5100	9.794	53.410	45.398	40.862	0.000	0.000	0.000
5200	9.827	53.600	45.554	41.843	0.000	0.000	0.000
5300	9.859	53.788	45.707	42.827	0.000	0.000	0.000
5400	9.890	53.972	45.859	43.815	0.000	0.000	0.000
5500	9.918	54.154	46.008	44.805	0.000	0.000	0.000
5600	9.945	54.333	46.155	45.798	0.000	0.000	0.000
5700	9.970	54.509	46.300	46.794	0.000	0.000	0.000
5800	9.992	54.683	46.443	47.792	0.000	0.000	0.000
5900	10.012	54.854	46.584	48.792	0.000	0.000	0.000
6000	10.030	55.022	46.723	49.795	0.000	0.000	0.000

Table F.7. Monatomic Hydrogen (H); Atomic Weight = 1.00797.

	cal/(mol K)			kcal/mol			
T/K	Cp°	S°	$-(G°-H°_{298})/T$	$H°-H°_{298}$	ΔHf°	ΔGf°	Log K
0	0.000	0.000	INFINITE	-1.481	51.634	51.634	INFINITE
100	4.968	21.964	31.808	-0.984	51.772	50.778	-110.973
200	4.968	25.408	27.846	-0.488	51.947	49.716	-54.327
298.15	4.968	27.392	27.392	0.000	52.103	48.588	-35.616
300	4.968	27.422	27.392	0.009	52.105	48.566	-35.380
400	4.968	28.852	27.587	0.506	52.255	47.364	-25.878
500	4.968	29.960	27.955	1.003	52.402	46.124	-20.160
600	4.968	30.866	28.367	1.500	52.549	44.854	-16.338
700	4.968	31.632	28.780	1.996	52.695	43.560	-13.600
800	4.968	32.295	29.179	2.493	52.839	42.245	-11.541
900	4.968	32.880	29.558	2.990	52.980	40.913	-9.935
1000	4.968	33.404	29.917	3.487	53.118	39.564	-8.647
1100	4.968	33.877	30.256	3.984	53.252	38.203	-7.590
1200	4.968	34.309	30.576	4.480	53.381	36.829	-6.707
1300	4.968	34.707	30.878	4.977	53.504	35.444	-5.959
1400	4.968	35.075	31.165	5.474	53.623	34.051	-5.315
1500	4.968	35.418	31.437	5.971	53.736	32.649	-4.757
1600	4.968	35.739	31.696	6.468	53.845	31.239	-4.267
1700	4.968	36.040	31.943	6.964	53.948	29.823	-3.834
1800	4.968	36.324	32.179	7.461	54.046	28.401	-3.448
1900	4.968	36.592	32.404	7.958	54.140	26.974	-3.103
2000	4.968	36.847	32.620	8.455	54.229	25.542	-2.791
2100	4.968	37.090	32.827	8.952	54.315	24.106	-2.509
2200	4.968	37.321	33.026	9.448	54.396	22.665	-2.252
2300	4.968	37.542	33.218	9.945	54.473	21.221	-2.016
2400	4.968	37.753	33.402	10.442	54.547	19.774	-1.801
2500	4.968	37.956	33.580	10.939	54.617	18.324	-1.602
2600	4.968	38.151	33.752	11.436	54.684	16.871	-1.418
2700	4.968	38.338	33.919	11.932	54.748	15.415	-1.248
2800	4.968	38.519	34.080	12.429	54.808	13.957	-1.089
2900	4.968	38.693	34.236	12.926	54.866	12.497	-0.942
3000	4.968	38.862	34.387	13.423	54.921	11.035	-0.804
3100	4.968	39.024	34.534	13.920	54.973	9.572	-0.675
3200	4.968	39.182	34.677	14.416	55.023	8.106	-0.554
3300	4.968	39.335	34.816	14.913	55.070	6.639	-0.440
3400	4.968	39.483	34.951	15.410	55.114	5.171	-0.332
3500	4.968	39.627	35.083	15.907	55.156	3.701	-0.231
3600	4.968	39.767	35.211	16.404	55.196	2.231	-0.135
3700	4.968	39.903	35.336	16.900	55.234	0.759	-0.045
3800	4.968	40.036	35.458	17.397	55.268	-0.714	0.041
3900	4.968	40.165	35.577	17.894	55.301	-2.188	0.123
4000	4.968	40.291	35.693	18.391	55.331	-3.662	0.200
4100	4.968	40.413	35.807	18.888	55.360	-5.138	0.274
4200	4.968	40.533	35.918	19.384	55.386	-6.613	0.344
4300	4.968	40.650	36.026	19.881	55.410	-8.090	0.411
4400	4.968	40.764	36.133	20.378	55.432	-9.567	0.475
4500	4.968	40.876	36.237	20.875	55.451	-11.045	0.536
4600	4.968	40.985	36.339	21.372	55.469	-12.522	0.595
4700	4.968	41.092	36.439	21.868	55.484	-14.001	0.651
4800	4.968	41.197	36.537	22.365	55.498	-15.479	0.705
4900	4.968	41.299	36.633	22.862	55.510	-16.958	0.756
5000	4.968	41.399	36.728	23.359	55.519	-18.437	0.806
5100	4.968	41.498	36.820	23.855	55.527	-19.916	0.853
5200	4.968	41.594	36.911	24.352	55.533	-21.395	0.899
5300	4.968	41.689	37.000	24.849	55.538	-22.875	0.943
5400	4.968	41.782	37.088	25.346	55.541	-24.354	0.986
5500	4.968	41.873	37.174	25.843	55.543	-25.834	1.027
5600	4.968	41.962	37.259	26.339	55.543	-27.313	1.066
5700	4.968	42.050	37.342	26.836	55.542	-28.793	1.104
5800	4.968	42.137	37.424	27.333	55.540	-30.272	1.141
5900	4.968	42.222	37.505	27.830	55.537	-31.752	1.176
6000	4.968	42.305	37.584	28.327	55.532	-33.232	1.210

Table F.8. Monatomic Oxygen (O); Atomic Weight = 16.00

	cal/(mol K)			kcal/mol			
T/K	Cp°	S°	$-(G°-H°_{298})/T$	$H°-H°_{298}$	ΔHf°	ΔGf°	Log K
0	0.000	0.000	INFINITE	-1.607	58.984	58.984	INFINITE
100	5.665	32.466	43.265	-1.080	59.164	57.988	-126.730
200	5.433	36.339	38.952	-0.523	59.374	56.728	-61.988
298.15	5.237	38.468	38.468	0.000	59.554	55.390	-40.602
300	5.234	38.500	38.468	0.010	59.557	55.364	-40.332
400	5.134	39.991	38.672	0.528	59.720	53.942	-29.472
500	5.081	41.130	39.054	1.038	59.865	52.480	-22.939
600	5.049	42.053	39.479	1.544	59.994	50.991	-18.573
700	5.029	42.830	39.904	2.048	60.109	49.481	-15.448
800	5.015	43.501	40.313	2.550	60.212	47.955	-13.101
900	5.006	44.091	40.700	3.051	60.306	46.418	-11.272
1000	4.999	44.618	41.066	3.552	60.393	44.870	-9.806
1100	4.994	45.094	41.411	4.051	60.473	43.314	-8.606
1200	4.990	45.528	41.736	4.550	60.548	41.751	-7.604
1300	4.987	45.927	42.043	5.049	60.619	40.181	-6.755
1400	4.984	46.297	42.334	5.548	60.685	38.607	-6.027
1500	4.982	46.641	42.610	6.046	60.748	37.027	-5.395
1600	4.981	46.962	42.872	6.544	60.808	35.444	-4.841
1700	4.979	47.264	43.122	7.042	60.865	33.857	-4.353
1800	4.978	47.549	43.360	7.540	60.919	32.267	-3.918
1900	4.978	47.818	43.587	8.038	60.970	30.673	-3.528
2000	4.978	48.073	43.805	8.536	61.018	29.078	-3.177
2100	4.978	48.316	44.014	9.033	61.063	27.480	-2.860
2200	4.978	48.548	44.215	9.531	61.106	25.879	-2.571
2300	4.980	48.769	44.408	10.029	61.146	24.277	-2.307
2400	4.981	48.981	44.595	10.527	61.183	22.673	-2.065
2500	4.983	49.184	44.774	11.025	61.219	21.068	-1.842
2600	4.986	49.380	44.948	11.524	61.252	19.461	-1.636
2700	4.990	49.568	45.115	12.023	61.282	17.854	-1.445
2800	4.994	49.750	45.277	12.522	61.311	16.245	-1.268
2900	4.999	49.925	45.435	13.021	61.338	14.635	-1.103
3000	5.004	50.094	45.587	13.522	61.362	13.023	-0.949
3100	5.010	50.259	45.735	14.022	61.386	11.412	-0.805
3200	5.017	50.418	45.879	14.524	61.407	9.799	-0.669
3300	5.024	50.572	46.019	15.026	61.428	8.187	-0.542
3400	5.032	50.722	46.155	15.528	61.447	6.573	-0.422
3500	5.041	50.868	46.288	16.032	61.465	4.959	-0.310
3600	5.050	51.011	46.417	16.537	61.482	3.344	-0.203
3700	5.060	51.149	46.543	17.042	61.498	1.729	-0.102
3800	5.070	51.284	46.666	17.549	61.514	0.113	-0.006
3900	5.080	51.416	46.786	18.056	61.529	-1.503	0.084
4000	5.091	51.545	46.903	18.565	61.543	-3.119	0.170
4100	5.102	51.671	47.018	19.075	61.557	-4.736	0.252
4200	5.114	51.794	47.130	19.585	61.571	-6.353	0.331
4300	5.126	51.914	47.240	20.097	61.584	-7.971	0.405
4400	5.137	52.032	47.348	20.610	61.597	-9.588	0.476
4500	5.149	52.148	47.453	21.125	61.610	-11.206	0.544
4600	5.162	52.261	47.557	21.640	61.622	-12.825	0.609
4700	5.174	52.372	47.658	22.157	61.634	-14.443	0.672
4800	5.186	52.481	47.757	22.675	61.646	-16.062	0.731
4900	5.198	52.588	47.855	23.194	61.658	-17.681	0.789
5000	5.210	52.693	47.950	23.715	61.669	-19.300	0.844
5100	5.222	52.797	48.044	24.236	61.680	-20.919	0.896
5200	5.234	52.898	48.137	24.759	61.690	-22.539	0.947
5300	5.246	52.998	48.228	25.283	61.699	-24.159	0.996
5400	5.257	53.096	48.317	25.808	61.709	-25.779	1.043
5500	5.269	53.193	48.405	26.335	61.717	-27.399	1.089
5600	5.280	53.288	48.491	26.862	61.724	-29.020	1.133
5700	5.291	53.381	48.576	27.391	61.731	-30.640	1.175
5800	5.302	53.473	48.660	27.920	61.736	-32.261	1.216
5900	5.313	53.564	48.742	28.451	61.740	-33.882	1.255
6000	5.323	53.654	48.823	28.983	61.743	-35.502	1.293

Table F.9. Hydroxyl (OH); Molecular Weight = 17.0074.

	cal/(mol K)			kcal/mol			
T/K	Cp°	S°	$-(G°-H°_{298})/T$	$H°-H°_{298}$	ΔHf°	ΔGf°	Log K
0	0.000	0.000	INFINITE	-2.192	9.175	9.175	INFINITE
100	7.798	35.727	50.399	-1.467	9.195	8.894	-19.438
200	7.356	40.985	44.542	-0.711	9.281	8.557	-9.350
298.15	7.167	43.881	43.881	0.000	9.318	8.192	-6.005
300	7.165	43.926	43.881	0.013	9.318	8.185	-5.963
400	7.087	45.974	44.161	0.725	9.328	7.806	-4.265
500	7.056	47.552	44.688	1.432	9.320	7.426	-3.246
600	7.057	48.838	45.275	2.137	9.298	7.049	-2.568
700	7.090	49.928	45.864	2.845	9.265	6.677	-2.085
800	7.150	50.878	46.433	3.556	9.225	6.309	-1.724
900	7.233	51.725	46.974	4.275	9.181	5.947	-1.444
1000	7.332	52.492	47.488	5.004	9.137	5.590	-1.222
1100	7.439	53.196	47.976	5.742	9.093	5.238	-1.041
1200	7.549	53.848	48.438	6.491	9.050	4.889	-0.890
1300	7.659	54.456	48.878	7.252	9.010	4.544	-0.764
1400	7.766	55.028	49.297	8.023	8.971	4.202	-0.656
1500	7.867	55.567	49.697	8.805	8.934	3.863	-0.563
1600	7.963	56.078	50.080	9.596	8.899	3.526	-0.482
1700	8.053	56.564	50.447	10.397	8.865	3.191	-0.410
1800	8.137	57.026	50.800	11.207	8.832	2.858	-0.347
1900	8.214	57.468	51.140	12.024	8.800	2.527	-0.291
2000	8.286	57.891	51.467	12.849	8.768	2.198	-0.240
2100	8.353	58.297	51.782	13.682	8.736	1.870	-0.195
2200	8.415	58.687	52.087	14.520	8.703	1.544	-0.153
2300	8.473	59.063	52.383	15.364	8.670	1.219	-0.116
2400	8.526	59.425	52.669	16.214	8.637	0.896	-0.082
2500	8.576	59.774	52.946	17.069	8.602	0.574	-0.050
2600	8.622	60.111	53.215	17.929	8.567	0.254	-0.021
2700	8.665	60.437	53.476	18.794	8.530	-0.065	0.005
2800	8.706	60.753	53.731	19.662	8.492	-0.383	0.030
2900	8.744	61.059	53.978	20.535	8.452	-0.699	0.053
3000	8.780	61.356	54.219	21.411	8.412	-1.014	0.074
3100	8.814	61.645	54.454	22.291	8.369	-1.327	0.094
3200	8.846	61.925	54.683	23.174	8.325	-1.640	0.112
3300	8.877	62.198	54.907	24.060	8.281	-1.950	0.129
3400	8.906	62.463	55.125	24.949	8.233	-2.260	0.145
3500	8.933	62.722	55.338	25.841	8.185	-2.567	0.160
3600	8.959	62.974	55.547	26.736	8.135	-2.874	0.174
3700	8.985	63.220	55.751	27.633	8.084	-3.179	0.188
3800	9.009	63.459	55.951	28.533	8.030	-3.483	0.200
3900	9.032	63.694	56.146	29.435	7.976	-3.785	0.212
4000	9.055	63.923	56.338	30.339	7.920	-4.086	0.223
4100	9.076	64.147	56.526	31.246	7.862	-4.386	0.234
4200	9.098	64.366	56.710	32.154	7.803	-4.683	0.244
4300	9.118	64.580	56.890	33.065	7.742	-4.980	0.253
4400	9.138	64.790	57.067	33.978	7.679	-5.275	0.262
4500	9.157	64.995	57.241	34.893	7.615	-5.569	0.270
4600	9.176	65.197	57.412	35.809	7.549	-5.861	0.278
4700	9.195	65.394	57.580	36.728	7.482	-6.152	0.286
4800	9.213	65.588	57.745	37.648	7.413	-6.441	0.293
4900	9.232	65.778	57.907	38.571	7.343	-6.729	0.300
5000	9.249	65.965	58.066	39.495	7.271	-7.016	0.307
5100	9.267	66.148	58.223	40.421	7.197	-7.300	0.313
5200	9.284	66.328	58.377	41.348	7.122	-7.584	0.319
5300	9.302	66.505	58.528	42.277	7.044	-7.866	0.324
5400	9.319	66.679	58.678	43.208	6.965	-8.147	0.330
5500	9.336	66.851	58.825	44.141	6.885	-8.426	0.335
5600	9.353	67.019	58.970	45.076	6.803	-8.703	0.340
5700	9.370	67.185	59.112	46.012	6.719	-8.979	0.344
5800	9.388	67.348	59.253	46.950	6.634	-9.254	0.349
5900	9.405	67.508	59.392	47.889	6.547	-9.527	0.353
6000	9.422	67.667	59.528	48.831	6.458	-9.799	0.357

Table F.10. Nitric Oxide (NO); Molecular Weight = 30.08.

	cal/(mol K)			kcal/mol			
T/K	Cp°	S°	$-(G°-H°_{298})/T$	$H°-H°_{298}$	ΔHf°	ΔGf°	Log K
0	0.000	0.000	INFINITE	-2.197	21.456	21.456	INFINITE
100	7.721	42.286	56.801	-1.451	21.503	21.256	-46.453
200	7.271	47.477	51.003	-0.705	21.558	20.984	-22.929
298.15	7.133	50.347	50.347	0.000	21.580	20.697	-15.171
300	7.132	50.392	50.348	0.013	21.580	20.692	-15.073
400	7.157	52.444	50.627	0.727	21.590	20.394	-11.142
500	7.287	54.053	51.157	1.448	21.594	20.095	-8.783
600	7.466	55.397	51.755	2.186	21.598	19.795	-7.210
700	7.655	56.562	52.360	2.942	21.601	19.494	-6.086
800	7.832	57.596	52.951	3.716	21.605	19.192	-5.243
900	7.988	58.528	53.520	4.507	21.610	18.890	-4.587
1000	8.123	59.377	54.064	5.313	21.615	18.588	-4.062
1100	8.238	60.157	54.583	6.131	21.620	18.285	-3.633
1200	8.336	60.878	55.078	6.960	21.624	17.981	-3.275
1300	8.419	61.548	55.550	7.798	21.628	17.678	-2.972
1400	8.491	62.175	56.001	8.644	21.631	17.373	-2.712
1500	8.552	62.763	56.432	9.496	21.633	17.069	-2.487
1600	8.605	63.317	56.845	10.354	21.635	16.765	-2.290
1700	8.651	63.840	57.242	11.217	21.635	16.461	-2.116
1800	8.692	64.335	57.622	12.084	21.633	16.156	-1.962
1900	8.727	64.806	57.988	12.955	21.630	15.853	-1.823
2000	8.759	65.255	58.340	13.829	21.626	15.548	-1.699
2100	8.788	65.683	58.680	14.706	21.619	15.244	-1.586
2200	8.813	66.092	59.007	15.587	21.611	14.941	-1.484
2300	8.837	66.484	59.324	16.469	21.601	14.637	-1.391
2400	8.858	66.861	59.630	17.354	21.589	14.336	-1.305
2500	8.877	67.223	59.927	18.241	21.574	14.033	-1.227
2600	8.895	67.571	60.214	19.129	21.558	13.732	-1.154
2700	8.912	67.908	60.493	20.020	21.540	13.432	-1.087
2800	8.927	68.232	60.763	20.911	21.520	13.132	-1.025
2900	8.941	68.545	61.026	21.805	21.498	12.834	-0.967
3000	8.955	68.849	61.282	22.700	21.474	12.535	-0.913
3100	8.968	69.143	61.531	23.596	21.449	12.237	-0.863
3200	8.980	69.427	61.773	24.493	21.421	11.940	-0.815
3300	8.991	69.704	62.010	25.392	21.392	11.644	-0.771
3400	9.002	69.973	62.240	26.291	21.361	11.349	-0.729
3500	9.012	70.234	62.464	27.192	21.329	11.054	-0.690
3600	9.022	70.488	62.684	28.094	21.294	10.762	-0.653
3700	9.032	70.735	62.898	28.997	21.259	10.470	-0.618
3800	9.041	70.976	63.108	29.900	21.222	10.179	-0.585
3900	9.050	71.211	63.312	30.805	21.185	9.889	-0.554
4000	9.058	71.440	63.513	31.710	21.145	9.598	-0.524
4100	9.066	71.664	63.709	32.616	21.104	9.311	-0.496
4200	9.074	71.882	63.901	33.523	21.063	9.024	-0.470
4300	9.082	72.096	64.089	34.431	21.021	8.739	-0.444
4400	9.090	72.305	64.273	35.340	20.977	8.452	-0.420
4500	9.097	72.509	64.454	36.249	20.932	8.169	-0.397
4600	9.105	72.709	64.631	37.159	20.887	7.888	-0.375
4700	9.112	72.905	64.805	38.070	20.841	7.605	-0.354
4800	9.119	73.097	64.976	38.982	20.794	7.324	-0.333
4900	9.125	73.285	65.144	39.894	20.747	7.040	-0.314
5000	9.132	73.470	65.308	40.807	20.699	6.763	-0.296
5100	9.139	73.651	65.470	41.720	20.650	6.484	-0.278
5200	9.145	73.828	65.629	42.634	20.601	6.207	-0.261
5300	9.152	74.002	65.786	43.549	20.551	5.932	-0.245
5400	9.158	74.173	65.939	44.465	20.501	5.654	-0.229
5500	9.164	74.342	66.091	45.381	20.451	5.383	-0.214
5600	9.170	74.507	66.239	46.298	20.400	5.107	-0.199
5700	9.176	74.669	66.386	47.215	20.348	4.835	-0.185
5800	9.182	74.829	66.530	48.133	20.297	4.566	-0.172
5900	9.188	74.986	66.672	49.051	20.245	4.292	-0.159
6000	9.194	75.140	66.812	49.970	20.192	4.024	-0.147

Table F.11. Monatomic Nitrogen (N); Atomic Weight = 14.008.

	cal/(mol K)			kcal/mol			
T/K	Cp°	S°	$-(G°-H°_{298})/T$	$H°-H°_{298}$	ΔHf°	ΔGf°	Log K
0	0.000	0.000	INFINITE	-1.481	112.530	112.530	INFINITE
100	4.968	31.186	41.030	-0.984	112.680	111.470	-243.615
200	4.968	34.630	37.068	-0.488	112.829	110.202	-120.422
298.15	4.968	36.613	36.613	0.000	112.975	108.882	-79.812
300	4.968	36.644	36.614	0.009	112.978	108.857	-79.301
400	4.968	38.073	36.808	0.506	113.126	107.460	-58.713
500	4.968	39.182	37.176	1.003	113.271	106.027	-46.344
600	4.968	40.088	37.588	1.500	113.412	104.565	-38.087
700	4.968	40.854	38.002	1.996	113.545	103.080	-32.182
800	4.968	41.517	38.400	2.493	113.670	101.576	-27.749
900	4.968	42.102	38.780	2.990	113.788	100.057	-24.297
1000	4.968	42.626	39.139	3.487	113.897	98.525	-21.532
1100	4.968	43.099	39.478	3.984	114.000	96.983	-19.269
1200	4.968	43.531	39.798	4.480	114.097	95.432	-17.380
1300	4.968	43.929	40.100	4.977	114.188	93.873	-15.781
1400	4.968	44.297	40.387	5.474	114.274	92.307	-14.410
1500	4.968	44.640	40.659	5.971	114.356	90.735	-13.220
1600	4.968	44.961	40.918	6.468	114.435	89.158	-12.178
1700	4.968	45.262	41.165	6.964	114.511	87.576	-11.258
1800	4.968	45.546	41.401	7.461	114.583	85.989	-10.440
1900	4.968	45.814	41.626	7.958	114.654	84.399	-9.708
2000	4.969	46.069	41.842	8.455	114.722	82.804	-9.048
2100	4.970	46.312	42.049	8.952	114.788	81.207	-8.451
2200	4.971	46.543	42.248	9.449	114.852	79.606	-7.908
2300	4.972	46.764	42.439	9.946	114.915	78.003	-7.412
2400	4.975	46.975	42.624	10.443	114.977	76.397	-6.957
2500	4.978	47.179	42.802	10.941	115.038	74.788	-6.538
2600	4.982	47.374	42.974	11.439	115.097	73.176	-6.151
2700	4.987	47.562	43.141	11.937	115.156	71.563	-5.793
2800	4.993	47.743	43.302	12.436	115.215	69.947	-5.460
2900	5.001	47.919	43.458	12.936	115.274	68.330	-5.149
3000	5.010	48.088	43.610	13.436	115.332	66.710	-4.860
3100	5.021	48.253	43.757	13.938	115.391	65.089	-4.589
3200	5.034	48.413	43.900	14.441	115.449	63.465	-4.334
3300	5.049	48.568	44.039	14.945	115.510	61.840	-4.095
3400	5.066	48.719	44.174	15.451	115.570	60.212	-3.870
3500	5.085	48.866	44.306	15.958	115.632	58.583	-3.658
3600	5.106	49.009	44.435	16.468	115.695	56.952	-3.457
3700	5.130	49.150	44.560	16.980	115.760	55.320	-3.268
3800	5.155	49.287	44.683	17.494	115.827	53.685	-3.088
3900	5.183	49.421	44.803	18.011	115.896	52.049	-2.917
4000	5.212	49.553	44.920	18.531	115.967	50.411	-2.754
4100	5.244	49.682	45.034	19.053	116.041	48.771	-2.600
4200	5.278	49.808	45.147	19.579	116.118	47.129	-2.452
4300	5.313	49.933	45.257	20.109	116.197	45.486	-2.312
4400	5.351	50.056	45.364	20.642	116.280	43.841	-2.178
4500	5.390	50.176	45.470	21.179	116.366	42.193	-2.049
4600	5.431	50.295	45.573	21.720	116.456	40.544	-1.926
4700	5.473	50.412	45.675	22.265	116.550	38.893	-1.808
4800	5.516	50.528	45.775	22.815	116.647	37.239	-1.696
4900	5.561	50.642	45.873	23.369	116.748	35.584	-1.587
5000	5.607	50.755	45.970	23.927	116.854	33.927	-1.483
5100	5.654	50.867	46.065	24.490	116.964	32.267	-1.383
5200	5.702	50.977	46.158	25.058	117.078	30.605	-1.286
5300	5.751	51.086	46.250	25.631	117.197	28.941	-1.193
5400	5.800	51.194	46.341	26.208	117.320	27.275	-1.104
5500	5.849	51.301	46.430	26.791	117.447	25.606	-1.017
5600	5.899	51.407	46.518	27.378	117.580	23.935	-0.934
5700	5.949	51.512	46.604	27.970	117.716	22.262	-0.854
5800	6.000	51.615	46.690	28.568	117.858	20.586	-0.776
5900	6.050	51.718	46.774	29.170	118.003	18.907	-0.700
6000	6.100	51.821	46.857	29.778	118.154	17.227	-0.627

Table F.12 Carbon (C); Reference State—Graphite; Molecular Weight = 12.011.

	cal/(mol K)			kcal/mol			
T/K	Cp°	S°	$-(G°-H°_{298})/T$	$H°-H°_{298}$	ΔHf°	ΔGf°	Log K
0	0.000	0.000	INFINITE	-0.251	0.000	0.000	0.000
100	0.400	0.228	2.597	-0.237	0.000	0.000	0.000
200	1.196	0.737	1.531	-0.159	0.000	0.000	0.000
298.15	2.036	1.372	1.372	0.000	0.000	0.000	0.000
300	2.051	1.385	1.372	0.004	0.000	0.000	0.000
400	2.824	2.083	1.462	0.248	0.000	0.000	0.000
500	3.495	2.787	1.657	0.565	0.000	0.000	0.000
600	4.026	3.474	1.903	0.942	0.000	0.000	0.000
700	4.430	4.126	2.174	1.366	0.000	0.000	0.000
800	4.739	4.739	2.457	1.825	0.000	0.000	0.000
900	4.977	5.311	2.743	2.312	0.000	0.000	0.000
1000	5.165	5.845	3.026	2.819	0.000	0.000	0.000
1100	5.316	6.345	3.306	3.343	0.000	0.000	0.000
1200	5.441	6.813	3.579	3.881	0.000	0.000	0.000
1300	5.546	7.253	3.845	4.431	0.000	0.000	0.000
1400	5.635	7.667	4.103	4.990	0.000	0.000	0.000
1500	5.713	8.059	4.354	5.558	0.000	0.000	0.000
1600	5.782	8.430	4.597	6.132	0.000	0.000	0.000
1700	5.843	8.782	4.833	6.714	0.000	0.000	0.000
1800	5.899	9.118	5.062	7.301	0.000	0.000	0.000
1900	5.950	9.438	5.284	7.893	0.000	0.000	0.000
2000	5.997	9.745	5.499	8.491	0.000	0.000	0.000
2100	6.042	10.038	5.708	9.093	0.000	0.000	0.000
2200	6.083	10.320	5.912	9.699	0.000	0.000	0.000
2300	6.123	10.592	6.109	10.309	0.000	0.000	0.000
2400	6.160	10.853	6.301	10.924	0.000	0.000	0.000
2500	6.196	11.105	6.489	11.541	0.000	0.000	0.000
2600	6.231	11.349	6.671	12.163	0.000	0.000	0.000
2700	6.265	11.585	6.848	12.788	0.000	0.000	0.000
2800	6.297	11.813	7.022	13.416	0.000	0.000	0.000
2900	6.329	12.035	7.191	14.047	0.000	0.000	0.000
3000	6.360	12.250	7.356	14.682	0.000	0.000	0.000
3100	6.391	12.459	7.517	15.319	0.000	0.000	0.000
3200	6.420	12.662	7.675	15.960	0.000	0.000	0.000
3300	6.450	12.860	7.829	16.603	0.000	0.000	0.000
3400	6.478	13.053	7.980	17.250	0.000	0.000	0.000
3500	6.507	13.241	8.127	17.899	0.000	0.000	0.000
3600	6.535	13.425	8.272	18.551	0.000	0.000	0.000
3700	6.563	13.604	8.414	19.206	0.000	0.000	0.000
3800	6.590	13.780	8.553	19.863	0.000	0.000	0.000
3900	6.617	13.951	8.689	20.524	0.000	0.000	0.000
4000	6.644	14.119	8.822	21.187	0.000	0.000	0.000
4100	6.671	14.284	8.954	21.853	0.000	0.000	0.000
4200	6.698	14.445	9.083	22.521	0.000	0.000	0.000
4300	6.724	14.603	9.209	23.192	0.000	0.000	0.000
4400	6.751	14.758	9.333	23.866	0.000	0.000	0.000
4500	6.777	14.910	9.456	24.542	0.000	0.000	0.000
4600	6.803	15.059	9.576	25.221	0.000	0.000	0.000
4700	6.828	15.205	9.694	25.903	0.000	0.000	0.000
4800	6.854	15.349	9.810	26.587	0.000	0.000	0.000
4900	6.880	15.491	9.925	27.274	0.000	0.000	0.000
5000	6.905	15.630	10.038	27.963	0.000	0.000	0.000
5100	6.931	15.767	10.149	28.655	0.000	0.000	0.000
5200	6.956	15.902	10.258	29.349	0.000	0.000	0.000
5300	6.982	16.035	10.366	30.046	0.000	0.000	0.000
5400	7.007	16.166	10.472	30.746	0.000	0.000	0.000
5500	7.032	16.294	10.577	31.448	0.000	0.000	0.000
5600	7.057	16.421	10.680	32.152	0.000	0.000	0.000
5700	7.082	16.546	10.782	32.859	0.000	0.000	0.000
5800	7.107	16.670	10.882	33.568	0.000	0.000	0.000
5900	7.132	16.792	10.981	34.280	0.000	0.000	0.000
6000	7.157	16.912	11.079	34.995	0.00	0.000	0.000

Table F.13. Ozone (O_3); Molecular Weight = 48.000.

	cal/(mol K)			kcal/mol			
T/K	Cp°	S°	$-(G°-H°_{298})/T$	$H°-H°_{298}$	ΔHf°	ΔGf°	Log K
0	0.000	0.000	INFINITE	-2.474	34.739	34.739	INFINITE
100	7.957	47.964	47.981	-1.679	36.141	37.573	-82.112
200	8.379	53.564	57.909	-0.869	34.254	37.411	-40.879
298.15	9.378	57.080	57.080	0.000	34.100	38.997	-28.585
300	9.400	57.138	57.080	0.017	34.098	39.028	-28.430
400	10.455	59.992	57.462	1.012	34.026	40.684	-22.227
500	11.296	62.419	58.217	2.101	34.019	42.351	-18.511
600	11.916	64.536	59.097	3.263	34.048	44.015	-16.032
700	12.369	66.409	60.011	4.479	34.097	45.672	-14.259
800	12.704	68.083	60.917	5.733	34.154	47.321	-12.927
900	12.956	69.595	61.799	7.017	34.217	48.963	-11.889
1000	13.151	70.971	62.648	8.323	34.282	50.599	-11.058
1100	13.303	72.232	63.463	9.646	34.347	52.227	-10.376
1200	13.426	73.395	64.243	10.982	34.411	53.850	-9.807
1300	13.526	74.473	64.989	12.330	34.474	55.468	-9.324
1400	13.611	75.479	65.702	13.687	34.535	57.080	-8.910
1500	13.682	76.420	66.386	15.052	34.593	58.688	-8.550
1600	13.743	77.305	67.041	16.423	34.649	60.293	-8.235
1700	13.796	78.140	67.670	17.800	34.703	61.895	-7.957
1800	13.843	78.930	68.273	19.182	34.751	63.492	-7.709
1900	13.885	79.680	68.854	20.569	34.795	65.088	-7.486
2000	13.922	80.393	69.413	21.959	34.835	66.680	-7.286
2100	13.957	81.073	69.953	23.353	34.872	68.272	-7.105
2200	13.988	81.723	70.473	24.750	34.901	69.861	-6.940
2300	14.017	82.345	70.976	26.150	34.927	71.449	-6.789
2400	14.045	82.943	71.462	27.554	34.948	73.039	-6.651
2500	14.070	83.516	71.933	28.959	34.961	74.623	-6.523
2600	14.094	84.069	72.389	30.368	34.972	76.211	-6.406
2700	14.117	84.601	72.831	31.778	34.975	77.797	-6.297
2800	14.139	85.115	73.261	33.191	34.973	79.383	-6.196
2900	14.160	85.611	73.678	34.606	34.966	80.971	-6.102
3000	14.180	86.092	74.084	36.023	34.954	82.557	-6.014
3100	14.199	86.557	74.479	37.442	34.937	84.145	-5.932
3200	14.218	87.008	74.864	38.863	34.915	85.731	-5.855
3300	14.236	87.446	75.238	40.285	34.889	87.318	-5.783
3400	14.254	87.871	75.604	41.710	34.857	88.908	-5.715
3500	14.272	88.285	75.960	43.136	34.822	90.496	-5.651
3600	14.288	88.687	76.308	44.564	34.783	92.090	-5.590
3700	14.305	89.079	76.648	45.994	34.740	93.682	-5.533
3800	14.321	89.460	76.980	47.425	34.694	95.278	-5.479
3900	14.337	89.833	77.305	48.858	34.645	96.869	-5.428
4000	14.353	90.196	77.623	50.293	34.591	98.464	-5.380
4100	14.369	90.550	77.934	51.729	34.535	100.064	-5.334
4200	14.384	90.897	78.238	53.166	34.477	101.661	-5.290
4300	14.399	91.235	78.536	54.605	34.416	103.266	-5.248
4400	14.414	91.567	78.829	56.046	34.352	104.864	-5.208
4500	14.429	91.891	79.116	57.488	34.287	106.468	-5.171
4600	14.444	92.208	79.397	58.932	34.220	108.078	-5.135
4700	14.458	92.519	79.673	60.377	34.150	109.682	-5.100
4800	14.473	92.823	79.943	61.824	34.080	111.291	-5.067
4900	14.487	93.122	80.209	63.272	34.009	112.894	-5.035
5000	14.501	93.415	80.471	64.721	33.935	114.504	-5.005
5100	14.515	93.702	80.727	66.172	33.861	116.121	-4.976
5200	14.529	93.984	80.979	67.624	33.786	117.730	-4.948
5300	14.543	94.261	81.227	69.078	33.711	119.352	-4.921
5400	14.557	94.533	81.471	70.533	33.635	120.962	-4.895
5500	14.571	94.800	81.711	71.989	33.559	122.585	-4.871
5600	14.585	95.063	81.947	73.447	33.481	124.200	-4.847
5700	14.598	95.321	82.180	74.906	33.404	125.818	-4.824
5800	14.612	95.575	82.408	76.366	33.327	127.447	-4.802
5900	14.625	95.825	82.634	77.828	33.250	129.067	-4.781
6000	14.639	96.071	82.856	79.292	33.173	130.695	-4.760

Table F.14. Octane (C_8H_{18}); Atomic Weight = 114.24 and 2,2,4-Trimethylpentane (C_8H_{18}); Atomic Weight = 114.24.

OCTANE

	cal/(mole °K)			kcal/mole			
$T°K$	$Cp°$	$S°$	$-(F°-H°_{298})/T$	$H°-H°_{298}$	$\Delta Hf°$	$\Delta Ff°$	Log Kp
298	45.14	111.55	111.55	0.00	-49.82	3.92	-2.872
300	45.35	111.83	111.56	0.09	-49.89	4.25	-3.093
400	57.36	126.55	113.48	5.23	-52.96	22.78	-12.445
500	68.32	140.56	117.51	11.53	-55.50	42.02	-18.364
600	77.67	153.86	122.47	18.84	-57.51	61.71	-22.475
700	85.66	166.45	127.86	27.02	-59.04	81.71	-25.511
800	92.50	178.34	133.43	35.93	-60.16	101.88	-27.832
900	98.43	189.59	139.05	45.49	-60.90	122.20	-29.672
1000	103.60	200.23	144.64	55.59	-61.29	142.58	-31.160

2,2,4-TRIMETHYLPENTANE

	cal/(mole °K)			kcal/mole			
$T°K$	$Cp°$	$S°$	$-(F-H°_{298})/T$	$H°-H°_{298}$	$\Delta Hf°$	$\Delta Ff°$	Log Kp
298	45.14	101.15	101.15	0.00	-53.57	3.27	-2.396
300	45.35	101.43	101.16	0.09	-53.64	3.62	-2.634
400	57.36	116.15	103.08	5.23	-56.71	23.19	-12.669
500	68.32	130.16	107.11	11.53	-59.25	43.47	-18.998
600	77.67	143.46	112.07	18.84	-61.26	64.20	-23.382
700	85.66	156.05	117.46	27.02	-62.79	85.24	-26.613
800	92.50	167.94	123.03	35.93	-63.91	106.45	-29.081
900	98.43	179.19	128.65	45.49	-64.65	127.81	-31.035
1000	103.60	189.83	134.24	55.59	-65.04	149.23	-32.613

REFERENCES

Stull, D. R., E. F. Westrum Jr., and G. C. Sinke (1969), *The Chemical Thermodynamics of Organic Compounds*, Wiley, New York.

JANAF Thermochemical Tables, (1971). 2nd ed., National Bureau of Standards Publications, NSRDS-N35 37, Washington D.C.

Index

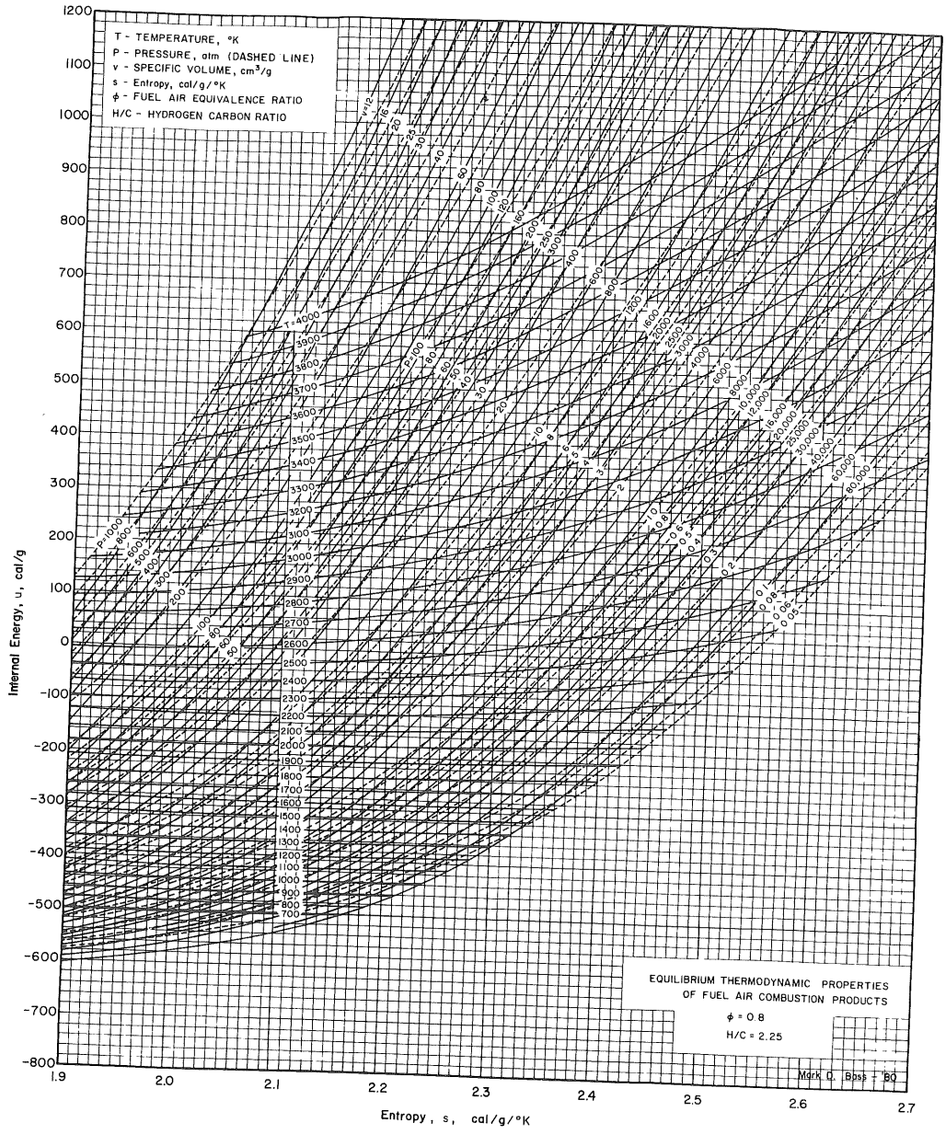

PURDUE UNIVERSITY, INDIANA

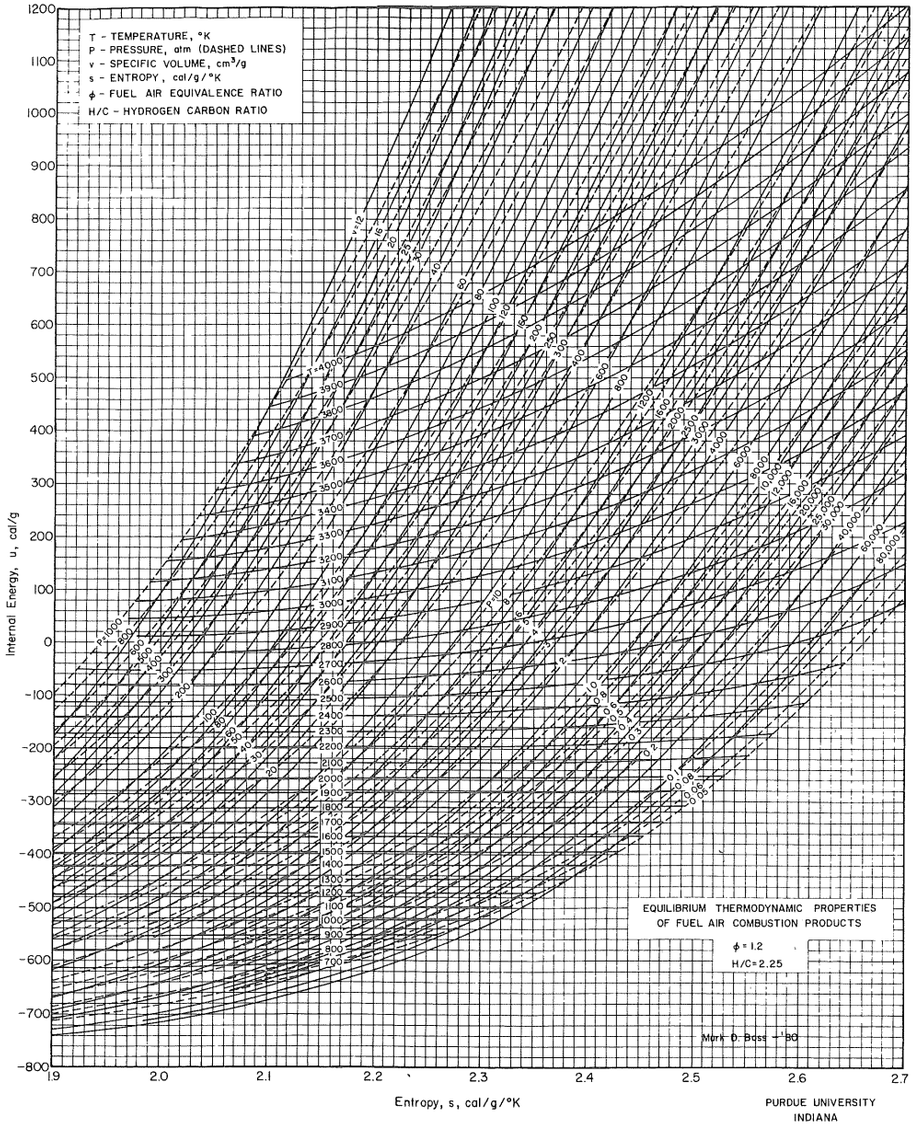
T - TEMPERATURE, °K
P - PRESSURE, atm (DASHED LINES)
v - SPECIFIC VOLUME, cm³/g
s - ENTROPY, cal/g/°K
ϕ - FUEL AIR EQUIVALENCE RATIO
H/C - HYDROGEN CARBON RATIO
EQUILIBRIUM THERMODYNAMIC PROPERTIES
OF FUEL AIR COMBUSTION PRODUCTS
ϕ = 1.2
H/C = 2.25
Mark D. Bass - '60
Internal Energy, u, cal/g
Entropy, s, cal/g/°K
PURDUE UNIVERSITY
INDIANA

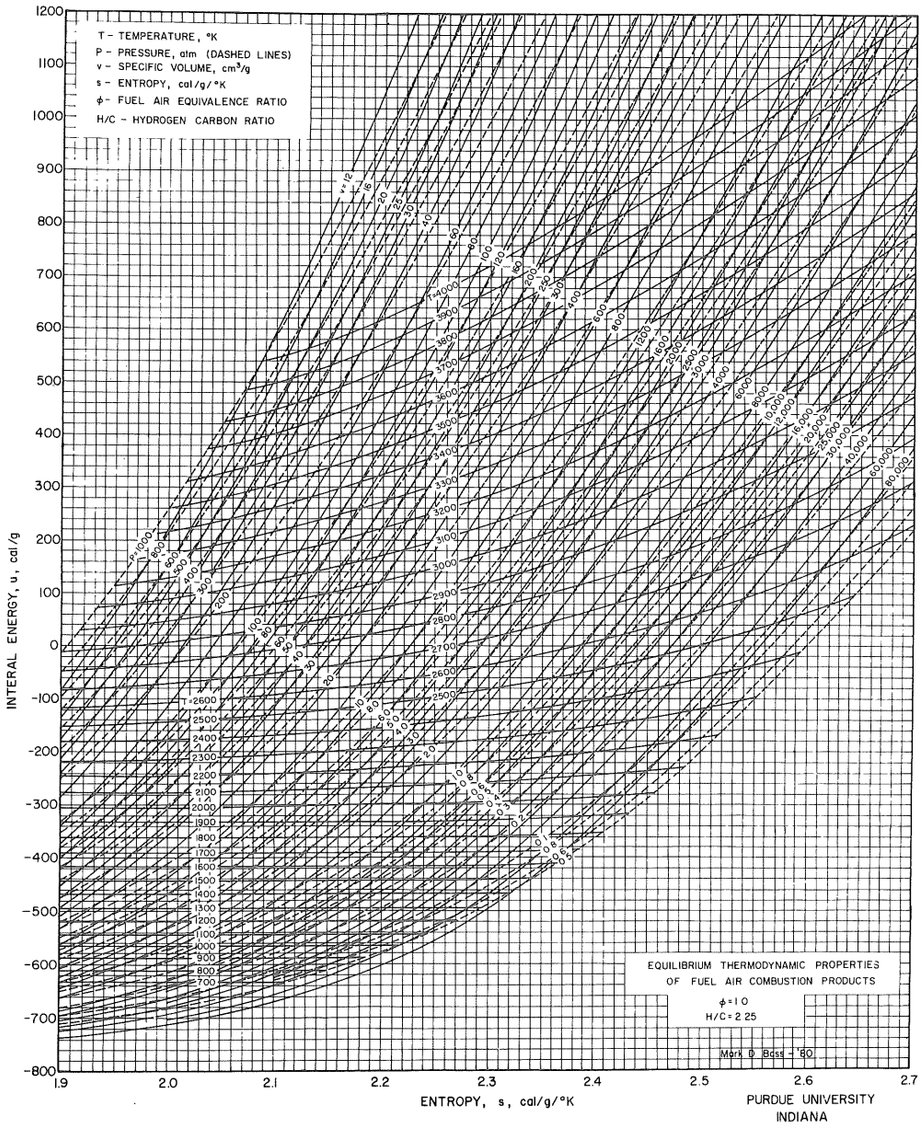
T - TEMPERATURE, °K
P - PRESSURE, atm (DASHED LINES)
v - SPECIFIC VOLUME, cm³/g
s - ENTROPY, cal/g/°K
ϕ - FUEL AIR EQUIVALENCE RATIO
H/C - HYDROGEN CARBON RATIO
EQUILIBRIUM THERMODYNAMIC PROPERTIES
OF FUEL AIR COMBUSTION PRODUCTS
ϕ = 1.0
H/C = 2.25
Mark D. Bass - '60
INTERAL ENERGY, u, cal/g
ENTROPY, s, cal/g/°K
PURDUE UNIVERSITY
INDIANA